Plankton dynamics of the open Southern Ocean and surrounding the (Sub)Antarctic islands

Luca Stirnimann

Supervised by Professor Sarah E. Fawcett, Professor Thomas G. Bornman and Dr Sir Hans M. Verheye

Dissertation of the degree of *Philosophiae Doctor* (Ph.D.)

Department of Oceanography

Faculty of Science

University of Cape Town

January 2023

University of Cape Town

The copyright of this thesis vests in the author. No quotation from it or information derived from it is to be published without full acknowledgement of the source. The thesis is to be used for private study or non-commercial research purposes only.

Published by the University of Cape Town (UCT) in terms of the non-exclusive license granted to UCT by the author.

University of Cape Town

Declarations

I hereby declare that except where specific reference is made to the work of others, the contents of this dissertation are original and have not been submitted in whole or in part for consideration for any other degree or qualification in this, or any other university. This dissertation is my own work and contains nothing which is the outcome of work done in collaboration with others, except as specified in the text and Acknowledgements.

I confirm that I have been granted permission by the University of Cape Town's Doctoral Degrees Board to include the following publication in my Ph.D. thesis, and where co-authorships are involved, my co-authors have agreed that I may include the publication:

Stirnimann, L., Bornman, T. G., Verheye, H. M., Bachèlery, M. L., Van der Poel, J., & Fawcett, S. E. (2021). Plankton community composition and productivity near the Subantarctic Prince Edward Islands archipelago in autumn. Limnology and Oceanography, 66(12), 4140-4158.

Luca Stirnimann

Cape Town, January 2023

A tutte le giovani strobilae che sognano di diventare grandi meduse

Acknowledgments

Someone once said that it’s the journey and not the destination that matters, and for me, this Ph.D. represented a truly amazing and intense journey. I'm glad I chose to study and live in the Mother City because it gave me the chance to pursue my interests, learn about a culture other than my own, forge new lasting friendships, and lay the groundwork for a future career in research. In fact, this thesis serves as both the culmination of a recently completed journey and the beginning of a brand new one.

My most profound appreciation goes to my supervisors Sarah Fawcett, Tommy Bornman and Hans Verheye; it would not have been possible to complete this Ph.D. without their guidance and support. Sarah has been enormously essential to my success, by supporting me both intellectually and emotionally. She has undoubtedly taught me a lot about oceanography and science in general, but what is most important to me is that she taught me to be organised, independent and consistent in my research, that there is no limit to what we can accomplish but to look for more, and that there is always a valuable result to be gained from anything we study. Though I regret not being able to spend more time with Tommy and Hans, the few times I have stayed with them have always been incredibly enjoyable, intense, and greatly appreciated. They have both been wonderful supervisors and amazingly supportive. I have learned so much from their massive intellectual knowledge and from their personal experiences. Tommy has also shown me that science can be ‘Jollie Patrollie’ besides being hard work. Hans has been particularly inspiring because, like me, he moved from his own Country to South Africa when he was still a young student to pursue his higher education, finally achieving amazing success.

I value each and every effort made to help me finish my assignments, no matter how big. I thank Loïc N. Michel and Eleonora Puccinelli for their assistance and intellectual contribution with the trophic analysis on zooplankton. I thank Marie-Lou Bachélery for assistance and support with satellite and physical data processing. I appreciate Heather Forrer, Giuseppe Suaria, and Thomas Ryan-Keogh sharing with me their samples and data since without them, I couldn't do this work. I thank Janine Van Der Poel and Elana Wright for help with the zooplankton incubation experiments and taxonomy. I particularly thank Renae Logston, Holly Nel, and Grant van der Heever for assistance with sample collection and processing and for being an amazing team during our expedition to Marion Island. I also acknowledge Raymond Roman, Ian Newton,

Julie Luyt, and the Stable Light Isotope Laboratory at the University of Cape Town (UCT) for assisting during my analysis. Furthermore, I want to thank Dr David V. P. Conway of the Marine Biological Association of the UK, Dr Holger Auel of the Universität Bremen, and Prof Delphine Thibault of the Aix-Marseille Université for their assistance with plankton identification, and Dr Luke Gregor of Eidgenössische Technische Hochschule Zürich for his valuable replies to my questions on 'Stack Overflow'.

I must acknowledge the Swiss Polar Institute, Captain Dimitri Alexandrovitch Karpenko and the crew of the Russian Polar Research Vessel *Akademik Treshnikov* for financial and logistical support during the Antarctic Circumnavigation Expedition (ACE); as well as, the Department of Forestry, Fisheries and the Environment (DFFE), Captain Gavin Syndercombe and the crew of the South African Polar Research Vessel MV *S.A. Agulhas II*, for financial and logistical support during the voyage to the Prince Edward Islands archipelago.

My Ph.D. was funded by the South African National Research Foundation's Antarctic Programme (SANAP), the Swiss Polar Institute through Antarctic Circumnavigation Expedition (ACE) Project XII, the South African Environmental Observation Network (SAEON), and by a UCT Science Faculty postgraduate fellowship. Support for the research was also made available by the Royal Society/African Academy of Sciences FLAIR programme, the UCT Vice Chancellor's Future Leaders 2030 initiative, the European Union H2020 TRIATLAS project, the Nansen-Tutu Centre for Marine Environmental Research at UCT, and the Department of Science and Innovation's Biogeochemistry Research Infrastructure Platform (BIOGRIP) and Shallow Marine and Coastal Research Infrastructure (SMCRI).

I would like to single out three outstanding colleagues/friends/amazing-girls from the 'THT group': Jess, Raquel and Sina. Thank you for keeping me sane during these last few years and making the time spent on ship fly by. A particular thank goes to Eleonora and Charlino that supported and tolerated me while working and living together with Giotto and Silvestro. I thank Jeremy for being an honest and friendly companion always ready to mockingly point out how pointless both our Ph.D. studies are. I would like to express my sincere gratitude to the UCT Marine Biogeochemistry Lab members for patiently listening to me talking about plankton isotopes, incubation of females (copepods), and about 'small islands in the middle of the ocean'. Thanks to all former and current members of the Department of Oceanography at the UCT, especially Cashifa, who looked out for me in the same way a mother would but in a light-hearted and

delightful way befitting a friend. I thank my first office mates Daneeja, Katherine, Majambo and Obadias *alias* ‘Square of the Good Hope’, and the colleagues of my second office Mishka, Ruan, Robyn and Ruru for distracting me and enabling my procrastination with your endless talks and coffee breaks. I appreciate the handy assistance and the extremely friendly support of Hazel Little and Pieter Truter. Without those two components, a Lab could not be considered a true Lab. I also thank Prof. Isabelle Ansorge and Prof. Marcello Vichi for their enthusiastic support of my research, and of me personally. I had such fun running into them in the corridors of the Department of Oceanography and talking to them about my research.

To my family that have cheered me on at every step of the way, in so many ways; despite the fact that they still believe that the only thing I do research on is the Antarctic krill.

Last but not least, I want to thank Marie-Lou for helping to make this journey more joyful by being helpful and supportive in her own manner.

Abstract

The Southern Ocean is a high-nutrient, low-chlorophyll region where primary productivity is limited mainly by iron and light availability, yet it accounts for ~30-40% of global ocean CO_2 absorption annually. Marine plankton play a major role in the Southern Ocean CO_2 sink as they fix dissolved atmospheric CO_2 into organic carbon biomass, much of which supports the ocean food web and a portion of which sinks into the ocean interior, thereby removing atmospheric CO_2 on decadal to centennial timescales (i.e., the biological carbon pump). The importance of plankton diversity and dynamics in modulating carbon production and export remains poorly understood, particularly around the many (Sub)Antarctic islands where physical and biogeochemical variability is high. The major motivation for the work presented in this thesis is an improved understanding of the role of the plankton system in Southern Ocean fertility and carbon export, and relatedly, the response of the plankton to environmental forcing such as changes in nutrient dynamics driven by hydrography and island mass effects. To that end, I investigated plankton community diversity and ecological dynamics in the context of nutrient cycling, primary production, and carbon export potential in the open Southern Ocean and in the vicinity of its many island systems. Specifically, I used carbon and nitrogen stable isotope ratios as a tool to quantify carbon export potential and food web dynamics across all major hydrographic zones and basins of the Southern Ocean. Five main findings emerged. Firstly, I developed insights into the major drivers of spatial and temporal variability in the carbon and nitrogen isotope ratios ($\delta^{13}C$ and $\delta^{15}N$) of the Southern Ocean's plankton system using circum-Antarctic carbon and nitrogen isoscapes. Along with the drivers commonly invoked by previous studies, I further determined a relationship between the $\delta^{13}C$ and $\delta^{15}N$ of suspended particulate matter (SPM) and phytoplankton community composition, with diatoms exerting a particularly strong influence on the $\delta^{13}C$ and $\delta^{15}N$ of the SPM, which is subsequently transferred to the zooplankton. Secondly, I observed that the (Sub)Antarctic islands tend to increase the $\delta^{13}C$ and $\delta^{15}N$ of phytoplankton and zooplankton relative to the open Southern Ocean. This trend can be explained by the input of terrestrially-derived iron and other nutrients (e.g., ammonium and/or urea from birds and seals) into the surface layer, which stimulate diatom growth on nitrate and/or exogenous reduced nitrogen sources that are high in $\delta^{15}N$. Thirdly, I applied a new approach using the $\delta^{15}N$ of seawater nitrate and SPM to quantify carbon export potential across the summertime Southern Ocean. I found that

carbon export potential is highest near the islands and melting sea ice, driven by the input of limiting nutrients (i.e., iron) and by the dominance of diatoms. Fourthly, I found that the $\delta^{15}N$ of SPM is a reliable baseline for trophic analysis of the zooplankton system over a large spatial extent of the Southern Ocean (i.e., circum-Antarctic). Since the collection and analysis of SPM samples for $\delta^{15}N$ is relatively straightforward, this result should be welcomed by researchers who use such data to reconstruct trophic flows through plankton food webs, as well as the movements and dietary histories of zooplankton in the Southern Ocean. Finally, my new zooplankton $\delta^{13}C$ and $\delta^{15}N$ isoscapes reveal that during the summer, the primary zooplankton consumers in the Subantarctic waters of the Southern Ocean occupy a low trophic position akin to herbivores, implying that the Subantarctic food web may act to retain organic carbon within the euphotic zone instead of exporting it to depth. By contrast, the primary consumers in Antarctic waters occupy a higher trophic position that suggests they are omnivores and carnivores, which potentially indicates a shorter food chain and thus a stronger biological pump. The work detailed in this thesis suggests new methodological approaches for studying the Southern Ocean plankton system and offers an improved understanding of plankton dynamics and their relationship(s) with the biogeochemical processes that govern the different zones of the Southern Ocean.

Contents

Chapter 1. Introduction

1.1. Motivation

Through their complex biological and chemical dynamics, marine phytoplankton and zooplankton in the world's oceans provide fundamental ecosystem services that are vital for life (Naselli-Flores and Padisák, 2022), such as producing the oxygen present in the atmosphere (Harris, 2012; Sekerci and Petrovskii, 2015), sustaining the marine system through their role as food sources (Frederiksen *et al.*, 2006), and contributing to the regulation of global climate by capturing carbon dioxide (a major greenhouse gas) from the atmosphere through photosynthesis and exporting it from the upper water column to the deep ocean, where it will be stored for hundreds of years (i.e., the biological pump; Volk and Hoffert 1985).

Although plankton have been studied for over a hundred years (e.g., Dolan 2021, 2022), there are still fundamental uncertainties surrounding their role in both carbon export and the marine food web, including the magnitude and drivers of fluxes of nutrients and biomass between plankton and other components of the marine system (Lalli and Parsons, 1997; Sarmiento, 2013). One implication of these uncertainties is that Earth system models (i.e., ESMs), which are tools used to study the ocean carbon cycle and its response to historical, present, and future changes in climate and other forcings (Sixth Assessment Report of the Intergovernmental Panel on Climate Change, 2022), are developed based on biogeochemical and plankton dynamics and relationships that may be too simplistic and/or incorrect (Séférian *et al.* 2020 and references therein). Advancing the availability of ocean biogeochemical data and our knowledge of plankton dynamics will allow us to better understand the role of plankton and the ecological services they provide to the marine system, including within its carbon cycle, with implications for improving ESMs.

My Ph.D. research is focused on the plankton dynamics that govern some of the ecosystem services provided by the Southern Ocean. The Southern Ocean is considered one of Earth's major carbon sinks because it takes up approximately one third of the CO_2 absorbed by the global ocean annually (DeVries, 2014). Furthermore, the Southern Ocean harbours habitats of important large marine species such as whales (Hill *et al.*, 2006) and supports large commercial fish stocks (upon which humans are also dependent; Croxall and Nicol 2004).

The remoteness and vast spatial extent of the Southern Ocean make it a challenging location for observational oceanography, with many of the existing observations studies being by necessity locally/regionally focused. Much of my observational research in the Southern Ocean was conducted on a circumpolar spatial scale in order to investigate the variability of the major hydrographic zones spanning the Southern Ocean, as well as regions affected by sea ice, glaciers, continental shelves, and islands. In particular, islands are regions where changes in the circulation and the retention of surface waters, inputs of island-derived nutrients, and the upwelling of deep nutrient-rich waters yield localized increases in phytoplankton biomass, which affect the entire marine system (i.e., the Island Mass Effect (IME); Doty and Oguri 1956). Although all the islands in the Southern Ocean influence the plankton system and their dynamics in some way (e.g., Perissinotto *et al.* 1992; Korb *et al.* 2004; Bakker *et al.* 2007; Jouandet *et al.* 2008; Jones *et al.* 2012), a particular focus of the research detailed in this thesis is the ocean properties and processes generated by the IME of the Subantarctic Prince Edward Islands archipelago (PEIs) in the southwest Indian sector of the Southern Ocean. This focus was motivated by 1) the long historical record of observations from the PEIs that span more than 70 years (Pakhomov and Froneman, 1999; Pakhomov *et al.*, 2000; this Ph.D. thesis); 2) the significance of this particular ecosystem for South Africa's heritage (e.g., Costanza *et al.* 1997); and 3) the importance of the PEIs as a habitat for hundreds of marine and terrestrial species of elevated conservation status and ecological importance (Chown and Froneman, 2008).

This thesis advances our quantitative understanding of carbon and nutrient export, recycling, and redistribution across the Southern Ocean and its islands, through transformations driven by the plankton system and their transfer across the pelagic food web.

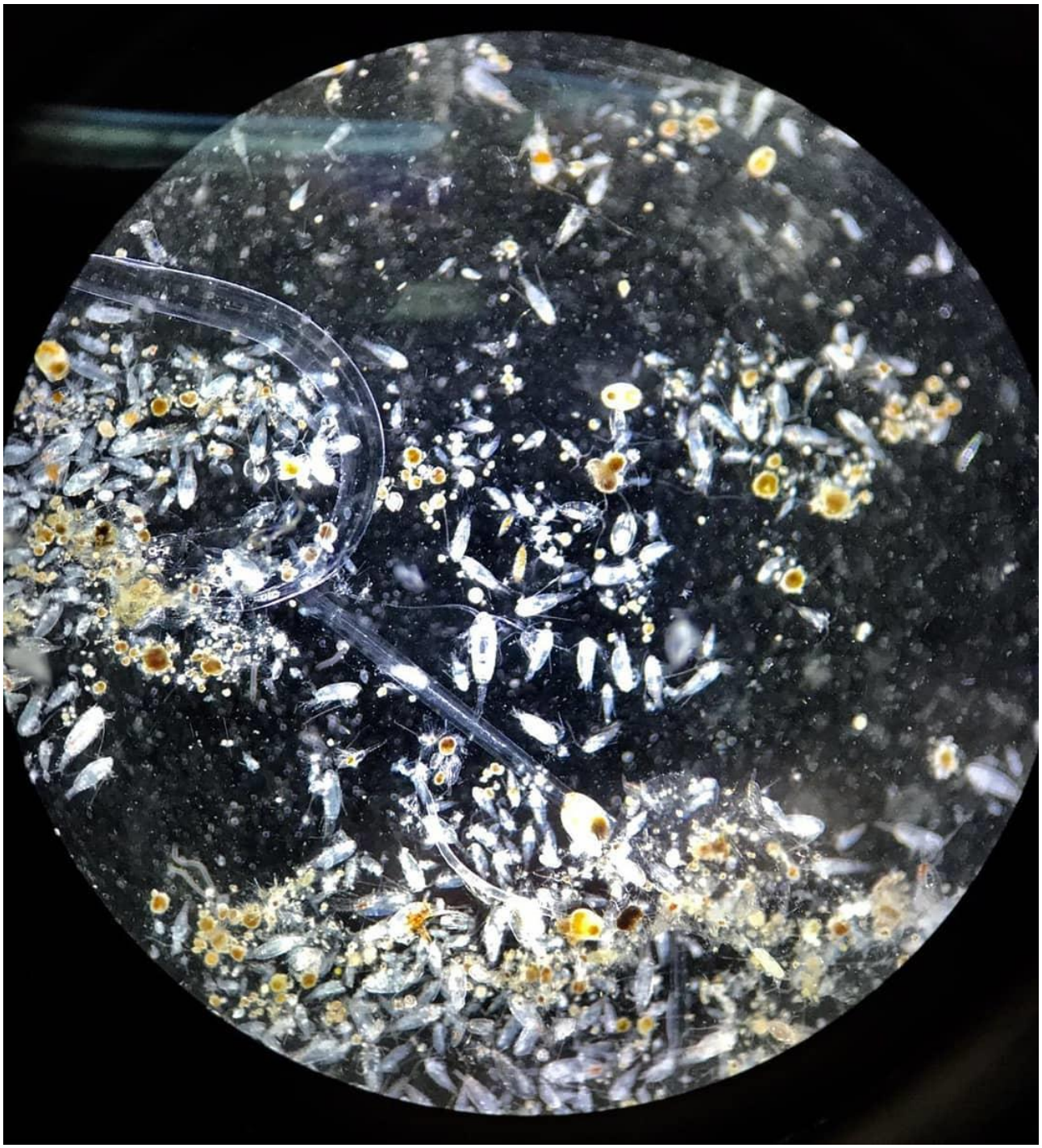

Figure 1.1 Numerous distinct taxonomic groups of varying sizes, morphologies, and physiologies make up the plankton communities, which are affected by and adapted to a wide range of environmental conditions. As such, plankton are not distributed randomly in the oceans (Castellani and Edwards 2017 and references therein). This image captures the researcher's vision while observing through a microscope a fresh sample of plankton collected using a net (200 µm mesh size) in the Southern Ocean (photo taken by Luca Stirnimann).

1.2. The importance of the plankton

The term *plankton* was introduced by Viktor Hensen (Hensen, 1887) and originates from the Greek word πλαγκτός meaning *errant* or *drifter* in the oceanographic context, in order to separate these marine organisms from those associated with the seafloor (βένθος or *benthos*) or those organisms capable of swimming against water currents (νηκτόν or *nekton*). Plankton span unicellular and small colonial organisms of only a few micrometres in size, and multicellular ones several meters long, and can be divided into three major categories: the autotrophic and mixotrophic phytoplankton and the heterotrophic zooplankton (Reynolds, 2006; Stoecker *et al.*, 2017 and references therein).

Phytoplankton (φυτόν + *plankton*, or drifter plant) are unicellular plants that live in the euphotic zone (i.e., sunlit upper layer) of the water column, amounting to approximately 25,000 recognized species, including eubacterial and eukaryotic species (Marañón *et al.*, 2009). Among the eukaryotic marine phytoplankton are significant contributors to major global processes, such as diatoms, dinoflagellates, haptophytes, and the small prasinophytes, some of which periodically form massive blooms visible in satellite images (Not *et al.*, 2012). All phytoplankton live in the sunlit surface layer of the water column, and through their activity provide ecological services that are fundamental to the regulation and sustenance of life on our planet (Naselli-Flores and Padisák, 2022). Through their photosynthesis, phytoplankton transform the inorganic carbon dioxide (CO_2) that is dissolved from the atmosphere in the water into organic compounds useful for cellular growth and division (i.e., primary production; Falkowski *et al.*, 1998; Field *et al.*, 1998; Falkowski and Woodhead, 2013). Indeed, phytoplankton are responsible for about half of global net primary production (~49% ≈ 108 Pg C year^{-1}) and produce half of the oxygen available in the atmosphere (Field *et al.*, 1998; Friend *et al.*, 2009). Phytoplankton, like the plants on land, require macronutrients such as nitrate and phosphate (with some requiring silicic acid) and micronutrients such as iron in different amounts depending on the species, and are fundamental to the biogeochemical cycles of all the inorganic elements, driving processes such as nutrient (re-)cycling and redistribution, which are necessary to support the food web (Falkowski, 1994).

Zooplankton (ζῷον + *plankton*, or drifter animal) are free-swimming animals, with this group containing thousands of species from all phyla of the Animal Kingdom, including Cnidaria, Ctenophora, Mollusca, and

the Crustacea, with the last representing the most abundant and diverse zooplankton phylum (Castellani and Edwards 2017 and references therein). Zooplankton contribute to the transfer and recycling of organic matter through the capture, sorting, filtration, and ingestion of food of diverse origin, such as phytoplankton, other zooplankton, faecal pellets, and/or other forms of particulate organic carbon (POC; Lalli and Parsons 1997). In turn, the zooplankton biomass (i.e., secondary productivity) is fed upon by a vast variety of predators including sea birds, fish, and whales, such that zooplankton provide a fundamental and global ecological service by contributing to sustaining the marine food webs (Fenchel, 1988; Frederiksen *et al.*, 2006). Zooplankton organisms can live throughout the entire water column, with some capable of swimming hundreds of meters from the deep- to the surface layer of the water column and *vice versa* (i.e., vertical migration; Lampert 1989). Zooplankton vertical migration enhances the rate of export of euphotic zone-produced organic carbon to depth where it is then remineralized into dissolved inorganic carbon (i.e., DIC, which includes dissolved CO_2, bicarbonate, and carbonate), the concentration of which consequently increases with depth. Zooplankton contribute to the removal of CO_2 from the atmosphere by exporting new biomass produced at the surface (primary productivity) to the bottom of the ocean where it can be stored for centuries (i.e., the biological pump) through, in addition to active vertical migration, the gravitational sinking of their faecal pellets, crustacean moults from ecdysis, dead bodies, and decaying cells (Figure 1.2; Longhurst and Glen Harrison 1989; Ducklow *et al.* 2001; Steinberg and Landry 2017)

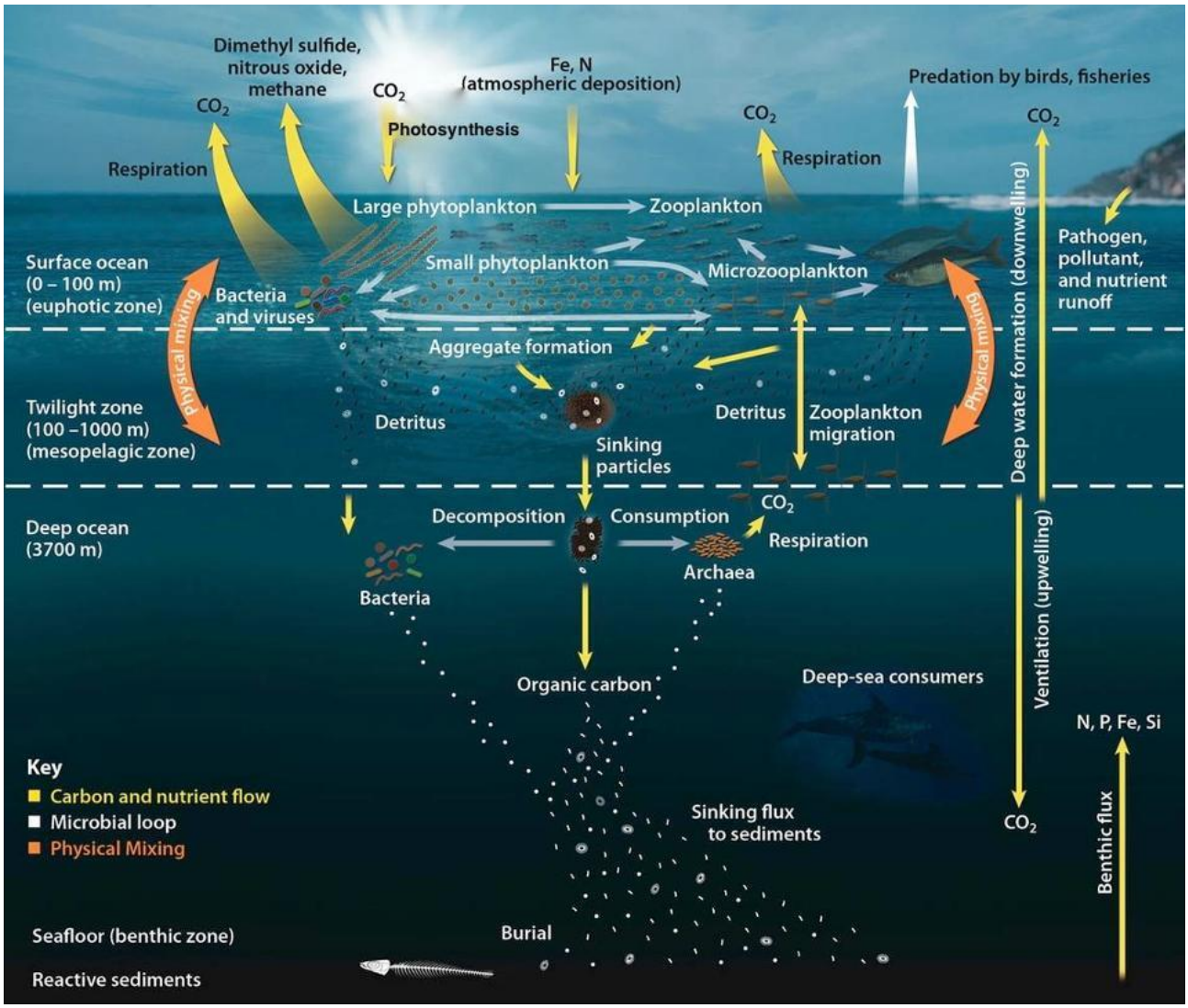

Figure 1.2 The biological pump and pelagic food web are two of the major ecosystem services governed by plankton. N, P, Fe, Si indicate nitrogen, phosphorus, iron, and silicon. From: Office of Biological and Environmental Research of the U.S. Department of Energy Office of Science (DOE, 2008).

1.2.1. Carbon export potential in the context of the biological pump

In the euphotic zone, much of the new carbon biomass (phytoplankton) produced by the photosynthetic fixation of DIC is consumed by zooplankton grazing (with these zooplankton then fuelling higher trophic levels including fish and whales) and heterotrophic microbial activity, which recycle it back to CO_2 that is eventually returned to the atmosphere (Robinson *et al.*, 2010; Turner, 2015; Steinberg and Landry, 2017). However, as mentioned above, a fraction of the organic carbon escapes recycling in the upper layer and is exported to the deep ocean where it is respired and can be sequestered for centuries (DeVries *et al.*, 2012; DeVries, 2014).

The amount of carbon that is exported and sequestered (with the former term referring to the transport of carbon out of the mixed layer, and the latter to the centennial-scale storage of regenerated nutrients and carbon in the ocean interior ocean before they are returned to the surface) is determined by two well-known mechanisms that control the surface-to-deep ocean gradient of DIC, the solubility pump and the biological pump (Volk and Hoffert, 1985; McKinley *et al.*, 2016; Boyd *et al.*, 2019). The solubility pump involves the transport of the DIC to depth through the dissolution of atmospheric CO_2 in cold, dense water masses that form at high latitudes and subduct into the ocean interior (Volk and Hoffert, 1985; Sarmiento, 2013). The biological pump, by contrast, involves two dominant mechanisms that transport POC from the surface to depth, the gravitational and migration pumps (Boyd *et al.*, 2019; Halfter *et al.*, 2020, 2022; Nowicki *et al.*, 2022). It has been suggested that the solubility pump drives approximately 10% of the vertical DIC gradient, with the remaining 90% driven by the biological pump (Sarmiento, 2013; Boyd *et al.*, 2019), in particular by the gravitational pump (i.e., the sinking of zooplankton faecal pellets, phytoplankton aggregates, detritus, and other organic particles), which is responsible for the export of ~4–9 Pg C yr^{-1} (Henson *et al.*, 2011; Siegel *et al.*, 2014; Nowicki *et al.*, 2022) and for the sequestration of 600–1,400 Pg C globally over the last *circa* 150 years (Boyd *et al.*, 2019; Nowicki *et al.*, 2022).

Although the direct quantification of the gravitational pump (e.g., through the deployment of sediment traps along bottom-tethered mooring platforms) gives a good estimate of effective carbon export and sequestration in the ocean (Honjo *et al.* 2008 and references therein), such measurements are difficult to make and coverage is sparse. Fortunately, it is also possible to estimate the strength (i.e., the rate of organic carbon export) and efficiency (i.e., the degree to which primary productivity contributes to export from the available nutrients) of the biological pump through the 'new production paradigm', which links surface nitrogenous nutrient assimilation to carbon export by mass balance (Dugdale and Goering, 1967; Eppley and Peterson, 1979).

The bioavailable nitrogen (N) forms present in the mixed layer include particulate and dissolved organic N (PON and DON, respectively), and the dissolved inorganic forms such as nitrite (NO_2^-), ammonium (NH_4^+), and the most common, nitrate (NO_3^-). These N forms can be characterized as either 'new' or 'regenerated' (Dugdale and Goering, 1967). In contrast to 'regenerated production', which is supported by N recycled in

the surface ocean (primarily NH_4^+, as well as forms of DON, and NO_2^- and NO_3^- produced and recycled within the surface layer[1]), 'new production' refers to phytoplankton growth fueled by new N (primarily deep NO_3^- mixed up into the surface layer) (Dugdale and Goering, 1967). The new production paradigm requires that new production must be balanced on an annual timescale by the export of organic matter from the surface layer ('export production'). In other words, the amount of new NO_3^- introduced and taken up by phytoplankton is equivalent to the amount of organic N (and through the application of a known organic matter carbon:N ratio, the amount of organic carbon) exported. By contrast, regenerated production yields no net organic matter export in a mass balance sense (Figure 1.3; Dugdale and Goering 1967). The proportion of new production (and hence, export) relative to total (i.e., new + regenerated) production in an ecosystem can be measured by the *f*-ratio, also known as the 'flux ratio' (Eppley and Peterson, 1979).

Whether phytoplankton assimilation new or regenerated N is controlled by several environmental factors, such as solar irradiance, temperature, and macro- and micro-nutrient availability, as well as physiological factors such as cell size (e.g., Price *et al.* 1991; Stolte and Riegman 1995; Sunda and Huntsman 1997; Hu and Smith 1998). In general, while the input of limiting nutrients such as iron stimulate the uptake of new NO_3^- (Traganza *et al.*, 1980; Timmermans *et al.*, 1994, 1998; Cochlan, 2008) leading to higher *f*-ratios and carbon export potential, warmer waters and conditions of nutrient limitation are associated with higher rates of regenereted NH_4^+ uptake and thus a lower *f*-ratio and carbon export potential (e.g., Lipschultz 2001; Fawcett *et al.* 2011; Prakash *et al.* 2015; Wallschuss *et al.* 2022). At the same time, NH_4^+ is less energetically expensive for phytoplankton to assimilate than NO_3^- (Dortch, 1990; Raven *et al.*, 1992; Glibert *et al.*, 2016), in addition to requiring less iron and irradiance (Dortch, 1990; Raven *et al.*, 1992; Glibert *et al.*, 2016). NO_3^- uptake is also controlled by the size of phytoplankton cells present in the water column, with large cells typically able to take up NO_3^- at a maximum rate for a greater period of time than small cells (Stolte and Riegman, 1995; Fawcett *et al.*, 2011). As such, marine systems where dependence on NO_3^- is high tend to be characterised by larger phytoplankton than regions where most productivity is fueled by NH_4^+ (Stolte and Riegman, 1995). On the other hand, as cell size increases, the diffusion-boundary layer around the cell

[1]In the original formulation of the new production paradigm (*sensu* Dugdale and Goering 1967), the 'surface layer' was taken to be the euphotic zone. However, if the mixed layer is deeper than the euphotic zone, as is often the case in the Southern Ocean (e.g., Cavagna *et al.* 2015; Mdutyana *et al.* 2020), then nutrient supply to, consumption and cycling within, and export from the entire mixed layer must be considered. Where the new production paradigm is invoked in this thesis, the relevant 'surface layer' is always defined.

thickens and nutrient diffusion per unit of cell volume decreases (Pasciak and Gavis, 1974; Kiørboe, 1993; Raven, 1998). As a result, the capacity of phytoplankton to obtain nutrients decreases faster than the volume-specific nutrient quotas as cells size increases, which means that small cells are more competitive in low-nutrient environments (Smith and Kalff, 1982; Litchman *et al.*, 2007). In the Southern Ocean, as in other regions, small phytoplankton appear to outcompete larger cells for NH_4^+ (Fawcett *et al.*, 2011; Smith *et al.*, 2022).

Concurrent to the fact that plankton depend on the marine N cycle for their productivity, a variety of (mainly photosynthetic) prokaryotes, known as diazotroph (e.g., filamentous cyanobacteria), are essential to the marine N cycle and to oceanic productivity. These plankton can 'fixing' dinitrogen (N_2) gas, which involves converting unreactive N_2 dissolved in seawater into bioavailable NH_4^+ (Gruber 2008 and references threin). Diazotrophs are thus essential for ocean fertility, while also compensating for N losses via denitrification (i.e., the dissimilatory reduction of NO_3^- to N_2 gas during organic matter oxidation; Gruber 2008; Voss *et al.* 2013 and references therein). N_2 fixation may represent a fundamental source of new N to N-limited surface waters (i.e., the (sub)tropical oceans), potentially even exceeding the supply of deep new N by physical processes, with implications for how carbon is cycled through the ecosystem and the proportion that is exported (i.e., N_2 fixation, like subsurface NO_3^-, fuels export production; Karl *et al.* 1997; Capone *et al.* 2005). In the Southern Ocean, the rate of N_2 should be low to zero given the cold temperatures, low light and iron conditions, and high mixed-layer NO_3^- concentrations (Kustka *et al.*, 2003; Knapp, 2012; Jiang *et al.*, 2018). N_2 fixation is therefore not considered in applications of the new production paradigm to the data collected for this thesis.

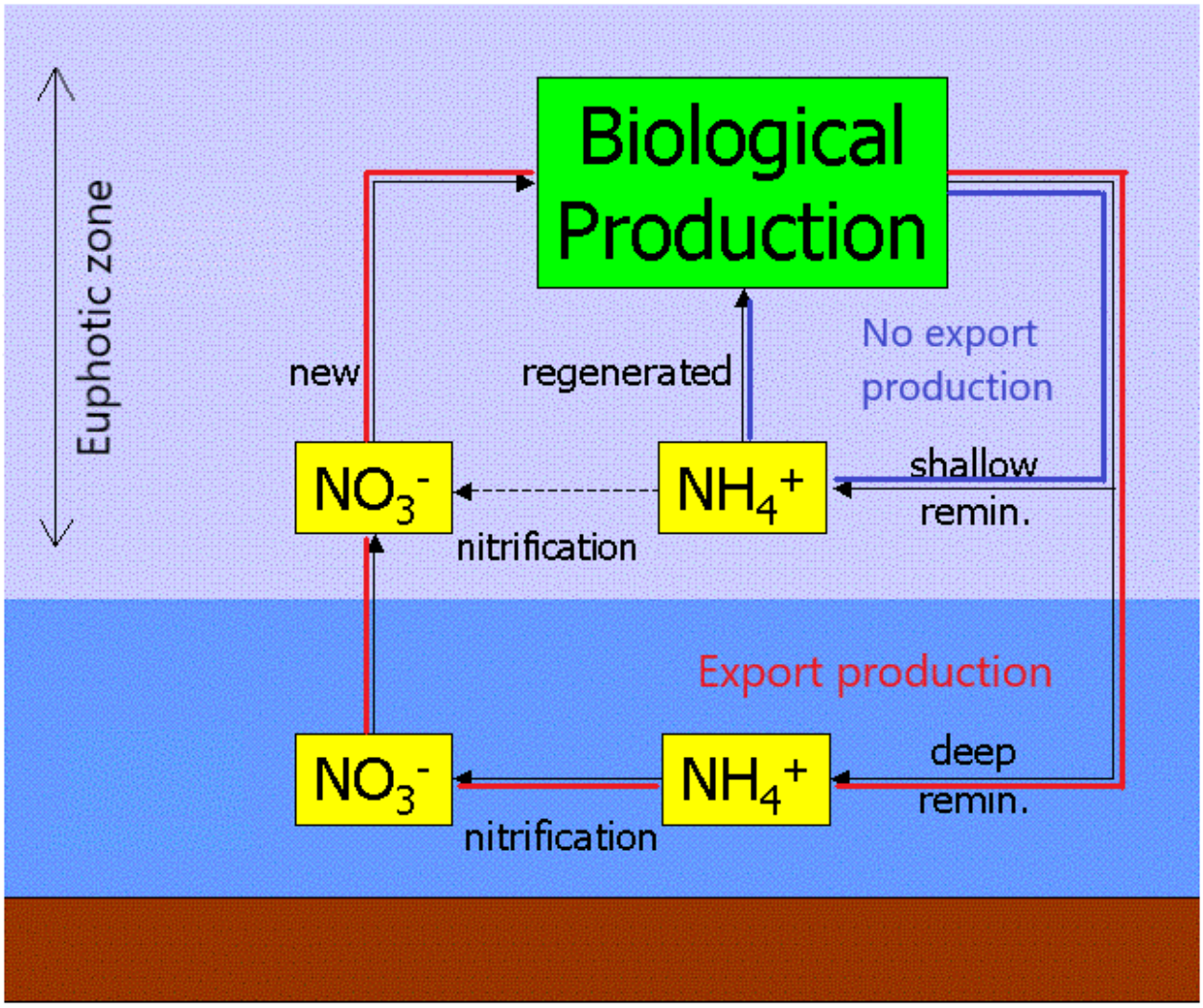

Figure 1.3 The new production paradigm as originally formulated by Dugdale and Goering (1967). New production – defined as primary production supported by 'new' nutrients (such as allochthonous nitrate mixed up into the surface layer from depth) – is quantitatively related to 'export production' over an annual cycle. Regenerated production, in contrast, which is fuelled by 'regenerated' nutrients (such as ammonium and nitrate regenerated within the surface layer), does not contribute to export (figure adapted from Plumbago 2006).

1.2.2. Carbon export through the food web

As mentioned above, zooplankton play a central role in elemental cycling, by ingesting and converting POC and nutrients into dissolved pools, and actively exporting nutrients to depth during diurnal and seasonal migrations (Figure 1.2; Steinberg and Landry 2017 and references therein; Halfter *et al.* 2020 and references therein), as well as in the trophic linkages between primary producers and higher trophic levels (such as fish and whales; Figure 1.4; e.g., Cavan *et al.* 2019 and references therein). However, the study of zooplankton participation in food webs and biogeochemical cycles is extremely complex due to their large diversity of

taxa, life histories, sizes, trophic ecology, and physiology (Steinberg and Landry 2017 and references there in). Zooplankton trophic roles and biological processes impact oceanic biogeochemical cycles and the efficiency of carbon export through the pelagic food web. The proportion of organic carbon that leaves the euphotic zone can vary significantly, as a function of the top-down regulation of the vertical flux due to the trophic behaviour of different types of zooplankton and the structure of the zooplankton community (Kiørboe, 1997; Wassmann, 1997; Nowicki *et al.*, 2022). Uncertainties regarding the pathways of carbon and nutrient flows through the food web can be reduced through the analysis of trophic structure and the roles of each consumer in the pelagic ecosystem (Steinberg and Landry, 2017). That said, assessing regional and temporal variability in the transfer of phytoplankton production to higher trophic levels requires knowledge of the mean trophic position of zooplankton relative to phytoplankton, which is still a significant unknown in most marine ecosystems. For instance, this thesis presents a novel assessment of the trophic positions of specific zooplankton species relative to phytoplankton, to better understand the plankton food web system across the Southern Ocean.

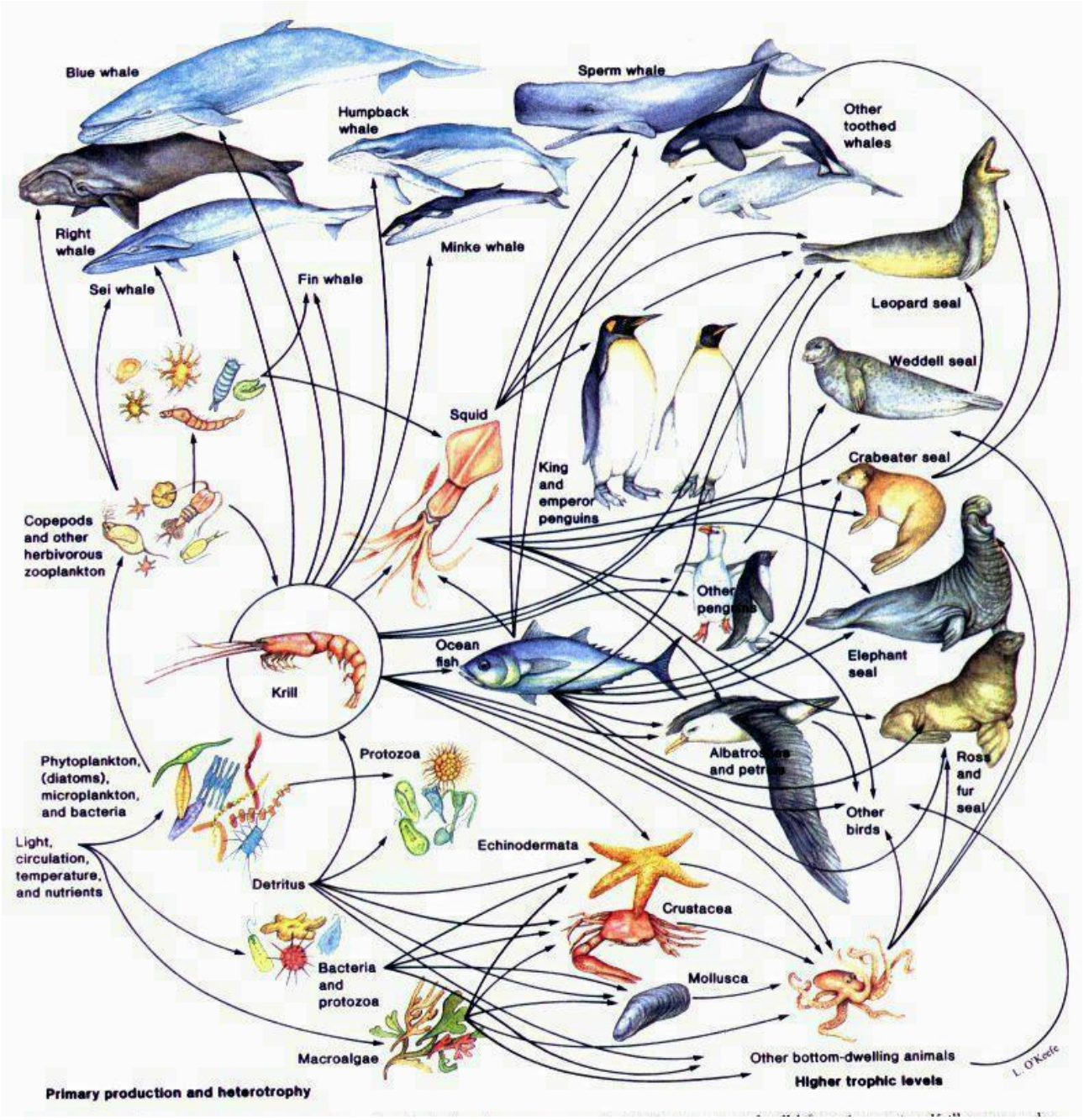

Figure 1.4 Example of an Antarctic marine food web and energy flows from prey to predator/grazer (black arrows). The keystone species of the Antarctic ecosystem are phytoplankton and zooplankton, especially Antarctic krill, since they are a vital source of food for whales, seals, squid, icefish, penguins, albatrosses, and several other bird species. Picture source: unknown

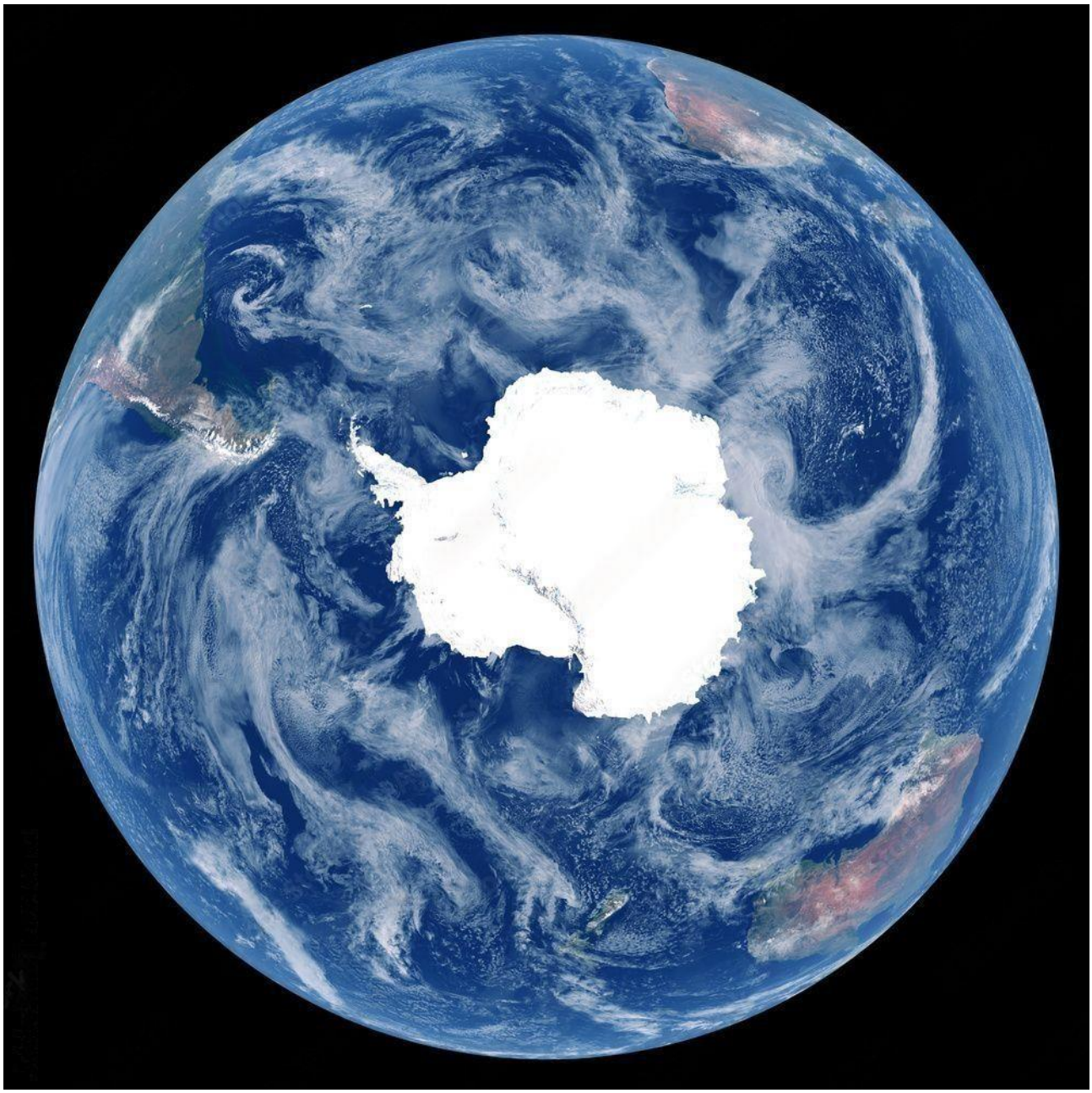

Figure 1.5 The Southern Ocean as seen from space: it surrounds the Antarctic continent without interruption and touches three of the world's continents: Africa (top-right), Australia (bottom-right), and South America (top-left). Satellite image courtesy of NASA.

1.3. The importance of the Southern Ocean

The Southern Ocean is a significant marine system that surrounds the Antarctic continent and accounts for around 20% of the world's ocean surface. It has a disproportionate influence on global climate and hosts vast and diverse marine ecosystems (e.g., Sarmiento and Toggweiler 1984; Murphy 1995; Sarmiento and Le Quere 1996; Takahashi *et al.* 2009; Deppeler and Davidson 2017).

The Southern Ocean is separated from the subtropical waters of the Atlantic, Pacific, and Indian Oceans by a steep gradient in sea surface temperature and salinity termed the Subtropical Front (Orsi *et al.*, 1995; Holliday and Read, 1998) and is subject to strong winds that generate the dominant eastward-flowing Antarctic Circumpolar Current (ACC; Trenberth *et al.* 1990). A series of fronts within the ACC driven by sea-wind interactions represent important physical and biological boundaries that separate hydrographic zones characterized by distinct environmental characteristics (Figure 1.6; Orsi *et al.* 1995; Chapman *et al.* 2020). From north to south, the Southern Ocean can be divided into two main oceanic regions: 1) the Subantarctic, which makes up more than half of the Southern Ocean's surface and can be further divided into two zones: the Subantarctic Zone (SAZ), between the Subtropical and Subantarctic Fronts (STF and SAF, respectively), and the Polar Frontal Zone (PFZ), between the SAF and the Antarctic Polar Front (APF or PF) (Orsi *et al.*, 1995); and to the south of the PF, 2) the Antarctic Ocean, which includes the permanently ice-free zone (or Open Antarctic Zone [OAZ]) to the north of the Southern Antarctic Circumpolar Current Front (SACCF) and the seasonal sea-ice zone to the south of the SACCF (Hempel 1985; Talley 2011; Figure 1.6), that can be further divided by the Antarctic Shelf Front (ASF) into the Antarctic Zone (AZ) between the SACCF and the ASF, and the Continental Zone (CZ) between the ASF and the continent (Orsi *et al.*, 1995; Post *et al.*, 2014).

While the hydrographic fronts of the Southern Ocean are regions of enhanced vertical exchange between deep- and surface water masses (e.g., Carter *et al.* 2008), they often coincide with dynamical mixing barriers or jets, which reduce the exchange of biogeochemical elements across fronts (Palter *et al.*, 2013). In addition, the extent of the seasonal variability in irradiance and temperature increases from north to south, leading to strong latitudinal (and thus hydrographic zone-related) differences in regional biogeochemical cycling and ecosystem functioning (Abbott *et al.*, 2000; Landry *et al.*, 2002; Chapman *et al.*, 2020).

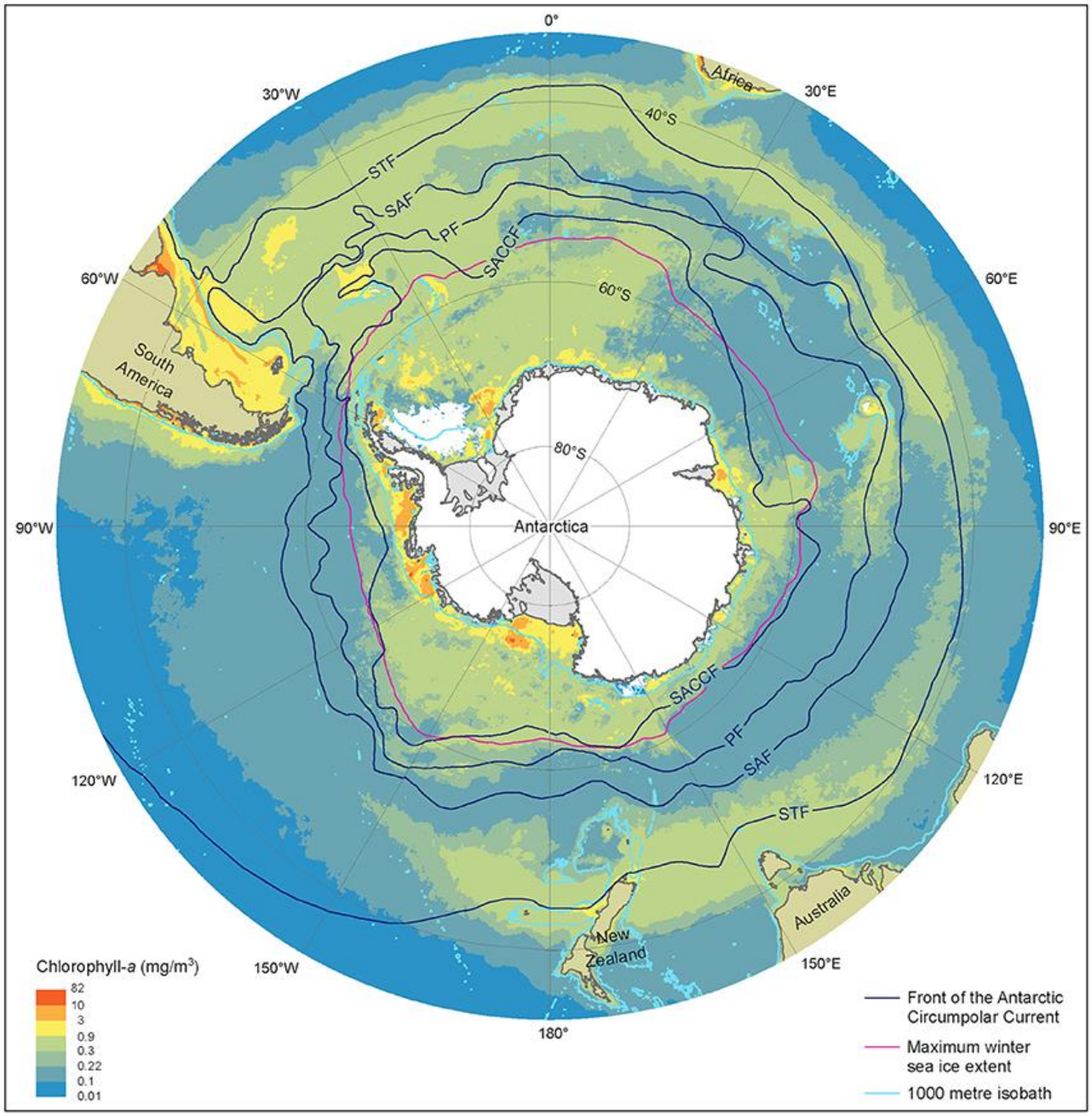

Figure 1.6 Average estimates of surface chlorophyll-a concentration (mg m^{-3}; background shading) from summer season between 2002/03 and 2015/16, frontal locations (black lines), and sea-ice extent (magenta line for the maximum winter extent and white shading for the minimum summer extent) in the Southern Ocean. Frontal positions are based on the definitions of Orsi *et al.* (1995) and are summertime climatological averages: STF = Subtropical Front, SAF = Subantarctic Front, PF = Antarctic Polar Front, SACCF = Southern Antarctic Circumpolar Current Front. The red line denotes the maximum extent of sea ice averaged over the 1979/80 to 2007/08 winter seasons. Figure from Deppeler and Davidson (2017).

It is estimated that the Southern Ocean south of 30°S removes about 3 Pg of carbon emitted to the atmosphere every year, which represents approximately 30-40% of the global ocean's total carbon flux (Schlitzer, 2002; DeVries, 2014; Frölicher *et al.*, 2015; Arteaga *et al.*, 2018); the Southern Ocean is therefore a significant contributor to the planet's oceanic CO_2 sink. Additionally, by the absorption of CO_2 through

solubility and biological pump processes and the release of CO_2 from the deep ocean, the Southern Ocean significantly modifies global climate over seasonal to millennial time-scales (e.g., Sarmiento and Le Quere 1996; Gruber *et al.* 2009; Takahashi *et al.* 2009; Sigman *et al.* 2010).

Although the Southern Ocean's biological pump plays a central role in the export and sequestration of carbon, the combined low concentrations of iron and, in some regions, manganese (Mn) and/or silicic acid (SiO_4^-), as well as reduced light availability for many months of the year, limit the consumption by phytoplankton of macronutrients such as new NO_3^- and phosphate (PO_4^{3-}; Martin *et al.* 1990; Sunda and Huntsman 1997; Bracher and Kroon 1999; Boyd 2002; Boyd *et al.* 2016; Hawco *et al.* 2022). As a consequence, the input of new nutrients from deep water does not yield as much carbon fixation and export as one might expect, such that the Southern Ocean is considered a 'leak' in the global ocean's biological pump (Sarmiento and Toggweiler, 1984). In this context, the (Sub)Antarctic islands, continental shelves, sea ice, and glaciers contribute significantly to alleviating phytoplankton from iron and silicic acid stress, largely as a result of bathymetric upwelling, terrestrial run-off, and ice melt, all of which are a manifestation of the 'island mass effect' (see section 1.4; e.g., Doty and Oguri 1956; Hamner and Hauri 1981; Pollard *et al.* 2009; Lourantou and Metzl 2011; Alderkamp *et al.* 2012). This thesis focuses on estimating the carbon export potential implied by phytoplankton consumption of new NO_3^- in the Southern Ocean and the effects of nutrient release from glaciers, sea-ice, continental shelves, and islands (particularly the Subantarctic islands).

Due in part to the prevalence of two main consumers in the Southern Ocean, *Euphausia superba*, a species of Antarctic krill, and several species of plankton-consuming whales (e.g., Murphy 1995; Baines *et al.* 2021, 2022; McBride *et al.* 2021; Johnston *et al.* 2022), the Antarctic food web is often referred to as a 'krill-whale food chain' (Figure 1.4), which is unique in the world's oceans because of its shorter, simpler, and more linear energy fluxes compared to marine food webs found at lower latitudes (Hempel, 1985; Murphy, 1995). Antarctic krill transfer energy through the food web after consuming phytoplankton biomass by becoming prey for higher trophic levels. They also contribute to driving the biogeochemical cycles in the Southern Ocean, including carbon, N, and iron, through the production and sinking of faecal pellets, which are then remineralized by microbial activity (Tarling and Johnson, 2006; Cavan *et al.*, 2019). It has been estimated that the sinking of krill faecal pellets contributes between 17% and 72% of total carbon export in Antarctic

waters (Gleiber *et al.*, 2012; Belcher *et al.*, 2019), such that krill are one of the most important actors in the region's biological pump. As a consequence, most of the models used to quantify carbon export are based on the role of *Euphausia superba* in the Antarctic food web (Hill *et al.* 2006; McCormack *et al.* 2021a; and references therein). However, the Antarctic plankton system is more intricate than the krill-whale food chain and several other organisms contribute substantially to the energy fluxes, and may become more important in future as the plankton trophic structure varies with global change (Atkinson *et al.*, 2004, 2019; Hill *et al.*, 2019; Johnston *et al.*, 2022). For instance, zooplankton organisms such as salps, copepods, amphipods, pteropods, and jellyfish (Voronina, 1998; Atkinson *et al.*, 2012a; Johnston *et al.*, 2022) contribute to the carbon and nutrient flows in Antarctica's marine system by providing substantial biomass to top predators such as seabirds (penguins and Procellariiformes, including albatrosses, shearwaters, storm- and diving petrels) and marine mammals (cetaceans, including whales and dolphins, and pinnipeds such as seals) (Clarke, 1985; Murphy, 1995; Grant *et al.*, 2013; Bestley *et al.*, 2020), and likely also influence the biogeochemical cycles. Indeed, it has been reported for the Southern Ocean that salps produce large amounts of faecal pellets, which sink 2.5-times faster than krill pellets (760 *versus* ~300 $m\,d^{-1}$; (Pakhomov *et al.*, 2006; Atkinson *et al.*, 2012b), contributing between 5% and 66% of the total flux of POC (Fischer *et al.*, 1988; Gleiber *et al.*, 2012). In addition, contrary to the widely held belief that salps are indiscriminate and continuous filter feeders (Andersen, 1998 and references therein; Pakhomov *et al.*, 2002) whose diets generally reflect the composition of the available plankton community, recent research on the stomach contents of Antarctic salps and the composition of plankton communities in the water column during autumn has revealed that salps exhibit selective feeding behaviour (Pauli *et al.*, 2021). Specifically, salps preferentially consume small flagellates and golden algae over other unicellular algae (Pauli *et al.*, 2021). This selective grazing behaviour of salps adds complexity to the study of the energy flow driven by these organisms and raises questions about whether other species exhibit different trophic behaviours than currently understood, with potential implications for our understanding of food web interactions and energy flows.

Marine species and the pelagic food web vary with the physical and biogeochemical environments of the different hydrographic zones of the Southern Ocean (Constable *et al.*, 2014; McCormack *et al.*, 2021b; Yang *et al.*, 2021; Johnston *et al.*, 2022). Notably, future changes in the distributions and ecological roles of

plankton and (related) food web structures in the hydrographic zones of the Southern Ocean (Hill *et al.*, 2021; McCormack *et al.*, 2021b) could have implications for ecosystem services such as carbon export and sequestration, ocean acidification, recovery of the great whales, and fisheries (Trebilco *et al.*, 2020; McCormack *et al.*, 2021b). As such, understanding the food web and the food requirements of different trophic levels in the Southern Ocean is crucial for understanding the energy fluxes between species and the implications for carbon export (Hill *et al.*, 2006; Melbourne-Thomas *et al.*, 2017).

In this thesis, the plankton contributions to carbon export and their trophic roles in the Southern Ocean's marine system, with implications for the major biogeochemical cycles, are investigated using sensitive ecological tools such as the stable isotopes of carbon and nitrogen (see section 1.5).

Figure 1.7 The Prince Edward Islands archipelago is formed by the Prince Edward Island (north-east) and Marion Island (south-west) and hosts one of the most biodiverse marine ecosystems of the Subantarctic Ocean. Satellite image courtesy of NASA.

1.4. The Island Mass Effect (IME)

The island mass effect (IME) describes a localized increase of the oceanic biota and primary production downstream and in close proximity to islands (Doty and Oguri, 1956) that results from a spectrum of physical and biogeochemical processes (e.g., Boden 1988; Perissinotto *et al.* 1992; Blain *et al.* 2007; Gove *et al.* 2016). The physical mechanisms responsible for the IME, such as current-island interactions, wind-island interactions, ocean-atmosphere coupled processes and interactions, and ocean mixing, control the circulation and retention of surface waters around islands and the by extension, the availability (i.e., supply and residence time) of nutrients in the upper water column, ultimately resulting in enhanced biological activity (Figure 1.8; De Falco *et al.*, 2022). Currents interacting with the bathymetry upstream of an island may lift the isotherms and cause upward vertical transport of nutrient-rich deep water (Hamner and Hauri, 1981; Gove *et al.*, 2006; Liu *et al.*, 2014), while anti-cyclonic (or cyclonic for the northern hemisphere) eddies often form downstream of an island due to barotropic or baroclinic instabilities (Dong *et al.*, 2007; Teinturier *et al.*, 2010) and flow divergence (Heywood *et al.*, 1990; Hasegawa *et al.*, 2004; Chang *et al.*, 2013), enhancing upwelling mechanisms and the retention of water (McCartney, 1976; Gordon *et al.*, 1978). Finally, the friction between strong currents or tidal waves and the sea floor can introduce cold water and nutrients (particularly iron, as many ocean islands are volcanic in origin) from the thermocline into the surface mixed layer (Hamner and Hauri 1981; De Falco *et al.* 2020 and references therein; Storlazzi *et al.* 2020).

In addition to bathymetry-induced mechanisms, nutrients can be imported into the surface layer near islands due to terrestrial run-off (Figure 1.8). Submarine groundwater, surface streams, and glacial run-off transport high concentrations of nutrients into near-shore waters surrounding the islands (Doty and Oguri, 1956; Hawkings *et al.*, 2014; Gove *et al.*, 2016; Pérez-Tribouillier *et al.*, 2020). In addition to supplying nutrients, the input of freshwater enhances upper water-column stability in the vicinity of the islands, generating a more stable mixed layer that reduces the likelihood of light limitation of phytoplankton, thus stimulating productivity (Perissinotto *et al.*, 1990, 1992). Because of the nutrient input and retention mechanisms associated with islands in the Southern Ocean, phytoplankton blooms can persist for periods of more than two weeks and extend spatially over thousands of kilometres (Perissinotto *et al.*, 1992; Mongin *et al.*, 2009).

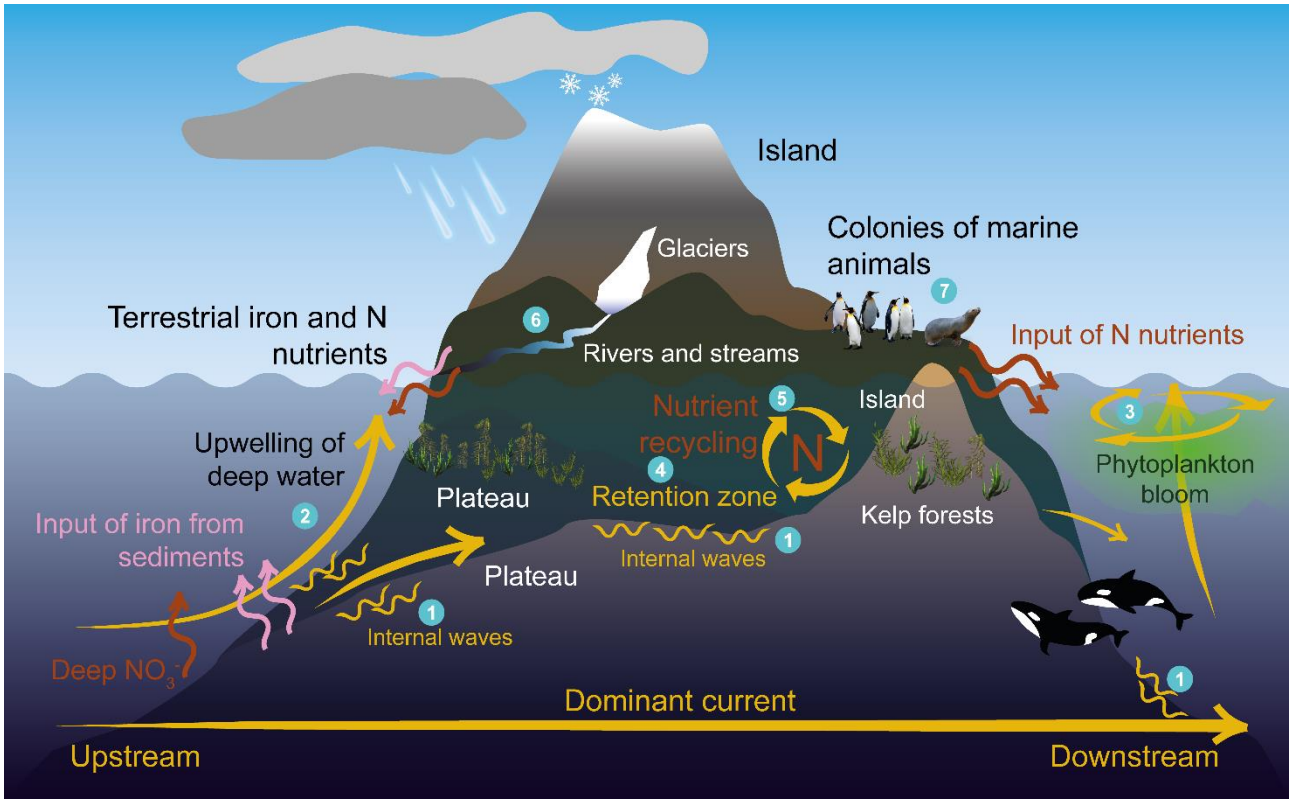

Figure 1.8 Multiple physical mechanisms drive the Island Mass Effect (IME) of (Sub)Antarctic island systems that ultimately results in enhanced plankton productivity. The vertical transport of nutrients to the surface (e.g., iron, nitrate and silicic acid) near the islands is promoted by the shoaling of the bathymetry, which leads to the development of (1) tidally-driven internal waves, (2) upwelling of deep waters on the upstream side of the islands, and (3) anti-cyclonic eddies downstream of the island/plateau region. The morphology of the island/plateau may also promote the formation of (4) retention areas where deep- and terrestrially-derived nutrients are concentrated and (5) nutrient recycling is favoured. Terrestrially-derived inputs into nearshore waters include (6) riverine outflow (including submarine groundwater discharge and glacially-derived flow) and (7) animal-derived runoff (figure made by Luca Stirnimann and adapted from Gove *et al.* 2016).

1.4.1. Subantarctic islands: The Prince Edward Islands archipelago

There are tens of islands (single islands or archipelagos) in the Southern Ocean, and most of them are located in the Atlantic and Indian Subantarctic. The productivity in the Subantarctic Ocean is highly variable due to the strong seasonality in solar irradiance, deep mixing, nutrient availability, frontal positions, and the IME (Pakhomov *et al.*, 2000b; Lamont *et al.*, 2019; Lamont and Toolsee, 2022). Because of the islands' basaltic (i.e., volcanic) nature, surface waters are enriched with micronutrients such as dissolved iron due to the re-suspension of shallow benthic sediments (Blain *et al.*, 2007; Jouandet *et al.*, 2008; Mongin *et al.*, 2008). In addition, many of the Subantarctic islands are sources of macronutrients such as SiO_4^{4-} derived from the

dissolution of deep-sea sediments and terrigenous rocks eroded by streams (Heath, 1974; Leblanc *et al.*, 2002; Tréguer, 2014), as well as nitrogen-based nutrients derived from remineralized soil and guano from colonies of sea birds and marine mammals (Blain *et al.*, 2001; Wing *et al.*, 2014; Treasure *et al.*, 2015). The input of these nutrients (particularly iron and SiO_4^4) into Subantarctic surface waters alleviate the phytoplankton from nutrient limitation (particularly the larger size classes and heavily-silicified diatoms), thus enhancing their productivity, abundance, and diversity, with a consequent enhancement of carbon export (Tréguer and Pondaven, 2000; Blain *et al.*, 2001; Hoffmann *et al.*, 2006; Shatova *et al.*, 2016).

Of the Subantarctic islands, the Prince Edward Islands archipelago (PEIs; Figure 1.7 and Figure 1.9), Crozet Islands, Kerguelen Island, and Heard Island are located in the Indian sector, and South Georgia, the South Sandwich Islands, and Bouvet Island are located in the Atlantic sector of the Southern Ocean. However, depending on the position of hydrographic fronts (i.e., the Antarctic Polar Front [APF]), some of these islands may variably experience Subantarctic or Antarctic Ocean conditions (Lutjeharms and Valentine, 1984; Belkin and Gordon, 1996; Graham *et al.*, 2012; Chapman *et al.*, 2020). This thesis focused particularly on the influence of the IME on the plankton system of the PEIs (e.g., on their rates of nutrient uptake and primary productivity), because this archipelago provides habitats of elevated ecological and conservation importance for hundreds of terrestrial and marine organisms (Figure 1.9; Chown and Froneman, 2008) and is an important offshore marine protected area in the exclusive economic zone of South Africa (Lombard *et al.*, 2007; Sink *et al.*, 2012).

The marine system surrounding the PEIs, which comprises two islands, Marion Island and Prince Edward Island (Figure 1.7 andFigure 1.9), has been studied since 1947. The establishment in 2014 of permanent moorings at fixed locations between the two islands (Verheye and Makhado, 2014) allows for daily monitoring of the physical dynamics (i.e., temperature, salinity, Sea Surface Hight (SSH); Lamont *et al.* 2019). The PEIs have long been used as a living laboratory to study the sensitivity and adaptation strategies of sub-polar ecosystems to long-term natural and anthropogenic changes, with evidence of climate change already described for the waters surrounding the islands (Smith, 2002; Le Roux and McGeoch, 2008; Ansorge *et al.*, 2012; Louise Allan *et al.*, 2013; von der Meden *et al.*, 2017). The plankton ecosystem at the

PEIs has been studied for more than 40 years, during which observations of plankton abundance, taxonomy, size, and productivity have been collected (Pakhomov and Froneman, 1999; Ansorge *et al.*, 2012).

Figure 1.9 View of the Prince Edward Island (island at the top of the image) from one of the Marion Island's cliffs, which formed a 'pocket beach' where sea birds (i.e., penguins, albatrosses, gulls) and marine mammals (i.e., seals) established large colonies (photo by Luca Stirnimann).

The PEIs lie in the path of the ACC between the SAF and the APF (Lutjeharms, 1985; Pakhomov *et al.*, 2000a). The fronts exhibit a significant degree of latitudinal fluctuation in this area (Ansorge *et al.*, 2009; Sokolov and Rintoul, 2009a), resulting in frequent exchange of Subantarctic and Antarctic surface- and intermediate water masses (Deacon, 1982), with implications for advective forcing around the archipelago and thus for the IME on plankton productivity (Ansorge *et al.*, 1999, 2009; Lamont and Toolsee, 2022). When the SAF is located in close proximity to the PEIs, its strong advective forcing impedes water retention around the archipelago (Perissinotto and Duncombe Rae, 1990; Pakhomov and Froneman, 1999; Pakhomov *et al.*, 2000a). In contrast, when the SAF is positioned far to the north of the archipelago, the advection of the ACC is relatively weak, leading to the formation of anti-cyclonic eddies downstream of the archipelago,

which concentrate and retain upwelled and island-derived nutrients (Allanson *et al.*, 1985; Perissinotto and Duncombe Rae, 1990; Pakhomov *et al.*, 2000a).

The Subantarctic waters around the PEIs host two groups of organisms that dominantly drive the input of energy into the ecosystem (Kaehler *et al.*, 2000); 1) the autochthonous phytoplankton, whose productivity is highly influenced by the IME (Boden and Parker, 1986), and 2) the allochthonous zooplankton, the distribution of which is determined by the availability of their food sources (Gallup, 1970; Paffenhöfer, 1983), as well as by the highly variable hydrographic environment near the PEIs (Bernard and Froneman, 2003; Ansorge and Lutjeharms, 2005; Ansorge *et al.*, 2012). Although considerable research has been conducted on the plankton of the PEIs, very little work to-date has focused on the variability of plankton dynamics relative to carbon fixation, nutrient uptake, and export, particularly using methodologies based on stable isotopes. Some of the work detailed in this thesis used stable isotope techniques to examine the effect of the PEIs on primary production and carbon export potential, and to investigate the transfer of energy from the producers to the first consumers.

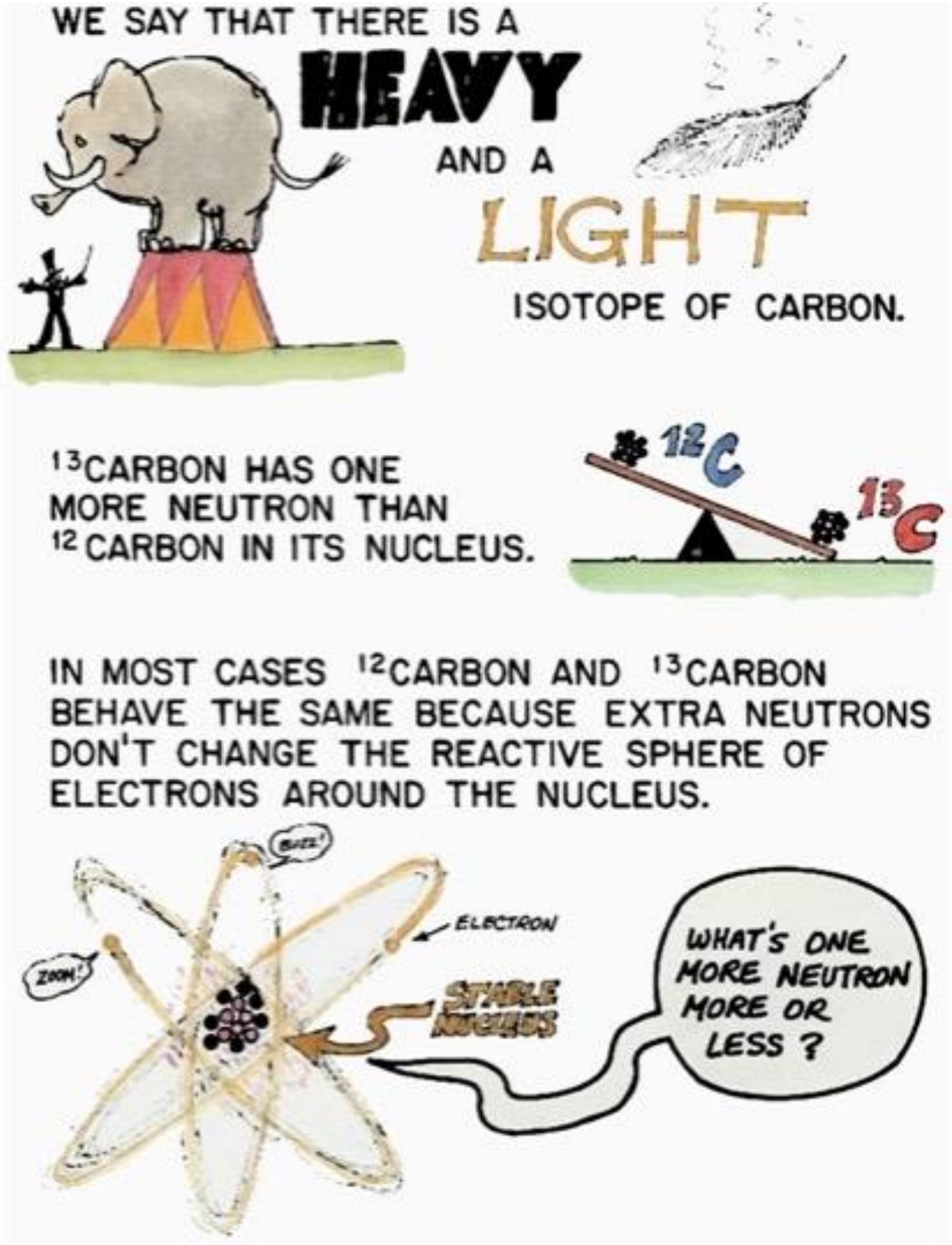

Figure 1.10 Comic illustration of Bryan Fry (from Fry 2006), showing that the 'light' and 'heavy' isotopes are atoms of the same element that differ by the number of neutrons.

1.5. The use of stable isotopes in ecology

Stable isotopes are non-radioactive elements with the same number of electrons and protons but differing numbers of neutrons, distinguishing the 'lighter' (less neutrons, e.g., ^{12}C and ^{14}N) from the 'heavier' (more neutrons, e.g., ^{13}C and ^{15}N) isotope (Figure 1.10). In the last few decades, isotopes have become commonly used in several fields, including ecology and biogeochemical oceanography, to identify food sources, infer biogeochemical and biological processes, monitor animal migrations, and define food web structures (Peterson and Fry, 1987; Michener and Lajtha, 2007). Methods of sample preparation and analysis vary for each isotope and substrate (Sharp 2017); however, the main goal is to convert a sample quantitatively into a gas that an isotope ratio mass spectrometer (IRMS) can analyse. The IRMS measures the ratio of heavy-to-light isotopes (e.g., $^{15}N/^{14}N$) relative to an internal (i.e., laboratory) standard, and the measured value must subsequently be converted and reported relative to an international reference, expressed in parts per thousand (*per mille* or ‰*)* deviations from that standard as:

$$\delta\ (‰) = \left(\frac{R_{sample}}{R_{standard}} - 1\right) \times 1000 \qquad \text{(Eqn. 1.1)}$$

where R_{sample} and $R_{standard}$ are the heavy-to-light isotope ratios in the sample and the standard, respectively (McKinney *et al.*, 1950).

The use of the stable isotopes of carbon and nitrogen ($\delta^{13}C$ and $\delta^{15}N$, respectively) has escalated in the last decades in ecology and oceanography to elucidate physiological and biogeochemical processes that involve the cycling of molecules such as CO_2, nitrate (NO_3^-), and ammonium (NH_4^+) through the organic biomass of marine organisms, including plankton (Peterson and Fry, 1987; Michener and Lajtha, 2007). In addition to the isotope ratios themselves, researchers are interested in the differences in velocity and bond strength among isotopes that lead to 'fractionation', or isotopic differences between the source and product of a chemical reaction (Michener and Lajtha, 2007). For instance, during a kinetic unidirectional reaction, the lighter isotopes are typically preferentially transformed because it requires less energy to react their lower mass while the heavier isotopes form stronger bonds with other elements and thus react more slowly (Figure 1.11). As such the extent to which the reactant pool is enriched in the heavy isotope relative to the product

pool can be quantified by the kinetic isotope effect (ε; (Eqn. 1.2), defined as the ratio of the rates by which the two isotopes are converted from reactant to product:

$$\varepsilon\ (‰) = \left(\left(\frac{k_l}{k_h}\right) - 1\right) \times 1000 \qquad \text{(Eqn. 1.2)}$$

where k_h and k_l are the rate coefficients for the reactant containing the heavy and light isotope, respectively.

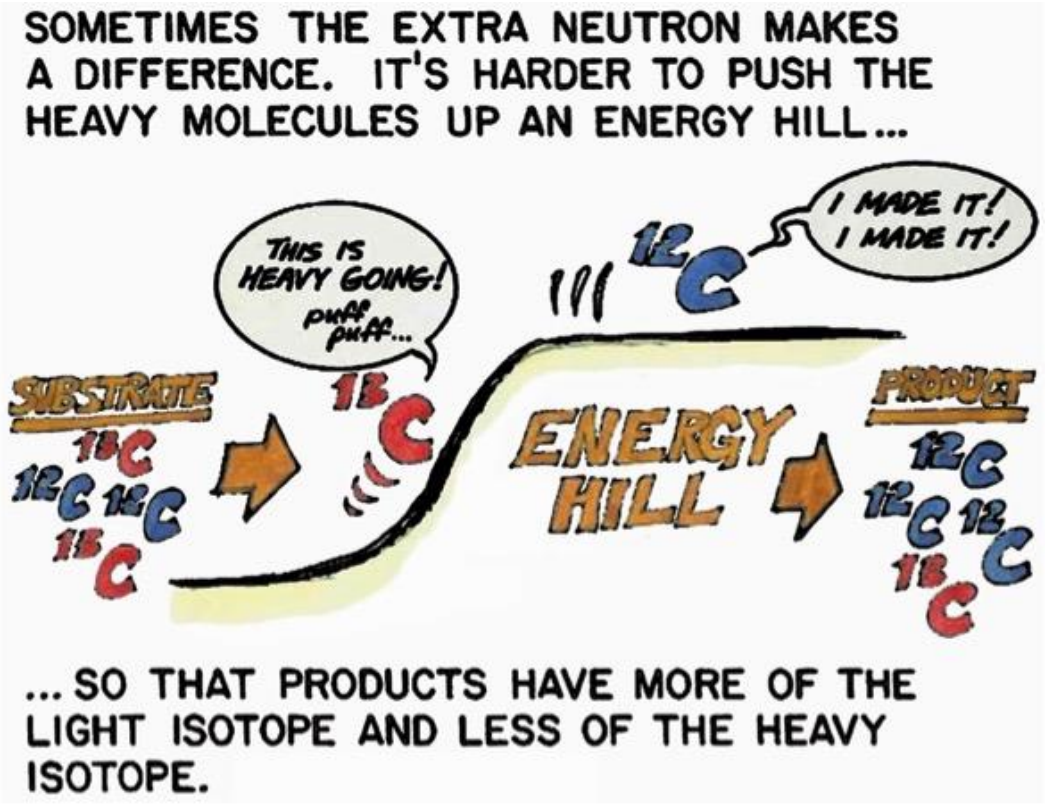

Figure 1.11 Comic illustration of Bryan Fry (from Fry 2006), showing that having an extra neutron does make a difference in chemical and biological reactions. Heavier isotopes form stronger chemical bonds than lighter ones, as such the lighter isotopes are preferentially transformed with faster reactions since their smaller mass needs less energy to react. The fractionation is the reaction difference.

In the context of marine plankton ecology, measurements of $\delta^{13}C$ are used to define the origin of a nutrient or food source to phytoplankton and zooplankton or as a tool for tracking the movements and migration of marine animals (e.g., McMahon *et al.* 2013; Trueman and St John Glew 2019). In contrast, measurements of $\delta^{15}N$ have been widely used to explore a variety of ecological and biogeochemical processes in the ocean, including the assessment of trophic levels of organisms in the food web (Post, 2002; Fry, 2006), N uptake

rates and the cycling of N nutrients (e.g., NO_3^- and NH_4^+; Sigman *et al.* 1999; Fawcett *et al.* 2011; Mdutyana *et al.* 2020), and for the estimation of the net primary production (NPP; Dugdale and Wilkerson 1986).

The $\delta^{13}C$ of phytoplankton is set by the fractionation between ^{13}C and ^{12}C that occurs during several transport- and biological reactions that occur in the cells, such as CO_2 diffusion across the cell membrane, carboxylation during photosynthesis, which can be catalysed by a few different carboxylase enzymes (O'Leary, 1981; Fry and Sherr, 1989; Descolas-Gros and Oriol, 1992), the organic carbon content of the cell (Laws *et al.*, 1997), the cell growth rate, and the ambient pCO_2 (François *et al.*, 1993; Goericke, 1994; Laws *et al.*, 1995). The $\delta^{15}N$ of phytoplankton is strongly influenced by the $\delta^{15}N$ of the available N source (i.e., $\delta^{15}N\text{-}NO_3^-$ or $\delta^{15}N\text{-}NH_4^+$), the degree of consumption of the different N sources (Sigman *et al.*, 1999; Altabet and Francois, 2001; DiFiore *et al.*, 2010; Fawcett *et al.*, 2011, 2014), and the fractionation between ^{15}N and ^{14}N that occurs during N-source assimilation (Mariotti *et al.*, 1981; Altabet and Francois, 1994; Waser *et al.*, 1998; Lourey *et al.*, 2003; Granger *et al.*, 2004, 2010; Lara *et al.*, 2010; Somes *et al.*, 2010). For example, when phytoplankton take up NO_3^-, they preferentially consume the lighter ^{14}N, meaning that the substrate pool remaining in the water column becomes progressively enriched in the heavier ^{15}N, such that it increases in $\delta^{15}N$. At the same time, the $\delta^{15}N$ of the phytoplankton consuming the NO_3^- will be lower than the $\delta^{15}N\text{-}NO_3^-$, and will increase as consumption of the source pool proceeds, to eventually converge upon the original $\delta^{15}N\text{-}NO_3^-$ once its consumption is complete (Mariotti *et al.*, 1981; Sigman *et al.*, 1999).

If the transformation of NO_3^- to biomass N proceeds unidirectionally with a constant ε (Eqn. 1.2) and if the N pools are neither replenished nor depleted from the system during transformation, then the process can be described in terms of Rayleigh fractionation kinetics, which quantify variations in the $\delta^{15}N$ of the reactant pool (e.g., NO_3^-) and the $\delta^{15}N$ of the generated product (e.g., phytoplankton biomass) as a function of the extent to which the reactant pool has been transformed (Mariotti *et al.*, 1981; Sigman *et al.*, 1999; Sigman and Fripiat, 2019). It is common practice to interpret N isotope data from the ocean in terms of the 'Rayleigh model' or alternatively, the 'steady-state' model. Key parameters in both of these models include the fraction of the reactant N pool that remains unconsumed in the water column (F), the initial $\delta^{15}N$ of the reactant pool ($\delta^{15}N_{initial}$), and isotope effect (ε).

The Rayleigh model is applicable to reactions that take place in a closed system (i.e., neither the reactant nor product N pools are replenished or depleted during the reaction, which proceeds with a constant isotope effect; Mariotti *et al.* 1981), such as phytoplankton nitrate assimilation in stratified surface waters. The Rayleigh model describes the $\delta^{15}N$ of the reactant N pool ($\delta^{15}N_{reactant}$), the instantly generated product pool (for example, organic biomass N produced from nitrate at any given moment; $\delta^{15}N_{instantaneous}$), and the integrated product N pool ($\delta^{15}N_{accumulated}$) as a given reservoir of reactant N is consumed. Since the purpose of this section is only introductory, I will not extend the description of the Rayleigh model here; rather, it is described and explored in great detail in Chapter 2.

The $\delta^{13}C$ and $\delta^{15}N$ of the first producers are propagated up the food web through to its higher trophic levels, following the general paradigm that "you are what you eat plus a few *per mille*" (DeNiro and Epstein, 1978, 1981). By this principle, both $\delta^{13}C$ and $\delta^{15}N$ progressively increase from the lower to the higher trophic levels of the food web, which makes their measurement a useful tool for defining the structure of the trophic web and tracking feeding ecology (Peterson and Fry, 1987; Herman *et al.*, 2000; Post, 2002; Fry, 2006). While the $\delta^{13}C$ of an organism predominantly reflects the different food sources they have assimilated and can thus be used to monitor the migration of the marine animals or to identify the food source(s) to specific organisms, their $\delta^{15}N$ provides insights into their role and trophic position within the food web(MacKenzie *et al.* 2011 and references therein).

Because of their numerous applications, measurements of $\delta^{13}C$ and $\delta^{15}N$ are the major tools used in this research. In the open Southern Ocean and in the vicinity of the (Sub)Antarctic islands, I use measurements of $\delta^{13}C$ and $\delta^{15}N$ to elucidate plankton ecological dynamics, such as variations in community composition and trophic behaviours, and characterize and quantify biogeochemical processes, including carbon production and export. For instance, I have studied the geographical and temporal variability of plankton $\delta^{13}C$ and $\delta^{15}N$, applied the Rayleigh model to determine the potential for carbon export, and assessed isotopic niches and trophic positions of zooplankton across the Southern Ocean.

1.6. Objectives and thesis outline

The overarching aim of this work is to advance our understanding of plankton dynamics in the open Southern Ocean and in the vicinity of the (Sub)Antarctic islands, particularly as they pertain to carbon fixation and uptake of nitrogenous nutrients during primary production, along with the transfer of carbon and N through the plankton trophic system, using novel methods and high-resolution observations. The thesis is comprised of four data chapters presented as scientific papers (one already published; Chapter 4; Stirnimann *et al.*, 2021) that address distinct topics, each with its own set of research questions. Below, I outlined the workflow of the thesis, contextualising each chapter's broad aims and specific research questions. The thesis concludes with a final chapter that briefly summarizes my major findings, outlines the main messages that emanate from this work, and suggests some research directions that could pursued in the future.

- **Chapter 2. A** circum-Antarctic plankton isoscape I: Carbon export potential across the Southern Ocean

Recent studies have reported the geographical distributions ('isoscapes') of the $\delta^{13}C$ and $\delta^{15}N$ of surface suspended particulate matter (SPM; $\delta^{13}C_{SPM}$ and $\delta^{15}N_{SPM}$) in the Southern Ocean (e.g., Espinasse *et al.*, 2019; St John Glew *et al.*, 2021). However, the mechanisms underlying the carbon and nitrogen isoscapes have not been fully explored, with key aspects remaining poorly understood. This chapter discusses the major drivers of geographical variability in phytoplankton community composition and relatedly, of $\delta^{13}C_{SPM}$ and $\delta^{15}N_{SPM}$ in the Southern Ocean. Sampling was conducted at a circumpolar scale, including in the vicinity of sea-ice and land masses, such as the (Sub)Antarctic islands and continental shelves. Here, I aimed to answer the following questions:

- How does the phytoplankton community composition differ between the hydrographic zones of the Southern Ocean?
- What are the main drivers affecting the $\delta^{13}C_{SPM}$ and $\delta^{15}N_{SPM}$ in the open Southern Ocean and in the vicinity of the islands?
- Is phytoplankton community composition a key determinant of $\delta^{13}C_{SPM}$ and $\delta^{15}N_{SPM}$ variability?

Following an assessment of the major processes affecting the $\delta^{13}C_{SPM}$ and $\delta^{15}N_{SPM}$ isoscapes of the Southern Ocean, I show that the $\delta^{15}N_{SPM}$ is a powerful tool for studying biogeochemical processes and quantifying carbon export potential in the Southern Ocean. In this context, I modified the Rayleigh model for isotopic fractionation during NO_3^- assimilation and combined its output with a simple isotope mixing model to quantify the fraction of organic carbon (i.e., primary production) produced through the uptake of 'new' *versus* 'regenerated' N by phytoplankton (i.e., a version of the *f*-ratio) to ultimately assess carbon export potential across the Southern Ocean. Here, I aimed to answer the following questions:

- Can measurements of $\delta^{15}N_{SPM}$ be used to assess carbon export potential in the Southern Ocean?
- What is the carbon export potential across the Southern Ocean implied from the $\delta^{15}N_{SPM}$, how does it differ among hydrographic zones, and how it is altered by proximity to ice and island systems?
- To what extent does phytoplankton community composition explain geographical variations in carbon export potential?

• Chapter 3. A circum-Antarctic plankton isoscape II: zooplankton isotope niches and trophic structure across Southern Ocean hydrographic zones

There are substantially more investigations and observations of $\delta^{13}C_{SPM}$ and $\delta^{15}N_{SPM}$ in the Southern Ocean than of zooplankton biomass $\delta^{13}C$ and $\delta^{15}N$. Having assessed the principal drivers of the carbon and N isoscape of SPM in the Southern Ocean (Chapter 2), in the present chapter, I describe the drivers of geographical variability in the $\delta^{13}C$ and $\delta^{15}N$ of zooplankton in the Southern Ocean at a circumpolar scale. In addition, I characterize the geographical variability in zooplankton community composition in the open Southern Ocean and near ice and land masses. Here, I aimed to answer the following questions:

- How does zooplankton community composition differ among the hydrographic zones of the Southern Ocean?
- What are the major drivers of the spatial variability in the $\delta^{13}C$ and $\delta^{15}N$ of zooplankton in the Southern Ocean?
- How do $\delta^{13}C_{SPM}$ and $\delta^{15}N_{SPM}$ contribute to the spatial variability in zooplankton $\delta^{13}C$ and $\delta^{15}N$?
- How do terrestrial systems affect zooplankton $\delta^{13}C$ and $\delta^{15}N$?

This study also assessed the validity of five different N isotopic baselines for trophic analysis. Ultimately, I used the $\delta^{15}N_{SPM}$ to determine the trophic position of the zooplankton and the ecological niches of the various communities present at the time of sampling. In this context, I aimed to answer the following questions:

- Is $\delta^{15}N_{SPM}$ a suitable baseline for trophic analysis of the zooplankton system?
- How do the latitudinal trends in phytoplankton community composition and isotope ratios (assessed in Chapter 5) influence zooplankton trophic structure in the Southern Ocean?
- Are there differences in zooplankton trophic structure among hydrographic zones and what are the implications thereof for the biological pump?

Before outlining the objectives of Chapters 4 and 5, I first need to briefly outline my motivation for undertaking the research described therein. I learned from Chapters 2 and 3 that, in addition to the well-known IME on plankton biomass and community composition, the (Sub)Antarctic Island systems increase the carbon and N isotope ratios of SPM and zooplankton. Specifically, during the Antarctic Circumnavigation Expedition (ACE; Landwehr *et al.*, 2021), I examined the plankton community near the Prince Edward Islands archipelago (PEIs) at the start of the austral summer of 2016–2017 (Chapters 2 and 3) and found that the higher $\delta^{13}C$ and $\delta^{15}N$ of the plankton community relative to that measured in the open Southern Ocean was due to the dominance in near-island waters of large diatoms and primary-consumer zooplankton that were likely herbivorous. I carried out a second excursion to the PEIs two months after the ACE cruise, in April-May 2017, to further investigate the plankton dynamics near this archipelago. The outcomes of these efforts are discussed in Chapters 7 and 8, with a brief summary of the aims and objectives provided below.

• Chapter 4. Plankton community composition and productivity near the Subantarctic Prince Edward Islands archipelago in autumn

I conducted a high-resolution study in autumn (April-May) of 2017 to determine how the PEIs affect the composition and productivity of the plankton community. I analysed biological, chemical, and ecological parameters, including grazing rates, primary and secondary production rates, and plankton species composition, with the aim of answering the following questions:

- How productive are the plankton in the vicinity of the Prince Edward Islands archipelago at the end of the summer growth season?
- What is the plankton community composition during this period?
- What are the major differences between the PEIs' plankton system and that of the nearby Subantarctic Islands (e.g., Crozet and Kerguelen Islands)?

- **Chapter 5. Short-term variations in plankton biomass, δ13C and δ15N and trophic structure near the Subantarctic Prince Edward Islands archipelago**

In addition to the biological and chemical observations detailed in Chapter 4, during the autumn expedition to the PEIs (April-May 2017), I collected samples for analysis of the $\delta^{13}C$ and $\delta^{15}N$ of SPM and zooplankton. I compared these measurements to similar data produced for four seasons (i.e., July to August 2015, April to May 2016, late December 2016, April to May 2017, and June to July 2017) in order to characterize the short-term temporal variability in the $\delta^{13}C$ and $\delta^{15}N$ of SPM and zooplankton near the PEIs archipelago. Here, I aimed to answer the following questions:

- What is the temporal variability in the isotope ratios of plankton near a Subantarctic Island system?
- What are the major drivers of the observed seasonal variability in $\delta^{13}C_{SPM}$ and $\delta^{15}N_{SPM}$?
- To what extent do the PEIs affect the isotope ratios of plankton?

- **Chapter 6. Summary and future research directions**

Each of the four data chapters in this thesis (Chapters 2 to 5) includes a comprehensive summary of the major findings, along with detailed conclusions. Therefore, this final chapter does not reiterate those conclusions in depth. Instead, following a brief summary of the main findings of the thesis work, this chapter suggests some potential future research directions, specifically related to better understanding the implications of climate change for the plankton ecosystems of the Southern Ocean.

Figure 1.12 Uncovering the mysteries of the Southern Ocean: a scientist (myself) is busy studying plankton samples collected from the deep sea using advanced microscopy techniques (photo taken by Sina Wallschuss).

1.7. Observations

1.7.1. Overview of the field campaigns

The datasets that underpin my research are *in situ* oceanographic observations collected during two projects and expeditions, the Antarctic Circumnavigation Expedition (ACE) and the 2017 Marion Island Relief Voyage 024.

The ACE cruise was conducted from December 2016 to March 2017 on board the Russian research vessel *Akademik Treshnikov*. Starting and ending in Cape Town, South Africa, the clockwise longitudinal circumnavigation around the Antarctic continent was split into three legs: Leg1, from Cape Town to Hobart, Australia, Leg2 from Hobart to Punta Arenas, Chile, and Leg3 from Punta Arenas to Cape Town (Figure 1.13). The ACE programme as a whole, which included 55 scientists from 30 nations working on 22 different projects, was developed to improve our collective understanding of the Southern Ocean and its ecosystems (https://swisspolar.ch/expeditions/ace/). The expedition followed the path of the largest oceanographic feature of the Southern Ocean, the eastward propagating, wind-driven Antarctic Circumpolar Current (ACC), which involved crossing a series of marine and terrestrial (i.e., islands and glaciers) environments. These included the Subantarctic and Antarctic islands (e.g., from the Prince Edward Islands archipelago to Heard Island [Leg1], from the Scott Islands to Diego Ramirez Islands [Leg2], and from South Georgia Island and the South Sandwich Islands to Bouvet Island [Leg3]), as well as the seasonal sea ice zone near Antarctica, which was the focus of Leg2.

This thesis uses data generated by the South African Project XII of ACE: *A multi-disciplinary, multi-resolution approach to understanding nutrient cycling and microbial diversity in changing Subantarctic ecosystems.* The overarching goal of ACE Project XII was to develop an integrated observational model of the Subantarctic Island systems based on the diversity of the pelagic system (phytoplankton, bacteria, and zooplankton) and metabolic activity, interpreted in the context of various chemical and physical parameters, in order to better understand their role in Southern Ocean productivity and CO_2 draw down.

Figure 1.13 Map showing the cruise track followed during the Antarctic Circumnavigation Expedition (ACE), and the Russian research vessel Akademik Treshnikov (*Академик Трёшников*; top-right) (picture from the Swiss Polar Institute). The research vessel circumnavigated Antarctica in a clockwise direction and was split into three legs: Leg1 in the Indian sector between Cape Town and Hobart (24th December 2016 – 17th January 2017); Leg2 in the Pacific sector between Hobart and Punta Arenas (23rd January – 19th February 2017); and Leg3 in the Atlantic sector between Punta Arenas and Cape Town (26th February – 16th March 2017).

This thesis also has a strong focus on the Prince Edward Islands archipelago (PEIs) , which was investigated between the 20th and 28th of December 2016 (austral summer) during the ACE cruise, and again from the 6th of April to the 12th of May 2017 (autumn) during the Marion Island Relief Voyage 024 conducted by the then South African National Department of Environmental Affairs (DEA). The latter voyage was conducted on board of the South African polar research vessel MV *S.A. Agulhas II* (Figure 1.14). This expedition occurred as part of a long-term monitoring effort managed by several South African research institutions and spear-headed by the DEA. During the annual Marion Island Relief Voyages, multi-disciplinary studies are routinely conducted to assess and monitoring changes in the marine environment, with a strong focus on microbial, planktonic and benthic communities in the near-shore zone around the PEIs (Verheye, 2017).

Figure 1.14 The MV *S.A. Agulhas II*, a state-of-the-art research vessel designed to support oceanographic and atmospheric research in the Southern Ocean and Antarctic waters (photo from Redit).

1.7.2. Sampling and analytical approaches

During both expeditions, a series of atmospheric and oceanic properties were measured while the ships were underway, and physical, biogeochemical, and biological samples were collected in both the open ocean and in the vicinity of the islands. The materials and methods for each study are described in detail in each of the following chapters; below, I include a brief summary of the main methodologies employed during this project.

Biogeochemical (e.g., nutrients, nitrate isotopes, primary production rates, chlorophyll-a and particulate organic carbon and nitrogen concentrations) and physical (e.g., temperature, mixed layer depth, salinity) data were collected and/or measured 1) throughout the water column (with a focus on the epipelagic layer) using a Conductivity Temperature Depth (CTD; Figure 1.15) profiling instrument augmented with various environmental sensors and equipped with 12L Niskin bottles for seawater collection, and 2) at the near-surface through the underway seawater supply system of the research vessels (intake at ~5-7 m).

For taxonomic analysis, phytoplankton were collected 1) using vertically towed nets with a mesh size of 60 µm, 2) from Niskin bottles fired at different euphotic zone depths during the CTD casts, and 3) by filtering the underway water supply through 20 µm nylon mesh filters, whereafter the samples were preserved with 1% glutaraldehyde. Zooplankton samples were also collected using nets, including via horizontal Neuston net tows and oblique and vertical Bongo net tows, both equipped with 200 µm mesh nets (Figure 1.15 and Figure 1.16). When vertical sampling was conducted, our goal was to investigate the epipelagic layer of the water column (between the surface and 200 m). Zooplankton samples were preserved in a 4% formaldehyde-seawater solution or 70% ethanol in plastic or glass bottles. To quantify species abundances in the different locations, a rigorous evaluation of community composition and species diversity was performed using optical microscopes and taxonomic keys available in the literature (Figure 1.12).

Analyses of carbon and N stable isotope ratios were performed on both biogeochemical and biological samples, including surface NO_3^-, bulk suspended particulate matter (SPM), and zooplankton species and/or size-fractionated classes. These samples were stored at -80°C until analysis ashore using isotope ratio mass spectrometers.

Figure 1.15 On board of the MV *S.A. Agulhas II*: (Centre) Plankton sample collection using a Bongo net requires rigorous net washing for plankton concentration in the Bongo net's cod-end. (Left) The Conductivity Temperature Depth (CTD) profiling instrument, crucial for determining the physical properties of seawater, is affixed to the rosette frame, which can also hold Niskin bottles used for water sampling (photo taken by Sina Wallschuss).

Figure 1.16 Bongo nets' cod-ends concentrate the plankton samples, which will be successively analysed for taxonomic identifications and for the examination of the chemical and biological properties of the plankton (photo taken by Sina Wallschuss).

Chapter 2. A circum-Antarctic plankton isoscape I: Carbon export potential across the Southern Ocean

Supplementary information of this Chapter can be found in Appendix A.

2.1. Abstract

The Southern Ocean accounts for >30% of the ocean's CO_2 sink, partly due to its biological pump that transfers surface-produced organic carbon into deeper waters. To estimate large-scale Southern Ocean carbon export potential and characterize its drivers, we measured the carbon and nitrogen isotope ratios of surface suspended particulate matter ($\delta^{13}C_{SPM}$ and $\delta^{15}N_{SPM}$) for samples collected in summer 2016/17 during the Antarctic Circumnavigation Expedition (364 stations). Concurrent measurements of phytoplankton community composition revealed the dominance of large diatoms in the Antarctic and nano-phytoplankton in open Subantarctic waters. As expected, $\delta^{13}C_{SPM}$ was strongly dependent on pCO_2, with local deviations in this relationship explained by phytoplankton community dynamics. $\delta^{15}N_{SPM}$ reflected the nitrogen sources consumed by phytoplankton, with higher inferred nitrate (*versus* recycled ammonium) dependence generally coinciding with higher micro-phytoplankton (mainly diatom-) abundances. Using $\delta^{15}N_{SPM}$ and a two-endmember isotope mixing model, we quantified the extent of nitrate- *versus* ammonium-supported phytoplankton growth, which yields a measure of carbon export potential. We estimated that across the Southern Ocean, 43 ± 28% of the surface-produced organic carbon was potentially exported during the growth season, with maximum export potential (50-99%) occurring in the Antarctic Circumpolar Current's southern Boundary Zone and near (Sub)Antarctic islands, reaching a minimum in the Subtropical Zone (<33%). Along with iron, phytoplankton community composition emerged as an important driver of the Southern Ocean's biological pump, with large diatoms dominating regions characterized by high nitrate dependence and elevated carbon export potential and smaller, mainly non-diatom taxa proliferating in waters where recycled ammonium supported most productivity.

2.2. Introduction

Phytoplankton are the foundation of marine food webs (Falkowski *et al.*, 2003; Reynolds, 2006) and contribute to climate regulation by fixing CO_2 into organic carbon biomass (i.e., primary production; Falkowski *et al.* 1998). In the Southern Ocean, iron and light limitation of phytoplankton growth lead to mixed-layer macronutrient concentrations (i.e., nitrate and phosphate) that are perennially high (Martin *et al.*, 1990a; de Baar *et al.*, 1995; Sunda and Huntsman, 1997). Nonetheless, the Southern Ocean is a major contributor to the global ocean CO_2 sink and is estimated to account for ~30% of the global ocean carbon flux (Schlitzer, 2002; DeVries, 2014; Frölicher *et al.*, 2015; Arteaga *et al.*, 2018). While CO_2 removal is largely attributed to the solubility pump (i.e., atmospheric CO_2 dissolved in the Southern Ocean's cold surface waters is subducted into the deep ocean), a key mechanism maintaining the surface-to-deep CO_2 gradient is the biological pump, which transfers a portion of the organic carbon produced by phytoplankton into the ocean interior where it may be stored for hundreds of years (Volk and Hoffert, 1985).

Of the 15.8 ± 3.9 Pg C yr^{-1} of net primary production (NPP) occurring in the Southern Ocean south of 30°S (Arteaga *et al.*, 2018), ~3 Pg C yr^{-1} is exported from surface waters (Schlitzer, 2002). NPP and carbon export have been shown to be elevated over the Antarctic continental shelf and near the various (Sub)Antarctic islands, as well as in the marginal ice zone (MIZ), with the Ross and Weddell Seas in particular emerging as productivity hotspots (Schlitzer, 2002; Arrigo *et al.*, 2008a, 2008b; Pollard *et al.*, 2009). Carbon production and export are thought to be enhanced in these regions because of local increases in the iron (and at times, silicic acid) supply and/or increased stratification (and thus light exposure) due to seasonal ice melt (e.g., Death *et al.* 2014; Lannuzel *et al.* 2016).

Experimental analyses, geochemical measurements, and satellite data coupled with biogeochemical models have been used to investigate carbon export in the Southern Ocean (e.g., Hirawake *et al.* 2011; Fan *et al.* 2020; Kerkar *et al.* 2020). However, this flux is challenging to quantify from satellite data (e.g., Strutton *et al.* 2012; Dubovik *et al.* 2021) and direct measurements require expensive sediment trap arrays and/or analysis of thorium-uranium disequilibria, both of which only record the

functioning of a small region of the ocean and are subject to limitations (Buesseler *et al.*, 2007; Clevenger *et al.*, 2021). Proxies for carbon export, such as measurements of surface seawater O_2/Ar ratios, are powerful in that they can be made at high spatial resolution (Kaiser *et al.*, 2005; Cassar *et al.*, 2009). However, the conversion of O_2/Ar ratios to export estimates involves numerous assumptions that are frequently violated (Wang *et al.*, 2020). Autonomous float-based measurements of the annual cycle of mixed-layer nitrate concentrations provide a promising alternative measure of export (Johnson *et al.*, 2017; Prend *et al.*, 2022), although as with satellite data, this approach must be calibrated against direct measurements. There thus remains a need for additional estimates of carbon export in the Southern Ocean based on *in situ* measurements. Furthermore, to better predict how the Southern Ocean's biological pump and CO_2 sink may change requires an improved understanding of the drivers of carbon export at large scales (Henley *et al.*, 2020).

The stable isotope ratios of carbon ($\delta^{13}C$, in ‰ *versus* Vienna Pee Dee Belemnite (VPDB) = $\{[(^{13}C/^{12}C)_{sample}/(^{13}C/^{12}C)_{VPDB}]-1)\times1000\}$) and nitrogen ($\delta^{15}N$, in ‰ *versus* N_2 in air = $\{[(^{15}N/^{14}N)_{sample}/(^{15}N/^{14}N)_{air}]-1)\times1000\}$) in suspended particulate matter (SPM) have been widely used to explore a variety of ecological and biogeochemical processes in the ocean. The $\delta^{13}C$ of phytoplankton biomass (often approximated by the $\delta^{13}C$ of SPM; $\delta^{13}C_{SPM}$) is largely set by discrimination between the ^{12}C and ^{13}C isotopes (i.e., fractionation) during CO_2 diffusion across the cell membrane and its subsequent carboxylation (O'Leary, 1981; Fry and Sherr, 1989). Variations in carbon isotope fractionation can arise due to changes in the partial pressure of CO_2 in seawater (pCO_2, which is strongly controlled by temperature), cell growth rate and cell membrane permeability, phytoplankton species and size, light availability, and sea-ice cover (Descolas-Gros and Fontungne, 1990; Rau *et al.*, 1991b; Dehairs *et al.*, 1997; Trull and Armand, 2001). pCO_2 appears to have a dominant effect on phytoplankton $\delta^{13}C$, with higher ambient pCO_2 associated with a higher degree of discrimination against ^{13}C by phytoplankton and thus a lower $\delta^{13}C_{SPM}$ (Rau *et al.*, 1989, 1991b, 1992a; François *et al.*, 1993). Phytoplankton $\delta^{13}C$ also depends on the environmental conditions and (related) photosynthetic activity. For example, conditions that favour a bloom (e.g., high light, micro- and macronutrient concentrations, and/or stratification) can enhance cell growth, resulting in a higher

$\delta^{13}C_{SPM}$ due to a reduction in the net fractionation associated with inter-cellular CO_2 carboxylation (Deuser, 1970; Dehairs *et al.*, 1997; Laws *et al.*, 1997; Raven, 1997; Tortell *et al.*, 1997; Keller, 1999).

Phytoplankton $\delta^{15}N$ (often approximated by the $\delta^{15}N$ of SPM; $\delta^{15}N_{SPM}$) is set by the $\delta^{15}N$ of the nitrogenous nutrients supporting growth (i.e., nitrate, ammonium, dissolved organic N; Altabet 1988; Lourey *et al.* 2003; Fawcett *et al.* 2011, 2014) as well as the associated kinetic isotopic fractionation occurring during N assimilation (e.g., Needoba *et al.* 2004; Granger *et al.* 2004). For example, phytoplankton preferentially consume the ^{14}N-bearing form of nitrate, causing the residual nitrate pool to become progressively enriched in ^{15}N as consumption proceeds (Mariotti *et al.*, 1981; Sigman *et al.*, 1999). In the summertime Southern Ocean, variations in $\delta^{15}N_{SPM}$ in surface waters have been largely attributed to isotope fractionation during nitrate consumption, with a strong negative correlation observed between the surface nitrate concentration and $\delta^{15}N_{SPM}$ (Altabet and Francois, 1994; Lourey *et al.*, 2003; Smart *et al.*, 2020). However, the $\delta^{15}N$ of primary producers (and thus SPM) is also influenced by other N species that support production, with the assimilation of recycled N (e.g., ammonium) yielding a lower $\delta^{15}N_{SPM}$ than the consumption of nitrate supplied from the subsurface (Altabet, 1988; Fawcett *et al.*, 2011, 2014; Treibergs *et al.*, 2014). Because of the different isotopic signals of nitrate *versus* ammonium assimilation, $\delta^{15}N_{SPM}$ can be leveraged to distinguish 'new' *versus* 'regenerated' N uptake by phytoplankton (e.g., Lourey *et al.* 2003; Fawcett *et al.* 2011, 2014; Van Oostende *et al.* 2017). Since the rate of new nitrate uptake by phytoplankton must be balanced by the downward flux of organic matter ('export production'), distinguishing nitrate- from ammonium-fuelled NPP using $\delta^{15}N_{SPM}$ provides a means of estimating carbon export potential (Dugdale and Goering, 1967; Eppley and Peterson, 1979).

While $\delta^{13}C_{SPM}$ and $\delta^{15}N_{SPM}$ are commonly used as a proxy for the bulk phytoplankton community (e.g., Van Oostende *et al.* 2017; Espinasse *et al.* 2019; St John Glew *et al.* 2021) and as a baseline for food web analyses (e.g., Lorrain *et al.* 2015; Pasotti *et al.* 2015; Puccinelli *et al.* 2020), SPM includes diverse living and dead autotrophic and heterotrophic material. As such, measurements of $\delta^{13}C_{SPM}$ and $\delta^{15}N_{SPM}$ that are not accompanied by phytoplankton assemblage data may yield a limited view of the

biogeochemical functioning of a system (Falkowski, 1991). For example, the strong correlation observed between surface $\delta^{15}N_{SPM}$ and nitrate in the Southern Ocean appears to be relevant only in spring to mid-summer when phytoplankton consume mainly mixed-layer nitrate (Lourey *et al.*, 2003; Smart *et al.*, 2020). In late summer when phytoplankton increase their reliance on recycled ammonium, surface $\delta^{15}N_{SPM}$ has been observed to be significantly lower than expected from nitrate assimilation (Lourey *et al.*, 2003; Smart *et al.*, 2020), while in winter when nitrate assimilation is light-limited and heterotrophic bacteria and detritus constitute a significant fraction of the SPM, $\delta^{15}N_{SPM}$ is decoupled from nitrate $\delta^{15}N$ and instead reflects heterotrophic processes (Smart *et al.*, 2020).

Maps showing the spatial distribution of $\delta^{13}C_{SPM}$ and $\delta^{15}N_{SPM}$ (i.e., 'isoscapes') are increasingly used to address large-scale ecological and biogeochemical questions (West *et al.*, 2009; Bowen, 2010; Espinasse *et al.*, 2019; St John Glew *et al.*, 2021). Such studies have described gradients in $\delta^{13}C_{SPM}$ and $\delta^{15}N_{SPM}$ across the Southern Ocean, with many reporting relatively stable values within each hydrographic zone but substantial differences among zones (e.g., François *et al.* 1993; Espinasse *et al.* 2019; St John Glew *et al.* 2021; Smith *et al.* 2022). Recently, St John Glew *et al.* (2021) used an Integrated Nested LaPlace Approximation-based approach constrained by measured environmental variables to predict $\delta^{13}C_{SPM}$ and $\delta^{15}N_{SPM}$ for the entire Southern Ocean. The authors found that $\delta^{13}C_{SPM}$ and $\delta^{15}N_{SPM}$ generally decreased southwards with latitudinal variations in sea surface temperature (SST) and changes in N nutrient availability. Additionally, $\delta^{13}C_{SPM}$ and $\delta^{15}N_{SPM}$ increased near Antarctica, the islands (e.g., Kerguelen Island), and within the MIZ, as has been observed by others (Federici *et al.*, 2003; Trull *et al.*, 2008; Espinasse *et al.*, 2019; Smart *et al.*, 2020). While the meta-analysis of St John Glew *et al.* (2021) represents a significant improvement in Southern Ocean isoscape coverage, particularly for regions where sample collection has been limited, more direct observations are needed to fill sampling gaps and validate isoscape models. Another shortcoming of $\delta^{15}N_{SPM}$ isoscapes in particular is that they often do not consider variations in the $\delta^{15}N$ of the nitrate supply as a potential driver of $\delta^{15}N_{SPM}$ variability (*cf.* Van Oostende *et al.* 2017). However, the $\delta^{15}N$ of the source nitrate to surface waters (e.g., Subantarctic Mode Water nitrate) can change by >2‰

zonally across the Southern Ocean (Rafter *et al.*, 2013; Fripiat *et al.*, 2021), such that for the same amount of nitrate consumption, and without varying any other environmental parameter, phytoplankton biomass $\delta^{15}N$ (and thus, $\delta^{15}N_{SPM}$) could also differ by >2‰.

Here, we use samples collected during the 2016/17 Antarctic Circumnavigation Expedition (ACE) to describe circum-Antarctic $\delta^{13}C_{SPM}$ and $\delta^{15}N_{SPM}$ isoscapes and phytoplankton community composition in summer. The ACE cruise provided a unique opportunity for direct high-resolution observations across all sectors of the Southern Ocean that could be used to confirm and expand upon the conclusions of previous more localized and/or model-based studies. A major advantage of our dataset is its high spatial resolution, which means that very little interpolation is required (Brault *et al.* 2018). We discuss the dominant drivers of isotopic variability among and within the hydrographic zones and, by applying a two-endmember isotope mixing model to our $\delta^{15}N_{SPM}$ data, initialized with measured and modelled nitrate concentration and $\delta^{15}N$ data, constrain phytoplankton reliance on new *versus* recycled N. We use this information to estimate carbon export potential across the Southern Ocean and further discuss the potential drivers of new, regenerated, and export production during the summer growth season.

Materials and methods

2.2.1. Sample collection

The ACE cruise occurred during the summer of 2016/17 onboard the R/V *Akademik Treshnikov* (*Академик Трёшников*) (Walton and Thomas, 2018; Landwehr *et al.*, 2021). The research vessel circumnavigated Antarctica in three legs (Figure 2.1): Leg1 in the Indian sector between Cape Town and Hobart (24th December 2016 – 17th January 2017; Figure 2.1b); Leg2 in the Pacific sector between Hobart and Punta Arenas (23rd January – 19th February 2017; Figure 2.1c); and Leg3 in the Atlantic sector between Punta Arenas and Cape Town (26th February – 16th March 2017; Figure 2.1d). Leg1 and Leg3 crossed the open Southern Ocean zonally, visiting the Prince Edward Islands (PEIs), Crozet, Kerguelen, and Heard Islands during Leg1, and South Georgia, the South Sandwich, and Bouvet Island during Leg3. Leg2 followed the Antarctic coastline, sampling the MIZ and visiting the Mertz Glacier, Balleny Islands, Scott Island, Siple Island, Peter 1st Island, and Diego Ramírez Islands.

Seawater samples were collected from the ship's underway system (~4.5 m subsurface intake) every one- to-three hours while the ship was steaming, at a total of 330 stations, and from Niskin bottles triggered between the surface and 200 m during CTD casts at 34 stations. In total, we collected 364 unique samples at 142, 132, and 90 stations during Leg1, Leg2, and Leg3, respectively.

At all the underway stations, samples for phosphate (PO_4^{3-}), silicic acid (SiO_4^{4-}), nitrate (NO_3^-+NO_2^-; hereafter referred to as NO_3^-), and nitrite (NO_2^-) concentrations were collected in sample-rinsed 50 mL Falcon tubes that were immediately stored at -20°C. Samples for ammonium (NH_4^+) concentrations were collected in 50 mL high-density polyethylene bottles (HDPE) that had been 'aged' with orthophthaldialdehyde working reagent (Holmes *et al.*, 1999; Smith *et al.*, 2022). Samples were analysed on board within 24 hours of collection, except for those from Leg1 which were frozen and measured on land. Nutrient samples were also collected at the CTD stations in 15 mL Falcon tubes (Janssen *et al.* 2020; Hassler and Ellwood, 2020). Iron concentrations were measured for samples collected at 17 CTD stations during Leg1 and Leg2 (Janssen *et al.*, 2020b). While iron data are not available for the whole transect, measurements were made near some (Sub)Antarctic islands (stations

16, 19, 43, 47, and 49), in the Mertz polynya (stations 26 and 36), near the Antarctic Peninsula (station 71), at open ocean stations (21 and 22), and on meridional transects to and from Antarctica (stations 23-25 and 56, 68, 72, and 73). We refer to these data in our analysis.

At all the underway and all but two of the CTD stations, duplicate 2L seawater aliquots were collected in sample-rinsed opaque HDPE bottles, then filtered through pre-combusted (450°C for 8h) glass fibre filters (GF-75s; 0.3 µm pore size) to capture the bulk suspended particulate matter (SPM). Filters were stored in pre-combusted aluminium foil envelopes at -80°C.

Samples for micro-phytoplankton (20-200 µm) taxonomy were collected at 83 underway stations. Seawater was filtered through a 20 µm nylon mesh with the volume filtered varying according to the concentration of cells in the water (range of 4.5 to 60 L). The nylon filter was then suspended in 5 mL of 0.2 µm-filtered seawater in a 10 mL polyethylene tube, fixed via the addition of 5 µL of 25% glutaraldehyde, and stored at 4°C in the dark.

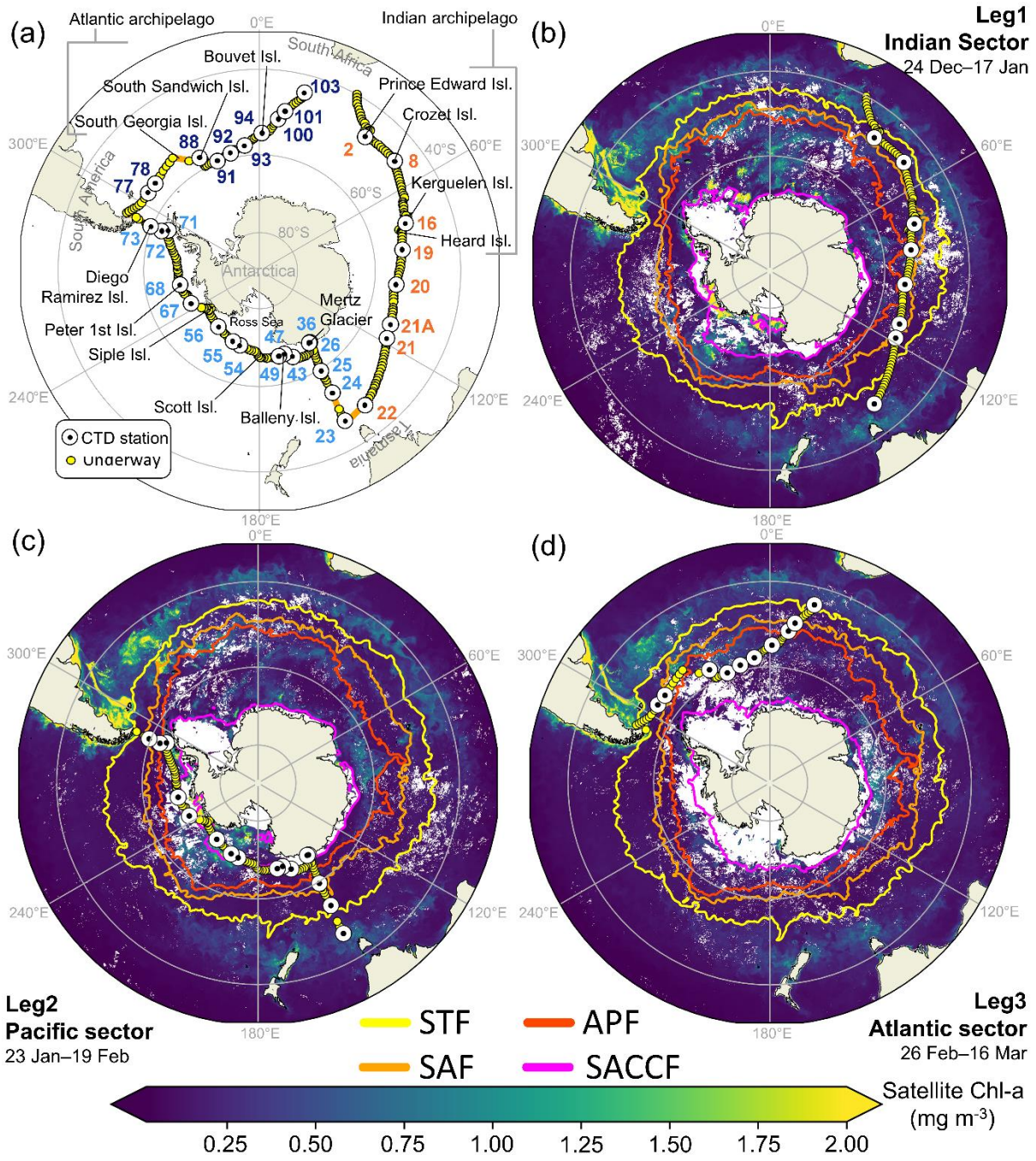

Figure 2.1 (a) Cruise track and stations sampled during the Antarctic Circumnavigation Expedition (ACE). Yellow dots indicate underway stations, white/black dots show CTD stations, and numbers are station identifiers, with the font colour corresponding to the cruise leg: Leg1 = orange, Leg2 = light blue, Leg3 = dark blue. b-d) Monthly satellite-based chlorophyll-a concentrations (mg m^{-3}; level-3 Chl-a from the Moderate Resolution Imaging Spectroradiometer (MODIS) Aqua satellite product (https://oceandata.sci.gsfc.nasa.gov/MODIS-Aqua/Mapped/Monthly/4km/chlor_a/) at 4 km spatial resolution for each cruise leg overlaid with monthly average frontal positions (coloured lines: yellow = Subtropical Front (STF), orange = Subantarctic Front (SAF), red = Antarctic Polar Front (APF), purple = Southern Antarctic Circumpolar Current Zone (SACCZ)). Fronts were determined from satellite-derived SST (UKMO 2005) according to Orsi *et al.* (1995).

2.2.2. Sample analysis

Underway nutrient concentrations were analysed in the Marine Biogeochemistry Lab at the University of Cape Town. NO_3^- and SiO_4^{4-} were measured using a Lachat QuickChem flow injection analysis platform (detection limit of 0.5 μM and precision of ≤0.5 μM) (Grasshoff, 1976; Diamond, 1994). PO_4^{3-} and NO_2^- were analysed manually using standard benchtop colorimetric methods (Bendschneider and Robinson, 1952; Strickland and Parsons, 1972) and a Thermo Scientific Genesys 30 Visible spectrophotometer (detection limit of 0.05 μM, precision of ≤ 0.05 μM). Certified reference materials (JAMSTEC) were analysed during all autoanalyzer and manual runs to ensure measurement accuracy. Nutrient samples collected at the CTD stations were analysed as described by Hassler and Ellwood (2020) and Janssen *et al.* (2020).

The SPM filters were dried for 24 h at 40°C, then subsamples were packaged into tin capsules and analysed for C and N content and $\delta^{13}C$ and $\delta^{15}N$ using a Flash 2000 elemental analyser coupled to a Delta V Plus isotope ratio mass spectrometer (IRMS) (detection limit of 2 μg C and 1 μg N, precision of ±0.2‰ for $\delta^{13}C$ and $\delta^{15}N$). Three in-house standards calibrated against certified reference materials were included in each IRMS run along with numerous blanks (unused pre-combusted filter + tin capsule). The particulate organic C and N (POC and PON) concentrations were calculated by normalizing C and N content to seawater volume filtered. The station-specific $\delta^{13}C_{SPM}$ and $\delta^{15}N_{SPM}$ values reported hereafter are the POC- and PON concentration-weighted averages of duplicate samples.

Phytoplankton taxonomic identification involved gently mixing each preserved sample, then transferring 0.08 mL onto two clean microscope slides. Cells with intact chloroplasts (i.e., alive at the time of sampling) were counted at 630x magnification using a Zeiss Axioscope A1 light microscope; all live cells on both slides were counted. The remaining volume of preserved sample was treated with 10% hydrochloric acid and 37% hydrogen peroxide to remove carbonate particles and organic matter, respectively. After a thorough rinsing with distilled water, permanent slides were prepared by pipetting the cleaned material onto acid-washed coverslips that were air-dried overnight and then mounted onto glass slides using Naphrax® mountant (refractive index of 1.7). The permanent slides

were examined using a Zeiss Axioscope A1 light microscope equipped with differential interference contrast at 1000x magnification (under oil immersion). Stubs were also prepared from the cleaned material for examination using a JEOL JSM-7001F field emission scanning electron microscope to visualize the morphological features not evident under the light microscope.

2.2.3. Supporting data products

Satellite data were used to supplement the ship-based surface hydrography measurements (Appendix A.a). Daily high-resolution SST (GHRSST) Level 4 data on a global 0.054° grid from the OSTIA database (https://podaac.jpl.nasa.gov/dataset/UKMO-L4HRfnd-GLOB-OSTIA; UKMO 2005) were used to determine the positions of the major oceanic fronts following Orsi *et al.* (1995). The Subtropical Zone (STZ) lies north of the Subtropical Front (STF) and is characterized by a SST of 20°C to 10°C. South of the STF and bounded to the south by the Subantarctic Front (SAF), the Subantarctic Zone (SAZ) has a SST of 10°C to 6°C, while the Polar Frontal Zone (PFZ) has a SST of 6°C to 4°C and is bounded to the south by the Antarctic Polar Front (APF). The PFZ is characterized by high physical variability and is often considered the transition zone between Antarctic and Subantarctic waters (Orsi *et al.*, 1995; Bowie *et al.*, 2011); here, we take the APF as the point of separation between these two predominant regions. South of the APF is the Southern Antarctic Circumpolar Current Zone (SACCZ), which remains ice-free year-round. The SACCZ has a SST of 4°C to 0.7°C and is bounded to the south by the Southern ACC Front (SACCF), which constitutes the southern edge of the ACC core (Orsi *et al.*, 1995). South of the SACCF is the southern Boundary Zone (sBZ), which experiences seasonal sea-ice cover (e.g., Squire 1998). Here, we group all stations south of the SACCF, including in the Antarctic Continental Zone, into the sBZ.

Phytoplankton pigment data were collected underway every three hours and analysed using High Performance Liquid Chromatography (HPLC) (Antoine *et al.*, 2020). We used the total chlorophyll-a concentrations (Chl-a; defined as the sum of monovinyl Chl-a, divinyl Chl-a, chlorophyllide a, and Chl-a allomers and epimers) as a proxy for biological activity. Seven marker pigments were weighted as per Uitz *et al.* (2006) and used to estimate the phytoplankton size classes present in each mixed

population (i.e., pico-phytoplankton (<2 μm), nano-phytoplankton (2–20 μm), and micro-phytoplankton (20–200 μm); Vidussi *et al.* 2001). In addition, monthly (December 2016 to March 2017) level-3 Chl-a concentrations from the Moderate Resolution Imaging Spectroradiometer (MODIS) Aqua satellite product (https://oceandata.sci.gsfc.nasa.gov/MODIS-Aqua/Mapped/Monthly/4km/chlor_a/) at 4 km spatial resolution were used to visualize phytoplankton biomass distributions (Figure 2.1b-d). For each leg, we used the monthly average of the data product corresponding to January for Leg1, February for Leg2, and March for Leg3.

Surface ocean pCO_2 (Pa), air-sea fluxes of CO_2 (fCO_2; mg m^{-2} h^{-1}), and pH were obtained from a monthly 1-degree resolution global reconstructed product (resources.marine.copernicus.eu/ product-detail/ MULTIOBS_GLO_BIO_CARBON_SURFACE_REP_015_008) that was created by interpolation using an ensemble of artificial neural networks (https://doi.org/10.48670/moi-00047). For each leg, we used the monthly average of the data product corresponding to January for Leg1, February for Leg2, and March for Leg3.

2.2.4. Isotope models to assess phytoplankton dependence on NO_3^- *versus* NH_4^+

$\delta^{15}N_{SPM}$ is strongly influenced by the $\delta^{15}N$ of the nitrogenous nutrients supporting phytoplankton growth (Altabet 1988; Lourey *et al.* 2003; Fawcett *et al.* 2011; 2014; Treibergs *et al.* 2014). Additionally, the extent to which phytoplankton rely on new N is quantitatively related to the fraction of NPP that escapes recycling to sink into the ocean interior (i.e., export production; Dugdale and Goering 1967; Eppley and Peterson 1979). A major goal of this study was to leverage these two concepts and, using our large SPM dataset, estimate the fraction of new production relative to total production (and thus, carbon export potential) across the summertime Southern Ocean.

We assume that surface SPM in summer comprises mainly actively growing phytoplankton (e.g., Trull and Armand, 2001; Popp *et al.* 1999). As such, $\delta^{15}N_{SPM}$ can be described by a two-endmember isotope mixing model (Fawcett *et al.*, 2011):

$$\delta^{15}N_{SPM} = \delta^{15}N_{new} \times f_{new} + \delta^{15}N_{RN} \times f_{RN} \quad \text{(Eqn. 1)}$$

where $\delta^{15}N_{new}$ and $\delta^{15}N_{RN}$ are the $\delta^{15}N$ of the new and regenerated N assimilated by phytoplankton and f_{new} and f_{RN} are the fraction of growth fuelled by new and regenerated N (with $f_{new} + f_{RN} = 1$). The fraction of new production can thus be computed as:

$$f_{new} = \frac{(\delta^{15}N_{SPM} - \delta^{15}N_{RN})}{(\delta^{15}N_{new} - \delta^{15}N_{RN})} \quad \text{(Eqn. 2)}$$

We assume that regenerated N is well represented by NH_4^+, the most abundant recycled N form to phytoplankton that is dominantly sourced in the surface layer from the remineralization of SPM. We did not directly measure $\delta^{15}N_{NH4}$ because it is near-impossible to analyse at the low NH_4^+ concentrations characteristic of the open ocean (Zhang *et al.*, 2007). However, $\delta^{15}N_{NH4}$ should be low given the isotope effects associated with its production (Macko *et al.*, 1986; Checkley and Miller, 1989; Silfer *et al.*, 1992; Möbius, 2013). We estimate $\delta^{15}N_{NH4}$ as:

$$\delta^{15}N_{NH_4^+} = \delta^{15}N_{SPM} - \varepsilon_{regen} \quad \text{(Eqn. 3)}$$

where ε_{regen} is the isotope effect associated with NH_4^+ production (i.e., regeneration), set here to 1.5‰. While ε_{regen} has been estimated under steady state conditions to be ~3‰ (i.e., the NH_4^+ instantaneously produced from organic N decomposition by heterotrophic bacteria is ~3‰ lower than the SPM being degraded; Möbius, 2013), we use a lower value for ε_{regen} because 1) processes other than regeneration are coincidentally acting on the SPM pool, violating the steady state assumption and altering $\delta^{15}N_{SPM}$; 2) while the primary fate of regenerated NH_4^+ is rapid consumption by phytoplankton, some NH_4^+ will nonetheless have accumulated over a variable time period and as such, is unlikely to have a $\delta^{15}N$ equal to that of NH_4^+ instantaneously produced from the *in situ* SPM; and 3) previous studies of SPM and our own preliminary data from elsewhere in the Southern Ocean suggest that the $\delta^{15}N_{NH4}$ in the summer is on the order of -1‰ (Lourey *et al.*, 2003; Smart *et al.*,

2020). The mean $\delta^{15}N_{NH4}$ computed for our dataset using Eqn. 3 is -0.99 ± 0.13‰. In the open ocean where NH_4^+ concentrations are <5 μM, NH_4^+ assimilation by phytoplankton is thought to occur with little to no isotopic fractionation (Hoch *et al.*, 1992; Pennock *et al.*, 1996; Liu *et al.*, 2013); thus, $\delta^{15}N_{RN} = \delta^{15}N_{NH_4^+}$.

Above, we have assumed that regenerated N is well-represented by NH_4^+. However, if nitrification (i.e., the chemoautotrophic oxidation of NH_4^+ to NO_2^- and then NO_3^-) occurs in the surface layer, the NO_3^- produced therefrom constitutes a regenerated rather than a new N source to phytoplankton. In a mass balance sense, productivity fuelled by this regenerated NO_3^- will yield no carbon export (Dugdale and Goering, 1967; Yool *et al.*, 2007). However, direct measurements of nitrification from across the summertime Southern Ocean indicate that regenerated NO_3^- production is negligible in open surface waters (Mdutyana *et al.*, 2020). Moreover, even if nitrification were occurring in the surface layer (as has been suggested near Kerguelen Island; Dehairs *et al.* 2015; Fripiat *et al.* 2015), the difference in the magnitude of the isotope effects associated with NH_4^+ oxidation (14-19‰; Casciotti *et al.* 2003) and NH_4^+ assimilation (negligible; Liu *et al.* 2013) means that the regenerated NO_3^- would be low in $\delta^{15}N$, akin to $\delta^{15}N_{RN}$ (DiFiore *et al.*, 2009; Fawcett *et al.*, 2011).

Determining $\delta^{15}N_{new}$ is more complex than estimating $\delta^{15}N_{RN}$ because NO_3^- is never fully consumed in Southern Ocean surface waters and undergoes isotopic fractionation during assimilation (Mariotti *et al.*, 1981; Granger *et al.*, 2004). The effect of this fractionation on the NO_3^- pool being consumed and the SPM produced therefrom can be characterized using the Rayleigh model. This model describes a unidirectional N transformation process (i.e., NO_3^- assimilation into SPM) that proceeds with a constant isotope effect (ε_{assim}) under conditions where the reactant NO_3^- is neither resupplied (e.g., by mixing) nor lost by any mechanism other than phytoplankton assimilation (Mariotti *et al.*, 1981). In the Southern Ocean in summer, the N isotope dynamics associated with NO_3^- assimilation are reasonably well described by the Rayleigh model since NO_3^- is supplied to the surface mainly during winter mixing, then assimilated in spring and summer following surface-layer stratification (Sigman *et al.*, 1999).

The Rayleigh model describes the isotopic evolution of the reactant pool ($\delta^{15}N_{reactant}$; Eqn. 4a), the instantaneously generated product pool ($\delta^{15}N_{instantaneous}$; Eqn. 4b), and the accumulated product pool ($\delta^{15}N_{accumulated}$; Eqn. 4c) (Mariotti *et al.*, 1981) as:

$$\delta^{15}\mathrm{N}_{\mathrm{reactant}} = \delta^{15}\mathrm{N}_{\mathrm{source}} - \varepsilon_{\mathrm{assim}} \times \ln(F) \quad \text{(Eqn. 4a)}$$

$$\delta^{15}\mathrm{N}_{\mathrm{instantaneous}} = \delta^{15}\mathrm{N}_{\mathrm{reactant}} - \varepsilon_{\mathrm{assim}} \quad \text{(Eqn. 4b)}$$

$$\delta^{15}\mathrm{N}_{\mathrm{accumulated}} = \delta^{15}\mathrm{N}_{\mathrm{source}} + \varepsilon_{\mathrm{assim}} \times \left\{\frac{F \times \ln(F)}{(1 - F)}\right\} \quad \text{(Eqn. 4c)}$$

where $\delta^{15}N_{source}$ is the initial $\delta^{15}N$ of the source NO_3^- supplied to surface waters in winter, F is the fraction of this NO_3^- supply remaining at the time of sampling (i.e., the measured surface NO_3^- concentration ($[NO_3^-]_{meas}$) divided by the source NO_3^- concentration ($[NO_3^-]_{source}$)), and ε_{assim} is the isotope effect of NO_3^- assimilation. The $\delta^{15}N_{instantaneous}$ is the SPM produced from NO_3^- at each moment of consumption, while the $\delta^{15}N_{accumulated}$ is the sum of all the SPM produced from NO_3^- since consumption began (Mariotti *et al.*, 1981). As such, both $\delta^{15}N_{instantaneous}$ and $\delta^{15}N_{accumulated}$ provide a measure of the $\delta^{15}N$ of SPM generated from the assimilation of NO_3^- (i.e., $\delta^{15}N_{new}$; Eqn. 2).

Whether $\delta^{15}N_{accumulated}$ or $\delta^{15}N_{instantaneous}$ best characterizes $\delta^{15}N_{new}$ depends on the extent to which the SPM produced from NO_3^- has been exported from the surface since NO_3^- consumption began. For $\delta^{15}N_{instantaneous}$ to approximate $\delta^{15}N_{new}$, almost all the SPM must have been exported. However, phytoplankton biomass is known to accumulate in surface waters during the growth season (e.g., Peloquin and Smith Jr. 2007; Swart *et al.* 2015; van Leeuwe *et al.* 2020), such that $\delta^{15}N_{instantaneous}$ unlikely approximates $\delta^{15}N_{new}$. On the other hand, if a significant portion of the accumulated SPM was exported by the time of our sampling, then $\delta^{15}N_{new}$ also cannot be approximated by $\delta^{15}N_{accumulated}$. We estimate the quantity of exported SPM (N_{export}) by comparing the $[NO_3^-]_{source}$ to the sum of the measured surface concentrations of NO_3^-, SPM, and NH_4^+:

$$\mathrm{N_{export}} = [\mathrm{NO_3^-}]_{\mathrm{source}} - ([\mathrm{NO_3^-}] + [\mathrm{SPM}] + [\mathrm{NH_4^+}])_{\mathrm{meas}} \quad \text{(Eqn. 5)}$$

$[NH_4^+]_{meas}$ is included in Eqn. 5 because unlike NO_3^-, NH_4^+ is not supplied by vertical mixing but is regenerated *in situ*, with a concentration at the start of the spring growth season that is below detection (Smith *et al.*, 2022); as such, the NH_4^+ present in the surface layer at the time of our sampling was regenerated from SPM produced from assimilation of the source NO_3^-. To apply Eqn. 5, we interpolated our NH_4^+ concentration measurements using DIVA (i.e., Data-Interpolating Variational Analysis; Barth *et al.* 2010), which allowed for the extraction of NH_4^+ concentrations at stations where measurements are lacking (195 out of 364 stations).

Mathematically, N_{export} should always be ≥0 µM. However, since the surface ocean is not truly at steady state, we allow for a confidence interval equal to the propagated error associated with the terms on the right-hand side of Eqn. 5 (±1.5 µM); all observations that fall within this confidence interval are included in our analysis. Using N_{export}, we then calculate the fraction of the source NO_3^- pool consumed since the start of the growth season that was exported by the time of our sampling as:

$$f_{\mathrm{export}} = \frac{\mathrm{N_{export}}}{[\mathrm{NO_3^-}]_{\mathrm{source}} - [\mathrm{NO_3^-}]_{\mathrm{meas}}} \in [0; 1] \quad \text{(Eqn. 6)}$$

For our dataset, the median concentration (± interquartile range) of N_{export} is 2.4 ± 3.8 µM and the median f_{export} is 0.6 ± 0.4, indicating that a significant portion of the SPM produced since the start of the growth season was exported prior to our sampling. Thus, $\delta^{15}N_{new}$ cannot be approximated by $\delta^{15}N_{accumulated}$.

We propose that $\delta^{15}N_{new}$ can instead be estimated by integrating $\delta^{15}N_{instantaneous}$ over the concentration of SPM + NH_4^+ measured in the surface layer at the time of sampling since this SPM + NH_4^+ represents the product of $NO_3^-{}_{source}$ consumption that has not been exported. As such, Eqn. 4a can be modified as:

$$\delta^{15}\mathrm{N}_{\mathrm{reactant\_sampling}} = \delta^{15}\mathrm{N}_{\mathrm{source}} - \varepsilon_{\mathrm{assim}} \times \ln \frac{([\mathrm{NO}_3^-] + \mathrm{SPM} + [\mathrm{NH}_4^+])_{\mathrm{meas}}}{[\mathrm{NO}_3^-]_{\mathrm{source}}} \quad \text{(Eqn. 7)}$$

where $\delta^{15}\mathrm{N}_{\mathrm{reactant\_sampling}}$ is the theoretical δ^{15}N of the surface NO_3^- pool at the concentration of total N (i.e., $([NO_3^-] + [SPM] + [NH_4^+])_{meas}$) present in the surface layer at the time of sampling. Using Eqn. 4c, but integrating over only the measured surface-layer SPM + NH_4^+, we compute $\delta^{15}N_{new}$ as:

$$\delta^{15}\mathrm{N}_{\mathrm{new}} = \delta^{15}\mathrm{N}_{\mathrm{reactant\_sampling}} + \varepsilon_{\mathrm{assim}} \times \frac{F_{\mathrm{meas}} \times \ln(F_{\mathrm{meas}})}{1 - F_{\mathrm{meas}}} \quad \text{(Eqn. 8)}$$

Where F_{meas} is the fraction of $NO_3^-{}_{source}$ remaining (i.e., measured as NO_3^-) in the surface at the time of sampling:

$$F_{\mathrm{meas}} = \frac{[\mathrm{NO}_3^-]_{\mathrm{meas}}}{([\mathrm{NO}_3^-] + \mathrm{SPM} + [\mathrm{NH}_4^+])_{\mathrm{meas}}} \quad \text{(Eqn. 9)}$$

We note that if $\delta^{15}N_{new}$ were well approximated by either the instantaneous or the accumulated product equations (Eqns 4b and 4c), our definition of $\delta^{15}N_{new}$ (Eqn. 8) will still return the correct value of $\delta^{15}N_{instantaneous}$ or $\delta^{15}N_{accumulated}$ (Figure A.2).

In applying Eqn. 8 to our dataset, we assume that the $NO_3^-{}_{source}$ to phytoplankton is the NO_3^- that was present directly following winter mixing, which we take to be represented by the NO_3^- below the summer mixed layer at the time of sampling and above the maximum depth of the winter mixed layer; we refer to these waters between the winter and summer mixed layer depths (MLDs) as W-S. Due to a paucity of vertically-resolved measurements from ACE, we use a data-constrained model output, the biogeochemical-Southern Ocean State Estimate (b-SOSE) (Mazloff *et al.*, 2010; Verdy and Mazloff, 2017), to estimate the summer (average of January to March 2017) and winter (average of June to August 2016) MLDs at each station, as well as the source NO_3^- concentrations, computed as the mean NO_3^- concentration over the W-S layer ($[\mathrm{NO}_3^-]_{(\mathrm{W-S})}$). Comparison of the b-SOSE-derived

$[NO_3^-]_{(W-S)}$ with measurements of the $[NO_3^-]_{(W-S)}$ from ACE (Hassler and Ellwood, 2020) reveals good agreement between the two datasets (Appendix A.b; Figure A.3). The $\delta^{15}N$ of the $NO_{3\,source}^-$ was approximated as the concentration-weighted average $\delta^{15}N_{NO_3^-(W-S)}$, with the $\delta^{15}N$ values extracted from the neural-network-based global ocean NO_3^- $\delta^{15}N$ database of Rafter *et al.* (2019). Comparison of the NO_3^- $\delta^{15}N$ from Rafter *et al.* (2019) with measurements of the NO_3^- $\delta^{15}N$ from ACE (Forrer, 2021) reveals good agreement between the two datasets (Appendix A.c; Figure A.4).

For stations located near islands and continents, we used the average NO_3^- concentration and $\delta^{15}N$ from 200-300 m to represent the source NO_3^- ($[NO_3^-]_{(200-300)}$ and $\delta^{15}N_{NO_3^-(200-300)}$, respectively) as land-adjacent waters are influenced by physical processes that can supply NO_3^- from below the winter mixed layer (e.g., wind stress, topographic upwelling, internal waves; De Falco *et al.* 2022). These stations (117 in total) were identified considering proximity to land, plateau bathymetry, and the extent of the Island Mass Effect (IME) (Mongin *et al.*, 2009).

While estimates of ε_{assim} for the summertime Southern Ocean have been observed to vary (from 4‰ to 10‰; Sigman *et al.* 1999; Karsh *et al.* 2003; Lourey *et al.* 2003; DiFiore *et al.* 2010; Fripiat *et al.* 2019), DiFiore *et al.* (2010) showed a strong linear correlation between the summer MLD and ε_{assim}, which we use to derive ε_{assim} at each station:

$$\varepsilon_{assim} = 0.07 \times MLD_{summer} + 4‰ \quad \text{(Eqn. 10)}$$

We then calculate a median ε_{assim} for each of the hydrographic zones.

In summary, via the approach outlined above, we can estimate the isotopic endmembers, $\delta^{15}N_{RN}$ and $\delta^{15}N_{new}$, that we then incorporate into Eqn. 2 to estimate f_{new} from our SPM data.

2.2.5. Statistical analysis

Data were analysed using a combination of tools and software, including R for statistical analysis (R Core Team, 2018) and Python (van Rossum, 1995) and Ocean Data View (Schlitzer, 2021) for data

visualization. Results are reported in the text as mean ± 1 standard deviation (SD), $\mathrm{median}_{Q1}^{Q3}$ where Q_1 = first quartile and Q_3 = third quartile, or median ± interquartile range (IQR), where IQR = $Q_3 - Q_1$.

Shapiro-Wilk tests, quantile-quantile plot analysis, and Levene's tests were performed to assess the normality and homogeneity of variance of data distributions. Data were sub-grouped according to geographical region (oceanic zones = STZ, SAZ, PFZ, SACCZ, and sBZ; and oceans = Subantarctic and Antarctic). While parametric assumptions were satisfied when data were grouped as either Subantarctic or Antarctic, the equal variance assumption was violated when data were sub-grouped into the five oceanic zones. As such, and given the differently-sized sample sets from each oceanic zone, non-parametric analyses were used to test for differences among zones. Parametric analysis included analysis of variance (ANOVA) and t-tests while non-parametric analysis included the Kruskal-Wallis test and multiple pairwise-Wilcoxon test. When multiple statistical tests were performed on a single dataset, the probability values were adjusted using the Bonferroni correction (Chen *et al.*, 2017). Hereafter, the probability values obtained from the parametric and non-parametric tests are denoted as *p*-value(s) and *p*-value(s)*, respectively.

The *stats* R-package was used for linear regression model analysis of the surface SPM data, with the *p*-value and R^2 reported for each model. Spearman's rank correlation (ρ) was performed as a nonparametric measure of how well the relationship between two variables is described using a monotonic function. A Principal Component Analysis (PCA) was performed to investigate how various parameters (e.g., SST, nutrient concentrations, $\delta^{15}N_{SPM}$) drive data variance and distribution, with clustering based on observational similarity. Biodiversity and evenness were determined for the taxonomic counts using the Shannon-Wiener index (*H'*).

2.3. Results

2.3.1. Oceanic setting

The satellite-based Chl-a concentrations and positions of the major oceanic fronts at the time of sampling are shown in Figure 2.1b-d. The surface distributions of the main contextual parameters (i.e., concentrations of NO_3^-, PO_4^{3-}, SiO_4^{4-}, NH_4^+, iron, pCO_2) are presented in Table 2.1 and Figure 2.2.

Surface NO_3^- and PO_4^{3-} concentrations and pCO_2 increased from the STZ to the SAF (from $8.37^{11.43}_{6.18}$ to $19.92^{21.70}_{17.82}$ µM, from $0.72^{1.32}_{0.56}$ to $1.46^{1.56}_{1.32}$ µM, and from $37.0^{38.4}_{35.9}$ to $39.0^{39.1}_{38.8}$ Pa, respectively; *p*-values* <0.001Figure 2.2a, b, and f) while the air-sea flux of CO_2 (fCO_2) decreased (from $3.54^{4.93}_{1.63}$ to $1.10^{1.37}_{0.75}$ mg m^{-2} h^{-1}; *p*-value* <0.001; Table 2.1 and Figure A.6). South of the SAF, the NO_3^- and PO_4^{3-} concentrations remained constant towards Antarctica ($23.40^{24.9}_{21.2}$ and $1.56^{1.66}_{1.43}$ µM; *p*-values* = 1). pCO_2 also changed minimally until ~65°S ($38.6^{39.0}_{37.2}$ Pa), south of which it decreased strongly towards Antarctica, with minimum values at the mouth of the Ross Sea and near Siple Island (~23.0 Pa). fCO_2 was highly variable in the PFZ (~0 to 5.59 mg m^{-2} h^{-1}), becoming more constant south of the APF to ~65°S ($1.82^{2.39}_{0.83}$ mg m^{-2} h^{-1}), beyond which it increased towards Antarctica to reach maxima where pCO_2 was lowest (>10 mg m^{-2} h^{-1}). The near-island waters hosted elevated surface NO_3^- and PO_4^{3-} concentrations, particularly over the Indian archipelago (formed by the PEIs, Crozet and Kerguelen Islands), the Balleny Islands, and Peter 1st Island (>25 µM and >1.8 µM, respectively). Waters adjacent to the Atlantic archipelago (formed by South Georgia, South Sandwich, and Bouvet Islands) were also local hotspots for NO_3^- and PO_4^{3-}, although their surface concentrations were lower than near the Indian and Pacific islands (20-25 µM and 1.3-1.8 µM, respectively). Surface pCO_2 was lower near the islands than in the surrounding offshore waters (<36 Pa), while fCO_2 was higher (>2.5 mg C m^{-2} h^{-1}).

The surface SiO_4^{4-} concentrations increased gradually from the STZ to the APF ($1.04^{1.34}_{0.92}$ µM to $9.30^{11.8}_{4.39}$ µM) before increasing sharply southwards (Antarctic = $40.60^{51.50}_{38.50}$ µM), reaching ~80 µM near the Balleny Islands (Figure 2.2c). The SiO_4^{4-} concentrations over the Atlantic archipelago were

higher than elsewhere on Leg3 because this region is in the SACCZ. In the Subantarctic, SiO_4^{4-} concentrations were highest downstream of Kerguelen Island (>15 µM).

The surface NH_4^+ concentrations were highly variable along the transect, ranging from relatively low values in the open ocean ($0.72^{1.02}_{0.50}$ µM) to higher concentrations near the islands ($1.17^{1.73}_{0.73}$ µM). While NH_4^+ concentrations near Peter 1st, Diego Ramírez, South Sandwich and Bouvet Islands exceeded 1.5 µM and reached up to 2.0 µM, maximum concentrations of 2.7 µM were measured within the Indian archipelago and near the Balleny Islands (Figure 2.2d).

Surface dissolved iron concentrations were higher in the eastern Indian sector (second half of Leg1; ranging from 0.14 to 0.43 nmol kg^{-1}) than on Leg2 (from 0.21 to 0.33 nmol kg^{-1}), with maxima at Kerguelen Island and downstream of Heard Island (0.28 nmol kg^{-1} and 0.43 nmol kg^{-1}, respectively), as well as at the Balleny Islands and the West Antarctic Peninsula (WAP) (Leg2; 0.31 nmol kg^{-1} and 0.25 nmol kg^{-1}, respectively) Figure 2.2e; Janssen *et al.* 2020a). No iron data are available for the first half of Leg1 or Leg3.

Table 2.1 Medians (± IQR) of the sea surface temperature (SST; °C), concentrations of nitrate (NO_3^-; µM), phosphate (PO_4^{3-}; µM), silicic acid (SiO_4^{4-}; µM), and ammonium (NH_4^+; µM), the partial pressure of CO_2 (pCO_2; Pa), and the air-sea flux of CO_2 (fCO_2; mg m^{-2} h^{-1}) in the different regions of the Southern Ocean during ACE: 'Subantarctic' includes the STZ = Subtropical Zone, SAZ = Subantarctic Zone, PFZ = Polar Frontal Zone while 'Antarctic' includes the SACCZ = Southern Antarctic Circumpolar Current Zone and sBZ = southern Boundary Zone. In parentheses are the numbers of observations used to calculate the medians ± interquartile ranges.

Region	SST (°C)	NO_3^- (µM)	PO_4^{3-} (µM)	SiO_4^{4-} (µM)	NH_4^+ (µM)	pCO_2 (Pa)	fCO_2 (mg $m^{-2}h^{-1}$)
Subantarctic	6.62 ± 3.44 (196)	20.29 ± 7.43 (177)	1.46 ± 0.39 (177)	2.64 ± 6.91 (177)	0.81 ± 0.65 (196)	38.80 ± 1.42 (196)	1.26 ± 1.54 (196)
Antarctic	1.86 ± 1.58 (166)	23.37 ± 3.68 (142)	1.56 ± 0.26 (142)	40.62 ± 21.05 (142)	0.88 ± 0.66 (166)	36.88 ± 2.84 (166)	2.23 ± 1.94 (166)
STZ	11.89 ± 2.25 (38)	8.37 ± 5.26 (35)	0.72 ± 0.44 (35)	1.04 ± 0.42 (35)	0.63 ± 0.39 (38)	37.03 ± 2.52 (38)	3.54 ± 3.30 (38)
SAZ	7.31 ± 1.44 (77)	19.92 ± 3.52 (71)	1.46 ± 0.24 (71)	2.31 ± 2.79 (71)	0.98 ± 0.62 (77)	39.02 ± 0.29 (77)	1.10 ± 0.62 (77)
PFZ	5.01 ± 0.72 (81)	23.37 ± 3.72 (71)	1.53 ± 0.20 (71)	9.30 ± 7.40 (71)	0.72 ± 1.20 (81)	38.66 ± 1.60 (81)	1.33 ± 1.75 (81)
SACCZ	2.28 ± 1.37 (141)	23.15 ± 3.50 (122)	1.56 ± 0.23 (122)	39.03 ± 23.04 (122)	0.94 ± 0.61 (141)	37.08 ± 2.07 (141)	2.08 ± 1.70 (141)
sBZ	0.45 ± 0.27 (25)	24.29 ± 4.46 (20)	1.56 ± 0.42 (20)	46.26 ± 11.28 (20)	0.42 ± 0.34 (25)	33.98 ± 7.68 (25)	3.76 ± 4.47 (25)

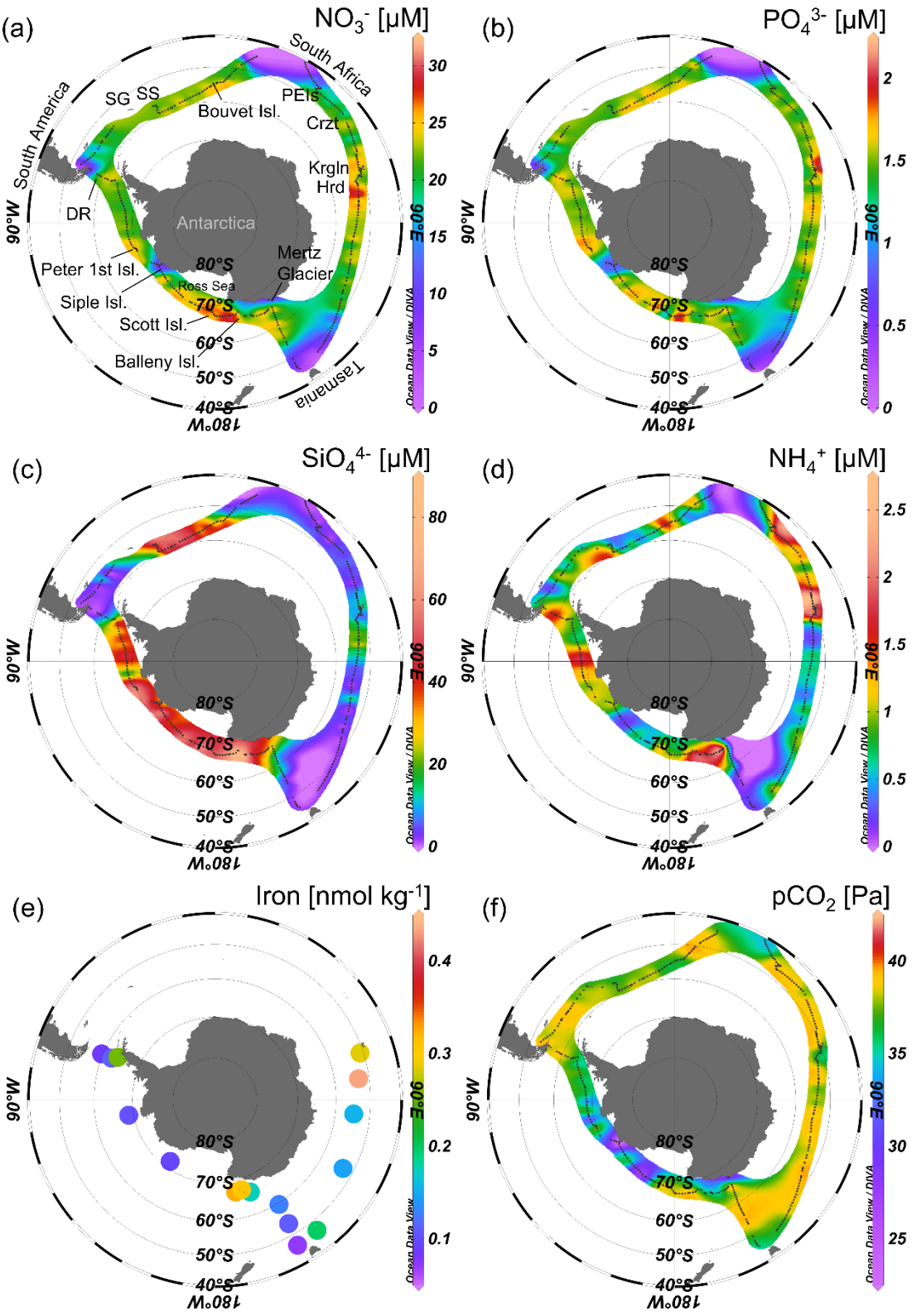

Figure 2.2 Surface distributions of the concentrations of (a) nitrate (NO_3^-; µM), (b) phosphate (PO_4^{3-}; µM), (c) silicic acid (SiO_4^{4-}; µM), (d) ammonium (NH_4^+; µM), and (e) iron (nmol kg^{-1}), and (f) the partial pressure of CO_2 (pCO_2; Pa) during ACE. The islands visited during the cruise are indicated on panel (a): PEIs = Prince Edward Islands, Crzt = Crozet Island, Krgln = Kerguelen Island, Hrd = Heard Island, DR = Diego Ramírez Island, SG = South Georgia Island, and SS = South Sandwich Islands.

2.3.2. POC and PON concentrations around the Southern Ocean

The POC and PON concentrations varied similarly along the transect, ranging from 1.9 to 70.7 µM ($7.4^{9.9}_{5.8}$ µM) and from 0.3 to 7.7 µM ($1.0^{1.4}_{0.8}$ µM), respectively Figure 2.3a, b). Variable concentrations were measured in the STZ (medians of $10.7^{11.0}_{4.0}$ µM and $1.3^{1.7}_{1.0}$ µM, respectively) and the sBZ (medians of $11.4^{19.2}_{9.2}$ µM and $1.5^{2.2}_{1.3}$ µM, respectively), and these values were significantly higher than those measured in the other zones (*p*-values* <0.01; Table 2.2). The POC and PON concentrations in the SAZ, PFZ, and SACCZ were statistically homogeneous (medians of $7.2^{8.9}_{5.6}$ µM and $1.0^{1.2}_{0.8}$ µM, respectively; *p*-values* = 1.0). Particularly high POC and PON concentrations were measured in the open STZ south of South Africa and in the sBZ near Siple Island (30.0-70.7 µM and 4.0-7.7 µM, respectively), with elevated concentrations also observed near Kerguelen and Bouvet Islands, the Mertz Glacier, at the mouth of the Ross Sea, near the WAP, and off South America (15.0-30.0 µM and 2.0-4.0 µM, respectively).

Table 2.2 Medians (± IQR) of the surface particulate organic carbon (POC) and nitrogen (PON) concentrations (µM) and $\delta^{13}C_{SPM}$ and $\delta^{15}N_{SPM}$ (‰) for different regions of the Southern Ocean sampled during ACE: 'Subantarctic' includes the STZ = Subtropical Zone, SAZ = Subantarctic Zone, PFZ = Polar Frontal Zone while 'Antarctic' includes the SACCZ = Southern Antarctic Circumpolar Current Zone and sBZ = southern Boundary Zone. In parentheses are the numbers of observations used to calculate the medians.

Region	POC (µM)	PON (µM)	$\delta^{13}C_{SPM}$ (‰)	$\delta^{15}N_{SPM}$ (‰)
Subantarctic	7.3 ± 3.6 (195)	1.0 ± 0.5 (195)	-25.2 ± 2.1 (194)	-0.1 ± 3.1 (194)
Antarctic	7.5 ± 4.9 (166)	1.1 ± 0.7 (166)	-28.4 ± 2.0 (166)	0.4 ± 2.6 (166)
STZ	10.7 ± 7.7 (37)	1.3 ± 0.7 (37)	-23.6 ± 2.3 (37)	2.1 ± 5.4 (37)
SAZ	6.8 ± 2.3 (77)	0.9 ± 0.3 (77)	-25.4 ± 1.3 (76)	-0.1 ± 3.1 (76)
PFZ	7.4 ± 3.3 (81)	1.1 ± 0.5 (81)	-26.1 ± 2.2 (81)	-0.8 ± 2.2 (81)
SACCZ	7.1 ± 3.8 (141)	1.0 ± 0.5 (141)	-28.4 ± 2.2 (141)	0.3 ± 2.8 (141)
sBZ	11.4 ± 10.0 (25)	1.5 ± 0.9 (25)	-28.4 ± 0.8 (25)	0.6 ± 1.3 (25)

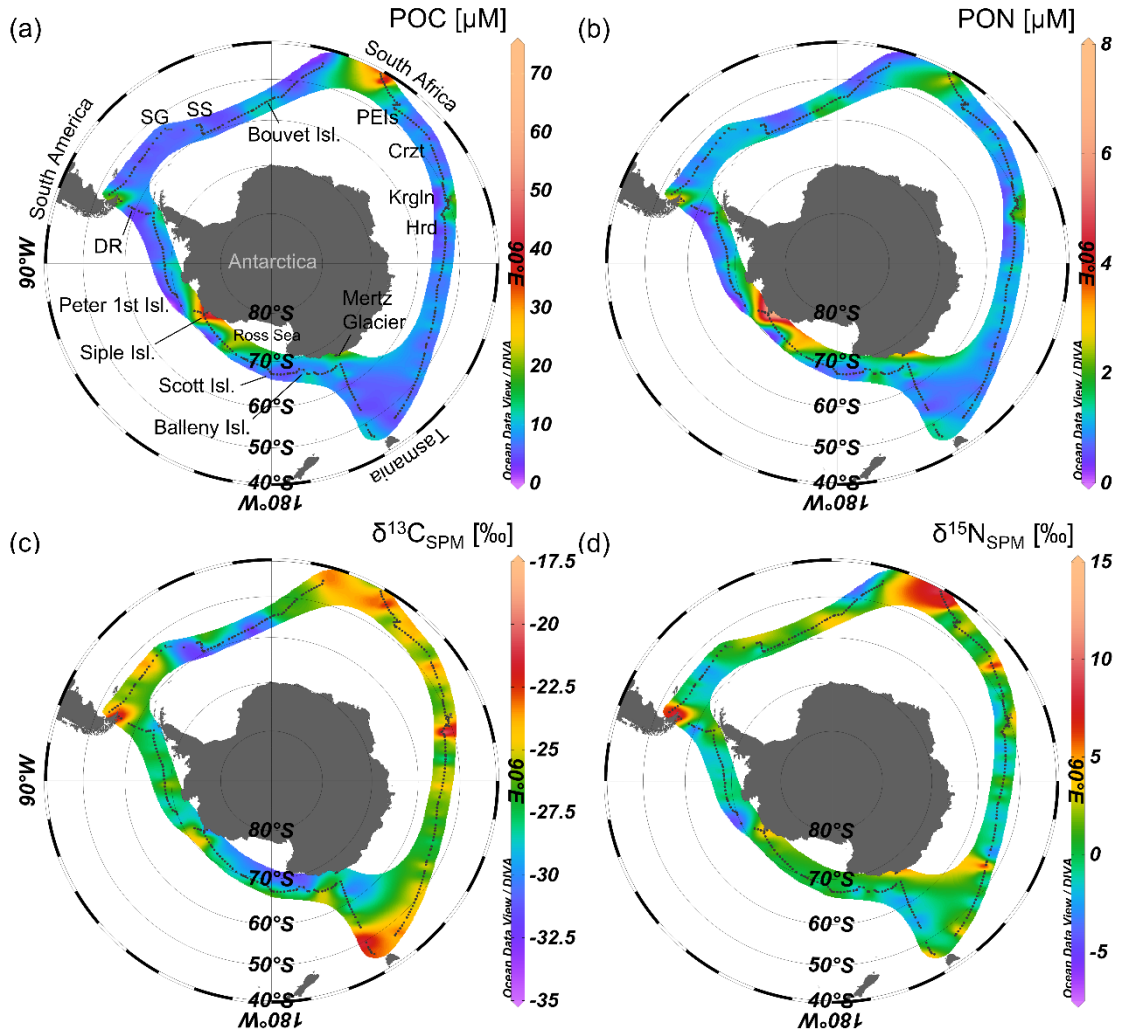

Figure 2.3 Surface concentrations (µM) of (a) particulate organic carbon (POC) and (b) particulate organic nitrogen (PON) and surface (c) $\delta^{13}C_{SPM}$ (‰) and (d) $\delta^{15}N_{SPM}$ (‰) for samples collected during ACE. The islands visited during the cruise are indicated on panel (a): PEIs = Prince Edward Islands, Crzt = Crozet Island, Krgln = Kerguelen Island, Hrd = Heard Island, DR = Diego Ramírez Island, SG = South Georgia Island, and SS = South Sandwich Islands.

2.3.3. POC and PON isoscapes around the Southern Ocean

For the entire transect, $\delta^{13}C_{SPM}$ and $\delta^{15}N_{SPM}$ ranged from -33.7‰ to -19.6‰ ($-26.6^{-25.1}_{-28.4}$‰) and -5.9‰ to 14.4‰ ($0.2^{+1.7}_{-1.1}$‰), respectively (Figure 2.3c, d). Local maxima in $\delta^{13}C_{SPM}$ and $\delta^{15}N_{SPM}$ were apparent in the STZ and near the Indian archipelago, South America, and Siple Island ($\delta^{13}C_{SPM}$ >-22.0‰ and $\delta^{15}N_{SPM}$ >5.0‰). Elsewhere, a negative relationship was observed between $\delta^{13}C_{SPM}$ and $\delta^{15}N_{SPM}$. For example, $\delta^{15}N_{SPM}$ at the mouth of the Ross Sea ($0.6^{1.8}_{0.2}$‰) and near the Atlantic archipelago ($1.5^{1.9}_{0.4}$‰) was higher than at the surrounding stations ($-0.8^{+0.6}_{-1.8}$‰ and $0.5^{+1.8}_{-1.5}$‰ for Leg2 and Leg3, respectively) while $\delta^{13}C_{SPM}$ was lower ($-27.6^{-26.2}_{-28.4}$‰ and $-29.9^{-29.1}_{-31.0}$‰ *versus*

$-28.4^{-27.5}_{-28.9}$‰ and $-25.7^{-24.8}_{-26.4}$‰). Below, we describe the broad latitudinal trends in $\delta^{13}C_{SPM}$ and $\delta^{15}N_{SPM}$ in detail, while the longitudinal and temporal patterns are presented in Appendix A.f and A.g, respectively.

In general, $\delta^{13}C_{SPM}$ decreased with increasing latitude and was significantly higher in the Subantarctic (-25.2 ± 1.9‰, mean ± 1SD) than the Antarctic (-28.4 ± 1.7‰; *p*-values <0.001; Table 2.2; Figure 2.4a). The boundary between these two regions (~55°S to 60°S) was characterized by a $\delta^{13}C_{SPM}$ minimum (reaching -33.7‰, average of -28.9 ± 2.5‰). $\delta^{15}N_{SPM}$ was high at many lower latitude (i.e., STZ) stations (>5‰), yet the median Subantarctic $\delta^{15}N_{SPM}$ was statistically similar to the median Antarctic $\delta^{15}N_{SPM}$ ($-0.1^{+1.9}_{-1.2}$‰ and $+0.4^{+1.6}_{-1.0}$‰, respectively; *p*-value* =0.63; Figure 2.4b).

For the hydrographic zones in the Subantarctic, significantly higher $\delta^{13}C_{SPM}$ and $\delta^{15}N_{SPM}$ were measured in the STZ ($-23.6^{-22.5}_{-24.8}$‰ and $2.1^{5.9}_{0.5}$‰, respectively) than in the SAZ and PFZ (*p*-values* <0.001) where the values were similar ($\delta^{13}C_{SPM}$ = $-25.4^{-24.7}_{-26.1}$‰ and $-26.1^{-24.7}_{-27.0}$‰, $\delta^{15}N_{SPM}$ = $-0.1^{+1.8}_{-1.3}$‰ and $-0.8^{+0.7}_{-1.5}$‰; *p*-values* >0.27; Table 2.2, Figure 2.4). The STZ values were also higher than those measured in the SACCZ ($\delta^{13}C_{SPM}$ = $-28.4^{-27.1}_{-29.3}$‰ and $\delta^{15}N_{SPM}$ = $0.3^{+1.6}_{-1.2}$‰) and for $\delta^{13}C_{SPM}$, higher than in the sBZ ($-28.4^{-28.1}_{-28.8}$‰; *p*-values* <0.001) while $\delta^{15}N_{SPM}$ in the sBZ was similar ($0.6^{+1.6}_{-1.2}$‰; *p*-value* = 0.37). For the Antarctic stations, $\delta^{13}C_{SPM}$ and $\delta^{15}N_{SPM}$ in the SACCZ and the sBZ were similar (*p*-values* >0.05). Additionally, $\delta^{15}N_{SPM}$ in the SACCZ was similar to that measured in the SAZ and PFZ (*p*-values* >0.18) but different from $\delta^{15}N_{SPM}$ in the STZ (*p*-values* <0.001).

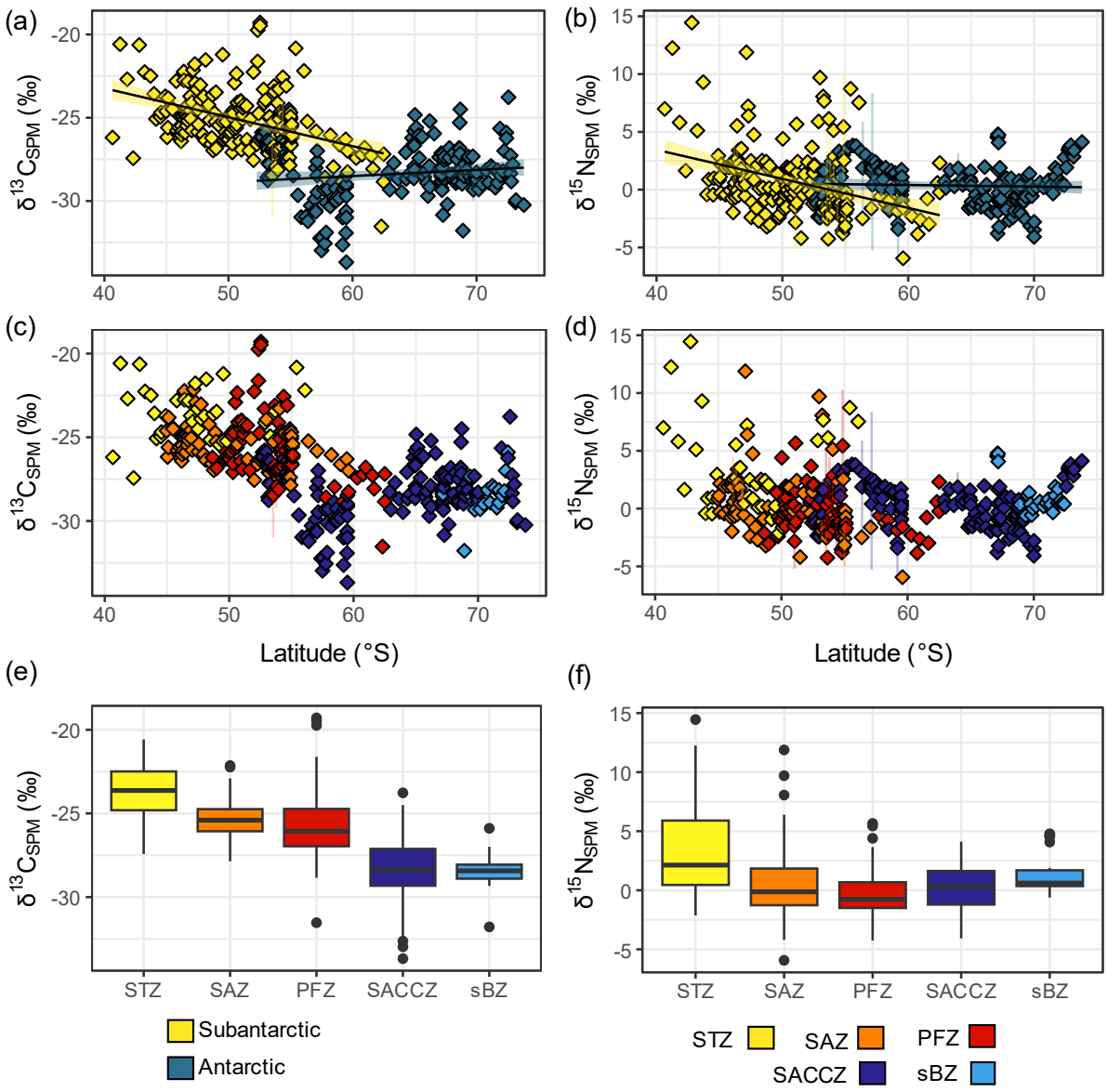

Figure 2.4 Latitudinal distribution of (a, c, e) $\delta^{13}C_{SPM}$ (‰) and (b, d, f) $\delta^{15}N_{SPM}$ (‰) for surface samples collected during ACE. Panels (a-b) show data coloured according to ocean: Subantarctic (yellow) and Antarctic (blue); panels (c-f) show data coloured according to hydrographic zone: STZ = Subtropical Zone (yellow), SAZ = Subantarctic Zone (orange), PFZ = Polar Frontal Zone (red), SACCZ = Southern Antarctic Circumpolar Current Zone (dark blue), and sBZ= southern Boundary Zone (light blue). Boxplots (panels e and f) show medians (thick horizontal lines), IQR (50% of the data; box within first and third quartiles), and whiskers (1.5 times the IQR).

2.3.4. Chlorophyll-a concentrations and phytoplankton community composition from pigment data

Total Chl-a concentrations ranged from 0.01 to 3.7 mg m^{-3} (median of $0.2^{0.4}_{0.1}$ mg m^{-3}) for the entire transect and were significantly higher (*p*-value* <0.001) in the sBZ and the STZ ($0.4^{1.0}_{0.2}$ mg m^{-3} and $0.3^{0.5}_{0.1}$ mg m^{-3}; *p*-value* = 0.18) than in the SAZ, PFZ, and SACCZ ($0.2^{0.4}_{0.1}$ mg m^{-3}, $0.2^{0.4}_{0.1}$ mg m^{-3}, and $0.1^{0.3}_{0.1}$ mg m^{-3}; *p*-values* >0.05; Table 2.3 and Figure 2.5a). Low Chl-a concentrations were recorded in the open ocean (0.01-0.3 mg m^{-3}) while elevated concentrations (>3 mg m^{-3}) occurred near Heard Island, Siple Island, and South America. Elevated Chl-a (1-2 mg m^{-3}) was also measured during Leg2 at the mouth of the Ross Sea and near the Mertz Glacier.

The relative contributions (%) of the different phytoplankton size classes to total Chl-a derived from the HPLC varied across the transect, from 11% to 99% and <1% to 89% for the micro-phytoplankton and nano-phytoplankton, respectively, and from 0% to 13% for the pico-phytoplankton (Figure 2.5b-d, Figure A.13, Table 2.3). The contributions of the micro-phytoplankton increased polewards (from $24.5^{33.4}_{19.1}$% in the STZ to $81.1^{90.7}_{62.4}$% in the sBZ) as the nano-phytoplankton contribution declined (from $72.3^{75.5}_{63.2}$% in the STZ to $18.9^{37.6}_{9.3}$% in the sBZ; Figure 2.5b). Pico-phytoplankton contributed $2.7^{4.5}_{1.7}$% and $0.8^{1.8}_{0.1}$% to the total Chl-a in the STZ and the SAZ, respectively, but in the PFZ, SACCZ, and sBZ, their median contributions were negligible. Consequently, the Subantarctic and Antarctic Oceans were dominated by nano-phytoplankton ($56.4^{68.5}_{41.5}$%) and micro-phytoplankton ($72.8^{83.1}_{55.7}$%), respectively. The highest micro-phytoplankton contributions (>75%) were observed near Heard Island, throughout Leg2, and between the South Sandwich and Bouvet Islands (Figure 2.5c). Nano-phytoplankton were dominant near South Africa and Tasmania, in the open ocean waters of Leg1, and between South America and South Georgia Island (Figure 2.5d).

Table 2.3 Median (± IQR) surface total chlorophyll-a concentrations (Chl-a; mg m^{-3}), relative contributions to total Chl-a (i.e., fraction; %), and biomass concentrations (mg m^{-3}; expressed as fraction × total Chl-a) of the various phytoplankton size classes (pico-phytoplankton (<2 µm; blue), nano-phytoplankton (2 – 20 µm; yellow), and micro-phytoplankton (20 – 200 µm; green) determined from HPLC pigment data from different regions of the Southern Ocean during the Antarctic Circumnavigation Expedition: 'Subantarctic' includes the STZ = Subtropical Zone, SAZ = Subantarctic Zone, and PFZ = Polar Frontal Zone; and 'Antarctic' includes the SACCZ = Southern Antarctic Circumpolar Current Zone and sBZ = southern Boundary Zone. In parentheses are the numbers of observations used to calculate the medians.

Region	Total Chl-a	Micro-phytoplankton (>20 µm)		Nano-phytoplankton (2-20 µm)		Pico-phytoplankton (<2 µm)	
	mg m^{-3}	Fraction (%)	mg m^{-3}	Fraction (%)	mg m^{-3}	Fraction (%)	mg m^{-3}
Subantarctic	0.2 ± 0.3 (208)	43.1 ± 29.8 (215)	0.1 ± 0.1 (208)	56.4 ± 27.0 (215)	0.1 ± 0.1 (208)	0.7 ± 1.8 (215)	0.0 ± 0.0 (208)
Antarctic	0.2 ± 0.3 (169)	72.8 ± 27.4 (169)	0.1 ± 0.2 (169)	26.1 ± 27.4 (169)	0.1 ± 0.1 (169)	0.0 ± 0.4 (169)	0.0 ± 0.0 (169)
STZ	0.3 ± 0.4 (39)	24.5 ± 14.3 (45)	0.1 ± 0.2 (39)	72.3 ± 12.3 (45)	0.2 ± 0.2 (39)	2.7 ± 2.7 (45)	0.0 ± 0.0 (39)
SAZ	0.2 ± 0.3 (81)	35.4 ± 20.3 (82)	0.1 ± 0.1 (81)	62.3 ± 18.4 (82)	0.1 ± 0.1 (81)	0.8 ± 1.7 (82)	0.0 ± 0.0 (81)
PFZ	0.2 ± 0.2 (88)	57.1 ± 19.3 (88)	0.1 ± 0.1 (88)	42.7 ± 19.3 (88)	0.1 ± 0.1 (88)	0.0 ± 0.6 (88)	0.0 ± 0.0 (88)
SACCZ	0.1 ± 0.2 (127)	71.2 ± 28.3(127)	0.1 ± 0.2 (127)	28.8 ± 28.4 (127)	0.1 ± 0.0 (127)	0.0 ± 0.5 (127)	0.0 ± 0.0 (127)
sBZ	0.4 ± 0.8 (42)	81.1 ± 28.3 (42)	0.3 ± 0.7 (42)	18.9 ± 28.3 (42)	0.1 ± 0.1 (42)	0.0 ± 0.0 (42)	0.0 ± 0.0 (42)

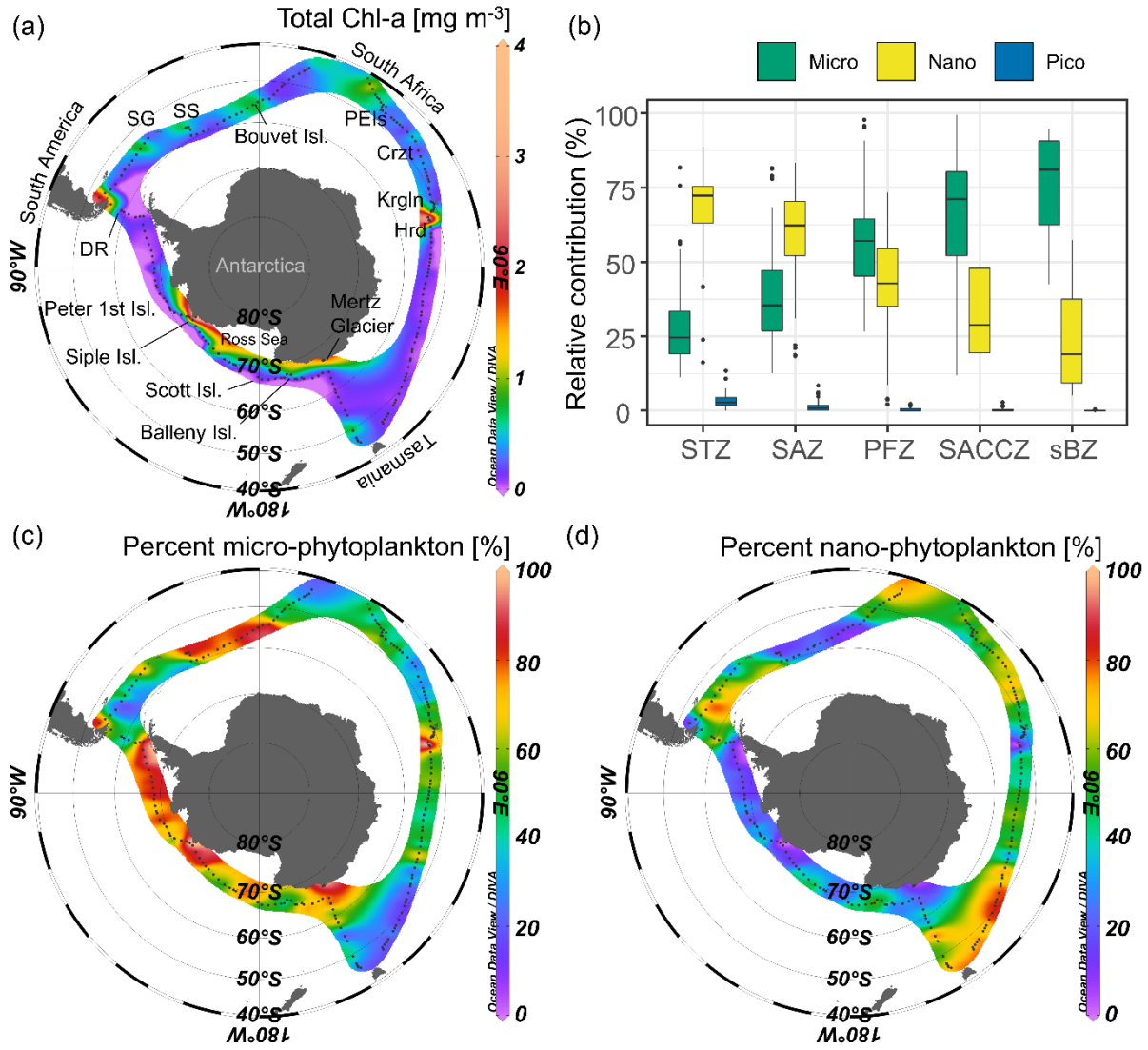

Figure 2.5 Pigment data collected during ACE (Antoine *et al.*, 2020). (a) Surface concentrations of total chlorophyll-a (Chl-a; mg m^{-3}); (b) boxplots showing the relative contributions (%) of three phytoplankton size classes to total Chl-a in each hydrographic zone (pico-phytoplankton (<2 µm; blue), nano-phytoplankton (2 – 20 µm; yellow), and micro-phytoplankton (20 – 200 µm; green)): STZ = Subtropical zone, SAZ = Subantarctic Zone, PFZ = Polar Frontal Zone, SACCZ = Southern Antarctic Circumpolar Current Zone, and sBZ = southern Boundary Zone. Also shown are the surface distributions of the percent contribution of (c) micro-phytoplankton and (d) nano-phytoplankton to total Chl-a. The islands visited during the cruise are indicated on panel (a): PEIs = Prince Edward Islands, Crzt = Crozet Island, Krgln = Kerguelen Island, Hrd = Heard Island, DR = Diego Ramírez Island, SG = South Georgia Island, and SS = South Sandwich Islands. Boxplots (panel (b)) show medians (think horizontal lines), IQR (50% of the data; box within first and third quartiles), and whiskers (1.5 times the IQR).

2.3.5. Micro-phytoplankton abundance and diversity from microscopy data

The total microplankton abundances ranged from 2 to 12056 cells L^{-1} (average of 1773 ± 2393 cells L^{-1} and median of 880^{2022}_{217} cells L^{-1} for the entire cruise) and 119 species of diatoms, 21 species of dinoflagellates, and 2 species of silicoflagellates were identified. Diatom abundances ranged from 0 to 11972 cells L^{-1}, with diatoms dominating at most stations and accounting for an average of 82.5 ± 30.6% of the total micro-phytoplankton (Figure 2.6a). Maximum diatom abundances occurred between South Sandwich and Bouvet Islands, with high abundances (>5000 cells L^{-1}) also observed near the PEIs, Kerguelen, and Heard Islands (Figure 2.6b and Figure 2.7a). Diatom abundances were particularly low (0 to 200 cells L^{-1}) in the open ocean over the Indian archipelago, at the end of Leg1, and for most of Leg2. Dinoflagellate abundances ranged from 0 to 762 cells L^{-1} and dinoflagellates accounted for an average of 17.1 ± 30.7% of the total micro-phytoplankton (Figure 2.6c). Near the end of Leg1 and east of South America, the dinoflagellate contribution increased to 70-100%, with abundances of >200 cells L^{-1} (and a maximum abundance near Tasmania of 762 cells L^{-1}), while for much of Leg1 and Leg2, dinoflagellate abundances were ≤20 cells L^{-1}. Silicoflagellates were rare, averaging 4 ± 23% of the total micro-phytoplankton and reaching a maximum abundance near the PEIs of 55.6 cells L^{-1} (data not shown).

In terms of phytoplankton species, *Fragilariopsis kerguelensis* (Figure 2.8a) dominated the diatom communities along the transect (average of 56 ± 28% of total diatom abundance), reaching particularly high abundances near the PEIs and Kerguelen Island (1000-5556 cells L^{-1}; Figure 2.7a-c). By contrast, the high diatom abundances near Heard Island (three stations) were due to *Odontella weissflogii* and *Eucampia antarctica* var. *antarctica* (Figure 2.8c) (1895 and 1519 cell L^{-1}, respectively), while the high abundances observed during Leg3 between the South Sandwich and Bouvet Islands were largely due to *Chaetoceros atlanticus* (3264 ± 2212 cells L^{-1}, ~40%) and *F. kerguelensis* (1861 ± 1254 cells L^{-1}, ~20%).

Micro-phytoplankton species richness was higher in the SAZ, PFZ, and SACCZ (108, 101, and 72 species, respectively) than in the STZ and sBZ (9 and 8 species, respectively), noting that of the 83

stations sampled for micro-phytoplankton, there were five in the STZ, 33 in the SAZ, 26 in the PFZ, 18 in the SACCZ, and one in sBZ. The average micro-phytoplankton abundance was highest in the PFZ (124 ± 551 cells L^{-1}), followed by the SACCZ and the SAZ (188 ± 653 and 145 ± 531 cells L^{-1}, respectively), with far lower abundances in the STZ and sBZ (6.6 ± 10.4 and 16.7 ± 14.6 cells L^{-1}; Table 2.4). *H'* ranged between 0.1 and 2.3 across the transect. Excluding the sBZ (one station only; *H'* = 1.8), the most diverse communities occurred in the PFZ (*H'* of $1.2^{1.4}_{0.9}$) and SACCZ (*H'* of $1.0^{1.5}_{0.7}$) followed by the SAZ (*H'* of $0.9^{1.2}_{0.6}$) and STZ (*H'* of $0.7^{0.9}_{0.6}$).

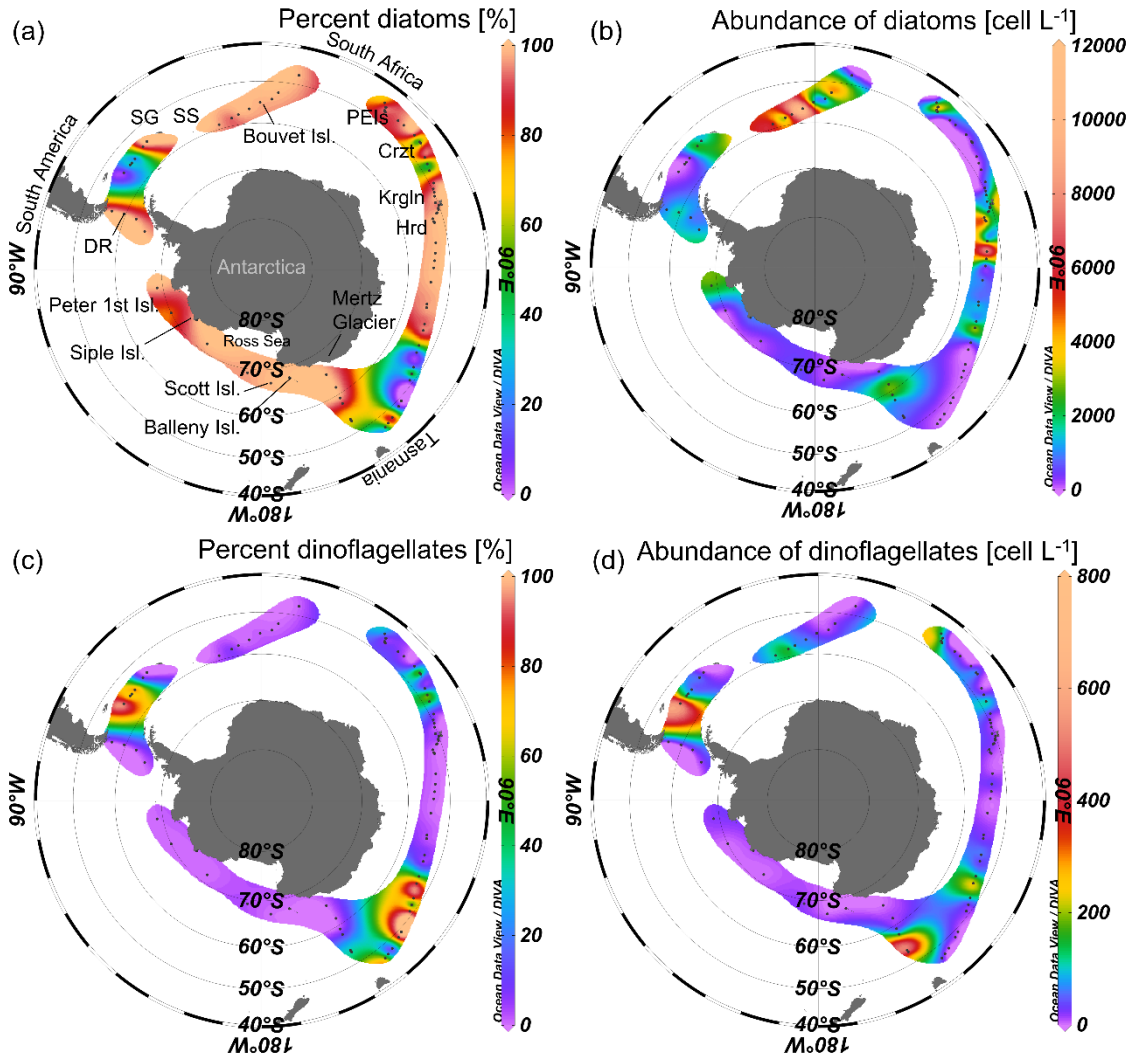

Figure 2.6 Surface distribution of the percent contribution (a, c; %) to the micro-phytoplankton and total abundances (cells L^{-1}; b, d) of (a-b) diatoms and (c-d) dinoflagellates sampled during ACE. The islands visited during the cruise are indicated on panel (a): PEIs = Prince Edward Islands, Crzt = Crozet Island, Krgln = Kerguelen Island, Hrd = Heard Island, DR = Diego Ramírez Island, SG = South Georgia Island, and SS = South Sandwich Islands.

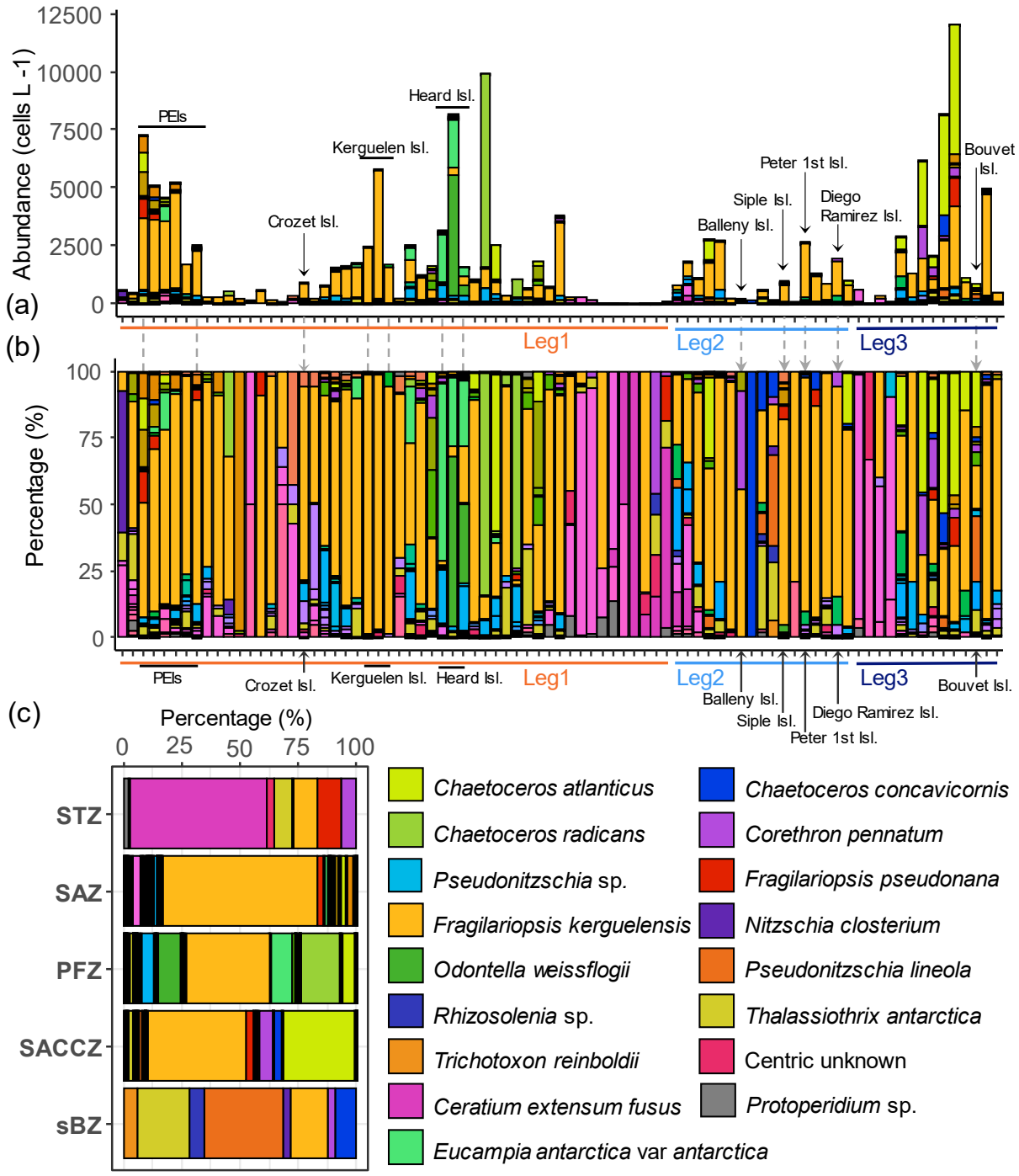

Figure 2.7 (a) Abundance (cells L^{-1}) and (b-c) percent contribution of different micro-phytoplankton species at each station (b) and in different hydrographic zones (c) of the Southern Ocean during ACE: STZ = Subtropical Zone, SAZ = Subantarctic Zone, PFZ = Polar Frontal Zone, SACCZ = Southern Antarctic Circumpolar Current Zone, and sBZ = southern Boundary Zone. Vertical arrows indicate island archipelagos, with PEIs = Prince Edward Islands, and horizontal lines denote the cruise legs. The percent contribution in panel (c) was estimated from the average abundance of the different micro-phytoplankton species in each zone.

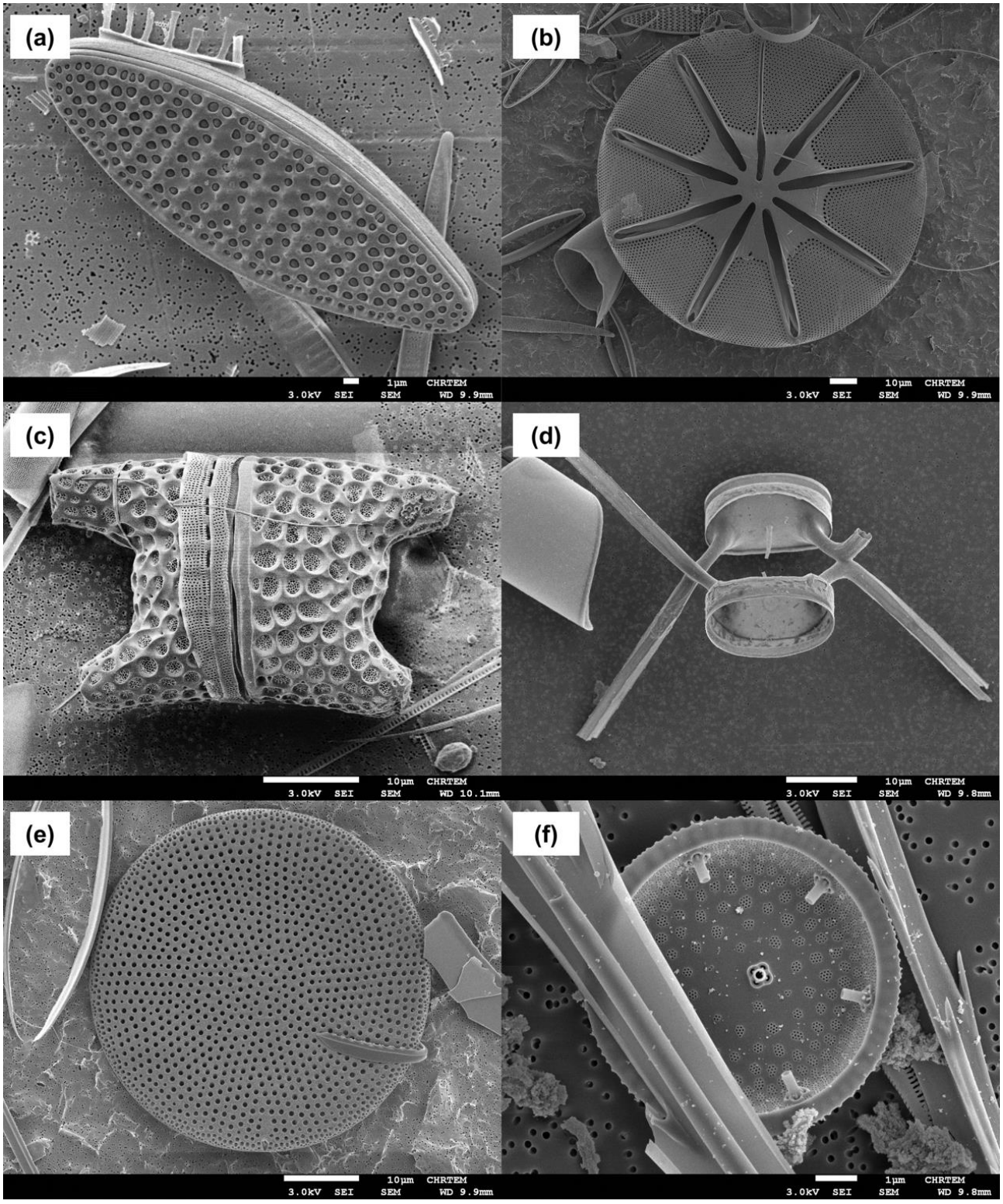

Figure 2.8. Examples of micro-plankton taxa collected during ACE and recorded using a scanning electron microscope. (a) *Fragilariopsis kerguelensis*, (b) *Asteromphalus roperianus*, (c) *Eucampia antarctica*, (d) *Chaetoceros dichaeta*, (e) *Thalassiosira lentignosa*, (f) *Thalassiosira gracilis* var. *gracilis*.

2.3.6. Estimates of f_{new}

The inputs to the Rayleigh model used to determine $\delta^{15}N_{new}$ (Figure A.14) and the resultant estimates of $\delta^{15}N_{NO_3^-(surf)}$ and $\delta^{15}N_{new}$ (Figure A.15) are listed in Table 2.4 and discussed in section S6.

Before applying the Rayleigh model to our dataset (total of 364 $\delta^{15}N_{SPM}$ observations), we excluded 32 datapoints that did not satisfy the conditions of $N_{export} \geq 0$ (-1.5) µM and $F_{export} \in (0, 1)$. For the resulting dataset (332 observations), the two-endmember isotope mixing model-derived estimates of f_{new} ranged from -7.0 to 35.2, with 86 values of $f_{new} \notin (0, 1)$. Most of these values occurred in the STZ and near or downstream of land masses, islands, or regions of sea-ice melt (Figure A.16) where the Rayleigh model requirement of a closed system was violated (e.g., by intermittent upward or lateral mixing of subsurface NO_3^- or allochthonous nutrient inputs). Excluding the out-of-range values yielded 246 estimates of $f_{new} \in (0, 1)$.

Our estimates of f_{new} ranged from 0.07 to 0.99 ($0.43^{0.60}_{0.31}$; Figure 8). High values of f_{new} (>0.7) were estimated for the waters near the PEIs, at the mouth of the Ross Sea, at Scott and Siple Islands, between the South Sandwich and Bouvet Islands, and downstream of South America, with values >0.9 at the stations near Kerguelen and Heard and to the east of the South Sandwich Islands. In addition, relatively high values (>0.5) were estimated for the Drake Passage and near the Mertz Glacier, with lower values (<0.5) for much of the open ocean, particularly in the STZ.

Values of f_{new} gradually increased from the STZ ($0.32^{0.47}_{0.24}$) to the SAZ and the PFZ ($0.39^{0.57}_{0.32}$ and $0.44^{0.55}_{0.33}$%, respectively) (Figure 2.9b, Table 2.4). In the SACCZ, f_{new} was $0.42^{0.61}_{0.31}$, increasing considerably to $0.60^{0.66}_{0.47}$% in the sBZ. The estimates of f_{new} in the SAZ, PFZ, and SACCZ were statistically similar (*p*-values* >0.1).

Table 2.4 Inputs to and outputs of the Rayleigh model. Medians (± IQR) of the isotope effect of NO_3^- assimilation (ε_{assim}; ‰), summer and winter mixed layer depth (MLD_{summer} and MLD_{winter}; m; from b-SOSE: Mazloff *et al.* 2010; Verdy and Mazloff 2017), and the concentration (µM) and $\delta^{15}N$ (‰) of the NO_3^- source (from b-SOSE and Rafter *et al.* (2019), respectively), taken to be either the water mass between the MLD_{summer} and the MLD_{winter} ($NO_{3\,(W\text{-}S)}^-$ and $\delta^{15}N_{NO_3^-(W-S)}$) or the water mass at 200-300 m ($NO_{3\,(200\text{-}300)}^-$ and $\delta^{15}N_{NO_3^-(200-300)}$), the $\delta^{15}N$ of regenerated N ($\delta^{15}N_{RN}$; ‰), the $\delta^{15}N$ of the new N (NO_3^-) consumed by phytoplankton ($\delta^{15}N_{new}$; ‰), and the fraction of phytoplankton growth fuelled by new N (f_{new}). In parentheses and in the column headed *n* are the number of observations used to calculate the medians. Medians of input parameters were calculated from the whole dataset (364 observations), while the medians of the outputs were calculated for a subset of the dataset that met certain criteria: $N_{export} \geq 0$ (-1.5) µM, $F_{export} \in (0, 1)$, and $f_{new} \in (0, 1)$ (270 observations). Values are shown for the Subantarctic and Antarctic Oceans, as well as for the STZ = Subtropical Zone, SAZ = Subantarctic Zone, PFZ = Polar Frontal Zone, SACCZ = Southern Antarctic Circumpolar Current Zone, and sBZ = southern Boundary Zone.

Region	Input to Rayleigh model								Output from Rayleigh model		
	ε_{assim} (‰)	MLD_{summer} (m)	MLD_{winter} (m)	$NO_{3\,(W\text{-}S)}^-$ (µM)	$\delta^{15}N\ NO_{3\,(W\text{-}S)}^-$ (‰)	$NO_{3\,(200\text{-}300)}^-$ (µM)	$\delta^{15}N\ NO_{3\,(200\text{-}300)}^-$ (‰)	$\delta^{15}N_{RN}$ (‰)	*n*	$\delta^{15}N_{new}$ (‰)	f_{new}
Subantarctic	6.5 ± 2.0 (189)	35.2 ± 28.8 (189)	105.0 ± 30.0 (189)	23.3 ± 6.2 (189)	6.7 ± 1.1 (189)	26.0 ± 9.5 (196)	5.7 ± 1.0 (187)	-1.6 ± 3.1 (194)	121	1.1 ± 2.4	0.41 ± 0.24
Antarctic	5.3 ± 0.5 (158)	18.6 ± 7.7 (158)	55.0 ± 20.0 (158)	28.8 ± 1.9 (158)	6.1 ± 0.5 (158)	34.0 ± 1.0 (158)	4.9 ± 0.1 (158)	-1.1 ± 2.6 (166)	125	1.8 ± 0.8	0.45 ± 0.31
STZ	5.8 ± 1.1 (34)	26.2 ± 16.3 (34)	105.0 ± 40.0 (34)	14.2 ± 4.9 (34)	8.2 ± 0.6 (34)	15.4 ± 4.7 (38)	6.8 ± 0.5 (33)	0.6 ± 5.4 (37)	27	4.5 ± 3.2	0.32 ± 0.22
SAZ	6.5 ± 1.3 (77)	35.2 ± 18.8 (77)	105.0 ± 20.0 (77)	21.7 ± 3.5 (77)	7.1 ± 0.7 (77)	25.1 ± 5.4 (77)	5.8 ± 0.3 (76)	-1.6 ± 3.1 (76)	50	1.1 ± 1.0	0.39 ± 0.25
PFZ	7.2 ± 2.0 (78)	45.0 ± 28.8 (78)	105.0 ± 61.5 (78)	26.1 ± 2.7 (78)	6.4 ± 0.5 (78)	31.3 ± 6.5 (81)	5.2 ± 0.2 (78)	-2.3 ± 2.2 (81)	44	0.3 ± 1.1	0.44 ± 0.21
SACCZ	5.3 ± 0.5 (138)	18.6 ± 7.7 (138)	55.0 ± 20.0 (138)	28.7 ± 2.0 (138)	6.2 ± 0.4 (138)	34.0 ± 1.2 (138)	4.9 ± 0.1 (138)	-1.2 ± 2.8 (141)	108	1.8 ± 0.8	0.42 ± 0.30
sBZ	5.3 ± 0.0 (20)	18.6 ± 0.0 (20)	50.0 ± 39.8 (20)	29.0 ± 0.7 (20)	5.9 ± 0.7 (20)	34.3 ± 0.2 (20)	4.9 ± 0.0 (20)	-0.9 ± 1.3 (25)	17	1.6 ± 1.1	0.60 ± 0.20

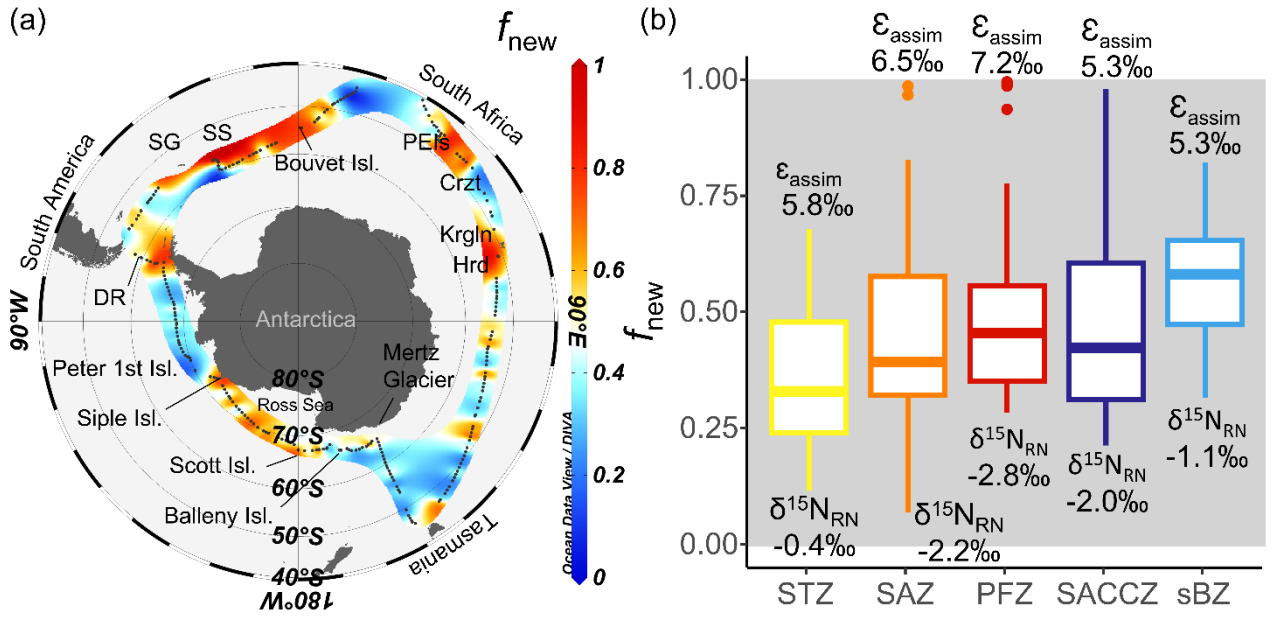

Figure 2.9 (a) Fraction of phytoplankton growth fuelled by new NO_3^- (f_{new}), and (b) boxplots of f_{new} for each hydrographic zone: yellow = Subtropical Zone (STZ), orange = Subantarctic Zone (SAZ), red = Polar Frontal Zone (PFZ), dark blue = Southern Antarctic Circumpolar Current Zone (SACCZ), light blue = southern Boundary Zone (sBZ). Numbers at the top of the boxplots are the median NO_3^- assimilation isotope effects derived for each zone (ε_{assim}; ‰; Eqn. 10) and used as inputs to the Rayleigh model. Numbers at the bottom of the boxplots are the median $\delta^{15}N$ computed for regenerated N ($\delta^{15}N_{RN}$; ‰; Eqn. 3) and used as inputs to the isotope mixing model. All values shown here, excluding ε_{assim}, were calculated for the subset of the data for which $N_{export} \geq 0$ (-1.5) µM, $F_{export} \in (0, 1)$, and $f_{new} \in (0,1)$ (270 observations). The islands visited during the cruise are indicated on panel (a): PEIs = Prince Edward Islands, Crzt = Crozet Island, Krgln = Kerguelen Island, Hrd = Heard Island, DR = Diego Ramírez Island, SG = South Georgia Island, and SS = South Sandwich Islands. Boxplots (panel (b)) show medians (thick horizontal lines), IQR (50% of the data; box within first and third quartiles), and whiskers (1.5 times the IQR).

2.3.7. Principal Component Analysis

The first and the second principal components (PC1 and PC2) together explained 55.79% of the variance, with the data clustering according to the five hydrographic zones (Figure 2.10). Observations in the STZ and SAZ were associated with higher values of SST, $\delta^{13}C_{SPM}$, $\delta^{15}N_{SPM}$, $\delta^{15}N_{new}$, the $\delta^{15}N$ of the NO_3^- sources (W-S and 200-300 m), and with higher relative contribution to the Chl-a of nano- and pico-phytoplankton (F-nano and F-pico, respectively). The higher latitude stations (SACCZ and sBZ) were negatively associated with these variables. The PCA revealed a generally positive relationship for the SAZ and PFZ with pCO_2 and a slight negative relationship with f_{new}. Observations from Kerguelen and Heard Islands were negatively associated with pCO_2 and positively associated with fCO_2, pH, $\delta^{15}N_{SPM}$, $\delta^{15}N_{new}$, and biomass (i.e., Chl-a, POC, PON), with a slight positive relationship with f_{new}. Data from the SACCZ and sBZ were associated with higher concentrations of SiO_4^{4-}, PO_4^{3-}, and NO_3^-, as well as with higher relative contributions of micro-phytoplankton (F-micro) to the Chl-a. Observations at the extreme latitudes (a few from the STZ and many

from the sBZ) were associated with higher concentrations of POC, PON, and Chl-a, high values of $\delta^{15}N_{SPM}$, $\delta^{15}N_{new}$, fCO_2, and pH, and low pCO_2. In addition, many observations from the sBZ and some from the SACCZ were slightly positively correlated with f_{new}. In the context of PC1 and PC2, NH_4^+ did not impact the data distribution, even though it was slightly positively related to the observations at higher latitudes.

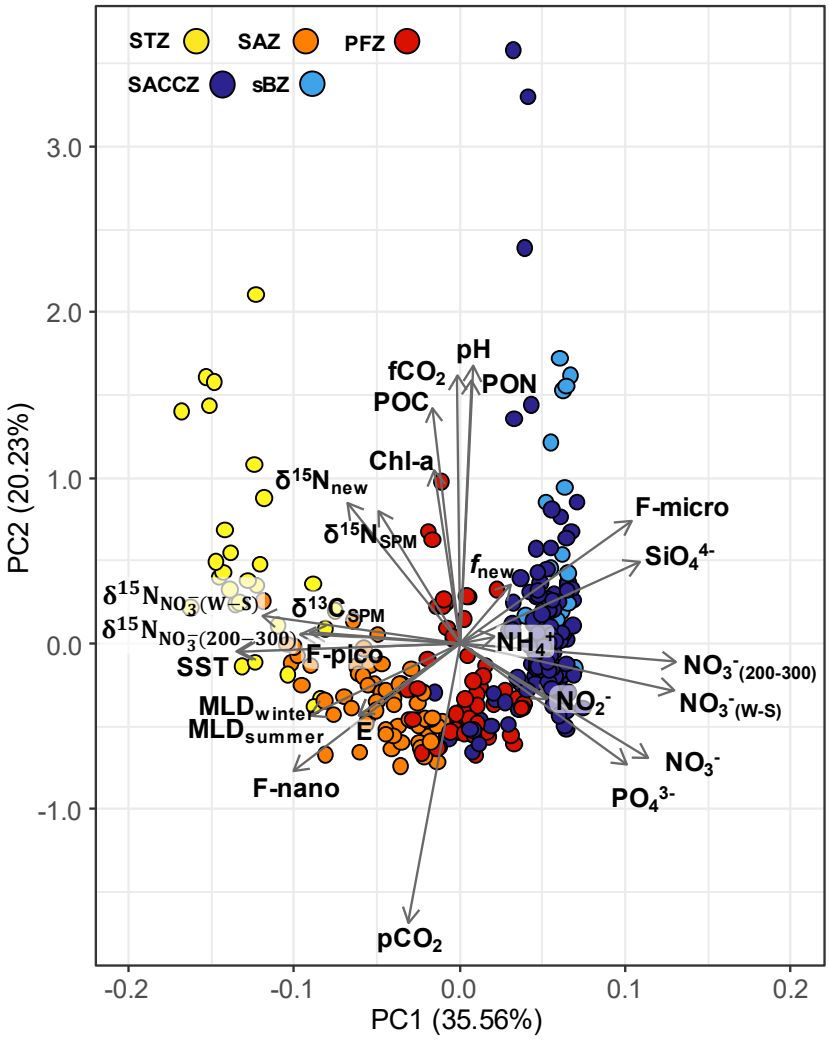

Figure 2.10 Principal Component Analysis (PCA) of our dataset from ACE. Surface parameters considered include observations of sea surface temperature (SST), the concentrations of nitrate (NO_3^-), nitrite (NO_2^-), phosphate (PO_4^{3-}), silicic acid (SiO_4^{4-}), and ammonium (NH_4^+), the partial pressure and air-sea flux of CO_2 (pCO_2 and fCO_2), pH, the concentrations of particulate organic carbon and nitrogen (POC and PON) and their isotopes ($\delta^{13}C_{SPM}$ and $\delta^{15}N_{SPM}$), total chlorophyll-a concentration (Chl-a) and the fractions of micro-, nano-, and pico-phytoplankton (F-micro, F-nano, and F-pico, respectively) derived using the HPLC data. Modelled parameters were also included, such as the winter and summer mixed layer depths (MLD_{winter} and MLD_{summer}), the concentration and $\delta^{15}N$ of the NO_3^- source ($NO_3^-{}_{(W-S)}$ and $\delta^{15}N_{NO_3^-(W-S)}$ and $NO_3^-{}_{(200-300)}$ and $\delta^{15}N_{NO_3^-(200-300)}$), the theoretical $\delta^{15}N$ of phytoplankton biomass produced from the assimilation of NO_3^- ($\delta^{15}N_{new}$), and the fraction of phytoplankton growth fuelled by NO_3^- (f_{new}). The symbol colours indicate the hydrographic zones: yellow = Subtropical Zone (STZ), orange = Subantarctic Zone (SAZ), red = Polar Frontal Zone (PFZ), dark blue = Southern Antarctic Circumpolar Current Zone (SACCZ), and light blue = southern Boundary Zone (sBZ).

2.4. Discussion

2.4.1. SPM isotopic differences among Southern Ocean zones reflect different biogeochemical regimes

Variability in physical forcings (e.g., SST) and mixed-layer nutrient concentrations is a major reason for the differentiation of the Southern Ocean's hydrographic zones (Orsi *et al.* 1995; Figure 2.9), driving differences in the solubility- and biological pumps, and in phytoplankton biomass and community composition (e.g., Pollard *et al.* 2002; Rigual-Hernández *et al.* 2015). Our dataset reveals that the physical, chemical, and biological differences among the zones, directly or indirectly, also control the $\delta^{13}C_{SPM}$ and $\delta^{15}N_{SPM}$ isoscapes. Below, we discuss the spatial trends in $\delta^{13}C_{SPM}$ and $\delta^{15}N_{SPM}$, evaluate potential drivers of the dominant patterns, and consider the implications for regional productivity and Southern Ocean food webs.

2.4.2. Spatial variability in $\delta^{13}C_{SPM}$

During photosynthesis, phytoplankton preferentially fix ^{12}C-bearing CO_2, producing biomass (SPM) that is lower in $\delta^{13}C$ than the CO_2 substrate (O'Leary, 1981). The remineralization of this SPM returns low-$\delta^{13}C$ CO_2 to the dissolved inorganic carbon (DIC) pool (e.g., McCorkle *et al.* 1985) such that upwelling of deeper waters, which introduces remineralized DIC, lowers the $\delta^{13}C$ of the surface DIC pool (Gruber *et al.*, 1999). The extent to which phytoplankton discriminate against $^{13}CO_2$ is strongly driven by their growth rate and the ambient pCO_2 (François *et al.*, 1993; Goericke, 1994; Laws *et al.*, 1995). For the same initial pCO_2, a higher growth rate yields less isotopic fractionation and thus a higher $\delta^{13}C_{SPM}$, while for phytoplankton growing at the same rate, higher surface-water pCO_2 is associated with higher isotopic fractionation and thus a lower $\delta^{13}C_{SPM}$ (Rau *et al.* 1991; Gruber *et al.* 1999). The $\delta^{13}C$ of the DIC available to phytoplankton will also affect $\delta^{13}C_{SPM}$ as it sets the isotopic baseline for the ecosystem (e.g., Tamelander *et al.* 2009). Net fractionation of CO_2 during photosynthesis is further influenced by the isotope effects associated with any process that brings DIC into the cell (i.e., passive diffusion and/or active uptake of bicarbonate (HCO_3^-) or CO_2) (Laws *et al.*, 1997; Keller, 1999).

We observed a general northward increase in $\delta^{13}C_{SPM}$, of ~12‰ between the Antarctic and the STZ, with a higher median (± IQR) $\delta^{13}C_{SPM}$ in the Subantarctic than the Antarctic (-25.2 ± 2.1‰ *versus* -28.4 ± 2.0‰; Figure 2.4a, c, e; Figure A.17a). This meridional trend has been reported previously and attributed to a

gradual northward decrease in isotopic fractionation during photosynthesis driven by a decline in surface pCO_2 and higher phytoplankton growth rates (François *et al.*, 1993; Popp *et al.*, 1999; Arteaga *et al.*, 2018; Espinasse *et al.*, 2019), along with a northward increase in DIC-$\delta^{13}C$ (of ~1‰ between ~60°S and the STF; Kroopnick 1985; François *et al.* 1993; Gruber *et al.* 1999). Across the Subantarctic, $\delta^{13}C_{SPM}$ was negatively correlated with pCO_2 (ρ = -0.41; Figure 2.11a-b) and (relatedly) positively correlated with pH, fCO_2, and SST (ρ = 0.50, 0.53, 0.37; *p*-values <0.05; Figure A.19), which indicates that ambient pCO_2 was a dominant driver of its $\delta^{13}C_{SPM}$ variability. DIC-$\delta^{13}C$ may also have played a role, although it changed by <1‰ across >20 degrees of latitude while $\delta^{13}C_{SPM}$ increased by >10‰ from the APF to the STZ. We also observed strong deviations from the expected pCO_2-driven latitudinal trend in $\delta^{13}C_{SPM}$. For instance, $\delta^{13}C_{SPM}$ reached a minimum in the southern PFZ and northern SACCZ (55-60°S; median of -29.3 ± 3.2‰, reaching -33.7‰). Furthermore, incidences of anomalously high $\delta^{13}C_{SPM}$ relative to expectations from pCO_2 were apparent near and/or downstream of some of the islands (e.g., the PEIs) and off South America, while in the SACCZ and sBZ where pCO_2 was the lowest, we observed anomalously low values of $\delta^{13}C_{SPM}$ (Figure 2.2f and Figure 2.3c).

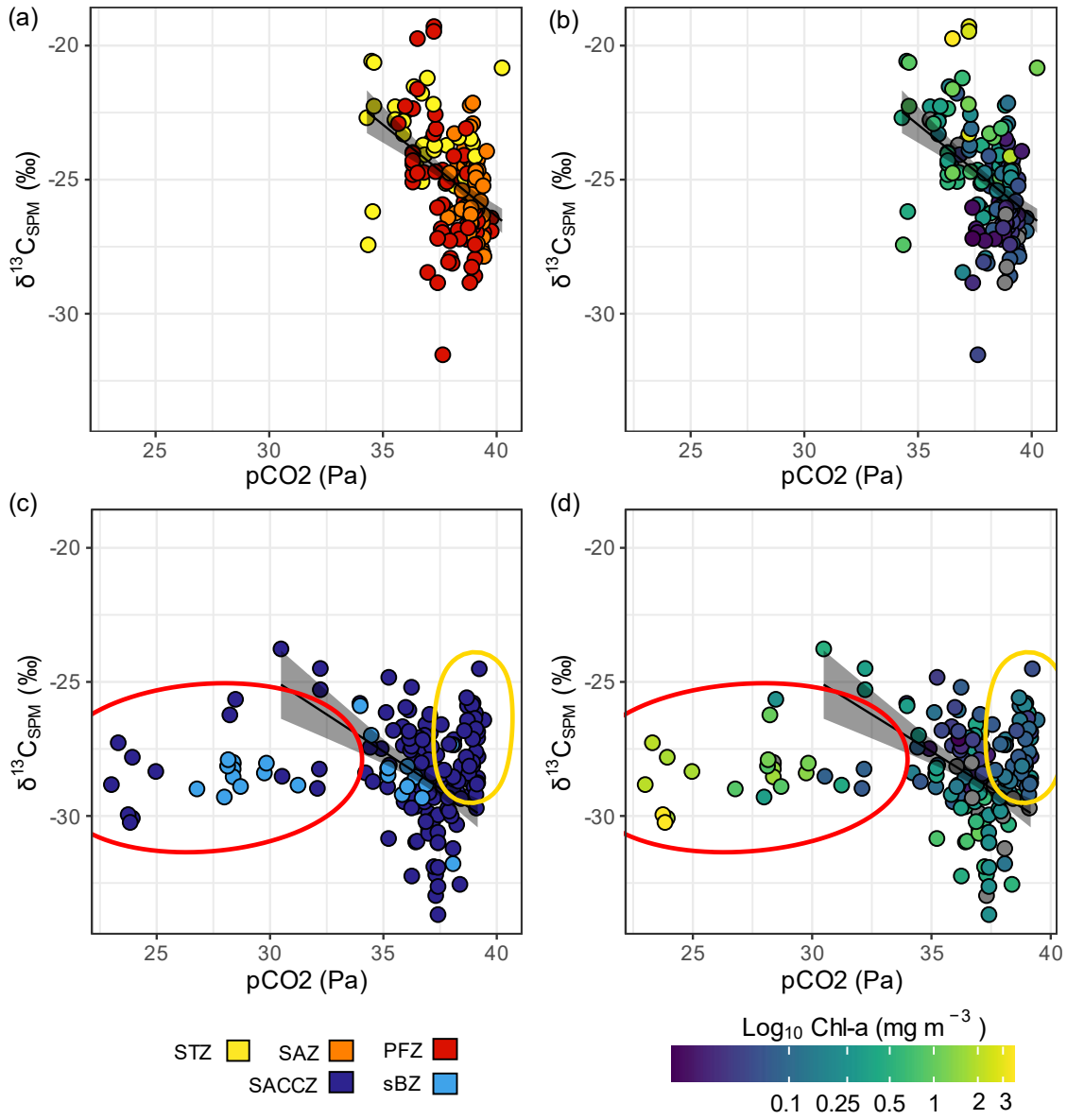

Figure 2.11 Relationship between the surface partial pressure of CO_2 (pCO_2; Pa) and $\delta^{13}C_{SPM}$ (‰) in the (a-b) Subantarctic and (c-d) Antarctic Oceans. Symbol colours in the left-hand panels (a, c) show the hydrographic zones: yellow = Subtropical Zone (STZ), orange = Subantarctic Zone (SAZ), red = Polar Frontal Zone (PFZ), dark blue = Southern Antarctic Circumpolar Current Zone (SACCZ), light blue = southern Boundary Zone (sBZ), while symbol colours in the right-hand panels (b, d) show total chlorophyll-a concentrations (HPLC data) on a $\log_{10}$ scale (Chl-a; mg m^{-3}). In panels (c) and (d), the ellipses highlight notable deviations from the expected pCO_2-$\delta^{13}C_{SPM}$ relationship. Solid lines are linear regressions with 95% confidence intervals shaded in grey.

The $\delta^{13}C_{SPM}$ minimum in the PFZ/SACCZ may be due to the low-$\delta^{13}C$ DIC that upwells in Upper Circumpolar Deep Water (UCDW), a water mass that outcrops south of the ACC where it is transformed into Antarctic Surface Water (AASW; Talley 2011). UCDW is relatively low in oxygen due to organic matter remineralization during its transit through the ocean and high in SiO_4^{4-}, NO_3^-, and iron that, once upwelled, favour diatom growth (Kang and Lee, 1995; Prézelin *et al.*, 2000). UCDW also hosts a remineralization-

driven high DIC concentration and low DIC-$\delta^{13}C$ (0.2–0.3‰; Kroopnick 1985; Eide *et al.* 2017; Williams *et al.* 2021). By contrast, the DIC-$\delta^{13}C$ of shallow Southern Ocean waters (upper 50 m) typically ranges from 0.75‰ to 1.75‰ in the Antarctic (>55°S) and 1.50‰ to 2.25‰ in the Subantarctic (40-55°S) (François *et al.*, 1993; Gruber *et al.*, 1999). Thus, the upwelling and subsequent photosynthesis of relatively low-$\delta^{13}C$ DIC in UCDW may explain the lower $\delta^{13}C_{SPM}$ in the PFZ/SACCZ upwelling region.

Although pCO_2 in the Subantarctic and Antarctic Oceans showed a similar range (except for a few incidences of particularly low pCO_2 (23-32 Pa) in the Antarctic; see below), $\delta^{13}C_{SPM}$ differed by ~3‰ between the two regions (Figure 2.11 and Table 2.2). Such a $\delta^{13}C_{SPM}$ shift could be driven by several co-occurring factors including phytoplankton growth rates and community composition, and species-specific physiological processes such as the transport of inorganic carbon across the cell membrane, the enzymes catalysing carboxylation, and cell size and geometry (Dehairs *et al.*, 1997; Popp *et al.*, 1998; Laws *et al.*, 2002; Cassar *et al.*, 2004). We observed a northward increase in the contribution of nano-phytoplankton and decrease in that of the micro-phytoplankton (Figure 2.5), along with an increase in dinoflagellate and decrease in diatom abundances (Figure 2.6 and Figure 2.7). These geographical differences in plankton community composition that are set by zone-specific biogeochemical environments likely influenced the latitudinal trends in $\delta^{13}C_{SPM}$ (Falkowski, 1991; Goericke, 1994; Tuerena *et al.*, 2019).

At high pCO_2, diffusion of CO_2 across the cell membrane is rate-limiting to photosynthesis and thus controls the extent of isotope fractionation, yielding a low $\delta^{13}C_{SPM}$ (Rau *et al.*, 1989, 1991b, 1992a; François *et al.*, 1993). In contrast, at lower pCO_2, fractionation associated with the intra-cellular carbon concentrating mechanism becomes rate-limiting, yielding a higher $\delta^{13}C_{SPM}$ (François *et al.*, 1993; Raven *et al.*, 2008). While all phytoplankton contain the RuBisCO enzyme, which has a large isotope effect (of ~29‰; Roeske and O'Leary 1984; Raven and Johnston 1991), some species may also have one or both types of β-carboxylation enzymes, including PEPcarboxylase (PEPc), which is typically found in dinoflagellates and small (pico- and nano-) phytoplankton, and PEPcarboxykinase (PEPk), which is possessed by diatoms (Descolas-Gros and Fontugne, 1985; Descolas-Gros and Oriol, 1992). PEPc catalyses the fixation of HCO_3^-, which has a higher $\delta^{13}C$ (~1.5‰, akin to DIC) than CO_2 (~ -10‰), the latter fixed by PEPk (Mook *et al.* 1974; François *et al.* 1993). In addition, PEPc has a smaller intrinsic isotope effect than PEPk (~2‰ *versus*

>20‰; O'Leary 1981; Guy *et al.* 1989; Arnelle and O'Leary 1992). As such, while the northward decrease in pCO_2 may explain much of the latitudinal rise in $\delta^{13}C_{SPM}$, the coincident increase in nano-phytoplankton and large dinoflagellates may also have increased $\delta^{13}C_{SPM}$ because of the lower net fractionation associated with their PEPc carboxylation pathway.

The higher $\delta^{13}C_{SPM}$ near the Subantarctic islands and continental shelves could be due to the coincidence of low pCO_2 and the composition and growth rates of the *in situ* phytoplankton community. During fast-growing blooms, large diatoms have been observed to have a higher $\delta^{13}C_{SPM}$ (i.e., lower isotopic fractionation) than smaller cells (Fry and Wainright, 1991), with Nakatsuka *et al.* (1992) reporting a positive correlation between phytoplankton growth rate and $\delta^{13}C_{SPM}$. However, Berg *et al.* (2011) observed a low $\delta^{13}C_{SPM}$ for diatoms growing rapidly following iron fertilization in the open PFZ, with $\delta^{13}C_{SPM}$ increasing later as the phytoplankton community became more diverse following the bloom. In our study, phytoplankton biomass at Heard Island was higher (Chl-a of 2.6 ± 1.2 mg m^{-3}) than that measured over the Atlantic archipelago (0.4 ± 0.2 mg m^{-3}) and the rest of the Indian archipelago (0.4 ± 0.2 mg m^{-3}) (Figure 2.5a). Higher phytoplankton growth rates at Heard Island, stimulated by an IME-related input of nutrients (e.g., Jena 2016) (Figure 2.2a-e), may have reduced net isotope fractionation, yielding values of $\delta^{13}C_{SPM}$ ($-19.7^{-19.6}_{-20.7}$‰) that were 5‰ to 10‰ higher than at the Atlantic ($-29.1^{-28.5}_{-29.8}$‰) and rest of the Indian archipelagos ($-25.0^{-24.4}_{-25.9}$‰).

The observed $\delta^{13}C_{SPM}$ differences among the islands were unlikely to be due only to pCO_2 and growth rates. The $\delta^{13}C_{SPM}$ at the Indian archipelago (excluding Heard Island) was higher than at the Atlantic archipelago, despite both regions having similar pCO_2 and phytoplankton biomass. Micro-phytoplankton were the major contributors to the total Chl-a at the Atlantic archipelago (73 ± 10%; Figure 5), presumably comprising mainly diatoms (i.e., as per the >5000 Ind. m^{-3} measured from -20°E to 0°E downstream of the South Sandwich Islands; no taxonomy data are available directly at the islands; Figure 7). At the Indian archipelago, the micro-phytoplankton contribution was lower, 49 ± 15% and 31 ± 6% at the PEIs and Crozet, increasing to 94 ± 3% at Heard Island. The taxonomy data show two distinct diatom communities, one dominated by *F. kerguelensis* (along most of the archipelago) and the second dominated by *Odontella weissflogii* and *Eucampia antarctica* var. *antarctica* (Heard Island only).

Assuming relief from iron limitation near the islands due to the IME (e.g., Schallenberg *et al.* 2018), the distinct phytoplankton communities of the Atlantic and Indian archipelagos (excluding Heard Island) may be analogous to two assemblages described by Berg *et al.* (2011) following artificial iron fertilization of open Southern Ocean waters. In that study, rapidly growing *Chaetoceros* spp. came to dominate the assemblage shortly after iron addition, with a $\delta^{13}C_{SPM}$ that was slightly higher than that measured prior to fertilization. The phytoplankton community then evolved into a more diverse assemblage of smaller cells (2–20 µm), as well *Pseudo-nitzschia* spp., *Fragilariopsis cylindrus*, and the haptophyte, *Phaeocystis antarctica* (Hoffmann *et al.*, 2006; Croot *et al.*, 2007; Berg *et al.*, 2011). This change coincided with a further ~1.5‰ rise in $\delta^{13}C_{SPM}$, attributed to a higher ratio of PEPc:RuBisCO activity and thus a decline in net isotopic fractionation (Descolas-Gros and Fontungne, 1990; Wada and Hattori, 1991; Bentaleb *et al.*, 1998). Our data may be similarly explained – we measured a higher $\delta^{13}C_{SPM}$ in waters dominated by a smaller, more diverse phytoplankton community (the Indian archipelago excluding Heard Island) and a lower $\delta^{13}C_{SPM}$ coincident with the dominance of large diatoms including *Chaetoceros* spp. (Atlantic archipelago).

From the APF to Antarctica, $\delta^{13}C_{SPM}$ appeared near-constant ($-28.4^{-27.3}_{-29.3}$‰, Figure 2.4), as has been observed previously (Rau *et al.* 1989; Freeman and Hayes, 1992; Goericke and Fry 1994; Espinasse *et al.* 2019), and was (weakly) correlated with only a few environmental parameters, including SiO_4^{4-}, Chl-a, and $\delta^{15}N_{SPM}$. Interestingly, $\delta^{13}C_{SPM}$ was not correlated with pCO_2 when all measurements from the SACCZ and sBZ were considered (ρ = -0.02, *p*-value = 0.52; Figure A.20). However, a closer inspection of the data reveals three different relationships of $\delta^{13}C_{SPM}$ to pCO_2 (Figure 2.11c-d). In the SACCZ and sBZ, $\delta^{13}C_{SPM}$ was significantly negatively correlated with pCO_2 between 32 and 38 Pa (ρ = -0.60, *p*-value <0.001), as was observed for the Subantarctic. Additionally, at the highest pCO_2 (~39 to 40 Pa; data from the SACCZ only), $\delta^{13}C_{SPM}$ was anomalously high (>-28‰; yellow ellipse in Figure 2.11c-d) while at a pCO_2 of 23 to 32 Pa, $\delta^{13}C_{SPM}$ was anomalously low (-30‰ to -28‰; red ellipse in Figure 2.11c-d) relative to the expected relationship of $\delta^{13}C_{SPM}$ to pCO_2.

As outlined above, Berg *et al.* (2011) reported a lower $\delta^{13}C_{SPM}$ for large, iron-replete diatoms than for the more mixed and generally smaller phytoplankton community that succeeded them. This dynamic may explain the anomalously low $\delta^{13}C_{SPM}$ at low pCO_2 observed near the Mertz Glacier, at the mouth of the Ross

Sea, and adjacent to Siple and Peter 1st Islands (Figure 2.2f, Figure 2.3c, and red ellipse in Figure 2.11c-d). Here, biomass was high (Figure 2.3a-b, Figure 2.5, and Figure 2.11d) and the phytoplankton community comprised near-exclusively large diatoms (mostly *F. kerguelensis*; Figure 2.7). However, the rapid growth rates typically associated with high biomass production occur with lower isotopic fractionation (Laws *et al.*, 1995), yielding higher values of $\delta^{13}C_{SPM}$, as at Heard Island (Figure 2.5 and Figure 2.6). The $\delta^{13}C_{SPM}$ difference between Heard Island and the Mertz Glacier/Ross Sea/Siple/Peter 1st Islands may instead involve the rate of CO_2 resupply to surface waters. At Heard Island, CO_2 depletion by phytoplankton may have been faster than its rate of resupply, causing $\delta^{13}C_{SPM}$ to increase due to a progressive ^{13}C-enrichment of the *in situ* CO_2 (Deuser, 1970; Villinski *et al.*, 2008). Such ^{13}C enrichment is typically negligible because rapid equilibration of CO_2 and HCO_3^- essentially renders the entire (large) DIC pool available to phytoplankton (Tortell *et al.*, 1997, 2008). However, if phytoplankton growth is particularly rapid, as is possible near Heard Island where conditions are extremely favourable (Mongin *et al.*, 2008, 2009), CO_2 can be so rapidly depleted as to raise its $\delta^{13}C$ (Deuser, 1970). In contrast, the Mertz Glacier/Ross Sea/Siple/Peter 1st Islands region is characterized by the highest fCO_2 of the Antarctic Ocean (>10 mg m^{-2} h^{-1} from atmosphere to ocean; Figure A.6), likely induced by high biological activity (Tagliabue and Arrigo, 2016) and intense CO_2 dissolution driven by low SSTs and enhanced ice melt (Fransson *et al.*, 2011; Tortell *et al.*, 2012). The resultant high rate of CO_2 resupply likely negates any ^{13}C-enrichment of the *in situ* CO_2 (and thus, the SPM) (Rau *et al.*, 1989; Freeman and Hayes, 1992).

The anomalously high-pCO_2 and high-$\delta^{13}C_{SPM}$ (yellow ellipse in Figure A.10c-d) occurred far downstream of Bouvet and Heard Islands in waters that were influenced by the APF. Phytoplankton biomass was low and comprised ~50% nano-phytoplankton (Figure A.5). We suggest that these phytoplankton were mainly a post-bloom, iron-limited community expressing a higher ratio of PEPc:RuBisCO activity, which would have yielded lower net isotope fractionation and thus a higher $\delta^{13}C_{SPM}$ (Descolas-Gros and Fontungne, 1990; Wada and Hattori, 1991; Bentaleb *et al.*, 1998).

Deducing the drivers of latitudinal variability in $\delta^{13}C_{SPM}$ across the Southern Ocean is crucial when such data are used as a baseline for food web analyses (e.g., McMahon *et al.* 2013; Alurralde *et al.* 2020). From our extensive dataset, we provide some insights into the possible role of regional biogeochemistry and

phytoplankton community composition in setting $\delta^{13}C_{SPM}$. However, the species-specific physiological mechanisms underlying the relationship of carbon isotopic fractionation to phytoplankton taxonomy remain uncertain.

2.4.3. Spatial variability in $\delta^{15}N_{SPM}$

In our dataset, $\delta^{15}N_{SPM}$ decreased by ~3‰ from the STZ (2.1 ± 5.4‰ [median ± IQR]) to the SAZ and PFZ where it reached a minimum (-0.1 ± 3.1‰ and -0.8 ± 2.2‰, respectively) before increasing by ~1.4‰ into the Antarctic (SACCZ = 0.3 ± 2.8‰ and sBZ = 0.6 ± 1.3‰; Table 2.2 and Figure A.2e). The $\delta^{15}N_{SPM}$ data from the entire transect were positively correlated with POC, PON, and Chl-a (ρ = 0.48, 0.44, and 0.45, respectively; *p*-value <0.001), which is qualitatively consistent with the expectation that higher biomass accompanies higher rates of NPP and greater NO_3^- utilization, the latter yielding higher values of $\delta^{15}N_{SPM}$ (Altabet and Francois, 1994; Somes *et al.*, 2010; St John Glew *et al.*, 2021). Generally, the latitudinal variability in $\delta^{15}N_{SPM}$ agrees well with previous observations (e.g., Espinasse *et al.* 2019; St John Glew *et al.* 2021). Using a Bayesian hierarchical spatial model applied to data collected over 50 years in the Southern Ocean, St John Glew *et al.* (2021) determined that SST and MLD are good predictors of $\delta^{15}N_{SPM}$; however, we find a positive relationship between $\delta^{15}N_{SPM}$ and SST only in the Subantarctic (ρ = 0.37, *p*-value <0.001; Figure A.19) and a positive correlation with MLD only in the Antarctic (ρ = 0.37, *p*-value <0.001; Figure A.20). The inconsistency of our findings with those of St John Glew *et al.* (2021) highlights the lack of a mechanistic understanding of the synergistic drivers of $\delta^{15}N_{SPM}$ across the Southern Ocean.

The $\delta^{15}N$ of phytoplankton biomass depends on the $\delta^{15}N$ of the N sources consumed, the degree of consumption of those N sources, and the isotope effect(s) expressed during N uptake (Sigman *et al.*, 1999; Altabet and Francois, 2001; DiFiore *et al.*, 2010; Fawcett *et al.*, 2011, 2014). The $\delta^{15}N$ of subsurface NO_3^- (i.e., $\delta^{15}N_{NO_3^-\,(source)}$) is influenced by vertical exchange with underlying deep-water NO_3^- and by N-cycle processes occurring in the surface and subsurface during water mass circulation (Sigman *et al.*, 2000; Rafter *et al.*, 2013). South of the SACCF, Lower Circumpolar Deep Water (LCDW) is the ultimate source of NO_3^- to the mixed layer, with a $\delta^{15}N$ of 4.8‰, while north of the SACCF, upwelling of UCDW supplies NO_3^- with a $\delta^{15}N$ of 5‰ (Sigman *et al.*, 2000; Rafter *et al.*, 2013; Smart *et al.*, 2015; Fripiat *et al.*, 2019). Partial consumption of NO_3^- in the northward-flowing AASW that derives from UCDW raises its $\delta^{15}N$ such that the

Antarctic Intermediate Water (AAIW) and Subantarctic Mode Water (SAMW) that form in the PFZ and SAZ are higher in $\delta^{15}N_{NO_3^-}$ than UCDW (5.7‰ and >6.3‰, respectively; Sigman *et al.* 1999; Rafter *et al.* 2013; Fripiat *et al.* 2019). As these water masses subduct and flow northwards, their higher-$\delta^{15}N_{NO_3^-}$ becomes the sub-mixed layer NO_3^- source across much of the Subantarctic. At the same time, surface processes continue to modify subsurface NO_3^- as sinking particles recording the $\delta^{15}N$ of surface N cycling are remineralized below the mixed layer (Sigman *et al.*, 1999; Rafter *et al.*, 2013). Here, we define the source NO_3^- to phytoplankton at the beginning of the growth season as that present in the winter mixed layer following NO_3^- recharge, a record of which is retained directly beneath the summer mixed layer. For the regions where we expect local upwelling of deeper waters (e.g., near the islands and coastal regions; De Falco *et al.* 2022), we take the mean properties of the 200-300 m layer as representative of the immediate source NO_3^-.

The $\delta^{15}N_{NO_3^-\,(source)}$ decreased by ~2‰ from the lower latitudes to the APF (STZ = 8.2 ± 0.7‰, SAZ = 6.8 ± 1.1‰, PFZ = 6.3 ± 0.6‰), after which it remained stable (Antarctic Ocean = 6.1 ± 0.5‰) (Table 2.4 and Figure A.21a). As expected, the $\delta^{15}N_{SPM}$ was generally lower than the $\delta^{15}N_{NO_3^-\,(source)}$ because of isotope fractionation during NO_3^- assimilation (Sigman *et al.*, 1999), with a median difference (i.e., $\delta^{15}N_{SPM} - \delta^{15}N_{NO_3^-\,(source)}$) of $-6.3^{-4.9}_{-7.7}$‰ and the highest variability observed in the lower latitudes (*p*-value < 0.05; Figure A.21b-c). The large-scale consistency of $\delta^{15}N_{SPM} - \delta^{15}N_{NO_3^-\,(source)}$ across the Southern Ocean suggests that the $\delta^{15}N$ of NO_3^- is a principal factor controlling $\delta^{15}N_{SPM}$ (e.g., Sigman *et al.* 1999) (Figure A.2).

The $\delta^{15}N_{SPM}$ is also strongly influenced by the $\delta^{15}N$ of regenerated N and the degree of consumption of NO_3^- *versus* regenerated N (Lourey *et al.*, 2003; Fawcett *et al.*, 2011, 2014). The derived values of f_{new} explain a variance of 2.7‰^{2} of the $\delta^{15}N_{SPM} - \delta^{15}N_{NO_3^-\,(source)}$, with larger negative differences in $\delta^{15}N_{SPM} - \delta^{15}N_{NO_3^-\,(source)}$ associated with a higher degree of regenerated N consumption (i.e., f_{new} < 0.5) and smaller differences associated with a higher proportion of NO_3^- consumption (i.e., f_{new} > 0.5; Figure A.21b-c). This trend is explained by the $\delta^{15}N$ of regenerated N, which is lower than that of the source NO_3^- (i.e., −5‰ to 0‰

versus 5‰ to 7‰; Mariotti *et al.* 1981; Checkley and Miller 1989; Sigman *et al.* 1999, 2000; Lourey *et al.* 2003; Fawcett *et al.* 2011).

Our estimates of f_{new} indicate that the degree of NO_3^- consumption increased poleward (Figure 2.9b). Such a trend could be related to latitudinal changes in nutrient concentrations, light and MLD, and/or phytoplankton community composition. Indeed, f_{new} was (weakly) positively correlated with the relative contributions of micro-phytoplankton to Chl-a, likely due to the dominance of the micro-phytoplankton by diatoms (Figure 2.5), which are NO_3^- specialists. Indeed, diatoms have been shown to take up NO_3^- faster than other phytoplankton groups at comparable substrate concentrations (Eppley *et al.*, 1969; Paasche *et al.*, 1984; Hildebrand and Dahlin, 2000), often achieving higher NO_3^- uptake and reduction rates than those required for growth, especially in cold, NO_3^--rich environments (Lomas and Glibert, 1999, 2000). f_{new} was negatively correlated with the relative contributions of nano-phytoplankton to Chl-a, which typically show a higher affinity for NH_4^+ (Probyn, 1985; Wafar *et al.*, 2004; Stirnimann *et al.*, 2021). The apparent preference of nano-phytoplankton for NH_4^+ over NO_3^- can be explained by their higher surface-area-to-volume ratio, which makes them more competitive for scarce nutrients than the larger diatoms (Marañón 2015 and references therein).

Of our 332 measurements of $\delta^{15}N_{SPM}$, 86 yielded values of f_{new} that fell outside the range of 0 to 1 (grey circles in Figure A.21b-c). These samples were mainly collected near the islands, the continents, and at the mouth of the Ross Sea (Figure A.14). Here, processes such as bathymetrically-induced mixing, ice melt, and/or terrestrial N inputs may have altered the mixed-layer NO_3^- and/or NH_4^+ pools (e.g., Cavagna *et al.* 2015; Smart *et al.* 2015; Shatova *et al.* 2016), violating the Rayleigh model assumption of a closed system and rendering estimates of f_{new} invalid. Mathematically, $\delta^{15}N_{new}$ must be higher than the measured $\delta^{15}N_{SPM}$ to produce an acceptable f_{new}; if $\delta^{15}N_{new} < \delta^{15}N_{RN}$, then $f_{new} < 0$ and if $\delta^{15}N_{RN} < \delta^{15}N_{new} < \delta^{15}N_{SPM}$, then $f_{new} > 1$ (Figure A.14a). The $\delta^{15}N_{SPM}$ at the sites where the model failed was on average 2.0 ± 2.0‰ higher than the $\delta^{15}N_{new}$ derived for those sites ($\delta^{15}N_{SPM} = 2.2^{3.3}_{0.9}$ and $\delta^{15}N_{new} = 0.8^{+1.6}_{-0.2}$‰ for $f_{new} \notin (0, 1)$) and 2.4 ± 3.5‰ higher than the $\delta^{15}N_{SPM}$ measured elsewhere ($\delta^{15}N_{SPM} = -0.5^{+0.6}_{-1.6}$‰ for $f_{new} \in (0, 1)$). These high $\delta^{15}N_{SPM}$ values likely reflect consumption of N sources other than subsurface NO_3^- and recycled NH_4^+ such as terrestrially-derived N, which can be very high in $\delta^{15}N$ (Erskine *et al.*, 1998; Wainright *et al.*, 1998), and/or

non-assimilation N-cycle processes such as bacterial decomposition of SPM, which raises its $\delta^{15}N$ (Möbius, 2013). Since our sampling was conducted during a period of active phytoplankton growth when SPM production would have exceeded its degradation, we suggest that the consumption of external N sources accounts for most of the anomalous $\delta^{15}N_{SPM}$ values.

We measured high concentrations of NH_4^+ near the islands and Antarctica (Figure 2.2d), which may have been partly supplied via terrestrial run-off and/or melting sea-ice and glaciers (Fripiat *et al.*, 2014; Otero *et al.*, 2018). Land-derived NH_4^+ is generally high in $\delta^{15}N$ due to trophic enrichment and/or volatilization of ammonia gas from guano and other organic matter deposited by sea birds and marine mammals (i.e., the $\delta^{15}N$ of guano can be >12‰; Mizutani *et al.* 1986; Wainright *et al.* 1998). Phytoplankton consumption of this high $\delta^{15}N_{NH_4^+}$ could yield higher values of $\delta^{15}N_{SPM}$ than is possible from the assimilation of subsurface NO_3^- (Wainright *et al.*, 1998).

In addition, the high $\delta^{15}N_{SPM}$ at the mouth of the Ross Sea and near Siple Island (Figure 2.3d; Figure A.14g) may have been influenced by the release of nutrients from melting sea-ice and/or coastal glaciers. Surface NH_4^+ concentrations were elevated relative to open ocean values almost everywhere during Leg2 ($0.9^{1.3}_{0.5}$ µM), particularly between the Mertz Glacier and Scott Island and downstream of Peter 1st Island, reaching concentrations >1.5 µM. Remineralization of organic N produced by ice algae and excretion by zooplankton feeding under the sea-ice produce NH_4^+ and other reduced N forms that accumulate in and under the ice from winter to early summer (Fripiat *et al.*, 2014, 2017; Roukaerts *et al.*, 2016; Louw *et al.*, 2022). Indeed, NH_4^+ can reach concentrations as high as 150 µM in Antarctic sea-ice (Priscu and Sullivan, 1998; Thomas and Dieckmann, 2002), although 10-20 µM is more common (Kattner *et al.*, 2004; Fripiat *et al.*, 2017; Louw *et al.*, 2022). This NH_4^+ appears to be relatively low in $\delta^{15}N$ (<0‰; Fripiat *et al.* 2014), as would be expected given the N isotope effects associated with its production (Macko *et al.*, 1986; Silfer *et al.*, 1992; Möbius, 2013). However, there may be times when coincident NH_4^+ assimilation, which occurs with little to no fractionation (Hoch *et al.*, 1992; Pennock *et al.*, 1996; Liu *et al.*, 2013), and NH_4^+ oxidation, which is associated with a large isotope effect (14-19‰; Casciotti *et al.* 2003), cause the $\delta^{15}N$ of the sea-ice NH_4^+ pool to rise significantly. In contrast to NH_4^+, algal NO_3^- consumption is a fractionating process, which in the spring/summer sea-ice yields a relatively low-concentration NO_3^- pool that can be very high in $\delta^{15}N$ (Fripiat

et al., 2014; Roukaerts *et al.*, 2016). When the ice melts, the N species contained within it are released, along with high concentrations of iron (Lannuzel *et al.*, 2016). This iron stimulates phytoplankton NO_3^- consumption in the water column (Timmermans *et al.*, 1994), including of the high-$\delta^{15}N$ NO_3^- released from the ice, resulting in the production of higher $\delta^{15}N_{SPM}$ than predicted by a Rayleigh model initialized with the underlying $\delta^{15}N_{NO_3^-(source)}$.

2.4.4. Estimating relative carbon export potential from $\delta^{15}N_{SPM}$

In this study, we aimed to assess carbon export potential in the Southern Ocean by estimating the fraction of organic matter produced via the uptake of new *versus* regenerated nutrients (i.e., subsurface NO_3^- *versus* recycled NH_4^+; Dugdale and Goering 1967; Eppley and Peterson 1979). The relative strength of the biological pump can be approximated by the *f*-ratio, assuming that the surface ocean is a steady state over an annual cycle (Eppley and Peterson, 1979). Here, we derive f_{new} (a measure of the *f*-ratio) using a two-endmember isotope mixing model, with the $\delta^{15}N$ of the consumed NO_3^- (i.e., $\delta^{15}N_{new}$) estimated via the Rayleigh model. However, instead of assuming that the $\delta^{15}N_{SPM}$ generated from the assimilation of subsurface NO_3^- can be approximated by the accumulated (or instantaneous) product equation, we account for the fact that some portion of the SPM would have been exported from the surface layer between the start of the growth season and our sampling. Above, we have discussed cases in which our isotope mixing model failed (e.g., due to an input of high-$\delta^{15}N$ allochthonous N; section 4.1.2). Below, we discuss our estimates of f_{new} and the implications for carbon export potential in the case where the $\delta^{15}N_{SPM}$ data are well described by the model (i.e., 74% of the observations).

In a mass balance sense, our data suggest that the Southern Ocean potentially exports almost half of the carbon produced during the summer (f_{new} = 43^{60}_{32}%), with minimal difference between the Subantarctic and Antarctic Oceans (41 ± 24% and 45 ± 31% [median ± IQR], respectively; Figure 2.9; Table 2.4). These values generally agree with existing estimates of the *f*-ratio (and export ratio) for the summertime Southern Ocean (which averages ~50%; e.g., (Sambrotto and Mace, 2000; Schlitzer, 2002; Joubert *et al.*, 2011; Prakash *et al.*, 2015; Le Moigne *et al.*, 2016; Mdutyana *et al.*, 2020), noting that the different methods integrate over different time-periods, complicating such a comparison. Examining our data by zone shows that f_{new} decreased by ~20% from the higher to the lower latitudes (Figure 2.9b) and was slightly negatively

correlated with SST (ρ = -0.18, *p*-value <0.01), consistent with previous (albeit poorly-understood) observations of an inverse correlation between export efficiency and temperature (Laws *et al.*, 2000; Ángel *et al.*, 2006; Cael and Follows, 2016; Britten *et al.*, 2017).

The mean f_{new} was highest in the sBZ, with 60 ± 20% of phytoplankton carbon potentially exported, reaching ~80% near the sea ice (e.g., at the mouth of the Ross Sea; Table 2.4 and Figure 2.9b). f_{new} was lowest in the STZ, although ~30% of NPP was still potentially exported. Across the SAZ, PFZ, and SACCZ, while f_{new} was highly variable (ranging between 7% and ~98%), similar median values were estimated for all three zones (39-44%). High values of f_{new} (>65%) were derived for stations near and downstream of many of the islands, with ~75% of NPP exported near the PEIs and >80% downstream of Kerguelen Island. Lower values of f_{new} (<50%) were derived for open ocean stations that were distant from the islands or covered with sea-ice (e.g., the open STZ, the waters south of Tasmania, and the SACCZ during the latter half of Leg2; Figure 2.9a). The apparent latitudinal trend in f_{new} may thus be driven principally by processes that occur at the regional scale, such as the alleviation of iron limitation that leads to proportionally higher NO_3^- dependence near the islands, at the hydrographic fronts, and off the continental shelves. For instance, the extensive area between the South Sandwich and Bouvet Islands that was characterized by a high degree of NO_3^- dependence (73 ± 33%) may have biased the mean SACCZ f_{new} estimate upwards, while most of the truly open ocean stations where regenerated production dominated were located at lower latitudes, potentially biasing those f_{new} estimates downwards.

NO_3^- uptake by Southern Ocean phytoplankton is typically enhanced by an increase in light, a stable upper water column, and a supply of limiting nutrients (i.e., iron and/or SiO_4^{4-}) via upwelling, terrestrial run-off, and/or melting sea-ice and glaciers (Cochlan 2008 and references therein). The IME is generally associated with upwelling, input of land-derived nutrients, and retention and stabilization of surface waters over shallow plateaus, which drive localized increases in phytoplankton biomass and nutrient and CO_2 drawdown near the islands (e.g., Planquette *et al.* 2011; Schallenberg *et al.* 2018; Holmes *et al.* 2019). In the Ross Sea, large and persistent polynyas reduce sea-ice cover, increasing stratification and light availability (Gordon *et al.*, 2000; Arrigo *et al.*, 2015), as well as iron availability (Alderkamp *et al.*, 2012). Relief from iron limitation enhances NO_3^- reductase activity in phytoplankton, particularly diatoms, allowing for higher NO_3^- uptake and

increased rates of phytoplankton biomass production (Timmermans *et al.*, 1994; De Baar *et al.*, 1997; Karsh *et al.*, 2003; Blain *et al.*, 2007). By contrast, low iron concentrations limit NO_3^- uptake and favour the growth of small phytoplankton reliant on regenerated N (Martin *et al.*, 1990b; Sunda and Hardison, 2007). In our dataset, the open ocean regions were characterized by low iron concentrations (<0.05 nmol kg^{-1}; Figure 2.2e) and supported low biomass and a high proportion of nano-phytoplankton (<0.1 mg Chl-a m^{-3} and >65%, respectively; Figure 2.5). By contrast, near the South Sandwich Islands, PEIs, and Heard Island, iron concentrations were higher (≥0.2 nmol kg^{-1}), biomass and micro-phytoplankton contributions to total Chl-a were elevated (>0.5 mg Chl-a m^{-3} and >65%, respectively), large diatoms were abundant (>5000 cell L^{-1}; Figure 2.7), and local minima in pCO_2 were apparent (Figure 2.2f). Interestingly, downstream of Crozet Island, the plankton system was dominated by nano-phytoplankton and diatom abundance was low (Figure 2.5 and Figure 2.6); here, regenerated N fuelled more than half of NPP and ~30-40% of the autotrophic carbon was potentially exported (Figure 2.2c).

Between Siple Island and the Drake Passage, biomass and f_{new} were low ($0.1^{0.16}_{0.05}$ mg Chl-a m^{-3} and 20-40%, respectively; Figure 2.5a and Figure 2.9b) and the NH_4^+ concentrations were high (0.9-2 µM). Near melting sea-ice, the specific rates of NO_3^- and NH_4^+ uptake have been observed to correlate positively with their respective concentrations (Zhang *et al.*, 2019). Thus, high NH_4^+ concentrations supplied by melting sea-ice (Fripiat *et al.*, 2014; Roukaerts *et al.*, 2016) could have decreased f_{new}. At the same time, the addition of relatively high NH_4^+ (1 µM) in regions with high dissolved iron and low NH_4^+ availability can both enhance NH_4^+ uptake and (partly) inhibit NO_3^- consumption by phytoplankton (Elskens *et al.*, 2002). Interestingly, our estimates of f_{new} from the Antarctic Ocean did not correlate with NH_4^+ concentration, while in the Subantarctic Ocean, f_{new} and NH_4^+ were weakly positively correlated ($\rho = 0.3$, p-value <0.001). This positive correlation, which seems counterintuitive, may be due to elevated regeneration of NH_4^+ following high biomass production that was fuelled predominantly by NO_3^- (Rönner *et al.*, 1983; Semeneh *et al.*, 1998), which would have resulted in high values of $\delta^{15}N_{SPM}$ (and thus, f_{new}) coincident with elevated NH_4^+ concentrations.

Across the Southern Ocean, f_{new} was slightly positively correlated with SiO_4^{4-} ($\rho = +0.25$, p-value < 0.001; Figure A.18). Since the availability of SiO_4^{4-} controls the distribution of diatoms (Hoffmann *et al.*, 2008),

which typically drive new production (Egge and Aksnes, 1992; Dugdale *et al.*, 1995), and given that the fraction of micro-phytoplankton was strongly positively correlated with SiO_4^{4-} (ρ = +0.70, *p*-value <0.001), the relationship of f_{new} to SiO_4^{4-} is not unexpected. Consistently, f_{new} was also slightly positively correlated with micro-phytoplankton biomass (ρ = +0.40, *p*-value <0.001) and showed no relationship with nano-phytoplankton biomass (Figure A.22c-d). The correlation of f_{new} to micro-phytoplankton biomass was high for the Antarctic, but weak for the Subantarctic Ocean (ρ = +0.56 and +0.28, respectively; Figure A.19 and Figure A.20). During a study conducted in Subantarctic waters south of Tasmania in summer, Elskens *et al.* (2002) similarly observed no relationship between phytoplankton community structure and new *versus* regenerated N uptake. Nonetheless, it is not a coincidence that the regions of our circumpolar transect characterized by a higher f_{new} were dominated by large diatoms. By contrast, low values of f_{new} occurred where nano-phytoplankton dominated, typically in open ocean waters. Here, low iron availability strongly limits diatom growth and their capacity to assimilate NO_3^- (Timmermans *et al.*, 2004), which leads to the development of regenerated N-fuelled systems dominated by nano-phytoplankton that are more competitive for scarce nutrients (Hare *et al.*, 2007).

2.4.5. Temporal trends in $\delta^{13}C_{SPM}$ and $\delta^{15}N_{SPM}$ differ among hydrographic zones due to latitudinal changes in the seasonal cycles of phytoplankton community composition and production

Over the three-month ACE cruise (early summer to early autumn), $\delta^{13}C_{SPM}$ for the entire Southern Ocean decreased by ~4‰ and $\delta^{15}N_{SPM}$ decreased by ~5‰ (Figure A.8a-b; Table A.3). These trends may not be entirely due to temporal changes, however, given the complicating influence of regional factors such as proximity to islands and fronts. However, excluding all the stations influenced by the IME or the continents does not change the general patterns; on average $\delta^{13}C_{SPM}$ still decreased by ~4‰ and $\delta^{15}N_{SPM}$ decreased by ~3‰ over the three-month period (Figure A.8c-d). The trends in $\delta^{13}C_{SPM}$ and $\delta^{15}N_{SPM}$ differed among zones, suggesting a latitudinal dependence of their driver(s). Throughout the sampling period, $\delta^{13}C_{SPM}$ remained stable in the STZ and SAZ while $\delta^{15}N_{SPM}$ decreased by ~4‰ and ~1‰, respectively. In the PFZ, both $\delta^{13}C_{SPM}$ and $\delta^{15}N_{SPM}$ by ~3‰ while in the SACCZ, $\delta^{13}C_{SPM}$ decreased by ~3‰ and $\delta^{15}N_{SPM}$ increased by ~2‰. In the sBZ, the temporal gradients for $\delta^{13}C_{SPM}$ and $\delta^{15}N_{SPM}$ were positive and negative, respectively, although the time-series duration was only 12 days and as such, cannot be taken to show temporal changes.

During the cruise, SST in the STZ decreased by ~2°C and did not change in the SAZ, PFZ, and SACCZ (Figure A.9a). Similarly, pCO_2 remained stable (Figure A.9b-c), such that the decrease in $\delta^{13}C_{SPM}$ cannot be attributed to changes in pCO_2.

Our estimates of f_{new} indicate that phytoplankton consumption of regenerated N relative to NO_3^- increased with time in the STZ and SAZ where nano-phytoplankton dominated while the proportion of NO_3^- consumption increased with time in the PFZ, SACCZ, and sBZ where micro-phytoplankton were generally more abundant (Figure A.10). The HPLC data show that over the three-month expedition, the contribution of nano-phytoplankton to total Chl-a remained stable (SAZ) or increased (STZ and PFZ) in the Subantarctic and decreased in the Antarctic where the fractional contribution of micro-phytoplankton increased (Figure A.11). For the whole Southern Ocean, the average contributions of the nano- and micro-phytoplankton were similar at the beginning of the cruise (51 ± 19% and 47 ± 20%, respectively, for the first two weeks) while by the end of the cruise, the nano-phytoplankton contribution to total Chl-a had decreased to 35 ± 21% and that of the micro-phytoplankton had increased to 65 ± 21%. The NH_4^+ concentrations also changed over time, apparently declining in all the hydrographic zones (Figure A.12a). However, the input of terrestrial NH_4^+ (e.g., derived from guano and/or faecal material from animal colonies on the islands) enhanced the NH_4^+ concentrations in near-island waters, complicating our temporal analysis. Excluding the near-island data reveals that the open-ocean NH_4^+ concentrations increased with time in all zones but the STZ where it declined (Figure A.12b).

As conditions in the Southern Ocean become favourable for phytoplankton growth in spring/early summer, diatoms come to dominate the phytoplankton assemblage (e.g., Garibotti *et al.* 2005; Kopczyńska *et al.* 2007; Alvain *et al.* 2008). This group uses both PEPk and RuBisCO for carboxylation (Arnelle and O'Leary, 1992; Descolas-Gros and Oriol, 1992), which yields a low $\delta^{13}C$ for their biomass (O'Leary, 1981; Guy *et al.*, 1989; Arnelle and O'Leary, 1992). They also tend to be NO_3^- specialists (Eppley *et al.*, 1969; Paasche *et al.*, 1984; Hildebrand and Dahlin, 2000), with the preferential consumption of this nutrient causing their biomass to be relatively high in $\delta^{15}N$ (Altabet, 1988; Lourey *et al.*, 2003; Fawcett *et al.*, 2011, 2014). As the growth season progresses, iron and SiO_4^{4-} become limiting, which, coupled with increased zooplankton grazing, decreases diatom productivity (Hunt and Hosie, 2006a, 2006b; Llort *et al.*, 2015; Arteaga *et al.*, 2020).

Generally, these conditions favour the growth of smaller phytoplankton, an upregulation of the microbial loop, and a (related) increase in NH_4^+ availability and consumption (Christaki *et al.*, 2021b; Smith *et al.*, 2022) since far less iron is required to assimilate NH_4^+ than NO_3^- (Price *et al.*, 1991; Geider and La Roche, 1994; Schoffman *et al.*, 2016). As such, $\delta^{13}C_{SPM}$ should decline from the spring to reach a minimum at the end of the productive season (St John Glew *et al.*, 2021) before rising through the late-summer and autumn due to an increase in the expression of PEPc:RuBisCO activity associated with increased nano-phytoplankton growth (Descolas-Gros and Fontungne, 1990; Wada and Hattori, 1991; Bentaleb *et al.*, 1998). At the same time, $\delta^{15}N_{SPM}$ should rise between spring and early-to-mid summer as a result of preferential NO_3^- assimilation by large diatoms before decreasing again due to enhanced consumption of low-$\delta^{15}N$ NH_4^+ to reach a minimum in autumn (Lourey *et al.*, 2003; Smart *et al.*, 2020; St John Glew *et al.*, 2021). However, it is unlikely that the seasonal cycles of the biogeochemical processes affecting $\delta^{13}C_{SPM}$ and $\delta^{15}N_{SPM}$ occur synchronously in each hydrographic zone. As such, we suggest that at the time of our sampling, the productive period was less advanced at the higher latitudes, which were dominated by diatoms relying on NO_3^-, while at the lower latitudes, the seasonal cycle was more advanced and ecosystems were dominated by nano-phytoplankton consuming proportionally more NH_4^+.

In the SACCZ (and presumably also the sBZ), micro-phytoplankton (i.e., diatoms) dominated the assemblage and their relative contribution to total Chl-a increased with time (Figure A.11), as did f_{new} (Figure A.10). Regenerated NH_4^+ progressively accumulated (Figure A.12b) due to increased bacterial remineralization of the accumulated biomass. As such, $\delta^{13}C_{SPM}$ decreased with time as a result of increasing PEPk (and RuBisCO) activity while $\delta^{15}N_{SPM}$ rose due to the continued dominant consumption of high-$\delta^{15}N$ NO_3^-.

By the end of our sampling, the seasonal cycle had advanced further in the PFZ than the SACCZ. The micro-phytoplankton contribution to total Chl-a had begun to decrease, with nano-phytoplankton biomass starting to increase (Figure A.11). Nonetheless, diatoms remained dominant throughout the sampling period (Figure 2.5 and Figure 2.6; Figure A.11), maintaining high PEPk and RuBisCO activity and inducing a general decrease in $\delta^{13}C_{SPM}$. At the same time, iron limitation would have caused higher reliance on regenerated NH_4^+, resulting in the observed seasonal decline in $\delta^{15}N_{SPM}$. That the NH_4^+ concentration remained roughly

stable over time (Figure A.12b) is consistent with this N form being consumed as rapidly as it was produced, with a higher rate of production (i.e., remineralization) expected later in the season in response to the accumulation of biomass. That said, ambient NH_4^+ concentration is not a particularly good measure of NH_4^+ availability since the flux of this nutrient can be large while its concentration remains very low (e.g., Smith *et al.* 2022; Mdutyana *et al.* 2022).

The SAZ phytoplankton community had evolved even more by the end of the cruise, towards an 'autumn assemblage' dominated by nano-phytoplankton (Figure A.11) and characterized by an f_{new} <50% (Figure A.10), indicative of dominant recycled N reliance (a notion supported by the decrease in NH_4^+ concentration). The combined increase in nano-phytoplankton abundance and NH_4^+ consumption would have been accompanied by an increase in the activity of PEPc relative to RuBisCO (Descolas-Gros and Fontugne, 1985; Descolas-Gros and Oriol, 1992), yielding new biomass that was high in $\delta^{13}C$ and low in $\delta^{15}N$. However, given the background $\delta^{13}C_{SPM}$ to which this new biomass was added (very low), along with the continued presence of some diatoms, the net effect by the end of our sampling of the addition of low-$\delta^{13}C$ biomass was to arrest the decline in $\delta^{13}C_{SPM}$ rather than to reverse it (i.e., evidenced by the very weak decrease in $\delta^{13}C_{SPM}$ with time; Figure A.8c). By contrast, the $\delta^{15}N_{SPM}$ decreased due to enhanced assimilation of low-$\delta^{15}N$ NH_4^+ by the nano-plankton, including the remaining diatoms.

In the STZ, the ecosystem had clearly shifted by the end of the cruise to one dominated by nano-phytoplankton expressing proportionally more PEPc during carboxylation, consistent with the increase in $\delta^{13}C_{SPM}$. At the same time, the observed decrease in NH_4^+ concentration and strong decline in f_{new} (Figure A.12b; Figure A.10) suggest that the STZ had hosted a predominantly regenerated N-fueled ecosystem for some time, which explains the fairly weak temporal decrease in $\delta^{15}N_{SPM}$ (Figure A.8d).

Our results indicate a latitudinal gradient in the seasonal cycle of phytoplankton community composition and production. The lower latitude zones appeared to have become regenerated production-dominated systems driven by nano-phytoplankton by the end of our sampling while the higher latitude zones were experiencing a proportional increase in new production and coincident rise in micro-phytoplankton biomass. This duality has implications for carbon export in the Southern Ocean, indicating that relative export potential increases over the growth season in the Antarctic but decreases in the Subantarctic.

2.5. Conclusions

In this circum-Antarctic study, , which is the first of its kind, we sought to 1) better understand the drivers of $\delta^{13}C_{SPM}$ and $\delta^{15}N_{SPM}$ isoscape variability across the summertime Southern Ocean and 2) quantify carbon export potential across the Southern Ocean from measurements of $\delta^{15}N_{SPM}$. In general, the latitudinal gradients in $\delta^{13}C_{SPM}$ and $\delta^{15}N_{SPM}$ were consistent with previous studies, with clear differences between the Subantarctic and Antarctic Oceans. As expected, $\delta^{13}C_{SPM}$ was highly dependent on seawater pCO_2, with phytoplankton community composition helping to explain measurements of $\delta^{13}C_{SPM}$ that deviated from the expected relationship with pCO_2. The observed trends in $\delta^{15}N_{SPM}$ were driven by the $\delta^{15}N$ of the N sources available to phytoplankton and the extent of their reliance on new *versus* regenerated N. Phytoplankton community composition also played a role as some taxa specialize in NO_3^- assimilation while others favour recycled NH_4^+ consumption. In contrast to previous isoscape studies, this work highlights the significant influence of phytoplankton community dynamics on $\delta^{13}C_{SPM}$ and $\delta^{15}N_{SPM}$. For instance, higher $\delta^{13}C_{SPM}$ and $\delta^{15}N_{SPM}$ usually coincided with high abundances of diatoms; for $\delta^{15}N_{SPM}$, this relationship can be explained by enhanced NO_3^- uptake while for $\delta^{13}C_{SPM}$, a mechanistic understanding remains elusive.

We employed a novel approach to determine relative carbon export potential using a two-endmember isotope mixing model that incorporated the Rayleigh equations for isotope fractionation during phytoplankton NO_3^- uptake. Our derived values of f_{new} are consistent with previous summertime measurements of the *f*-ratio, which validates our approach, although we also note that different methods for estimating the *f*-ratio integrate over different time scales, making a direct comparison difficult. For example, *f*-ratios determined from ^{15}N-tracer-based measurements of NO_3^- and NH_4^+ uptake (Joubert *et al.*, 2011; Mdutyana *et al.*, 2020) reflect the conditions of the water column at the time of sampling while our $\delta^{15}N_{SPM}$-based approach integrates over weeks to months, and geochemical estimates (e.g., float-based measurements of NO_3^- consumption) integrate over even longer periods. We estimate that on average, almost half of the carbon produced in Southern Ocean surface waters was potentially exported, with higher ratios near the (Sub)Antarctic islands and in regions of melting sea-ice, induced by an increase in phytoplankton growth rates and NO_3^- uptake, likely in response to an input of iron. The onset of iron limitation should result in Southern Ocean phytoplankton consuming proportionally more NH_4^+ as the growth season progresses

(Cochlan, 2008; Smith *et al.*, 2022). As such, f_{new} is likely to have declined following our sampling. By the same logic, however, f_{new} would have been considerably higher at the beginning of the growth season, with most of the organic N then produced already exported by the time of our sampling. We thus conclude that our estimates of f_{new} provide a reasonable approximation of the fraction of NPP exported from the Southern Ocean surface during the summer growth period.

Bulk SPM is easily sampled and $\delta^{13}C_{SPM}$ and $\delta^{15}N_{SPM}$ are already widely analysed. Here we show how $\delta^{15}N_{SPM}$ can be used in the framework of a simple isotope model to infer relative carbon export potential, an approach that could be applied to other ocean regions. We find that the $\delta^{15}N_{NO_3^-\,(source)}$ is a critical variable that should be measured alongside $\delta^{15}N_{SPM}$; indeed, the $\delta^{15}N_{NO_3^-\,(source)}$ varies by >3‰ across the Southern Ocean, meaning that 3‰ of the variability in $\delta^{15}N_{SPM}$ could be explained by changes in NO_3^- $\delta^{15}N$ alone, before changes in new *versus* regenerated N uptake or phytoplankton community dynamics need to be invoked. As such, we recommend that studies using measurements of $\delta^{15}N_{SPM}$ (e.g., trophic analyses) consider the influence of $\delta^{15}N_{NO_3^-\,(source)}$.

Chapter 3. A circum-Antarctic plankton isoscape II: zooplankton isotope niches and trophic structure across Southern Ocean hydrographic zones

Supplementary information of this Chapter can be found in Appendix B.

3.1. Abstract

Phylogenetically and functionally diverse assemblages of zooplankton occupy different trophic levels in the marine food web, facilitating complex pathways of carbon flow through the trophic system, as well as carbon export to the ocean interior, which modulates atmospheric CO_2. The Southern Ocean plays an important role in Earth's climate system and carbon cycle, yet much remains unknown about the functioning of its planktonic ecosystems, which form the base of all Southern Ocean food webs. We recently showed, for samples collected across the Southern Ocean during the Antarctic Circumnavigation Expedition (ACE) during the austral summer 2016/2017, strong latitudinal gradients in phytoplankton community composition and carbon and nitrogen isotope ratios ($\delta^{13}C_{SPM}$ and $\delta^{15}N_{SPM}$, where SPM denotes suspended particulate matter). To assess the influence of these phytoplankton trends on the zooplankton system and to investigate the large-scale variability in zooplankton ecology, we measured the $\delta^{13}C$ and $\delta^{15}N$ of numerous zooplankton species collected from the neuston layer at 28 stations sampled during ACE. Coupled with information on zooplankton taxonomy, these data were used to determine the isotopic niches of zooplankton communities and species-specific trophic positions in various hydrographic zones across the Southern Ocean. We observed a strong difference between the isotopic niches of Subantarctic and Antarctic Ocean zooplankton, implying that the trophic roles of Subantarctic first consumers were more herbivory, in contrast to the same zooplankton in the Antarctic that occupied higher trophic positions associated with omnivorous and carnivorous behaviour. One implication of this finding is that the zooplankton trophic web in the Antarctic may enable greater carbon export than that of the Subantarctic because the sinking of phytoplankton cells to the deep ocean is likely to be higher where there are less grazing (Antarctic) and lower where herbivory behaviour is predominant. As part of this study, we compared five possible $\delta^{15}N$ baselines for trophic analysis and found that $\delta^{15}N_{SPM}$ is an appropriate baseline for assessing the trophic positions of zooplankton species over large spatial scales such as the major hydrographic zones of the Southern Ocean.

3.2. Introduction

Phytoplankton and zooplankton play fundamental roles in sustaining marine life and modulating the climate (Longhurst and Glen Harrison, 1989). Phytoplankton produce organic biomass by fixing atmospheric carbon dioxide (CO_2) during photosynthesis, the bulk of which is transferred to higher trophic levels through zooplankton grazing (Ducklow *et al.*, 2001; Steinberg and Landry, 2017). However, a portion of this organic matter sinks into the ocean interior (i.e., either as individual phytoplankton cells or following aggregation into marine snow), facilitating the removal of atmospheric CO_2 to deep waters where it can be stored for centuries (i.e., the biological pump; Volk and Hoffert 1985). Zooplankton, through their active vertical migration and the gravitational sinking of their faecal pellets, carcasses and crustacean moults, also facilitate organic carbon export to the deep ocean (Longhurst, 1991; Halfter *et al.*, 2020, 2022; Nowicki *et al.*, 2022). It has been proposed that the efficiency of this so-called 'biological pump' in different latitudinal zones of the Southern Ocean can be predicted from the trophic composition of the zooplankton communities (Pakhomov *et al.*, 2000c). Zooplankton are mid-level trophic consumers that support higher consumers including fish, seabirds, and marine mammals (Rau *et al.*, 1992b; Bost *et al.*, 2009); as such, geographic and temporal fluctuations in zooplankton food sources, as well as how these impact on the feeding dynamics and overall structure of zooplankton communities, have implications for the entire marine food web.

The Southern Ocean is a highly variable marine system due to the interplay of its numerous water masses, sea ice, and the atmosphere (Mayewski *et al.*, 2009), which together determine its biogeochemical properties and the distribution of marine organisms (Henley *et al.* 2020 and references therein). The Southern Ocean can be divided into five major latitudinal hydrographic zones (Figure 3.1a-b) differentiated mainly by the sea surface temperature (SST) of their respective water masses (Orsi *et al.*, 1995; Pollard *et al.*, 2002; Chapman *et al.*, 2020): three warmer zones form the Subantarctic Ocean at the lower latitudes, including the Subtropical Zone (STZ; SST of 20-10°C) located north of the Subtropical Front (STF), the Subantarctic Zone (SAZ; SST of 10-6°C) between the STF and the Subantarctic Front (SAF), and the Polar Frontal Zone (PFZ; SST of 6-4°C that is bounded by the SAF to is north and the Antarctic Polar Front (APF) to its south. The PFZ is characterized by high physical variability and is often considered the transition zone between the Subantarctic Ocean and the cooler waters of the Antarctic Ocean, the latter comprising the Southern

Antarctic Circumpolar Current Zone (SACCZ; SST of 4-0.7°C) between the APF and the Southern ACC Front (SACCF), which constitutes the southern edge of the ACC core and remains ice-free year-round, and the southern Boundary Zone (sBZ; SST of <0.7°C) of the ACC, which is partially sea-ice covered but still biologically active (Whitworth III and Nowlin Jr., 1987; Orsi *et al.*, 1995; Pollard *et al.*, 2002).

Physico-chemical parameters such as temperature, salinity, oxygen, and micro- and macronutrient concentrations are typically homogeneous within the upper mixed layer of each zone (Orsi *et al.*, 1995; Pollard *et al.*, 2002) and play a central role in driving variability in plankton community composition (Atkinson *et al.*, 2012a; Vereshchaka *et al.*, 2021). Southern Ocean surface waters are generally iron-limited, except near the (Sub)Antarctic islands where iron-rich deep waters upwell to the surface (Sherrell *et al.*, 2018; De Falco *et al.*, 2022) and terrestrial iron can be supplied via wind-blown dust and/or island run-off (Planquette *et al.*, 2011). Due to perennial iron limitation of phytoplankton, open Southern Ocean surface waters host elevated concentrations of nitrate and phosphate year-round (Martin *et al.*, 1990b; Hoffmann *et al.*, 2008; Moore *et al.*, 2013), with higher values in the Antarctic than the Subantarctic mixed layer (Janssen *et al.*, 2020a). Nitrate and phosphate only become limiting to phytoplankton growth in the STZ in summer (Pollard *et al.*, 2002). The concentrations of silicate are also higher in Antarctic waters, particularly south of the SACCF, but decrease rapidly northward/equatorward to near-zero values at the SAF where the growth of siliceous phytoplankton (i.e., diatoms) becomes silicate-limited during summer (Laubscher *et al.*, 1993; Sullivan *et al.*, 1993; Froneman *et al.*, 1995; M. Franck *et al.*, 2000; Pollard *et al.*, 2002).

We recently demonstrated that the summertime phytoplankton community composition varies across the Southern Ocean's hydrographic zones: the communities in the lower latitudes (i.e., STZ and SAZ) were dominated by nano-phytoplankton and large dinoflagellates such as *Ceratium* spp., those in the PFZ were composed by the same proportions of micro- and nano-phytoplankton but with the large *Fragilariopsis kerguelensis* highly abundant, and those in the higher latitudes (i.e., SACCZ and sBZ) were dominated by micro-phytoplankton such as the diatoms *Fragilariopsis* spp. and *Chaetoceros* spp. (Chapter 2). Other studies have observed a similar latitudinal zonation in the phytoplankton community composition across the Indian sector of the Southern Ocean (e.g., Kopczynska *et al.* 1986; Wright *et al.* 1996). These trends suggest that the fronts of the Southern Ocean are biogeochemical and biological barriers to the distribution of

nutrients and marine species (Froneman *et al.*, 1995, 2000; Pakhomov and McQuaid, 1996; Pakhomov *et al.*, 2000c; Bost *et al.*, 2009), possibly leading to unique plankton trophic systems within each hydrographic zone that support different carbon cycles and marine food webs.

The food web structure, the feeding ecology of various species, and the biogeochemical processes occurring in the oceans can be inferred from measurements of the stable isotope ratios of nitrogen (N) and carbon (C) ($\delta^{15}N$ and $\delta^{13}C$, respectively; Peterson and Fry 1987; Fry 1988; Hansson *et al.* 1997). The $\delta^{13}C$ of organic material provides information about the food source(s) being assimilated by consumers as different food sources often have distinct $\delta^{13}C$ signatures (Herman *et al.*, 2000). By contrast, the $\delta^{15}N$ of organic matter is an indicator of the trophic level of the consumers in a food chain, as biomass $\delta^{15}N$ becomes progressively higher with an increase in an organism's trophic position (Peterson and Fry, 1987). The $\delta^{13}C$ of phytoplankton is largely the result of discrimination between ^{13}C and ^{12}C (i.e., isotopic fractionation) during the carboxylation of CO_2, and is also influenced by growth rate and community composition (Descolas-Gros and Fontungne, 1990; Fontugne *et al.*, 1991; Rau *et al.*, 1991a; Dehairs *et al.*, 1997; Trull and Armand, 2001). The $\delta^{15}N$ of phytoplankton is set by the $\delta^{15}N$ of the available N sources (e.g., nitrate and ammonium) and isotopic fractionation between ^{14}N and ^{15}N during N assimilation (e.g., Mariotti *et al.* 1981; Altabet and Francois 1994; Waser *et al.* 1998; Lourey *et al.* 2003; Granger *et al.* 2010; Lara *et al.* 2010; Somes *et al.* 2010; Fawcett *et al.* 2011). Phytoplankton $\delta^{13}C$ and $\delta^{15}N$ are transmitted through the food chain, with isotopic enrichment from one trophic level to the next estimated to be 1‰ for $\delta^{13}C$ and 2.3‰ for $\delta^{15}N$ (McCutchan Jr *et al.*, 2003; Schwamborn and Giarrizzo, 2015).

The isotopic composition of suspended particulate matter (SPM) is often used in aquatic research as a proxy for phytoplankton and as baseline for the calculation of trophic position (TP, defined as the trophic level at which a consumer feeds; Post 2002). However, recent studies have discouraged the use of the $\delta^{15}N$ of SPM ($\delta^{15}N_{SPM}$) as a trophic baseline (Pakhomov *et al.* 2019 and references therein) because SPM constitutes a diverse mixture of particles including phytoplankton, bacteria, zooplankton, and detritus (e.g., Rau *et al.* 1990). As such, SPM may incorporate two to three TPs by itself, leading some researchers to suggest that trophic studies involving stable isotopes should instead be normalized to the isotopic composition of the first consumers.

In ecological research, stable isotopes have been used extensively to characterize trophic niches (Layman *et al.*, 2007, 2012). The trophic niche of a single species, community, or ecosystem represents a cumulative index of interactions between its members and the ecosystem (Elton, 1927) and is thus a good indicator of the properties of a habitat and trophic level (Leibold, 1995). Trophic niche can be inferred from isotopic niche (e.g., from a plot of organism $\delta^{13}C$ *versus* $\delta^{15}N$; Layman *et al.* 2007) and quantitative measures of trophic niche can be used to verify ecological theory, probe trophic responses to anthropogenic perturbations, and disentangle the extent of overlap between different trophic niches (Layman *et al.*, 2007; Schmidt *et al.*, 2007; Jackson *et al.*, 2011).

Here, we seek to investigate the trophic niche and structure of the zooplankton systems in each hydrographic zone of the Southern Ocean. Using the SPM as baseline, we undertake a traditional trophic-level analysis based on stable isotope measurements of zooplankton specimens collected during the Antarctic Circumnavigation Expedition (Walton and Thomas, 2018; Landwehr *et al.*, 2021). To ascertain whether the SPM is an appropriate baseline for such analyses at the ocean-basin scale, we compared the trophic positions of zooplankton assessed using five potentially good baselines for trophic analysis.

While a number of SPM isoscapes have been generated for the Southern Ocean (Espinasse *et al.* 2019; St John Glew *et al.* 2021; including Chapter 2), zooplankton stable isotope data are scarce and usually do not include inter-species differences, instead grouping species at higher taxonomic levels (e.g., Family/Order). In addition, most of the studies are restricted on a spatial scale/spatially (e.g., Brault *et al.* 2018; Walsh and Reiss 2020). There is therefore a need to develop larger-scale zooplankton isoscapes developed coincident with measurements of the stable isotopes of SPM that can be used to infer variations in ecosystem niches (e.g., Polito *et al.* 2013) and, ultimately, to provide eco-geochemical tools that can be used to reconstruct dietary histories in the Southern Ocean and animal movements within and among zones.

Using measurements of the $\delta^{13}C$ and $\delta^{15}N$ of zooplankton collected from every hydrographic zone of the Southern Ocean in austral summer and interpreted in the context of SPM $\delta^{13}C$ and $\delta^{15}N$ ($\delta^{13}C_{SPM}$ and $\delta^{15}N_{SPM}$) isoscapes generated for the same ACE cruise (Chapter 2), we aim to answer the following questions:

1. Given the latitudinal gradients in the Southern Ocean SPM $\delta^{13}C$ and $\delta^{15}N$ isoscapes described in Chapter 2, do the $\delta^{13}C$ and $\delta^{15}N$ of simultaneously collected zooplankton reflect the spatial variability in the isotopic composition of their food source(s)?
2. If the $\delta^{13}C$ and $\delta^{15}N$ of the zooplankton track the SPM isoscapes, is SPM a suitable baseline for zooplankton trophic analysis?
3. Do the trophic positions and isotopic niches of zooplankton differ between the Southern Ocean's hydrographic zones?

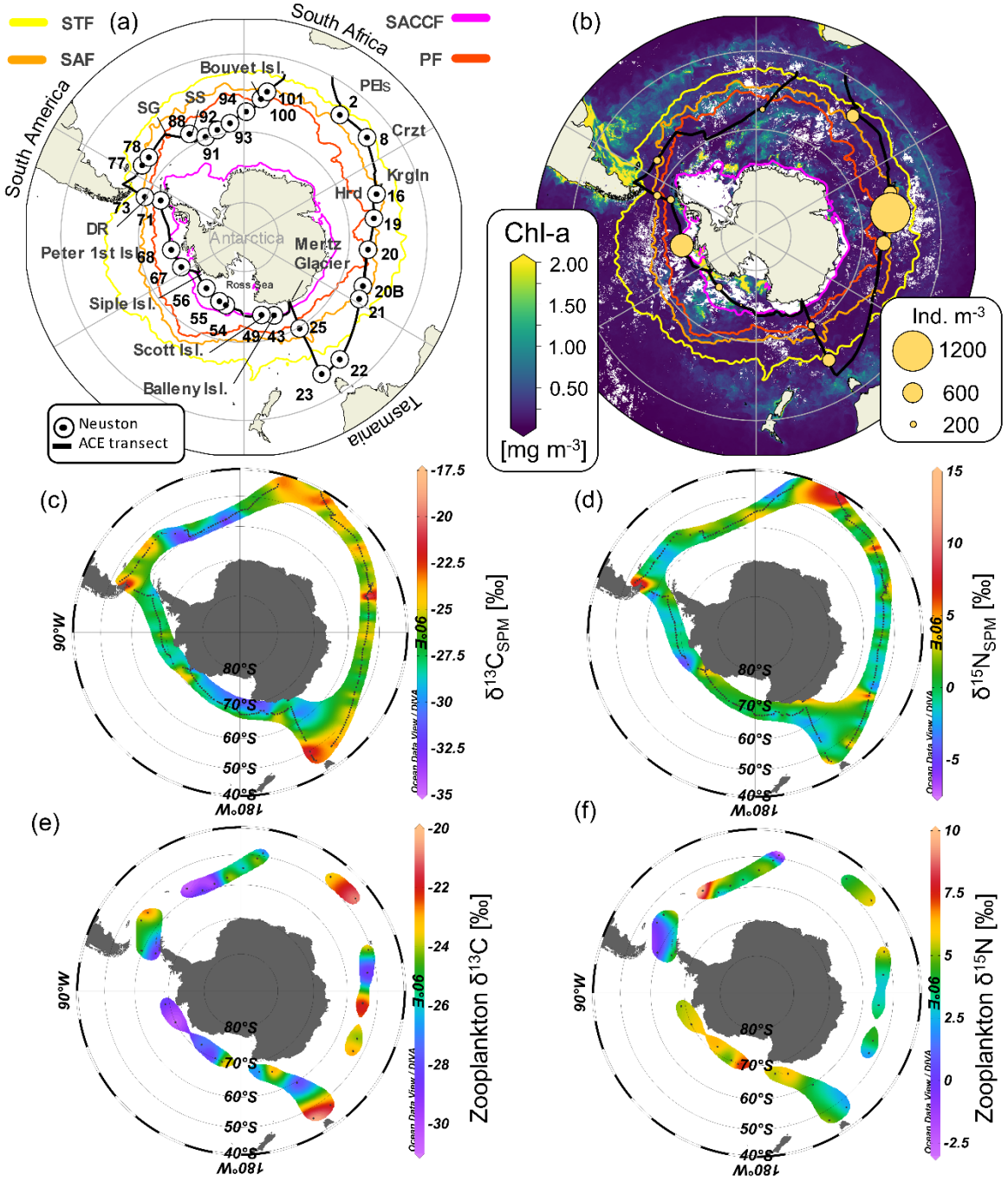

Figure 3.1 a) Cruise transect and station positions during the Antarctic Circumnavigation Expedition (ACE). The white/black dots indicate Neuston collection stations, the black line shows the cruise transect, and the numbers are station identifiers. Islands and land masses are labelled as follows: PEIs = Prince Edward Islands archipelago, Crzt = Crozet Island, Krgln = Kerguelen Island, Hrd = Heard Island, DR = Diego Ramirez Island, SG = South Georgia Island, and SS = South Sandwich Island. Line colours correspond with the various hydrographic fronts: yellow = Subtropical Front (STF), orange = Subantarctic Front (SAF), red = Antarctic Polar Front (APF), purple = Southern Antarctic Circumpolar Current Front (SACCF). b) Distribution of monthly-averaged satellite-based chlorophyll-a concentrations (mg m^{-3}; level-3 Chl-a from the Moderate Resolution Imaging Spectroradiometer (MODIS) Aqua satellite product (https://oceandata.sci.gsfc.nasa.gov/MODIS-Aqua/Mapped/Monthly/4km/chlor_a/) at 4 km spatial resolution) and monthly average frontal positions (coloured lines) during the cruise. The black line shows the cruise transect and the orange dots indicate stations where taxonomic analyses of samples were undertaken, with the dot size indicating zooplankton abundance (Ind. m^{-3}). Also shown are the surface (i.e., ~5 m) c) $\delta^{13}C_{SPM}$ [‰] and d) $\delta^{15}N_{SPM}$ [‰] for suspended particulate matter (SPM) collected during the cruise (Chapter 2), as well as zooplankton e) $\delta^{13}C$ [‰] and f) $\delta^{15}N$ [‰] for samples collected using a Neuston net.

3.3. Materials and methods

3.3.1. Sample collection

Samples were collected during the Antarctic Circumnavigation Expedition (ACE) conducted during austral summer of 2016/2017 on board the Russian polar vessel R/V *Akademik Treshnikov* (*Академик Трёшников*) (Figure 3.1a) (Walton and Thomas 2018; Landwehr *et al.* 2021). The expedition was divided into three legs: Leg1 in the Indian sector between Cape Town and Hobart (24th December 2016 – 17th January 2017); Leg2 in the Pacific sector between Hobart and Punta Arenas (23rd January – 19th February 2017); and Leg3 in the Atlantic sector between Punta Arenas and Cape Town (26th February – 16th March 2017). Leg1 and Leg3 crossed the open Southern Ocean sectors zonally and purposefully sampled near the islands including Prince Edward, Crozet, Kerguelen, and Heard Islands (Leg1), and South Georgia, South Sandwich Islands and Bouvet Island (Leg3). Leg2 closely followed the Antarctic continent coastline, crossing the marginal ice zone and transiting near Balleny, Scott, Siple, Peter 1st, and Diego Ramirez Islands. Sampling for zooplankton was conducted at eight stations on Leg1, 11 on Leg2, and nine on Leg3 (in total of 28 stations).

In this study, we used samples that were originally collected for the determination of microplastic concentrations, using a Neuston net (200 µm mesh) towed horizontally at the surface for 15 minutes at an average speed of ~2 knots (Suaria *et al.*, 2020). Samples were preserved in 70% ethanol and stored in glass jars at room temperature until analysis. The zooplankton collected in the Neuston net represent the surface community present at the time of sampling, which may include/exclude specimens and species that vertically migrate into/out of the surface layer. The sampling approach thus precluded consideration of diel vertical migration of zooplankton. As such, we do not treat our results as quantitatively representative of the plankton community present in the upper water column. Instead, our data represent the neuston zooplankton communities associated with the surface SPM that was sampled coincidentally and is described at length in Chapter 2.

From the underway seawater supply (intake at ~4.5 m), SPM and micro-phytoplankton (>20 µm) samples were collected by filtering surface seawater through pre-combusted (450°C for 8 hr) 0.3 µm glass fibre filters (GF-75s; Sterlitech) and 20 µm clean nylon filters, respectively, at 341 underway stations along the ACE transects and at 34 stations where CTD casts were also made (refer to Chapter 2 for details on SPM and

micro-plankton sample collection and preservation). All the Neuston net stations coincided with a CTD cast station at which SPM and micro-plankton were collected, but not *vice versa*.

Taxonomic identification of zooplankton was conducted in a shore-based laboratory using a ZEISS Stemi 508 stereo microscope and ZEISS Primo Star phase-contrast microscope following Boltovskoy's taxonomic key (Boltovskoy, 1999) (Figure 3.2). Specimens were identified and enumerated from 19 stations only as the material collected at stations 8, 43, 49, 55, 88, 91, 92, 93, and 101 was not sufficiently preserved to perform a full taxonomic analysis. However, specimens were collected for stable isotope analysis at all 28 stations, although there were sometimes insufficient specimens available for reliable species-specific isotope analysis. As such, the taxonomic and stable isotope data are not always coinciding. Zooplankton taxa were identified to the species level or to the lowest possible taxonomic level for samples where sample preservation was inadequate (e.g., Chaetognatha, Ostracoda, Euphausiacea, Thaliacea, Clausocalanidae). Where possible, Amphipoda (Figure 3.2a-d) and Copepoda (Figure 3.2g-i) were also identified to the developmental stage level. For isotope analysis only, whenever different species of Amphipoda or Copepoda could not be identified, they were analysed collectively and labelled as 'mixed-amphipods' and 'mixed-copepods', respectively. Likewise, specimens of Euphausiacea were grouped as 'mixed-euphausiids' (Figure 3.2m) and/or size-fractionated into five size classes based on total body length (i.e., krill 0-5, 5-10, 10-20, 20-50, and >50 mm) by direct measurement of the specimens using a calibrated stage micrometre. Copepoda specimens were also size-fractionated into two size classes based on their total length (i.e., mixed-copepods 200-500 and >500 µm). Nauplii of Copepoda were sorted and measured separately according to their morphology, with specimens falling into two main groups, putative nauplii of Pontellidae ('Nauplii*'; Figure 3.2g) and a mixed group of smaller nauplii that excludes the Nauplii* ('Nauplii'). In addition, juveniles of the amphipod *Themisto gaudichaudii* were labelled as 'Themisto-J' (Figure 3.2a). All counts were converted to abundances of individuals per volume of water filtered (Ind. m^{-3}).

Zooplankton specimens for stable isotope analysis were processed four years after their collection. They were sorted using cleaned tweezers, then rinsed with Milli Q water to remove all traces of ethanol. The carbonate shells of the thecate Pteropoda were manually removed to avoid biasing the $\delta^{13}C$ of the soft tissue (Mateo *et al.*, 2008). While most of the zooplankton specimens were placed directly onto pre-combusted foil,

some of the smaller gelatinous plankton (e.g., Thaliacea, Chaetognatha, and Hydrozoa) were transferred onto pre-combusted glass fibre filters that were analysed with the zooplankton specimens. All samples were then freeze-dried (Scanvac Coolsafe 55-4 cooling trap) for 24h at -60°C. The non-filter samples were ground using a clean mortar and pestle, with subsamples of the ground material (0.35 -0.5 mg, with a minimum weight for reliable isotope measurements of ~0.25 mg) and the filters were transferred into tin cups for isotope analysis.

Analyses were conducted using a Flash 2000 elemental analyzer coupled to a Delta V Plus isotope ratio mass spectrometer (IRMS) in the Stable Light Isotope Laboratory at the University of Cape Town. Three in-house standards, calibrated against IAEA reference materials, were included in each IRMS run along with several blanks (unused pre-combusted filter + tin capsule or tin capsule alone). The detection limit was 2 μg for C and 1 μg for N, and precision was ± 0.2‰ for C and N. Results are expressed in standard unit notation as follows:

$$\delta X\ (‰) = \frac{\left(R_{sample} - R_{standard}\right)}{R_{standard}} x\ 1000 \qquad \text{(Eqn. 3.1)}$$

where X is ^{13}C or ^{15}N and R is the ratio of $^{13}C/^{12}C$ or $^{15}N/^{14}N$, with $R_{standard}$ = 1.07% for C and 0.366% for N. The $\delta^{13}C$ and $\delta^{13}C$ data are reported relative to Vienna-PeeDee Belmnite and N_2 in air, respectively.

The $\delta^{13}C$ data were not corrected for the presence of high concentrations of lipids (as per Post *et al.* 2007) given that preservation in ethanol decreases sample lipid content due to dissolution (Arrington and Winemiller, 2002; Sarakinos *et al.*, 2002; Sweeting *et al.*, 2004; Syväranta *et al.*, 2008; Ventura and Jeppesen, 2009). Nevertheless, it has been shown that ethanol does not alter the $\delta^{13}C$ or $\delta^{15}N$ of zooplankton tissue (Hobson *et al.*, 1997; Sarakinos *et al.*, 2002; Syväranta *et al.*, 2008). With the exception of the thecate Pteropoda (see above), we analysed whole organisms that had been homogenized, which means that our measurements include stomach contents, chitin, and muscular tissue. While some researchers depurate organisms after collection to eliminate potential isotopic biases associated with gut contents and endo- or exoskeletons (Peterson and Fry, 1987; Gorokhova and Hansson, 1999; Ventura and Catalan, 2008; Hill and McQuaid, 2011; Seyboth *et al.*, 2018), this is not always possible for smaller zooplankton specimens.

Nevertheless, we expect small gut contents in the zooplankton specimens because a long-term net sampling exposes organisms to additional stress and physical damages that raises gut evacuation by regurgitation (Lusher *et al.* 2017 and references therein). In any case, gut contents do not appear to influence the $\delta^{15}N$ of zooplankton (Hill and McQuaid, 2011). In addition, we did not correct for the potential effect of gut contents and skeletal material on zooplankton $\delta^{13}C$ due to uncertainties in the endmembers required to make such a correction, and because chitin correction appears not to have any effects on either the zooplankton $\delta^{15}N$ or $\delta^{13}C$ (Ventura and Catalan, 2008).

3.3.2. Baselines and assessment of trophic position

Because of our large SPM dataset, we used $\delta^{15}N_{SPM}$ as the baseline to derive the TPs of zooplankton species at all the stations occupied during the ACE cruise. However, the use of $\delta^{15}N_{SPM}$ as a trophic baseline has been questioned because it can be highly variable in space and time due to small-scale biogeochemical and hydrographic forcings, meaning that $\delta^{15}N_{SPM}$ may not accurately represent the food source to zooplankton (Zanden and Rasmussen, 1999; Puccinelli *et al.*, 2018). As such, we derived the TPs of zooplankton using five different baselines: (1) $\delta^{15}N_{SPM}$ in surface waters (Figure 3.1d; described in detail by Chapter 2); (2) the theoretical $\delta^{15}N$ for phytoplankton biomass produced as a result of nitrate assimilation ($\delta^{15}N_{new}$), calculated using the Rayleigh model for isotope fractionation, with the *in situ* nitrate concentration and $\delta^{15}N$ as constraints, as detailed in Chapter 2. This choice of baseline assumes that the extent to which phytoplankton consume the subsurface nitrate supply sets the $\delta^{15}N$ of the plankton system; (3) the $\delta^{15}N$ of large (>20 μm) diatoms (diatom-$\delta^{15}N$) collected during the ACE cruise (Forrer, 2021) given that diatoms dominated the phytoplankton biomass from the SAZ to the sBZ during ACE; and the $\delta^{15}N$ of the primary consumers, represented by (4) Salpidae (salp-$\delta^{15}N$) or (5) the small Copepoda size class (i.e., mixed-copepods 200-500 μm; copepods-$\delta^{15}N$). Salpidae and small Copepoda are supposedly herbivores, which means they should have the lowest $\delta^{15}N$ of the zooplankton specimens collected (Cherel *et al.*, 2008; Richoux and Froneman, 2009; Stowasser *et al.*, 2012; Ménard *et al.*, 2014). Because Salpidae were not present at every station (i.e., we collected only two specimens in the STF and PFZ and six in the SACCZ), combined with the fact that we found no significant difference in salp-$\delta^{15}N$ among hydrographic zones (Kruskal-Wallis, *p*-value > 0.05), we use the averaged salp-$\delta^{15}N$ as baseline (4) across the transect.

A baseline comparison was undertaken for the stations at which data were available for most of the baseline options. Baselines (1) to (4) were all assessed at Neuston stations 2, 8, 16, 19, 20, 21, and 22. However, copepods-$\delta^{15}N$ was only analysed at four of these stations (i.e., stations 2, 16, 19, 22) so that we cannot use copepods-$\delta^{15}N$ as a baseline at stations 8, 20, and 21.

The TP of each sample was calculated following Deniro and Epstein (1981) as:

$$TP = \frac{\delta^{15}N_{consumer} - \delta^{15}N_{baseline}}{TEF} + b \qquad \text{(Eqn. 3.2)}$$

where b = 1 if the baseline is a primary producer and b = 2 if the baseline is a primary consumer, $\delta^{15}N_{consumer}$ and $\delta^{15}N_{baseline}$ are the $\delta^{15}N$ of the zooplankton specimen and the baseline, respectively (DeNiro and Epstein, 1981; Vander Zanden *et al.*, 1997), and TEF is the trophic enrichment factor (2.3‰; McCutchan Jr *et al.* 2003; Schwamborn and Giarrizzo 2015). Here, we used a TEF of 2.3‰ for ^{15}N based on the meta-analysis by McCutchan *et al.* (2003), which suggested that this value is more representative of the average TEF across different taxa and conditions than the commonly used value of 3.4‰, which was derived from a more limited study by Minagawa and Wada (1984). This choice means that the TPs calculated will be higher than those obtained using a TEF of 3.4‰.

3.3.3. Layman metrics: isotopic niche assessment

Isotopic niches were defined using the geometric approach of Layman *et al.* (2007) who defined a series of metrics related to niche structure based on carbon and nitrogen isotope measurements (convex hull or polygonal areas based on $\delta^{15}N$ and $\delta^{13}C$) of individuals to entire communities. These metrics include:

1. $\delta^{15}N$-range, which provides information on the vertical structure of a food web;
2. $\delta^{13}C$-range, which gives an estimate of the diversity of basal resources and niche diversity;
3. total area (TA) of the convex hull encompassing the data points, which is a proxy for the extent of trophic diversity within a food web;
4. mean distance to centroid (CD), which provides a measure of the average degree of trophic diversity within a food web;

5. mean nearest neighbour distance (MNND), which yields a measure of density and clustering of species within the community (i.e., niche divergence); and
6. standard deviation of the nearest neighbour distance (SDNND), which is a measure of the evenness of spatial density and data spread.

The six Layman metrics are standard arguments for describing the isotope niches of ecological communities. For instance, we still display their values for report proposals even though we do not use the CD, MNND, or SDNND for the proposes of this study.

3.3.4. Supporting data products

Daily high-resolution SST (GHRSST) level-4 data on a global 0.054° grid from the Operational Sea Surface Temperature and Sea Ice Analysis (OSTIA) database (https://podaac.jpl.nasa.gov/dataset/UKMO-L4HRfnd-GLOB-OSTIA; UKMO 2005) were used to determine the averaged the positions of the major hydrographic fronts during the 3 months of cruise using the definitions of Orsi *et al.* (1995) (Figure 3.1a-b).

Monthly averaged (24th December 2016 - 16th March 2017) level-3 Chl-a concentrations from the Moderate Resolution Imaging Spectroradiometer (MODIS) Aqua satellite product (https://oceandata.sci.gsfc.nasa.gov/MODIS-Aqua/Mapped/Monthly/4km/chlor_a/) at a 4-km spatial resolution were used to visualize the phytoplankton biomass distribution across the Southern Ocean at the time of the cruise (Figure 3.1b).

3.3.5. Statistical analysis

Data were analysed using a combination of tools and software, including R for statistical analysis (R Core Team, 2018) and ODV (Schlitzer, 2021) for data visualization. To compare the $\delta^{13}C$ and $\delta^{15}N$ of zooplankton taxa within and among regions, we used an analysis of variance (ANOVA) and multiple paired Student t-test with Bonferroni adjustment (Armstrong, 2014). Because of the relatively small size of our dataset (<30 stations), some taxa were analysed using the non-parametric Kruskal-Wallis and Wilcoxon tests. When data are sub-grouped according to geographical region (i.e., hydrographic zones: STZ, SAZ, PFZ, SACCZ, sBZ; or ocean: Subantarctic *versus* Antarctic), values are reported as average (mean ± 1SD) or median (median_{Q1}^{Q3} or median ± IQR where Q1 = first quartile, Q3 = third quartile, and IQR = interquartile range which is

defined as Q3-Q1). Linear regression model (*lm*) analysis of zooplankton observations was conducted using the *stats* R-package.

3.4. Results

3.4.1. Zooplankton abundances and distribution around the Southern Ocean

From the neuston layer of the water column, we collected different life stages of various Copepoda including *Calanus propinquus*, *Calanus simillimus*, *Candacia varicans* (*sensu lato*), *Clausocalanus* spp., *Clausocalanus laticeps*, *Metridia gerlachei*, *Metridia lucens*, *Microcalanus* spp., *Oithona* spp., *Oncea* spp., *Paraeuchaeta antarctica*, and a few unidentified species. We also sampled two genera of Amphipoda, *Themisto gaudichaudii* (Figure 3.2a-b) and *Cyllopus* spp. (likely *C. lucasi* and *C. magellanicus*; Figure 3.2c-d), four groups of Pteropoda including the shelled *Creseis* spp., *Limacina helicina antarctica* (Figure 3.2q)., and *Clio pyramidata* (Euthecosomata; Figure 3.2r), and the two naked species, *Spongiobranchaea australis* and *Clione limacina antarctica* (Gymnosomata). Other plankton groups included Appendicularia (e.g., *Frittillaria* spp. and *Oikopleura* spp.), Chaetognatha, Enteropneusta, Euphausiacea (Figure 3.2m), Foraminifera (Figure 3.2n), Hydrozoa, larvae of Lepadiformes (Figure 3.2o), Ostracoda (Figure 3.2p), fish larvae, Radiozoa, Thaliacea (e.g., Doliolida and Salpida; Figure 3.2s-t), and planktonic Polychaeta (*Tomopteris* spp.; Figure 3.2u).

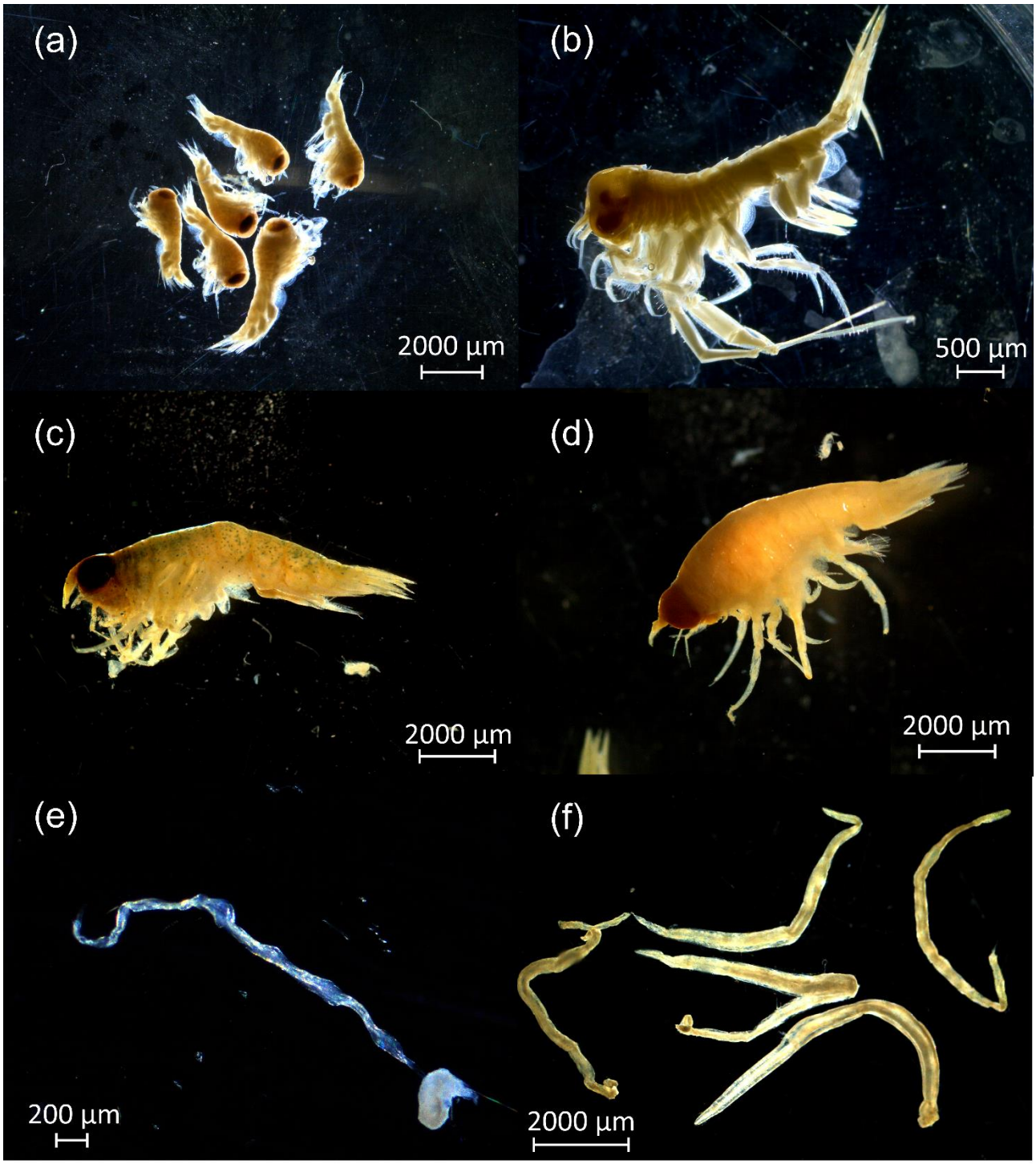

Continues…

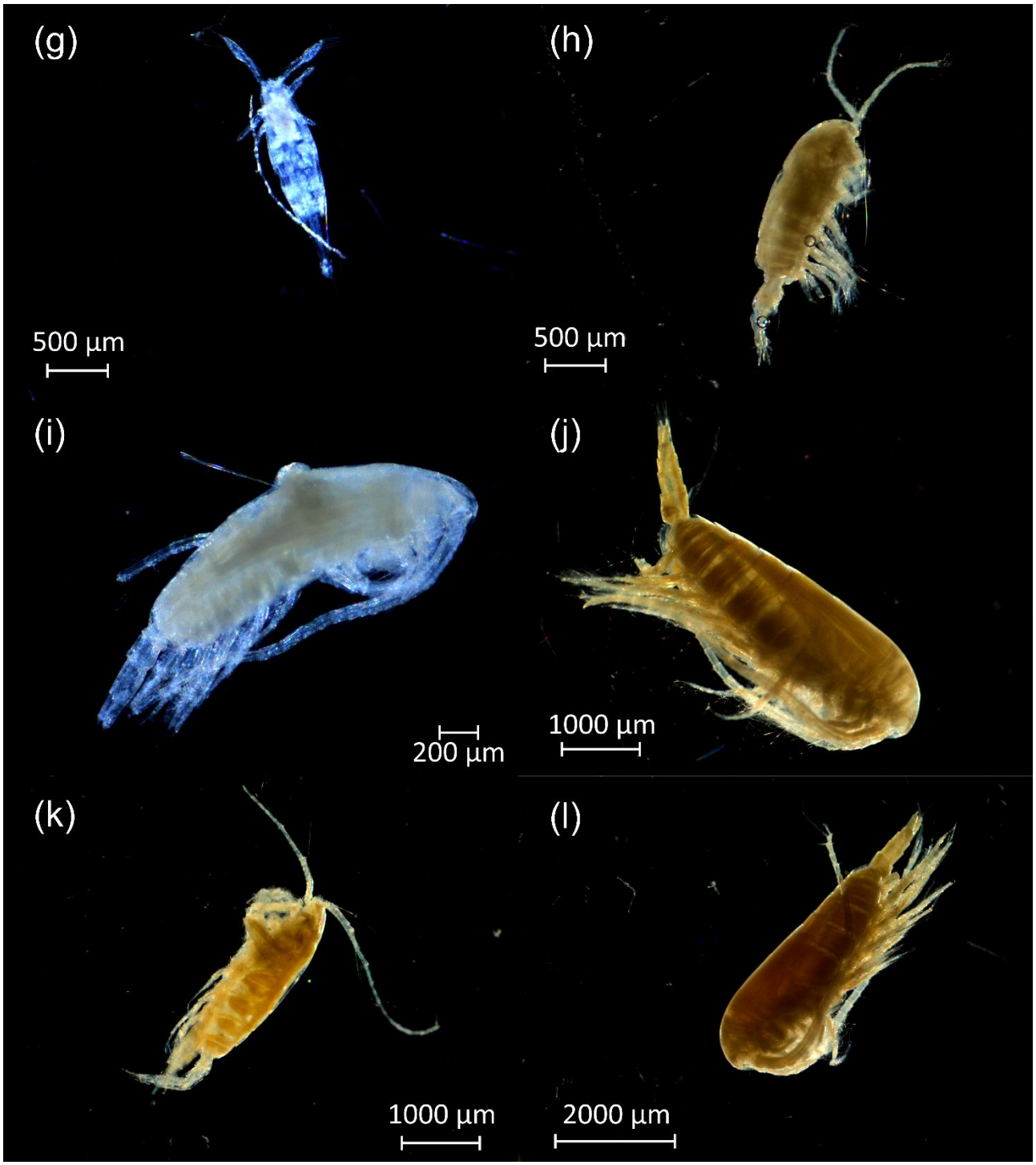

Continues…

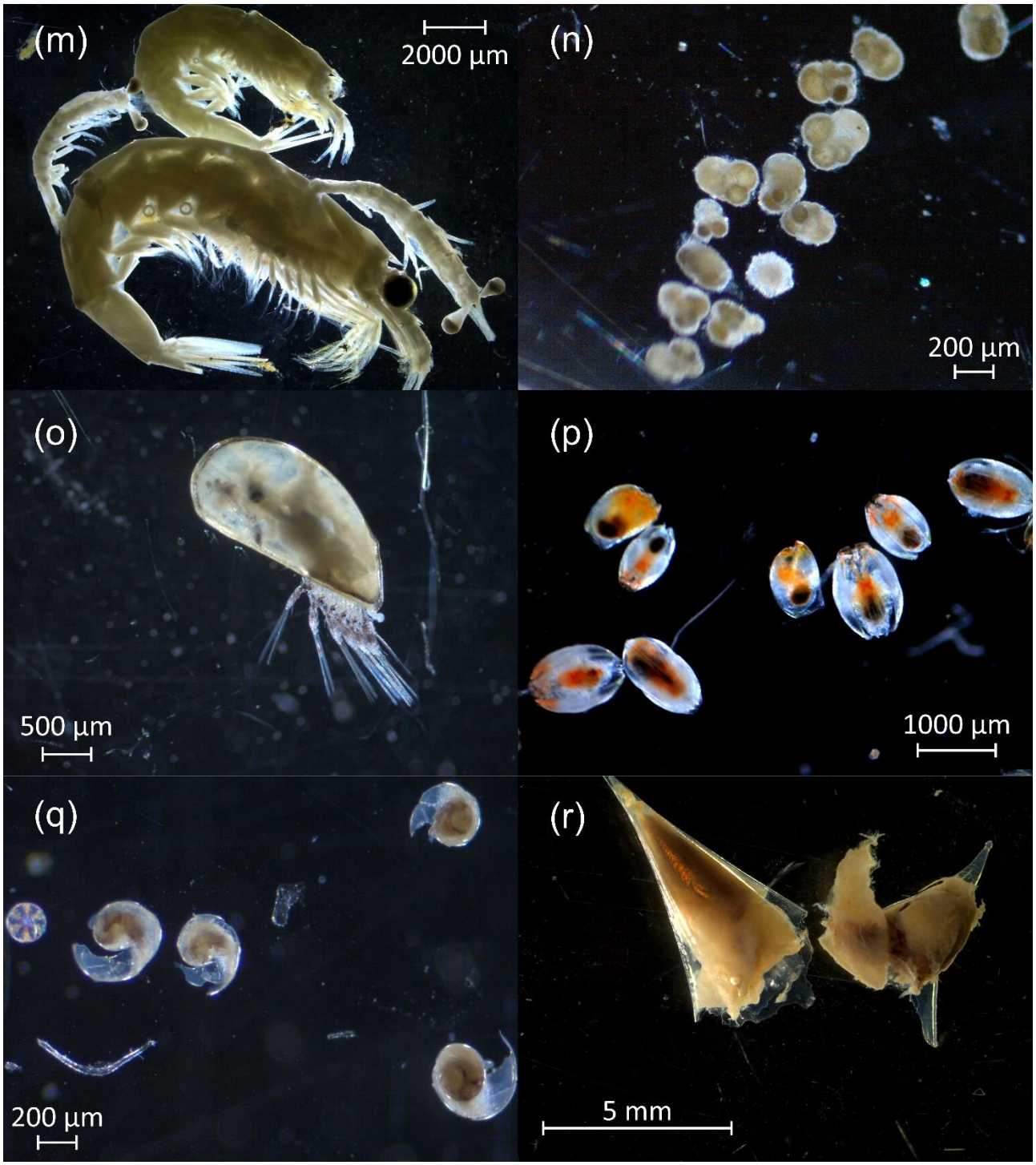

Continues…

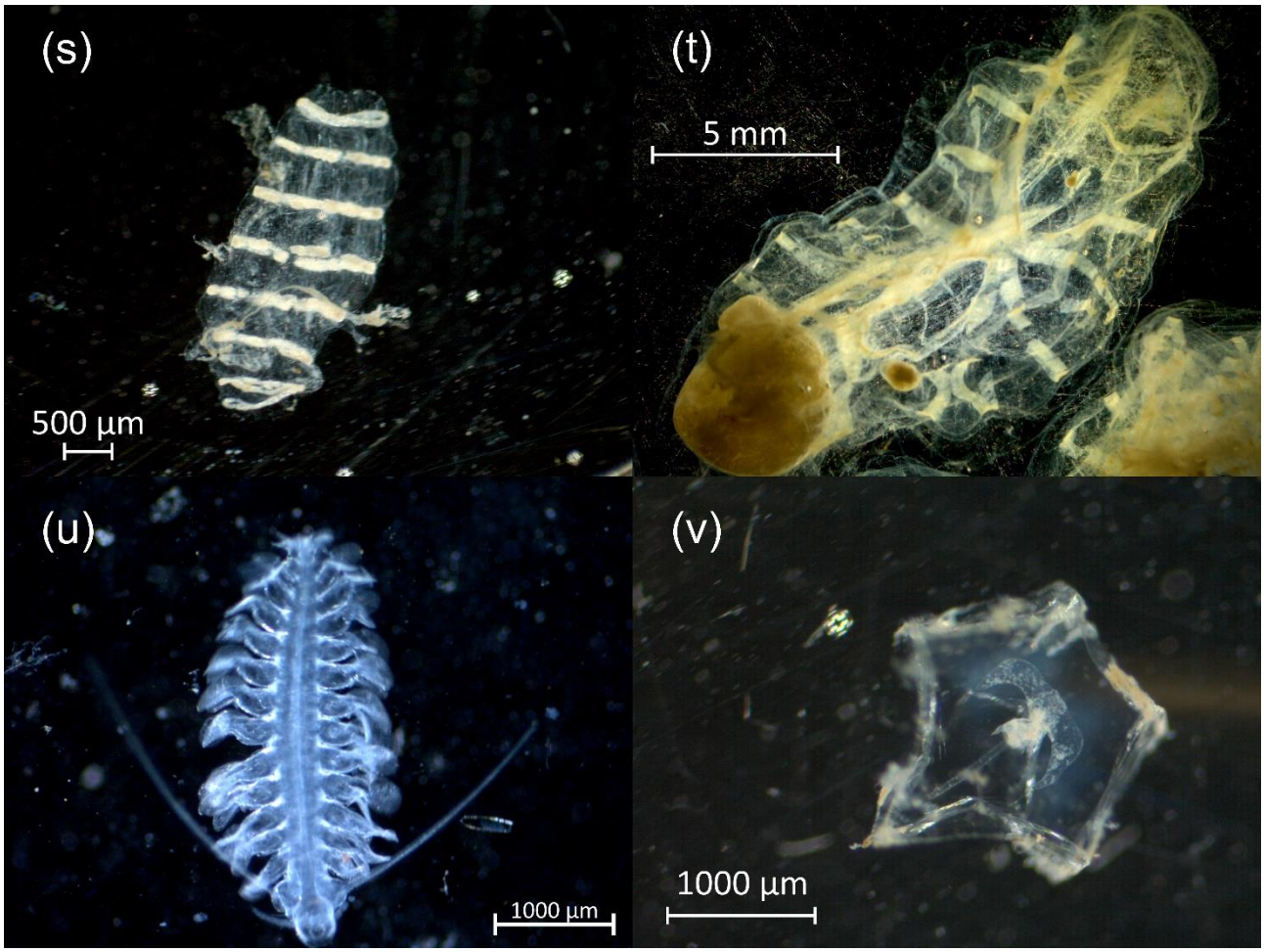

Figure 3.2 Zooplankton taxa collected during the Antarctic Circumnavigation Expedition. Micrographs were taken using a ZEISS Axiocam ERc 5s mounted on a ZEISS Stemi 508 stereo microscope (by Luca Stirnimann). (a) Juveniles (Themisto-J) and (b) adult of *Themisto gaudichaudii*; (c) *Cyllopus magellanicus* s.l.; (d) *Cyllopus lucasi s.l.*; (e) *Oikopleura* spp.; (f) Chaetognatha; (g) suspected nauplius of Pontellidae (Nauplii*); (h) Pontellidae *s.l.*; (i) Calanidae CIV; (j) *Calanus* spp. (female); (k) *Paraeuchaeta antarctica*; (l) *Metridia* spp.; (m) Euphausiacea (mixed-euphausiids); (n) Foraminifera; (o) Lepadiformes larva (Cirripedia); (p) Ostracoda; (q) *Limacina helicina antarctica*; (r) Pteropoda thecosomata; (s) Doliolida; (t) Salpida; (u) *Tomopteris* spp; (v) eudoxid of *Abylopsis eschscholtzi*. Different size bars scales are included in each panel.

Neustonic zooplankton abundance (median of $57.3_{3.1}^{106.0}$ Ind. m^{-3}) varied among stations, with the number of specimens per sample ranging from comparatively few (e.g., at the mouth of the Ross Sea (station 54) where only 90 specimens of *Oikopleura* spp., one Hydrozoa, and three Euphausiacea (10-20 mm) were collected) to richer samples such as near Heard Island, where the sample contained 1150 specimens (station 19; Figure 3.1b). Abundances were generally lower at open ocean stations, with six stations characterised by <5 Ind. m^{-3} (stations 20B, 21, 22, 54, 67, 68). At five stations near land (i.e., stations 2, 25, 56, 73, and 77 near the Prince Edward Islands, Diego Ramirez Islands, Antarctic coast, and South America), zooplankton abundances ranged from 60 to 100 Ind. m^{-3}, and hotspots of even higher abundances were observed near and downstream of Kerguelen and Heard Islands (stations 16, 19, and 20 with 143.7, 1189.1 and 143.5 Ind. m^{-3}, respectively) as well as near Tasmania (station 23; 120.8 Ind. m^{-3}) and east of Siple Island (station 67; 540 Ind. m^{-3}).

High variability made the assessment of general patterns in the composition and distribution of the neuston challenging. Excluding station 54 where Copepoda were absent, their abundances ranged from 0.03 (station 22) to 1182.2 Ind. m^{-3} (station 19), becoming the most abundant taxon (>75% of all specimens) at 14 stations (Figure 3.3a and Table B.1), with relative contributions across the transect that ranged from 8.0 to 99.6% (median of 79.1 ± 24.6%). At station 94 between South Sandwich and Bouvet Islands, Radiozoa and Pteropoda dominated the neuston (15.7 and 11.4 Ind. m^{-3}, 51.4 and 37.4%, respectively); near the Prince Edward Islands, fish larvae were dominant (46.6 Ind.m^{-3}, 51.6%; station 2); and near Tasmania and South America, low abundances but high contributions of Euphausiacea and Hydrozoa (0.02 and 0.02 Ind. m^{-3}, 27.8 and 27.8%, respectively; station 22) and Appendicularia (1.3 Ind. m^{-3}, 50.9%; station 78) were found.

Grouping the stations by hydrographic zone (where the sampling stations were considered as replicates within each hydrographic zone, and absent species were counted but with null abundance), the average Copepoda abundance varied from 28.2 ± 24.8 (mean ± 1SD; SAZ) to 303.1 ± 478.3 Ind. m^{-3} (SACCZ), contributing 63.4% in the SAZ to 97.7% in both the STZ and SACCZ (Figure 3.3b and Table B.2), noting that we sampled only two stations in each of the STZ and sBZ, *versus* four or five stations in the other zones. Fish larvae were particularly abundant in the SAZ, averaging 9.3 ± 20.8 Ind. m^{-3} (21.0%; Figure 3.3b and Table B.2). All other taxa averaged <5 Ind. m^{-3} in each zone.

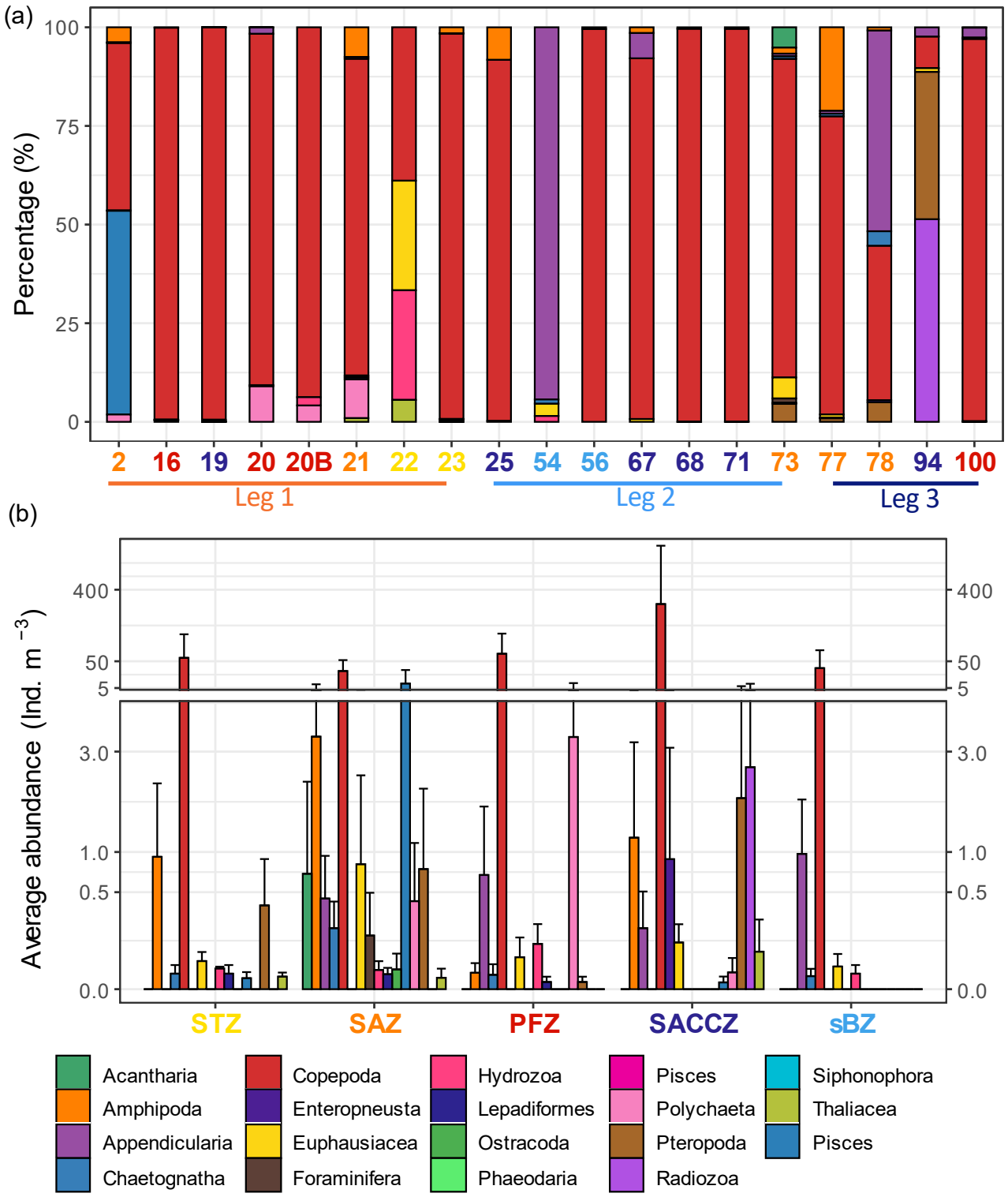

Figure 3.3 Composition of the zooplankton community sampled in the neuston layer during the Antarctic Circumnavigation Expedition. (a) Percent contribution of zooplankton taxa at each station, where numbers on the x-axes refer to the stations and their font colour refers to the hydrographic zone: yellow = Subtropical Zone (STZ), orange = Subantarctic Zone (SAZ), red = Polar Frontal Zone (PFZ), dark blue = Southern Antarctic Circumpolar Current Zone (SACCZ), and light blue = southern Boundary Zone (sBZ). Horizontal lines on the x-axis denote each leg of the cruise. (b) Average abundances (Ind. m^{-3}) of zooplankton taxa in each hydrographic zone. For panel (b), data were assessed considering each sampling station as single replicate for the relative hydrographic zone, and the absent species were counted as null abundance. Note that the y-axis is non-linear and vertical error bars = 1SD.

At the species level, *Oithona* spp. and Clausocalanidae (i.e., *Microcalanus* spp. and *Clausocalanus* spp.) were most abundant at 9 stations. Abundances of *Oithona* spp. ranged from 0.1 to 482.6 Ind. m^{-3} (50 to 95% of all individuals) at six stations distributed across the transect including near Kerguelen Island (station 16; 96.3 Ind. m^{-3}, 52.0%) and downstream of Heard Island (station 19; 482.6 Ind. m^{-3}, 40.6%). *Clausocalanus* spp. were also particularly abundant downstream of Heard Island (station 19; 534.2 Ind. m^{-3}, 44.9%) and *Microcalanus* spp. near Tasmania and Peter 1st Island (stations 23 and 68; 115.6 and 104 Ind. m^{-3}, 95.6 and 20.1%).

By hydrographic zone, adults of *Oithona* spp. constituted 32.5 ± 32.5, 45.4 ± 23.4, and 156.3 ± 93.7 Ind. m^{-3} of the zooplankton sampled in the sBZ , PFZ, and the SACCZ respectively (92.3, 60.2 and 50.2%), while in the SAZ, and STZ, they accounted for <20% (Table B.3). Clausocalanidae (i.e., *Clausocalanus* spp. and *C. laticeps*) were abundant in the SACCZ (95.6 ± 93.1 Ind. m^{-3}, 30.1%). In the STZ, most of the Copepoda were *Microcalanus* spp., which were particularly abundant at station 23 (58.0 ± 57.8 Ind. m^{-3}, 95%; Table B.3). Adult *C. varicans* (*sensu lato*), *P. antarctica*, *M. gerlachei*, *Oncaea* spp., and *C. propinquus* were the least abundant Copepoda across the transect (0.1 to 0.9 Ind. m^{-3}).

Among the non-copepod community, Amphipoda, Pteropoda, Radiolaria, Appendicularia (*Oikopleura* spp. and *Frittillaria* spp.), and fish larvae were the most abundant taxa, and were unevenly distributed among stations and Legs (Table B.1 and S2). Juvenile and adult *T. gaudichaudii* were generally the dominant Amphipoda, particularly near Tasmania, downstream of Heard Island and South America, and along the Antarctic coast (0.01 to 12.1 Ind. m^{-3}). *L. helicina antarctica* were the most abundant Pteropoda, particularly in the SACCZ on Leg3 (station 94, 11.4 Ind. m^{-3}). Pteropoda Thecosomata, such as *Clio recurva*, *C. pyramidata f. martensi*, and *C. pyramidata f. sulcata* were mainly encountered during Leg1 and Leg3, with abundances ranging from 0.01 to 11.4 Ind. m^{-3}. *Spongiobranchia australis* was the only Gymnosomata pteropod sampled and was present only at station 23 (0.7 Ind. m^{-3}). We found the hydrozoan *Physalia physalis* near Tasmania (0.03 Ind. m^{-3}, station 23), eudoxid of *Abylopsis eschscholtzii* at station 54 (0.02 Ind. m^{-3}; Figure 3.2v), unidentified Cnidaria downstream of Heard Island and along Leg1 (0.02 to 0.2 Ind. m^{-3}; stations 16, 20, and 21), while the Scyphozoa were found near South America (0.03 Ind. m^{-3}; station 77). The

planktonic Polychaeta *Tomopteris* spp. were sampled only near the Prince Edward Islands and the Diego Ramirez Islands (0.02 and 1.7 Ind. m^{-3}, respectively).

3.4.2. Zooplankton isoscapes around the Southern Ocean

In total, 327 zooplankton specimens from 47 taxa were collected and processed for $\delta^{13}C$ and $\delta^{15}N$, with values for the entire dataset ranging from -33.2 to -12.6‰ (median of $-24.6^{-22.1}_{-28.4}$‰) and -4.1 to 12.7‰ (median of $4.1^{5.9}_{2.7}$‰), respectively (Figure 3.1e-f). The median $\delta^{13}C$ and $\delta^{15}N$ for the entire zooplankton community at each station ranged from -30.5 to -20.5‰ ($-24.1^{-22.9}_{-27.9}$‰) and -2.2 to 10.0‰ ($3.8^{5.0}_{3.1}$‰), respectively, with the trend in $\delta^{13}C$ across the transect generally opposite that of $\delta^{15}N$. For instance, zooplankton $\delta^{13}C$ was low near Siple and Peter 1st Island ($-28.2^{-26.7}_{-30.1}$‰) and downstream of the South Sandwich Islands ($-29.7^{-27.0}_{-30.5}$‰) while $\delta^{15}N$ was high ($5.3^{6.9}_{4.6}$ and $4.3^{5.6}_{2.4}$‰, respectively). Zooplankton $\delta^{13}C$ was notably elevated near Crozet Island and off Tasmania ($-20.8^{-20.4}_{-22.4}$ and $-20.9^{-20.0}_{-21.8}$‰, respectively), and at one station in the open PFZ (station 20; $-21.9^{-20.7}_{-24.1}$‰). Maxima in $\delta^{15}N$ occurred at the mouth of the Ross Sea ($7.3^{8.6}_{4.1}$‰) and near the South Sandwich Islands (although we note that only the larger size class of Copepoda (>500 µm) was measured here; $\delta^{15}N$ = 10.0 ± 4.0‰; mean ± 1SD), while $\delta^{15}N$ minima were observed at the lower latitudes, such as near South America and South Africa ($+0.2^{+2.8}_{-1.3}$‰).

Over 340 samples (excluding duplicates) were measured for bulk $\delta^{13}C_{SPM}$ and $\delta^{15}N_{SPM}$ (Figure 3.1c-d; Chapter 2). Both $\delta^{13}C_{SPM}$ and $\delta^{15}N_{SPM}$ decreased latitudinally, with clear differences between the Subantarctic and Antarctic Oceans (Figure 3.4a-b). The trends in $\delta^{13}C_{SPM}$ and $\delta^{15}N_{SPM}$ were driven mainly by the partial pressure of CO_2 and the dominant nitrogen source consumed by phytoplankton (i.e., nitrate *versus* recycled ammonium), respectively. Both $\delta^{13}C_{SPM}$ and $\delta^{15}N_{SPM}$ were higher near the islands and in the vicinity of sea ice, which we attribute to increased phytoplankton productivity and nitrate consumption in these waters driven mainly by the alleviation of iron limitation, possibly augmented by the assimilation of high-$\delta^{15}N$ ammonium supplied via terrestrial run-off at the islands (Chapter 2).

3.4.3. Latitudinal gradients in zooplankton $\delta^{13}C$ and $\delta^{15}N$

3.4.3.1. Bulk zooplankton community trends

We observed a clear gradient in the $\delta^{13}C$ of the bulk zooplankton community between the Subantarctic and the Antarctic Oceans, decreasing from a mean ± 1SD ($[\text{median}_{Q1}^{Q3}]$) of -22.9 ± 3.5‰ $[-23.2_{-24.6}^{-20.8}‰]$ to -26.9 ± 3.6‰ $[-28.0_{-29.4}^{-24.8}‰]$ (t-test, *p*-value < 0.001; Figure 3.4a). In contrast, $\delta^{15}N$ was significantly lower in the Subantarctic (3.3 ± 2.7‰ $[3.3_{2.2}^{5.3}‰]$) than the Antarctic Ocean (5.0 ± 2.3‰ $[4.6_{3.7}^{6.6}‰]$) (t-test, *p*-value < 0.001; Figure 3.4b).

Zooplankton $\delta^{13}C$ decreased from the STZ (-20.8 ± 1.3‰ $[-20.7_{-21.9}^{-20.2}‰]$) to the SACCZ (-27.8 ± 2.8‰ $[-28.6_{-29.8}^{-26.7}‰]$) (pairwise t-test with Bonferroni adjustment, *p*-values < 0.05) where values reached a minimum between 55°S and 60°S (-27.2 ± 2.7‰ $[-27.0_{-29.3}^{-25.3}‰]$) (Figure 3.4c, e; Table 3.1). The $\delta^{13}C$ of zooplankton in the PFZ and the SAZ were comparable (t-test; *p*-values = 1; -23.8 ± 3.4‰ $[-23.9_{-26.4}^{-21.4}‰]$ and -22.7 ± 4.1‰ $[-23.3_{-24.7}^{-22.5}‰]$, respectively) with slightly lower values in the sBZ (-25.4 ± 4.2‰ $[-26.7_{-28.7}^{-22.2}‰]$; although higher than in the SACCZ; t-tests; *p*-value < 0.01). Zooplankton $\delta^{15}N$ decreased from the STZ (4.4 ± 1.7‰ $[4.4_{2.9}^{6.1}‰]$) to the SAF (2.2 ± 2.3‰ $[2.4_{0.1}^{3.5}‰]$) (pairwise t-test, p-value < 0.01) where values reached a minimum (pairwise t-test, p-values < 0.01; Figure 3.4d, f; Table 3.1) before increasing southwards to a maximum in the sBZ (6.2 ± 2.3‰ $[6.4_{4.3}^{7.2}‰]$; pairwise t-test, p-values < 0.001). Zooplankton $\delta^{15}N$ values in the PFZ and the SACCZ (3.1 ± 3.2‰ $[3.8_{1.8}^{5.2}‰]$ and 4.3 ± 2.3‰ $[4.0_{2.9}^{5.3}‰]$, respectively) were similar to those measured in the SAZ (pairwise t-test, p-values < 0.01).

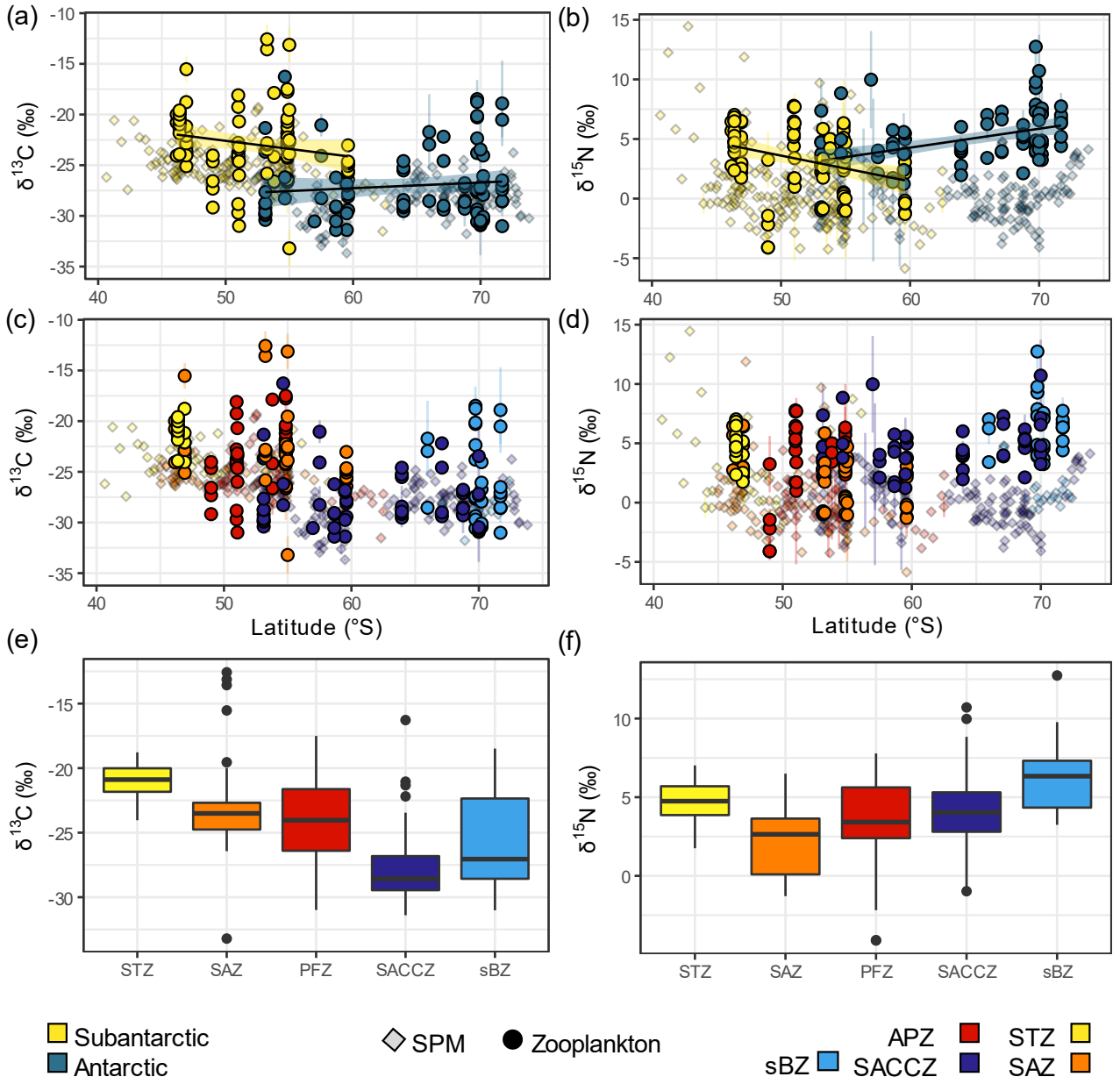

Figure 3.4 Latitudinal distribution of (a, c, e) $\delta^{13}C$ [‰] and (b, d, f) $\delta^{15}N$ [‰] for zooplankton (circles) and SPM (opaque diamonds) samples collected from the neuston layer during the Antarctic Circumnavigation Expedition. Panels a and b show data coloured according to Subantarctic (yellow) and Antarctic (blue) Ocean, while panels c-f show data coloured according to hydrographic zone: STZ = Subtropical Zone (yellow), SAZ = Subantarctic Zone (orange), PFZ = Polar Frontal Zone (red), SACCZ = Southern Antarctic Circumpolar Current Zone (dark blue), and sBZ = southern Boundary Zone (light blue). Boxplots (panels e and f) show medians (thick horizontal lines), interquartile range (IQR = 50% of the data; box within first and third quartiles), and whiskers (1.5 times the IQR).

Table 3.1 $\delta^{13}C$ [‰] and $\delta^{15}N$ [‰] of zooplankton collected during the Antarctic Circumnavigation Expedition, presented by hydrographic zone: STZ = Subtropical Zone, SAZ = Subantarctic Zone, PFZ = Polar Frontal Zone, SACCZ = Southern Antarctic Circumpolar Current Zone, and sBZ = southern Boundary Zone. n = number of observations (specimens), min and max = minimum and maximum values, Q1 = first quartile, Q3 = third quartile, 1SD = 1 standard deviation.

Zone		n	min	max	median	Q1	Q2	mean	1SD
STZ	$\delta^{13}C$ (‰)	38	-24.0	-18.0	-20.7	-21.9	-20.2	-20.8	1.3
	$\delta^{15}N$ (‰)	37	1.5	7.1	4.4	2.9	6.1	4.4	1.8
SAZ	$\delta^{13}C$ (‰)	68	-34.5	-11.6	-23.3	-24.7	-22.5	-22.7	4.1
	$\delta^{15}N$ (‰)	64	-1.6	6.7	2.4	0.1	3.5	2.2	2.3
PFZ	$\delta^{13}C$ (‰)	70	-31.3	-16.6	-23.9	-26.4	-21.4	-23.8	3.4
	$\delta^{15}N$ (‰)	65	-4.7	8.5	3.8	1.9	5.2	3.1	3.2
SACCZ	$\delta^{13}C$ (‰)	90	-31.5	-16.3	-28.6	-29.7	-26.7	-27.8	2.8
	$\delta^{15}N$ (‰)	86	-1.0	12.9	4.0	2.9	5.3	4.2	2.1
sBZ	$\delta^{13}C$ (‰)	52	-31.1	-15.9	-26.7	-28.7	-22.2	-25.4	4.3
	$\delta^{15}N$ (‰)	51	3.1	13.1	6.4	4.4	7.2	6.2	2.3

The $\delta^{13}C$ and $\delta^{15}N$ measured for the various zooplankton taxa and species are summarized in Table 3.2 and Table 3.3, respectively, with the broad trends outlined below for the Subantarctic and Antarctic Oceans and the hydrographic zones. Because of complications during analysis, we do not report species-specific Copepoda $\delta^{13}C$ and $\delta^{15}N$ for the STZ and instead present only the bulk values of the smaller group of Copepoda (mixed-copepods 200-500 µm, comprising mainly Oithonidae and Oncaeidae). For all other zones, several species-specific and size fractionated Copepoda (200-500 and >500 µm) $\delta^{13}C$ and $\delta^{15}N$ values are reported.

Table 3.2 Medians (± IQR) of $\delta^{13}C$ [‰], $\delta^{15}N$ [‰], and trophic position (TP) of zooplankton taxa collected during the Antarctic Circumnavigation Expedition, for the Subantarctic and Antarctic Oceans. The number of observations is given in parentheses.

Order	Subantarctic			Antarctic		
	$\delta^{13}C$ (‰)	$\delta^{15}N$ (‰)	TP	$\delta^{13}C$ (‰)	$\delta^{15}N$ (‰)	TP
Amphipoda	-23.4 ± 3.0 (43)	2.2 ± 2.7 (41)	2.4 ± 1.2 (36)	-27.4 ± 3.5 (15)	3.8 ± 1.0 (15)	2.4 ± 1.7 (15)
Appendicularia	-25.3 ± 1.2 (8)	0.0 ± 3.8 (8)	2.4 ± 1.0 (6)	-30.2 ± 2.3 (8)	4.3 ± 0.9 (7)	3.0 ± 1.3 (7)
Chaetognatha	-23.3 ± 1.7 (14)	6.4 ± 2.6 (14)	3.9 ± 1.3 (12)	-18.8 ± 0.1 (2)	12.7 ± 0.4 (2)	6.4 ± 0.2 (2)
Copepoda	-24.4 ± 3.9 (48)	3.4 ± 2.8 (42)	2.2 ± 2.1 (38)	-28.5 ± 2.7 (73)	4.9 ± 2.9 (68)	3.1 ± 1.6 (68)
Euphausiacea	-22.0 ± 0.3 (18)	2.4 ± 2.5 (18)	2.2 ± 1.0 (18)	-26.2 ± 3.5 (23)	4.9 ± 1.8 (24)	3.0 ± 0.8 (24)
Foraminifera	-15.5 ± 2.9 (6)	4.0 ± 1.4 (6)	2.7 ± 1.3 (6)	-27.9 ± 0.8 (2)	7.6 ± 2.3 (2)	4.2 ± 1.0 (2)
Hydrozoa	-19.9 ± 0.9 (2)	7.0 ± 0.1 (2)	3.0 ± 0.0 (2)	-23.4 ± 8.5 (4)	4.7 ± 6.4 (4)	2.7 ± 3.1 (4)
Lepadiformes	-19.9 ± 1.7 (18)	4.2 ± 2.0 (17)	3.3 ± 1.2 (15)			
Ostracoda	-26.4 ± 0.1 (2)	2.1 ± 0.8 (2)	4.5 ± 0.3 (2)			
Phaeodaria	-24.1 ± 0.6 (2)	2.5 ± 0.7 (2)	0.3 ± 0.3 (2)	-30.0 ± 0.4 (2)	-0.9 ± 0.1 (2)	-0.1 ± 0.1 (2)
Polychaeta				-30.5 (1)	7.2 (1)	4.0 (1)
Pteropoda	-19.3 ± 3.1 (11)	1.1 ± 4.6 (10)	1.7 ± 0.6 (10)	-23.4 ± 4.6 (5)	4.0 ± 0.7 (5)	2.3 ± 0.1 (5)
Thaliacea	-22.4 ± 3.0 (4)	0.3 ± 3.5 (4)	1.4 ± 0.6 (4)	-29.1 ± 4.7 (7)	1.7 ± 0.6 (7)	1.5 ± 0.5 (7)

Table 3.3 Averages (± 1SD) of $\delta^{13}C$ [‰], $\delta^{15}N$ [‰], and trophic position (TP) of zooplankton taxa collected during the Antarctic Circumnavigation Expedition in each hydrographic zone: STZ = Subtropical Zone, SAZ = Subantarctic Zone, PFZ = Polar Frontal Zone, SACCZ = Southern Antarctic Circumpolar Current Zone, and sBZ = southern Boundary Zone. *N* = the number of specimens analysed as whole-body (*versus* a subsample of ground material, denoted by an empty cell).

Order	Species / Taxa	STZ				SAZ				PFZ			
		$\delta^{13}C$ (‰)	$\delta^{15}N$ (‰)	*N*	TP	$\delta^{13}C$ (‰)	$\delta^{15}N$ (‰)	*N*	TP	$\delta^{13}C$ (‰)	$\delta^{15}N$ (‰)	*N*	TP
Amphipoda	*Cyllopus* spp.	-20.6 ± 0.0 (4)	4.4 ± 0.3 (4)		1.7 ± 0.2	-23.4 (1)	2.2 (1)	1	2.8	-26.6 ± 0.1 (2)	-4.1 ± 0.5 (2)		0.5 ± 0.3
	mixed-amphipods	-23.9 (1)	6.6 (1)	2	2.7	-23.9 (1)	-		-				
	Themisto-J	-21.0 (1)	4.7 (1)	4	1.9	-23.2 ± 0.2 (11)	1.9 ± 0.1 (11)	13	2.4 ± 0.5				
	Themisto gaudichaudii	-21.3 ± 0.9 (2)	4.8 (1)		1.9	-23.1 ± 1.0 (6)	3.4 ± 1.2 (5)		3.1 ± 1.0	-23.0 ± 0.5 (12)	3.4 ± 0.5 (12)	2	1.1 ± 2.1
	Vibilia antarctica									-27.3 ± 0.4 (2)	-4.1 ± 0.3 (2)		0.5 ± 0.2
Appendicularia	*Oikopleura* spp.					-24.5 ± 0.6 (6)	0.2 ± 0.9 (6)	21	2.5 ± 0.6	-26.2 ± 0.2 (2)	3.0 ± 2.1 (2)	14	0.9 ± 0.0
Chaetognatha	Chaetognatha	-19.6 ± 0.5 (2)	6.8 ± 0.2 (2)		2.8 ± 0.1	-23.4 ± 0.4 (7)	4.6 ± 0.5 (7)	1.5	4.3 ± 1.0	-23.7 ± 0.7 (5)	7.5 ± 0.4 (5)	5	3.3 ± 1.7
Copepoda	Calanidae CIII												
	Calanidae CIV					-20.9 ± 2.0 (7)	2.6 ± 1.1 (6)	7	3.2 ± 0.4	-22.5 ± 0.6 (4)	3.6 ± 1.0 (4)	12	0.8 ± 2.0
	Calanidae CV									-22.1 ± 0.3 (3)	4.7 ± 1.5 (3)	6	1.4 ± 2.4
	Calanoides spp.												
	Calanus propinquus CV												
	Calanus propinquus F												
	Calanus spp.												
	Clausocalanus laticeps									-25.2 ± 2.2 (3)	4.3 ± 1.6 (2)	7	-0.3 ± 0.0
	Metridia gerlachei									-28.8 (1)	6.0 (1)	1	3.5
	Microcalanus spp.					-23.3 (1)	3.0 (1)		3.7				
	mixed-copepods (>500µm)					-25.8 ± 0.0 (2)	3.4 ± 0.1 (2)	13	3.3 ± 0.1	-22.6 ± 0.4 (2)	3.0 ± 0.4 (2)	16	0.0 ± 0.2
	mixed-copepods (200-500µm)	-21.6 ± 1.2 (3)	4.2 ± 1 (3)		1.9 ± 0.4	-24.7 ± 0.7 (4)	0.9 ± 1.2 (4)	60	2.5 ± 0.7	-26.8 ± 1.1 (7)	0.6 ± 1.4 (7)	75	2.0 ± 0.9
	Nauplii												
	Nauplii*									-26.6 ± 0.0 (2)	5.7 ± 1.7 (2)	4	1.1 ± 1.0
	Oithona spp.					-33.2 ± 1.3 (2)	-		-	-27.8 ± 0.8 (7)	5.0 ± 0.6 (5)	158	1.3 ± 0.4
	Paraeuchaeta antarctica												

	Pontellidae spp.												
Euphausiacea	krill 0-5 mm									-20.4 (1)	3.2 (1)	2	0.0
	krill 5-10 mm	-21.2 ± 0.2 (4)	1.8 ± 0.2 (4)	2.2	1.3 ± 0.2								
	krill 10-20 mm	-22.1 ± 0.0 (3)	2.5 ± 0.2 (3)	0.8	1.6 ± 0.2								
	krill 20-50 mm	-22.1 ± 0.1 (3)	4.0 ± 0.2 (3)		2.3 ± 0.2								
	Krill 50 mm												
	Calyptopis I												
	Calyptopis II									-24.4 (1)	5.2 (1)	2	3.1
	mixed-euphausiids	-21.8 ± 0.0 (2)	5.7 ± 0.4 (2)		2.3 ± 0.2	-22.7 ± 0.3 (4)	-0.1 ± 0.2 (4)		2.9 ± 0.6				
Foraminifera	Foraminifera					-14.1 ± 1.0 (4)	3.7 ± 0.7 (4)	105	2.8 ± 0.2	-17.5 ± 0.6 (2)	4.0 ± 0.2 (2)	37	0.4 ± 0.1
Hydrozoa	*Abylopsis eschscholtzii*												
	Halicreatidae												
	Physalia physalis	-19.9 ± 0.9 (2)	7.0 ± 0.1 (2)		2.9 ± 0.1								
Lepadiformes	Lepadiformes larvae	-19.0 ± 0.5 (5)	5.1 ± 0.6 (5)	4	2.6 ± 0.7	-21.4 ± 0.8 (6)	4.3 ± 0.7 (6)	3	2.8 ± 0.7	-19.7 ± 0.4 (7)	4.2 ± 0.5 (6)	5	3.2 ± 0.5
Ostracoda	Ostracoda					-26.4 ± 0.1 (2)	2.1 ± 0.8 (2)		4.5 ± 0.5				
Phaeodaria	Phaeodaria									-24.1 ± 0.6 (2)	2.5 ± 0.7 (2)		-0.3 ± 0.4
Polychaeta	*Tomopteris* spp.												
Pteropoda	*Clio pyramidata*	-20.4 ± 0.2 (2)	3.9 ± 0.4 (2)		1.5 ± 0.2	-26.4 ± 2.3 (2)	-0.9 ± 0.4 (2)		2.0 ± 0.3				
	Clione Continue antarctica												
	Limacina helicina antarctica					-13.6 ± 0.2 (2)	-0.9 ± 0.3 (2)	11	1.5 ± 0.2	-17.9 ± 0.7 (3)	1.1 ± 0.5 (2)	55	0.2 ± 1.9
	Limacina retroversa												
	Spongiobranchaea australis	-19.6 ± 0.3 (2)	6.5 ± 0.2 (2)	2	2.7 ± 0.1								
Thaliacea	Doliolidae												
	Salpidae	-20.9 ± 0.1 (2)	2.4 ± 0.5 (2)		0.9 ± 0.3					-24 ± 0.3 (2)	-1.4 ± 0.2 (2)		1.7 ± 0.1

Continues…

Order	Species / Taxa	SACCZ				sBZ			
		$\delta^{13}C$ (‰)	$\delta^{15}N$ (‰)	*N*	TP	$\delta^{13}C$ (‰)	$\delta^{15}N$ (‰)	*N*	TP
Amphipoda	*Cyllopus* spp.	-26.3 ± 0.5 (4)	3.2 ± 0.4 (4)		1.4 ± 0.3				
	mixed-amphipods					-20.3 (1)	4.0 (1)		2.6
	Themisto-J	-23 ± 1.6 (2)	5.7 ± 1.0 (2)		3.9 ± 2.3				
	Themisto gaudichaudii	-29.1 ± 0.5 (7)	3.8 ± 0.6 (7)		2.9 ± 1.5				
	Vibilia antarctica								
Appendicularia	*Oikopleura* spp.	-30.7 ± 0.2 (4)	4.2 ± 0.1 (3)		4 ± 1.0	-28.2 ± 0.7 (4)	5.2 ± 0.7 (4)		2.9 ± 0.5
Chaetognatha	Chaetognatha					-18.8 ± 0.1 (2)	12.7 ± 0.4 (2)		6.4 ± 0.2
Copepoda	Calanidae CIII	-28.1 ± 0.5 (3)	3.3 ± 0.5 (3)	10	1.7 ± 0.3				
	Calanidae CIV	-28.5 ± 1.0 (6)	4.1 ± 0.2 (6)	7	2.7 ± 0.9	-27.8 ± 0.4 (3)	4.8 ± 1.1 (3)	2	2.8 ± 0.6
	Calanidae CV								
	Calanoides spp.	-27.2 ± 0.2 (2)	3.3 ± 0.2 (2)	1	4.2 ± 0.1	-27.6 ± 0.1 (2)	4.0 ± 0.0 (2)	1	2.6 ± 0.0
	Calanus propinquus CV					-30.2 ± 0.2 (2)	3.7 ± 0.6 (2)		2.5 ± 0.4
	Calanus propinquus F	-27.1 ± 0.6 (2)	5.3 ± 0.0 (2)	2	3.2 ± 0.0				
	Calanus spp.					-29.1 ± 0.5 (4)	7.1 ± 0.5 (4)	3	3.8 ± 0.6
	Clausocalanus laticeps	-28.7 ± 0.1 (3)	3.7 ± 0.3 (3)	78	1.9 ± 0.2				
	Metridia gerlachei					-28.5 ± 0.1 (2)	6.7 ± 0.1 (2)		3.4 ± 0.0
	Microcalanus spp.								
	mixed-copepods (>500µm)	-27.9 ± 0.6 (8)	6.4 ± 1.0 (8)	4	3.7 ± 1.2	-27.1 ± 3.5 (3)	7.3 ± 0.1 (3)		4.0 ± 0.1
	mixed-copepods (200-500µm)	-29.1 ± 0.3 (8)	4.1 ± 0.4 (8)	0	2.5 ± 0.8	-21.6 ± 0.8 (9)	6.0 ± 0.5 (9)		3.3 ± 0.8
	Nauplii	-29.2 ± 0.6 (2)	7.4 ± 1.8 (2)	23	3.5 ± 1.1				
	Nauplii*	-23.1 ± 6.8 (2)	6.1 ± 2.7 (2)	5	3.1 ± 1.8				
	Oithona spp.	-29.6 ± 0.3 (6)	4.8 ± 0.6 (2)	46	2.4 ± 0.7	-31.0 ± 0.1 (2)	-		-
	Paraeuchaeta antarctica					-30.1 (1)	4.6 ± 0.4 (2)		2.9 ± 0.2
	Pontellidae spp.	-22.7 (1)	8.6 (1)		6.5	-18.9 ± 3.0 (2)	7.7 ± 0.8 (2)		3.9 ± 0.5
Euphausiacea	krill 0-5 mm	-28.1 ± 1.6 (4)	4.8 ± 1.0 (4)	1	3.3 ± 1.5				
	krill 5-10 mm								
	krill 10-20 mm								
	krill 20-50 mm								
	Krill 50 mm	-26 ± 0.5 (4)	5.6 ± 0.2 (4)		3.0 ± 0.2				

	Calyptopis I		2.8 (1)	2	1.5			
	Calyptopis II							
	mixed-euphausiids	-26.9 ± 1.3 (8)	3.6 ± 0.5 (8)		3.5 ± 0.7	-24.6 ± 0.6 (7)	5.2 ± 0.4 (7)	3.1 ± 0.5
Foraminifera	Foraminifera					-27.9 ± 0.8 (2)	7.6 ± 2.3 (2)	4.2 ± 1.4
	Abylopsis eschscholtzii					-18.5 ± 1.3 (2)	9.8 ± 2.5 (2)	5.1 ± 1.6
Hydrozoa	Halicreatidae	-28.3 ± 1.3 (2)	2.1 ± 0.0 (2)		1.5 ± 0.0			
	Physalia physalis							
Lepadiformes	Lepadiformes larvae							
Ostracoda	Ostracoda							
Phaeodaria	Phaeodaria	-30 ± 0.4 (2)	-0.9 ± 0.1 (2)		-0.1 ± 0.1			
Polychaeta	*Tomopteris* spp.					-30.5 (1)	7.2 (1)	4.0
	Clio pyramidata							
	Clione limacina antarctica	-21.8 ± 0.9 (3)	4.9 ± 0.8 (3)		3.4 ± 1.9			
Pteropoda	*Limacina helicina antarctica*							
	Limacina retroversa					-26.7 ± 0.3 (2)	3.2 ± 0.2 (2)	2.3 ± 0.1
	Spongiobranchaea australis							
Thaliacea	Doliolidae					-22.4 (1)	9.3 (1)	4.9
	Salpidae	-27.8 ± 1.0 (6)	1.6 ± 0.1 (6)		1.4 ± 0.4			

3.4.3.2. Trends in zooplankton taxonomic groups: Subantarctic *versus* Antarctic

With few exceptions, the major zooplankton taxonomic groups were significantly higher in $\delta^{13}C$ and lower in $\delta^{15}N$ in the Subantarctic than the Antarctic Ocean (pairwise t-test and Wilcoxon's test, *p*-values <0.05; Figure 3.5; Table 3.2). The largest $\delta^{13}C$ difference between the Subantarctic and Antarctic Oceans was measured for the Foraminifera (12.4‰), followed by Thaliacea and Phaeodaria (6.7‰ and 5.8‰, respectively) (Figure 3.5a). For all other zooplankton groups, the median Subantarctic $\delta^{13}C$ was 3.5‰ to 4.9‰ higher than in the Antarctic. Only the Chaetognatha were higher in $\delta^{13}C$ in the Antarctic than in Subantarctic (by 4.6‰), noting that we analysed only two specimens in the Antarctic *versus* 12 in the Subantarctic. The median $\delta^{15}N$ measured for the Chaetognatha, Appendicularia, and Foraminifera were respectively 6.3‰, 4.3‰, and 3.6‰ lower in the Subantarctic than the Antarctic, while 1.4‰ to 2.6‰ lower for all other groups (Figure 3.5b). Only the Hydrozoa and Phaeodaria were higher in $\delta^{15}N$ in the Subantarctic than in the Antarctic, by 2.3‰ and 3.4‰, respectively. There was no significant difference in $\delta^{15}N$ between the Subantarctic and Antarctic for Pteropoda and Thaliacea (Wilcoxon's test, *p*-values >0.05). Some organisms were only found in one of the oceans (e.g., Lepadiformes larvae, Medusozoa, Ostracoda, Polychaeta, and Siphonophora) so their regional $\delta^{13}C$ and $\delta^{15}N$ could not be compared.

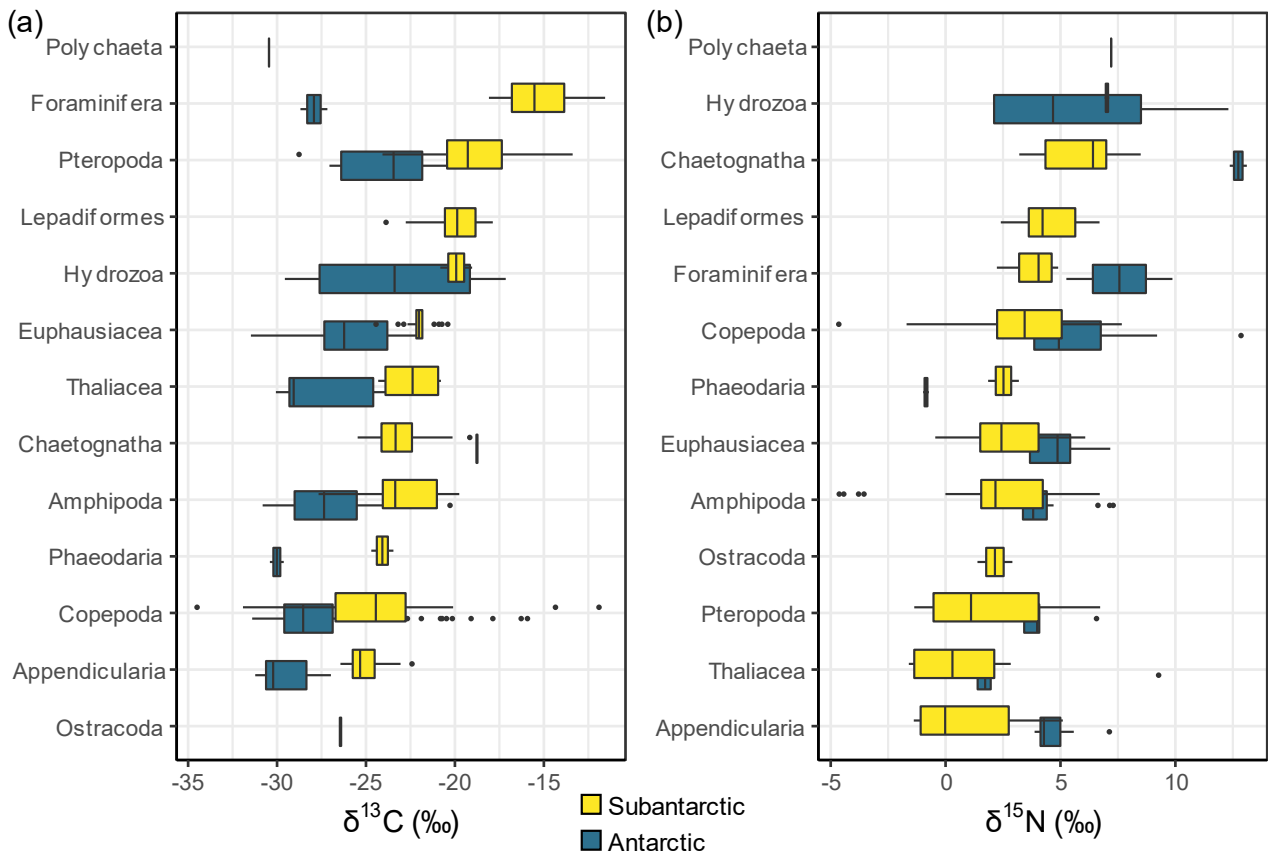

Figure 3.5 Boxplots of (a) $\delta^{13}C$ [‰] and (b) $\delta^{15}N$ [‰] for zooplankton taxa (y-axes) collected during the Antarctic Circumnavigation Expedition in the Subantarctic Ocean (yellow) and Antarctic Ocean (blue). Taxa have been ordered from the most isotopically-deplete to the most isotopically-enriched, as measured for the Subantarctic samples. Boxplots show medians (thick vertical lines), interquartile range (IQR = 50% of the data; box within first and third quartiles), and whiskers (1.5 times the IQR). The black dots indicate outliers.

3.4.3.3. Trends in zooplankton taxonomic groups: hydrographic zones

In the STZ, the $\delta^{13}C$ and $\delta^{15}N$ of the different taxa varied by 6.0‰ and 5.6‰, respectively (Figure 3.5a, Table 3.3). The Chaetognatha, *Physalia physalis*, and *Spongiobranchea australis* had the highest $\delta^{13}C$ and $\delta^{15}N$ (-19.9‰ to -19.6‰ and 6.5‰ to 7.0‰, respectively), an unidentified Amphipoda had the lowest $\delta^{13}C$ (-23.9‰; mixed-amphipods), and the smaller Euphausiacea (5-10 µm) and Salpidae had the lowest $\delta^{15}N$ (1.8 ± 0.2‰ and 2.4 ± 0.5‰). The $\delta^{15}N$ of the Euphausiacea increased with size, from 1.8 ± 0.2‰ (5-10 mm) to 4.1 ± 0.3‰ (20-50 mm) and was 5.7 ± 0.4‰ for the mixed-euphausiids, while Euphausiacea $\delta^{13}C$ varied little with size (-22.1‰ to -21.2‰).

The $\delta^{13}C$ and $\delta^{15}N$ of the SAZ taxa varied by 12.8‰ and 7.8‰, respectively (Figure 3.6b, Table 3.3). Ostracoda and *Clio pyramidata* had the lowest $\delta^{13}C$ (-26.4 ± 0.1 and -26.4 ± 2.3‰) and *C. pyramidata* also had the lowest $\delta^{15}N$ (-0.9 ± 0.4‰). The Chaetognatha and Lepadimorphes larvae had the highest $\delta^{15}N$ (4.6 ±

0.5‰ and 4.3 ± 0.7‰) and a higher $\delta^{13}C$ than most of the other zooplankton (-23.4 ± 04‰ and -21.4 ± 0.8‰), although the highest $\delta^{13}C$ was measured for the Foraminifera and *Limacina helicina antarctica* (-14.1 ± 1.0‰ and -13.1 ± 0.2‰).

In the PFZ, the $\delta^{13}C$ and $\delta^{15}N$ of the zooplankton varied by 12.3‰ and 11.9‰, respectively (Figure 3.6c, Table 3.3). *Metridia gerlachei* and *Oithona* spp. had the lowest $\delta^{13}C$ (-28.8‰ and -27.8 ± 0.8‰), while Foraminifera, *L. helicina antarctica,* and Lepadimorphes larvae had the highest (-17.5 ± 0.6‰, -17.9 ± 0.7‰, and -19.7 ± 0.4‰). *Vibilia antarctica* and *Cyllopus* spp. had the lowest $\delta^{15}N$ (-4.1 ± 0.3‰ and -4.1 ± 0.5‰) and a relatively low $\delta^{13}C$ (-27.3 ± 0.4‰ and -26.6 ± 0.1‰), while the Chaetognatha had the highest $\delta^{15}N$ (7.5 ± 0.4‰). Interestingly, the Calyptopis II (5.2‰, n = 1) and the Nauplii* (5.7 ± 2.3‰) were higher in $\delta^{15}N$ than their more developed stages, such as the smaller Euphausiacea group (krill, 0-5µm; 3.2‰, n=1) and most of the Copepoda (range of 3.0‰ to 4.7‰).

The $\delta^{13}C$ and $\delta^{15}N$ of zooplankton taxa in the SACCZ varied by 10.4‰ and 10.9‰, respectively (Figure 3.6d, Table 3.3). *Oikopleura* spp. and Phaeodaria had the lowest $\delta^{13}C$ (-30.7 ± 0.2‰ and -30.0 ± 0.4‰), although several other taxa were almost as low in $\delta^{13}C$ (e.g., *Oithona* spp. and *T. gaudichaudii,* -29.6 ± 0.3‰ and 29.1 ± .5‰). Phaeodaria also had the lowest $\delta^{15}N$ (-0.9 ± 0.1‰). The highest mean $\delta^{13}C$ was measured for *Clione limacina antarctica* (-21.8 ± 0.9‰), although the $\delta^{13}C$ of the Nauplii* ranged considerably, between -29.8‰ and -16.3‰, and Pontellidae had the highest $\delta^{15}N$ (8.6‰). Interestingly, the $\delta^{13}C$ of two *T. gaudichaudii* juveniles (Themisto-J; -23.0 ± 1.6‰) and two Nauplii* (-23.1 ± 6.8‰) were >4‰ higher than the $\delta^{13}C$ of the more-developed stages. In addition, the $\delta^{15}N$ of the Nauplii* (6.1 ± 2.7‰) and the Nauplii (7.4 ± 1.8‰) were both higher than most of the more developed life cycle-stages of Copepoda (e.g., Calanidae CIII, *Calanoides* spp.). The $\delta^{15}N$ of the Themisto-J (5.7 ± 1.0‰) was also ~1.8‰ higher than that of the adult *Cyllopus* spp.

In the sBZ, the $\delta^{13}C$ and $\delta^{15}N$ of the different zooplankton taxa varied by 12.5‰ and 9.5‰, respectively (Figure 3.6e, Table 3.3). *Tomopteris* spp., *Calanus propinquus* CV, and *Paraeuchaeta antarctica* had the lowest $\delta^{13}C$ (-30.5‰, -30.2 ± 0.2‰, and -30.1‰), while the Chaetognatha, *Abylopsis eschscholtzii*, and Pontellidae had the highest $\delta^{13}C$ (-18.8 ± 0.1, -18.5 ± 0.3, -18.9 ± 3.0). While the *Limacina retroversa* and *Calanus propinquus* CV had the lowest $\delta^{15}N$ (3.2 ± 0.2‰ and 3.7 ± 0.6‰), the Chaetognatha were highest in

$\delta^{15}N$ (12.7 ± 0.4‰). The only specimen of Doliolida ($\delta^{15}N$ = 9.3‰ and $\delta^{13}C$ = -22.4‰; Figure 3.2s) was higher in $\delta^{13}C$ and $\delta^{15}N$ (by 4.7‰ to 8.1‰ and 1.7‰ to 2.6‰, respectively) than most of the Copepoda (e.g., *M. gerlachei*, *Calanus* spp., and the mixed-copepods >500 µm), the *Tomopteris* spp. (planktonic Polychaeta), and the Foraminifera.

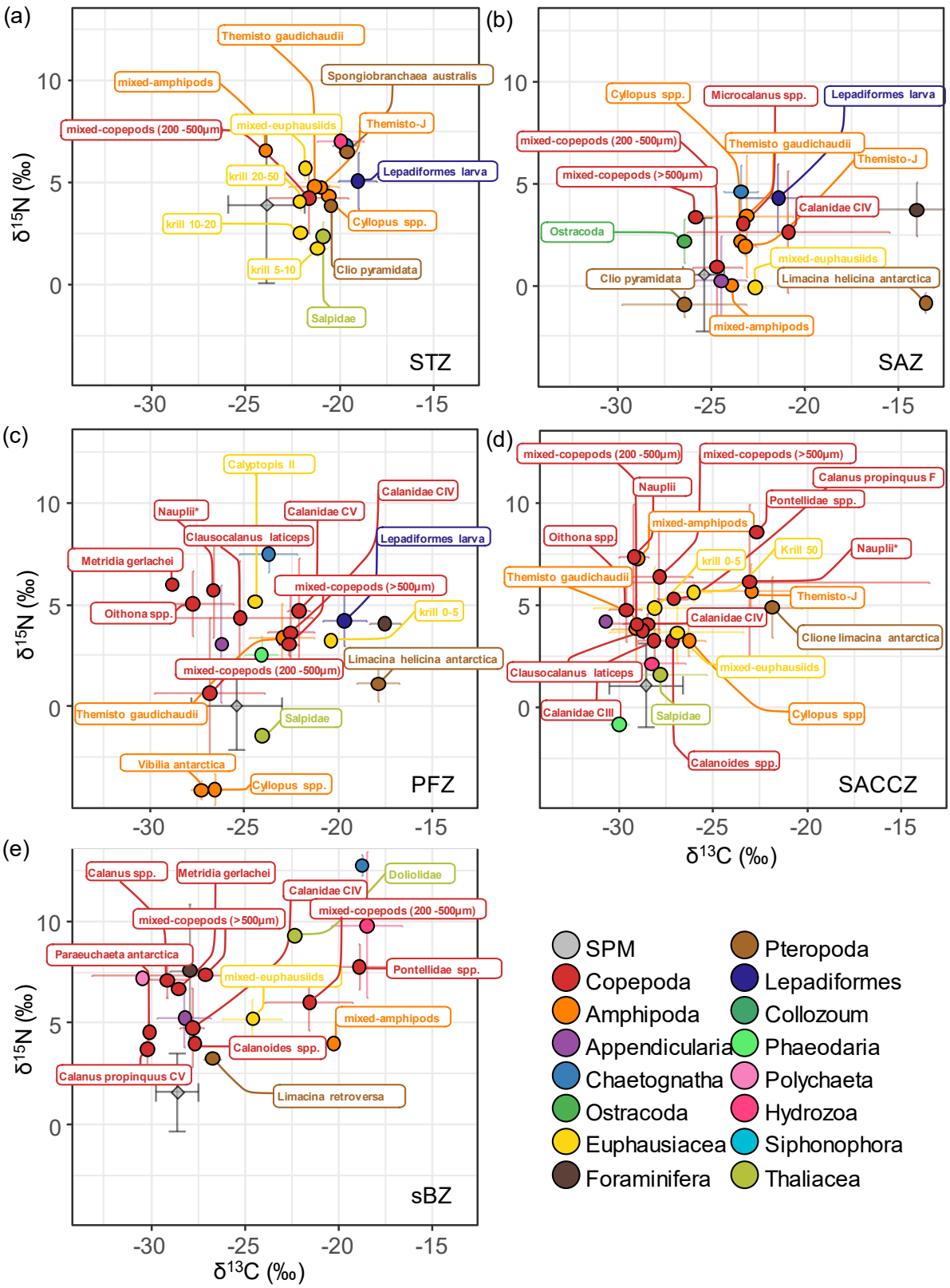

Figure 3.6 Average $\delta^{13}C$ [‰] and $\delta^{15}N$ [‰] of zooplankton taxa (colours) collected from the neuston layer during the Antarctic Circumnavigation Expedition in each hydrographic zone: a) STZ = Subtropical Zone, b) SAZ = Subantarctic Zone, c) PFZ = Polar Frontal Zone, d) SACCZ = Southern Antarctic Circumpolar Current Zone, and e) sBZ = southern Boundary Zone. Error bars show one standard deviation (SD) about the mean. The grey diamonds indicate the average (± 1SD) $\delta^{13}C$ and $\delta^{15}N$ of surface suspended particulate matter (SPM) collected from the underway seawater supply and the CTD in each zone.

3.4.4. Longitudinal (temporal) variability in zooplankton $\delta^{13}C$ and $\delta^{15}N$

During the ACE, the ship steamed along a longitudinal transect over a three-month period, such that analysing our dataset for longitudinal variability required consideration of temporal variability (Chapter 2). The $\delta^{13}C$ of bulk zooplankton collected during Leg1 (-23.2 ± 4.0‰ [$-23.3^{-21.2}_{-25.6}$‰]) was higher than the zooplankton sampled during Leg2 and Leg3 (ANOVA, *p*-value < 0.005; -25.7 ± 3.7‰ [$-26.5^{-22.4}_{-28.9}$‰] and -25.6 ± 4.2‰ [$-25.5^{-23.3}_{-29.1}$‰] for Leg2 and Leg3, respectively), with no difference between the Leg2 and Leg3 values. In contrast, bulk zooplankton $\delta^{15}N$ differed among all three legs (multiple t-tests with Bonferroni adjustment, *p*-values < 0.05; Leg1 = 2.0 ± 0.2‰ [$3.5^{5.0}_{2.2}$‰], Leg2 = 2.5 ± 0.2‰ [$4.9^{6.6}_{3.8}$‰], and Leg3 = 2.4 ± 3.4‰ [$2.6^{4.2}_{0.2}$‰]). For the Southern Ocean as a whole, zooplankton $\delta^{13}C$ and $\delta^{15}N$ decreased over the three months of the cruise, from a mean of -23.7 ± 2.9‰ and 4.1 ± 2.0‰ for the first 15 days to -25.6 ± 4.2‰ and 2.4 ± 3.4‰ for the last 15 days (*lm* for $\delta^{13}C$: *p*-value < 0.001, R^2=0.08; *lm* for $\delta^{15}N$ = *p*-value < 0.05, R^2=0.03; dashed black lines in Figure 3.7). The same trends were apparent in the Subantarctic (*lm*, *p*-values < 0.01) but not the Antarctic where $\delta^{13}C$ and $\delta^{15}N$ were roughly constant with time (*lm*, *p*-values > 0.05; Table B.4 and Figure B.1).

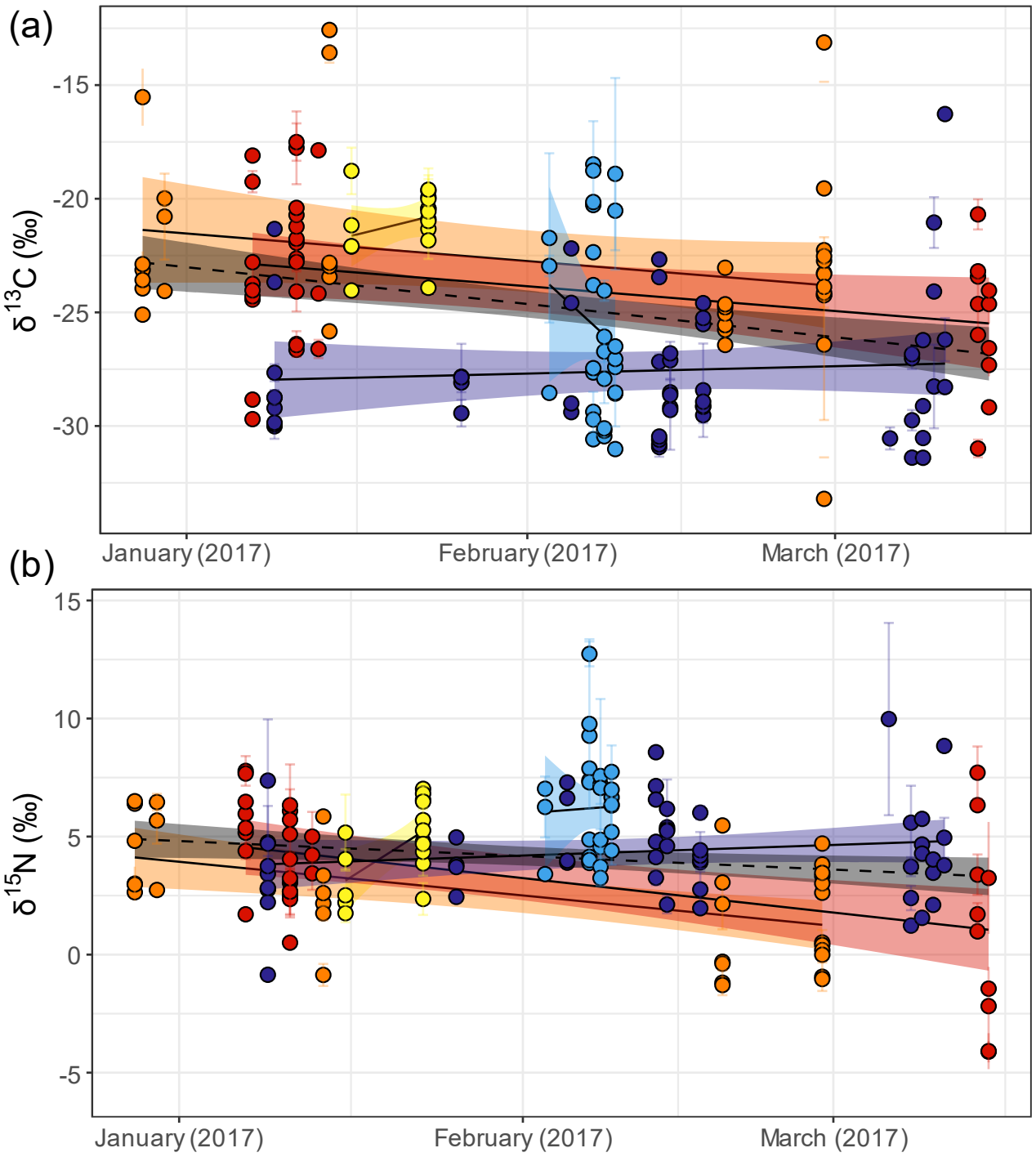

Figure 3.7 Temporal variability in (a) $\delta^{13}C$ [‰] and (b) $\delta^{15}N$ [‰] for zooplankton collected from the neuston layer during the Antarctic Circumnavigation Expedition. The coloured dots indicate the hydrographic zones: yellow = Subtropical Zone, orange = Subantarctic Zone, red = Polar Frontal Zone, dark blue = Southern Antarctic Circumpolar Current Zone, light blue = southern Boundary Zone. Linear regressions with 95% confidence intervals are shown for each hydrographic zone by the similarly coloured solid lines and shading, as well as for the whole ACE transect (dashed black line and grey shading).

3.4.5. Comparison of different baselines for zooplankton trophic analysis

While we ultimately used $\delta^{15}N_{SPM}$ as a baseline for our whole-Southern Ocean trophic analysis, we first compared the zooplankton TPs at seven stations on Leg1 (Figure 3.8) that were derived using five different baselines ($\delta^{15}N_{SPM}$, $\delta^{15}N_{new}$, diatom-$\delta^{15}N$, salp-$\delta^{15}N$, and copepods-$\delta^{15}N$; Table 3.4). Unsurprisingly, the derived TPs were dependent on the baseline used. For the same station (colours in Figure 3.8), the TPs calculated using different baselines (shapes in Figure 3.8) were offset by a constant value for all zooplankton specimens, with the magnitude of the offset changing between stations. At stations 2, 8, and 16, the diatom-$\delta^{15}N$ baseline gave the lowest TPs, with TPs calculated using the other baselines being higher by 0.3-2.2. At stations 21 and 22, the lowest TPs were obtained from the $\delta^{15}N_{new}$ baseline, with TPs derived using the other baselines being 0.4-1.9 units higher. Finally, at stations 19 and 20, the TPs were lowest when $\delta^{15}N_{SPM}$ was used as a baseline, with the other baselines yielding TPs that were 0.1-2.3 units higher. Across all the stations, the salp-$\delta^{15}N$ baseline generally yielded the highest TPs.

Table 3.4 $\delta^{15}N$ [‰] of the baselines used in the Leg1 trophic position comparison. The $\delta^{15}N_{SPM}$ and diatom-$\delta^{15}N$ are averages (± 1SD), $\delta^{15}N_{new}$ is a derived parameter and is therefore represented by only one value per station, the salp-$\delta^{15}N$ is the averaged value computed for all stations during all legs of the cruise at which Salpidae were collected, and copepods-$\delta^{15}N$ is the averaged $\delta^{15}N$ of the small Copepoda size class (i.e., mixed-copepods 200-500 µm; copepods-$\delta^{15}N$) observed at each station.

Station	diatom-$\delta^{15}N$	$\delta^{15}N_{SPM}$	$\delta^{15}N_{new}$	salp-$\delta^{15}N$	copepods-$\delta^{15}N$
16	2.9 ± 0.0	0.4 ± 0.7	-0.6	1.1 ± 1.4	4.4 ± 0.3
19	-1.6 ± 0.0	1.7 ± 0.2	1.4		2.8 ± 0.3
2	3.9 ± 0.1	0.8 ± 1.0	1.4		3.0 ± 0.4
20	0.5 ± 0.3	4.1 ± 5.9	-1.1		
21	0.5 ± 0.1	-1.7 ± 1.1	1.3		
22	0.6 ± 0.1	0.8 ± 1.1	3.3		2.2
8	3.5 ± 0.1	2.6 ± 1.9	-0.1		

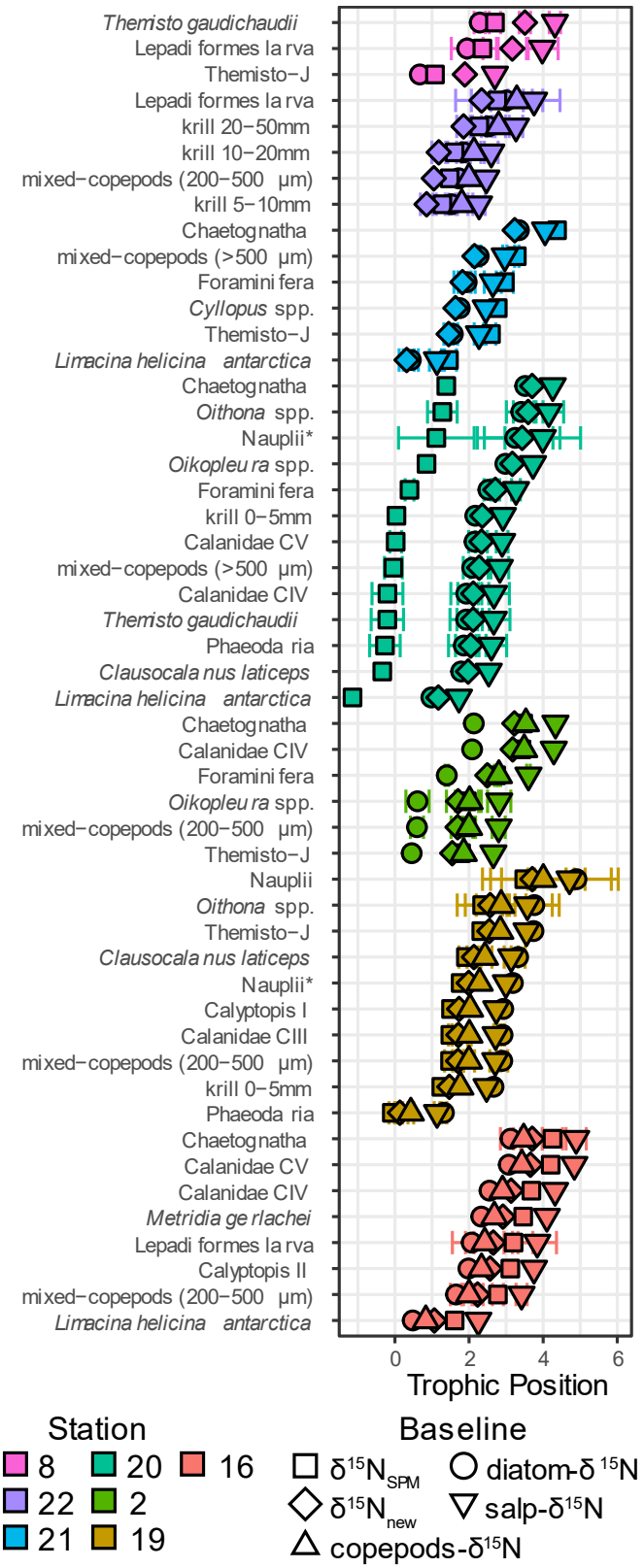

Figure 3.8 Comparison of zooplankton trophic positions derived using five different baselines at seven stations (colours) on Leg1 of the Antarctic Circumnavigation Expedition cruise. The baselines are indicated by the different symbol shapes: $\delta^{15}N_{SPM}$ (square), $\delta^{15}N_{new}$ (diamond), diatom-$\delta^{15}N$ (circle), salp-$\delta^{15}N$ (downward-triangle) and copepods-$\delta^{15}N$ (upward-triangle). The error bars show one standard deviation about the mean.

The lowest TPs derived for *Limacina helicina antarctica* (station 20) and Phaeodaria (station 19) were < 0 because the measured $\delta^{15}N$ of these organisms (0.5‰ and -0.9 ± 0.2‰, respectively) was lower than the average $\delta^{15}N$ of all the baselines at their respective stations (Table 3.4). This result suggests that these species consumed a food source that was particularly low in $\delta^{15}N$ (e.g., a specific fraction of the SPM rather than the bulk pool). Several other zooplankton TPs were < 2, which implies that these species occupied the same TP as the primary producers (TP=1) or that they, too, consumed a lower-$\delta^{15}N$ food source than represented by the baselines.

As result, our baseline comparison has not shown advantages or disadvantages in selecting one baseline over another one for determining the TPs of the zooplankton in the stations considered, suggesting that the SPM may be just as effective as the other four baselines here considered for trophic analysis (see section 3.5.2 for further discussion). For instance, we proceeded our analysis on isotope niche and trophic structure in zooplankton system using as baseline the parameter that was the most widely distributed and present along the transect, the $\delta^{15}N_{SPM}$. We also briefly discuss the trophic positions of zooplankton determined using the $\delta^{15}N_{new}$ as baseline (see section 3.5.2 and Appendix B).

3.4.6. Trophic analysis

3.4.6.1. Layman metrics and isotopic niches

We used Layman metrics to assess the isotopic niche differences among the hydrographic zones of the Southern Ocean inferred from the $\delta^{13}C$ and $\delta^{15}N$ of the SPM and the zooplankton. While we describe the isotopic niches implied by all the SPM samples (underway (UDW) + Neuston stations) in order to characterize the variability across the whole-Southern Ocean plankton system, we consider the SPM collected at the Neuston stations (i.e., coincident with the zooplankton samples) as a more accurate representation of the food source available to the zooplankton at the time of sampling.

The greatest similarity in SPM and zooplankton niches, indicated by overlap in the convex hulls, was observed for the hydrographic zones of the same ocean (i.e., the STZ, SAZ, and PFZ for the Subantarctic Ocean and the SACCZ and sBZ for the Antarctic Ocean; Figure 3.9a-c). This result reveals a distinct difference between the zooplankton niches of the Subantarctic *versus* the Antarctic Ocean, even if they

partially overlap (Figure B.2; Table B.5). A closer examination of the positions of each zone-hull indicates that the isotopic niches of the SPM and the zooplankton from the STZ and the SAZ are more distant from the niches in the SACCZ and the sBZ, while the PFZ niche falls between them (Figure 3.9a-b). If we consider only the SPM samples collected at the Neuston stations (Figure 3.9c), the difference in the $\delta^{13}C$-ranges of the Subantarctic *versus* the Antarctic is more evident because of the lesser overlap between hulls, suggesting distinct food sources to the zooplankton in these two regions (see below).

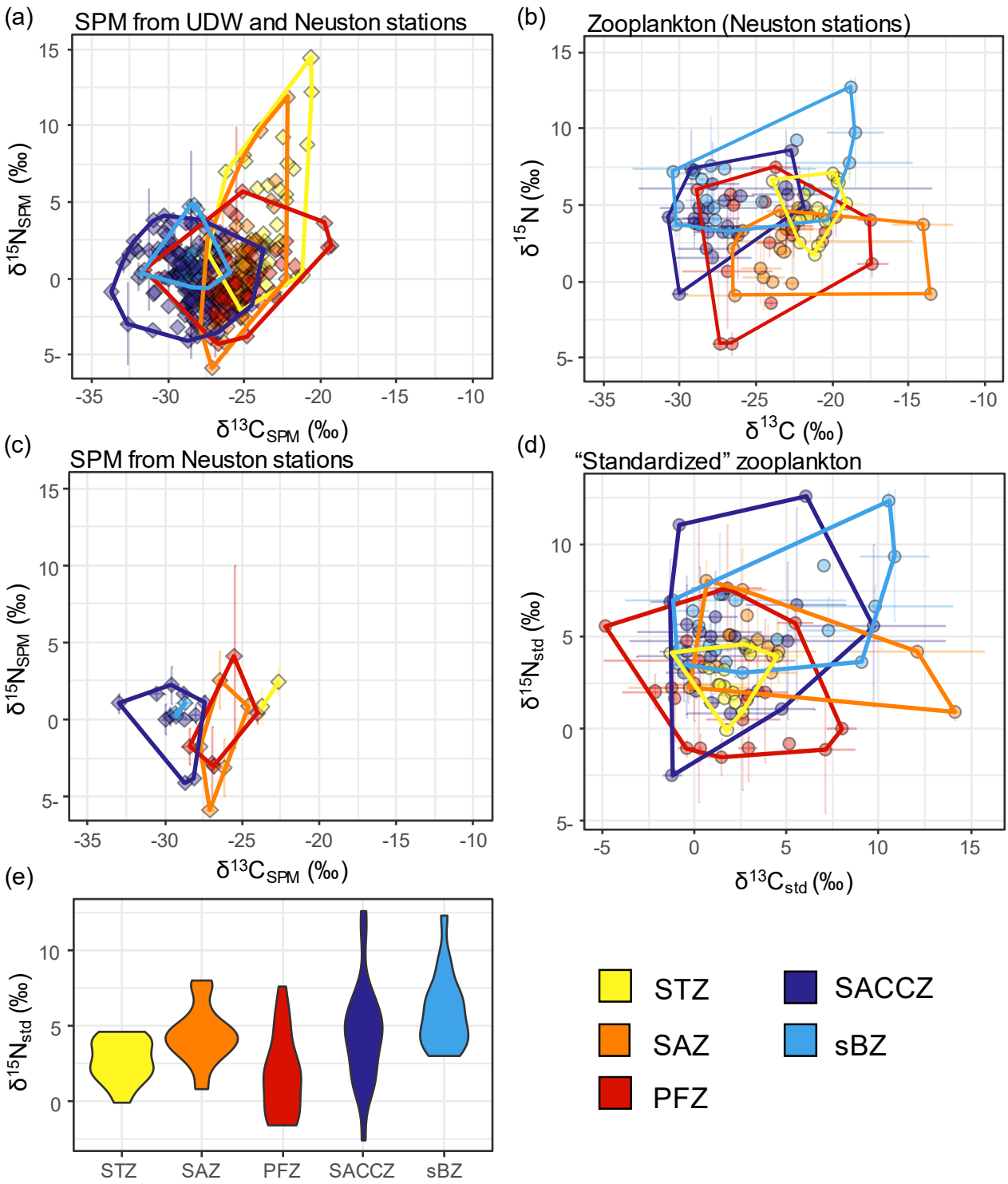

Figure 3.9 Isotopic niches based on Layman metrics analysis for (a) SPM collected from the ship's underway seawater supply (UDW), including at the Neuston stations (diamonds; n = 358), (b) zooplankton from the Neuston stations (circles; n = 91), and (c) SPM from the Neuston stations only (diamonds; n = 26). (d) Layman metrics calculated using standardized zooplankton $\delta^{13}C$ and $\delta^{15}N$ (where $\delta^{13}C_{std}$ = zooplankton $\delta^{13}C$ – $\delta^{13}C_{SPM}$ and $\delta^{15}N_{std}$ = zooplankton $\delta^{15}N$ – $\delta^{15}N_{SPM}$; ‰). In panels a-d, the solid lines show the convex hulls assessed from the Layman metrics analysis. Error bars show one standard deviation about the mean. (e) Density plot of zooplankton $\delta^{15}N_{std}$ (‰) in each hydrographic zone: yellow = Subtropical Zone (STZ), orange = Subantarctic Zone (SAZ), red = Polar Frontal Zone (PFZ), dark blue = Southern Antarctic Circumpolar Current Zone (SACCZ), and sBZ = southern Boundary Zone.

For the SPM (UDW + Neuston; Figure 3.9a), the δ^{15}N-range (defined as maximum δ^{15}N – minimum δ^{15}N) was greater for the Subantarctic zones (STZ = 16.6‰, SAZ = 17.7‰, PFZ = 9.9‰) than the Antarctic zones (SACCZ = 8.2‰, sBZ= 5.4‰; Figure 3.9a; Table 3.5). However, the total areas of the convex hulls were comparable (TA ranging between 58.5 and 67.6‰^{2}), except for the sBZ where the TA was only 17‰^{2}. The large δ^{15}N-range in the STZ is partly due to the higher $\delta^{15}N_{SPM}$ of the samples collected at the lowest latitudes, far north of the Neuston stations (Chapter 2).

For the zooplankton, STZ trophic diversity (i.e., δ^{15}N-range and δ^{13}C-range of 5.3‰ and 4.9‰, respectively, and TA of 15.2‰^{2}) was the lowest among the zones, indicating a limited diversity of food source(s) to STZ zooplankton compared to zooplankton in the SAZ, PFZ, SACCZ, and sBZ (Figure 3.9b; Table 3.5). In contrast, trophic diversity was the highest in the PFZ (i.e., δ^{15}N-range = 11.5‰, δ^{13}C-range = 11.6‰ and TA = 85.8‰^{2}; Figure 3.9b; Table 3.5). SAZ basal source diversity was the highest among the hydrographic zones (i.e., δ^{13}C-range = 12.9‰) indicating that primary producers were important for that zooplankton community, but much less trophic diversity was present along the vertical axis (as little diversity as in the STZ), lowering the overall trophic diversity (i.e., δ^{15}N-range and TA of 5.5‰, 62.4‰^{2}, respectively; Figure 3.9b; Table 3.5). At higher latitudes instead, niches at the SACCZ and sBZ had similar vertical structures (i.e., δ^{15}N-range of 9.4 and 9.5‰, respectively), but the SACCZ source diversity was 3.1‰ lower than in sBZ (i.e., δ^{13}C-range of 8.9 and 12.0‰, respectively) resulting in the second lowest trophic diversity among the zones (i.e., TA of 49.0 and 71.1‰^{2}, respectively; Figure 3.9b; Table 3.5).

Table 3.5 Layman metrics computed for the δ^{13}C and δ^{15}N of SPM collected from all underway (UDW) stations, zooplankton from the Neuston stations, SPM from the Neuston stations, and 'standardized zooplankton' in each hydrographic zone: STZ = Subtropical Zone, SAZ = Subantarctic Zone, PFZ = Polar Frontal Zone, SACCZ = Southern Antarctic Circumpolar Current Zone, and sBZ = southern Boundary Zone. δ^{15}N-range and δ^{13}C-range = distances between the two species with the most enriched and most depleted δ^{15}N or δ^{13}C values (e.g., maximum δ^{15}N – minimum δ^{15}N); TA = total area; MNND = mean nearest neighbour distance; SDNND = standard deviation of the nearest neighbour distance; std = values for 'standardized zooplankton'. UDW + Neuston stations = observations from both underway and stations coinciding with the Neuston stations.

Zone	δ^{15}N-range (‰)	δ^{13}C-range (‰)	TA (‰^{2})	CD (‰)	MNND (‰)	SDNND (‰)
			SPM (UDW + Neuston Stations)			
STZ	16.6	6.9	66.1	3.5	0.8	0.6
SAZ	17.7	5.7	58.7	2.3	0.5	0.5
PFZ	9.9	12.2	67.6	2.4	0.5	0.4
SACCZ	8.2	9.9	58.5	2.3	0.3	0.3
sBZ	5.4	5.9	17.0	1.5	0.5	0.5

			Zooplankton			
STZ	5.3	4.9	15.2	1.8	0.8	0.5
SAZ	5.5	12.9	62.4	3.2	1.5	1.3
PFZ	11.6	11.5	85.8	3.7	1.5	0.9
SACCZ	9.4	8.9	49.0	2.7	0.9	0.8
sBZ	9.5	12.0	71.1	4.4	1.6	0.9
			SPM (Neuston Stations)			
STZ	1.6	1.1		1.0	1.9	
SAZ	8.4	3.1	12.3	2.9	2.4	0.3
PFZ	7.1	4.4	14.3	2.9	2.0	1.9
SACCZ	6.3	5.6	18.8	2.1	0.9	0.6
sBZ	0.8	0.6	0.1	0.4	0.4	0.4
Zone	δ^{15}N-range$_{std}$ (‰)	δ^{13}C-range$_{std}$ (‰)	TA$_{std}$ (‰^{2})	CD$_{std}$ (‰)	MNND$_{std}$ (‰)	SDNND$_{std}$ (‰)
			Standardized zooplankton			
STZ	4.7	5.8	13.9	1.6	0.7	0.6
SAZ	7.1	14.4	58.2	3.2	1.2	1.2
PFZ	9.2	12.9	76.4	3.6	1.5	1.2
SACCZ	15.2	11.1	107.4	3.5	1.8	1.5
sBZ	9.3	12.0	70.5	4.3	1.6	1.0

Subtracting the $\delta^{13}C_{SPM}$ and $\delta^{15}N_{SPM}$ from the coincidently measured zooplankton $\delta^{13}C$ and $\delta^{15}N$ at the Neuston stations yields 'standardized' values of zooplankton $\delta^{13}C$ and $\delta^{15}N$ (i.e., $\delta^{13}C_{std}$ and $\delta^{15}N_{std}$; Figure 3.9d), which provide more insight into the influence of the SPM on the zooplankton food web structure (e.g., Black and Armbruster 2021). Compared to the original zooplankton analysis (Figure 3.9b), the convex hulls of the standardized isotopic niches overlap more, although differences between the Subantarctic and Antarctic remain consistent. The highest basal source diversity was found in the SAZ, followed by the PFZ (i.e., δ^{13}C-range$_{std}$ of 14.4 and 12.9‰, respectively), suggesting that communities from those zones depended on more primary producers than the zooplankton in the STZ, SACCZ and the sBZ. In contrast, the SACCZ and sBZ vertical trophic structures (i.e., δ^{15}N-range$_{std}$ of 9.3 and 15.2‰, respectively) were higher than the STZ, SAZ, and PFZ (even though the PFZ δ^{15}N-range$_{std}$ was relatively high; i.e., δ^{15}N-range$_{std}$ of 4.7, 7.1, and 9.2‰, respectively; Figure 3.9d; Table 3.5), suggesting that zooplankton consumers at higher latitudes belonged to more and higher trophic levels and the food chain was longer than at lower latitudes. In addition, the TAs of the standardized isotopic niches are similar to the original zooplankton TAs for all zones except the SACCZ where the TA was more than doubled (107.4‰^{2}), indicating that the SACCZ trophic diversity

was highest compared to any of the other hydrographic zones. Zooplankton niche in the STZ still showed the most limited isotopic diversity (i.e., δ^{15}N-range$_{std}$, δ^{13}C-range$_{std}$, and TA of 4.7‰, 5.8‰, and 13.9‰^{2}; Figure 3.9d; Table 3.5).

The $\delta^{15}N_{std}$ data distribution (Figure 3.9e) provides more insights into the vertical structure of a community. In addition to indicating that the SACCZ food chain was the longest among the zones (as shown by the high δ^{15}N-range$_{std}$; see above), our analysis revealed three other important results, all suggesting that the Antarctic zooplankton belonged to higher trophic levels than the Subantarctic consumers: 1) the mode of the zooplankton $\delta^{15}N_{std}$ in the SACCZ and the sBZ was roughly twice that in the STZ and PFZ (5.3‰ and 4.9‰ *versus* 1.4‰ and 1.3‰), while the $\delta^{15}N_{std}$ mode in the SAZ was comparable to the Antarctic zone modes (5.1‰); 2) the $\delta^{15}N_{std}$ of zooplankton in the SACCZ and the sBZ reached a maximum of 12.5‰, considerably higher than the maxima in the Subantarctic zones (4.6-8.0‰); and 3) most of the zooplankton in the sBZ were higher in $\delta^{15}N_{std}$ than most of the zooplankton in the Subantarctic zones.

3.4.6.2. Assessment of zooplankton trophic positions using SPM as the baseline

The average and median derived TPs derived for all zooplankton taxa appeared lower in the Subantarctic than the Antarctic (Figure 3.10 and Table 3.2); however, only the Chaetognatha, Copepoda, Euphausiacea, and Pteropoda TPs were significantly different between the two regions (pairwise Wilcoxon test, p-values < 0.05) as the number of specimens available for the other taxa was insufficient to warrant a reliable analysis. The Chaetognatha occupied the highest TP in both the Subantarctic (3.9 ± 1.3) and Antarctic Oceans (6.4 ± 0.2), with an Antarctic TP that was 2.5 positions higher than in the Subantarctic. In both oceans, the Phaeodaria TPs were <1, suggesting that these organisms occupy the same trophic level as the SPM and/or consume only a specific portion of the SPM.

The TPs of the various zooplankton species were also distinct among Southern Ocean zones (Figure 3.11, Table 3.3). In the STZ, the trophic structure ranged from Salpidae at a TP of 1.0 ± 0.3 to Chaetognatha at 2.9 ± 0.1 and *Physalia physalis* at 3.0 ± 0.1. In the SAZ, *Limacina helicina antarctica* occupied the lowest TP of 1.4 ± 1.4, with the Ostracoda and Chaetognatha occupying the highest TP (4.5 ± 0.5 and 4.3 ± 1.0, respectively). In the PFZ, C. laticeps, Phaeodaria and larger mixed-copepods (> 500µm) were at TP < 0, while several other species were associated with 0 < TP < 1, including the smaller krill (0-5 mm), *L. helicina*

antarctica, Foraminifera, *Vibilia antarctica*, *Cyllopus* spp.. In contrast, Chaetognatha occupied the highest TP (4.3 ± 1.5). In the SACCZ, Phaeodaria were the only taxon with a TP < 1 (-0.1 ± 0.1), the Salpidae had a TP of 1.3 ± 0.4, and an adult specimen from the Family Pontellidae (*sensu latu*) occupied the highest TP of 6.5. In the sBZ, the lowest TP was occupied by *Limacina retroversa* (2.3 ± 0.1) while the Chaetognatha were associated with the highest TP (6.4 ± 0.2).

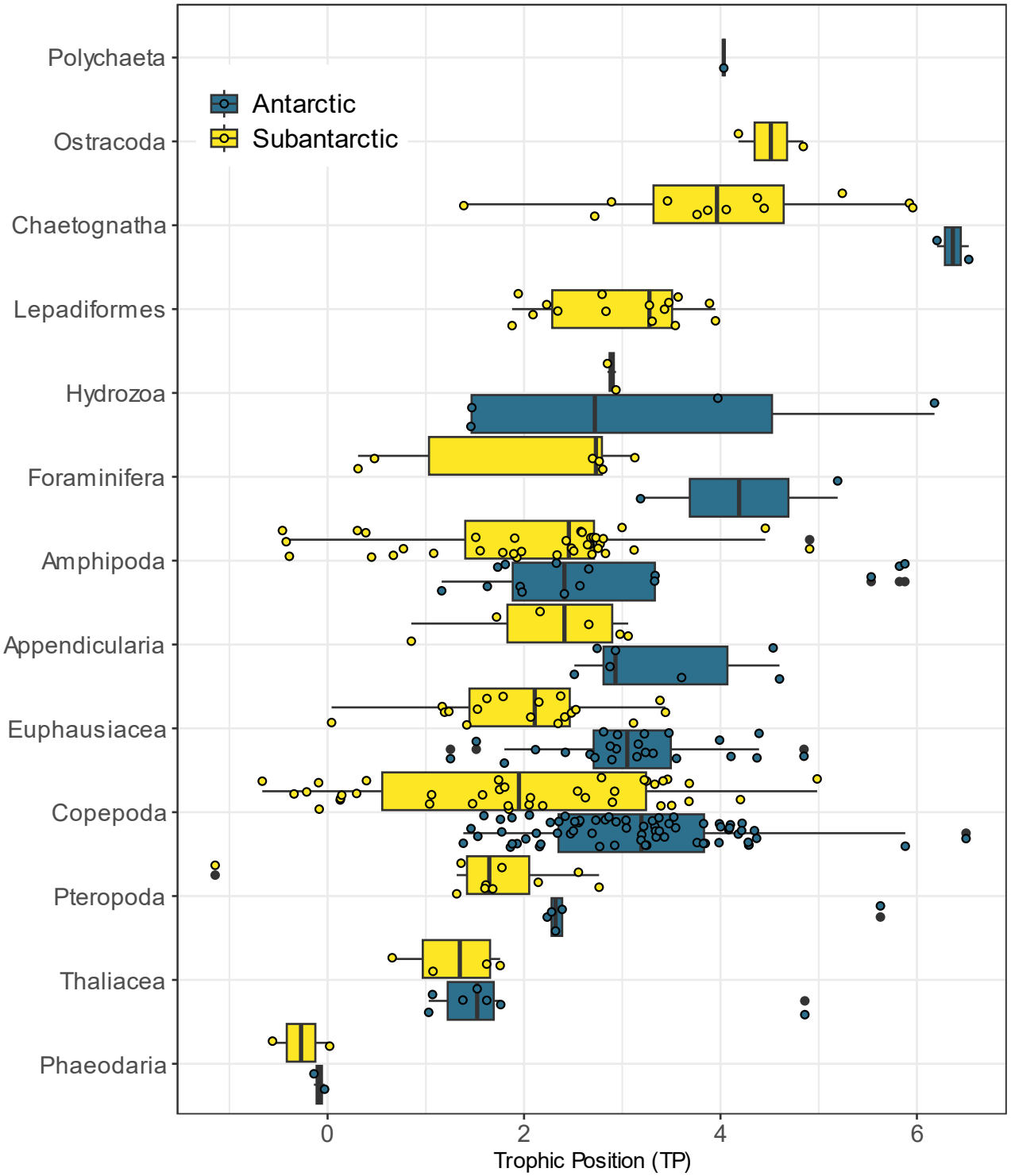

Figure 3.10 Boxplots of a) trophic positions derived using $\delta^{15}N_{SPM}$ as the baseline for zooplankton taxa (y-axis) collected across the Subantarctic (yellow) and Antarctic (blue) Oceans during the Antarctic Circumnavigation Expedition. Taxa have been ordered from the most isotopically-deplete to the most isotopically-enriched, as measured for the Subantarctic samples. Boxplots show medians (thick vertical lines), interquartile range (IQR = 50% of the data; box within first and third quartiles), and whiskers (1.5 times the IQR). The black dots indicate outliers.

Figure 3.11 Average trophic positions derived using $\delta^{15}N_{SPM}$ as the baseline for zooplankton taxa (y-axis) collected during the Antarctic Circumnavigation Expedition in each hydrographic zone (colours): yellow = Subtropical Zone (STZ), orange = Subantarctic Zone (SAZ), red = Polar Frontal Zone (PFZ), dark blue = Southern Antarctic Circumpolar Current Zone (SACCZ), and light blue = southern Boundary Zone (sBZ). Taxa have been ordered from the most isotopically-deplete to the most isotopically-enriched in each zone. The error bars indicate one standard deviation about the mean.

3.4.7. Influence of the island mass effect on zooplankton stable isotopes and trophic structure

A comparison between the $\delta^{13}C$ and $\delta^{15}N$ of bulk zooplankton collected near the islands (9 stations) and zooplankton $\delta^{13}C$ and $\delta^{15}N$ at open water stations (19) reveals no significant geographic differences (t-test, *p*-values > 0.1; $\delta^{13}C$ = -25.2 ± 3.7‰ [$-25.1^{-23.0}_{-28.6}$‰] near the islands and -24.4 ± 4.2‰ [$-24.0^{-21.4}_{-27.5}$‰] in the open ocean, and $\delta^{15}N$ = 4.2 ± 2.7‰ [$4.5^{5.9}_{2.8}$‰] near the islands and 3.8 ± 2.7‰ [$3.9^{5.3}_{2.2}$‰] in the open ocean). When grouping the data by hydrographic zone, the only significant difference was for $\delta^{15}N$ in the PFZ, with a near-island zooplankton $\delta^{15}N$ ($5.6^{6.7}_{4.5}$‰) that was higher (pairwise t-test, *p*-value = 0.03) than that in the open ocean stations ($3.2^{4.2}_{1.6}$‰; Table 3.6).

For the Layman metrics analysis of bulk zooplankton data grouped by hydrographic zone, the convex hulls overlapped for the island and open ocean data (Figure B.3). In each zone, the island and open ocean $\delta^{13}C$-ranges were similar, as was also the case for the $\delta^{15}N$-ranges except in the PFZ where the island $\delta^{15}N$-range was narrower than the open ocean range (Table B.6).The median TPs varied among island stations, ranging from $2.2^{2.8}_{1.8}$ at the Prince Edward Islands to $4.6^{5.3}_{4.0}$ at the South Sandwich Islands (Table 3.7; Figure B.4). Grouping by hydrographic zone shows no significant differences between the zooplankton TPs at the islands and the ones at the open ocean (pairwise t-test, p-values > 0.8 for STZ, SAZ, PFZ, SACCZ; Wilcox test, p-values = 0.5 for sBZ; Figure 3.12, Table 3.6).

Table 3.6 Median (± IQR) $\delta^{13}C$ [‰], $\delta^{15}N$ [‰], and trophic position (TP) of zooplankton collected from the neuston layer near the islands and at open ocean stations in each hydrographic zone during the Antarctic Circumnavigation Expedition: STZ = Subtropical Zone, SAZ = Subantarctic Zone, PFZ = Polar Frontal Zone, SACCZ = Southern Antarctic Circumpolar Current Zone, and sBZ = southern Boundary Zone. The numbers in parentheses indicate the number of observations.

Zone	Region	$\delta^{13}C$ (‰)	$\delta^{15}N$ (‰)	TP
STZ	Islands	-	-	-
	Open Ocean	-20.7 ± 1.7 (38)	4.4 ± 3.2 (37)	2.1 ± 0.9 (37)
SAZ	Islands	-23.9 ± 2.4 (29)	2.9 ± 5.4 (27)	2.9 ± 1.2 (27)
	Open Ocean	-23.1 ± 1.6 (39)	2.0 ± 2.8 (37)	2.6 ± 0.7 (29)
PFZ	Islands	-23.9 ± 3.9 (14)	5.6 ± 2.2 (12)	3.2 ± 1.0 (12)
	Open Ocean	-23.9 ± 5.1 (56)	3.2 ± 2.7 (53)	1.1 ± 1.9 (46)
SACCZ	Islands	-28.0 ± 2.6 (22)	5.3 ± 2.3 (22)	3.2 ± 1.4 (22)
	Open Ocean	-28.8 ± 3.1 (68)	3.8 ± 2.0 (64)	2.2 ± 1.8 (64)
sBZ	Islands	-23.3 ± 1.7 (5)	6.9 ± 1.8 (5)	4.0 ± 0.8 (5)
	Open Ocean	-27.1 ± 7.0 (47)	6.3 ± 2.9 (46)	3.3 ± 1.4 (46)

Table 3.7 Median (± IQR) $\delta^{13}C$ [‰], $\delta^{15}N$ [‰], and trophic position (TP) of zooplankton collected in neuston layer in the vicinity of the several islands investigated during the Antarctic Circumnavigation Expedition. The numbers in parentheses indicate the number of observations.

Island	Station	$\delta^{13}C$ (‰)	$\delta^{15}N$ (‰)	TP
Prince Edward Island	2	-23.6 ± 1.2 (10)	3.5 ± 2.2 (9)	2.2 ± 1.0 (9)
Crozet Island	8	-20.4 ± 2.4 (6)	5.9 ± 1.6 (6)	2.5 ± 0.7 (6)
Kerguelen Island	16	-23.9 ± 3.9 (14)	5.6 ± 2.2 (12)	3.2 ± 1.0 (12)
Balleny Island	43	-23.3 ± 1.7 (5)	6.9 ± 1.8 (5)	4.0 ± 0.8 (5)
Scott Island	49	-24.6 ± 6.8 (5)	4.0 ± 2.7 (5)	4.4 ± 1.2 (5)
Peter 1st Island	68	-28.1 ± 1.8 (11)	5.3 ± 0.4 (11)	3.2 ± 0.2 (11)
Diego Ramirez Islands	73	-25.3 ± 0.9 (13)	-0.4 ± 2.7 (12)	3.4 ± 1.2 (12)
South Sandwich Island	88	-30.5 ± 0.3 (2)	10.0 ± 2.9 (2)	4.6 ± 1.3 (2)
Bouvet Island	94	-26.2 ± 4.0 (4)	5.0 ± 2.2 (4)	2.7 ± 0.9 (4)

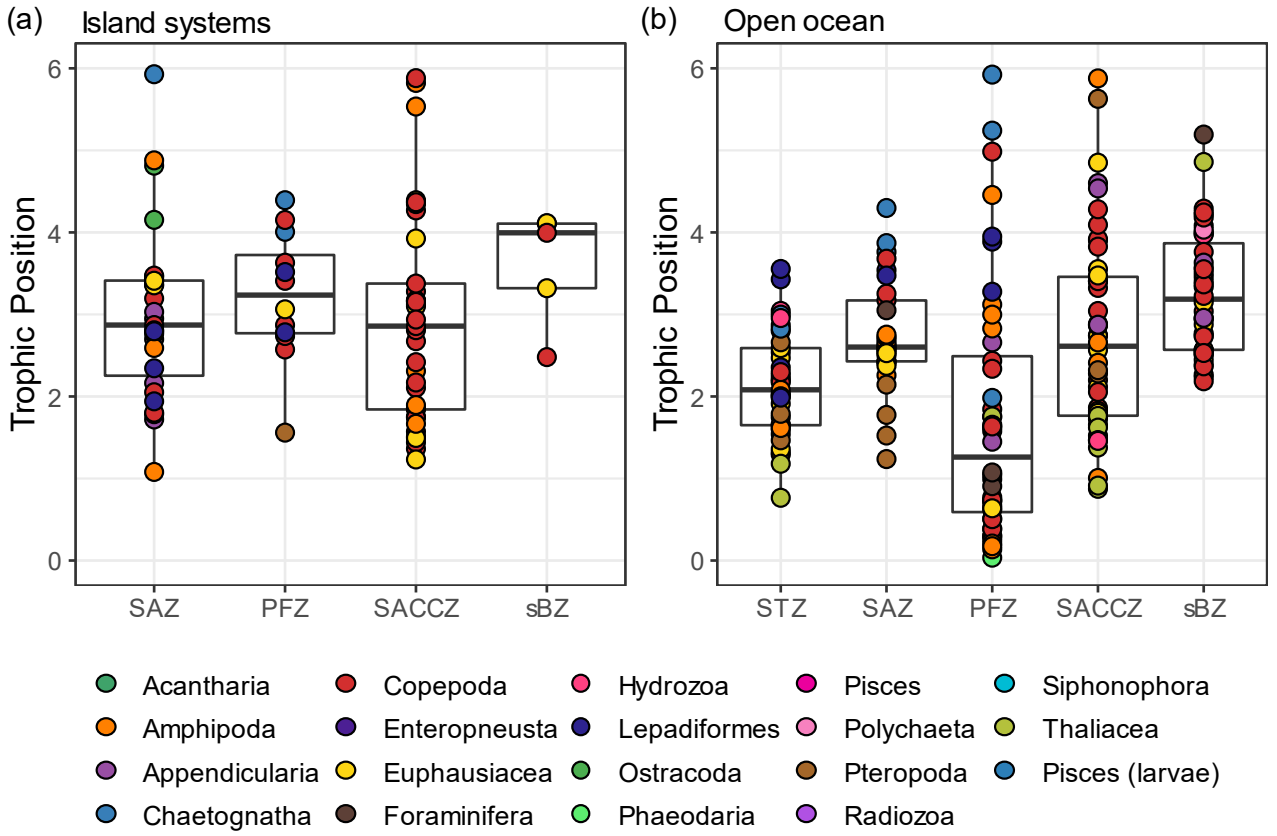

Figure 3.12 Boxplots of zooplankton trophic positions derived using $\delta^{15}N_{SPM}$ as the baseline for samples collected a) near the islands and b) at the open ocean stations in each hydrographic zone during the Antarctic Circumnavigation Expedition: STZ = Subtropical Zone, SAZ = Subantarctic Zone, PFZ = Polar Frontal Zone, SACCZ = Southern Antarctic Circumpolar Current Zone, and sBZ = southern Boundary Zone. The coloured symbols show the different zooplankton taxa while the boxplots show the median (thick horizontal lines), interquartile range (IQR = 50% of the data; box within first and third quartiles), and whiskers (1.5 times the IQR) for each zone.

3.5. Discussion

3.5.1. Zooplankton $\delta^{13}C$ and $\delta^{15}N$ vary with $\delta^{13}C_{SPM}$ and $\delta^{15}N_{SPM}$ across Southern Ocean zones

We observed strong opposing latitudinal gradients in zooplankton $\delta^{13}C$ and $\delta^{15}N$ across the summertime Southern Ocean. Zooplankton $\delta^{13}C$ decreased by ~10‰ from the STZ to the SACCZ, before increasing again by ~2.5‰ in the sBZ (Table 3.1 and Figure 3.4c-f). In contrast, zooplankton $\delta^{15}N$ increased by ~4‰ from the SAZ to the sBZ, with similarly high values in the STZ as in the PFZ and the SACCZ. This trend is consistent with the findings of Richoux and Froneman (2009) of a higher zooplankton $\delta^{15}N$ (by ~4‰) in the STZ than the SAZ in the Indian sector of the Southern Ocean. Our results are also aligned with the findings of Brault *et al.* (2018) who observed strong gradients in zooplankton $\delta^{15}N$ and $\delta^{13}C$ for samples (with lipid extraction) collected in the austral summer from the eastern Ross Sea, along the coast of Antarctica to the West Antarctic Peninsula, and across the Drake Passage to South America. Zooplankton $\delta^{15}N$ was significantly higher in the Ross Sea and Amundsen Sea (6.2 ± 0.8‰) than in the SACCZ (3.7 ± 0.6‰) and the PFZ/SAZ (3.3 ± 0.6‰), while zooplankton $\delta^{13}C$ increased with decreasing latitude, from a minimum in the Ross Sea (−27.5 ± 1.6‰) to a maximum in the PFZ/SAZ (−24.2 ± 0.9‰; Brault *et al.* 2018). Across the Scotia Sea (south of the APF) in the austral summer, Stowasser *et al.* (2012) measured zooplankton $\delta^{13}C$ and $\delta^{15}N$ (without lipid extraction) that varied from -30.5‰ to -16.4‰ and 2.7‰ to almost 10‰, respectively. We measured a similar range in zooplankton $\delta^{13}C$ across the Antarctic Ocean, while the lower end of our zooplankton $\delta^{15}N$ range was <-5‰. Finally, Yang *et al.* (2021) recently developed the first summer isoscapes of Euphausiacea (without lipid extraction) at the circumpolar scale, reporting higher $\delta^{13}C$ and $\delta^{15}N$ values for *Euphausia superba* in the Pacific and Atlantic sectors (-28.5‰ to -24.0‰ and 3.0‰ to 6.0‰, respectively) compared to the western and eastern Indian sector (-30.0‰ to -27.0‰ and 2.0‰ to 3.5‰, respectively).

Along the ACE transect, the $\delta^{13}C_{SPM}$ decreased southward by ~12‰ from the STZ to the Antarctic Ocean, reaching a minimum at 55°S-60°S coincident with the upwelling of Upper Circumpolar Deep Water (UCDW). At the same time, the $\delta^{15}N_{SPM}$ decreased by ~3‰ from the STZ to the SAZ and the PFZ where it reached a minimum, before gradually increasing across the Antarctic Ocean by ~1.4‰ (Figure 3.4a-b; see Chapter 2). The spatial gradients in $\delta^{13}C_{SPM}$ and $\delta^{15}N_{SPM}$ were broadly reflected in the spatial gradients in

zooplankton $\delta^{13}C$ and $\delta^{15}N$ (Figures 3.1c-f, 3.4a-d, and B.5), consistent with the fundamental principle that the isotopic composition of the main food source to an ecosystem (i.e., SPM) will be reflected in the $\delta^{13}C$ and $\delta^{15}N$ of the first consumers (i.e., zooplankton) and will propagate up the food web through several trophic levels (i.e., "you are what you eat plus a few *per mille*"; DeNiro and Epstein 1978, 1981). Propagation of the isotopic signature of SPM to zooplankton can also explain the apparently anomalous isotopic variability observed in two specific regions: 1) the zone of minimum zooplankton $\delta^{13}C$ and $\delta^{15}N$ at 55°S-60°S coincides with lower $\delta^{13}C_{SPM}$ and $\delta^{15}N_{SPM}$, the latter set by the upwelling of UCDW that brings a high concentration of DIC and NO_3^- to the surface that are relatively low in $\delta^{13}C$ and $\delta^{15}N$ (Chapter 2); and 2) near the islands, where the $\delta^{13}C$ and $\delta^{15}N$ of zooplankton are higher than in the surrounding open waters (e.g., at the Prince Edward Islands, Kerguelen Island, and the South Sandwich Islands; Figure 3.1e-f and Table 3.4), and the input of upwelled and/or land-derived nutrients (i.e., iron) stimulate diatom productivity, which manifests in elevated $\delta^{13}C_{SPM}$ and $\delta^{15}N_{SPM}$ (Chapter 2).

In addition, we suggest that isotopic propagation from the SPM to the zooplankton occurred over the three months of the investigation, with changes in $\delta^{13}C_{SPM}$ and $\delta^{15}N_{SPM}$ over time driving the decrease in zooplankton $\delta^{13}C$ and $\delta^{15}N$ in the SAZ and the PFZ and the increase in the SACCZ (Figure 3.7, Figure B.1, and Table B.4). In Chapter 2, we suggested that the decline in $\delta^{13}C_{SPM}$ and $\delta^{15}N_{SPM}$ in the Subantarctic from early to late summer is attributed to a decrease in phytoplankton productivity and nitrate uptake driven by seasonal iron limitation, accompanied by a shift in the autotrophic community towards (mainly non-diatom) nano-phytoplankton and the upregulation of the microbial loop. In contrast, the $\delta^{15}N_{SPM}$ increase with time in the SACCZ can be explained by regional factors such as proximity to the many island systems encountered during the latter half of Leg3 (Chapter 2). This seasonal rise in $\delta^{15}N_{SPM}$, and in the drivers thereof, likely explains the temporal increase in zooplankton $\delta^{15}N$ in the SACCZ (Figure B.1i).

The difference between the median $\delta^{13}C$ of zooplankton and the median $\delta^{13}C_{SPM}$ (= 2.7‰, 2.0‰, 2.1‰, 0.1‰, and 1.3‰, respectively, for the STZ, SAZ, PFZ, SACCZ, and sBZ) was generally smaller than the difference between the $\delta^{15}N$ of zooplankton and the $\delta^{15}N_{SPM}$ (= 2.6‰, 2.8‰, 4.2‰, 3.8‰, and 5.7‰), consistent with the fact that the mean trophic enrichment factor for $\delta^{13}C$ is smaller than for $\delta^{15}N$ (i.e., 1‰ and 2.3‰, respectively; DeNiro and Epstein 1978, 1981; McCutchan Jr *et al.* 2003). That we compute higher

$\delta^{13}C$ and $\delta^{15}N$ differences between the zooplankton and SPM than the trophic enrichment factors determined by McCutchan Jr *et al.* (2003) and Schwamborn and Giarrizzo (2015) can be attributed to the fact that the median isotopic ratios determined for the bulk zooplankton include organisms occupying a variety of trophic positions, many of which are higher than that of the primary consumer.

It could be argued that our observations of zooplankton $\delta^{13}C$ and $\delta^{15}N$ are influenced by species richness and composition of the zooplankton community and thus by our ability to collect and/or consider particular specimens (and inability to consider others) during our analysis. However, our findings suggest that variability in the $\delta^{13}C$ and $\delta^{15}N$ of zooplankton in the neuston layer, as well as in their trophic positions, is unlikely to be driven by changes in zooplankton composition only since, even when examined at the lowest taxonomic levels of genus and species, the $\delta^{13}C$ and $\delta^{15}N$ of the zooplankton groups followed the same trends in space and time as the bulk community (Figure 3.4, 3.6 and 3.7; Figure B.5).

3.5.2. SPM can be used as a baseline in trophic analysis over a large spatial scale

Above, we used five different baselines to derive the TPs of zooplankton: measured surface $\delta^{15}N_{SPM}$, $\delta^{15}N_{new}$ calculated using an amended version of the Rayleigh model (Chapter 2), measured diatom-$\delta^{15}N$, and the measured $\delta^{15}N$ of two primary consumers, Salpidae (salp-$\delta^{15}N$) and the smaller size class of Copepoda (copepods-$\delta^{15}N$). While $\delta^{15}N_{SPM}$ is the most commonly used baseline for TP analysis, its reliability is widely debated (e.g., Cherel *et al.* 2008; Stowasser *et al.* 2012; Pakhomov *et al.* 2019 and references therein). SPM is a complex mixture of particles that may include bacteria, detritus, and zooplankton in addition to the phytoplankton that form the base of the food web. In addition, the short (hourly to daily) turnover rates of carbon and nitrogen isotopes in phytoplankton cells means that phytoplankton (i.e., SPM) $\delta^{13}C$ and $\delta^{15}N$ represent a near-instantaneous measure of the local oceanographic conditions, such as nutrient availability (Aberle and Malzahn, 2007; Treibergs *et al.*, 2014), temperature, and CO_2 concentrations (Goericke and Fry, 1994), while the longer (weekly to monthly) turnover time of zooplankton tissue means that these organisms do not have time to mirror such 'instant' isotopic variations (e.g., O'Reilly *et al.* 2002; Schmidt *et al.* 2006; Hannides *et al.* 2009).

To resolve these issues, several researchers have suggested using Salpidae (primary consumers) as baseline surrogates instead of SPM (Cherel *et al.*, 2008; Richoux and Froneman, 2009; Stowasser *et al.*, 2012; Ménard *et al.*, 2014). However, Salpidae may reflect specific food chains only because they selectively prey on bacteria, ciliates, and autotrophic and heterotrophic dinoflagellates (Vargas and Madin, 2004; Sutherland *et al.*, 2010; Pakhomov *et al.*, 2019; Pauli *et al.*, 2021). Indeed, Pakhomov *et al.* (2019) concluded that Salpidae (Tunicata in general) may be a promising baseline surrogate for the food webs of which they form an integral part (i.e., food webs in which they are consumed) but will be 'erroneous' surrogates in other (e.g., crustacean-dominated) food webs. In the latter case, using Salpidae as a baseline surrogate may result in progressively increasing uncertainty associated with the derived TPs of higher-order consumers. Instead, the authors suggested that herbivorous Copepoda (i.e., other primary consumers more commonly consumed by higher consumers) would be a more appropriate baseline surrogate, also because they are usually ubiquitous and omnipresent.

Although some specimens showed herbivorous behaviour in specific hydrographic zones, our analysis suggests that no species of Copepoda were strictly herbivorous in all Southern Ocean zones (Table B.7). This result may however be due to our Neuston net collections lacking sufficient material to allow for detection of herbivorous Copepoda such as *Calanoides acutus* and possibly *Rhincalanus gigas* (Graeve *et al.*, 1994). The few specimens of *Calanoides* spp. that were collected in the SACCZ and sBZ only occupied TPs of 4.2 ± 0.1 and 2.6, respectively, indicating carnivorous and/or omnivorous behaviour, while adults of *Calanus* spp. were assigned a TP of 3.8 ± 0.6 in the sBZ, characterizing them as predators. In other words, under certain environmental conditions, *Calanoides* spp. and *Calanus* spp. should be considered opportunistic feeders, able to switch their diets according to the available food source present at the time and/or in a particular region or depth of their environment. In contrast, *Oithona* spp. emerged as herbivorous in the PFZ (TP of 1.9 ± 0.4) and herbivorous/omnivorous in the SACCZ (TP of 2.3 ± 0.7). A similar signal was detected in the smaller class of Copepoda (i.e., mixed-copepods; comprising mainly Oithonidae and Oncaeidae), which occupied a TP of 2-2.5 in all hydrographic zones but the sBZ where they were associated with a TP of 3.3 ± 0.8. This finding supports the idea that pure herbivory does not exist among Copepoda due to their feeding modes (Atkinson *et al.*, 2012a). Some Copepoda species (e.g., Calanoides acutus; not collected in this study) are often considered herbivorous (Graeve *et al.*, 1994), but they are actually suspension-feeders that capture

any particle near their mouthparts, including algae, microzooplankton, and micrometazoa (Atkinson *et al.*, 2012a and references therein). They differ from other feeding modes such as raptorial, cruising or ambush feeding that target more motile and animal-like prey, as seen in Eucheatidae, Metridinidae and Oithonidae (Atkinson *et al.*, 2012a and references therein). That said, if exclusively herbivorous Copepoda do not exist, they are unlikely to be an appropriate baseline surrogate.

Within each station, each baseline returned the same trophic order for the zooplankton species but with different TPs, although the difference was always ≤2 positions (Figure 3.8). However, the difference between TPs was not constant among baselines, with a particular baseline in some instances yielding a lower TP and in other instances a higher TP than the position suggested by a different baseline. For example, the TPs derived using salp-$\delta^{15}N$ were the highest (by 0.5-2 positions) at four of the seven stations, while the TPs suggested by $\delta^{15}N_{SPM}$ and diatom-$\delta^{15}N$ were often, although not always, the lowest. As such, we cannot evaluate the reliability of one baseline relative to the others, the implication of which is that the TPs of zooplankton may be over- or underestimated depending on the chosen baseline. Without a measure of the 'true TP, it is arguably impossible to denote one baseline as more appropriate than the others. Nonetheless, this comparative exercise yields a number of important insights.

First, it would be advisable to use diatom-$\delta^{15}N$ as a baseline if diatoms were the only food source available to zooplankton. However, the trophic behaviours of many zooplankton (e.g., Copepoda) are still uncertain and unpredictable (e.g., Atkinson 1995; Schmidt *et al.* 2003; Atkinson *et al.* 2012; Pauli *et al.* 2021). In addition, our results suggest that omnivory is widespread (see section 3.4.3), such that using diatom-$\delta^{15}N$ as a baseline, particularly for analysis of our Antarctic Ocean dataset, is not advisable.

Second, to the best of our knowledge, this is the first time a derived theoretical parameter (i.e., $\delta^{15}N_{new}$, the SPM produced as a result of nitrate assimilation) has been applied as a baseline for assessing the TPs of zooplankton. As for the other baselines, the results obtained using $\delta^{15}N_{new}$ were variable. However, since an estimate of $\delta^{15}N_{new}$ is available for all the Neuston stations, we can compare the $\delta^{15}N_{new}$- *versus* $\delta^{15}N_{SPM}$-derived TPs for the entire Southern Ocean. For the same species, the TPs computed using $\delta^{15}N_{new}$ were generally lower than or similar to those derived using $\delta^{15}N_{SPM}$, except in the PFZ (Figure B.6; Table B.7). The resulting variance between the two derived TPs (σ^2TPs) was lowest in the STZ and the sBZ (0.5 and 0.2,

respectively), as well as for most of the SACCZ TPs (total σ^2 TPs = 0.7, with σ^2TPs increasing as the TP increased), while the variances in the SAZ and the PFZ were higher (1.8 and 2.2, respectively). This finding suggests that assimilation by phytoplankton may not be a dominant process acting on the surface nitrate pool across the summertime SAZ and PFZ. The Rayleigh model assumes a closed system with no nitrate resupply (Mariotti *et al.*, 1981; Sigman *et al.*, 1999); if this condition is violated (e.g., due to upwelling and/or vertical or lateral mixing), then the $\delta^{15}N$ of the biomass actually produced from nitrate assimilation could be considerably lower than that predicted by $\delta^{15}N_{new}$. This scenario may explain some of our PFZ data. By contrast, in the SAZ, nitrate assimilation may not have exerted the dominant control on $\delta^{15}N_{SPM}$. Indeed, in Chapter 2 I concluded that the consumption of high-$\delta^{15}N$ ammonium derived from guano and other higher-trophic-level organic matter (Mizutani *et al.* 1986; Wainright *et al.* 1998) that was supplied from land near the islands (e.g., the Prince Edward, Crozet, Kerguelen, and Heard Islands) may account for observations of $\delta^{15}N_{SPM}$ that were significantly higher than the $\delta^{15}N_{new}$ assessed with the Rayleigh model (Chapter 2). In summary, our analysis showed that $\delta^{15}N_{new}$ worked as well as $\delta^{15}N_{SPM}$ as a baseline in those hydrographic zones governed by more stable biogeochemical processes, while in those regions affected by island inputs and/or enhanced mixing, $\delta^{15}N_{SPM}$ is likely a more appropriate baseline.

Finally, our findings suggest that $\delta^{15}N_{SPM}$ can be used as a baseline at the scale of the Southern Ocean hydrographic zones because the large-scale variability in zooplankton $\delta^{15}N$ (and $\delta^{13}C$) followed the trends in $\delta^{15}N_{SPM}$ (and $\delta^{13}C_{SPM}$), both geographically and temporally (see section 3.5.1). This observation strongly implies that the SPM is a reasonable representation of the average food source available to zooplankton. However, we do not recommend using $\delta^{15}N_{SPM}$ at smaller spatial scales (i.e., station level). It is possible that in these cases, Salpidae may be a more appropriate baseline surrogate since our analysis indicates that they were the primary consumers (Pakhomov *et al.* 2019); however, we could not investigate their TP in the food web sufficiently to draw any strong conclusion regarding the utility of salp-$\delta^{15}N$.

3.5.3. The Subantarctic and Antarctic Oceans are characterized by distinct plankton ecological niches

This study assessed for the first time at the spatial extent of the entire Southern Ocean, the isotopic niches and trophic structure of the zooplankton systems across hydrographic zones. The Layman metrics analysis indicates a clear distinction between the respective plankton food webs of the Subantarctic and Antarctic Oceans, with the PFZ emerging as an isotopic divide between these two regions (Figure 3.4). The different $\delta^{13}C$ values of the convex hulls in the various zones suggest a major shift in the plankton food source from the Subantarctic to the Antarctic Ocean, consistent with the $\delta^{13}C_{SMP}$ data, while the different $\delta^{15}N$ values indicate a difference in the mean trophic positions of the zooplankton communities (Figure 3.9a-c). These isotopic signals propagate up the food web, yielding two major zooplankton niches, evident in the isotope distributions (Figure B.5a) and the only partial overlap of the convex hulls derived for the Subantarctic and Antarctic Oceans (Figure B.2).

It is possible that latitudinal gradients in SST and pCO_2 affected phytoplankton carboxylation rates and thus the $\delta^{13}C_{SPM}$ (O'Leary 1981; Fry and Sherr 1989; St John Glew *et al.* 2021; Chapter 2). At the same time, Chapter 2 I observed a meridional shift in the size distribution of the phytoplankton community, from a predominance of nano-phytoplankton in the Subantarctic to micro-phytoplankton in the Antarctic Ocean. Furthermore, the Subantarctic Ocean was dominated by dinoflagellates (e.g., *Ceratium* spp.) and diatoms (e.g., *Fragilariopsis* spp.) whereas at higher latitudes, diatoms such as *Chaetoceros* spp. and *Fragilariopsis* spp. proliferated. These different phytoplankton communities may have implications for food availability, thus altering zooplankton grazing and competition behaviours, while the top-down control by zooplankton grazing will have simultaneously influenced the abundance, composition, and distribution of the phytoplankton community (Smetacek *et al.*, 2004; Smith and Lancelot, 2004; Atkinson *et al.*, 2012a). Layman *et al.* (2012) note that isotopic (dis)similarity does not necessarily mean ecological (dis)similarity, as two individuals can occupy the same isotopic niche but distinct ecological niches. For the Southern Ocean, we hypothesize that the hydrographic conditions (e.g., SST, pCO_2, and nutrient availability) and phytoplankton community composition were equally responsible for setting the $\delta^{13}C_{SPM}$, which was then transferred to the zooplankton. As such, the different isotopic niches observed for the zooplankton communities of the Subantarctic and Antarctic Oceans are at least partly attributable to their distinct

ecological niches, with the zooplankton communities of these two major ocean regions relying on different phytoplankton food sources.

This idea of two distinct ecological niches is supported by the difference in trophic variability that we detected between the Subantarctic and Antarctic Oceans. Overall, the zooplankton niche in the Antarctic Ocean (SACCZ + sBZ) had a wider δ^{15}N-range and greater trophic diversity than that of the Subantarctic Ocean (δ^{15}N-ranges of 13.6‰ and 11.1‰, and TA of 105.1 and 77.2‰^{2}, respectively; Table B.5). Furthermore, by removing the isotopic signals of the SPM from the zooplankton (i.e., $\delta^{13}C_{std}$ and $\delta^{15}N_{std}$) we show that, in addition to the variability induced by baseline shifts (i.e., $\delta^{13}C_{SPM}$ and $\delta^{15}N_{SPM}$), the zooplankton niches in the Subantarctic and Antarctic Oceans differed in their ecological structure insofar as trophic diversity is represented by the size of the convex hulls (Figure 3.9d; Table 3.5). Trophic diversity was lowest in the STZ (TA_{std} = 13.9‰^{2}; Table 3.5), indicating a more homogeneous trophic structure and less variable food source than in the SAZ (TA_{std} = 58.2‰^{2}; Table 3.5) and in the PFZ and sBZ where food web diversity was higher and comparable (TA_{std} = 76.4 and 70.5‰^{2}, respectively) although still lower than in the SACCZ (TA_{std} = 107.4‰^{2}). These data show that the Antarctic hosted a higher density of ^{15}N-enriched zooplankton than the Subantarctic (Figure 3.9e), indicating a higher density of zooplankton at high trophic positions in the Antarctic *versus* a higher density of zooplankton at lower trophic positions in the Subantarctic Ocean (see below).

We estimated higher TPs for the zooplankton taxa in the Antarctic Ocean (Figure 3.10), suggesting that zooplankton south of the APF were primarily omnivorous/carnivorous, in contrast to the Subantarctic Ocean where zooplankton were more herbivorous (Figure 3.11, Table 3.3). Several studies have suggested that variability in primary producer biomass and productivity can contribute to changes in the TPs of the primary consumers (e.g., McMeans *et al.* 2015). For example, Henschke *et al.* (2015) showed that omnivorous zooplankton (e.g., Copepoda and Euphausiacea) increased their TPs to a similar level as carnivorous zooplankton (Chaetognatha) in response to a lower abundance and reduced diversity of phytoplankton in oligotrophic waters near Tasmania. Likewise, Michel *et al.* (2019) reported that during periods of high food availability, such as the sinking of high concentrations of sea-ice algae, benthic invertebrates shift to a lower

TP, with omnivorous consumers engaging in herbivory (i.e., grazing) rather than predation and/or scavenging.

During the ACE cruise, the total chlorophyll-a concentrations (Chl-a) in the surface were higher throughout the Subantarctic Ocean ($0.2^{0.4}_{0.1}$mg m^{-3}) and in the sBZ ($0.4^{1.0}_{0.3}$mg m^{-3}) than in the SACCZ ($0.1^{0.3}_{0.1}$mg m^{-3}), with the relative contributions of different phytoplankton size classes (i.e., micro- or nano-phytoplankton) varying among regions (see above; Chapter 2). The higher Chl-a in the Subantarctic Ocean may indicate an abundance of phytoplankton available to sustain the herbivorous zooplankton (i.e., Thaliacea, Pteropoda, Euphausiacea and Copepoda, the TPs of which were ≤ 2, indicating that these zooplankton were primary consumers; Figure 3.10). In contrast, the lower phytoplankton biomass in the SACCZ may have been insufficient to sustain herbivorous zooplankton, leading them to adapt their trophic behaviour by switching preferentially to omnivory and/or carnivory engaged in by their taxa (primary consumers would occupy a TP >2-3). However, our results from the sBZ are inconsistent with this explanation as this zone was characterized by relatively high phytoplankton biomass yet its zooplankton occupied high TPs (comparable to those in the SACCZ; Figure 3.11). It is possible that at the time of our sampling, Chl-a had recently increased in the sBZ (e.g., in response to the release of iron from melting sea ice; Chapter 2) but the associated trophic switch in the zooplankton had not yet manifested in their biomass δ^{15}N. For example, O'Reilly *et al.* (2002) showed that after an upwelling event, the δ^{15}N of zooplankton still reflected the average δ^{15}N of phytoplankton prior to the upwelling-induced bloom because zooplankton have slower growth rates and longer turnover times for N-containing molecules than phytoplankton, such that their δ^{15}N varies over a longer time scale. One way to avoid such an 'isotopic mismatch' between producer and consumer and to capture a TP switch in the consumers in near-real time is to analyse the δ^{15}N of individual amino acids instead of bulk organisms (e.g., Schmidt *et al.* 2006; Hannides *et al.* 2009).

In this study, we briefly investigated whether the islands influence the trophic structure of zooplankton, with our analysis showing no substantial differences between the island and open-ocean stations (Figure 3.12 and Figure B.3). However, the absence of any island mass effect (IME) is unlikely . The (Sub)Antarctic islands have been shown to enhance phytoplankton productivity and favour the dominance of larger species (i.e., diatoms) as a result of their influence on the local circulation (e.g., upwelling and/or the retention of surface

waters near the islands), augmented by inputs of island-derived nutrients (e.g., Pakhomov and Froneman 1999; Borrione and Schlitzer 2013; Lamont *et al.* 2022). We would expect that an increase in phytoplankton biomass due to the IME would catalyse a switch in zooplankton diet from omnivory/carnivory to herbivory, thus lowering their TPs. However, given the time required for a TP switch to be reflected in the $\delta^{15}N$ of zooplankton biomass, and considering that the IME can manifest more than 1000 km downstream of some of the islands (e.g., in elevated concentrations of phytoplankton biomass; Mongin *et al.* 2009), it is possible that the effect on the zooplankton isotopic composition and trophic behaviour would be more apparent downstream than in the vicinity of the islands. The larger-scale circulation may also play a role; for example, the meandering of the hydrographic fronts in the Southern Ocean has been hypothesized to retain plankton near the islands in some seasons and separate them in others (Chapter 4).

3.5.3.1. Different plankton food webs have implications for the Southern Ocean's biological pump

Our findings raise the questions whether and how the trophic differences in the zooplankton systems among hydrographic zones might be reflected throughout the food web and influence carbon export in the Southern Ocean. Zooplankton are integral to the biological pump via their ingestion of lower trophic levels, production of faecal pellets, moults and carcasses, and respiration of organic matter (Mayzaud and Pakhomov, 2014; Turner, 2015; Steinberg and Landry, 2017; Halfter *et al.*, 2020, 2022). According to the theory of top-down regulation of the vertical flux (Kiørboe, 1997; Wassmann, 1997), the percentage of phytoplankton carbon that leaves the euphotic zone can vary widely (by 33-70%) depending on the trophic behaviour of the zooplankton and the structure of the zooplankton community. The model developed by Wassmann (1997) indicates that a herbivory-based food web promotes organic matter recycling and retention of nutrients in the upper layer, as well as the export of biogenic matter by faecal pellet sinking. In contrast, when omnivory and carnivory are dominant, grazing pressure on phytoplankton decreases, which may favour the export of aggregated cells and phytodetritus. These two food-web scenarios are referred to as '*retention chain*' and '*export chain*', respectively, with the former and the latter leading respectively to a weaker and a more intense biological pump. In addition, under conditions where zooplankton exhibit a high degree of omnivory, including predation on micro-heterotrophs and possibly cannibalism by large or small Copepoda, production

originating from the microbial loop is transferred to depth, increasing the strength of the biological pump (Froneman *et al.*, 2000; Zeldis *et al.*, 2002; Zeldis and Décima, 2020).

Halfter *et al.* (2020) recently reviewed the importance of zooplankton community species and size composition in modifying the downward carbon flux in high- and low-productivity regions of the Subantarctic Ocean, such as near the islands and in the open ocean, respectively. They concluded that contrary to the expectation that high productivity results in high export, regions of iron fertilization support low rates of carbon export relative to their surface productivity, while the iron-deplete waters of the open ocean are areas of significant carbon export. The major difference between the two regions appears to be the variable control on phytoplankton biomass accumulation by zooplankton grazing and the efficiency of upper water column remineralization. The islands are hotspots for elevated photosynthetic biomass and support a larger and more diverse zooplankton community than the open ocean (e.g., Pakhomov *et al.* 2000a). The higher abundance of omnivorous and detritivorous zooplankton in waters surrounding islands may retain carbon in the mesopelagic zone, first through grazing and the ingestion and fragmentation of particles (e.g., faecal pellets), and then through microbial respiration and the recycling of nutrients (Iversen and Poulsen, 2007; Quéguiner, 2013; Dagg *et al.*, 2014). As a result in such a system, carbon export flow to the deep ocean is lowered for the most of the year by the effective transfer of carbon to higher trophic levels and by the microbial loop in surface waters (Rembauville *et al.*, 2014, 2015). In contrast, the low abundance of omnivorous and detritivorous copepods in the open Subantarctic Ocean limits the ability of the zooplankton community to attenuate the sinking flux. Instead, the dominance of protozooplankton, small Copepoda, and Salpida enhances grazing on the pico-phytoplankton (0.3–3 μm), allowing phytoplankton aggregates and other large particles to be exported below the mixed layer (Pearce *et al.*, 2011). Consequently, more particles are exported from the iron-deplete open Subantarctic surface as faecal aggregates (pellets and faecal material reaggregated with phytodetritus; Ebersbach and Trull 2008; Laurenceau-Cornec *et al.* 2015).

Considering the above, we hypothesize that the mainly omnivore- and carnivore-based food web in the Antarctic Ocean may lead to higher carbon export, in contrast to the largely herbivore-based food web in the Subantarctic where carbon may have been preferentially retained in the upper layer. Furthermore, a different

carbon export regime may have been established near the islands where a higher relative abundance of omnivores and an upregulated microbial loop may have attenuated the carbon flux.

Carbon retention and/or export depend on the food source available and the zooplankton species composition. According to Koski *et al.* (2017), a community dominated by small particle-feeders (e.g., *Oncea* spp.) would mainly consume sinking aggregates, whereas dispersed phytoplankton cells and microzooplankton would be the major food source for a community dominated by Calanoida. These latter organisms could repackage phytoplankton into large faecal pellets that sink rapidly along with zooplankton carcasses, especially when diatoms are their main food source (Besiktepe, 2002; Manno *et al.*, 2015; Halfter *et al.*, 2022). A study using sediment traps in the Scotia Sea (Southern Ocean) indicated that the faecal pellet contribution to export varies considerably among seasons, with the sinking-fluxes being up to 40% lower in the autumn–winter season compared to spring and summer (Manno *et al.*, 2015). The faecal pellet analysis of Manno *et al.* (2015) indicated a shift in the zooplankton community composition from herbivory in spring to omnivory in autumn, while detritivory remained relatively constant throughout the year. These findings are consistent with our study results. Another factor that may affect the carbon flux is diel vertical migration (DVM) of zooplankton, which can increase the depth at which faecal pellets are released (Buesseler and Boyd, 2009; Wallace *et al.*, 2013). A recent global modelling study estimated that DVM may contribute as much as 18% of the gravitational carbon flux, but observations are scarce and the mechanisms of DVM are poorly understood (Aumont *et al.*, 2018).

The observations summarized above suggest that the behaviour of zooplankton may modulate the strength of the biological pump in a variety of ways across the different regions of the Subantarctic Ocean, with the availability and quality of food resources and DVM identified as potentially important drivers. Therefore, characterizing the zooplankton community composition and identifying the trophic role of each species may improve estimates of the carbon fluxes and must be included in global models tasked with quantifying carbon export.

In our framework above, we do not consider the trophic level and role of the microzooplankton (i.e., <200 µm, e.g., ciliates and dinoflagellates). Microzooplankton are known to feed preferentially on pico- (0-2 µm) and nanoplankton (2-20 µm), including bacteria and phytoplankton, thus occupying the lowest trophic level

of primary consumers and exhibiting principally herbivory and sometimes, omnivory (Schmoker *et al.*, 2013). The carbon flux and biological pump efficiency can be modulated by the trophic structure and interactions of microzooplankton with other plankton groups (Steinberg and Landry 2017 and references therein). Microzooplankton can affect the carbon flux in different ways: (1) by grazing on phytoplankton and reducing the food available to mesozooplankton (i.e., >200 μm) herbivores (Sherr and Sherr, 2002; Calbet and Landry, 2004), (2) by stimulating regenerated production through nutrient remineralization and dissolved organic matter production (Goldman *et al.*, 1987; Caron *et al.*, 1990), and (3) by serving as a food source for mesozooplankton omnivores or carnivores (e.g., Christaki *et al.* 2021b).

The size distribution of the phytoplankton assemblages in the Southern Ocean affects the amount of carbon grazed by microzooplankton and thus, the efficiency of the biological pump (Froneman and Perissinotto, 1996a; Froneman *et al.*, 1996; Christaki *et al.*, 2021a). When larger phytoplankton cells dominate the biomass (i.e., summer), grazing impact microzooplankton is relatively low and most of the photosynthetic biomass is directly transferred to the mesozooplankton, which rapidly export organic carbon to the deep ocean through vertical migration and large faecal pellet production (Froneman and Perissinotto 1996a; b). On the other hand, when pico- and nano-phytoplankton are most dominant (i.e., autumn and winter), microzooplankton grazing impact is higher and phytoplankton biomass is rapidly reduced thus lowering the efficiency of the biological pump (Froneman and Perissinotto, 1996a) because carbon is largely recycled in the upper mixed layer rather than transferred into deep waters (Christaki *et al.*, 2021b).

Microzooplankton community succession and grazing have been found to differ with region and season in the Southern Ocean. This variability appears to follow a latitudinal gradient and to be influenced by sea ice dynamics (Froneman and Perissinotto, 1996a; Safi *et al.*, 2007; Price, 2012; Yang *et al.*, 2016). We suggest that microzooplankton phenology would follow a latitudinal gradient similar to the seasonal cycles observed in phytoplankton and larger zooplankton, as discussed in above. In the Antarctic, the microzooplankton system may have been more characteristic of a winter-to-spring community, with intense ciliate and dinoflagellate grazing on pico- and nano-phytoplankton transferring biomass to higher trophic levels (i.e., mesozooplankton; >200 μm) (e.g., Christaki *et al.* 2021b). In this scenario, large phytoplankton would experience minimal grazing, allowing them to grow unchecked and ultimately contribute significantly to

carbon export. Furthermore, microzooplankton may have constituted the major food source to mesozooplankton, explaining the omnivore- and carnivore-based food web determined in the Antarctic. Since microzooplankton would essentially act as a conduit of the small phytoplankton stock to the carnivorous mesozooplankton, their production of large faecal pellets and DVM would then enhance the downward carbon flux in the Antarctic (Froneman and Perissinotto 1996a; b; Christaki *et al.* 2021b). In contrast, during the same expedition period, the Subantarctic microzooplankton may have resembled a summer-to-autumn system, similar to the Subantarctic phytoplankton. We hypothesize that the microzooplankton were increasing their abundances and grazing rates from summer to autumn (Froneman and Perissinotto 1996a; b) coincident with the increase in their preferred food source (i.e., pico- and nano-phytoplankton). At the same time, the large dinoflagellates found in the Subantarctic may have been engaging in heterotrophy and/or mixotrophy, potentially feeding on the micro-phytoplankton (>20 µm) size class, including diatoms (Suttle *et al.*, 1986). In this scenario, micro- and mesozooplankton could be grazing across the size-spectrum of phytoplankton, limiting phyto-aggregation and biomass sinking. Furthermore, enhanced microzooplankton activity would likely have increased the recycling of nutrients and thus, regenerated production (Goldman *et al.*, 1987; Caron *et al.*, 1990), reducing carbon export (Christaki *et al.*, 2021b).

The influence of microzooplankton on carbon export remains uncertain due to the scarcity of data and trophic analysis across vast areas of the oceans, including the Southern Ocean. A major knowledge gap is the extent and impact of mixotrophy and trophic cascades among microzooplankton, which are still poorly understood (Schmoker *et al.* 2013; Stoecker *et al.* 2017; Steinberg and Landry 2017 and references therein). These processes may have significant implications for the carbon flux and warrant future attention.

3.5.3.2. Zooplankton species-specific trophic roles in the Southern Ocean

In the Southern Ocean, five major zooplankton taxa are notable for their biomass and abundance: Euphausiacea, Copepoda, Pteropoda, Amphipoda, and Salpidae (Atkinson *et al.*, 2012a). Although zooplankton have been investigated in the Southern Ocean for decades and several recent studies have reviewed their role in the structure and function of the Southern Ocean carbon cycle and food webs (e.g.,

Atkinson *et al.* 2012a; Steinberg and Landry 2017; Johnston *et al.* 2022), new data that offer insights into their ecological behaviour and dynamics remain essential.

Euphausiacea have a significant influence on the structure and functioning of the marine system, *inter alia* by supporting large populations of predators (Trathan and Hill, 2016). They are omnivorous and able to feed on a large variety of prey (e.g., phytoplankton, micro-zooplankton [< 200 µm] and meso-zooplankton [>200 µm], and detritus; Pakhomov 2000; Schmidt *et al.* 2014, 2018). Our results show distinct trophic behaviours for Euphausiacea in the various oceanic regions. In the Subantarctic Ocean, a larger proportion of specimens were herbivorous (median of TP of 2.2 ± 1) while in the Antarctic, more specimens were carnivorous (TP of 3.0 ± 0.8; Figure 3.10 and Table 3.1), in line with the trophic structures defined for the two regions (see section 3.4.3). In the STZ, we determined an increase in TP from the smaller (5-10 mm; TP of 1.3 ± 0.2) to the bigger (20-50 mm; TP of 2.3 ± 0.2) size classes of Euphausiacea from an increase in $\delta^{15}N$ by ~2.2‰ (Figure 3.6a, Table 3.3). This observation is noteworthy because it suggests that Euphausiacea may alter their trophic behaviours — and therefore, their food sources — as they mature, with the younger juveniles being more herbivorous and the adults more carnivorous. Our findings are consistent with those of Schmidt *et al.* (2003), who assessed that the stable isotope ratios of *Euphausia superba* increased from juvenile to adult stages during a long-term incubation experiment at various dietary regimes. We have also assessed the TP of the larvae stages of Euphausiacea, such as Calyptopis I in the SACCZ, which occupied a TP of 1.5 suggesting mixotrophy (Table 3.3), and Calyptopis II in the PFZ that had a TP of 3.1, which was much higher than the TP of the 0-5 mm Euphausiacea size class (TP of 0). However, we cannot entirely rely on these results because only one specimen from each of these two groups was analysed. In any case, even if those results are accurate, it would be too difficult to define the origin of such trophic difference.

Copepoda are one of the most abundant and diverse components of the plankton system and can feed on a wide variety of organisms depending on the Copepoda species and developmental stage, as well as the season and environmental conditions (Atkinson, 1998). In this study, the analysed Copepoda species were more herbivorous in the Subantarctic (TP of 2.2 ± 2.1; median ± IQR) than in the Antarctic Ocean where they tended to be carnivorous (TP of 3.1 ± 1.6; Figure 3.10 and Table 3.1). The smaller Copepoda (200-500 µm, comprising mainly Oithonidae and Oncaeidae) were generally at a lower TP than the larger ones (>500

µm), although we note that large Copepoda like *Calanus* spp. and *Calanoides* spp. may adopt different feeding behaviours at different times during their life cycle, demonstrating that they are more opportunistic feeders and omnivorous (Atkinson, 1998).

Small Copepoda like *Oithona* spp. were at TPs of 1.9 ± 0.4 and 2.3 ± 0.7 in the PFZ and SACCZ, respectively (Table 3.3). This observation is consistent with the general consensus that *Oithona* spp. feed on small heterotrophic proto-zooplankton and detritus colonised by bacteria, as well as on large diatoms (Atkinson, 1995, 1996; Nielsen and Sabatini, 1996; Lonsdale *et al.*, 2000; Stowasser *et al.*, 2012). As suggested by Nielsen and Sabatini (1996), these food sources (except the large diatoms) are typically available year-round, allowing *Oithona* spp. to maintain stable populations almost continuously.

Remaining among the small Copepoda, *Clausocalanus laticeps* were at TPs of 2.6 ± 2.3 and 1.9 ± 0.2 in PFZ and SACCZ, respectively (Figure 3.11 and Table 3.3), suggesting opportunistic omnivorous behaviour. In contrast, the only one specimen of the small *Microcalanus* spp. from the SAZ was strongly enriched in ^{15}N ($\delta^{15}N$ = 3‰), indicating a TP of 3.7 (strictly carnivorous), which was even higher than that of the bigger Copepoda (>500 µm; TP of 3.3 ± 0.1).

Calanidea such as *Calanus* spp. and *Calanoides* spp. are widely reported as being preferentially herbivorous when phytoplankton are present in high concentrations, but will alter their diet with developmental stage and in response to seasonal changes in food availability (Drits *et al.*, 1993; Pasternak and Schnack-Schiel, 2001). The consensus is that *Calanoides acutus* are the most herbivorous species of Copepoda (Hopkins and Torres, 1989; Atkinson *et al.*, 1996; Schmidt *et al.*, 2003) while *Calanus simillimus* and *C. propinquus* are more omnivorous, able to switch their feeding to raptorial mode, ingesting a large variety of prey (Hopkins and Torres, 1989; Atkinson, 1995; Burghart *et al.*, 1999; Schmidt *et al.*, 2003). We derived different TPs for specimens of Calanidae that were related to their developmental stage. While adults of *Calanus* spp. occupied TPs of between 3 and 4, *Calanoides* spp. were at a TP of 4.2 ± 0.1 and 2.9 ± 0.6 in the SACCZ and the sBZ, respectively, indicative of carnivorous behaviour while the TPs of copepodite stages (CIII-CV) of Calanidae were between 1 and 3 (except for Calanidae CIV in SAZ that occupied a TP of 3.2 ± 0.4; Figure 3.11 and Table 3.3). These results indicate that trophic behaviour changes with life-cycle stage.

In the sBZ, *Paraeuchaeta antarctica* occupied a TP of 3 (Figure 3.11 and Table 3.3), consistent with its role as a carnivore that preys on other Copepoda by raptorial feeding, ambush or suspension modes (Hopkins, 1985; Hopkins and Torres, 1989; Yen, 1991; Øresland and Ward, 1993). Although *Metridia gerlachei* has previously been characterized as omnivorous (Hopkins and Torres, 1989; Atkinson, 1995; Burghart *et al.*, 1999; Schmidt *et al.*, 2003), our measurements of *M. gerlachei* from the Antarctic Ocean indicate that it is strictly carnivorous (TP of 3.4 ± 0.0; PFZ and sBZ) as has been previously observed in the Antarctic waters (Øresland, 1991; Huntley and Escritor, 1992).

We collected one specimen of Pontellidae from the Antarctic Ocean (Figure 3.2h), with our measurement of its $\delta^{15}N$ suggesting that it is at the top of the plankton food chain in the SACCZ (TP of 6.5).

Our data show that the early life-cycle stages of certain taxa such as Copepoda nauplii, the Calyptopis of Euphausiacea, and the juveniles of the Amphipoda *Themisto* spp. were more ^{15}N-enriched and therefore occupied a higher TP than their adult stages. Contrary to the ontogenetic enrichment observed in Euphausiacea, which has been attributed to changes in trophic behaviour, these taxa deviate from this pattern, prompting further investigation into why early life-stages exhibit higher $\delta^{15}N$ values than more mature stages. Studies on mammals showed a species-dependent isotopic fractionation from the mother to the offspring, for which the $\delta^{13}C$ and $\delta^{15}N$ of the new-born are higher than those of their mother because of the consumption of maternal resources during gestation and nursing, although not necessarily a trophic level effect (e.g., Hobson and Sease 1998; Jenkins *et al.* 2001; Habran *et al.* 2010; Miller *et al.* 2011; Lübcker *et al.* 2020). For example, the transfer of amino acids from the mother's placenta to the foetus illustrates the mechanism underlying the isotopic enrichment in the foetus $\delta^{15}N$ (Lübcker *et al.*, 2020). Consecutively, when the offspring is weaned, its isotopic signature resemble that of the mother in proportion to the percentage of its overall nutrition that comes from an adult-type diet (e.g., Jenkins *et al.* 2001; Miller *et al.* 2011). Considering above, it is possible that during the embryonic development in invertebrates (e.g., Crustacea), the maternal isotopic signal can be imparted to the eggs causing them and the new nauplii to become enriched in the heavier isotopes. The first naupliar stages of zooplankton Crustacea would then lower their isotopic composition once they begin feeding on the available food, that may differ according to the life-cycle stages because of the different body size and feeding strategy (Uye and Kayano, 1994). This

suggestion may explain previous field studies that have found the $\delta^{15}N$ of adult Copepoda to be ~3‰ higher than that of the early copepodites (e.g., Schmidt *et al.* 2003). It is possible that by the time Schmidt *et al.* (2003) collected their samples, the nauplii had time to shift their isotopic signal to lower values as a result of the food source they had consumed. Excluding the incubation experiment on larval and post-larval Euphausiacea conducted by Schmidt *et al.* (2003), to the best of our knowledge, there have not been any studies specifically designed to investigate (e.g., via incubation experiments) isotopic flow between eggs, early life-cycle stages, and adults of zooplankton, as would be required to better understand our observations and those of others.

The various genera of Amphipoda investigated here occupied a range of TPs. The genus *Cyllopus*, comprising mainly *C. lucasi* and *C. magellanicus*, along with a few specimens of *Vibilia antarctica* in the PFZ, generally occupied a slightly lower TP than *Themisto gaudichaudii*, (TP of 1.7 ± 0.2 for *Cyllopus* spp. *versus* 1.9 for *T. gaudichaudii* in the STZ; 2.8 *versus* 3.1 ± 1 in the SAZ; 0.5 ± 0.3 *versus* 1.1 ± 2.1 in the PFZ; and 1.4 ± 0.3 *versus* 2.9 ± 1.5 in the SACCZ; no data are available for the sBZ; Table 3.3). *T. gaudichaudii* has been described as highly adapted predator, with raptorial gnathopods designed for grasping live and active prey, making them major predators of meso- and microzooplankton such as Euphausiacea and Copepoda (Lange *et al.*, 2005; Havermans *et al.*, 2019). Consistent with previous studies (Wada *et al.*, 1987; Gurney *et al.*, 2001; Stowasser *et al.*, 2012), we derived disparate TPs for *T. gaudichaudii*, which were sometimes comparable to the TPs of smaller Copepoda or even lower than the TPs of Euphausiacea (i.e., in the STZ). However, it is not reasonable that *T. gaudichaudii* behaves as an herbivore (Atkinson *et al.*, 2012a). The observed low $\delta^{15}N$ values in adult *Themisto* may indicate that the species employ diverse feeding strategies to maintain a balanced diet or that their amino acid composition significantly influences their $\delta^{15}N$, as proposed by (Schmidt *et al.*, 2004). In addition, even the TP of the juvenile stages of *T. gaudichaudii* was variable between zones, ranging from 2.0 to 3.9, with values sometimes higher than the co-occurring adult stage (e.g., in SACCZ; Figure 3.6d; Table 3.3). All these observations are consistent with several previous studies that have shown diverse trophic behaviours for *Themisto* at different life stages (Havermans *et al.* 2019 and references therein).

Pteropoda are another important member of the Southern Ocean zooplankton community (Hunt *et al.*, 2008; Roberts *et al.*, 2014). Our results suggest that Pteropoda were mostly herbivorous in both the Subantarctic and Antarctic Oceans (TP of 1.7 ± 0.6 and 2.3 ± 0.1, respectively; Figure 3.10 and Table 3.1). Two suborders of Pteropoda are known to have two distinct trophic behaviours – Gymnosomata are specialist predators, often preying on other Pteropoda, while Thecosomata are considered largely herbivorous, capturing their food with a mucous web (Hunt *et al.*, 2008; Roberts *et al.*, 2014; Weldrick *et al.*, 2019). In particular, the Thecosomata *Limacina helicina antarctica* is a dominant grazer that feeds predominantly on diatoms and dinoflagellates and supplements its diet with ciliates and foraminifera (Thibodeau *et al.*, 2022). We investigated three species of Thecosomata (*L. helicina antarctica* [Figure 3.2e], *L. retroversa*, and *Clio pyramidata* [Figure 3.2r]), and two species of Gymnosomata (*Clione limacina antarctica* and *Spongiobranchaea australis*). Our results are consistent with the expectation that *L. helicina antarctica* (TP = 1.5 ± 0.2 in the SAZ and 0.2 ± 1.9 in the PFZ, respectively), *L. retroversa* (2.3 ± 0.1 in the sBZ), and *C. pyramidata* are predominantly herbivorous species (1.5 ± 0.2 in the STZ and 2.0 ± 2.0 in the SAZ; Figure 3.11 and Table 3.3). Once more as expected, the Gymnosomata *C. limacina antarctica* (3.4 ± 1.9 in the SACCZ) and *S. australis* (2.8 ± 0.1 in the STZ) were carnivorous (Figure 3.11 and Table 3.3).

Salpidae are generally assumed to be non-selective filter feeders (Andersen, 1998; Pakhomov *et al.*, 2002), with diets that closely reflect the composition of the available plankton community (Bone *et al.*, 2003). However, Pauli *et al.* (2021) recently compared the stomach contents of Salpidae from the ambient plankton community, leading the authors to conclude that Salpidae are selective feeders of unicellular organisms only, such as small flagellates, Chrysophyceae and dinoflagellates, rather than of generalist continues and non-selective filter feeders (Andersen, 1998; Pakhomov *et al.*, 2002). While our study was not designed to investigate feeding behaviours in detail, we nevertheless determined low TPs for Salpidae, at times comparable to the primary producers (TP of 1.0 ± 0.3 in the STZ, 1.7 ± 0.1 in the PFZ, and 1.4 ± 0.4 in the SACCZ, with no observations for the SAZ and the sBZ; Figure 3.11 and Table 3.3). The very low TPs can be explained if the Salpidae were preferentially filtering specific organisms out of the SPM that were lower in $\delta^{15}N$ than the $\delta^{15}N_{SPM}$.

3.6. Conclusions

The major objectives of this work were to describe the zooplankton $\delta^{13}C$ and $\delta^{15}N$ isoscapes in the Southern Ocean and determine the trophic structures of the plankton communities in each of the hydrographic zones, thereby assessing trophic differences that may influence the functioning of the biological pump. In this study and a parallel one (Chapter 2), we characterized for the first time over a large spatial extent of the Southern Ocean in a single season, the spatial and temporal variability in the $\delta^{13}C$ and $\delta^{15}N$ of SPM and zooplankton. We observed clear latitudinal changes in the zooplankton isoscapes and community composition across the different hydrographic zones of the Southern Ocean, corroborating previous findings that the oceanic fronts dividing the hydrographic zones may represent barriers to pelagic organisms (Deacon, 1982; Koubbi, 1993; Pakhomov and McQuaid, 1996; Pakhomov *et al.*, 1999). We conclude that the hydrographic conditions, nutrient availability, and phytoplankton processes are reflected in the zooplankton stable isotopes and the food web (i.e., bottom-up control), with likely consequences for carbon flow such as preferential retention or export of the carbon produced in the euphotic zone. These drivers resulted in unique and defined $\delta^{13}C$ and $\delta^{15}N$ values for plankton in each zone, which could be leveraged as an *ecogeochemical* tool to reconstruct the movements and dietary histories of marine animals in the Southern Ocean.

This work compared five baselines for trophic analysis: the measured surface $\delta^{15}N_{SPM}$; the theoretical $\delta^{15}N$ for phytoplankton biomass produced as a result of nitrate assimilation ($\delta^{15}N_{new}$), calculated using the Rayleigh model for isotope fractionation with the in situ nitrate concentration and $\delta^{15}N$ as constraints; diatom-$\delta^{15}N$; and the $\delta^{15}N$ of a primary consumer, which in this study was represented by Salpidae and by the smaller class of Copepoda (200-500 µm, comprising mainly Oithonidae and Oncaeidae). We conclude that $\delta^{15}N_{SPM}$ is a good baseline for assessing the trophic position of zooplankton at large spatial scales such as the Southern Ocean hydrographic zones because 1) SPM is commonly collected during scientific expeditions and is straightforward and inexpensive to analyse, 2) the food source to the zooplankton system was well-represented by the SPM, perhaps partly because our sampling occurred during a period of active phytoplankton growth, and 3) using $\delta^{15}N_{SPM}$ as a baseline worked well even in regions with intense biogeochemical processes such as in the PFZ and SAZ, which are affected by upwelling, and the vicinity of the islands. However, $\delta^{15}N_{new}$ derived using the Rayleigh model could potentially be a good substitute for

$\delta^{15}N_{SPM}$, particularly in regions where the biogeochemical fluxes are in quasi 'steady-state', when measurements of $\delta^{15}N_{SPM}$ are not available.

We established that, contrary to expectations, the plankton systems in the Subantarctic and Antarctic Oceans have significantly distinct trophic structures. In the Subantarctic, the primary consumers occupied low TPs aligned with herbivory, possibly resulting in a food web defined as a *retention chain* where carbon was perhaps retained within the surface layer and slowing down the sinking of phytoplankton cells and thus of the biological pump. By contrast, the same primary consumers occupied higher TPs in the Antarctic, suggesting a dominance of omnivory/carnivory and a food web characterized as an *export chain*, which may stimulate enhanced carbon export and thus a more intense biological pump.

This study advances our understanding of plankton dynamics and their relationships with biogeochemical processes across the Southern Ocean. However, there remain significant uncertainties in our knowledge of trophic structure that must be resolved if we are to improve our understanding of carbon flows through zooplankton in food webs. Given the complex spatial and temporal dynamics of the Southern Ocean, future studies should additionally focus on species-specific responses to physical and chemical changes and variations in isotopic niches in relation to regional abundances and distributions of marine animals.

Chapter 4. Plankton community composition and productivity near the Subantarctic Prince Edward Islands archipelago in autumn

Supplementary information of this Chapter can be found in Appendix C.

4.1. Abstract

The Subantarctic Ocean is a sink for atmospheric CO_2, largely due to its biological pump, which is enhanced by the influence of the Subantarctic islands on the plankton ecosystem (the so-called 'island mass effect'). The influence of the Prince Edward Islands archipelago in the Indian Subantarctic on the surrounding hydrography and benthos have been well-studied; however, over the last two decades, little attention has been paid to the functioning and productivity of its plankton ecosystem. Here, we present the first measurements of primary production at the archipelago in over twenty years and the first-ever rates of secondary production, interpreted in the context of hydrographic, biogeochemical, and plankton community composition data. In autumn 2017 after the late-summer bloom, nano-phytoplankton dominated the near-island waters and regenerated nutrients fuelled 76% of phytoplankton growth. Primary production and carbon export potential (inferred from nitrate uptake) reached a local maximum in the inter-island region, which we attribute to water-mass retention and stratification over the inter-island plateau (a manifestation of the island mass effect). We observed a diverse mesozooplankton community, likely a remnant of the late-summer bloom rather than representing the consumers feeding on the *in situ* (nano)phytoplankton. We estimate that even after the decay of the late-summer bloom, roughly a quarter of the planktonic carbon was potentially exportable. This finding implies that the archipelago's upper-ocean ecosystem sequesters atmospheric CO_2 at least through autumn despite high rates of recycling and inefficient trophic transfer, thereby contributing to the island mass effect-associated strengthening of the Subantarctic Ocean's biological pump.

4.2. Introduction

The Southern Ocean is a high-nutrient, low-chlorophyll (HNLC) region where primary productivity is co-limited by iron and light availability (Sunda and Huntsman, 1997), yet it is a major regulator of atmospheric carbon dioxide (CO_2) (Gruber *et al.*, 2019). The solubility pump, combined with the fixation, transformation, and transportation of carbon during photosynthesis and food-web flows (i.e., the biological pump), allows the Southern Ocean to take up roughly 40% of the CO_2 absorbed by the global ocean annually (DeVries, 2014). In particular, the Subantarctic and Polar Frontal Zones (SAZ and PFZ; hereafter, 'the Subantarctic'), located between the Subtropical Front and the Antarctic Polar Front (APF) and comprising more than half of the area of the Southern Ocean (Orsi *et al.*, 1995), constitute the largest sink for atmospheric CO_2 south of 30°S (DeVries, 2014).

The Subantarctic Ocean's biological pump is strengthened by the influence of a number of island systems (e.g., Bakker *et al.* 2007). This 'island mass effect' typically yields a localized increase in phytoplankton biomass driven by changes in circulation and the retention of surface waters around the islands, augmented by inputs of island-derived nutrients (e.g., Planquette *et al.* 2011). For example, shoaling bathymetry upstream of islands facilitates the upwelling of deep nutrient-rich waters, which can alleviate iron limitation of surface phytoplankton (Schallenberg *et al.*, 2018), while downstream, eddies often form, creating a retention zone for nutrients and plankton (Planquette *et al.*, 2007). Additionally, the interaction of internal waves with the near-island bathymetry can drive upwelling of deeper waters (Leichter *et al.*, 2003) that can be particularly high in iron following interaction with iron-rich basaltic sediments (Zhang *et al.*, 2008). Enhanced iron availability allows phytoplankton to consume more of the available macronutrients (including nitrate; NO_3^-), with implications for the biological pump. Annually, net primary production (NPP) fuelled by NO_3^- supplied from depth ('new production') must be balanced by the export of sinking organic matter (Dugdale and Goering, 1967), which transfers atmospheric CO_2 to the deep ocean (Volk and Hoffert, 1985). By contrast, phytoplankton growth on recycled nitrogen (e.g., ammonium; NH_4^+) produced in the euphotic zone due to heterotrophy ('regenerated production') yields no net removal of CO_2 to depth (Dugdale and Goering, 1967).

The Prince Edward Islands archipelago in the Indian sector of the Subantarctic is a system of two islands (Marion Island and Prince Edward Island) that lies between the Subantarctic Front (SAF) and the APF (Figure 4.1). Phytoplankton are the main producers of energy for the marine ecosystem of this archipelago (Treasure *et al.*, 2019), and the rate at which they generate carbon biomass is influenced by the availability of nutrients (e.g., iron; supplied via upwelling, aeolian deposition, or terrestrial run-off) and water-column stability (Perissinotto and Duncombe Rae, 1990). Zooplankton also play a critical role in the biological pump by repackaging and exporting phytoplankton biomass to depth. Their distribution is determined by food availability and influenced by the hydrographic environment of the archipelago (Bernard and Froneman, 2003).

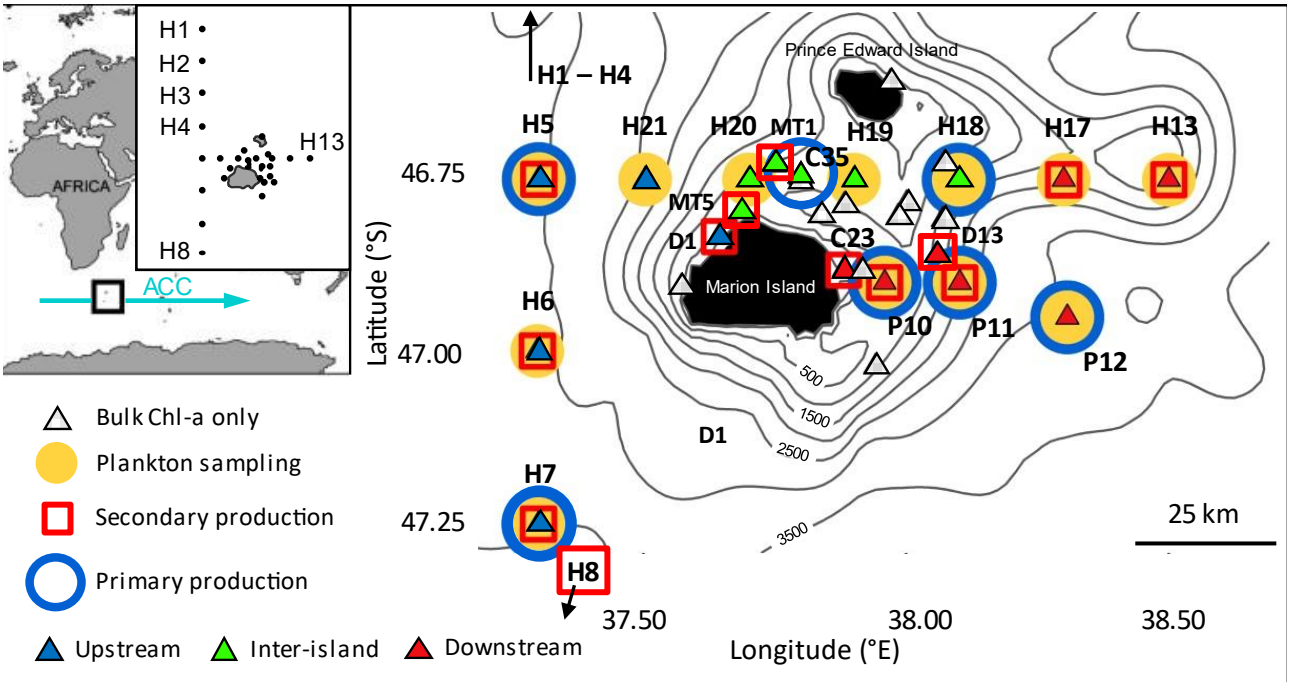

Figure 4.1 Map of the Prince Edward Islands archipelago and the sampling stations, with dark grey lines denoting the bathymetry (GEBCO_2020; www.gebco.net/data_and_products/gridded_bathymetry_data). The triangles show the sampling stations: diagonal black stripes = samples collected for bulk chlorophyll-a only; filled = stations sampled for multiple analyses, classified into three regions: blue = upstream, green = inter-island, red = downstream. The yellow circles indicate stations sampled for nutrients, plankton taxonomy, and zooplankton gut contents; blue rings show the location of primary production experiments; open red squares denote the location of secondary production experiments. The light blue arrow indicates the direction of the Antarctic Circumpolar Current (ACC). The locations of stations H1-H4 and H8 are shown on the map inset.

Since the 1950s, the Antarctic Circumpolar Current (ACC), of which the SAF is the northern boundary and the APF is a component, has increased in intensity (Sokolov and Rintoul, 2009b), temperature (Gille, 2002) and freshness (Oke and England, 2004), and appears to have migrated poleward (Sokolov and Rintoul,

2009a). These changes are projected to modify the intensity and frequency of eddies formed in the Antarctic PFZ and to drive the SAF southward (Sokolov and Rintoul, 2009a), resulting in more frequent SAF flow between the Prince Edward and Marion Islands. Atmospheric investigations have confirmed an increase in air temperature and hours of sunshine over the archipelago (Rouault *et al.*, 2005), along with a decrease of nearly 500 mm in annual precipitation and an increase in terrestrial ice melt (Le Roux and McGeoch, 2008). Furthermore, mean sea surface temperature near the archipelago rose by >1°C between 1949 and 1998 (Melice *et al.*, 2003), coinciding with an increase in the abundance of subtropical zooplankton species and a decrease in Antarctic species (by ~20%) over the past three decades (Ansorge *et al.*, 2012). Changes in plankton community composition and productivity are likely to propagate throughout the marine food web, from the benthos (e.g., von der Meden *et al.* 2017) to the top predators (e.g., Carpenter-Kling *et al.* 2019). However, no integrated monitoring of the biogeochemistry or plankton system of the Prince Edward Islands archipelago waters has occurred for over 20 years. The resultant paucity of information makes it difficult to evaluate the extent to which climate change is altering the regional plankton community or the biological pump, both of which have implications for the food supply to the surrounding ecosystems, and for CO_2 uptake, export, and sequestration.

Here, we investigate the influence of the island mass effect on the productivity and functioning of the plankton ecosystem at the Prince Edward Islands archipelago in autumn, after the main growing season. We present the first (primary and new) productivity data for the archipelago in over 20 years and the first-ever measurements of mesozooplankton secondary production. We focus on autumn because this is the season during which most of the historical Prince Edward Islands studies were conducted (Ansorge *et al.*, 2012), and it is also a period of transition that directly follows the late-summer phytoplankton bloom. Moreover, a recent community-led report emphasizes the need for 'non-summer' season observations if the future state of the Southern Ocean is to be understood or predicted (Newman *et al.* 2019). While summer is considered the most important season for carbon production and export in the Subantarctic, significant CO_2 sequestration may still occur in the autumn while light levels remain high, augmenting the contribution of the archipelago to carbon drawdown on an annual basis. Indeed, our autumn rate data imply that while net primary production is fairly low, carbon export potential is not trivial, with new production accounting for ~25% of total phytoplankton productivity. We conclude that while the Prince Edward Islands do not have the same

productivity footprint in the Indian Subantarctic as the larger island plateaus to the east, the island mass effect of this archipelago nonetheless enhances the fertility of the surrounding ecosystem and its capacity to sequester atmospheric CO_2.

4.3. Materials and Methods

4.3.1. Sampling location and strategy

Marion Island Relief Voyage 024 to the Prince Edward Islands archipelago (6 April to 12 May 2017) occurred on board the MV *S.A. Agulhas II*. Marion Island (46°54'S, 37°45'E) is separated from the smaller Prince Edward Island (46°38'S, 37°57'E) by a 40 m- to 200 m-deep inter-island plateau that is surrounded by steep slopes descending to ~1000 m within 10 km of the coast (Figure 4.1). In total, 34 stations near the islands were sampled on different days over two weeks, during the day (D) and/or at night (N) (see Table C.1 for details). Of these, 12 stations (yellow circles in Figure 4.1) were sampled over 24 h each for hydrography, nutrients, size-fractionated chlorophyll-a, plankton taxonomy, and zooplankton gut contents. Experiments were conducted for primary production and nitrate uptake at seven stations (blue rings in Figure 4.1) and for secondary production at 13 stations (red squares in Figure 4.1). The remaining stations were sampled for hydrography, nutrients, and/or bulk (i.e., >0.3 µm) Chl-a. The stations were separated into three clusters: 'upstream', 'inter-island', and 'downstream,' and sampling was restricted to the upper 200 m of the water column where the bulk of the plankton of interest here are resident and active (Harris *et al.*, 2000).

4.3.2. Hydrography and biogeochemical sampling

A Sea-Bird SBE 9/11 Plus package with conductivity-temperature-depth (CTD), dissolved oxygen, and fluorescence sensors, and a rosette of 24 x 12-L Niskin bottles was deployed at each station. The mixed layer depth (MLD) was estimated as the depth in the upper 200 of maximum Brunt-Väisälä frequency squared. Nutrient samples were collected in acid-washed, sample-rinsed 50 mL centrifuge tubes that were stored at -20°C until analysis ashore. Nitrate+nitrite (NO_3^-+NO_2^-) and silicic acid (SiO_4^{4-}) concentrations were measured using a Lachat QuikChem® flow injection autoanalysis platform, with precision and detection limits of ± 0.5 µmol L^{-1} and 0.4 µmol L^{-1} for NO_3^-+NO_2^- and ± 0.5 µmol L^{-1} and 0.5 µmol L^{-1} for SiO_4^{4-}.

Ammonium (NH_4^+) concentrations were measured using the fluorometric method of Holmes *et al.* (1999), with a precision and detection limit of ± 0.05 μmol L^{-1} and 0.05 μmol L^{-1}, respectively.

4.3.3. Plankton collections and analysis of community composition

At the stations circled in yellow in Figure 4.1, phytoplankton samples were collected in Niskin bottles from the near-surface (~10 m) and the depth of maximum fluorescence (F-max; between 50 m and 70 m, identified during the CTD down-casts). Samples were preserved in 1% glutaraldehyde and stored in the dark at 5°C. Ashore, plankton (3-200 μm) abundance (cells L^{-1}) was determined by settling 100 mL of sample in an Utermöhl chamber, then counting the settled cells along multiple transects using an inverted microscope (ZEISS AXIO Vert. A1) at 200x magnification. To achieve an acceptable precision for each sample (confidence limit ± 20% at 95% significance level), at least 500 total cells and 100 units of the most dominant group were counted. Cell volumes were calculated from measurements of the average linear dimensions of at least 25 cells per species using geometric formulae that approximated cell shape (Sun and Liu 2003). Cellular carbon content was then estimated using the empirical relationships included in Table C.2.

Mesozooplankton samples were collected using a Bongo net (200 μm) that was towed vertically from 200 m to the surface at a constant speed of 0.5 m s^{-1}. Samples were fixed with buffered formalin (4% v/v final solution) for microscope analysis ashore (ZEISS Stemi 508 and ZEISS Primo Star). Euphausiacea were only identified to Order level. Mesozooplankton biomass (mg C m^{-3}) was estimated using body area, determined by averaging a minimum of 25 digitized images per species at a given development stage, and using species-specific dry mass conversion formulas (Lehette and Hernández-León, 2009).

4.3.4. Chlorophyll-a, net primary production, and nitrate uptake rates

Water samples were collected from the near-surface at all stations for the analysis of Chl-a concentrations. At 12 stations (coloured triangles in Figure 4.1), samples were also collected from six depths throughout the euphotic zone. Duplicate 500 mL aliquots of seawater were filtered through 0.3 μm- and 2.7 μm glass fibre filters (Sterlitech, GF-75 and Grade D; GF/F) and 25 μm nylon mesh filters. Chlorophyll-a was measured following the non-acidified method of Welschmeyer (1994) using a Turner Designs Trilogy fluorometer.

Rates of size-fractionated (i.e., pico- [0.3-2.7 µm], nano- [2.7-25 µm], and micro-phytoplankton [>25 µm]) net primary production (NPP) and NO_3^- uptake were measured at 7 stations (blue circles in Figure 4.1) at the near-surface and F-max. These two depths were chosen as representative of the range of rates likely to occur in the euphotic zone. Duplicate 2 L seawater samples were collected in clear polycarbonate bottles at midday, pre-screened (200 µm mesh) to remove large grazers, and amended with $NaH^{13}CO_3$ and $K^{15}NO_3$ (100 µM and 2 µM final concentration, respectively). Bottles were incubated for 4-6 h in an on-deck incubator equipped with neutral-density filters to simulate the 55% (i.e., surface) and 5-10% (i.e., F-max) light levels, and cooled with running near-surface seawater.

After incubation, 500 mL subsamples from each bottle were filtered through 0.3 µm and 2.7 µm pre-combusted GF/F and 1 L was filtered through a 25 µm nylon mesh from which the captured particles were resuspended in 0.2 µm-filtered seawater and re-filtered onto a 0.3 µm GF/F. Filters were stored in pre-combusted foil envelopes at -80°C. Ashore, each filter was freeze-dried for 24 h at -60°C, then packaged into a tin capsule and analysed for carbon (C) and nitrogen (N) content using a Flash 2000 Elemental Analyzer coupled to a Delta V Plus isotope ratio mass spectrometer. Three in-house standards, calibrated against IAEA reference materials, were included in each run along with numerous blanks (unused pre-combusted filter + tin capsule). The detection limit was 2 µg C and 1 µg N, and precision was ± 0.005 atom% for C and N.

Rates of NPP (nmol C L^{-1} h^{-1}) and NO_3^- uptake (nmol N L^{-1} h^{-1}) were calculated as:

$$V_t = atom\%_{xs} \,/\, (atom\%_{enr} - F) \times T \qquad \text{(Eqn. 4.1)}$$

$$\rho_t = V_t \times B_t \qquad \text{(Eqn. 4.2)}$$

where V_t is the specific uptake rate (h^{-1}) and ρ_t is the transport rate (nmol C or N L^{-1} h^{-1}), $atom\%_{xs}$ is the excess ^{13}C or ^{15}N (relative to F, the naturally-occurring atom% of 1.07% for ^{13}C and 0.366% for ^{15}N) in the particulate organic C or N (POC or PON) sample, $atom\%_{enr}$ is the atom% of ^{13}C or ^{15}N in the substrate pool (dissolved inorganic carbon or NO_3^-) upon tracer addition, B is the POC or PON concentration (nmol L^{-1}), and T is the incubation length (h) (Dugdale and Wilkerson, 1986).

Eppley and Peterson (1979) defined the *f*-ratio as the ratio of new- to total production, calculated as:

$$f\text{-ratio} = \frac{\mathrm{NO_3^-\ uptake}}{\mathrm{NO_3^- + NH_4^+\ uptake}} \quad \text{(Eqn. 4.3)}$$

Since we did not measure NH_4^+ uptake, we computed the *f*-ratio as:

$$f\text{-ratio}_{NPP} = \frac{\mathrm{NO_3^-\ uptake}}{\mathrm{NPP} \times 16/106}$$

Here, 16/106 is the average ratio in which phytoplankton take up N and fix CO_2 (Redfield, 1934). Our *f*-ratio$_{NPP}$ formulation thus assumes that phytoplankton were behaving according to 'Redfieldian' expectations, which is reasonable given that non-diatom phytoplankton C:N ratios do not appear to vary much from 106:16 (Garcia *et al.*, 2018). If anything, the C:N ratio of nano-phytoplankton relying mainly on recycled N may be higher than 106:16 (Garcia *et al.*, 2018), which would yield a higher *f*-ratio$_{NPP}$. The *f*-ratio$_{NPP}$ also accounts for productivity supported by regenerated N forms other than NH_4^+, such as urea, which has been shown to fuel 13-27% of regenerated production (4-24% of total production) near the archipelago in autumn (Thomalla *et al.*, 2011).

Mixed layer-integrated NPP and NO_3^- uptake rates (mg m^{-2} h^{-1}) were calculated assuming that photosynthesis decreases as light attenuates with depth (Loisel and Morel, 1998). Since NO_3^- reduction is energy-intensive, the rate of NO_3^- uptake should also decline with decreasing light (e.g., Mdutyana *et al.* 2020). For each station, we fitted an exponential regression curve using the two measured rates (surface and F-max) and setting NPP and NO_3^- uptake to zero at the base of the euphotic zone, defined as the depth at which light was attenuated to 1% of its surface value. The Euphotic zone depth was calculated as:

$$E_z = E_0 \times e^{-kz}$$

where *E* is irradiance, *z* is euphotic zone depth, *0* is the surface, and *k* is the attenuation coefficient, determined from light attenuation data available for April and May 2017 near the archipelago (doi:10.5067/ORBVIEW-2/SEAWIFS_OC.2014.0); for k = 0.03 m^{-1}, z = 153.5 m. The MLD at each station

was significantly shallower than *z*, driven by a strong thermocline at 90-100 m that isolated the lower euphotic zone waters below it. We therefore integrated to the MLD instead of to *z*, deriving the NPP or NO_3^- uptake rate at the MLD from the regression equation. Our results are thus more likely to underestimate than overestimate productivity.

4.3.5. Daily egg production and grazing rate estimates

Egg production (i.e., 'secondary production') was measured for *Calanus simillimus*, the dominant copepod species in our study area, at 13 stations up- and downstream of the islands (red squares in Figure 4.1). Specimens were gently collected from the near-surface using a 300 µm driftnet. Following the bottle incubation method (Peterson *et al.*, 1991), single undamaged mature adult females were transferred to opaque 1 L polycarbonate bottles filled with pre-filtered (63 µm) surface water. The bottles were incubated at 4°C and gently agitated by the movement of the ship. After 24 h, the females were removed, their condition was assessed (experiments wherein females were found dead or moribund were excluded), and the eggs produced during the incubations were counted using a dissecting microscope. Secondary production can be estimated as carbon-specific egg production (C-SEP; d^{-1}) following Jakobsen *et al.* (2018) as:

$$C - SEP = EPR \times (C_e / C_f)$$

where *EPR* (egg production rate) = the number of eggs female^{-1} day^{-1} (eggs f^{-1} d^{-1}), C_e = egg C content, and C_f = female C content. C_e was estimated from egg volume (average egg diameter of *C. simillimus* = 150 µm*;* Ward and Shreeve (1995)) and a conversion factor of 0.139×10^{-6} µg C µm^{-3} (Huntley, 1992), and C_f was estimated from the body area conversion formulas of Lehette and Hernández-León (2009). Due to temperature differences between the ambient seawater (5-6°C) and incubation environment (4°C), egg production rates were scaled using a Q_{10} factor of 2.9 (Hansen *et al.*, 1997).

Sample collection and analysis for gut fluorescence and grazing rates were based on the protocol of Decima *et al.* (2016). After each Bongo net cast, the contents of one cod-end were rapidly anesthetized with CO_2 (via the addition of soda water) to prevent gut-content evacuation, then fractionated into four size-classes: 200-500 µm, 500-1000 µm, 1000-2000 µm, and >2000 µm. Each fraction was concentrated onto a 47 mm glass fibre filter, flash frozen in liquid nitrogen, and stored at -80°C. In the laboratory, two quarters of each filter

were transferred to borosilicate test tubes containing 7 mL of 90% acetone that were sonicated for 20 seconds, then left in the dark at -20°C for 24 h to allow for pigment extraction. The supernatant obtained by centrifuging the extracted samples at 3000 rpm for 5 min was analysed using a Turner Designs Trilogy fluorometer equipped with a Chl-a 'acidified module,' before and after acidification with 1 drop of 10% HCl, yielding total Chl-a and phaeopigments, respectively. Pigment content was estimated from the equations of Lorenzen (1967). While non-degraded Chl-a can be found in the gut of copepods along with phaeopigments, we used only phaeopigment content in our grazing rate calculations to avoid including any phytoplankton aggregates caught in the net (Decima *et al.*, 2016). Gut pigment content was trapezoidally depth-integrated to 200 m.

Ingestion (or grazing) rates (I; µg pigment m^{-3} d^{-1}) were calculated following the equation of Mackas and Bohrer (1976):

$$I = G \times K$$

where G is the depth-integrated gut pigment content and K is the gut passage rate of 0.019 min^{-1}, determined empirically for copepods living in 5°C seawater (Dam and Peterson, 1988). This K value agrees with gut passage rates estimated for *C. simillimus* collected from PFZ waters west of the Prince Edward Islands (K = 0.0053-0.0238 min^{-1}; Bernard and Froneman 2003). A carbon/Chl-a ratio of 50:1 (weight:weight) was used to convert measured gut-content Chl-a (inferred from phaeopigment measurements) to autotrophic carbon (Atkinson, 1996).

4.3.6. Remote sensing data

We examined monthly (October 2016 to May 2017) level-3 Chl-a concentrations from the MODIS Aqua satellite product (https://oceandata.sci.gsfc.nasa.gov/MODIS-Aqua/Mapped/Monthly/4km/chlor_a/) near the archipelago at 4 km spatial resolution. Additionally, 1/4-degree horizontal resolution daily sea surface height (SSH) and derived geostrophic currents were acquired from the multi-mission level-4 satellite gridded product (SEALEVEL_GLO_PHY_L4_REP_OBSERVATIONS_008_047; http://marine.copernicus.eu). Positions of the northern (N), middle (M), and southern (S) branches of the SAF and APF were determined

using the SSH data: N-SAF = 0.240 m, M-SAF = 0.030 m, S-SAF = −0.170 m, N-APF = −0.300 m, M-APF = −0.480 m, and S-APF = −0.630 m (Sokolov and Rintoul, 2009b, 2009a; Lamont *et al.*, 2019).

4.3.7. Statistical analyses

Plankton abundance data were log-transformed prior to statistical analysis (Curran-Everett, 2018). To test for differences in community structure among the different regions (i.e., upstream, inter-island, downstream), a permutation multivariate analysis of variance (PERMANOVA) was undertaken using the Primer-E software (ver.7, 2009). Maps of the horizontal distributions of physical and biogeochemical parameters were produced using the multilevel B-splines method of the R-package 'MBA'. The distribution about the population mean or median is presented as ± standard deviation (± STDEV) if observations were replicated (e.g., species abundance) or as ± standard error (± SE) if experiments were replicated (e.g., NPP).

4.4. Results

4.4.1. Evolution of the surface Chl-a distribution and hydrographic conditions

The evolution of the surface Chl-a distribution between spring and autumn 2017 appeared strongly influenced by the eastward movement of the oceanic fronts (Figure 4.2). In January, the phytoplankton biomass remaining after the spring bloom was trapped in a meander of the S-SAF (Figure 4.2d) that transported it eastward until it dissipated in May (Figure 4.2h). The late-summer (i.e., February and March) phytoplankton bloom augmented the biomass contained within this meander (Figure 4.2e and f). By the time of our sampling, Chl-a had declined and the S-SAF was transporting the remnants of the late-summer bloom to the northeast of the archipelago, leaving the upstream region depleted of phytoplankton (Figure 4.2g-h).

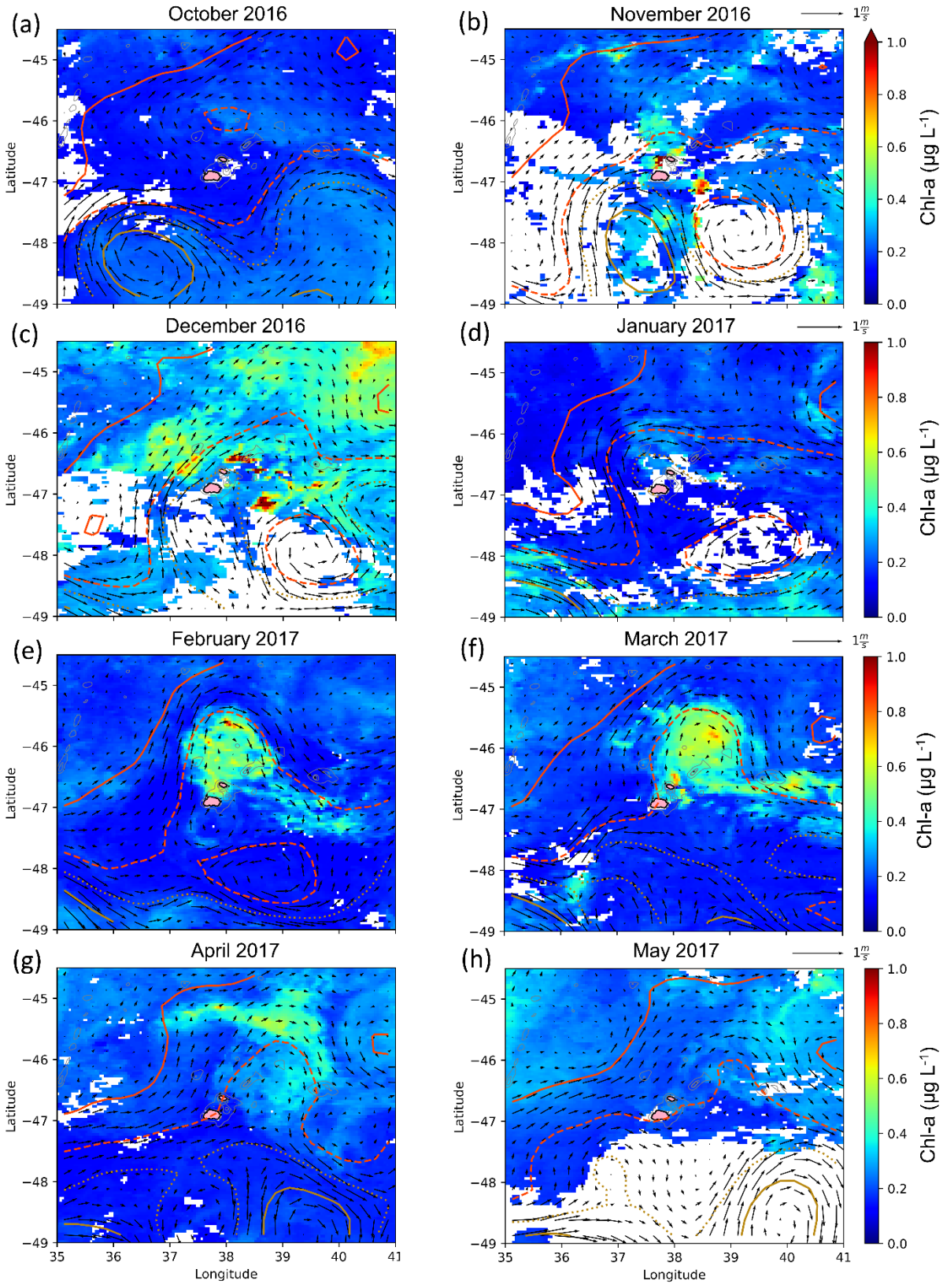

Figure 4.2 Monthly-averaged MODIS satellite-derived surface Chl-a concentrations around the Prince Edward Islands from October 2016 (a) to May 2017 (h). Solid orange line = M-SAF; dashed orange line = S-SAF; dotted yellow line = N-APF; solid yellow line = M-APF (see text for acronym definitions). The overlaid black arrows show the magnitude and direction of the geostrophic currents.

4.4.2. Oceanographic setting

The position of the S-SAF in April 2017 resulted in warmer (6.5-7°C), more saline (~33.90), lower-oxygen (~275-280 μM) waters to the northwest of Marion Island, separated from the cooler (5.5-6.0°C) and fresher (<33.85) waters to the south and east that were influenced by the N-APF (Figures 4.3a and C.1a-b). South of the S-SAF, the inter-island stations were slightly warmer (≥6.0°C) and more saline (≥33.85) than the stations to the south and east of the archipelago (5.0-6.0°C and 33.75-33.85). All the stations were characterized by a stable pycnocline, with MLDs of ~120 m at the upstream and downstream sites and ~90-100 m in the inter-island region (except at station H20 where the MLD was ~150 m).

Between the surface and 200 m, the concentrations of NO_3^-+NO_2^- (hereafter, NO_3^-), SiO_4^{4-}, and NH_4^+ ranged from 16.5 to 23.0 μmol L^{-1}, 2.0 to 12.5 μmol L^{-1}, and 0.1 to 1.6 μmol L^{-1}, respectively, with higher values generally observed between the islands and downstream (Figure 4.3b-c; Figure C.1c; surface concentrations only).

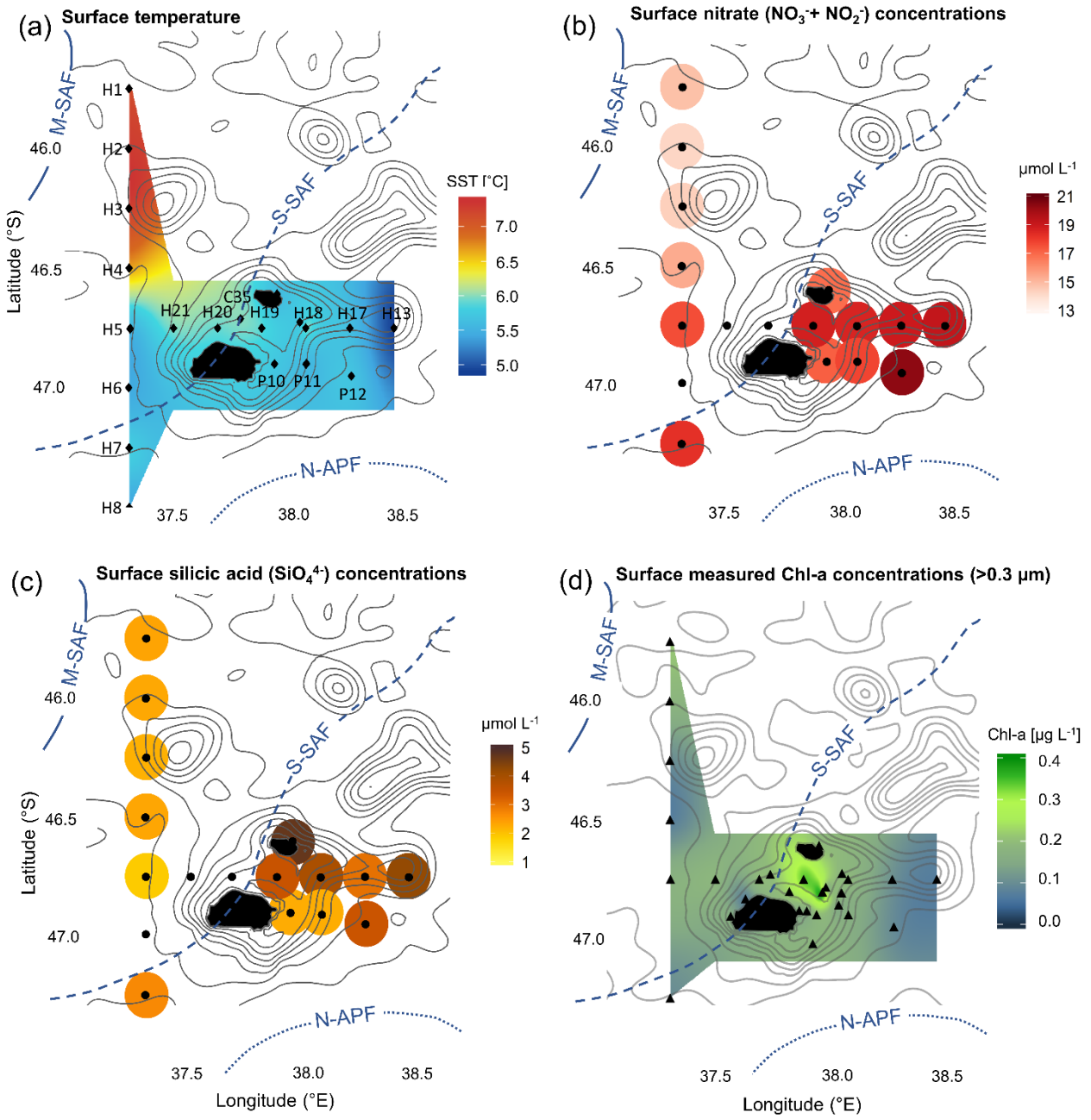

Figure 4.3 Surface maps of the major hydrographic and biogeochemical parameters measured around the Prince Edward Islands: (a) temperature, (b) nitrate+nitrite (NO_3^-+NO_2^-), (c) silicic acid (SiO_4^{4-}), and (d) Chl-a. Solid grey lines = bathymetry (see Figure 4.1 for depths); solid blue line = M-SAF; dashed blue line = S-SAF; dotted blue line = N-APF (see text for acronym definitions). The black dots indicate the positions of the stations, with station numbers included on panel (a).

4.4.3. Plankton (<200 µm) biomass and community composition

Total phytoplankton Chl-a (>0.3 µm) was relatively invariant around the archipelago at 0.2 to 0.3 µg L^{-1}, increasing slightly between the two islands to 0.4 µg L^{-1} (Figures 4.3d and C.2). The lowest Chl-a concentrations were observed at the most downstream stations, H13N and P12D, and at the southernmost upstream station H7 where the influence of the N-APF was greatest. Chl-a was relatively homogenous throughout the mixed layer (Figure C.2b), with the nanoplankton size-class contributing most to total Chl-a (60%; 0.1 < Chl-a < 0.3 µg L^{-1}), followed by the pico- (32%; <0.2 µg L^{-1}) and microplankton (8%; <0.1 µg L^{-1}).

The average bulk (0.3-200 µm) POC concentration across the archipelago was 75.2 ± 52.1 mg C m^{-3} (median of 50 mg C m^{-3}), reaching a maximum at inter-island station H18D (190 mg C m^{-3} at the surface and 100 mg C m^{-3} at the F-max). In general, higher POC (≥100 mg C m^{-3}) occurred throughout the euphotic zone in the inter-island and upstream areas, while at the downstream stations, POC was ~50 ± 10 mg C m^{-3} (Figure C.3). These values are 10- to 20-times higher than the summed nano+microplankton biomass values, estimated by converting species-specific biovolumes to carbon (Figure 4.4a-b). Average nano+microplankton biomass was 5.1 ± 2.0 mg C m^{-3}, reaching a maximum of 8-9.8 mg C m^{-3} at upstream stations H5N and H7D and inter-island station H18D. On average, nano- and microplankton contributed ~30% and ~70% of the total biomass, with ciliates (i.e., heterotrophs) constituting 43 ± 16% on average (50% upstream, 31% in inter-island waters, 51% downstream). The contribution of photoautotrophs (flagellates, cryptophytes, coccolithophores, diatoms) to nano+microplankton carbon ranged from 0.3 to 2.7 mg C m^{-3} (average across the study region of 1.4 ± 0.6 mg C m^{-3}; 25 ± 5% of total nano+microplankton biomass). This estimate would likely be higher if a dinoflagellate contribution were included since this group accounted for an average of 1.4 ± 0.8 mg C m^{-3} (28 ± 14% of the total nano+microplankton biomass). However, because the extent of dinoflagellate autotrophy *versus* mixotrophy is unclear (Stoecker, 1999), we exclude dinoflagellates from our calculations of autotrophic carbon.

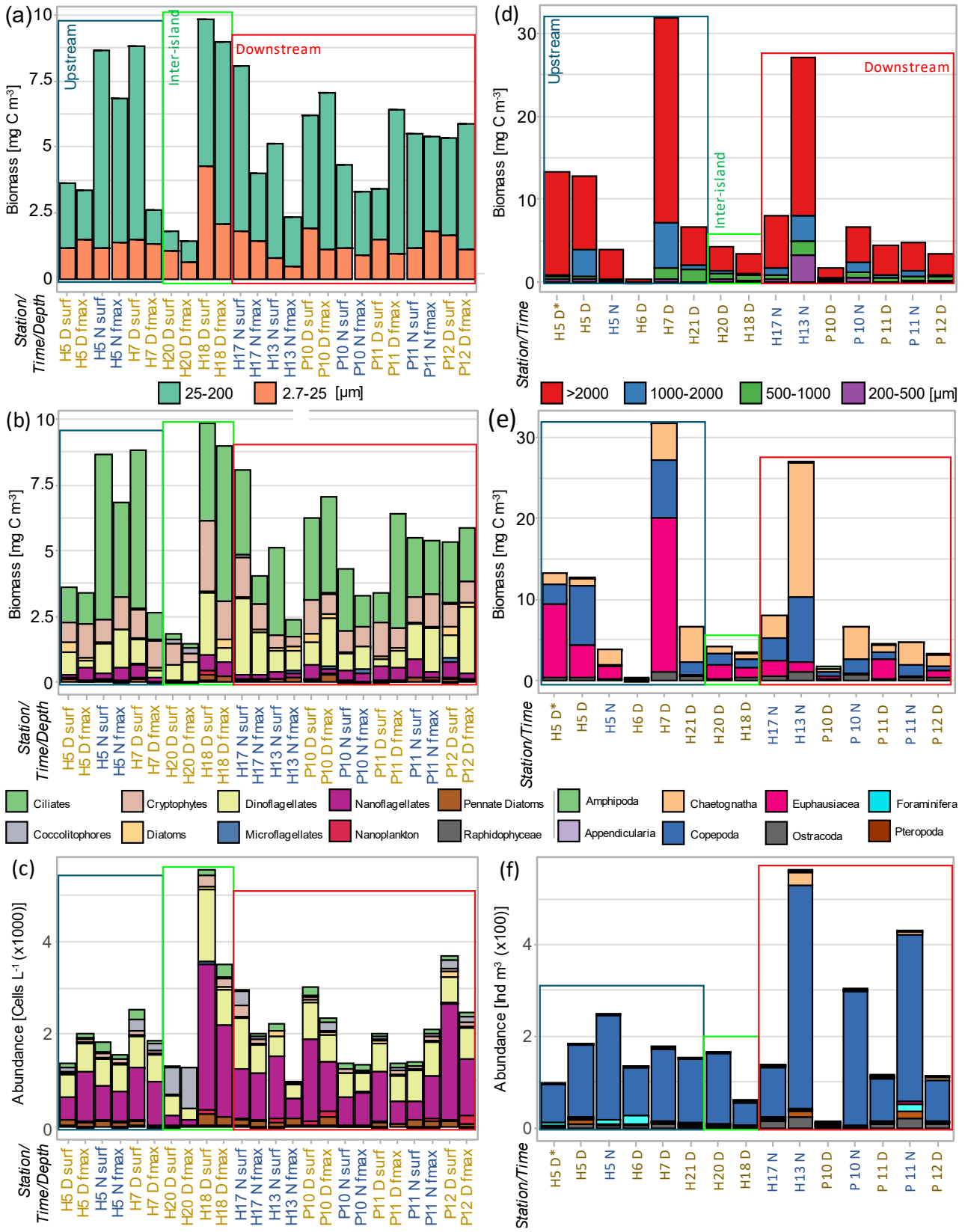

Figure 4.4 Biomass (mg C m^{-3}) and abundance (cells L^{-1} and ind. m^{-3}) of plankton <200 µm (mainly phytoplankton; (a-c) and mesozooplankton >200 µm (d-f). (a, d) Biomass in each size class; (b, e) biomass at the taxon level; and (c, f) abundance at the taxon level. Panels b and c share a legend. The large open squares indicate the area sampled: dark blue = upstream, green = inter-island, red = downstream. The x-axes show the stations, water depth (surface and F-max; panels a-b only), and time of sampling (D = day, yellow; N = night, blue).

At all the NPP stations, the POC-to-PON ratio (C:N) of bulk samples exceeded that expected for typical marine biomass (6.63; Redfield, 1934), ranging from 8.2 to 12.1 (Table C.3). The biomass C:N ratios were similar in the upstream and inter-island regions (10.5 ± 0.7 and 10.4 ± 2.5), while downstream, C:N was lower (8.4 ± 0.1). Biomass C:N varied among size-classes, with picoplankton characterized by the lowest C:N ratio (4.6 ± 2.3), while nano- and microplankton had higher ratios (10.1 ± 1.7 and 27.7 ± 7.4).

Although not dominant in terms of biomass, nanoflagellates (3-10 µm) numerically dominated the phytoplankton community (average abundance of 10.5 ± 7.1 cells mL^{-1}), followed by the dinoflagellates and pennate diatoms (6.3 ± 2.6 cells mL^{-1} and 0.9 ± 0.6 cells mL^{-1}) (Figure 4.4c, Table C.4). Across the archipelago, nanoplankton (nanoflagellates, cryptophytes, coccolithophorids) and dinoflagellates comprised an average of 60% and 30% of the total phytoplankton cells, respectively. Centric diatoms were minor contributors at all stations (1.7 ± 1.1%), with slightly higher downstream abundances (2.1 ± 1.7% on average, reaching 4.0 ± 1.4% at station H13N). Station H18D (inter-island) had the highest abundances of nano- and microplankton (40.5 ± 14.6 cells mL^{-1} and 5.0 ± 0.2 cells mL^{-1}). Nonetheless, phytoplankton biomass and community composition were relatively homogenous around the archipelago, with no significant differences among areas (PERMANOVA; $R^2 = 0.17$, $p = 0.07$).

4.4.4. Rates of net primary production and nitrate uptake

Similar trends were observed for NPP and NO_3^- uptake (Figure 4.5a and b; Table C.3), with surface rates that were typically 1.5- to 2-times those measured at the F-max, and generally highest in the inter-island region. Additionally, the rates were slightly higher downstream (mainly at stations P11 and P12) than upstream. Maximum rates for the total phytoplankton community were recorded at inter-island station C35, where NPP and NO_3^- uptake were 3- and 2-times higher, respectively, than the average rates for the plateau (55.3 ± 9.2 nmol C L^{-1} h^{-1} and 1.3 ± 0.1 nmol N L^{-1} h^{-1} *versus* 15.9 ± 13.5 nmol C L^{-1} h^{-1} and 0.5 ± 0.4 nmol N L^{-1} h^{-1}). The lowest rates of NPP and NO_3^- uptake were observed at stations H7 (upstream; 5.4 ± 5.1 nmol C L^{-1} h^{-1} and 0.15 ± 0.1 nmol N L^{-1} h^{-1}) and P10 (downstream; 6.8 ± 3.1 nmol C L^{-1} h^{-1} and 0.35 ± 0.1 nmol N L^{-1} h^{-1}).

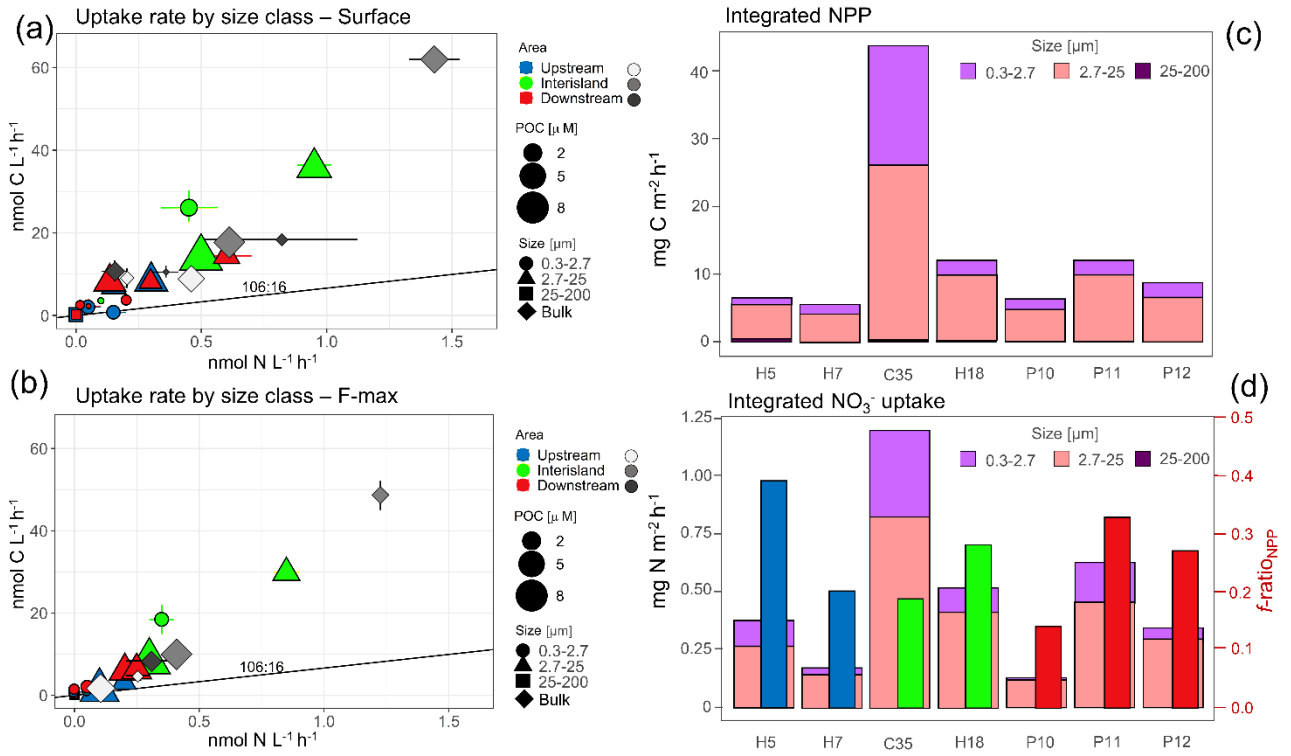

Figure 4.5 Rates of NPP (nmol C L^{-1} h^{-1}) and NO_3^- uptake (nmol N L^{-1} h^{-1}) in the waters surrounding the Prince Edward Islands at the (a) surface and (b) F-max. Symbol shape indicates the phytoplankton size-class: circle = picoplankton (0.3 - 2.7 µm), triangle = nanoplankton (2.7 - 25 µm), square = microplankton (25 - 200 µm), and diamond = bulk (0.3 - 200 µm). The colours represent the different regions: blue and grey = upstream, green and light-grey = inter-island, and red and dark-grey = downstream. The size of the symbols is proportional to the POC concentration. Also shown are the mixed layer-integrated rates of (c) NPP (mg C m^{-2} h^{-1}) and (d) NO_3^- uptake (mg N m^{-2} h^{-1}). Here, the colours of the wide bars indicate the size classes: bright purple = picoplankton, pink = nanoplankton, and dark purple = microplankton. The secondary y-axis and narrow coloured bars on panel (d) show the *f*-ratio$_{NPP}$, with the bar colours indicating the sampling regions (as per panels (a) and (b).

The nanoplankton size-class was the most productive, contributing 73 ± 8% of total NPP and 79 ± 9% of total NO_3^- uptake, followed by the picoplankton at 25 ± 9% and 20 ± 11% (Figure 4.5c-d). The microplankton accounted for <1.8% of both NPP and NO_3^- uptake.

The bulk *f*-ratio$_{NPP}$ ranged from 0.13 to 0.39 (whole-plateau average of 0.24 ± 0.09), indicating that recycled N fuelled 61-87% (average of 76%) of NPP (Figure 4.5d). On average, the *f*-ratio$_{NPP}$ was similar for the pico- and nanoplankton (0.26 ± 0.26 and 0.23 ± 0.05; Table C.3). We observed no clear differences in the *f*-ratio$_{NPP}$ among the upstream, inter-island, and downstream regions, and no strong relationship with productivity. For example, the station characterized by the highest rates of NPP and NO_3^- uptake (C35D) had one of the lowest *f*-ratios$_{NPP}$ (0.18 ± 0.01), while the highest *f*-ratio$_{NPP}$ (0.38 ± 0.03) was estimated for station H5D where NPP was low and NO_3^- uptake occurred at a moderate rate (Figure 4.5c-d; Table C.3).

4.4.5. Mesozooplankton biomass and community composition

Mesozooplankton biomass in the upper 200 m was quite variable across the study region (Figure 4.4d-e). For stations sampled during the day (D) and at night (N), no clear diel pattern emerged. For example, biomass at station H5 was three-times higher during the day (H5D* and H5D) than at night (H5N), biomass at P10 was four-times lower during the day than at night, and at P11, day and night biomass was similar. Stations H7D (far upstream) and H13N (far downstream) were characterised by the highest biomass, and stations H6D (upstream) and P10D (immediately downstream) supported the lowest biomass. Across the archipelago, total mesozooplankton biomass averaged 8.8 ± 9.1 mg C m^{-3} and was dominated by the >2000 µm size-class and by non-copepod species (collectively ~70% of total biomass; Figure 4.4d-e). Chaetognatha, Euphausiacea, and Copepoda constituted the three major taxa in terms of biomass, with the large size of the latter two groups elevating the biomass of the 1000-2000 µm and >2000 µm size-classes compared to the more numerically abundant 200-500 µm and 500-1000 µm fractions (which constituted ~8% and ~5% of the biomass).

Mesozooplankton abundance was dominated by copepods (~86% of the total organisms counted, ~2500 ind. m^{-3}; Figure 4.4f, Table 4.1). More generally, the main contributors were the 200-500 µm and 500-1000 µm size-classes, responsible for ~40% and ~30% of the total individuals counted. The remaining organisms were apportioned between the 1000-2000 µm (~21%) and >2000 µm size-classes (~9%).

Table 4.1 Abundances (ind. m^{-3}) of mesozooplankton sampled near the Prince Edward Islands in autumn 2017. Taxa are arranged in order of decreasing average abundance. Italicized U = upstream, I = inter-island, D = downstream.

Station	H5D	H5N	H5D*	H6D	H7D	H21D	H20D	H18D	H17D	H13D	P10D	P10N	P11D	P11N	P12D	Average	STDEV
Area / Taxa	U	U	U	U	U	U	I	I	D	D	D	D	D	D	D		
Copepoda	87.54	159.15	229.01	106.1	156.5	139.7	156.50	50.40	107.87	487.19	5.77	295.67	93.72	361.64	89.30	168.41	127.14
Ostracoda	4.46	7.32	6.26	7.71	9.69	5.87	4.81	3.71	13.23	22.35	1.28	2.32	7.75	21.43	9.66	8.52	6.22
Chaetognatha	0.64	1.49	1.31	2.72	5.69	2.76	1.84	3.93	8.21	33.39	0.26	1.75	5.62	8.98	8.70	5.82	8.18
Foraminifera	4.90	5.20	10.43	17.75	3.75	3.36	1.63	0.21	5.48	3.54	2.09	0.11	4.24	15.92	5.34	5.60	5.21
Limacina spp.	0.25	8.56	0.35	0.85	0.71	0.18	0.21	0.25	3.22	13.44	2.46	0.45	2.62	13.72	0.21	3.17	4.76
Copepod nauplii	1.77		2.83	0.28	1.91	1.03	3.57	3.57	0.04	1.06	0.09	3.28	3.71	0.28	3.86	1.82	1.52
Euphausiacea	0.34	2.02	0.99	0.21	1.41	1.17	1.10	1.31	0.25	1.98	0.17	2.26	0.21	7.85	0.11	1.43	1.92
Amphipoda	0.16	0.04	0.50	0.50	0.39	0.39	0.32	0.71	0.39	1.70	0.58	1.53	0.50	1.63	0.18	0.63	0.54
Cryptoniscus larvae (Isopod)	0.05	0.07	0.04	0.04	0.21	0.21	0.18	0.18	0.21	0.21		0.06	0.04		0.25	0.12	0.09
Oikopleura spp.	0.02			0.04		0.14		0.07	0.04	0.35		0.28	0.14	0.35	0.04	0.10	0.13
Cnidaria											0.09	0.06	0.04			0.01	0.03
Fritillaria spp.								0.04					0.07			0.01	0.02
Creseis spp.													0.11			0.01	0.03
Enteropneusta										0.07							0.02

Mesozooplankton assemblages were similar across the archipelago, albeit with variable relative abundances of the different groups (Figure 4.4f). While there was no significant difference in species distribution as a function of environmental parameter (temperature, salinity, oxygen, and nutrients; PERMANOVA; R^2 = 0.17, p = 0.25) or location (upstream, inter-island, downstream; PERMANOVA; R^2 = 0.18, p = 0.15), abundances were higher at night at the three stations that were sampled over a diel cycle – H5 (upstream; 254 ind. m^{-3} at night *versus* 142 ± 60 ind. m^{-3} in the day), P10 (downstream; 308 *versus* 15 ind. m^{-3}), and P11 (downstream; 443 *versus* 119 ind. m^{-3}), with the highest abundances recorded downstream at night (stations H13N and P11N; 566 and 443 ind. m^{-3}, respectively). For the stations with day- and night data, all size-classes were more abundant at night (200-500 µm, 152 ± 73 ind. m^{-3} at night *versus* 46 ± 32 ind. m^{-3} in the day; 500-1000 µm, 86 ± 86 *versus* 47 ± 38 ind. m^{-3}; 1000-2000 µm, 79 ± 53 *versus* 21 ± 14 ind. m^{-3}; >2000 µm, 22 ± 18 *versus* 11 ± 7 ind. m^{-3}). Average copepod abundances increased from 76 ± 47 ind. m^{-3} during the day to 384 ± 98 ind. m^{-3} at night (*t-test*, p-value <0.01). This trend was strongest for smaller copepod species such as *Oithona* spp. (from 67 ± 49 to 171 ± 81 ind. m^{-3}; p-value <0.01) and species of the family Clausocalanidae (from 20 ± 13 to 66 ± 53 ind. m^{-3}; p-value <0.01) (Table C.5). We do not have enough data to robustly address the potential effects of diel vertical migration on the zooplankton distributions at the time of sampling. However, given that most of the zooplankton of interest here reside and are active in the upper 200 m (rather than migrating to depth) (Harris *et al.*, 2000), we consider the combined day- and night dataset to broadly characterize the composition and role of zooplankton in the plankton system of the Prince Edward Islands archipelago, specifically with regards to carbon transfer within and from the euphotic zone.

The copepod community was dominated by Cyclopoida (*Oithona similis*; >63% of total copepods) and Clausocalanidae (mostly *Clausocalanus* spp.; ~21%) (Table C.5). Adult Calanidae (1.3%) were abundant at the downstream stations, while juveniles were well-represented across the archipelago (7.6%) (Table C.6). Key Antarctic species such as *Calanus simillimus, C. propinquus, Rhincalanus gigas, Heterorhabdus austrinus, Paraeuchaeta antarctica, Pleuromamma robusta, Metridia gerlachei*, and *M. lucens* were present at low abundances (0.07% to 1.15% of total copepods). *C. simillimus* and *R. gigas* were mainly found at the downstream stations, while Metrinidae *(P. robusta, M. gerlachei, M. lucens*; 3.4%), were more homogenously distributed across the archipelago. *P. antarctica* was present only at the upstream stations

(0.1%), while *Microcalanus* spp., common in previous studies of this region (e.g., Boden and Parker 1986), were not observed.

The non-copepod mesozooplankton community (14.2% of total mesozooplankton abundance) was dominated by Ostracoda (30.2%), Chaetognatha (20.6%), and Foraminifera (19.9%) (Figure 4.4f; Table C.7). While Ostracoda were homogenously distributed among regions (30.3%, 27.2%, and 30.5% of all non-copepod mesozooplankton in the upstream, inter-island, and downstream areas, respectively), Chaetognatha were more abundant downstream (56.7% *versus* 10.3% [upstream] and 46.3% [inter-island]) and Foraminifera were more abundant upstream (32.9% *versus* 10.2% [inter-island] and 14.3% [downstream]). Different life-cycle stages of Euphausiacea (200 µm to <4 cm) comprised 4.7% of the non-copepod community. Those in the 500-1000 µm and 1000-2000 µm size-classes were most abundant, accounting for 46.5% and 39.9% of the total krill.

4.4.6. Egg production and grazing rates

Of the 48 *C. simillimus* females that were individually incubated, 17 spawned between 1 and 22 eggs, while the remaining 31 produced no eggs (Table 4.2). The C-SEP was on average 17 ± 4% d^{-1} (n = 48; EPR = 3.7 ± 0.1 eggs f^{-1} d^{-1}) and was lower at the upstream (10 ± 7% d^{-1}, n = 12) and inter-island (11 ± 11% d^{-1}, n = 2) than the downstream stations (20 ± 5% d^{-1}, n = 34), with one specimen at P11 producing the maximum number of eggs (EPR = 22.5 eggs f^{-1} d^{-1}).Table 4.3 shows the EPRs for *C. simillimus* measured in Subantarctic waters during voyages to the Prince Edward Islands archipelago in autumn 2013 through 2016 and on winter cruises in 2012 and 2015 (Verheye, 2017) , as well as in summer 2011/2012 during a voyage along the Greenwich meridian *en route* to Antarctica (Kattner, 2012). The EPR estimated for autumn 2017 was on average four-times lower than in summer, and while higher than the EPR measured in winter 2015 and similar to winter 2012 and autumn 2014, was three- to six-times lower than the EPR measured in autumn 2013, 2015, and 2016.

Table 4.2 Egg production rates (EPR; eggs f^{-1} d^{-1}) and carbon-specific egg production rates scaled for temperature (C-SEP; d-1) for *C. simillimus* measured near the Prince Edward Islands in autumn 2017. '-' indicates no data because the number of spawned eggs = 0 or 1. In the column headed 'Stations', D = Day, N = Night. In the column headed 'Area', U = Upstream, I = Inter-island, D = Downstream. The rates aligned with 'TOTAL PEIs', 'Upstream', 'Inter-island', and 'Downstream' are the averages ± SE for all stations in these locations, with PEIs referring to Prince Edward Islands.

Stations	Area	n females	mean EPR (eggs f^{-1} d^{-1})	max EPR (eggs f^{-1} d^{-1})	mean C-SEP (d^{-1})	max C-SEP (d^{-1})
H5D	U	1	-	-	-	-
H6D	U	2	-	-	-	-
H7D	U	3	3.5 ± 3.5	10.5	0.2 ± 0.3	0.5
H8D	U	5	0.2 ± 0.3	0.9	0.01 ± 0.01	0.04
D1D	U	1	-	16.8	-	0.8
MT1N	I	1	-	4.9	-	0.2
MT5N	I	1	-	-	-	-
D13D	D	1	-	-	-	-
C23D	D	1	-	20.0	-	0.9
P10D	D	2	4.7 ± 4.7	9.4	0.4 ± 0.4	0.7
P11D	D	27	4.3 ± 1.3	22.5	0.2 ± 0.1	0.9
H17N	D	1	-	-	-	-
H13N	D	2	-	-	-	-
TOTAL PEIs		**48**	**3.7 ± 0.1**	**22.5**	**0.2 ± 0.04**	**0.9**
	Upstream	12	2.4 ± 1.5	16.8	0.1 ± 0.1	0.8
	Inter-island	2	2.5 ± 0.1	5.0	0.1 ± 0.1	0.2
	Downstream	34	4.3 ± 1.1	22.5	0.2 ± 0.05	1.0

Table 4.3 Average and maximum egg production rates (EPR; eggs f^{-1} d^{-1}) for *C. simillimus* measured in Subantarctic waters prior to 2017 during summer along the Greenwich meridian (Kattner, 2012), and during autumn and winter near the Prince Edward Islands (Verheye, 2017), with our new data shown in bold. N = number of observations.

Year	**Summer** (Dec-Jan)			**Autumn** (Apr-May)			**Winter** (Jul-Aug)		
	N	mean EPR	max. EPR	N.	mean EPR	max. EPR	N.	mean EPR	max. EPR
2011	17	16	44						
2012							95	4	13
2013				136	12	57			
2014				43	5	27			
2015				40	15	45	5	0	0
2016				2	24	47			
2017				**48**	**4**	**23**			

Zooplankton grazing rates ranged from 4 to 28 µg Chl-a m^{-2} h^{-1} upstream, 4 to 18 µg Chl-a m^{-2} h^{-1} in the inter-island region, and 5 to 70 µg Chl-a m^{-2} h^{-1} downstream, with no significant differences among stations and regions (PERMANOVA; R^2 = 0.17, p = 0.09; Figure 4.6a). The median grazing rate was 12.5 µg Chl-a m^{-2} h^{-1} (0.62 mg C m^{-2} h^{-1}). Elevated grazing rates were observed at night at some stations, such as at downstream stations H13 and P11 (75.6 and 59.4 µg Chl-a m^{-2} h^{-1}, or 3.7 and 2.9 mg C m^{-2} h^{-1}). Grazing rates at H7D (upstream) were higher than the median, reaching 27.5 µg Chl-a m^{-2} h^{-1} (1.4 mg C m^{-2} h^{-1}). The contribution of Euphausiacea to grazing over the upper 200 m was 2.3 µg Chl-a m^{-2} h^{-1}, corresponding to ~20% of the community grazing rate and reaching a maximum of 20.2 µg Chl-a m^{-2} h^{-1} at P11N (Figure C.5; see also Appendix C.b).

Community grazing rates showed a positive relationship with zooplankton abundance (p < 0.001, R^2 = 0.74; Figure C.4). Additionally, although we did not observe a significant relationship between the depth-integrated rates of NPP and zooplankton grazing rates (R^2 = 0.02), phytoplankton production in all areas of the archipelago was sufficient to sustain mesozooplankton grazing (i.e., all data points fall below the 1:1 line in Figure 4.6b), assuming the zooplankton were actually grazing on the extant phytoplankton.

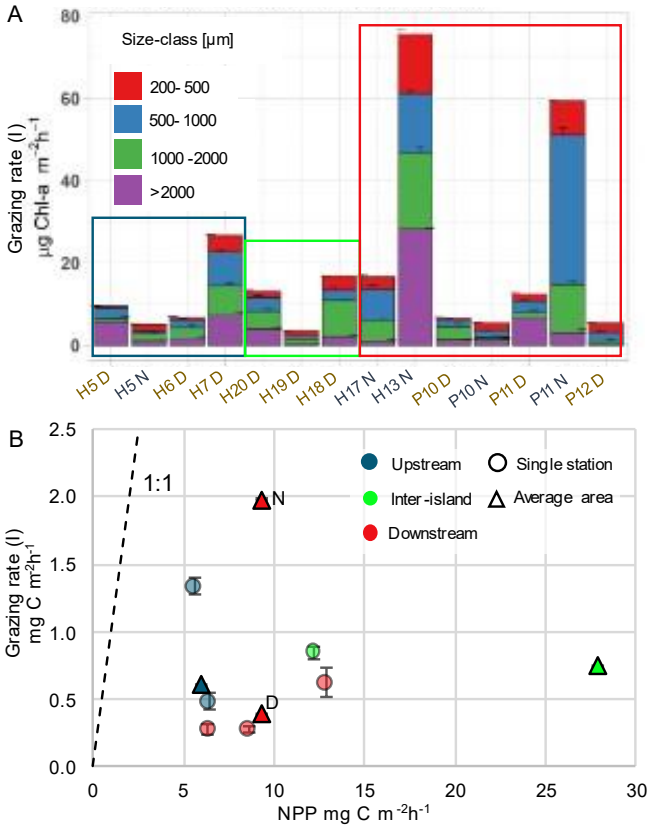

Figure 4.6 (a) Grazing rates (µg Chl-a m^{-2} h^{-1}) estimated for the different mesozooplankton size-classes and (b) mesozooplankton grazing rates *versus* bulk NPP at the stations where both parameters were measured (circles) and averaged for each region using all the available data (triangles). Dark blue = upstream, green = inter-island, red = downstream, with day- and night samplings in the downstream region distinguished by D and N.

4.5. Discussion

4.5.1. Plankton ecology, carbon production, and carbon export potential

The satellite-derived Chl-a data clearly show the influence of the Prince Edward Islands on phytoplankton growth in 2016/2017, with elevated Chl-a observed near the archipelago compared to the open Subantarctic, particularly in February and March (Figure 4.2). Just prior to our sampling in April, phytoplankton had bloomed for the second time following an initial summer bloom in November and December (Figure C.6). The dominant direction of surface water flow from south-west to north-east through the archipelago concentrated the phytoplankton biomass produced in late-summer within a meander of the S-SAF that persisted until May.

Our dataset suggests that plankton community composition and ecology near the Prince Edward Islands in autumn 2017 were influenced by the 'trapped' late-summer bloom, even though phytoplankton biomass had declined by the time of our sampling (Figure 4.2g). The nano- and dinoflagellates (<10 µm) that dominated the phytoplankton community across the archipelago likely succeeded larger diatoms that had proliferated earlier in the season (Seeyave *et al.*, 2007), before decreasing in abundance and productivity due to unfavourable nutrient conditions (e.g., iron- and/or SiO_4^{4-} depletion) and grazing. We hypothesize that at least some of the mesozooplankton sampled in autumn had been feeding on these diatoms, as the observed mesozooplankton community composition is inconsistent with that expected to be supported by the phytoplankton present at the time of our sampling. Most of the nano-phytoplankton, which dominated photoautotrophic abundance and biomass (Figure 4.4b-c), were too small to have been consumed by bigger (>500 µm) zooplankton species such as Euphausiacea, adults of Calanoida (e.g., *C. simillimus*), and other key Antarctic copepod species. Despite being opportunistic feeders, these large grazers prefer bigger phytoplankton cells such as diatoms (e.g., Nejstgaard *et al.* 1995). If their preferred food source is unavailable or because of seasonal feeding behaviour, they can switch their diets to carnivory or become detritivores (e.g., Euphausiacea (e.g., Hagen *et al.* 2007) and Calanoida (e.g., Saage *et al.* 2008)), or resort to using their stored lipid reserves (Lee and Hagen, 2006). The nano-phytoplankton were instead likely grazed by the smaller zooplankton that numerically dominated the archipelago (Figure 4.4d), such as ciliates and small copepods (*Oithona spp.* and *Clausocalanus spp.*), as well as Ostracoda and other filter feeders (e.g.,

Tunicata) (Sherr and Sherr, 2007; Steinberg and Landry, 2017). One consequence of abundant microzooplankton and detritivorous mesozooplankton is enhanced nutrient recycling and energy loss (Steinberg and Landry, 2017).

While our measurements suggest that herbivorous zooplankton grazing could have been sustained by ~10% of total NPP (Figure 4.6), we conclude that mesozooplankton composition and productivity in autumn was not controlled by the *in situ* phytoplankton community. Instead, these zooplankton appear to be a remnant of the preceding late-summer bloom, during which they would have fed on large phytoplankton (Vargas *et al.*, 2006). The subsequent shift in their diet to a less-nutritious food source (e.g., detritus) may have had deleterious effects on EPR and C-SEP (Table 4.3), as well as on the quantity and quality of the organic matter exported to the benthos (Gulati and Demott, 1997). The dominance of microzooplankton (e.g., ciliates) probably also negatively affected the downward flux of organic matter because their smaller faecal pellets are more easily retained and remineralized within the euphotic zone (Steinberg and Landry, 2017). The decoupling of the extant mesozooplankton and phytoplankton communities at the archipelago in autumn, along with the predominance of microzooplankton, would thus have led to enhanced organic matter remineralization by the microbial loop, retention of food in the surface layer, and slow rates of carbon transfer through the food web and to depth. This conclusion is consistent with our N uptake data that indicate a tendency for regenerated production across the archipelago.

Although our study was conducted after the residual late-summer phytoplankton bloom had been advected away from the islands, relatively high concentrations of Chl-a, phytoplankton biomass, and rates of NPP were observed in the inter-island region. Such elevated inter-island Chl-a, which is a persistent feature of the Prince Edward Islands archipelago, is typically associated with the entrapment of eddies originating from the interaction of the ACC and South-West Indian Ridge (Lamont and van den Berg, 2020). These eddies enhance water-column stability and residence time, favouring phytoplankton growth (Venkatachalam *et al.*, 2019). However, no such eddy was present at the time of our sampling, due to the close proximity of the S-SAF to the archipelago (Figure 4.2) (Lamont *et al.* 2019). The local increase in inter-island Chl-a and phytoplankton productivity (i.e., the island mass effect) may instead have resulted from i) the retentive effect of the shallow inter-island plateau and/or ii) an external input of iron or other limiting nutrient.

While we did not measure iron concentrations, our productivity experiments suggest that the modest observed island mass effect was mainly driven by physical processes related to the stability of the water column rather than by biogeochemical fluxes associated with the islands, such as the input of iron from land or via upwelling. Indeed, the *f*-ratio$_{NPP}$ <0.5 at all stations (Figure 4.5d) indicates that phytoplankton growth across the archipelago was largely fuelled by regenerated nutrients (NH_4^+ and other recycled N forms), the assimilation of which has a far lower iron requirement than that of NO_3^- (Morel *et al.*, 1991). If iron had been supplied to the upper-ocean ecosystem, higher-than-observed NPP, NO_3^- uptake rates, and *f*-ratios$_{NPP}$ would be expected, particularly given that the mixed layer was well within the euphotic zone at all stations, rendering light limitation of phytoplankton unlikely. Further evidence for iron limitation is the integrated rates of regenerated N uptake (inferred from the integrated NO_3^- uptake rates and the *f*-ratio$_{NPP}$ to range from 0.06-0.47 mmol m^{-2} h^{-1}, average of 0.15 mmol m^{-2} h^{-1}). These were fairly low compared to previous late-summer measurements from the Indian Subantarctic, including near the Prince Edward Islands (0.15-1.2 mmol m^{-2} h^{-1}), that were made under similar light conditions (e.g., Prakash *et al.* 2015). Additionally, nano- and dinoflagellates dominated the phytoplankton community, while diatoms were rare. The high surface-area-to-volume ratio of nano-flagellates makes them more competitive than micro-phytoplankton for scarce nutrients such as iron (Hare *et al.*, 2007), and iron limitation has been shown to most effectively impede diatoms (Timmermans *et al.*, 2004) because their large size prevents them from acquiring this nutrient fast enough to maintain rapid growth. Finally, many dinoflagellates are mixotrophic (Stoecker, 1999), such that under conditions of depletion they can obtain iron directly by ingesting particles. The composition of the phytoplankton community in autumn 2017 was thus consistent with an iron-limited ecosystem, which we expect (and observe) to be fairly unproductive and fuelled largely by recycled N.

We hypothesize that the phytoplankton retained between the two islands in autumn experienced light-replete, iron-limited conditions that drove them to rely mainly on reduced N forms that, at least in the case of NH_4^+, were available at relatively high concentrations (Figure C.1c). The large difference between the bulk POC concentration (higher) and the estimated carbon biomass of <200 µm planktonic organisms (lower) suggests that detritus may have been a source of regenerated nutrients to the nano-phytoplankton following microbial remineralization. Elevated levels of detritus, remnant of the earlier bloom, are further implicated by the high C:N ratio of the bulk biomass, consistent with the accumulation of carbon-rich particulate matter such as

non-living, partially-degraded organic material, faecal pellets, and mucus associated with gelatinous zooplankton and transparent exopolymer particles. The accumulation of detritus, along with NH_4^+ excreted by zooplankton, is expected for a maturing, lower-productivity water mass in a 'post-bloom' stage (Turner, 2015).

Despite the low productivity status of the ecosystem of the archipelago in autumn 2017, the average *f*-ratio$_{NPP}$ of 0.24 implies that roughly a quarter of the carbon biomass was potentially available for export. We estimate a carbon export flux of 2.2-2.7 mmol C m^{-2} d^{-1} (with the range dependent on the number of daylight hours, 8 to 10 h in April and May 2017; carbon export = 1.14 mmol C m^{-2} h^{-1} (i.e., average integrated NPP) × 0.24 (i.e., average *f*-ratio$_{NPP}$) × number of daylight hours = 2.2-2.7 mmol C m^{-2} d^{-1}). The annual mean carbon export flux in the open Subantarctic, away from the influence of land, is estimated from Community Earth System Model simulations to range from 0.8-1.6 mmol C m^{-2} d^{-1} (Harrison *et al.* 2018). While some months will be more important for carbon export than others, this value is nonetheless comparable to our estimates for the upstream stations located furthest from the archipelago (e.g., at station H7, located in >3500 m of water, carbon export = 0.7 mmol C m^{-2} d^{-1}), but lower than the average carbon export flux derived for the islands in autumn 2017 (2.2-2.7 mmol C m^{-2} d^{-1}). In other words, carbon export potential in the waters surrounding the Prince Edward Islands is enhanced three- to four-fold relative to the surrounding open Subantarctic (see also Appendix C.a). Thus, the island mass effect associated with this archipelago *does* enhance the productivity of the Subantarctic, driving atmospheric CO_2 sequestration at least through autumn, despite a tendency towards regenerated production and inefficient trophic transfer in this season.

4.5.2. The Prince Edward Islands in the context of other Subantarctic islands

The island mass effect has been well-documented near the Subantarctic islands with larger plateaus, such as Crozet (e.g., Bakker *et al.* 2007), Kerguelen (e.g., Lourantou and Metzl 2011), and South Georgia (e.g., Borrione and Schlitzer 2013), but is infrequently discussed for the Prince Edward Islands, particularly with respect to the plankton system. There appear to be broad similarities among the islands, with phytoplankton typically blooming (often in two separate events) between October and late March (Seeyave *et al.*, 2007; Borrione and Schlitzer, 2013). These blooms are initially dominated by diatoms that are succeeded by

nanoplankton as iron becomes exhausted (e.g., Mongin *et al.* 2008), accompanied by a shift from predominantly new- to predominantly regenerated production (Trull *et al.*, 2008).

There are also clear differences in the island mass effect associated with the various islands. Elevated Chl-a often persists for hundreds of kilometres beyond Crozet and Kerguelen (in the path of the ACC; Seeyave *et al.* 2007; Mongin *et al.* 2009), while the localized increase in phytoplankton biomass associated with the Prince Edward Islands is far less extensive (Figure C.7). Downstream of South Georgia, the summertime phytoplankton blooms are so vast and long-lived (e.g., Borrione and Schlitzer 2013) that they fuel the largest drawdown of CO_2 observed in the ACC (Jones *et al.*, 2012). The variable enhancement of NPP by the island mass effect at the different archipelagos has implication for carbon export potential. For example, a comparison of the carbon sink estimated for the waters downstream of the Kerguelen plateau in autumn (3.3-10.8 mmol C m^{-2} d^{-1} based on 20 years of data; Lourantou and Metzl 2011) with our estimate for the Prince Edward Islands (2.2-2.7 mmol C m^{-2} d^{-1}) reveals the greater importance of Kerguelen for the Subantarctic's biological pump. Moreover, the absolute carbon export flux at the Kerguelen plateau relative to the Prince Edward Islands will actually be much greater given the far larger spatial extent over which its island mass effect manifests. We attribute the fairly modest island mass effect of the Prince Edward Islands to the archipelago's small, steep plateau, which limits the degree to which nutrients (particularly iron) can be supplied to the upper-ocean ecosystem by upwelling or run-off, and/or retained in shallow waters that are trapped on the plateau (Planquette *et al.*, 2011).

4.5.3. Historical variability in the plankton ecosystem of the Prince Edward Islands

Our measurements of Chl-a, rates of NPP, and plankton community composition and biomass are similar to recent historical data from the same region, the majority of which were collected in autumn (Table C.8 and S9; Ansorge *et al.* 2012 and references there in). We observed the dominance of pico- and nano-phytoplankton across the archipelago, consistent with other measurements made after 1990. By contrast, earlier studies report autumn phytoplankton assemblages dominated by diatoms (>20 µm, present at abundances of 10^6-10^9 cells L^{-1}; Ansorge *et al.* 2012). Along with biases introduced by data paucity, the apparent differences in phytoplankton metrics over the last three decades could be due to changes in

sampling equipment and/or analysis techniques. Alternatively, the temporal trends in community composition may be real and related to changes in the regional hydrography. The ACC has migrated 50-70 km southwards over the past 50 years (Gille, 2002), altering the intensity and frequency of eddies spawned at the South-West Indian Ridge (Gille, 2003) and driving a southward migration of the S-SAF that has consequences for the through-flow regime at the Prince Edward Islands (Ansorge *et al.*, 2009). For instance, Venkatachalam *et al.* (2019) recently used mooring- and microbial data collected at the archipelago between 2012 and 2015 to show that the positions of the SAF and APF have a major impact on microbial community structure.

It has also been reported that key Antarctic zooplankton species dominate the waters surrounding the archipelago when the SAF is situated north of the islands and Antarctic Surface Water intrudes onto the plateau (Ansorge *et al.*, 2012). By contrast, when the SAF lies proximate to or south of the archipelago, more temperate surface waters surround the islands, introducing Subantarctic and subtropical species (Ansorge *et al.*, 2012). Since the 1990s, subtropical copepod species (e.g., *Clausocalanus* spp.) have become more abundant than Antarctic species near the Prince Edward Islands (Ansorge *et al.*, 2012), and similar warm-water species were also dominant during our study (Tables S5 and S6). A climate-driven shift towards a plankton ecosystem dominated by temperate zooplankton species has implications for the entire archipelago food web. For example, changes observed in the ecology and composition of the benthic community at Prince Edward Islands over the last three decades have been attributed to changes in food source(s) linked to the plankton (von der Meden *et al.*, 2017; Puccinelli *et al.*, 2018).

4.6. Conclusions

While this study was conducted in one season of a single year, our findings are nonetheless valuable given the paucity of recent data on the drivers and functioning of the plankton system proximate to the Prince Edward Islands archipelago. We conclude that 1) in autumn 2017 following the late-summer bloom, the Prince Edward Islands plankton system was dominated by small organisms (e.g., pico- and nano-phytoplankton, and microzooplankton) and characterized by retention and recycling of detritus and nutrients within the upper mixed layer; 2) the island mass effect associated with the archipelago manifests regardless of whether eddies form between the islands, provided that the irradiance-mixing conditions can support phytoplankton growth; 3) due to the proximity of the incident fronts, the phytoplankton biomass that evinces the (summertime) island mass effect can be retained within and transported a considerable distance from the islands by frontal meanders, with implications for the food supply to the benthos of the archipelago and the offshore pelagic ecosystem; 4) while phytoplankton blooms last longer near the Prince Edward Islands than in the open ocean, likely due to enhanced stratification and/or elevated iron inputs, these blooms are smaller and less productive than those associated with other Subantarctic islands – we attribute this to the smaller size of the archipelago's plateau and its steeply sloping shelves, which decrease the residence time of waters near the islands and may dampen the upward iron flux; 5) despite the tendency towards regenerated production in autumn, carbon export potential at the Prince Edward Islands was three- to four-fold higher than in the open Subantarctic, implying that through its island mass effect, the archipelago contributes to the enhancement of the Subantarctic Ocean's biological pump, even after the main bloom period; and 6) our data appear to confirm previous assertions that the plankton community at the Prince Edward Islands has changed in recent years, possibly due to a southward migration of the SAF.

Further studies are required to fully understand ongoing fluctuations in plankton community composition and function, as well as the impacts on the biological pump and marine ecosystems of the Prince Edward Islands. We recommend extending the long-term monitoring efforts at the archipelago to include observations of the plankton system through measurements of primary and secondary production in different seasons (particularly spring and summer), as well as quantification of the nutrient supply (particularly that of iron) to phytoplankton from upwelling, recycling, and terrestrial sources.

Chapter 5. Short-term variations in plankton biomass $\delta^{13}C$ and $\delta^{15}N$ and trophic structure near the Subantarctic Prince Edward Islands archipelago

Supplementary information of this Chapter can be found in Appendix D.

5.1. Abstract

We present and describe the principal factors driving temporal variability in the $\delta^{13}C$ and $\delta^{15}N$ of suspended particulate matter (SPM; $\delta^{13}C_{SPM}$ and $\delta^{15}N_{SPM}$) and zooplankton collected in the vicinity of the Subantarctic Prince Edward Islands archipelago in five near-consecutive seasons over two years, including winter 2015 and 2017, early summer 2016, and autumn 2016 and 2017. We find that the seasonal trends in $\delta^{13}C_{SPM}$ and $\delta^{15}N_{SPM}$ are mainly attributable to changes in the availability of nitrogenous nutrients (i.e., nitrate and ammonium) and the extent of their consumption by phytoplankton, as well as to (related) changes in phytoplankton community composition. The input of subsurface nitrate during winter mixing, which fuels mainly diatom growth in spring and early summer, drives a decrease in $\delta^{13}C_{SPM}$ and $\delta^{15}N_{SPM}$ relative to the winter when $\delta^{13}C_{SPM}$ and $\delta^{15}N_{SPM}$ are high, which we interpret at the result of bacterial decomposition of organic matter. From mid-summer to autumn, the now-iron-limited phytoplankton community becomes dominated by nano-phytoplankton that consume less nitrate in favour of recycled ammonium, which is low in $\delta^{15}N$. As such, $\delta^{13}C_{SPM}$ increases and $\delta^{15}N_{SPM}$ decreases to reach a maximum and minimum by autumn, respectively. Zooplankton biomass $\delta^{13}C$ and $\delta^{15}N$ tend to reflect the temporal variability in $\delta^{13}C_{SPM}$ and $\delta^{15}N_{SPM}$. However, we observed a mismatch between the zooplankton isotope ratios and the $\delta^{13}C_{SPM}$ and $\delta^{15}N_{SPM}$ in autumn 2017, which we attribute to the low isotopic turnover rate of zooplankton biomass and to changes of their food source(s) driven by the local hydrography.

5.2. Introduction

Measurements of carbon and nitrogen isotope ratios ($\delta^{13}C$ and $\delta^{15}N$) have been employed extensively in the last few decades as tools for researching marine ecosystems and food webs (e.g., Peterson and Fry, 1987; Fry, 1988; Hobson and Welch, 1992; Doi *et al.*, 2005; Hanson *et al.*, 2010; Pethybridge *et al.*, 2018) and biogeochemical processes (e.g., Sigman *et al.*, 2000; Pantoja *et al.*, 2002; Tamelander *et al.*, 2009; Newsome *et al.*, 2010). In general, the $\delta^{13}C$ and $\delta^{15}N$ of inorganic substrates (e.g., dissolved inorganic carbon (DIC) and nitrate) and organism tissue in the upper ocean are influenced by nutrient availability and biological activities, as well as the isotopic composition of the nutrient source(s) or organism diets (e.g., Post, 2002; Wada, 2009). Isotope-based studies of food webs and biogeochemical cycles can yield insights into geographical differences and temporal variations in ecosystem dynamics, food web structure, trophic relationships among species, and the flows of carbon and energy through ecosystems (e.g., Middelburg, 2014; Welti *et al.*, 2017). In particular, planktonic primary producers and consumers (i.e., herbivorous zooplankton) represent useful baselines for food web studies and for tracking animal migrations because their biomass $\delta^{13}C$ and $\delta^{15}N$ changes seasonally with changes in the environmental conditions (e.g., McMahon *et al.*, 2013; Pakhomov *et al.*, 2019).

Phytoplankton $\delta^{13}C$ is dependent on the pathway of carbon fixation during enzymatic carboxylation and carbon transport through the cell membrane (O'Leary, 1981, 1988; Fry and Sherr, 1984; Bidigare *et al.*, 1997; Pedentchouk and Zhou, 2018), and is also strongly influenced by seawater pH and pCO_2 (Arthur *et al.*, 1985; Rau *et al.*, 1989; Jasper and Hayes, 1990; Hinga *et al.*, 1994; Rickaby *et al.*, 2010), as well as temperature and salinity (Wong and Sackett, 1978; Hinga *et al.*, 1994; Lara *et al.*, 2010), cell growth rate (Nakatsuka *et al.*, 1992; François *et al.*, 1993; Laws *et al.*, 1995), cell geometry (Fry and Wainright, 1991; Popp *et al.*, 1998), phytoplankton community composition (Falkowski, 1991; Fry and Wainright, 1991; Van Oostende *et al.*, 2017; Chapter 2), and the availability of various nitrogenous nutrients that trigger variable carboxylation in different plankton species (Dehairs *et al.*, 1997 and references therein). By contrast, the $\delta^{15}N$ of phytoplankton is set by the $\delta^{15}N$ of the nutrient sources consumed (e.g., nitrate *versus* ammonium), the degree of consumption of those nutrients, and the isotopic fractionation expressed during consumption (e.g., Sigman *et al.*, 1999; Altabet and Francois, 2001; DiFiore *et al.*, 2010; Fawcett *et al.*, 2011, 2014).

Phytoplankton preferentially take up the lighter isotope (^{12}C or ^{14}N) during substrate consumption such that their biomass $\delta^{13}C$ and $\delta^{15}N$ are initially lower than those of the substrate. In response, nitrate (a dominant nitrogen substrate available to Southern Ocean phytoplankton) becomes progressively enriched in the heavier isotope (^{15}N) and its $\delta^{15}N$ rises as consumption proceeds, as does the $\delta^{15}N$ of the phytoplankton biomass. However, because of rapid equilibration among the DIC species (i.e., CO_2, bicarbonate, and carbonate), the $\delta^{13}C$ of the surface CO_2 pool changes minimally during photosynthesis as CO_2 is constantly being replenished (Popp *et al.*, 1989; Rau *et al.*, 1989, 1992; Freeman and Hayes, 1992). One exception to this scenario occurs when the phytoplankton growth rate is particularly high and CO_2 is consumed faster than it can be resupplied by equilibration, resulting in a ^{13}C enrichment of the CO_2 pool and thus a higher $\delta^{13}C$ of phytoplankton (Deuser, 1970).

The $\delta^{13}C$ and $\delta^{15}N$ of zooplankton (or consumers in general) generally resemble the $\delta^{13}C$ and $\delta^{15}N$ of their food source(s) but with an offset imparted by isotopic fractionation associated with metabolism (DeNiro and Epstein, 1978, 1981; Fry *et al.*, 1978). As such, the $\delta^{15}N$ of heterotrophic organisms is indicative of their trophic position in the food web (e.g., primary or secondary consumer) (Peterson and Fry, 1987), with an estimated isotopic enrichment of ~2.3‰ from one trophic level to the next (McCutchan Jr *et al.*, 2003). The $\delta^{13}C$ of heterotrophs provides information about the origins and transformations of organic matter within the food web, with an increase in $\delta^{13}C$ from the source to the consumer of ~1‰ (Fry and Sherr, 1989; Herman *et al.*, 2000).

Recent large spatial-scale studies conducted in the Southern Ocean have developed detailed geographical distributions (isoscapes) of the $\delta^{13}C$ and $\delta^{15}N$ of suspended particulate matter (i.e., SPM; $\delta^{13}C_{SPM}$ and $\delta^{15}N_{SPM}$; Espinasse *et al.*, 2019; St John Glew *et al.*, 2021; and Chapter 2) and zooplankton (Yang *et al.*, 2021; Chapter 3), providing valuable insights into Southern Ocean biogeochemistry, fertility, and plankton ecology. In particular, $\delta^{13}C_{SPM}$ and $\delta^{15}N_{SPM}$ decrease latitudinally in response to physical and/or biogeochemical processes (e.g., Rau *et al.*, 1992; François *et al.*, 1993; Somes *et al.*, 2010) taking place in each hydrographic zone, while in the vicinity of (Sub)Antarctic islands, sea ice, and continental shelfs, $\delta^{13}C_{SPM}$ and $\delta^{15}N_{SPM}$ increase as a result of local dynamics (e.g., St John Glew *et al.*, 2021; Chapter 2). In contrast to the spatial variability characterised by isoscapes, temporal changes in plankton $\delta^{13}C$ and $\delta^{15}N$ in

the Southern Ocean are less well understood. St John Glew *et al.* (2021) recently explored four seasonal prediction methods to model temporal changes in $\delta^{13}C_{SPM}$ and $\delta^{15}N_{SPM}$ across the Southern Ocean, reporting values consistent with the (at times, limited) observations available for each season for several sectors of the Southern Ocean. However, the mechanisms underpinning this seasonal variability have yet to be thoroughly elucidated, in part because the St John Glew *et al.* (2021) model does not capture all the biogeochemical processes operating in the Southern Ocean (e.g., those associated with sea ice), but mainly due to a paucity of temporally-resolved observations of plankton $\delta^{13}C$ and $\delta^{15}N$.

Additionally, there are only a few studies on temporal variations in zooplankton $\delta^{13}C$ and $\delta^{15}N$, mainly based on observations of a limited number of taxa inhabiting lake environments (e.g., Yoshioka *et al.*, 1994; Gu and Schelske, 1996; Matthews and Mazumder, 2005a), which are a poor analogue for the Southern Ocean (e.g., Dehairs *et al.*, 1997; Schmidt *et al.*, 2003). This lack of temporal observations of plankton $\delta^{13}C$ and $\delta^{15}N$ in the Southern Ocean limits our understanding of the factors that lead to seasonal changes in plankton ecology and by extension, the entire food web, as well as the migration patterns of some marine animals (Schmidt *et al.*, 2003; Matthews and Mazumder, 2005b, 2005a).

This work seeks to improve our understanding of the factors that influence plankton carbon and nitrogen isotopes throughout the year in the Southern Ocean. We report and describe the processes driving temporal variability in the $\delta^{13}C$ and $\delta^{15}N$ of SPM and zooplankton collected in five near-consecutive seasons in the vicinity of the Subantarctic Prince Edward Islands archipelago (PEIs) , which is a system of two islands (Marion Island and Prince Edward Island) that lies between the Subantarctic Front and the Antarctic Polar Front. Here, phytoplankton are the main producers of energy that is transferred by zooplankton to hundreds of marine and terrestrial organisms, such that the PEIs support numerous habitats of elevated ecological and conservation importance (Pakhomov *et al.*, 2000a; Chown and Froneman, 2008; Treasure *et al.*, 2019). Additionally, plankton $\delta^{15}N$ and $\delta^{13}C$ have been used historically as baselines for studying the marine ecosystems offshore and in the vicinity of the PEIs (e.g., Gurney *et al.*, 2001; Allan, 2011; Puccinelli *et al.*, 2018, 2020; Smart *et al.*, 2020). Furthermore, the plankton system around the PEIs is comparable to that of other Subantarctic islands such as Crozet and Kerguelen Island (Chapter 4) where plankton $\delta^{13}C$ and $\delta^{15}N$

have been employed in food web studies of higher trophic animals such as seabirds and marine mammals (e.g., Hilton *et al.*, 2006; Cherel *et al.*, 2007; Hunt *et al.*, 2021).

5.3. Materials and methods

5.3.1. Cruise tracks and sample collection

Samples were collected in different areas of the Southern Ocean between South Africa and ~50ºS, focusing sample collection near the PEIs (Figure 5.1a). In July and August 2015, surface SPM was collected along the Good Hope Line (0°E) on board of the South African MV *S.A. Agulhas II* (VOY016, with the bulk suspended particulate organic nitrogen [PON] data published previously; Smart *et al.*, 2020; https://www.bco-dmo.org/dataset/805324/data). Samples for stable isotope analysis of SPM and mesozooplankton were collected in the vicinity of the PEIs (Figure 5.1b and g) aboard the MV *S.A. Agulhas II* from April to May 2016 and 2017 (VOY019; Smart *et al.*, 2020; and VOY024; Chapter 4) and on board the Russian polar vessel MV *Akademik Treshnikov* (*Академик Трёшников*) during the Antarctic Circumnavigation Expedition (ACE; Walton and Thomas 2018; Landwehr *et al.* 2021) in late December 2016. Moreover, surface SPM samples were collected on board the MV *S.A. Agulhas II* in June and July 2017, (VOY025; Smith, 2020; https://doi.org/10.5281/zenodo.3884606).

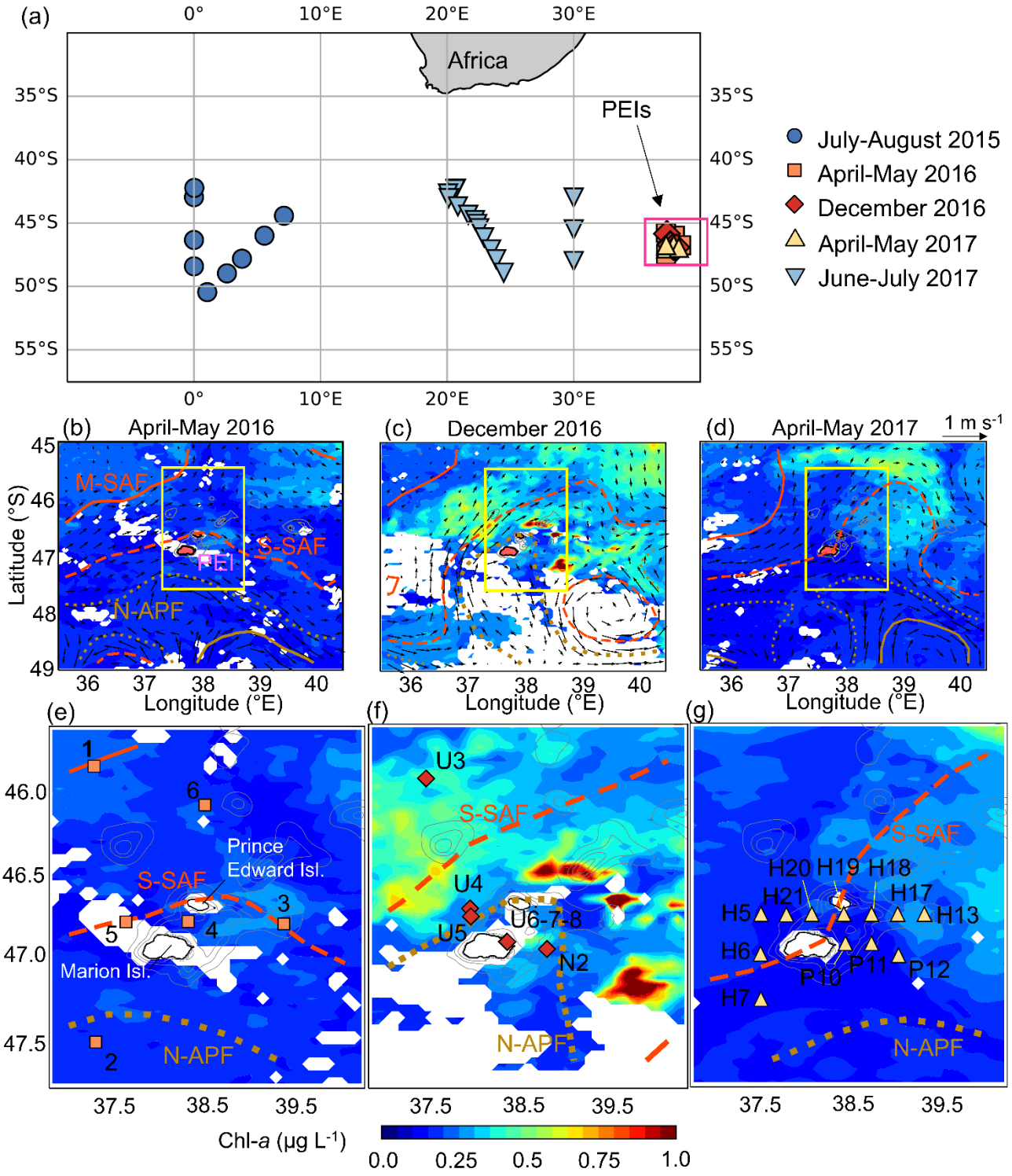

Figure 5.1 (a) Station positions during the five expeditions that are the focus of this study (shapes and colours). The pink rectangle in panel (a) indicates the position of the zoomed-in panels (b-d), which show monthly-averaged level 3 Chl-a concentrations from the MODIS Aqua satellite product (https://oceandata.sci.gsfc.nasa.gov/MODIS-Aqua/Mapped/Monthly/4km/chlor_a/) during (b-e) April-May 2016, (c-f) December 2016, and (d-g) April-May 2017. Solid orange line = Middle Subantarctic Front (M-SAF); dashed orange line = Southern Subantarctic Front (S-SAF); dotted yellow line = Northern Antarctic Polar Front (N-APF); and solid yellow line = Middle Antarctic Polar Front (M-APF). The overlaid black arrows (b-d) show the magnitude and direction of the geostrophic currents and the yellow rectangles indicate the position of the zoomed-in area near the Prince Edward Islands archipelago (PEIs) shown in panels (e-g).

At every station during each expedition, the SPM samples were collected by filtration of seawater (from 2 to 8 L) from the ship's underway seawater intake system (intake at ~7 m depth) through a pre-combusted (450°C for 24h) 0.3 µm pore-sized glass fibre filter (GF-75; Sterlitech). The GF-75s filters were stored in combusted foil envelopes at −80°C.

In April and May 2016, mesozooplankton were collected at every station (6 stations) by towing a Bongo net (200 µm mesh) at a depth between 25 and 90 m, targeting the depth of maximum chlorophyll-a concentration as determined by the preceding CTD casts. Once retrieved, the contents of the cod-end were sieved through 5000-, 2000-, 1000-, 500-, 250-µm mesh sieves, concentrated onto pre-combusted 0.7 µm pore-size glass fibre filters (GF/Fs) and frozen at −20 °C (see Smart *et al* (2020) for further details of the sampling strategy). In April and May 2017, mesozooplankton were collected at 11 of 12 stations (zooplankton samples were no collected at Station H21) by towing a Bongo net (200 µm mesh) vertically from 200 m to surface. Once retrieved, the contents of one cod-end were sieved through 2000-, 1000-, 500-, and 200-µm mesh sieves, concentrated onto pre-combusted 0.7-µm pore-size (GF/Fs) and frozen at -20°C, while the contents of the second cod-end were poured into a HDPE plastic bottle and fixed with buffered formalin (4% v/v final solution) (see Chapter 4 for further details of the sampling strategy). All sieved samples were stored at −20°C until analysis ashore.

Because some of the sieve mesh sizes varied between the two expeditions, the size fractionated zooplankton samples were categorized into the following size classes.: 250-500 µm, 500-1000 µm, 1000-2000 µm, 2000-5000 µm, and >5000 µm for the voyage in 2016; and 200-500 µm, 500-1000 µm, 1000-2000 µm, and >2000 µm for the voyage in 2017.

On 27th of December 2016 during the ACE cruise, mesozooplankton were collected at station N2 (46.918°S; 38.106°E) only by towing a Neuston net (200 µm mesh) horizontally for 15 minutes at approximately 2 knots. The material collected in the cod-end were preserved in 70% ethanol and stored in glass jars at room temperature until analysis (see Chapter 3 for further details of sampling during ACE). Mesozooplankton samples were not collected during the winter voyages (July-August 2015 and June-July 2017).

Ashore, the fixed zooplankton samples were rinsed of formalin or ethanol in Type 1 Milli-Q water to remove excess formalin or ethanol. Specimens were sorted and identified to species level under a dissecting microscope (ZEISS Stemi 508). During the taxonomic analysis, efforts were made to identify specimens at the species level, however, in some cases, the identification was limited to higher taxonomic levels such as family or order. An arbitrary number (from one to 10-20) of organisms belonging to specific taxon were selected to achieve a final dry weight within the range of 0.35 to 0.5 mg. These samples were transferred to pre-combusted foil envelopes and stored at -20°C until taxon-specific stable isotope analysis was conducted. Similar treatment was carried out on some size fractionated samples collected from April to May 2016; the most recognisable zooplankton specimens were selected for further taxon-specific isotopic analysis after the samples were defrosted and examined under the dissecting microscope.

The carbonate shells of shelled pteropods were manually removed as the isotopic composition of these shells is typically very different from the $\delta^{13}C$ of the animal tissue (Mateo *et al.*, 2008). We did not correct for the potential effect of chitin on the measured $\delta^{13}C$ and $\delta^{15}N$ because its effect is still poorly understood (e.g., Brault *et al.*, 2018), and in any case chitin correction appears not to have any effects on zooplankton isotopes ratios (Ventura and Catalan, 2008).

5.3.2. Carbon and nitrogen isotope analysis

In preparation for $\delta^{13}C$ and $\delta^{15}N$ analysis, three types of samples were obtained: SPM, taxon-specific zooplankton, and size-fractionated zooplankton samples. Each of these samples were then freeze-dried. (Scanvac Coolsafe 55-4 cooling trap) for 24h at -60°C. The samples were not fumed with acid to remove inorganic carbon because this process has been observed to alter the nitrogen isotope ratios (Pinnegar and Polunin, 1999; Grey *et al.*, 2001). After freeze drying, the GF-75s containing SPM were encapsulated in tin cups while the mesozooplankton samples (both size-fractionated and manually-sorted specimens) were pulverized initially with agate mortar and pestle and then packaged in a tin cup. All packaged samples were stored in a desiccator until analysis. Replicates (n = 2-4) of each sample were analysed for carbon (C) and nitrogen (N) content using a Flash 2000 Elemental Analyzer connected to a Delta V Plus isotope ratio mass spectrometer. Three in-house standards, calibrated against IAEA reference materials, were included in each run (Choc: $\delta^{15}N$ = 4.31‰, $\delta^{13}C$ = -17.75‰; Merck Gel: $\delta^{15}N$ = 7.50‰, $\delta^{13}C$ = -20.05‰; Valine: $\delta^{15}N$ =

12.14‰, $\delta^{13}C$ = -26.8‰) along with a number of blanks (combusted unused filter + tin capsule). The detection limit was 2 µg C and 1 µg N and precision was ± 0.2‰ for both C and N. Replicate $\delta^{13}C_{SPM}$ and $\delta^{15}N_{SPM}$ measurements were weighted by POC and PON concentration to yield the average and standard deviation (± 1SD). The POC-to-PON (hereafter, C:N) ratio of SPM is reported as a molar ratio, while the C:N ratio of zooplankton is reported as a gram ratio.

Zooplankton are typically rich in lipids (Wainman, 1997; Syväranta and Rautio, 2010), which are depleted in ^{13}C relative to proteins and carbohydrates (Parker, 1964; Tieszen *et al.*, 1983) and thus lower bulk zooplankton $\delta^{13}C$ relative to lipid-extracted tissue. However, since our aim in this study is to assess the dietary fluctuations recorded in the zooplankton isotopes, the samples for stable isotope analysis were not subject to lipid extraction (Schmidt *et al.*, 2003; Matthews and Mazumder, 2005).

5.3.3. Supporting data product

We used 'global' and 'local' approaches for determining the position of the hydrographic fronts in the open Southern Ocean and in the vicinity of the PEIs, respectively (Chapman *et al.*, 2020). For the open ocean (relevant to the July-August 2015 and June-July 2017 datasets) frontal positions were determined from sharp gradients in potential temperature, salinity, potential density, and oxygen concentrations (Lutjeharms and Valentine, 1984; Orsi *et al.*, 1995; Belkin and Gordon, 1996) that were measured using the ship's hull-mounted thermosalinograph, supported by temperature, salinity, and oxygen concentration data from CTD measurements (Smart *et al.*, 2020; Smith *et al.*, 2022). Near the PEIs (April-May 2016 and 2017 and December 2016 dataset), surface circulation patterns and positions of the major Southern Ocean fronts were determined, respectively, from derived geostrophic currents and daily Sea Surface Height (SSH) acquired from the multi mission level-4 satellite gridded product (SEALEVEL_GLO_PHY_L4_REP_OBSERVATIONS_008_047) distributed by the Copernicus Marine Environment Monitoring Service (CMEMS, http://marine.copernicus.eu). The positions of the northern (N), middle (M), and southern (S) branches of the Subantarctic Front (SAF) and Antarctic Polar Front (APF) were identified from optimised values of the SSH data as in Lamont *et al.*, (2019) and Chapter 4: N-SAF = 0.240 m, M-SAF = 0.030 m, S-SAF = −0.170 m, N-APF = −0.300 m, M-APF = −0.480 m, and S-APF = −0.630 m.

The large-scale distribution of phytoplankton biomass during each sampling period was investigated using monthly (October 2016–May 2017) Level 3 chlorophyll-a (Chl-a) concentrations from the MODIS Aqua satellite product (https://oceandata.sci.gsfc.nasa.gov/MODIS-Aqua/Mapped/Monthly/4km/chlor_a/) retrieved near the PEIs at 4 km spatial resolution. In addition, we used as a proxy of the phytoplankton biomass the observed Chl-a concentrations measured through fluorometer were conducted (for detailed methodology for Chl-a measuerements see Smart *et al.*, 2020; Smith *et al.*, 2022 and Chapters 2 and 4).

5.3.4. Statistical analysis

Numerical and descriptive analyses were performed using the R software. Data normality was tested using a Kolmogorov-Smirnov test and variance equality was tested using the F-test. If populations were normally distributed and the variance among groups was equal, differences between groups were tested using an analysis of variance (ANOVA) and Student's t-test followed by a post hoc test such as the Bonferroni correction. These results are reported as the mean ± 1SD. In contrast, if populations were not normally distributed, differences among groups were tested using a Kruskal-Wallis test by rank as a non-parametric alternative to the one-way ANOVA test, and the two-sample Wilcoxon test. These results are reported as medians with interquartile ranges ($median_{Q1}^{Q3}$ or median ± interquartile range [hereafter, IQR], where IQR = third quartile [Q3] – first quartile [Q1]).

5.4. Results

5.4.1. Hydrographic front positions and chlorophyll-a distribution.

In July-August 2015, the STF, SAF and APF along the Good Hope Line were encountered at 40.7°S, 43.8°S, and 50.6°S (Smart *et al.*, 2020), while in June-July 2017, the STF, SAF, and APF in the western Indian sector of the Southern Ocean were located at 42.1°S, 45.6°S, and 49.6°S, respectively (Smith *et al.*, 2022). The region between the STF and SAF is the Subantarctic Zone (SAZ) and between the SAF and APF is the Polar Frontal Zone (PFZ); these two hydrographic zones are the focus of our analysis. In both July-August 2015 and June-July 2017, the observed Chl-a concentrations increased from south to north, and ranged between 0.40 µg L^{-1} and 0.80 µg L^{-1} (Smart *et al.*, 2020; Smith *et al.*, 2022).

In April-May 2016, the S-SAF was located north of the PEIs and the N-APF was located to the south, and an eastward-flowing current of ~0.3 m s^{-1} dominated the surface circulation (Figure 5.1b, e). Stations 1 and 6 were located in the SAZ and stations 2 and 4 were in the PFZ with the former at the margin of a cyclonic eddy, while stations 3 and 5 were located on the S-SAF. The Chl-a concentrations were low across the region (regional average of 0.1 ± 0.2 µg L^{-1}), with local maxima of 0.3 µg L^{-1} observed downstream of the PEIs near Stations 3 and 4 (Figure 5.1e).

In December 2016, the PEIs was influenced by the northern margin of a cyclonic eddy transporting water from the APF, and the N-APF was located north of the islands (Figure 5.1c and f). As such, the S-SAF was pushed considerably further north than in April-May. Station U3 was located north of the S-SAF in the SAZ, with all the other stations located in the PFZ between the S-SAF and the margin of the eddy. The Chl-a concentration averaged 0.4 ± 0.6 µg L^{-1} across the region (Figure 5.1f). While lower concentrations were observed near the islands (0.3 ± 0.2 µg L^{-1}), extensive phytoplankton blooms to the north-west of the archipelago were associated with Chl-a concentrations of 0.7 ± 0.4 µg L^{-1} and to the north- and south-east, with patchy concentrations as high as 1.2 µg L^{-1}.

In April-May 2017, the S-SAF crossed the PEIs from the south-west to the north-east, forming a large meander to the north-east that originated in the downstream region of the PEIs (Figure 5.1d and g). The meander encapsulated a cyclonic eddy characterized by a weak surface flow (~0.2 m s^{-1}; Figure 5.1c). Given

the position of the S-SAF, three of the stations (H5, H6 and H20) were located in the SAZ, with the remaining eight (H7, H13, H17, H18, H19, P10, P11 and P12) in the PFZ. That said, Stations H6, H7, H19 and H20 were situated very close to the S-SAF such that they can be taken to represent the transition between the two hydrographic zones. The meander to the north-east of PEIs confined a water mass with a higher Chl-a concentration (0.4-0.6 µg L^{-1}) than the waters to the south-west of the archipelago and in vicinity of the islands where the concentrations were relatively invariant and low (0.2-0.3 µg L^{-1}), increasing slightly between the two islands to 0.4 µg L^{-1} (Figure 5.1g).

5.4.2. Particulate organic carbon and nitrogen (POC and PON

The concentrations of bulk surface POC and PON were significantly different among seasons (ANOVA, *p*-values < 0.001). POC and PON from the winter samplings (July-August 2015 = 5.5 ± 3.6 µM and 0.7 ± 0.4 µM; June-July 2017 = 3.3 ± 5 µM and 0.5 ± 0.9 µM) were significantly lower (pairwise t-test, *p*-values < 0.001) than the concentrations measured in the late-spring and autumn (April-May 2016 = 6.5 ± 1.8 µM and 1.0 ± 0.3 µM; December 2016 = 6.3 ± 3 µM and 1.0 ± 0.5 µM; April-May 2017 = 6.2 ± 0.4 µM and 1.0 ± 0.5µM), while the values from the latter two seasons were similar (pairwise t-test, *p*-values > 0.05; Table 5.1, Figures 5.2a-b and 5.3a).

Table 5.1 Average (mean ± 1SD; error propagated according to standard statistical practices) particulate organic carbon and nitrogen concentrations (POC and PON [µM]), POC to PON ratios (C:N), linear regression formulas for the C:N ratio, and carbon and nitrogen isotope ratios ($\delta^{13}C_{SPM}$ and $\delta^{15}N_{SPM}$ [‰]) measured for the surface suspended particulate matter collected in the open Southern Ocean or near the Prince Edward Islands archipelago (PEIs) in July-August 2015, April-May 2016, December 2016, April-May 2017, and June-July 2017.

Sampling period	POC (µM)	PON (µM)	C:N	Regression line C:N	$\delta^{13}C$ (‰)	$\delta^{15}N$ (‰)
July-August 2015	5.5 ± 3.6	0.7 ± 0.4	7.5 ± 0.7	5.21 x + 1.68 ($p < 0.05$)	-23.3 ± 9.2	3.2 ± 2.3
April-May 2016	6.5 ± 1.8	1.0 ± 0.3	6.2 ± 0.3	5.61 x + 0.63 ($p < 0.01$)	-23.4 ± 1.5	-2.7 ± 1.3
December 2016	6.3 ± 3.0	1.0 ± 0.5	6.1 ± 0.4	7.01 x + -0.96 ($p < 0.001$)	-25.7 ± 2.3	0.7 ± 1.6
April-May 2017	6.2 ± 0.4	1.0 ± 0.5	6.6 ± 0.5	5.60 x + 0.84 ($p < 0.01$)	-21.8 ± 0.1	-0.9 ± 1.0
June-July 2017	3.3 ± 5.0	0.5 ± 0.9	7.2 ± 1.0	5.38 x + 0.83 ($p < 0.001$)	-24.7 ± 3.3	1.7 ± 7.40

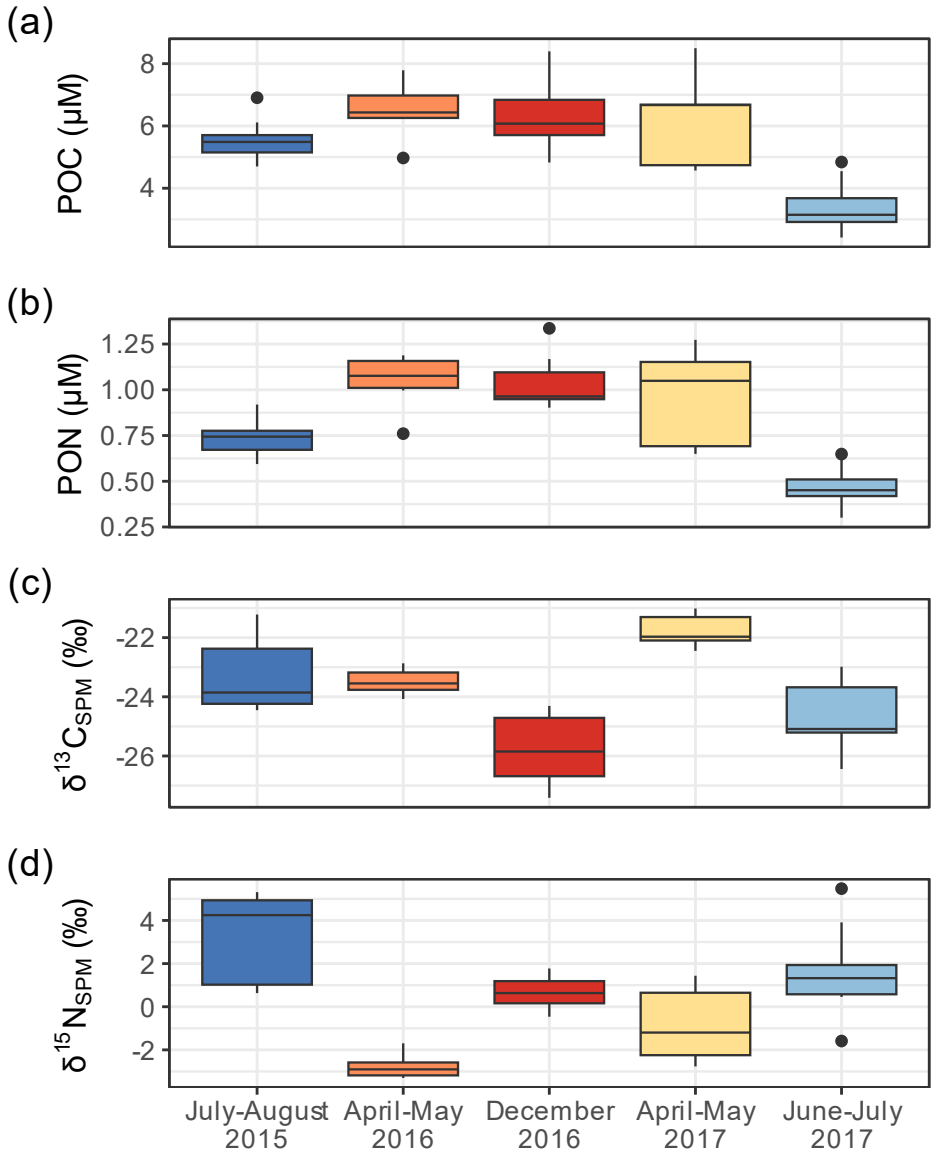

Figure 5.2 Concentrations of particulate organic carbon and nitrogen (POC and PON [µM]) and carbon and nitrogen isotope ratios ($\delta^{13}C_{SPM}$ and $\delta^{15}N_{SPM}$ [‰]) for the surface suspended particulate matter collected in the open Southern Ocean or near the Prince Edward Islands archipelago (PEIs) in July-August 2015 (dark-blue), April-May 2016 (orange), December 2016 (red), April-May 2017 (yellow), and June-July 2017 (light-blue). The colours correspond to season, with winter samplings in cool colours and summer and autumn data in warm colours. The boxplots show the median (thick horizontal line), interquartile range (IQR = 50% of the data; box within first and third quartiles), and whiskers (1.5 times the IQR).

For the whole dataset, the POC and PON concentrations differed among hydrographic zones (t-test, *p*-value < 0.05), with higher POC and PON in the PFZ (5.5 ± 1.6 µM and 0.8 ± 0.3 µM) than in the SAZ (4.4 ± 1.6 µM and 0.6 ± 0.3 µM, respectively; Figure 5.3a). The POC and PON concentrations also varied according to the location of the stations relative to the PEIs (i.e., open ocean, upstream- and downstream of the PEIs; ANOVA, *p*-value < 0.001; Figure 5.3b). Concentrations of POC and PON in the western open ocean were

significantly lower than in any other area (4.1 ± 8.9 µM and 0.6 ± 1.4 µM, respectively; pairwise t-test, *p*-values < 0.001), which is likely due to the sampling of these waters occurring only in winter. Although the POC and PON concentrations in the inter-island waters were generally higher (7.5 ± 3.1 µM and 1.2 ± 0.5 µM, respectively) than the concentrations from all the other areas, they were not significantly different on average from the concentrations measured upstream and downstream of the PEIs (6.0 ± 1.9 µM and 1.0 ± 0.5 µM upstream and 5.6 ± 0.5 µM and 1.0 ± 0.3 µM downstream; pairwise t-test, *p*-values > 0.05).

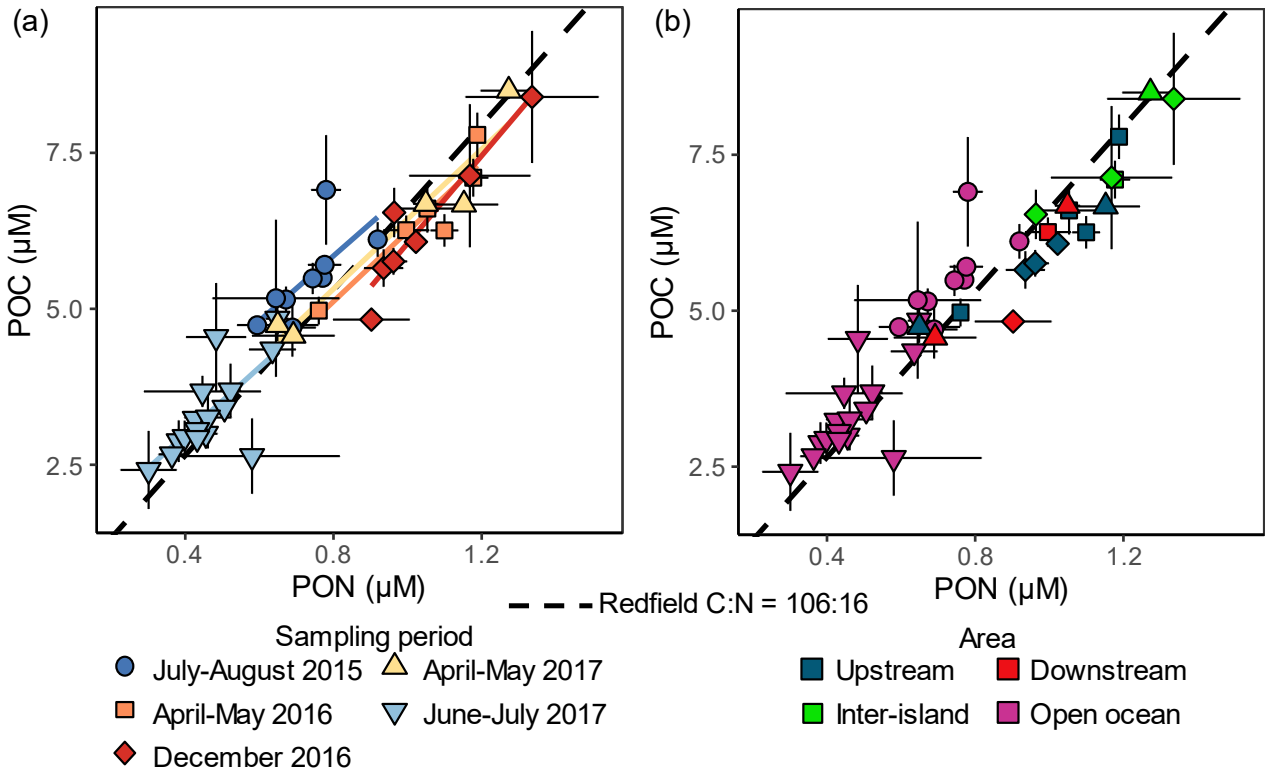

Figure 5.3 Concentrations of particulate organic carbon and nitrogen (POC and PON [µM]) for surface suspended particulate matter collected in the open Southern Ocean or near the Prince Edward Islands archipelago (PEIs) during five expeditions in July-August 2015 (circles), April-May 2016 (squares), December 2016 (diamonds), April-May 2017 (triangles), and June-July 2017 (inverted triangles). In panel (a), the symbol colours correspond to season, with winter samplings in cool colours and summer and autumn data in warm colours. In panel (b), the colours indicate sampling location relative to the PEIs: purple = open ocean, blue = upstream, green = inter-island, and red = downstream. In both panels, the diagonal dashed lines indicate the Redfield C:N ratio (C:N = 106:16), while in panel (a), the coloured diagonal lines show the linear regressions for each sampling period. Note that neither the x- nor y-axes scales begin from zero.

The C:N ratios of the SPM differed significantly with season (ANOVA, *p*-value < 0.001). For the entire dataset, C:N ranged from 4.5 to 9.4, with higher average values in winter (July-August 2015 = 7.5 ± 0.7 and June-July 2017 = 7.2 ± 1.0; both winter periods showed similar results: t-test, *p*-value > 1) than in summer and autumn (April-May 2016 = 6.2 ± 0.3, December 2016 = 6.1 ± 0.4; April-May 2017 = 6.6 ± 0.5; all three

periods showed similar results: ANOVA, *p*-value >0.05; Table 5.1 and Figure 5.3a). The C:N ratios for samples collected from the western open ocean (7.3 ± 0.9; winter) were significantly different from that those observed at all stations near the PEIs (6.3 ± 0.4; pairwise t-test, *p*-values <0.01), with the latter stations all similar to each other, regardless of sampling period. In addition, there was no significant difference in C:N ratios among the different hydrographic zones (t-test, *p*-value = 0.45). Moreover, if we consider all the sampling periods individually, there were no differences in the POC and POC concentrations or C:N ratios among hydrographic zones or by sampling region (ANOVA, *p*-values >0.05; Tables D.1 and D.2).

5.4.3. Carbon and nitrogen isotopes of suspended particulate matter ($\delta^{13}C_{SPM}$ and $\delta^{15}N_{SPM}$)

For the entire dataset, $\delta^{13}C_{SPM}$ and $\delta^{15}N_{SPM}$ ranged from -27.4‰ to -21.0‰ and from-3.3‰ to 5.5‰, respectively, with values differing among sampling periods (ANOVA, *p*-values <0.001) (Table 5.1; Figures 5.2c-d and 5.4; Figure D.1a). The $\delta^{13}C_{SPM}$ and $\delta^{15}N_{SPM}$ measured in April-May 2016 and 2017 were significantly similar (pairwise t-test, *p*-values >0.05), with $\delta^{13}C_{SPM}$ varying from -24.1‰ to -22.9‰ (average of -23.4 ± 1.5‰) and from -22.4‰ to -21.0‰ (average of -21.8 ± 0.1‰), respectively, while $\delta^{15}N_{SPM}$ varied from -3.3‰ to -1.7‰ (average of -2.7 ± 1.3‰) and from -2.8‰ to 1.4‰ (average of -0.9 ± 1.0‰). In December 2016, $\delta^{13}C_{SPM}$ was similar to that measured in June-July 2017 and $\delta^{15}N_{SPM}$ was similar to that measured in April-May 2017 (pairwise t-test, *p*-values >0.05), while both isotope ratios were significantly different from the $\delta^{13}C_{SPM}$ and $\delta^{15}N_{SPM}$ of the other periods (pairwise t-test, *p*-values <0.001). The $\delta^{13}C_{SPM}$ and $\delta^{15}N_{SPM}$ varied in December 2016 from -27.4‰ to -24.3‰ (average of -25.7 ± 2.3‰) and from -0.5‰ to 1.8‰ (average of 0.7 ± 1.6‰), respectively. The $\delta^{13}C_{SPM}$ and $\delta^{15}N_{SPM}$ from July-August 2015 and June-July 2017 were also significantly similar (pairwise t-test, *p*-values >0.05), with $\delta^{13}C_{SPM}$ varying from -24.5‰ to -21.2‰ and -26.4‰ to -23.0‰, respectively (averages of -23.3 ± 9.2 and -24.7 ± 3.3‰), and $\delta^{15}N_{SPM}$ varying from 0.6‰ to 5.3‰ and -1.6‰ to 5.5‰, respectively (averages of -0.9 ± 1.0‰ and 1.7 ± 7.4‰; Table 5.1; Figure 5.2c-d).

The average $\delta^{15}N_{SPM}$ for the winter samplings (July-August 2015 and June-July 2017; 2.3 ± 2.0‰) was ~1.6‰ and ~4.2‰ higher than the averages for early summer (December 2016; 0.7 ± 1.6‰; t-test, *p*-values <0.05) and autumn, with the latter season having the lowest values (April-May 2016 and 2017; -1.9 ± 1.6‰;

t-test, *p*-values <0.05). By contrast, the average $\delta^{13}C_{SPM}$ for autumn (-22.7 ± 1.0‰) was ~1.4‰ and ~3.0‰ higher than that measured in winter (-24.1 ± 1.3‰) and early summer (-25.7 ± 2.3‰), which had the lowest values (5. 4 and D.1a).

There were statistical differences in the $\delta^{13}C_{SPM}$ and $\delta^{15}N_{SPM}$ among hydrographic zones. During July-August 2015, $\delta^{13}C_{SPM}$ and $\delta^{15}N_{SPM}$ were, respectively, higher and lower in the SAZ (-21.8 ± 1.5‰ and 0.8 ± 0.2‰) than in the PFZ (-23.7 ± 7.7‰ and 3.9 ± 1.8‰; t-test, *p*-values <0.05; Table D.1; Figure D.1b). During April-May 2016 and 2017, $\delta^{15}N_{SPM}$ was higher in the SAZ (-2.2 ± 0.3‰ and 0.9 ± 1.5‰, respectively) than in PFZ (-3.1 ± 1.0‰ and -2.0 ± 1.0‰; *p*-values <0.001), while $\delta^{13}C_{SPM}$ was significantly different between the SAZ and the PFZ in April-May 2016 (-23.0 ± 0.5‰ and -23.7 ± 1.1‰, respectively; *p*-value <0.05) but not in April-May 2017 (-22.2 ± 0.0‰ and -21.6 ± 0.1 ‰, respectively; *p*-value > 0.05). During December 2016 and June-July 2017, there was no difference in the $\delta^{13}C_{SPM}$ and $\delta^{15}N_{SPM}$ between the SAF and the PFZ (*p*-values >0.05).

Considering the $\delta^{13}C_{SPM}$ and $\delta^{15}N_{SPM}$ observations from near the PEIs (i.e., the December 2016, April-May 2016 and 2017 samplings), there was no clear pattern among areas (Table D.2; Figure D.1c). In December 2016, $\delta^{13}C_{SPM}$ and $\delta^{15}N_{SPM}$ were higher in the inter-island waters and downstream of the PEIs (average $\delta^{13}C_{SPM}$ = -24.9 ± 0.7‰ and $\delta^{15}N_{SPM}$ = 1.1 ± 0.6‰) than in the upstream region ($\delta^{13}C_{SPM}$ = -26.9 ± 0.6‰ and $\delta^{15}N_{SPM}$ = 0.0 ± 0.6‰; ANOVA; *p*-value < 0.05). While there was no difference in the $\delta^{13}C_{SPM}$ among areas in April-May 2017 (ANOVA, *p*-value = 0.112), the $\delta^{15}N_{SPM}$ was higher downstream (0.9 ± 1.5‰) than in the inter-island region and upstream, with the latter region characterized by the lowest values (-1.2 ± 0.5 and -2.5 ± 0.4‰, respectively; ANOVA, *p*-value < 0.001). In contrast, the $\delta^{13}C_{SPM}$ and $\delta^{15}N_{SPM}$ measured in April-May 2016 did not differ among areas (ANOVA, *p*-values > 0.05).

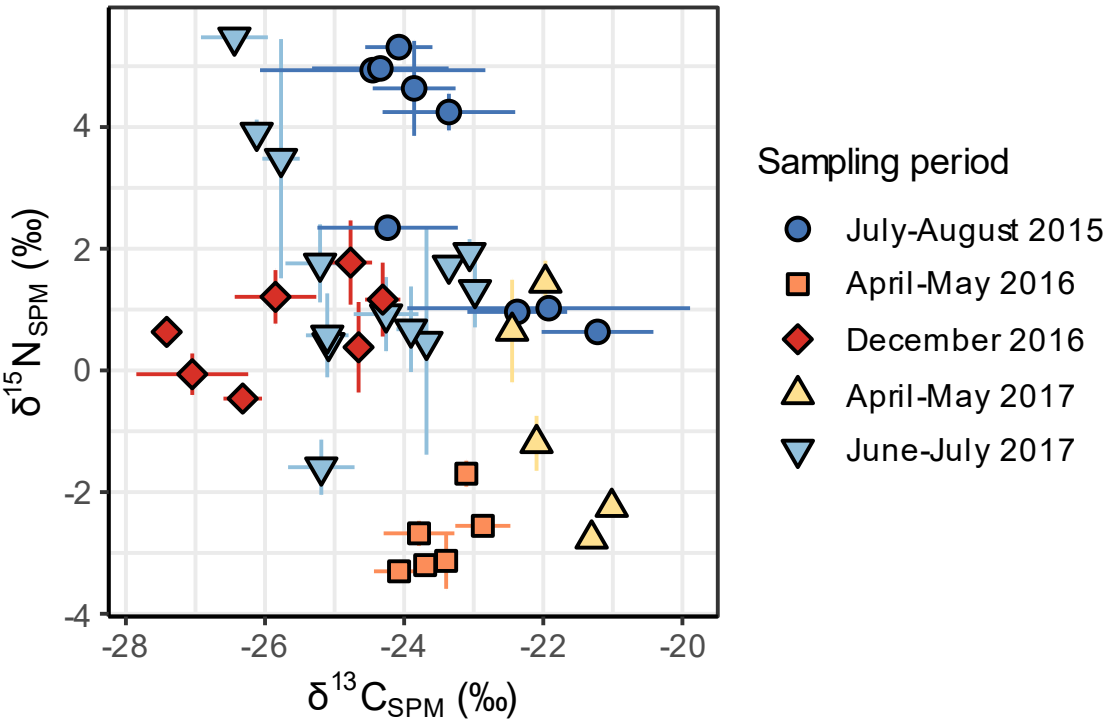

Figure 5.4 Carbon and nitrogen isotope ratios of suspended particulate matter ($\delta^{13}C_{SPM}$ and $\delta^{15}N_{SPM}$ [‰]) collected in the open Southern Ocean or near the Prince Edward Islands archipelago (PEIs) during five expeditions in July-August 2015 (circles), April-May 2016 (squares), December 2016 (diamonds), April-May 2017 (triangles), and June-July 2017 (inverted triangles). The colours correspond to season, with winter data in cool colours and summer and autumn data in warm colours. Error bars show ± 1SD.

5.4.4. Carbon-to-nitrogen ratio (C:N) and stable isotopes ($\delta^{13}C$ and $\delta^{15}N$) of zooplankton body tissue

For each sampling, zooplankton were collected and analysed 1) as single specimens identified at the species level and/or at the highest taxonomic level that could be determined, and 2) as size-fractionated classes. The number of species or specimens representing a single taxon differed among samplings, with four, six, and 13 taxa collected and analysed during April-May 2016, December 2016, and April-May 2017, respectively.

For the specimen data, the C:N, $\delta^{13}C$, and $\delta^{15}N$ of the zooplankton body tissue did not differ among sampling periods (Kruskal-Wallis test, *p*-values > 0.1), with median C:N ratios of $4.1^{4.3}_{3.8}$, $4.3^{4.4}_{3.7}$, and $3.8^{4.2}_{3.7}$ (Figure 5.5a), median $\delta^{13}C$ values of $-23.1^{-21.4}_{-23.6}$‰, $-23.4^{-21.4}_{-23.9}$‰, and $-23.5^{-22.7}_{-24.5}$‰ (Figure 5.5b), and median $\delta^{15}N$ values of $2.4^{3.9}_{1.3}$‰, $3.9^{3.8}_{3.0}$‰, and $3.8^{5.8}_{1.0}$‰ (Figure 5.5c), respectively, for April-May 2016, December 2016, and April-May 2017 (Table 5.2). There was no difference in the C:N ratio, $\delta^{13}C$, or $\delta^{15}N$ of zooplankton specimens among hydrographic zones or regions of the PEIs when the data from the three

sampling periods were grouped (Kruskal-Wallis test, *p*-values > 0.1). Below, we report the results of each sampling period separately.

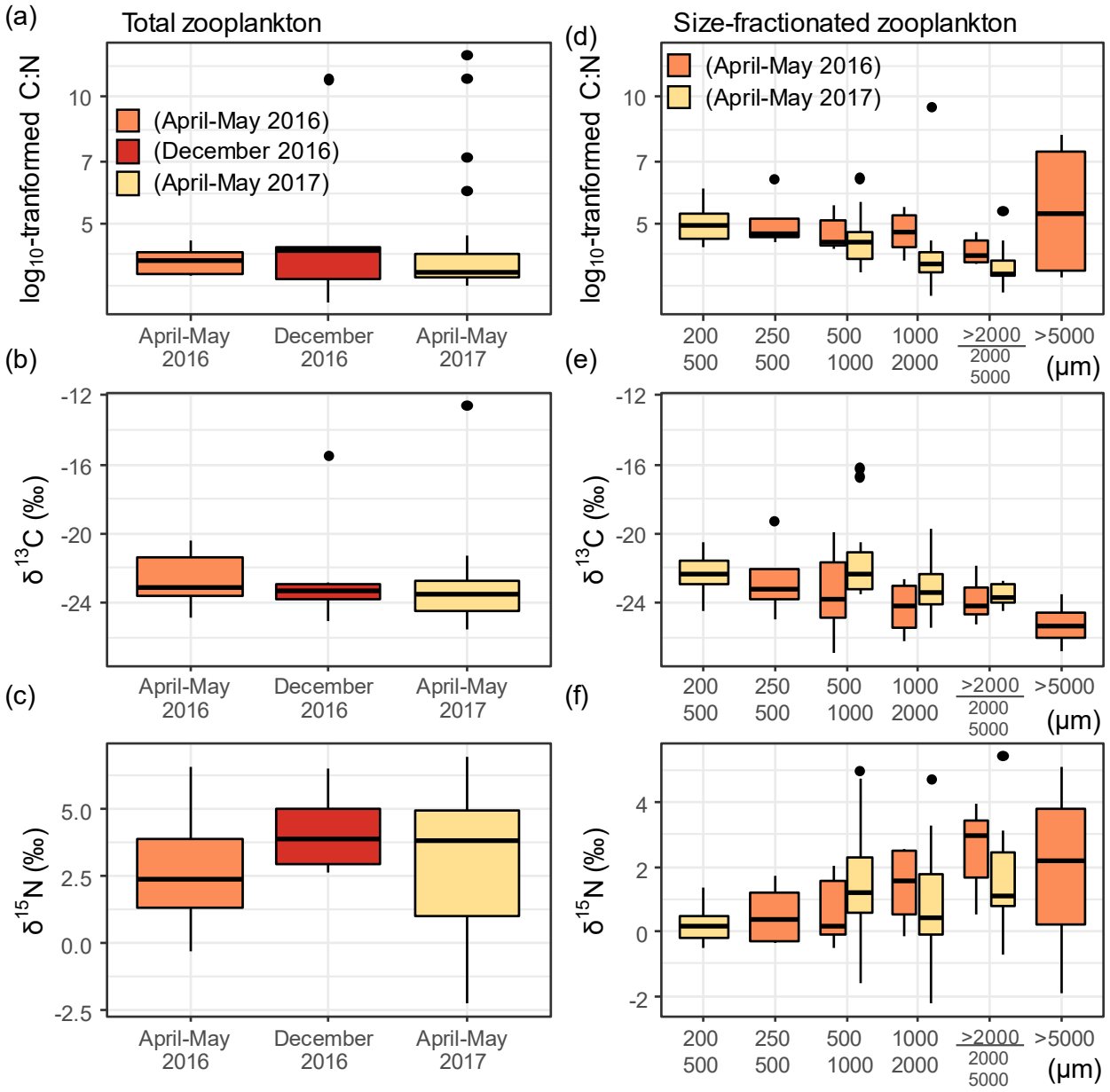

Figure 5.5 Boxplots of the carbon-to-nitrogen (C:N) ratio and carbon and nitrogen isotopes ($\delta^{13}C$ and $\delta^{15}N$; ‰) of the (a-c) zooplankton specimens and the (d-f) size-fractionated classes of zooplankton (i.e., 200-500 µm, 250-500 µm, 500-1000 µm, 1000-2000 µm, >2000 µm, and >5000 µm) collected during the different samplings: April-May 2016 (orange), December 2016 (red), and April-May 2017 (yellow). The y-axes of panels (a) and (b) are $\log_{10}$-transformed.

Table 5.2 Medians (± IQR) of the carbon-to-nitrogen (C:N) ratios and carbon and nitrogen isotopes ($\delta^{13}C$ and $\delta^{15}N$; ‰) of the zooplankton specimens. Data are grouped by sampling period (i.e., April-May 2016, December 2016, April-May 2017), by area of the PEIs (i.e., upstream, inter-island, and downstream), and by hydrographic zone (i.e., Subantarctic Zone [SAZ] and Polar Frontal Zone [PFZ]). N = number of observations.

Sampling period	C:N	$\delta^{13}C$ (‰)	$\delta^{15}N$ (‰)	N
April-May 2016	4.1 ± 0.5	-23.1 ± 2.2	2.4 ± 2.6	7
December 2016	4.3 ± 0.7	-23.4 ± 0.9	3.9 ± 3.0	6
April-May 2017	3.8 ± 0.5	-23.5 ± 1.8	3.8 ± 4.0	41

Area	C:N	$\delta^{13}C$ (‰)	$\delta^{15}N$ (‰)	N
Upstream	3.8 ± 0.5	-23.2 ± 2.0	3.8 ± 2.3	23
Inter-island	3.8 ± 0.5	-22.7 ± 0.6	4.5 ± 2.3	4
Downstream	3.8 ± 0.7	-23.7 ± 1.5	3.0 ± 4.4	27

Hydrographic zone	C:N	$\delta^{13}C$ (‰)	$\delta^{15}N$ (‰)	N
SAZ	3.8 ± 0.7	-22.7 ± 2.1	3.8 ± 2.2	17
PFZ	3.8 ± 0.6	-23.7 ± 1.5	3.0 ± 4.4	37

During April-May 2016, the fish larvae and the Copepoda had the highest and the lowest C:N ratios (4.6 and 3.8, respectively; Table 5.3). One specimen of Copepoda had the highest $\delta^{13}C$ and $\delta^{15}N$ (-21.3‰ and 6.6‰, respectively; Table 5.3 and Figure 5.6a), while the Euphausiacea (-23.7 ± 1.7‰ and 1.8 ± 2.0‰,respectively) and the fish larvae (-23.1‰ and 0.8‰, respectively [median ± IQR]) had the lowest $\delta^{13}C$ and $\delta^{15}N$. The $\delta^{13}C$ and $\delta^{15}N$ of the zooplankton were significantly higher in the SAZ ($-21.4^{-21.3}_{-23.1}$‰ and $2.4^{3.8}_{1.8}$‰, respectively) than in the PFZ ($-24.2^{-23.3}_{-24.5}$‰‰ and $1.9^{3.0}_{0.8}$‰, respectively; five taxa in SAZ *versus* two taxa in PFZ; Wilcoxon test, *p*-values > 0.5; Figure D.2a and Table D.4). The C:N ratios of the zooplankton body tissue did not differ among hydrographic zones (Kruskal-Wallis test, *p*-value = 0.6). The zooplankton samples were all collected in the upstream waters of the PEIs, precluding a regional comparison (Figure D.3a).

In December 2016, Foraminifera had the highest C:N ratio of 11.0, while the C:N of the other specimens ranged from 3.2 for the Chaetognatha to 4.4 for the Calanidae CIV and mixed Copepoda (200-500 µm; Table 5.3). The $\delta^{13}C$ of the Foraminifera (of -15.5‰) was ≥7.4‰ higher than the $\delta^{13}C$ of the other taxa, with a $\delta^{13}C$ for the Chaetognatha and Calanidae CIV of -22.9‰ and 23.1‰, respectively, while *Oikopleura* spp. had the lowest $\delta^{13}C$ of -25.1‰ (Table 5.3 and Figure 5.6b). Chaetognatha and the Calanidae CIV were similarly high in $\delta^{15}N$ (6.5‰ and 6.4‰, respectively), while the juveniles of *T. gaudichaudii* and *Oikopleura* spp. were similarly low (2.6‰ and 3.0‰, respectively). In December 2016, the zooplankton samples were all collected upstream of the PEI, with all stations located in the PFZ (Figure D.3b and D.4b; Tables D.4 and D.5).

During April-May 2017, the C:N ratio for most of the taxa ranged between 3.7 (Chaetognatha, *Calanus* spp., and Euphausiacea) and 4.4 (Amphipoda), although the C:N of the Lepadiformes larvae and *Limacina* spp. was considerably higher (11.8 ± 0.8 and 7.2, respectively; Table 5.3). The $\delta^{13}C$ of most of the zooplankton was lower than (by 0.5‰ to 3.8‰) the average $\delta^{13}C_{SPM}$, ranging between -25.3‰ (*Calanus* spp.) and -22.8 ± 0.9‰ (Euphausiacea). The exception was *Limacina* spp., which had a very high $\delta^{13}C$ of -12.6‰ (Table 5.3 and Figure 5.6c). The *Limacina* spp. $\delta^{15}N$ was the lowest measured in April-May 2017 (-2.3‰), while that of *Candacia* spp. and the Chaetognatha was the highest (5.9 ± 1.1‰ and 5.0 ± 2.0‰, respectively). Among the Copepoda, $\delta^{15}N$ increased from -1‰ for the *Calanus* spp., through *M. gerlachei*, *Paraeuchaeta antarctica*, and *Pleauromamma* spp., to reach a maximum of 5.9 ± 1.1‰ for *Candacia* spp. Neither the $\delta^{13}C$ nor the $\delta^{15}N$ of the zooplankton differed significantly between the SAZ and PFZ (Wilcoxon test, *p*-value = 0.058 and *p*-value = 0.207, respectively; Figure D.2c; Table D.4) or among the upstream, inter-island, and downstream waters of the PEIs (Kruskal-Wallis test, *p*-values > 0.5; Figure D.3c; Table D.5).

Table 5.3 Medians (± IQR) of the carbon-to-nitrogen (C:N) ratios and carbon and nitrogen isotopes ($\delta^{13}C$ and $\delta^{15}N$; ‰) of the zooplankton specimens. Data are grouped by Taxonomic classes, such as Family, Class and species or groups of mixed organisms. N = number of observations.

Family/Class	Family/group/Species	April-May 2016				December 2016				April-May 2017			
		C:N	$\delta^{13}C$ (‰)	$\delta^{15}N$ (‰)	N	C:N	$\delta^{13}C$ (‰)	$\delta^{15}N$ (‰)	N	C:N	$\delta^{13}C$ (‰)	$\delta^{15}N$ (‰)	N
Amphipoda	Amphipoda									4.4 ± 0.1	-23 ± 1.3	1.5 ± 3.2	4
Amphipoda	*Themisto gaudichaudii*									3.9 ± 0.1	-23.4 ± 1.9	3.6 ± 0.3	2
Amphipoda	*Themisto gaudichaudii* Juvenile					3.5	-23.9	2.6	1				
Appendicularia	*Oikopleura* spp.					4.3	-25.1	3.0	1				
Chaetognatha	Chaetognatha	4.0 ± 0.2	-21.9 ± 1.5	3.2 ± 0.9	2	3.2	-22.9	6.5	1	3.7 ± 0.1	-23.4 ± 0.0	5.0 ± 2.0	2
Copepoda	Calanidae CIV					4.4	-23.1	6.4	1				
Copepoda	*Calanus* spp.									3.7	-25.3	-1.0	1
Copepoda	*Candacia* spp.									4.0 ± 0.1	-24.6 ± 0.4	5.9 ± 1.1	2
Copepoda	Copepoda	3.8	-21.3	6.6	1								
Copepoda	*Metridia gerlachei*									3.8	-24.3	1.0	1
Copepoda	Mixed-copepods (200-500µm)					4.4	-23.6	3.0	1				
Copepoda	*Paraeuchaeta antarctica*									3.9 ± 0.5	-24.5 ± 0.9	5.0 ± 0.6	3
Copepoda	*Pleuromamma* spp.									3.8 ± 0.1	-24.4 ± 0.5	4.7 ± 0.8	7
Euphausiacea	Euphausiacea	4.1 ± 0.3	-23.7 ± 1.7	1.8 ± 2.0	3					3.7 ± 0.1	-22.8 ± 0.9	1.5 ± 4.0	13
Foraminifera	Foraminifera					11	-15.5	4.8	1				
Lepadiformes	Lepadiformes larva									11.8 ± 0.8	-24.4 ± 1.2	5.0 ± 1.4	2
Ostracoda	Ostracoda									4.2	-23.2	4.4	1
Phaeodaria	Phaeodaria									4.3 ± 0.4	-23 ± 0.5	4.1 ± 1.2	2
Pisces	Fish larvae	4.6	-23.1	0.8	1								
Pteropoda	*Limacina* spp.									7.2	-12.6	-2.3	1

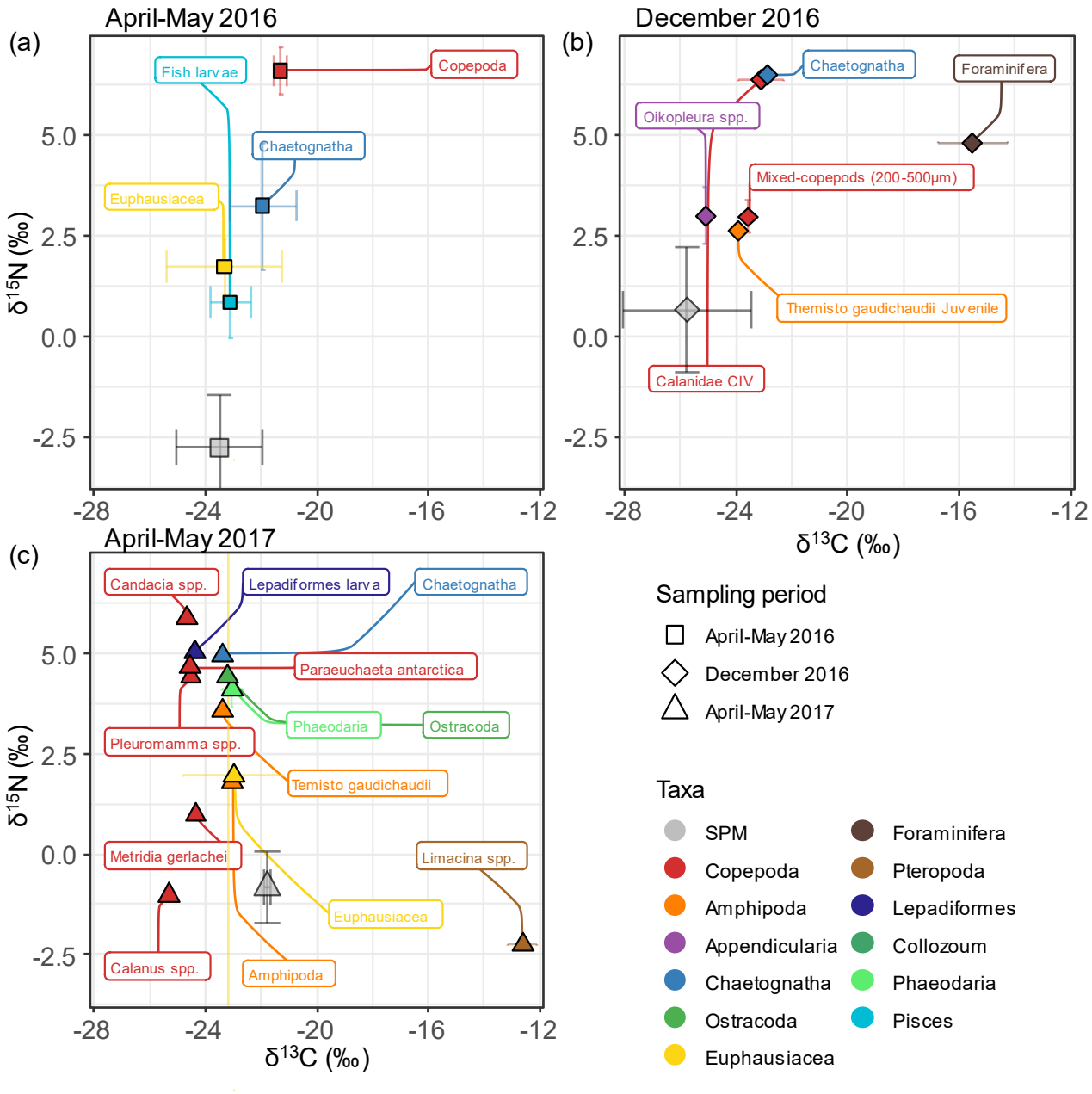

Figure 5.6 Carbon and nitrogen isotope ratios ($\delta^{13}C$ and $\delta^{15}N$ [‰]) of zooplankton specimens collected near the Prince Edward Islands archipelago (PEIs) during three sampling periods: a) April-May 2016, b) December 2016, and c) April-May 2017, with the different colours indicating the different taxa (i.e., family or class) and the labels denoting the species, family, or class. The grey symbols show the averaged carbon and nitrogen isotope ratios of the SPM ($\delta^{13}C_{SPM}$ and $\delta^{15}N_{SPM}$ [‰]). Error bars show ± 1SD about the mean value, propagated according to standard statistical practices. Where error bars are not visible, values represent one measurement only.

For the size-fractionated zooplankton samples, the C:N ratios, $\delta^{13}C$, and $\delta^{15}N$ measured in April-May 2016 showed similar trends to those measured in April-May 2017 – the C:N and $\delta^{13}C$ tended to decrease and the $\delta^{15}N$ to increase with an increase in size class (Table 5.4; Figure 5.5d-f). In addition, the C:N ratio, $\delta^{13}C$, and $\delta^{15}N$ of the same size classes were statistically similar in 2016 and 2017 (Wilcoxon test, *p*-values > 0.05),

except for the C:N ratio of the 500-1000 µm and 1000-2000 µm size classes, which were significantly higher in 2016 than in 2017 (Wilcoxon test, *p*-values < 0.05).

Analysing each year individually revealed no significant difference in the C:N ratio, $\delta^{13}C$, and $\delta^{15}N$ among the size classes in April-May 2016 (Kruskal-Wallis test, *p*-values > 0.05; Table 5.4). The C:N ratio varied from 3.7 to 8.2, with a median of $4.6^{5.2}_{4.3}$ (Figure 5.5d), while the $\delta^{13}C$ ranged between -26.9‰ and -19.3‰ (median of $-24.2^{-22.9}_{-25.0}$‰), with values gradually decreasing with increasing size class (from $-23.3^{-22.1}_{-23.9}$‰ for the 250-500 µm size class to $-25.4^{-24.6}_{-26.0}$‰ for the >5000 µm size class; Figure 5.5e). The $\delta^{15}N$ ranged from -1.9‰ to 5.1‰ (median of $1.2^{2.6}_{0.1}$‰), increasing slightly from $0.4^{+1.2}_{-0.3}$‰ for the 250-500 µm size class to $2.2^{3.8}_{0.4}$‰ for the >5000 µm size class (Figure 5.5f). In contrast to 2016, the April-May 2017 C:N ratios, $\delta^{13}C$, and $\delta^{15}N$ differed significantly by size class (Kruskal-Wallis test, *p*-values < 0.01). The C:N ratios ranged from 3.4 to 9.4, with medians for the smaller size classes ($5.0^{5.3}_{4.6}$ and $4.5^{4.8}_{4.1}$ for the 200-500 µm and 500-1000 µm classes, respectively) that were significantly higher than those of the 1000-2000 µm and >2000 µm classes ($4.0^{4.3}_{3.8}$ and $3.8^{4.1}_{3.8}$, respectively; pairwise Wilcoxon test, *p*-values < 0.001). Although the $\delta^{13}C$ appeared to decrease from the smaller to the larger size classes (from $-22.3^{-21.6}_{-22.9}$‰ to $-23.7^{-22.9}_{-24.0}$‰ for the 200-500 µm to the >2000 µm size classes), only the $\delta^{13}C$ of the >2000 µm size class was significantly different from the others (pairwise Wilcoxon test, *p*-values < 0.001). The $\delta^{15}N$ ranged from -2.3‰ to 5.4‰, and the $\delta^{15}N$ of the 500-1000 µm and >2000 µm size classes ($1.2^{2.3}_{0.6}$‰ and $1.1^{2.4}_{0.8}$‰, respectively) were significantly different (pairwise Wilcoxon test, *p*-values < 0.05) from the $\delta^{15}N$ of the 200-500 µm size class ($0.2^{+0.5}_{-0.2}$ ‰) (Table 5.4).

Table 5.4 Medians (± IQR) of the carbon-to-nitrogen (C:N) ratios and carbon and nitrogen isotopes ($\delta^{13}C$ and $\delta^{15}N$; ‰) of the size-fractionated zooplankton samples (i.e., 200-500 µm or 250-500, 500-1000 µm, 1000-2000 µm, >2000 µm or 2000-5000 µm, and >5000 µm) collected near the Prince Edwards Islands (PEIs) in April-May 2016 and April-May 2017. N = number of observations.

Size class (µm)	April-May 2016				April-May 2017			
	C:N	$\delta^{13}C$ (‰)	$\delta^{15}N$ (‰)	N	C:N	$\delta^{13}C$ (‰)	$\delta^{15}N$ (‰)	N
200-500					5.0 ± 0.7	-22.3 ± 1.4	0.2 ± 0.7	15
250-500	4.7 ± 0.5	-23.3 ± 1.8	0.4 ± 1.5	4				
500-1000	4.5 ± 0.7	-23.8 ± 3.2	0.2 ± 1.7	6	4.5 ± 0.7	-22.3 ± 2.2	1.2 ± 1.7	15
1000-2000	4.8 ± 0.8	-24.2 ± 2.4	1.6 ± 2.0	6	4.0 ± 0.4	-23.4 ± 1.8	0.4 ± 1.9	14
2000-5000	4.2 ± 0.5	-24.2 ± 1.6	3.0 ± 1.8	6				
>2000					3.8 ± 0.3	-23.7 ± 1.1	1.1 ± 1.6	15
>5000	5.5 ± 3.5	-25.4 ± 1.4	2.2 ± 3.6	4				

5.5. Discussion

5.5.1. Temporal variability in the $\delta^{13}C$ and $\delta^{15}N$ of SPM near the Prince Edward Islands

This study compared measurements of the C:N ratio, $\delta^{13}C$, and $\delta^{15}N$ of SPM collected from the open Southern Ocean and the waters near the Subantarctic PEIs. We collected samples over five *quasi*-consecutive seasons between winter 2015 and winter 2017 (Figure 5.1), and while sampling did not always occur in the same locations, we assume that measurements from the open Southern Ocean south of Africa in winter are a reasonable representation of the upstream waters near the PEIs during this season. This assumption is supported by 1) the fact that the samplings in winter occurred upstream and within the same hydrographic zones as the sampling conducted near the PEIs, as well as 2) the latitudinal homogeneity of $\delta^{13}C$ and $\delta^{15}N$ of SPM and zooplankton within the several hydrographic zones determined in Chapters 2 and 3. The measured C:N ratio of the SPM in each season and region (average of 6.7 ± 0.2; Figure 5.3) was similar to that expected for typical marine biomass (Redfield, 1934), suggesting that the SPM was composed mainly of phytoplankton (Garcia *et al.*, 2018). That said, the C:N ratio during winter was slightly higher than that measured in the early summer (7.4 ± 0.2 and 6.3 ± 0.1, respectively; Figure 5.3), which indicates that during winter, microbial degradation of organic matter and N remineralization were dominant (Azam *et al.*, 1991; Manganelli *et al.*, 2009), while in early summer, phytoplankton were rapidly consuming nutrients in order to build biomass (i.e., SPM) (Mengesha *et al.*, 1998; Semeneh *et al.*, 1998; Mdutyana *et al.*, 2020).

Throughout the study, $\delta^{13}C_{SPM}$ and $\delta^{15}N_{SPM}$ varied (from minimum to maximum average values) by 4‰ and 6‰, respectively (Table 5.1 and Figure 5.2). The summer $\delta^{13}C_{SPM}$ was the lowest of all seasons sampled (-25.7 ± 2.3‰) and the POC and PON concentrations were high (6.3 ± 3.0 µM and 1.0 ± 0.5 µM, respectively), while in winter, $\delta^{15}N_{SPM}$ was the highest of the study (1.7 ± 7.4‰ in 2015 and 3.2 ± 2.3‰ in 2017) and the POC and PON concentrations reached a minimum (5.5 ± 3.6µM and 0.7 ± 0.4 µM in 2015 and 3.3 ± 5.0 µM and 0.5 ± 0.9 µM in 2017). In autumn, we observed high $\delta^{13}C_{SPM}$ (-23.4 ± 1.5‰ in 2016 and -21.8 ± 0.1‰ in 2017) and the lowest $\delta^{15}N_{SPM}$ of the study (-2.7 ± 1.3‰ in 2016 and -0.9 ± 1.0‰ in 2017), coincident with high POC and PON concentrations (~6.3 µM and ~1.0 µM, respectively). Both the absolute values and trends in $\delta^{13}C_{SPM}$ and $\delta^{15}N_{SPM}$ agree with the seasonal cycle determined for the Indian sector of

the Subantarctic Ocean by St John Glew *et al.* (2021) using a Bayesian hierarchical modelling framework and in situ observations. They predicted an average seasonal variability of approximately ± 4‰ for both $\delta^{13}C_{SPM}$ and $\delta^{15}N_{SPM}$, with changes in $\delta^{15}N_{SPM}$ of up to ± 16‰ in some regions (e.g., in the open ocean waters of the Indian sector). The St John Glew *et al.* (2021) study also predicted that the highest $\delta^{13}C_{SPM}$ would occur in autumn (March and April; -25‰ to -21‰) and the lowest in summer (January and February; -29‰ to -27‰), while the $\delta^{15}N_{SPM}$ would be highest in spring (November and December; 2‰ to 7‰) when phytoplankton production is high and lowest in autumn (March and April; -5‰ to 0‰). Unfortunately, St John Glew *et al.* (2021) offered little explanation for the causes of the seasonal fluctuations that they observed. Below, using our new data, we examine the variables influencing the observed temporal evolution of $\delta^{13}C_{SPM}$ and $\delta^{15}N_{SPM}$ in Subantarctic waters (Figure 5.7 and Figure 5.8).

While spatial $\delta^{13}C_{SPM}$ variability in the Southern Ocean is mostly attributed to changes in the concentration of CO_2 in the surface layer, largely induced by variations in sea surface temperature (SST), and phytoplankton growth rates (Rau *et al.*, 1989, 1991b; François *et al.*, 1993; Popp *et al.*, 1999; Chapter 2), it has been suggested that seasonal fluctuations in $\delta^{13}C_{SPM}$ can be explained by variations in the N uptake regime (e.g., Dehairs *et al.*, 1997) and possibly, phytoplankton community composition (Fry and Wainright, 1991; Popp *et al.*, 1998; Chapter 2) (Figure 5.7). During winter in the Subantarctic, deep mixed layers induced by low SSTs and strong winds (McCartney, 1979; Dong *et al.*, 2008) entrain subsurface nutrients into the surface layer but productivity is low. In spring and summer, a progressive increase in irradiance due to mixed-layer shoaling and enhanced solar radiation, coupled with initially high (micro- and macro-) nutrient availability, drives increased phytoplankton productivity, particularly of diatoms (Mengesha *et al.*, 1998; Mdutyana *et al.*, 2020). The availability of NO_3^- (the assimilation of which should not be iron-limited early in the growing season) triggers the expression of both RuBisCO and PEPcarboxykinase (PEPk) in diatoms during carboxylation (Descolas-Gros and Oriol, 1992), both of which are associated with a large isotope effect (i.e., >20‰; Arnelle and O'Leary, 1992). As such, photosynthetic NO_3^- assimilation by diatoms should drive a $\delta^{13}C_{SPM}$ decrease from early spring to summer (Dehairs *et al.*, 1997) when it reaches a minimum (St John Glew *et al.* 2021). Indeed, in Chapter 2 I observed a temporal decline of ~4‰ in $\delta^{13}C_{SPM}$ from early- to late summer 2016/2017 for the whole Southern Ocean.

From summer to autumn in the Subantarctic, the depletion of essential nutrients (particularly iron, but also silicate (SiO_4^{4-}) in some regions) coupled with weak upward nutrient supply due to enhanced upper water-column stratification leads to a decrease in diatom (and other large phytoplankton) productivity (Llort *et al.*, 2015; Arteaga *et al.*, 2020) while zooplankton grazing increases (e.g., Hunt and Hosie 2006a; b) (Figure 5.7). Together, these conditions favour the growth of smaller phytoplankton (i.e., nano-phytoplankton) and an upregulation of the microbial loop (Dennett *et al.*, 2001; Lourey *et al.*, 2003; Morley *et al.*, 2020; Christaki *et al.*, 2021; Chapter 4). In Chapter 4, I determined that subsurface NO_3^- fuelled roughly a quarter of the primary productivity near the PEIs in autumn 2017, with the remaining 75% supported by regenerated N (i.e., recycled ammonium; NH_4^+). At the same time, the phytoplankton community was dominated by nano-phytoplankton (60% of the total abundance), particularly nanoflagellates. The assimilation of NH_4^+ requires far less iron and energy (i.e., light) than that of NO_3^- (Dortch, 1990; Raven *et al.*, 1992; Glibert *et al.*, 2016), which explains the summer to autumn shift in the dominant N source consumed by Southern Ocean phytoplankton (i.e., from mostly NO_3^- to mostly recycled NH_4^+) (Lourey *et al.*, 2003; Smart *et al.*, 2015). A similar seasonal trend has also been oberved in the subarctic North Pacific (Yoshikawa *et al.*, 2022). Additionally, an increase in the concentration of NH_4^+ in the Southern Ocean mixed layer in late summer and autumn (Smith *et al.* 2022) may even inhibit NO_3^- uptake by phytoplankton (Elskens *et al.*, 2002; Flynn *et al.*, 2021). Enhanced NH_4^+ uptake is associated with the expression of the PEPcarboxylase (PEPc) enzyme, which is present in pico- and nano-phytoplankton (e.g., Cryptophyceae, Chlorophyceae, and Prasinophyceae) and in some dinoflagellates (e.g., *Prorocentrum* spp.; Descolas-Gros and Fontugne 1985; Descolas-Gros and Oriol 1992). The expression of PEPc occurs with a small isotope effect (~2‰), thus yielding higher $\delta^{13}C_{SPM}$ than photosynthetic carbon production associated with PEPk and/or RuBisCo (O'Leary, 1981; Guy *et al.*, 1989; Arnelle and O'Leary, 1992). The PEPc carboxylation pathway is also associated with enhanced uptake of bicarbonate (HCO_3^-), which has a higher $\delta^{13}C$ than CO_2 in seawater (~1.5‰ *versus* ~-10‰; Mook *et al.*, 1974; François *et al.*, 1993), thus also contributing to the $\delta^{13}C_{SPM}$ reaching a maximum in autumn (St John Glew *et al.*, 2021).

From autumn to winter, $\delta^{13}C_{SPM}$ decreased by as much as 3‰ (Figure 5.2), coincident with the seasonal light- (and possibly temperature-) driven decrease in phytoplankton activity (Boyd *et al.*, 2001) and increase in the rates of nutrient recycling relative to consumption in the mixed layer (Ratnarajah *et al.*, 2018;

Mdutyana *et al.*, 2020, 2022; Smith *et al.*, 2022). Experiments using SPM collected from lakes have shown that bacterial degradation of SPM causes its $\delta^{13}C_{SPM}$ to decrease, which the authors hypothesize is due to the selective retention of organic matter in the SPM pool that is low in $\delta^{13}C$ (Lehmann *et al.*, 2002). To our knowledge, there are no studies characterising the alteration of the $\delta^{13}C$ of marine phytoplankton-dominated SPM during bacterial degradation. Nonetheless, the autumn-to-winter rise in the C:N ratio of the SPM, which occurs when biomass decomposition exceeds new biomass production (i.e., decomposition outpaces primary production), strongly suggests a remineralization-related explanation for the observed autumn-to-winter decline in $\delta^{13}C_{SPM}$. The seasonal trend in the $\delta^{15}N_{SPM}$ data is also consistent with this hypothesis (see below).

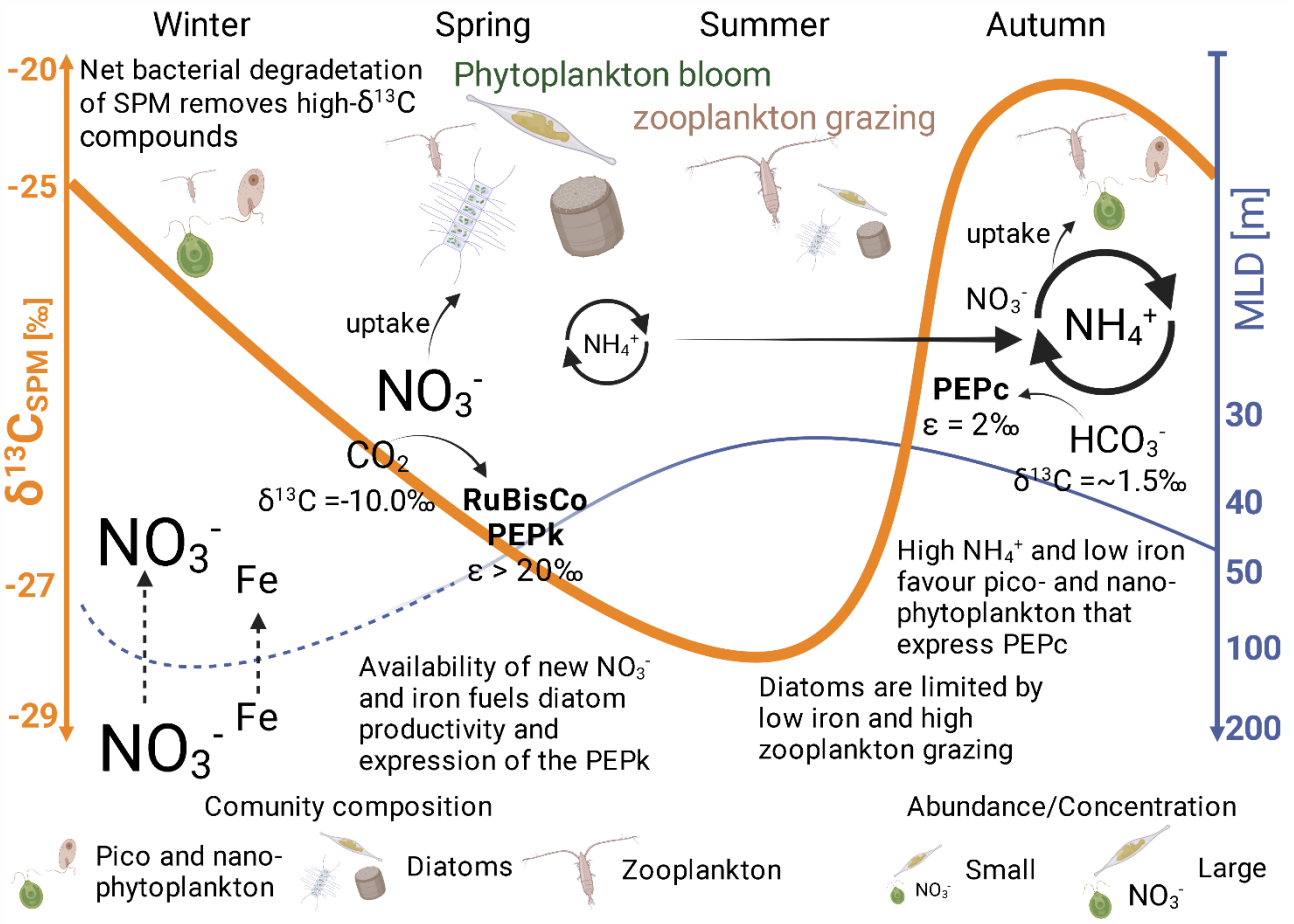

Figure 5.7 The seasonal cycle of $\delta^{13}C_{SPM}$ (‰; orange curve) in the Subantarctic. Diatoms, which have RuBisCo and PEPcarboxykinase (PEPk) for the carboxylation of CO_2, bloom as irradiance increases from winter to spring and summer, allowing them to consume the nutrients supplied during winter mixing (i.e., when the mixed layer depth (MLD; blue curve) is greatest). The $\delta^{13}C_{SPM}$ declines due to strong isotopic fractionation during diatom carboxylation to reach a minimum in the summer. In late summer and autumn, due mainly to iron (Fe) limitation of nitrate (NO_3^-) uptake and elevated zooplankton grazing, diatoms are succeeded by pico- and nano-phytoplankton and the microbial loop is upregulated. The remineralization of organic matter causes an increase in the ammonium (NH_4^+) concentration, which activates the PEPcarboxylase (PEPc) enzyme possessed by pico- and nano-phytoplankton and in some dinoflagellates and may even further inhibit NO_3^- uptake. The $\delta^{13}C_{SPM}$ rises due to the weak isotopic fractionation associated with carboxylation by PEPc and the high-$\delta^{13}C$ of HCO_3^- relative to CO_2, the former species being the substrate for PEPc carboxylation, to reach a maximum in the autumn. Between autumn and winter, $\delta^{13}C_{SPM}$ declines, likely due to bacterial degradation of organic matter, which has been hypothesized to drive a decrease in $\delta^{13}C_{SPM}$ because of the selective retention of organic compounds that are low in $\delta^{13}C$. The typical plankton community composition in each season is represented near to the top of the figure, with symbol size providing a qualitative estimation of their relative abundance and biomass. The blue curve indicates the approximate depth of the mixed layer (m), with the dashed portion indicating the high variability in MLD expected during the winter. The dashed vertical lines show the upwelling of subsurface NO_3^- and iron (Fe), with the different font sizes indicating that iron rather than NO_3^- becomes limiting to phytoplankton growth.

Similar to $\delta^{13}C_{SPM}$, the seasonal cycle in $\delta^{15}N_{SPM}$ (i.e., highest in winter, decreasing through summer to a minimum in autumn) can be explained by seasonal variability in the N sources consumed by phytoplankton, as well as the relative importance of different N cycle processes (Figure 5.8). The $\delta^{15}N$ of subsurface NO_3^- transported into the surface layer during winter is higher than the $\delta^{15}N$ of NH_4^+ recycled by the microbial loop (5‰ to 7‰ *versus* -5‰ to 0‰; (Mariotti *et al.*, 1981; Checkley and Miller, 1989; Sigman *et al.*, 1999, 2000; Lourey *et al.*, 2003; DiFiore *et al.*, 2009; Smart *et al.*, 2015; Mirkin *et al.*, 2023), with the latter N form observed to accumulate in the mixed layer from late-summer to winter, particularly in the southern region of the SAZ (Smith *et al.*, 2022). The dominant uptake of NO_3^- in spring and summer, despite occurring with an isotope effect of 5‰ to 7‰ (Sigman *et al.*, 1999; DiFiore *et al.*, 2010; Fripiat *et al.*, 2019), will yield phytoplankton biomass that is higher in $\delta^{15}N$ than that generated from the preferential assimilation of NH_4^+ in autumn (e.g., Altabet *et al.*, 1999; Fawcett *et al.*, 2011, 2014; Treibergs *et al.*, 2014), resulting in a decline in $\delta^{15}N_{SPM}$ over the growing season (Lourey *et al.*, 2003; Smart *et al.*, 2020; St John Glew *et al.*, 2021). By winter, NO_3^- assimilation has reached a minimum and the low rates of phytoplankton growth are near-exclusively supported by NH_4^+ (Mdutyana *et al.*, 2020, 2022; Smith *et al.*, 2022). However, $\delta^{15}N_{SPM}$ reaches a maximum (e.g., 2.5‰ higher in winter than autumn 2017), which has previously been explained by bacterial decomposition of SPM (Smart *et al.*, 2020). This heterotrophic process preferentially removes ^{14}N, increasing the $\delta^{15}N_{SPM}$ as its concentration declines (Möbius, 2013). At the same time, low rates of mixed-layer NH_4^+ assimilation in winter occur coincident with NH_4^+ oxidation (Mdutyana *et al.*, 2020, 2022). The latter pathway is associated with a large isotope effect (14-19‰; Casciotti *et al.*, 2003) while the former occurs with little to no isotopic fractionation (Hoch *et al.*, 1992; Pennock *et al.*, 1996; Liu *et al.*, 2013). As a result, the $\delta^{15}N$ of the residual NH_4^+ pool may rise above the $\delta^{15}N$ of the subsurface NO_3^-. Any consumption of this high-$\delta^{15}N$ NH_4^+ will yield SPM that is similarly high in $\delta^{15}N$.

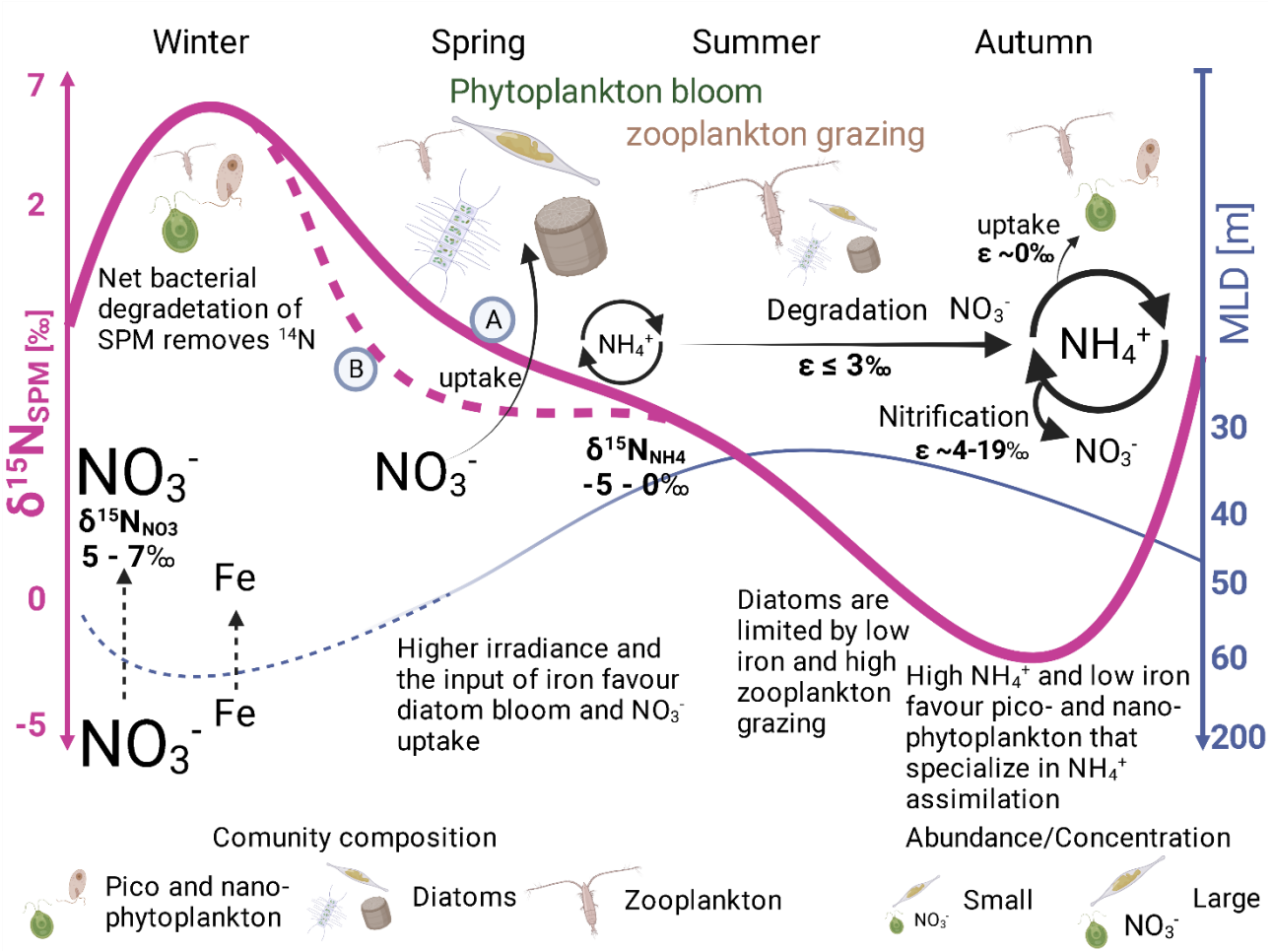

Figure 5.8 The seasonal cycle of $\delta^{15}N_{SPM}$ (‰; purple curve) in the Subantarctic. The $\delta^{15}N_{SPM}$ is highest in winter because heterotrophic bacterial degradation of organic matter, which preferentially removes the light isotope from the SPM pool, exceeds new biomass production. At the same time, nitrate (NO_3^-) and iron (Fe) are supplied to the surface layer during deep winter mixing (i.e., when the mixed layer depth (MLD; blue curve) is greatest). As irradiance increases from winter to spring due to both an increased light flux and MLD shoaling, diatoms begin to consume the NO_3^-, (and iron) which is relatively high in $\delta^{15}N$. However, isotope fractionation associated with NO_3^- assimilation causes the biomass initially produced from NO_3^- consumption to be low in $\delta^{15}N$; the combination of this low- $\delta^{15}N$ biomass with the high- $\delta^{15}N$ degraded SPM remaining from the winter causes the combined $\delta^{15}N_{SPM}$ to decline. By summer, the $\delta^{15}N_{SPM}$ largely represents the integrated signal of seasonal nitrate consumption. The summertime $\delta^{15}N_{SPM}$ could be (A) lower than or (B) higher than that of the spring, depending on the quantity of new biomass produced in both these seasons relative to the quantity of degraded biomass present at the end of winter and their respective isotopic compositions (we have illustrated this uncertainty by using a dashed purple curve throughout the spring season). In late summer and autumn, due mainly to iron limitation of NO_3^- uptake and elevated zooplankton grazing, diatoms are succeeded by pico- and nano-phytoplankton and the microbial loop is upregulated. The remineralization of organic matter causes an increase in the concentration of ammonium (NH_4^+), which is low in $\delta^{15}N$. The phytoplankton community switches to dominant reliance on this low- $\delta^{15}N$ NH_4^+, which causes a strong decrease in the $\delta^{15}N_{SPM}$, to reach a minimum in autumn. The typical plankton community composition in each season is represented near to the top of the figure, with symbol size providing a qualitative estimation of their relative abundance and biomass. The blue curve indicates the approximate depth of the mixed layer (m), with the dashed portion indicating the high variability in MLD expected during the winter. The dashed vertical lines show the upwelling of subsurface NO_3^- and iron (Fe), with the different font sizes indicating that iron rather than NO_3^- becomes limiting to phytoplankton growth.

5.5.2. Temporal variability in zooplankton δ13C and $\delta^{15}N$ and trophic structure at the PEIs

In this study, taxon-specific and size-fractionated zooplankton samples were collected in autumn of two consecutive years (i.e., April-May 2016 and 2017) and on one day of the intervening summer (December 2016). We use these data to explore temporal changes in the Subantarctic zooplankton community near the PEIs between summer and autumn.

The $\delta^{13}C_{SPM}$ and $\delta^{15}N_{SPM}$ for samples collected in April-May 2016 and December 2016 were on average lower than the $\delta^{13}C$ and $\delta^{15}N$ of the zooplankton specimens from the same samplings (by 0.8‰ and 5.4‰ [$\delta^{13}C$ and $\delta^{15}N$] in April and by 3.3‰ and 3.7‰ in December; Figure 5.6), consistent with the expectation that the $\delta^{13}C$ and $\delta^{15}N$ of a predator will resemble that of its food source "plus a few *per mille*" (DeNiro and Epstein, 1978, 1981; Fry *et al.*, 1978). This result is also congruent with previous studies that have shown a direct dependence of zooplankton $\delta^{13}C$ and $\delta^{15}N$ on the isotopic composition of surface SPM in the Southern Ocean during summer (e.g., Corbisier *et al.*, 2004; Chapter 3) and at the PEIs in autumn (e.g., Kaehler *et al.*, 2000).

In contrast, the $\delta^{13}C_{SPM}$ measured in April-May 2017 (Table 5.1) was on average 2.0‰ higher than the $\delta^{13}C$ of most of the zooplankton specimens (Table 5.3; Figure 5.6c), suggesting that the sampled SPM pool was not the dominant food source to the zooplankton. In a parallel study conducted on the same cruise in April-May 2017 (Chapter 4), I deduced that the plankton biomass present near the PEIs was the remanent summer bloom that had been 'trapped' within an eddy formed to the north-east of the archipelago in late summer (between March and April 2017) through the meandering of the S-SAF that was slowing migrating eastward (Figure 5.1d). Here, we show that the $\delta^{13}C$ and $\delta^{15}N$ of the zooplankton community did not change from December 2016 to April-May 2017, yet the $\delta^{13}C_{SPM}$ increased by 3.9‰ and the $\delta^{15}N_{SPM}$ decreased by 1.6‰ (Table 5.1). In other words, the SPM collected within the eddy during autumn appears to reflect the seasonal change in phytoplankton biomass $\delta^{13}C$ and $\delta^{15}N$ between December 2016 and April-May 2017 while the zooplankton collected in autumn still resemble the $\delta^{13}C$ and $\delta^{15}N$ of the food source(s) they consumed the previous summer. It is possible that the isotope ratios and community composition of the plankton system outside the meander differ from those reported here, but unfortunately, we have no data with which to evaluate this hypothesis. Phytoplankton cells represent a near instantaneous measure of the local

oceanographic conditions, such as nutrient availability (Aberle and Malzahn, 2007), temperature, and CO_2 concentration (Goericke and Fry, 1994), and their isotopic turnover rates are much quicker (hours to days) than those of zooplankton (weeks to months). As such, changes in zooplankton biomass $\delta^{13}C$ and $\delta^{15}N$ will be delayed relative to isotopic changes in their food source(s) (e.g., O'Reilly *et al.* 2002; Schmidt *et al.* 2006; Hannides *et al.* 2009; Chapter 3) and will likely also be muted compared to variations in $\delta^{13}C_{SPM}$ and $\delta^{15}N_{SPM}$ because of the longer time period over which zooplankton biomass integrates the isotopes. We thus hypothesize that the $\delta^{13}C$ of the zooplankton sampled in April-May 2017 was strongly biased towards the $\delta^{13}C_{SPM}$ of the previous summer (rather than the $\delta^{13}C_{SPM}$ measured coincidentally in April-May 2017) because of the relatively slow isotopic turnover rates associated with zooplankton (e.g., O'Reilly *et al.* 2002; Schmidt *et al.* 2006; Hannides *et al.* 2009) and the fact that summer represents a period of elevated feeding and biomass production (e.g., Atkinson *et al.*, 2012a; Arteaga *et al.*, 2020).

In addition, it is possible that the zooplankton consumed very little of the SPM present in the eddy from which they were sampled in April-May 2017, increasing the isotopic mismatch between SPM and zooplankton biomass. Indeed, in Chapter 4 I suggested that grazing by larger zooplankton herbivores (e.g., Euphausiacea and *Calanus simillimus*) near the PEIs in April-May 2017 was limited due to the dominance of the photoautotrophic community by small (i.e., pico- and nano-) phytoplankton, along with the near-absence of diatoms, the preferred prey of such zooplankton. As such, the zooplankton may have 1) switched their trophic behaviour from herbivory to omnivory (e.g., Hagen *et al.*, 2007) and/or 2) increased consumption of their reserves of lipids and fatty acids (e.g., Lee and Hagen, 2006). Both scenarios could increase the mismatch between SPM and zooplankton $\delta^{13}C$. Below, we use measurements of grazing rates (Chapter 4) and the C:N ratios of zooplankton biomass to address each of these possibilities.

The median zooplankton grazing rate near the PEIs in April-May 2017 corresponded to 5-10% of the rate of photosynthetic carbon production (i.e., 0.62 mg C m^{-2} h^{-1} *versus* 5-12 mg C m^{-2} h^{-1}; Chapter 4). In addition, the Euphausiacea accounted for ~20% of the total community grazing rate, suggesting that the larger zooplankton herbivores were still grazing (even if slowly) on the in situ phytoplankton assemblage, although perhaps on the less dominant and less productive diatoms rather than indiscriminately on the bulk SPM pool (Chapter 4). At the same time, we observe no differences in $\delta^{15}N$ for the various zooplankton taxa among the

three sampling periods. Predators such as Chaetognatha, *Candacia* spp., *Pleuromamma* spp., and *Paraeuchaeta antarctica* were high in $\delta^{13}C$ and $\delta^{15}N$ compared to the other taxa (potential prey), while the $\delta^{15}N$ of Euphausiacea was similarly low in both autumns (1.8 ± 2.0‰ in 2016 and 1.5 ± 4.0‰ in 2017; Table 5.3 and Figure 5.6), suggesting a lower trophic position for the krill and possibly confirming their herbivorous behaviour. Similarly, the $\delta^{15}N$ of *Calanus* spp. (most likely *Calanus simillimus*) in April-May 2017 was as low as that of *Limacina* spp. (-1‰ and -2.3‰, respectively), with the latter known to be strictly herbivorous and to feed predominantly on diatoms and dinoflagellates (Thibodeau *et al.*, 2022). We conclude that the bigger zooplankton grazers in April-May 2017 may have maintained the same trophic behaviour that they reportedly display when diatom abundances are high (i.e., in summer; Atkinson, 1998; Atkinson *et al.*, 2012a; Chapter 4), leading us to discount the idea that zooplankton grazers switched from herbivory in summer to omnivory or carnivory in autumn. That said, the relatively low $\delta^{15}N$ of the larger grazers in autumn 2017 could still reflect their summertime trophic role because of the low turnover rate of the isotope composition of their body tissue. In this case, we may not have detected a summer-to-autumn shift in their trophic behaviour.

Zooplankton biomass $\delta^{13}C$ and C:N are indicators of lipid content, and both can be used to estimate seasonal variability in zooplankton diet (Matthews and Mazumder, 2005b). Since C:N is positively related to lipid content (McConnaughey and McRoy, 1979; Lesage, 1999; Schmidt *et al.*, 2003) and lipids are usually depleted in ^{13}C relative to proteins and carbohydrates (Parker, 1964; Tieszen *et al.*, 1983), zooplankton with a high lipid content will likely have a lower $\delta^{13}C$ and higher C:N ratio than those with a low lipid content. A notable caveat, however, is that the slow turnover rates of zooplankton tissue and the isotopic variability of their food source(s) can overprint the relationship between C:N and $\delta^{13}C$, complicating the inference of consumer dietary carbon sources (France, 1995; Matthews and Mazumder, 2005b).

From December 2016 to April-May 2017, the C:N ratio of bulk zooplankton biomass decreased from 4.3 ± 0.7 to 3.8 ± 0.5, with a lower C:N ratio measured in April-May 2017 than April-May 2016 (4.1 ± 0.5 for the latter season; Figure 5.5a; Table 5.2). In general, our zooplankton samples had a lower C:N ratio than that reported previously for the open PFZ in autumn. For example, Schmidt *et al.*, (2003) reported higher C:N ratios for *Calanus propinquus*, *Calanus simillimus*, *Metridia lucens*, and *Metridia gerlachei* (8.1, 6.8, 7.4,

and 7.8, respectively) than we determined for *Calanus* spp. and *M. gerlachei* near the PEIs in April-May 2017 (3.7 and 3.8, respectively; Table 5.3). This discrepancy suggests that the zooplankton observed in the eddy near the PEIs could have a lower lipid content than zooplankton outside the meander, supporting our hypothesis that zooplankton increased consumption of their reserves of lipids and fatty acids from summer to autumn.

For our samples from autumn 2016 and 2017, the smaller zooplankton size classes (250-500 µm and 200-500 µm) may have been richer in lipids (higher C:N of ~4.7-5.0) and associated with a lower trophic position in the food web (lower $\delta^{15}N$ of ~0.2-0.4‰) than some of the bigger size classes (i.e., 2000-5000 µm and >2000 µm; lower C:N of ~3.8-4.2 and higher $\delta^{15}N$ of 1.1-3.0‰; Figure 5.5d; Table 5.4). These data suggest that the grazers (i.e., smaller size classes) were feeding on lipid-rich food sources and/or that they had stored substantial amounts of dietary lipids for the upcoming winter season (Wainman, 1997; Syväranta and Rautio, 2010), including for reproductive processes that occur in late winter/early spring (Hagen and Auel, 2001). In contrast to its C:N and $\delta^{15}N$, biomass $\delta^{13}C$ decreased from the smaller to the larger zooplankton size classes, by 1.4-2.1‰ (Figure 5.5e), yielding a positive relationship between C:N and $\delta^{13}C$ with increasing size, likely related to changes in food source. For instance, if we assume dominance of grazers in the smaller size classes, their higher $\delta^{13}C$ may be caused by the summer-to-autumn increase in $\delta^{13}C_{SPM}$ (Figure 5.2c). In addition, in April-May 2017, the zooplankton C:N ratios were lower and $\delta^{13}C$ was higher for each size class than in April-May 2016 (Figure 5.5d-e). For example, Euphausiacea collected in April-May 2017 had a C:N ratio of 3.7 ± 0.1 and $\delta^{13}C$ of -22.8 ± 0.9‰, *versus* 4.1 ± 0.3 and -23.7 ± 1.7‰ in April-May 2016 (Table 5.3). These findings suggest that zooplankton were more depleted in lipids in autumn 2017 than 2016. We thus hypothesize that while the autumn 2017 zooplankton community must have been feeding on the in situ phytoplankton (or at least a component of it), as suggested by the grazing rates measured in Chapter 4, they may also have experienced a higher degree of starvation than in April-May 2016 due to the dominantly small size of the phytoplankton cells inhabiting the near-island eddy from which the samples were collected (Chapter 4). Zooplankton starvation would have contributed to the observed $\delta^{13}C$ mismatch between the zooplankton and the SPM.

5.6. Conclusions

This work contributes to our understanding of the major drivers of temporal variability in the $\delta^{13}C$ and $\delta^{15}N$ of SPM and zooplankton in the Subantarctic Ocean. We generated SPM and zooplankton data for samples collected during five near-consecutive seasons over two years in the region of the Subantarctic Prince Edward Islands archipelago, including July-August 2015 (winter), April-May 2016 (autumn), December 2016 (summer), April-May 2017 (autumn), and June-July 2017 (winter). We suggest that while the major drivers of the geographical distribution of $\delta^{13}C_{SPM}$ in the Southern Ocean are surface water pCO_2 and phytoplankton growth rates, as has been shown by others (St John Glew *et al.*, 2021; Chapter 2), seasonal variability in $\delta^{13}C_{SPM}$ depends largely on the availability of different nitrogenous nutrient sources (i.e., nitrate *versus* ammonium) and phytoplankton community composition, which together induce different carboxylation pathways associated with variable carbon isotope effects (Figure 5.7). The seasonal evolution of $\delta^{15}N_{SPM}$ is also governed by the dominant N source being consumed by phytoplankton, related changes in phytoplankton community composition, and the relative rates of microbial processes that regenerate N *versus* photosynthetic N assimilation (Figure 5.8).

The upwelling of subsurface NO_3^- during winter supplies new N to the surface layer that is relatively high in $\delta^{15}N$. Along with the coincident supply of iron, this NO_3^- fuels diatom productivity in spring, which is associated with carboxylation catalysed by PEPk. Because of the large isotope effect inherent to PEPk, diatom biomass will be low in $\delta^{13}C$, causing $\delta^{13}C_{SPM}$ to decrease over the growing season (Dehairs *et al.*, 1997) to reach a minimum by mid-summer when diatom productivity is greatest (St John Glew *et al.*, 2021). The $\delta^{15}N_{SPM}$ is highest in winter because of isotope fractionation during heterotrophic bacterial decomposition of particulate organic N, which exceeds the rate of new biomass formation, the latter limited by low seasonal light availability (Smart *et al.*, 2020; Mdutyana *et al.*, 2022). When phytoplankton begin to consume the upwelled NO_3^- in spring, they generate biomass that is initially low in $\delta^{15}N$ (i.e., due to isotopic fractionation associated with the NO_3^- reductase enzyme; Granger *et al.*, 2004) but that rises over the growing season as NO_3^-consumption proceeds (Mariotti *et al.*, 1981; Sigman *et al.*, 1999). Following the peak summertime phytoplankton bloom, concentrations of low-$\delta^{15}N$ NH_4^+ increase in the mixed layer due to heterotrophic recycling (i.e., bacterial decomposition and zooplankton grazing; Smith *et al.*, 2022). The

consumption of this NH_4^+ by phytoplankton, which is favoured over NO_3^- because of the limiting iron concentrations (Raven, 1988; Maldonado and Price, 1996), decreases $\delta^{15}N_{SPM}$ to a minimum by autumn. Simultaneously, the phytoplankton community shifts from one dominated by large diatom cells to one dominated by nano-phytoplankton. These smaller cells express PEPc during carboxylation, which has a low intrinsic isotope effect, ultimately yielding organic matter in late-summer through autumn that is high in $\delta^{13}C$.

Zooplankton $\delta^{13}C$ and $\delta^{15}N$ tend to reflect the temporal isotopic variability of their principal food source(s), which in this study was determined to be the SPM. However, we also observed an isotopic mismatch between zooplankton and SPM $\delta^{13}C$ and $\delta^{15}N$ in one season (April-May 2017). We suggest that this mismatch can be explained by the relatively slow turnover rate of zooplankton biomass, coupled with the possibility that the larger zooplankton herbivores could not efficiently graze on the nano-sized phytoplankton present in the water column at the time of sampling such that they experienced starvation, which forced them to decrease their lipid stores. We encourage future studies to collect and analyse species-specific zooplankton $\delta^{13}C$ and $\delta^{15}N$ and lipid content during multiple seasons in the Southern Ocean in order to better characterize the seasonal variability of the plankton trophic system and their food source(s).

This study highlights the importance of accounting for seasonal variability when using plankton stable isotopes to understand carbon and nutrient cycling, decipher food web dynamics, and track animal migrations, and underscores the complexity of using SPM and zooplankton as isotopic baselines in the Southern Ocean. For instance, while $\delta^{15}N_{SPM}$ may be an appropriate baseline for trophic analysis during summer when the biomass is overwhelmingly comprised of actively growing phytoplankton, its suitability during autumn and winter are questionable because of the importance of other (i.e., non-assimilation) N cycle processes and the fact that SPM and zooplankton isotopes can become decoupled by their different turnover times. Primary consumers may provide a more suitable baseline for trophic analysis during autumn and winter, although additional seasonally-resolved data are required to confirm this idea.

Chapter 6. Summary and future research directions

Instead of reiterating the conclusions and implications that have been comprehensively discussed in the final sections of each previous data chapter (Chapters 2 to 5), in this section I provide the 'take-home' messages of my work and, given my findings, suggest future research directions that may improve our understanding of the potential consequences of the climate change for the plankton ecosystem in the Southern Ocean.

The work detailed in this thesis intended to provide novel information on the spatial and temporal variability of the drivers of ecological and biogeochemical dynamics within the plankton ecosystem of the open Southern Ocean and (Sub)Antarctic Islands, from a carbon production and export perspective (i.e., focused on the biological pump). This goal was achieved through high-resolution observations of plankton community composition and the carbon and nitrogen isotope ratios ($\delta^{13}C$ and $\delta^{15}N$) of suspended particulate matter (SPM; $\delta^{13}C_{SPM}$ and $\delta^{15}N_{SPM}$) and zooplankton body tissue for samples collected from all around the Southern Ocean and in the vicinity of (Sub)Antarctic islands, with a particular focus on the Prince Edward Islands archipelago. Geographical and seasonal variability in biogeochemical processes and phytoplankton dynamics govern the carbon and nitrogen isotopic composition of SPM (Chapter 2), which subsequently influences the zooplankton $\delta^{13}C$ and $\delta^{15}N$ such that it largely mimics the spatial and temporal variability in $\delta^{13}C_{SPM}$ and $\delta^{15}N_{SPM}$ (Chapter 3). In particular, while the latitudinal trends in $\delta^{13}C_{SPM}$ and $\delta^{15}N_{SPM}$ are strongly dependent on the ambient seawater pCO_2 and the $\delta^{15}N$ of the N sources available to phytoplankton, along with the extent to which phytoplankton rely on new *versus* regenerated N (i.e., the *f*-ratio), respectively (Chapter 2), I found that seasonal variations in both $\delta^{13}C_{SPM}$ and $\delta^{15}N_{SPM}$ are highly influenced by the N sources available to phytoplankton and to their seasonal cycles (Chapter 5). In addition, the composition of the phytoplankton community has an impact on the spatial and temporal variability in $\delta^{13}C_{SPM}$ and $\delta^{15}N_{SPM}$ because of taxonomic differences in the carboxylase enzymes expressed during photosynthesis and in the capacity to assimilate particular N sources (Chapters 2 and 5).

A central theme of this work is the differences in plankton productivity, dynamics, and $\delta^{13}C$ and $\delta^{15}N$ among oceanic systems of the Southern Ocean, such as open waters, islands and archipelagos, continental shelves, sea ice zones, and glaciers. While I preferentially focused my study on the effects of the Subantarctic Island systems on plankton dynamics and their isotope ratios (Chapters 4 and 5), I found that in all the more

dynamical systems, plankton $\delta^{13}C$ and $\delta^{15}N$ are elevated relative to the open Southern Ocean. This trend can be explained by the input of micro-and macronutrients such as iron and ammonium, albeit not always due to the same physical and biogeochemical processes (Chapter 2). Ultimately, I conclude that measurements of $\delta^{13}C_{SPM}$ and $\delta^{15}N_{SPM}$ from the various hydrographic zones of the Southern Ocean are useful for 1) assessing the biogeochemical processes occurring in the upper water column and 2) estimating carbon export potential, and that they 3) provide reliable baselines for trophic analysis of the zooplankton system.

In Chapter 2, I evaluated the potential for summertime carbon export through the application of a simple isotope mixing model, finding that export potential is stronger at higher latitudes (i.e., the *f*-ratio was higher in the Antarctic than the Subantarctic). Moreover, I estimated higher values close to the (Sub)Antarctic islands and in areas where the sea ice was melting. These higher values can be explained by an increase in phytoplankton growth rates and nitrate uptake, probably in response to the input of iron. At the same time, my findings detailed in Chapter 3 suggest that Antarctic waters host a zooplankton trophic web dominated by carnivores and omnivores, which favours carbon export rather than retention, in contrast to the more herbivore-based zooplankton trophic web in the Subantarctic Ocean, which likely retains and recycles more carbon in the upper layer of the water column. These results are complementary and indicate that the Antarctic Ocean may facilitate enhanced carbon export compared to the Subantarctic, which has implications for the role of the Southern Ocean in global climate regulation.

I also discovered that Subantarctic Island systems not only increase marine productivity in adjacent waters by supporting highly biodiverse marine ecosystems, but they also prolong the potential for carbon export during periods that are typically unproductive such as autumn (Chapter 4). By alleviating iron limitation of phytoplankton in particular, the island mass effect may stimulate more complete drawdown of the available macronutrients, which amounts to a net removal of atmospheric CO_2. To better understand the role that the more dynamical systems of the Southern Ocean, including the Subantarctic islands, play in regulating climate, it would be interesting to pursue the idea that some food webs promote carbon export while others favour retention.

Despite the promising results of the models presented in this thesis, there are some limitations that need to be acknowledged. One such limitation is the finding that systems near islands or continental shelves are not well

characterized by the Rayleigh model. A possible way to address this issue is to perform studies designed to evaluate models that may better describe and quantify N uptake processes and isotopic variability where supply and uptake are simultaneous (e.g., the steady state model; Sigman and Fripiat, 2019). Island- and continental shelf systems may be near-continuously supplied with deep (i.e., upwelled) N and/or terrestrial run-off, although it is unlikely that the latter flux will be constant. Nonetheless, dedicated studies employing a variety of isotope models would likely yield important insights. It would also be valuable to improve our understanding of the geographical and temporal distribution of the $\delta^{15}N$ of nutrients and SPM in the Southern Ocean, particularly in the vicinity of islands, sea ice regions, and continental shelves. Although the work described in this thesis does provides new measurements of the $\delta^{15}N$ of SPM near such features, these data are not sufficient to train or produce accurate prediction models. Such models are currently unable to accurately predict variability near the islands, sea ice, and continental shelves due to the lack of observations (St John Glew *et al.*, 2021). Two potential solutions are to collect more data through the use of moorings, floats, and gliders.

The work detailed in this thesis also shows that the study of zooplankton isotope ratios and trophic structure may inform our understanding of the fate of photosynthetic carbon produced in the mixed layer. However, there are currently no models that describe or predict the geographical and/or temporal variability of zooplankton isotope ratios. More species-specific studies on the trophic role of zooplankton are needed to better understand the structure of the food web, energy transfer through plankton systems, and carbon flow within and out of the mixed layer. It would be valuable to collect more observations of zooplankton isotope ratios at the species level, along with information on their vertical migration, egg production rates, trophic role, grazing rates, and contribution to the recycling of organic matter within the mixed layer. These studies could be coupled with measurements of the flux of faecal pellet from the mixed layer using sediment traps, although these are also subject to limitations in terms of geographical coverage (a few square meters), as well as how quantitatively they record the amount of composition of the material leaving the surface. All these observations must then be incorporated into models to better estimate and predict the geographical and seasonal trends in carbon export across the Southern Ocean. Combining improved modelled *f*-ratio estimates with model output related to zooplankton dynamics and carbon flow would be a valuable contribution to estimating export production and the carbon export efficiency (i.e., e-ratio which is defined as the fraction of

organic carbon fixed through net primary production that is exported out of the surface productive layer of the ocean; Fan *et al.*, 2020 and references therein).

Finally, it is important to consider how climate change may impact the plankton system in the open Southern Ocean and at and near the (Sub)Antarctic islands. The Southern Ocean is a dynamic marine ecosystem and is a major actor in the regulation of Earth's climate. Nonetheless, the Southern Ocean is a major contributor to the global ocean CO_2 sink and is estimated to account for ~30% of the global ocean carbon flux (Schlitzer 2002; DeVries 2014; Frölicher *et al.* 2015; Arteaga *et al.* 2018; Chapter 2). In this thesis, I have discussed the many roles of the phytoplankton and zooplankton in exporting and sequestering carbon in the deep ocean, and in supporting (Sub)Antarctic marine food webs. Like all other systems on Earth, the Southern Ocean is affected by global warming, which is inducing changes in plankton dynamics and consequently, in (Sub)Antarctic marine ecosystems and the biological carbon pump (e.g., Petrou *et al.*, 2016; Deppeler and Davidson, 2017 and references therein; Henley *et al.* 2020 and references therein).

As mentioned in Chapter 3, the Southern Ocean is already experiencing an increase in the intensity of the Antarctic Circumpolar Current (ACC), an increase in sea surface temperature (SST), the southward migration of hydrographic fronts, and changes in sea-ice coverage (e.g., Gille, 2002; Sokolov and Rintoul, 2009a, 2009b; Constable *et al.*, 2014; Hobbs *et al.*, 2016). Climate projections suggest that heating of the surface mixed layer in the Subantarctic Ocean will increase upper water-column stratification, enhancing the amount of light available to the phytoplankton that will also experience higher iron concentrations due to stronger eastward winds and storms that will supply more terrestrial dust to the open ocean (Orr *et al.*, 2005; Marinov *et al.*, 2010; Boyd *et al.*, 2016; Petrou *et al.*, 2016; Deppeler and Davidson, 2017). However, the effects on the phytoplankton are still uncertain and highly debated (Deppeler and Davidson, 2017 and references therein). Some studies suggest that an increase in the iron concentration and temperature within a more stratified mixed layer could lead to a doubling of diatom growth rates (e.g., Boyd *et al.*, 2016). By contrast, other studies propose that stronger stratification of the mixed layer will diminish the upward transport of subsurface nutrients, limiting phytoplankton production and the sinking of biogenic carbon, and thus the strength of the biological pump (e.g., Matear and Hirst, 1999; Marinov *et al.*, 2010; Petrou *et al.*, 2016). Speculating on possible future scenarios based on my findings and recent climate change projections,

the role of the Subantarctic Ocean as a major sink for atmospheric CO_2 may be significantly affected by increased stratification of the upper water layer. During winter, a shallower mixed layer depth would reduce the entrainment of iron into the surface, limiting nitrate uptake and decreasing carbon export potential (Dugdale and Goering, 1967; Yool *et al.*, 2007). Assuming that winter mixing could reset the nutrient conditions required to facilitate carbon export (e.g., Tagliabue *et al.*, 2014; Nicholson *et al.*, 2019), however, a more stratified mixed layer from spring to autumn might impede the gravitational sinking of particulate matter (e.g., phytoplankton cells, faecal pellets, dead bodies of zooplankton, etc.), thereby weakening the biological pump. In addition, regardless of the phytoplankton community that would be favoured during such a hypothetical scenario (e.g., diatoms *versus* nano-phytoplankton), the photosynthetic growth rate would potentially increase due to the favourable iron, light, and temperature conditions, resulting in more biomass available to zooplankton (from micro- to macro-zooplankton), which will increase the number of herbivores and their grazing rates. The increase in herbivory could lead to higher retention of the carbon biomass within the food web, which would decrease the sinking flux, thus weakening the biological pump. On the other hand, increased biomass production, if by large, ballasted phytoplankton (e.g., diatoms) could lead to enhanced direct carbon export (i.e., sinking of phytoplankton cells) and thus a strengthening of the biological pump.

For the permanently ice-free waters of the Antarctic Ocean, models are predicting a slower increase in SST than the global ocean rate of increase (0.02°C *versus* 0.08°C per decade; Armour *et al.*, 2016), a poleward migration of the Polar Frontal Zone, which will move the permanently ice-free zone southward (Sokolov and Rintoul, 2009a), and a strengthening of the westerly winds, which is likely to deepen the mixed layer (Orr *et al.*, 2005; Meijers, 2014; Leung *et al.*, 2015; Armour *et al.*, 2016; Haumann *et al.*, 2016). In addition, iron concentrations will increase due to more intense dust transport and an increase in the number of icebergs in the permanently ice-free zone (Scambos *et al.*, 2000), which will melt at faster rates, enriching the surrounding water with iron (Cefarelli *et al.*, 2011; Lin *et al.*, 2011; Shaw *et al.*, 2011; Vernet *et al.*, 2011, 2012). Moreover, models suggest that the deepening of the mixed layer will yield a higher input of subsurface nutrients (i.e., iron) to the surface, resulting in increased phytoplankton growth rates (when light is not limiting) and thus higher carbon export (Lovenduski and Gruber, 2005; Hauck *et al.*, 2013, 2015; Laufkötter *et al.*, 2015).

At the same time, with the increasing temperature, the northernmost extent of sea-ice cover will move southwards, thereby increasing the area of the permanently ice-free zone of the Antarctic (Bracegirdle *et al.*, 2008; Boyd *et al.*, 2015). According to a recent review (Eayrs *et al.*, 2021 and references therein), surface sea ice coverage around the Southern Ocean increased between 1979 and 2016, but then abruptly decreased between 2016 and today, with values significantly below the average sea ice cover of the past 40 years. The authors attribute this rapid decline to the combined effects of a decades-long ocean warming trend and an early spring southward advection of atmospheric heat, compounded by an exceptional weakening of the Southern Hemisphere mid-latitude westerlies in late spring. However, it is important to note that the general circum-Antarctic trend may not manifest at smaller spatial scales. For example, the seasonal sea-ice cover around the west Antarctic Peninsula has decreased by ~40% over the past decades (Smith and Stammerjohn, 2001; Ducklow *et al.*, 2007; Parkinson and Cavalieri, 2012) and the ice-free season is now three months longer than it was during the 1980s (Stammerjohn *et al.*, 2012). Furthermore, observations from the western Ross Sea suggest that the ice-free season has shortened by ~2.5 months because the sea ice is retreating later and advancing earlier than it was 30 years ago (Stammerjohn *et al.*, 2012), reducing the phytoplankton bloom duration and seasonal productivity (Arrigo and van Dijken, 2004).

The timing of phytoplankton blooms is highly dependent on the southward migration and seasonal retreat of the marginal ice zone (Arrigo and van Dijken, 2004; Pearce *et al.*, 2010; Westwood *et al.*, 2010). However, contradictory observations and model predictions of sea-ice extent and the duration of ice-free seasons illustrate the intricate interplay of variables affecting the quantity and distribution of sea ice around Antarctica (Gupta *et al.*, 2009; Parkinson and Cavalieri, 2012; Turner *et al.*, 2013), which makes it very complex to hypothesise future scenarios for the marine ecosystem (Petrou *et al.*, 2016; Deppeler and Davidson, 2017). Deppeler and Davidson (2017) discuss possible scenarios for the phytoplankton, the organisms at higher trophic levels, and the algae present in the sea ice. They postulate that the deepening of the mixed layer in the permanently ice-free zone and its larger area will yield higher phytoplankton growth rates and more extensive blooms of large diatoms, which will supply more food to the primary consumers. I would potentially investigate if the deeper mixed layer and weaker stratification of the upper water column could potentially strengthen the biological pump by increasing gravitational sinking of larger biogenic particles such as phytoplankton cells produced during more intense photosynthetic blooms and faecal pellets.

At the same time, I would expect that the phytoplankton community composition would shift toward smaller diatoms and/or flagellates, which will affect the larger grazers and possibly the trophic web (Deppeler and Davidson, 2017). Moreover, the reduced sea-ice cover will also decrease the abundance of ice algae, reducing an essential winter food source to zooplankton grazers (Deppeler and Davidson, 2017). Due to an increase in sea-ice melt (Maksym *et al.*, 2012 and references therein; Lannuzel *et al.*, 2016 and references there in), the iron supply will rise, increasing nitrate uptake for a relatively short period of time. A longer period of iron limitation will follow as sea ice extent is further reduced, perhaps reducing the relatively high carbon export potential that sea-ice-adjacent waters are known for (Chapter 2).

I recommend that future studies include measurements of species-specific phytoplankton and zooplankton $\delta^{13}C$ and $\delta^{15}N$, which would improve our understanding of the biogeochemical processes and ecological dynamics governing the plankton systems and biological pump of the Southern Ocean. Furthermore, there is a need to extend and intensify the spatial and temporal resolution of the available observations, especially during winter and in and near the marginal ice zone, in order to provide high-resolution data for biogeochemical and predictive models.

References

Abbott, M. R., Richman, J. G., Letelier, R. M., and Bartlett, J. S. 2000. The spring bloom in the Antarctic Polar Frontal Zone as observed from a mesoscale array of bio-optical sensors. Deep Sea Research Part II: Topical Studies in Oceanography, 47: 3285–3314. Elsevier.

Aberle, N., and Malzahn, A. M. 2007. Interspecific and nutrient-dependent variations in stable isotope fractionation: experimental studies simulating pelagic multitrophic systems. Oecologia, 154: 291–303.

Alderkamp, A.-C., Mills, M. M., van Dijken, G. L., Laan, P., Thuróczy, C.-E., Gerringa, L. J. A., de Baar, H. J. W., *et al.* 2012. Iron from melting glaciers fuels phytoplankton blooms in the Amundsen Sea (Southern Ocean): Phytoplankton characteristics and productivity. Deep Sea Research Part II: Topical Studies in Oceanography, 71–76: 32–48.

Allan, E. L. 2011. Trophodynamics of the benthic and hyperbenthic communities inhabiting the sub-Antarctic Prince Edward islands: stable isotope and fatty acid signatures. Rhodes University.

Allanson, B. R., Boden, B., Parker, L., and Rae, C. D. 1985. A Contribution to the Oceanology of the Prince Edward Islands BT - Antarctic Nutrient Cycles and Food Webs. *In* pp. 38–45. Ed. by W. R. Siegfried, P. R. Condy, and R. M. Laws. Springer Berlin Heidelberg, Berlin, Heidelberg.

Altabet, M. A. 1988. Variations in nitrogen isotopic composition between sinking and suspended particles: implications for nitrogen cycling and particle transformation in the open ocean. Deep Sea Research Part A. Oceanographic Research Papers, 35: 535–554.

Altabet, M. A. 1989. A time-series study of the vertical structure of nitrogen and particle dynamics in the Sargasso Sea. Limnology and Oceanography, 34: 1185–1201. John Wiley & Sons, Ltd.

Altabet, M. A., and Francois, R. 1994. Sedimentary nitrogen isotopic ratio as a recorder for surface ocean nitrate utilization. Global Biogeochemical Cycles, 8: 103–116. John Wiley & Sons, Ltd.

Altabet, M. A., Pilskaln, C., Thunell, R., Pride, C., Sigman, D., Chavez, F., and Francois, R. 1999. The nitrogen isotope biogeochemistry of sinking particles from the margin of the Eastern North Pacific. Deep Sea Research Part I: Oceanographic Research Papers, 46: 655–679. Pergamon.

Altabet, M. A., and Francois, R. 2001. Nitrogen isotope biogeochemistry of the Antarctic Polar Frontal Zone at 170°W. Deep Sea Research Part II: Topical Studies in Oceanography, 48: 4247–4273.

Alurralde, G., Fuentes, V. L., De Troch, M., and Tatián, M. 2020. Suspension feeders as natural sentinels of the spatial variability in food sources in an Antarctic fjord: A stable isotope approach. Ecological Indicators, 115: 106378.

Alvain, S., Moulin, C., Dandonneau, Y., and Loisel, H. 2008. Seasonal distribution and succession of dominant phytoplankton groups in the global ocean: A satellite view. Global Biogeochemical Cycles, 22. Wiley Online Library.

Andersen, V. 1998. The Biology of Pelagic Tunicates, ed Bone Q. Oxford Univ Press, New York.

Ángel, L.-U., Elena, S. M., P., H. R., and Xabier, I. 2006. Scaling the metabolic balance of the oceans. Proceedings of the National Academy of Sciences, 103: 8739–8744. Proceedings of the National Academy of Sciences.

Ansorge, I. J., Froneman, P. W., Pakhomov, E. A., Lutjeharms, J. R. E., Perissinotto, R., and Van Ballegooyen, R. C. 1999. Physical-biological coupling in the waters surrounding the Prince Edward Islands (Southern Ocean). Polar Biology, 21: 135–145.

Ansorge, I. J., and Lutjeharms, J. R. E. 2005. Direct observations of eddy turbulence at a ridge in the Southern Ocean. Geophysical Research Letters, 32. Wiley Online Library.

Ansorge, I. J., Durgadoo, J. V, and Pakhomov, E. A. 2009. Dynamics of physical and biological systems of the Prince Edward Islands in a changing climate. Papers and Proceedings of the Royal Society of Tasmania, 143: 15–18.

Ansorge, I. J., Froneman, W. P., and Durgadoo, J. V. 2012. The Marine Ecosystem of the Sub-Antarctic, Prince Edward Islands. Marine Ecosystems: 61–76. IntechOpen.

Antoine, D., Thomalla, S., Berliner, D., Little, H., Moutier, W., Olivier-Morgan, A., Robinson, C., *et al.* 2020. Phytoplankton pigment concentrations of seawater sampled during the Antarctic Circumnavigation Expedition (ACE) during the Austral Summer of 2016/2017. (1.1) [Data set]. Zenodo.

Armour, K. C., Marshall, J., Scott, J. R., Donohoe, A., and Newsom, E. R. 2016. Southern Ocean warming delayed by circumpolar upwelling and equatorward transport. Nature Geoscience, 9: 549–554. Nature Publishing Group.

Armstrong, R. A. 2014. When to use the Bonferroni correction. Ophthalmic and Physiological Optics, 34: 502–508. John Wiley & Sons, Ltd.

Arnelle, D. R., and O'Leary, M. H. 1992. Binding of carbon dioxide to phosphoenolpyruvate carboxykinase deduced from carbon kinetic isotope effects. Biochemistry, 31: 4363–4368. ACS Publications.

Arrigo, K. R., and van Dijken, G. L. 2004. Annual changes in sea-ice, chlorophyll a, and primary production in the Ross Sea, Antarctica. Deep Sea Research Part II: Topical Studies in Oceanography, 51: 117–138. Elsevier.

Arrigo, K. R., van Dijken, G. L., and Bushinsky, S. 2008a. Primary production in the Southern Ocean, 1997–2006. Journal of Geophysical Research: Oceans, 113. John Wiley & Sons, Ltd.

Arrigo, K. R., van Dijken, G., and Long, M. 2008b. Coastal Southern Ocean: A strong anthropogenic CO2 sink. Geophysical Research Letters, 35. John Wiley & Sons, Ltd.

Arrigo, K. R., van Dijken, G. L., and Strong, A. L. 2015. Environmental controls of marine productivity hot spots around Antarctica. Journal of Geophysical Research: Oceans, 120: 5545–5565. John Wiley & Sons, Ltd.

Arrington, D. A., and Winemiller, K. O. 2002. Preservation Effects on Stable Isotope Analysis of Fish Muscle. Transactions of the American Fisheries Society, 131: 337–342. Taylor & Francis.

Arteaga, L., Haëntjens, N., Boss, E., Johnson, K. S., and Sarmiento, J. L. 2018. Assessment of Export Efficiency Equations in the Southern Ocean Applied to Satellite-Based Net Primary Production. Journal of Geophysical Research: Oceans, 123: 2945–2964. John Wiley & Sons, Ltd.

Arteaga, L. A., Boss, E., Behrenfeld, M. J., Westberry, T. K., and Sarmiento, J. L. 2020. Seasonal modulation of phytoplankton biomass in the Southern Ocean. Nature Communications, 11: 5364.

Arthur, M. A., Dean, W. E., and Claypool, G. E. 1985. Anomalous 13C enrichment in modern marine organic carbon. Nature, 315: 216–218. Springer.

Atkinson, A. 1995. Omnivory and feeding selectivity in five copepod species during spring in the Bellingshausen Sea, Antarctica. ICES Journal of Marine Science, 52: 385–396.

Atkinson, A. 1996. Subantarctic copepods in an oceanic, low chlorophyll environment: ciliate predation, food selectivity and impact on prey populations. Marine Ecology Progress Series, 130: 85–96.

Atkinson, A., Shreeve, R. S., Pakhomov, E. A., Priddle, J., Blight, S. P., and Ward, P. 1996. Zooplankton response to a phytoplankton bloom near South Georgia, Antarctica. Marine Ecology Progress Series, 144: 195–210.

Atkinson, A. 1998. Life cycle strategies of epipelagic copepods in the Southern Ocean. Journal of Marine Systems, 15: 289–311.

Atkinson, A., Siegel, V., Pakhomov, E. A., and Rothery, P. 2004. Long-term decline in krill stock and increase in salps within the Southern Ocean. Nature, 432: 100–103.

Atkinson, A., Ward, P., Hunt, B. P. V, Pakhomov, E. A., and Hosie, G. W. 2012a. An overview of Southern Ocean zooplankton data: abundance, biomass, feeding and functional relationships. Ccamlr Science, 19: 171–218. CCAMLR.

Atkinson, A., Schmidt, K., Fielding, S., Kawaguchi, S., and Geissler, P. A. 2012b. Variable food absorption by Antarctic krill: Relationships between diet, egestion rate and the composition and sinking rates of their fecal pellets. Deep Sea Research Part II: Topical Studies in Oceanography, 59: 147–158. Elsevier.

Atkinson, A., Hill, S. L., Pakhomov, E. A., Siegel, V., Reiss, C. S., Loeb, V. J., Steinberg, D. K., *et al.* 2019. Krill (Euphausia superba) distribution contracts southward during rapid regional warming. Nature Climate Change, 9. Springer US.

Aumont, O., Maury, O., Lefort, S., and Bopp, L. 2018. Evaluating the Potential Impacts of the Diurnal Vertical Migration by Marine Organisms on Marine Biogeochemistry. Global Biogeochemical Cycles, 32: 1622–1643. John Wiley & Sons, Ltd.

Azam, F., Smith, D. C., and Hollibaugh, J. T. 1991. The role of the microbial loop in Antarctic pelagic ecosystems. Polar Research, 10: 239–244. John Wiley & Sons, Ltd.

Baines, M., Kelly, N., Reichelt, M., Lacey, C., Pinder, S., Fielding, S., Murphy, E., *et al.* 2021. Population abundance of recovering humpback whales Megaptera novaeangliae and other baleen whales in the Scotia Arc, South Atlantic. Marine Ecology Progress Series, 676: 77–94.

Baines, M., Jackson, J. A., Fielding, S., Warwick-Evans, V., Reichelt, M., Lacey, C., Pinder, S., *et al.* 2022. Ecological interactions between Antarctic krill (Euphausia superba) and baleen whales in the South Sandwich Islands region – Exploring predator-

prey biomass ratios. Deep Sea Research Part I: Oceanographic Research Papers, 189: 103867.

Bakker, D. C. E., Nielsdóttir, M. C., Morris, P. J., Venables, H. J., and Watson, A. J. 2007. The island mass effect and biological carbon uptake for the subantarctic Crozet Archipelago. Deep-Sea Research Part II: Topical Studies in Oceanography, 54: 2174–2190.

Balarin, M. G. 1999. Size-fractionated phytoplankton biomass and primary production in the Southern Ocean. (Doctoral dissertation, Rhodes University).

Barth, A., Alvera-Azcárate, A., Troupin, C., Ouberdous, M., and Beckers, J.-M. 2010. A web interface for griding arbitrarily distributed in situ data based on Data-Interpolating Variational Analysis (DIVA). Adv. Geosci., 28: 29–37. Copernicus Publications.

Belcher, A., Henson, S. A., Manno, C., Hill, S. L., Atkinson, A., Thorpe, S. E., Fretwell, P., *et al.* 2019. Krill faecal pellets drive hidden pulses of particulate organic carbon in the marginal ice zone. Nature communications, 10: 1–8. Nature Publishing Group.

Belkin, I. M., and Gordon, A. L. 1996. Southern Ocean fronts from the Greenwich meridian to Tasmania. Journal of Geophysical Research: Oceans, 101: 3675–3696. John Wiley & Sons, Ltd.

Bendschneider, K., and Robinson, R. J. 1952. A new spectrophotometric method for the determination of nitrite in sea water.

Bentaleb, I., Fontugne, M., Descolas-Gros, C., Girardin, C., Mariotti, A., Pierre, C., Brunet, C., *et al.* 1998. Carbon isotopic fractionation by plankton in the Southern Indian Ocean: relationship between δ13C of particulate organic carbon and dissolved carbon dioxide. Journal of Marine Systems, 17: 39–58. Elsevier.

Berg, G. M., Mills, M. M., Long, M. C., Bellerby, R., Strass, V., Savoye, N., Röttgers, R., *et al.* 2011. Variation in particulate C and N isotope composition following iron fertilization in two successive phytoplankton communities in the Southern Ocean. Global Biogeochemical Cycles, 25. John Wiley & Sons, Ltd.

Bernard, K., and Froneman, P. 2002. Mesozooplankton community structure in the Southern Ocean upstream of the Prince Edward Islands. Polar Biology, 25: 597–604.

Bernard, K. S., and Froneman, P. W. 2003. Mesozooplankton community structure and grazing impact in the Polar Frontal Zone of the south Indian Ocean during austral autumn 2002. Polar Biology, 26: 268–275.

Bernard, K. S., and Froneman, P. W. 2005. Trophodynamics of selected mesozooplankton in the west-Indian sector of the Polar Frontal Zone, Southern Ocean. Polar Biology, 28: 594–606.

Bernard, K. S. 2006. The role of the euthecosome pteropod, Limacina retroversa, in the Polar Frontal Zone, Southern Ocean. (Doctoral dissertation, Rhodes University).

Bernard, K. S., and Froneman, P. W. 2009. The sub-Antarctic euthecosome pteropod, Limacina retroversa: Distribution patterns and trophic role. Deep Sea Research Part I: Oceanographic Research Papers, 56: 582–598.

Besiktepe, S. 2002. Coupling of ingestion and defecation as a function of diet in the calanoid copepod Acartia tonsa . Marine Ecology Progress Series, 229: 151–164.

Bestley, S., Ropert-Coudert, Y., Bengtson Nash, S., Brooks, C. M., Cotté, C., Dewar, M., Friedlaender, A. S., *et al.* 2020. Marine Ecosystem Assessment for the Southern Ocean: Birds and Marine Mammals in a Changing Climate.

Bidigare, R. R., Fluegge, A., Freeman, K. H., Hanson, K. L., Hayes, J. M., Hollander, D., Jasper, J. P., *et al.* 1997. Consistent fractionation of 13C in nature and in the laboratory: Growth-rate effects in some haptophyte algae. Global Biogeochemical Cycles, 11: 279–292. John Wiley & Sons, Ltd.

Black, C. R., and Armbruster, J. W. 2021. New method of isotopic analysis: baseline-standardized isotope vector analysis shows trophic partitioning in loricariids. Ecosphere, 12: e03503. John Wiley & Sons, Ltd.

Blain, S., Tréguer, P., Belviso, S., Bucciarelli, E., Denis, M., Desabre, S., Fiala, M., *et al.* 2001. A biogeochemical study of the island mass effect in the context of the iron hypothesis: Kerguelen Islands, Southern Ocean. Deep Sea Research Part I: Oceanographic Research Papers, 48: 163–187.

Blain, S., Quéguiner, B., Armand, L., Belviso, S., Bombled, B., Bopp, L., Bowie, A., *et al.* 2007. Effect of natural iron fertilization on carbon sequestration in the Southern Ocean. Nature, 446: 1070–1074.

Boden, B. P., and Parker, L. D. 1986. The plankton of the Prince Edward Islands. Polar Biology, 5: 81–93.

Boden, B. P. 1988. Observations of the island mass effect in the Prince Edward archipelago. Polar Biology, 9: 61–68.

Boltovskoy, D. 1999. South Atlantic zooplankton. Backhuys, London. 1706 pp.

Bone, Q., Carré, C., and Chang, P. 2003. Tunicate feeding filters. Journal of the Marine Biological Association of the United Kingdom, 83: 907–919. Cambridge University Press.

Borrione, I., and Schlitzer, R. 2013. Distribution and recurrence of phytoplankton blooms around South Georgia, Southern Ocean. Biogeosciences, 10: 217–231.

Bost, C. A., Cotté, C., Bailleul, F., Cherel, Y., Charrassin, J. B., Guinet, C., Ainley, D. G., *et al.* 2009. The importance of oceanographic fronts to marine birds and mammals of the southern oceans. Journal of Marine Systems, 78: 363–376.

Bowen, G. J. 2010. Isoscapes: spatial pattern in isotopic biogeochemistry. Annual review of earth and planetary sciences, 38: 161–187.

Bowie, A. R., Brian Griffiths, F., Dehairs, F., and Trull, T. W. 2011. Oceanography of the subantarctic and Polar Frontal Zones south of Australia during summer: Setting for the SAZ-Sense study. Deep Sea Research Part II: Topical Studies in Oceanography, 58: 2059–2070.

Boyd, P. W., Crossley, A. C., DiTullio, G. R., Griffiths, F. B., Hutchins, D. A., Queguiner, B., Sedwick, P. N., *et al.* 2001. Control of phytoplankton growth by iron supply and irradiance in the subantarctic Southern Ocean: Experimental results from the SAZ Project. Journal of Geophysical Research: Oceans, 106: 31573–31583. John Wiley & Sons, Ltd.

Boyd, P. W. 2002. Environmental factors controlling phytoplankton processes in the southern ocean1. Journal of Phycology, 38: 844–861. John Wiley & Sons, Ltd.

Boyd, P. W., Lennartz, S. T., Glover, D. M., and Doney, S. C. 2015. Biological ramifications of climate-change-mediated oceanic multi-stressors. Nature Climate Change, 5: 71–79. Nature Publishing Group.

Boyd, P. W., Dillingham, P. W., McGraw, C. M., Armstrong, E. A., Cornwall, C. E., Feng, Y. -y., Hurd, C. L., *et al.* 2016. Physiological responses of a Southern Ocean diatom to complex future ocean conditions. Nature Climate Change, 6: 207–213.

Boyd, P. W., Claustre, H., Levy, M., Siegel, D. A., and Weber, T. 2019. Multi-faceted particle pumps drive carbon sequestration in the ocean. Nature, 568: 327–335.

Bracegirdle, T. J., Connolley, W. M., and Turner, J. 2008. Antarctic climate change over the twenty first century. Journal of Geophysical Research: Atmospheres, 113. Wiley Online Library.

Bracher, A. U., and Kroon, B. M. A. 1999. Primary production, physiological state and composition of phytoplankton in the Atlantic Sector of the Southern Ocean. Marine Ecology Progress Series, 190: 1–16.

Brault, E., Koch, P., McMahon, K., Broach, K., Rosenfield, A. P., Sauthoff, W., Loeb, V., *et al.* 2018. Carbon and nitrogen zooplankton isoscapes in West Antarctica reflect oceanographic transitions. Marine Ecology Progress Series, 593: 29–45.

Britten, G. L., Wakamatsu, L., and Primeau, F. W. 2017. The temperature-ballast hypothesis explains carbon export efficiency observations in the Southern Ocean. Geophysical Research Letters, 44: 1831–1838. John Wiley & Sons, Ltd.

Buesseler, K. O., Antia, A. N., Chen, M., Fowler, S. W., Gardner, W. D., Gustafsson, O., Harada, K., *et al.* 2007. An assessment of the use of sediment traps for estimating upper ocean particle fluxes. Journal of Marine Research, 65: 345–416. Sears Foundation for Marine Research.

Buesseler, K. O., and Boyd, P. W. 2009. Shedding light on processes that control particle export and flux attenuation in the twilight zone of the open ocean. Limnology and Oceanography, 54: 1210–1232. Wiley Online Library.

Burghart, S. E., Hopkins, T. L., Vargo, G. A., and Torres, J. J. 1999. Effects of a rapidly receding ice edge on the abundance, age structure and feeding of three dominant calanoid copepods in the Weddell Sea, Antarctica. Polar Biology, 22: 279–288.

Cael, B. B., and Follows, M. J. 2016. On the temperature dependence of oceanic export efficiency. Geophysical Research Letters, 43: 5170–5175. John Wiley & Sons, Ltd.

Calbet, A., and Landry, M. R. 2004. Phytoplankton growth, microzooplankton grazing, and carbon cycling in marine systems. Limnology and Oceanography, 49: 51–57. John Wiley & Sons, Ltd.

Capone, D. G., Burns, J. A., Montoya, J. P., Subramaniam, A., Mahaffey, C., Gunderson, T., Michaels, A. F., *et al.* 2005. Nitrogen fixation by Trichodesmium spp.: An important source of new nitrogen to the tropical and subtropical North Atlantic Ocean. Global Biogeochemical Cycles, 19. Wiley Online Library.

Caron, D. A., Goldman, J. C., and Dennett, M. R. 1990. Carbon utilization by the omnivorous flagellate Paraphysomonas imperforata. Limnology and oceanography, 35: 192–201. Wiley Online Library.

Carpenter-Kling, T., Handley, J. M., Connan, M., Crawford, R. J. M., Makhado, A. B., Dyer, B. M., Froneman, W., *et al.* 2019. Gentoo penguins as sentinels of climate change at the sub-Antarctic Prince Edward Archipelago, Southern Ocean. Ecological Indicators, 101: 163–172.

Carter, L., McCave, I. N., and Williams, M. J. M. 2008. Circulation and water masses of the Southern Ocean: a review. Developments in earth and environmental sciences, 8: 85–114. Elsevier.

Casciotti, K. L., Sigman, D. M., and Ward, B. B. 2003. Linking diversity and stable isotope fractionation in ammonia-oxidizing bacteria. Geomicrobiology Journal, 20: 335–353. Taylor & Francis.

Cassar, N., Laws, E. A., Bidigare, R. R., and Popp, B. N. 2004. Bicarbonate uptake by Southern Ocean phytoplankton. Global Biogeochemical Cycles, 18. John Wiley & Sons, Ltd.

Cassar, N., Barnett, B. A., Bender, M. L., Kaiser, J., Hamme, R. C., and Tilbrook, B. 2009. Continuous High-Frequency Dissolved O2/Ar Measurements by Equilibrator Inlet Mass Spectrometry. Analytical Chemistry, 81: 1855–1864. American Chemical Society.

Castellani, C., and Edwards, M. 2017. Marine Plankton: A practical guide to ecology, methodology, and taxonomy. Oxford University Press.

Cavagna, A. J., Fripiat, F., Elskens, M., Mangion, P., Chirurgien, L., Closset, I., Lasbleiz, M., *et al.* 2015. Production regime and associated N cycling in the vicinity of Kerguelen Island, Southern Ocean. Biogeosciences, 12: 6515–6528.

Cavan, E. L., Belcher, A., Atkinson, A., Hill, S. L., Kawaguchi, S., McCormack, S., Meyer, B., *et al.* 2019. The importance of Antarctic krill in biogeochemical cycles. Nature Communications, 10: 4742.

Cefarelli, A. O., Vernet, M., and Ferrario, M. E. 2011. Phytoplankton composition and abundance in relation to free-floating Antarctic icebergs. Deep Sea Research Part II: Topical Studies in Oceanography, 58: 1436–1450. Elsevier.

Chang, M., Tang, T. Y., Ho, C., and Chao, S. 2013. Kuroshio-induced wake in the lee of Green Island off Taiwan. Journal of Geophysical Research: Oceans, 118: 1508–1519. Wiley Online Library.

Chapman, C. C., Lea, M.-A., Meyer, A., Sallée, J.-B., and Hindell, M. 2020. Defining Southern Ocean fronts and their influence on biological and physical processes in a changing climate. Nature Climate Change, 10: 209–219.

Checkley, D. M., and Miller, C. A. 1989. Nitrogen isotope fractionation by oceanic zooplankton. Deep Sea Research Part A. Oceanographic Research Papers, 36: 1449–1456.

Chen, S.-Y., Feng, Z., and Yi, X. 2017. A general introduction to adjustment for multiple comparisons. Journal of thoracic disease, 9: 1725–1729. AME Publishing Company.

Cherel, Y., Hobson, K. A., Guinet, C., and Vanpe, C. 2007. Stable isotopes document seasonal changes in trophic niches and winter foraging individual specialization in diving predators from the Southern Ocean. Journal of Animal Ecology, 76: 826–836. John Wiley & Sons, Ltd.

Cherel, Y., Ducatez, S., Fontaine, C., Richard, P., and Guinet, C. 2008. Stable isotopes reveal the trophic position and mesopelagic fish diet of female southern elephant seals breeding on the Kerguelen Islands. Marine Ecology Progress Series, 370: 239–247.

Chown, S., and Froneman, P. W. 2008. The Prince Edward Islands: land-sea interactions in a changing ecosystem. African Sun Media. 469 pp.

Christaki, U., Skouroliakou, I.-D., Delegrange, A., Irion, S., Courcot, L., Jardillier, L., and Sassenhagen, I. 2021a. Microzooplankton diversity and potential role in carbon cycling of contrasting Southern Ocean productivity regimes. Journal of Marine Systems, 219: 103531.

Christaki, U., Gueneugues, A., Liu, Y., Blain, S., Catala, P., Colombet, J., Debeljak, P., *et al.* 2021b. Seasonal microbial food web dynamics in contrasting Southern Ocean productivity regimes. Limnology and Oceanography, 66: 108–122. John Wiley & Sons, Ltd.

Clarke, A. 1985. Energy Flow in the Southern Ocean Food Web BT - Antarctic Nutrient Cycles and Food Webs. *In* pp. 573–580. Ed. by W. R. Siegfried, P. R. Condy, and R. M. Laws. Springer Berlin Heidelberg, Berlin, Heidelberg.

Clevenger, S. J., Benitez-Nelson, C. R., Drysdale, J., Pike, S., Puigcorbé, V., and Buesseler, K. O. 2021. Review of the analysis of 234Th in small volume (2–4 L) seawater samples: improvements and recommendations. Journal of Radioanalytical and

Nuclear Chemistry, 329: 1–13.

Cochlan, W. P. 2008. Nitrogen uptake in the Southern Ocean. Nitrogen in the Marine Environment, edited by: Capone, DG, Bronk, DA, Mulholland, MR, and Carpenter, EJ, 2nd Edition, Academic Press, Elsevier: 569–596.

Constable, A. J., Melbourne-Thomas, J., Corney, S. P., Arrigo, K. R., Barbraud, C., Barnes, D. K. A., Bindoff, N. L., *et al.* 2014. Climate change and Southern Ocean ecosystems I: how changes in physical habitats directly affect marine biota. Global Change Biology, 20: 3004–3025. John Wiley & Sons, Ltd.

Corbisier, T. N., Petti, M. A. V, Skowronski, R. S. P., and Brito, T. A. S. 2004. Trophic relationships in the nearshore zone of Martel Inlet (King George Island, Antarctica): δ13C stable-isotope analysis. Polar Biology, 27: 75–82.

Costanza, R., d'Arge, R., de Groot, R., Farber, S., Grasso, M., Hannon, B., Limburg, K., *et al.* 1997. The value of the world's ecosystem services and natural capital. Nature, 387: 253–260.

Croot, P. L., Passow, U., Assmy, P., Jansen, S., and Strass, V. H. 2007. Surface active substances in the upper water column during a Southern Ocean Iron Fertilization Experiment (EIFEX). Geophysical Research Letters, 34. John Wiley & Sons, Ltd.

Croxall, J. P., and Nicol, S. 2004. Management of Southern Ocean fisheries: global forces and future sustainability. Antarctic Science, 16: 569–584. Cambridge University Press.

Curran-Everett, D. 2018. Explorations in statistics: the log transformation. Advances in Physiology Education, 42: 343–347. American Physiological Society.

Dagg, M. J., Jackson, G. A., and Checkley, D. M. 2014. The distribution and vertical flux of fecal pellets from large zooplankton in Monterey bay and coastal California. Deep Sea Research Part I: Oceanographic Research Papers, 94: 72–86.

Dam, H. G., and Peterson, Vv. T. 1988. The effect of temperature on the gut clearance rate. Journal of Experimental Marine Biology and Ecology, 123: 1–14.

de Baar, H. J. W., de Jong, J. T. M., Bakker, D. C. E., Löscher, B. M., Veth, C., Bathmann, U., and Smetacek, V. 1995. Importance of iron for plankton blooms and carbon dioxide drawdown in the Southern Ocean. Nature, 373: 412–415.

De Baar, H. J. W., Van Leeuwe, M. A., Scharek, R., Goeyens, L., Bakker, K. M. J., and Fritsche, P. 1997. Nutrient anomalies in Fragilariopsis kerguelensis blooms, iron deficiency and the nitrate/phosphate ratio (A. C. Redfield) of the Antarctic Ocean. Deep Sea Research Part II: Topical Studies in Oceanography, 44: 229–260.

De Falco, C., Bracco, A., and Pasquero, C. 2020. Climatic and oceanographic controls on coral bleaching conditions in the Maldivian region. Frontiers in Marine Science, 7: 539869. Frontiers Media SA.

De Falco, C., Desbiolles, F., Bracco, A., and Pasquero, C. 2022. Island Mass Effect: a review of oceanic physical processes. Frontiers in Marine Science: 1252. Frontiers.

Deacon, G. E. R. 1982. Physical and biological zonation in the Southern Ocean. Deep Sea Research Part A. Oceanographic Research Papers, 29: 1–15.

Death, R., Wadham, J. L., Monteiro, F., Le Brocq, A. M., Tranter, M., Ridgwell, A., Dutkiewicz, S., *et al.* 2014. Antarctic ice sheet fertilises the Southern Ocean. Biogeosciences, 11: 2635–2643. Copernicus Publications.

Decima, M., Landry, M. R., Stukel, M. R., Lopez-Lopez, L., and Krause, J. W. 2016. Mesozooplankton biomass and grazing in the Costa Rica Dome: Amplifying variability through the plankton food web. Journal of Plankton Research, 38: 317–330.

Dehairs, F., Kopczynska, E., Nielsen, P., Lancelot, C., Bakker, D. C. E., Koeve, W., and Goeyens, L. 1997. δ13C of Southern Ocean suspended organic matter during spring and early summer: regional and temporal variability. Deep Sea Research Part II: Topical Studies in Oceanography, 44: 129–142.

Dehairs, F., Fripiat, F., Cavagna, A.-J., Trull, T. W., Fernandez, C., Davies, D., Roukaerts, A., *et al.* 2015. Nitrogen cycling in the Southern Ocean Kerguelen Plateau area: evidence for significant surface nitrification from nitrate isotopic compositions. Biogeosciences, 12: 1459–1482. Copernicus GmbH.

DeNiro, M. J., and Epstein, S. 1978. Influence of diet on the distribution of carbon isotopes in animals. Geochimica et cosmochimica acta, 42: 495–506. Elsevier.

DeNiro, M. J., and Epstein, S. 1981. Influence of diet on the distribution of nitrogen isotopes in animals. Geochimica et Cosmochimica Acta, 45: 341–351.

Dennett, M. R., Mathot, S., Caron, D. A., Smith, W. O., and Lonsdale, D. J. 2001. Abundance and distribution of phototrophic and

heterotrophic nano- and microplankton in the southern Ross Sea. Deep Sea Research Part II: Topical Studies in Oceanography, 48: 4019–4037.

Deppeler, S. L., and Davidson, A. T. 2017. Southern Ocean phytoplankton in a changing climate. Frontiers in Marine Science, 203: 135–150.

Descolas-Gros, C., and Fontugne, M. R. 1985. Carbon fixation in marine phytoplankton: carboxylase activities and stable carbon-isotope ratios; physiological and paleoclimatological aspects. Marine Biology, 87: 1–6. Springer.

Descolas-Gros, C., and Fontungne, M. 1990. Stable carbon isotope fractionation by marine phytoplankton during photosynthesis. Plant, Cell & Environment, 13: 207–218. John Wiley & Sons, Ltd.

Descolas-Gros, C., and Oriol, L. 1992. Variations in carboxylase activity in marine phytoplankton cultures. β-carboxylation in carbon flux studies. Marine Ecology Progress Series, 85: 163–169. Inter-Research Science Center.

Deuser, W. G. 1970. Isotopic Evidence for Diminishing Supply of Available Carbon during Diatom Bloom in the Black Sea. Nature, 225: 1069–1071.

DeVries, T., Primeau, F., and Deutsch, C. 2012. The sequestration efficiency of the biological pump. Geophysical Research Letters, 39. John Wiley & Sons, Ltd.

DeVries, T. 2014. The oceanic anthropogenic CO2 sink: Storage, air-sea fluxes, and transports over the industrial era. Global Biogeochemical Cycles, 28: 631–647. John Wiley & Sons, Ltd.

Diamond, D. 1994. QuikChem Method 10-114-21-1-B: Silicate by flow injection analysis. Lachat Instruments.

DiFiore, P. J., Sigman, D. M., and Dunbar, R. B. 2009. Upper ocean nitrogen fluxes in the Polar Antarctic Zone: Constraints from the nitrogen and oxygen isotopes of nitrate. Geochemistry, Geophysics, Geosystems, 10. John Wiley & Sons, Ltd.

DiFiore, P. J., Sigman, D. M., Karsh, K. L., Trull, T. W., Dunbar, R. B., and Robinson, R. S. 2010. Poleward decrease in the isotope effect of nitrate assimilation across the Southern Ocean. Geophysical Research Letters, 37. John Wiley & Sons, Ltd.

DOE, U. S. 2008. Carbon cycling and biosequestration: Report from the March 2008 Workshop. Doe/Sc, 108.

Doi, H., Matsumasa, M., Toya, T., Satoh, N., Mizota, C., Maki, Y., and Kikuchi, E. 2005. Spatial shifts in food sources for macrozoobenthos in an estuarine ecosystem: Carbon and nitrogen stable isotope analyses. Estuarine, Coastal and Shelf Science, 64: 316–322.

Dolan, J. R. 2021. Pioneers of plankton research: Victor Hensen (1835–1924). Journal of Plankton Research, 43: 507–510.

Dolan, J. R. 2022. Pioneers of plankton research: Alister Hardy (1896–1985). Journal of Plankton Research, 44: 477–485.

Dong, C., McWilliams, J. C., and Shchepetkin, A. F. 2007. Island wakes in deep water. Journal of Physical Oceanography, 37: 962–981. American Meteorological Society.

Dong, S., Sprintall, J., Gille, S. T., and Talley, L. 2008. Southern Ocean mixed-layer depth from Argo float profiles. Journal of Geophysical Research: Oceans, 113. John Wiley & Sons, Ltd.

Dortch, Q. 1990. The interaction between ammonium and nitrate uptake in phytoplankton. Marine ecology progress series. Oldendorf, 61: 183–201.

Doty, M. S., and Oguri, M. 1956. The island mass effect. ICES Journal of Marine Science, 22: 33–37. Oxford University Press.

Drits, A. V, Pasternak, A. F., and Kosobokova, K. N. 1993. Feeding, metabolism and body composition of the Antarctic copepod Calanus propinquus Brady with special reference to its life cycle. Polar Biology, 13: 13–21.

Dubovik, O., Schuster, G. L., Xu, F., Hu, Y., Bösch, H., Landgraf, J., and Li, Z. 2021. Grand Challenges in Satellite Remote Sensing.

Ducklow, H. W., Steinberg, D. K., and Buesseler, K. O. 2001. Upper ocean carbon export and the biological pump. Oceanography, 14: 50–58.

Ducklow, H. W., Baker, K., Martinson, D. G., Quetin, L. B., Ross, R. M., Smith, R. C., Stammerjohn, S. E., *et al.* 2007. Marine pelagic ecosystems: the west Antarctic Peninsula. Philosophical Transactions of the Royal Society B: Biological Sciences, 362: 67–94. The Royal Society London.

Dugdale, R. C., and Goering, J. J. 1967. Uptake of new and regenerated forms of nitrogen in primary productivity. Limnology and Oceanography, 12: 196–206. John Wiley & Sons, Ltd.

Dugdale, R. C., and Wilkerson, F. P. 1986. The use of 15N to measure nitrogen uptake in eutrophic oceans; experimental considerations. Limnology and Oceanography, 31: 673–689. John Wiley & Sons, Ltd.

Dugdale, R. C., Wilkerson, F. P., and Minas, H. J. 1995. The role of a silicate pump in driving new production. Deep Sea Research Part I: Oceanographic Research Papers, 42: 697–719.

Eayrs, C., Li, X., Raphael, M. N., and Holland, D. M. 2021. Rapid decline in Antarctic sea ice in recent years hints at future change. Nature Geoscience, 14: 460–464.

Ebersbach, F., and Trull, T. W. 2008. Sinking particle properties from polyacrylamide gels during the KErguelen Ocean and Plateau compared Study (KEOPS): Zooplankton control of carbon export in an area of persistent natural iron inputs in the Southern Ocean. Limnology and Oceanography, 53: 212–224. John Wiley & Sons, Ltd.

Egge, J. K., and Aksnes, D. L. 1992. Silicate as regulating nutrient in phytoplankton competition. Marine ecology progress series. Oldendorf, 83: 281–289.

Eide, M., Olsen, A., Ninnemann, U. S., and Johannessen, T. 2017. A global ocean climatology of preindustrial and modern ocean δ13C. Global Biogeochemical Cycles, 31: 515–534. John Wiley & Sons, Ltd.

El-Sayed, S. Z., Benon, P., David, P., Grindley, J. R., Murail, J. F., Arnaud, P. M., and Hureau, J. C. 1979. Some aspects of the biology of the water column studied during the Marion-Dufresne cruise 08. Comité National Français des Recherches Arctiques et Antarctiques - CNFRA, 44: 127–134.

Elskens, M., Baeyens, W., Cattaldo, T., Dehairs, F., and Griffiths, B. 2002. N uptake conditions during summer in the Subantarctic and Polar Frontal Zones of the Australian sector of the Southern Ocean. Journal of Geophysical Research: Oceans, 107: 3–11. John Wiley & Sons, Ltd.

Elton, C. 1927. The animal community (Chapter 5). Animal ecology. London: Sidgwick & Jackson. Retrieved from http://www. lancaster. ac. uk/users/philosophy/awaymave/onlineresources/animal% 20community. pdf.

Eppley, R. W., Rogers, J. N., and McCarthy, J. J. 1969. Half-saturation constants for uptake of nitrate and ammonium by marine phytoplankton 1. Limnology and oceanography, 14: 912–920. Wiley Online Library.

Eppley, R. W., Reid, F. M. H., and Strickland, J. D. H. 1970. The ecology of the plankton off La Jolla, California, in the period April through September 1967. Bulletin of the Scripps Institution of Oceanography, 17: 33–42.

Eppley, R. W., and Peterson, B. J. 1979. Particulate organic matter flux and planktonic new production in the deep ocean. Nature, 282: 677–680.

Erskine, P. D., Bergstrom, D. M., Schmidt, S., Stewart, G. R., Tweedie, C. E., and Shaw, J. D. 1998. Subantarctic Macquarie Island – a model ecosystem for studying animal-derived nitrogen sources using 15N natural abundance. Oecologia, 117: 187–193.

Espinasse, B., Pakhomov, E., and Hunt, B. P. V. 2019. Latitudinal gradient consistency in carbon and nitrogen stable isotopes of particulate organic matter in the Southern Ocean. Marine Ecology Progress Series, 631: 19–30.

Falkowski, P. G. 1991. Species variability in the fractionation of 13C and 12C by marine phytoplankton. Journal of Plankton Research, 13: 21–28.

Falkowski, P. G. 1994. The role of phytoplankton photosynthesis in global biogeochemical cycles. Photosynthesis Research, 39: 235–258.

Falkowski, P. G., Barber, R. T., and Smetacek, V. 1998. Biogeochemical controls and feedbacks on ocean primary production. Science, 281: 200–206.

Falkowski, P. G., Laws, E. A., Barber, R. T., and Murray, J. W. 2003. Phytoplankton and Their Role in Primary, New, and Export Production BT - Ocean Biogeochemistry: The Role of the Ocean Carbon Cycle in Global Change. *In* pp. 99–121. Ed. by M. J. R. Fasham. Springer Berlin Heidelberg, Berlin, Heidelberg.

Falkowski, P. G., and Woodhead, A. D. 2013. Primary productivity and biogeochemical cycles in the sea. Springer Science & Business Media.

Fan, G., Han, Z., Ma, W., Chen, S., Chai, F., Mazloff, M. R., Pan, J., *et al.* 2020. Southern Ocean carbon export efficiency in relation to temperature and primary productivity. Scientific Reports, 10: 13494.

Fawcett, S. E., Lomas, M. W., Casey, J. R., Ward, B. B., and Sigman, D. M. 2011. Assimilation of upwelled nitrate by small eukaryotes in the Sargasso Sea. Nature Geoscience, 4: 717–722.

Fawcett, S. E., Lomas, M. W., Ward, B. B., and Sigman, D. M. 2014. The counterintuitive effect of summer-to-fall mixed layer deepening on eukaryotic new production in the Sargasso Sea. Global Biogeochemical Cycles, 28: 86–102. John Wiley & Sons, Ltd.

Federici, L., Dunbar, R. B., and Mucciarone, D. A. 2003. Variations in Particulate Organic Matter Across the Drake Passage. *In* AGU Fall Meeting Abstracts, pp. B21B-0714.

Fenchel, T. 1988. Marine plankton food chains. Annual Review of Ecology and Systematics: 19–38. JSTOR.

Field, C. B., Behrenfeld, M. J., Randerson, J. T., and Falkowski, P. 1998. Primary Production of the Biosphere: Integrating Terrestrial and Oceanic Components. Science, 281: 237–240. American Association for the Advancement of Science.

Fischer, G., Fütterer, D., Gersonde, R., Honjo, S., Ostermann, D., and Wefer, G. 1988. Seasonal variability of particle flux in the Weddell Sea and its relation to ice cover. Nature, 335: 426–428. Nature Publishing Group.

Flynn, R. F., Bornman, T. G., Burger, J. M., Smith, S., Spence, K. A. M., and Fawcett, S. E. 2021. Summertime productivity and carbon export potential in the Weddell Sea, with a focus on the waters adjacent to Larsen C Ice Shelf. Biogeosciences, 18: 6031–6059. Copernicus GmbH.

Fontugne, M., Descolas-Gros, C., and de Billy, G. 1991. The dynamics of CO2 fixation in the Southern Ocean as indicated by carboxylase activities and organic carbon isotopic ratios. Marine Chemistry, 35: 371–380.

Forrer, H. 2021. Toward an improved understanding of the Southern Ocean's biological pump: phytoplankton group-specific contributions to nitrogen and carbon cycling across the Subantarctic Indian Ocean. Unpublished MSc dissertation, Faculty of Science, Deparment of Oceanography, University of Cape Town.

France, R. L. 1995. Carbon isotopic variability in the composite pelagic foodweb of four oligotrophic lakes: feeding diversity or metabolic fractionations? Journal of Plankton Research, 17: 1993–1997. Oxford University Press.

François, R., Altabet, M. A., Goericke, R., McCorkle, D. C., Brunet, C., and Poisson, A. 1993. Changes in the δ13C of surface water particulate organic matter across the subtropical convergence in the SW Indian Ocean. Global Biogeochemical Cycles, 7: 627–644. John Wiley & Sons, Ltd.

Fransson, A., Chierici, M., Yager, P. L., and Smith Jr., W. O. 2011. Antarctic sea ice carbon dioxide system and controls. Journal of Geophysical Research: Oceans, 116. John Wiley & Sons, Ltd.

Frederiksen, M., Edwards, M., Richardson, A. J., Halliday, N. C., and Wanless, S. 2006. From plankton to top predators: bottom-up control of a marine food web across four trophic levels. Journal of Animal Ecology, 75: 1259–1268. John Wiley & Sons, Ltd.

Freeman, K. H., and Hayes, J. M. 1992. Fractionation of carbon isotopes by phytoplankton and estimates of ancient CO2 levels. Global Biogeochemical Cycles, 6: 185–198. John Wiley & Sons, Ltd.

Friend, A. D., Geider, R. J., Behrenfeld, M. J., and Still, C. J. 2009. Photosynthesis in global-scale models. *In* Photosynthesis in silico, pp. 465–497. Springer.

Fripiat, F., Sigman, D. M., Fawcett, S. E., Rafter, P. A., Weigand, M. A., and Tison, J.-L. 2014. New insights into sea ice nitrogen biogeochemical dynamics from the nitrogen isotopes. Global Biogeochemical Cycles, 28: 115–130. John Wiley & Sons, Ltd.

Fripiat, F., Elskens, M., Trull, T. W., Blain, S., Cavagna, A.-J., Fernandez, C., Fonseca-Batista, D., *et al.* 2015. Significant mixed layer nitrification in a natural iron-fertilized bloom of the Southern Ocean. Global Biogeochemical Cycles, 29: 1929–1943. John Wiley & Sons, Ltd.

Fripiat, F., Meiners, K. M., Vancoppenolle, M., Papadimitriou, S., Thomas, D. N., Ackley, S. F., Arrigo, K. R., *et al.* 2017. Macro-nutrient concentrations in Antarctic pack ice: Overall patterns and overlooked processes. Elementa: Science of the Anthropocene, 5: 13.

Fripiat, F., Martínez-García, A., Fawcett, S. E., Kemeny, P. C., Studer, A. S., Smart, S. M., Rubach, F., *et al.* 2019. The isotope effect of nitrate assimilation in the Antarctic Zone: Improved estimates and paleoceanographic implications. Geochimica et Cosmochimica Acta, 247: 261–279.

Fripiat, F., Marconi, D., Rafter, P. A., Sigman, D. M., Altabet, M. A., Bourbonnais, A., Brandes, J., *et al.* 2021, September 28. Compilation of nitrate δ15N in the ocean. PANGAEA.

Frölicher, T. L., Sarmiento, J. L., Paynter, D. J., Dunne, J. P., Krasting, J. P., and Winton, M. 2015. Dominance of the Southern Ocean in anthropogenic carbon and heat uptake in CMIP5 models. Journal of Climate, 28: 862–886.

Froneman, P., and Perissinotto, R. 1996a. Microzooplankton Grazing in the Southern Ocean: Implications for the Carbon Cycle.

Marine Ecology, 17: 99–115. John Wiley & Sons, Ltd.

Froneman, P. W., Perissinotto, R., McQuaid, C. D., and Laubscher, R. K. 1995. Summer distribution of netphytoplankton in the Atlantic sector of the Southern Ocean. Polar Biology, 15: 77–84.

Froneman, P. W., Perissinotto, R., and McQuaid, C. D. 1996. Seasonal variations in microzooplankton grazing in the region of the Subtropical Convergence. Marine biology, 126: 433–442. Springer.

Froneman, P. W., and Perissinotto, R. 1996b. Microzooplankton grazing and protozooplankton community structure in the South Atlantic and in the Atlantic sector of the Southern Ocean. Deep Sea Research Part I: Oceanographic Research Papers, 43: 703–721.

Froneman, P. W., and Balarin, M. G. 1998. Structure and grazing impact of the protozooplankton community in the waters surrounding the Prince Edward Islands (Southern Ocean). Polar Biology, 20: 198–205. Springer.

Froneman, P. W., Pakhomov, E. A., and Meaton, V. 1998. Surface distribution of microphytoplankton of the south-west Indian Ocean along a repeat transect between Cape Town and the Prince Edward Islands. South African journal of science, 94: 124–129. Sabinet.

Froneman, P. W., Pakhomov, E. A., Perissinotto, R., and McQuaid, C. D. 2000. Zooplankton structure and grazing in the Atlantic sector of the Southern Ocean in late austral summer 1993: Part 2. Biochemical zonation. Deep Sea Research Part I: Oceanographic Research Papers, 47: 1687–1702.

Fry, B., Joern, A., and Parker, P. L. 1978. Grasshopper food web analysis: use of carbon isotope ratios to examine feeding relationships among terrestrial herbivores. Ecology, 59: 498–506. Wiley Online Library.

Fry, B., and Sherr, E. B. 1984. S13C measurements as indicators of car bon flow in marine food webs. Contrib Mar Sei, 27: 15–47.

Fry, B. 1988. Food web structure on Georges Bank from stable C, N, and S isotopic compositions. Limnology and Oceanography, 33: 1182–1190. John Wiley & Sons, Ltd.

Fry, B., and Sherr, E. B. 1989. δ13C Measurements as Indicators of Carbon Flow in Marine and Freshwater Ecosystems. *In* pp. 196–229. Ed. by P. W. Rundel, J. R. Ehleringer, and K. A. Nagy. Springer New York.

Fry, B. 2006. Stable isotope ecology. Springer, New York, NY. 308 pp.

Fry, R., and Wainright, S. C. 1991. Diatom sources of 13C-rich carbon in marine food webs. Mar Ecol Prog Ser: 76–149.

Gallup, D. N. 1970. Zooplankton distribution and zooplankton-phytoplankton relationships in a mesotrophic lake. (Doctoral dissertation, University of New Hampshire).

Garcia, N. S., Sexton, J., Riggins, T., Brown, J., Lomas, M. W., and Martiny, A. C. 2018. High Variability in Cellular Stoichiometry of Carbon, Nitrogen, and Phosphorus Within Classes of Marine Eukaryotic Phytoplankton Under Sufficient Nutrient Conditions.

Garibotti, I. A., Vernet, M., and Ferrario, M. E. 2005. Annually recurrent phytoplanktonic assemblages during summer in the seasonal ice zone west of the Antarctic Peninsula (Southern Ocean). Deep Sea Research Part I: Oceanographic Research Papers, 52: 1823–1841.

Geider, R. J., and La Roche, J. 1994. The role of iron in phytoplankton photosynthesis, and the potential for iron-limitation of primary productivity in the sea. Photosynthesis Research, 39: 275–301.

Giglio, D., and Johnson, G. C. 2016. Subantarctic and Polar Fronts of the Antarctic Circumpolar Current and Southern Ocean Heat and Freshwater Content Variability: A View from Argo. Journal of Physical Oceanography, 46: 749–768. American Meteorological Society, Boston MA, USA.

Gille, S. T. 2002. Warming of the Southern Ocean Since the 1950s. Science, 295: 1275 LP – 1277.

Gille, S. T. 2003. Float Observations of the Southern Ocean. Part II: Eddy Fluxes. Journal of Physical Oceanography, 33: 1182–1196.

Gleiber, M. R., Steinberg, D. K., and Ducklow, H. W. 2012. Time series of vertical flux of zooplankton fecal pellets on the continental shelf of the western Antarctic Peninsula. Marine Ecology Progress Series, 471: 23–36.

Glibert, P. M., Wilkerson, F. P., Dugdale, R. C., Raven, J. A., Dupont, C. L., Leavitt, P. R., Parker, A. E., *et al.* 2016. Pluses and minuses of ammonium and nitrate uptake and assimilation by phytoplankton and implications for productivity and community composition, with emphasis on nitrogen-enriched conditions. Limnology and Oceanography, 61: 165–197. John Wiley &

Sons, Ltd.

Goericke, R. 1994. Physiology of isotopic fractionation in algae and cyanobacteria. Stable isotopes in ecology and environmental science.: 187–221. Blackwell.

Goericke, R., and Fry, B. 1994. Variations of marine plankton δ13C with latitude, temperature, and dissolved CO2 in the world ocean. Global Biogeochemical Cycles, 8: 85–90. John Wiley & Sons, Ltd.

Goldman, J. G., Caron, D. A., and Dennett, M. R. 1987. Nutrient cycling in a microflagellate food chain: IV. Phytoplankton-microflagellate interactions. Marine Ecology Progress Series: 75–87. JSTOR.

Gordon, A. L., Molinelli, E., and Baker, T. 1978. Large-scale relative dynamic topography of the Southern Ocean. Journal of Geophysical Research: Oceans, 83: 3023–3032. Wiley Online Library.

Gordon, L. I., Codispoti, L. A., Jennings, J. C., Millero, F. J., Morrison, J. M., and Sweeney, C. 2000. Seasonal evolution of hydrographic properties in the Ross Sea, Antarctica, 1996–1997. Deep Sea Research Part II: Topical Studies in Oceanography, 47: 3095–3117.

Gorokhova, E., and Hansson, S. 1999. An experimental study on variations in stable carbon and nitrogen isotope fractionation during growth of Mysis mixta and Neomysis integer. Canadian Journal of Fisheries and Aquatic Sciences, 56: 2203–2210. NRC Research Press.

Gove, J. M., Merrifield, M. A., and Brainard, R. E. 2006. Temporal variability of current-driven upwelling at Jarvis Island. Journal of Geophysical Research: Oceans, 111. Wiley Online Library.

Gove, J. M., McManus, M. A., Neuheimer, A. B., Polovina, J. J., Drazen, J. C., Smith, C. R., Merrifield, M. A., *et al.* 2016. Near-island biological hotspots in barren ocean basins. Nature Communications, 7: 10581.

Graeve, M., Hagen, W., and Kattner, G. 1994. Herbivorous or omnivorous? On the significance of lipid compositions as trophic markers in Antarctic copepods. Deep Sea Research Part I: Oceanographic Research Papers, 41: 915–924.

Graham, R. M., de Boer, A. M., Heywood, K. J., Chapman, M. R., and Stevens, D. P. 2012. Southern Ocean fronts: Controlled by wind or topography? Journal of Geophysical Research: Oceans, 117. John Wiley & Sons, Ltd.

Granger, J., Sigman, D. M., Needoba, J. A., and Harrison, P. J. 2004. Coupled nitrogen and oxygen isotope fractionation of nitrate during assimilation by cultures of marine phytoplankton. Limnology and Oceanography, 49: 1763–1773. John Wiley & Sons, Ltd.

Granger, J., Sigman, D. M., Rohde, M. M., Maldonado, M. T., and Tortell, P. D. 2010. N and O isotope effects during nitrate assimilation by unicellular prokaryotic and eukaryotic plankton cultures. Geochimica et Cosmochimica Acta, 74: 1030–1040.

Grant, S. M., Hill, S. L., Trathan, P. N., and Murphy, E. J. 2013. Ecosystem services of the Southern Ocean: trade-offs in decision-making. Antarctic Science, 25: 603–617. Cambridge University Press.

Grasshoff, K. 1976. Automated chemical analysis. Methods of seawater analysis: 263–297. Verlag Chemie.

Grey, J., Jones, R. I., and Sleep, D. 2001. Seasonal changes in the importance of the source of organic matter to the diet of zooplankton in Loch Ness, as indicated by stable isotope analysis. Limnology and Oceanography, 46: 505–513. John Wiley & Sons, Ltd.

Grindley, J. R., and Lane, S. B. 1979. Zooplankton around Marion and Prince Edward Islands. CNFRA, 44: 111–125.

Gruber, N., Keeling, C. D., Bacastow, R. B., Guenther, P. R., Lueker, T. J., Wahlen, M., Meijer, H. A. J., *et al.* 1999. Spatiotemporal patterns of carbon-13 in the global surface oceans and the oceanic suess effect. Global Biogeochemical Cycles, 13: 307–335. John Wiley & Sons, Ltd.

Gruber, N. 2008. The marine nitrogen cycle: overview and challenges. Nitrogen in the marine environment, 2: 1–50. Elsevier Amsterdam.

Gruber, N., Gloor, M., Mikaloff Fletcher, S. E., Doney, S. C., Dutkiewicz, S., Follows, M. J., Gerber, M., *et al.* 2009. Oceanic sources, sinks, and transport of atmospheric CO2. Global biogeochemical cycles, 23. Wiley Online Library.

Gruber, N., Landschützer, P., and Lovenduski, N. S. 2019. The Variable Southern Ocean Carbon Sink. Annual Review of Marine Science, 11: 159–186.

Gu, B., and Schelske, L. 1996. Temporal and spatial variations in phytoplankton carbon isotopes in a polymictic subtropical lake. Journal of Plankton Research, 18: 2081–2092. Oxford University Press.

Gulati, R., and Demott, W. 1997. The role of food quality for zooplankton: remarks on the state-of-the-art, perspectives and priorities. Freshwater Biology, 38: 753–768. John Wiley & Sons, Ltd.

Gupta, A. Sen, Santoso, A., Taschetto, A. S., Ummenhofer, C. C., Trevena, J., and England, M. H. 2009. Projected changes to the Southern Hemisphere ocean and sea ice in the IPCC AR4 climate models. Journal of Climate, 22: 3047–3078. American Meteorological Society.

Gurney, L. J., Froneman, P. W., Pakhomov, E. A., and McQuaid, C. D. 2001. Trophic positions of three euphausiid species from the Prince Edward Islands (Southern Ocean): implications for the pelagic food web structure. Marine Ecology Progress Series, 217: 167–174.

Guy, R. D., Vanlerberghe, G. C., and Turpin, D. H. 1989. Significance of Phosphoenolpyruvate Carboxylase during Ammonium Assimilation: Carbon Isotope Discrimination in Photosynthesis and Respiration by the N-Limited Green Alga Selenastrum minutum 1. Plant Physiology, 89: 1150–1157.

Habran, S., Debier, C., Crocker, D. E., Houser, D. S., Lepoint, G., Bouquegneau, J.-M., and Das, K. 2010. Assessment of gestation, lactation and fasting on stable isotope ratios in northern elephant seals (Mirounga angustirostris). Marine Mammal Science, 26: 880–895. John Wiley & Sons, Ltd.

Hagen, W., and Auel, H. 2001. Seasonal adaptations and the role of lipids in oceanic zooplankton. Zoology, 104: 313–326.

Hagen, W., Yoshida, T., Virtue, P., Kawaguchi, S., Swadling, K. M., Nicol, S., and Nichols, P. D. 2007. Effect of a carnivorous diet on the lipids, fatty acids and condition of Antarctic krill, Euphausia superba. Antarctic Science, 19: 183. Cambridge University Press.

Halfter, S., Cavan, E. L., Swadling, K. M., Eriksen, R. S., and Boyd, P. W. 2020. The Role of Zooplankton in Establishing Carbon Export Regimes in the Southern Ocean – A Comparison of Two Representative Case Studies in the Subantarctic Region.

Halfter, S., Cavan, E. L., Butterworth, P., Swadling, K. M., and Boyd, P. W. 2022. "Sinking dead"—How zooplankton carcasses contribute to particulate organic carbon flux in the subantarctic Southern Ocean. Limnology and Oceanography, 67: 13–25. John Wiley & Sons, Ltd.

Hamner, W. M., and Hauri, I. R. 1981. Effects of island mass: water flow and plankton pattern around a reef in the great barrier reef lagoon, Australia 1. Limnology and Oceanography, 26: 1084–1102. Wiley Online Library.

Hannides, C. C. S., Popp, B. N., Landry, M. R., and Graham, B. S. 2009. Quantification of zooplankton trophic position in the North Pacific Subtropical Gyre using stable nitrogen isotopes. Limnology and Oceanography, 54: 50–61. John Wiley & Sons, Ltd.

Hansen, J., Bjornsen, P. K., and Hansen, B. W. 1997. Zooplankton grazing and growth: Scaling within the 2-2,-µm body size range. Limnology and Oceanography, 42: 687–704.

Hanson, C. E., Hyndes, G. A., and Wang, S. F. 2010. Differentiation of benthic marine primary producers using stable isotopes and fatty acids: Implications to food web studies. Aquatic Botany, 93: 114–122.

Hansson, S., Hobbie, J. E., Elmgren, R., Larsson, U., Fry, B., and Johansson, S. 1997. The stable nitrogen isotope ratio as a marker of food-web interactions and fish migration. Ecology, 78: 2249–2257. Wiley Online Library.

Hare, C. E., DiTullio, G. R., Riseman, S. F., Crossley, A. C., Popels, L. C., Sedwick, P. N., and Hutchins, D. A. 2007. Effects of changing continuous iron input rates on a Southern Ocean algal assemblage. Deep Sea Research Part I: Oceanographic Research Papers, 54: 732–746.

Harris, G. 2012. Phytoplankton ecology: structure, function and fluctuation. Springer Science & Business Media.

Harris, R., Wiebe, P., Lenz, J., Skjoldal, H.-R., and Huntley, M. 2000. ICES zooplankton methodology manual. Elsevier. 684 pp.

Harrison, C. S., Long, M. C., Lovenduski, N. S., and Moore, J. K. 2018. Mesoscale Effects on Carbon Export: A Global Perspective. Global Biogeochemical Cycles, 32: 680–703. John Wiley & Sons, Ltd.

Hasegawa, D., Yamazaki, H., Lueck, R. G., and Seuront, L. 2004. How islands stir and fertilize the upper ocean. Geophysical research letters, 31. Wiley Online Library.

Hassler, C., and Ellwood, M. 2020. Nutrient concentration in seawater samples, collected from the underway supply, CTD and trace metal rosettes in the Southern Ocean during the austral summer of 2016/2017, on board the Antarctic Circumnavigation Expedition (ACE). (Version 1.1) [Data set]. Zenodo.

Hauck, J., Völker, C., Wang, T., Hoppema, M., Losch, M., and Wolf-Gladrow, D. A. 2013. Seasonally different carbon flux changes in the Southern Ocean in response to the southern annular mode. Global Biogeochemical Cycles, 27: 1236–1245. Wiley

Online Library.

Hauck, J., Völker, C., Wolf-Gladrow, D. A., Laufkötter, C., Vogt, M., Aumont, O., Bopp, L., *et al.* 2015. On the Southern Ocean CO2 uptake and the role of the biological carbon pump in the 21st century. Global Biogeochemical Cycles, 29: 1451–1470. Wiley Online Library.

Haumann, F. A., Gruber, N., Münnich, M., Frenger, I., and Kern, S. 2016. Sea-ice transport driving Southern Ocean salinity and its recent trends. Nature, 537: 89–92. Nature Publishing Group.

Haumann, F. A., Robinson, C., Thomas, J., Hutchings, J., Estany, C. P., Tarasenko, A., Gerber, F., *et al.* 2020. Physical and biogeochemical oceanography data from underway measurements with an AquaLine Ferrybox during the Antarctic Circumnavigation Expedition (ACE).

Havermans, C., Auel, H., Hagen, W., Held, C., Ensor, N. S., and A. Tarling, G. 2019. Chapter Two - Predatory zooplankton on the move: Themisto amphipods in high-latitude marine pelagic food webs. *In* pp. 51–92. Ed. by C. B. T.-A. in M. B. Sheppard. Academic Press.

Hawco, N. J., Tagliabue, A., and Twining, B. S. 2022. Manganese Limitation of Phytoplankton Physiology and Productivity in the Southern Ocean. Global Biogeochemical Cycles, 36: e2022GB007382. John Wiley & Sons, Ltd.

Hawkings, J. R., Wadham, J. L., Tranter, M., Raiswell, R., Benning, L. G., Statham, P. J., Tedstone, A., *et al.* 2014. Ice sheets as a significant source of highly reactive nanoparticulate iron to the oceans. Nature communications, 5: 1–8. Nature Publishing Group.

Heath, G. R. 1974. Dissolved silica and deep-sea sediments. Special Publications of SEPM.

Hempel, G. 1985. Antarctic marine food webs. *In* Antarctic nutrient cycles and food webs, pp. 266–270. Springer.

Henley, S. F., Cavan, E. L., Fawcett, S. E., Kerr, R., Monteiro, T., Sherrell, R. M., Bowie, A. R., *et al.* 2020. Changing Biogeochemistry of the Southern Ocean and Its Ecosystem Implications.

Henschke, N., Everett, J. D., Suthers, I. M., Smith, J. A., Hunt, B. P. V, Doblin, M. A., and Taylor, M. D. 2015. Zooplankton trophic niches respond to different water types of the western Tasman Sea: A stable isotope analysis. Deep Sea Research Part I: Oceanographic Research Papers, 104: 1–8.

Hensen, V. 1887. Ueber die Bestimmung des Plankton's oder des im Meere treibenden Materials an Pflanzen und Thieren.

Henson, S. A., Sanders, R., Madsen, E., Morris, P. J., Le Moigne, F., and Quartly, G. D. 2011. A reduced estimate of the strength of the ocean's biological carbon pump. Geophysical Research Letters, 38. John Wiley & Sons, Ltd.

Herman, P. M. J., Middelburg, J. J., Widdows, J., and Lucas, C. H. 2000. Stable isotopes as trophic tracers: combining field sampling and manipulative labelling of food resources for macrobenthos. Marine Ecology Progress Series, 204: 79–92.

Heywood, K. J., Barton, E. D., and Simpson, J. H. 1990. The effects of flow disturbance by an oceanic island. Journal of Marine Research, 48: 55–73. Sears Foundation for Marine Research.

Hildebrand, M., and Dahlin, K. 2000. Nitrate transporter genes from the diatom Cylindrotheca fusiformis (Bacillariophyceae): mRNA levels controlled by nitrogen source and by the cell cycle. Journal of Phycology, 36: 702–713. Wiley Online Library.

Hill, J. M., and McQuaid, C. D. 2011. Stable isotope methods: The effect of gut contents on isotopic ratios of zooplankton. Estuarine, Coastal and Shelf Science, 92: 480–485.

Hill, S. L., Murphy, E. J., Reid, K., Trathan, P. N., and Constable, A. J. 2006. Modelling Southern Ocean ecosystems: krill, the food-web, and the impacts of harvesting. Biological Reviews, 81: 581–608. Cambridge University Press.

Hill, S. L., Atkinson, A., Pakhomov, E. A., and Siegel, V. 2019. Evidence for a decline in the population density of Antarctic krill Euphausia superba Dana, 1850 still stands. A comment on Cox et al. Journal of Crustacean Biology.

Hill, S. L., Pinkerton, M. H., Ballerini, T., Cavan, E. L., Gurney, L. J., Martins, I., and Xavier, J. C. 2021. Robust model-based indicators of regional differences in food-web structure in the Southern Ocean. Journal of Marine Systems, 220: 103556.

Hillebrand, H., Dürselen, C., Kirschtel, D., Pollingher, U., and Zohary, T. 1999. Biovolume calculation for pelagic and benthic microalgae. Journal of Phycology, 35: 403–424. Wiley Online Library.

Hilton, G. M., Thompson, D. R., Sagar, P. M., Cuthbert, R. J., Cherel, Y., and Bury, S. J. 2006. A stable isotopic investigation into the causes of decline in a sub-Antarctic predator, the rockhopper penguin Eudyptes chrysocome. Global Change Biology, 12: 611–625. John Wiley & Sons, Ltd.

Hinga, K. R., Arthur, M. A., Pilson, M. E. Q., and Whitaker, D. 1994. Carbon isotope fractionation by marine phytoplankton in culture: The effects of CO2 concentration, pH, temperature, and species. Global Biogeochemical Cycles, 8: 91–102. John Wiley & Sons, Ltd.

Hirawake, T., Takao, S., Horimoto, N., Ishimaru, T., Yamaguchi, Y., and Fukuchi, M. 2011. A phytoplankton absorption-based primary productivity model for remote sensing in the Southern Ocean. Polar Biology, 34: 291–302.

Hobbs, W. R., Massom, R., Stammerjohn, S., Reid, P., Williams, G., and Meier, W. 2016. A review of recent changes in Southern Ocean sea ice, their drivers and forcings. Global and Planetary Change, 143: 228–250. Elsevier.

Hobson, K. A., and Welch, H. E. 1992. Determination of trophic relationships within a high Arctic marine food web using δ 13 C and δ 15 N analysis. Marine Ecology Progress Series, 84: 9–18. Inter-Research Science Center.

Hobson, K. A., Gloutney, M. L., and Gibbs, H. L. 1997. Preservation of blood and tissue samples for stable-carbon and stable-nitrogen isotope analysis. Canadian Journal of Zoology, 75: 1720–1723. NRC Research Press.

Hobson, K. A., and Sease, J. L. 1998. Stable isotope analyses of tooth annuli reveal temporal dietary records: an example using steller sea lions. Marine Mammal Science, 14: 116–129. John Wiley & Sons, Ltd.

Hoch, M. P., Fogel, M. L., and Kirchman, D. L. 1992. Isotope fractionation associated with ammonium uptake by a marine bacterium. Limnology and Oceanography, 37: 1447–1459. John Wiley & Sons, Ltd.

Hoffmann, L. J., Peeken, I., Lochte, K., Assmy, P., and Veldhuis, M. 2006. Different reactions of Southern Ocean phytoplankton size classes to iron fertilization. Limnology and Oceanography, 51: 1217–1229. John Wiley & Sons, Ltd.

Hoffmann, L. J., Peeken, I., and Lochte, K. 2008. Iron, silicate, and light co-limitation of three Southern Ocean diatom species. Polar Biology, 31: 1067–1080. Springer.

Holliday, N. P., and Read, J. F. 1998. Surface oceanic fronts between Africa and Antarctica. Deep Sea Research Part I: Oceanographic Research Papers, 45: 217–238.

Holmes, R. M., Aminot, A., Kérouel, R., Hooker, B. A., and Peterson, B. J. 1999. A simple and precise method for measuring ammonium in marine and freshwater ecosystems. Canadian Journal of Fisheries and Aquatic Sciences, 56: 1801–1808. NRC Research Press.

Holmes, T. M., Wuttig, K., Chase, Z., van der Merwe, P., Townsend, A. T., Schallenberg, C., Tonnard, M., *et al.* 2019. Iron availability influences nutrient drawdown in the Heard and McDonald Islands region, Southern Ocean. Marine Chemistry, 211: 1–14. Elsevier.

Honjo, S., Manganini, S. J., Krishfield, R. A., and Francois, R. 2008. Particulate organic carbon fluxes to the ocean interior and factors controlling the biological pump: A synthesis of global sediment trap programs since 1983. Progress in Oceanography, 76: 217–285.

Hopkins, T. L. 1985. Food web of an Antarctic midwater ecosystem. Marine Biology, 89: 197–212.

Hopkins, T. L., and Torres, J. J. 1989. Midwater food web in the vicinity of a marginal ice zone in the western Weddell Sea. Deep Sea Research Part A. Oceanographic Research Papers, 36: 543–560.

Hu, S., and Smith, W. O. 1998. The effects of irradiance on nitrate uptake and dissolved organic nitrogen release by phytoplankton in the Ross Sea. Continental Shelf Research, 18: 971–990.

Hunt, B. P. V, and Hosie, G. W. 2006a. The seasonal succession of zooplankton in the Southern Ocean south of Australia, part I: The seasonal ice zone. Deep Sea Research Part I: Oceanographic Research Papers, 53: 1182–1202.

Hunt, B. P. V, and Hosie, G. W. 2006b. The seasonal succession of zooplankton in the Southern Ocean south of Australia, part II: The Sub-Antarctic to Polar Frontal Zones. Deep Sea Research Part I: Oceanographic Research Papers, 53: 1203–1223.

Hunt, B. P. V, Pakhomov, E. A., Hosie, G. W., Siegel, V., Ward, P., and Bernard, K. 2008. Pteropods in Southern Ocean ecosystems. Progress in Oceanography, 78: 193–221.

Hunt, B. P. V, Espinasse, B., Pakhomov, E. A., Cherel, Y., Cotté, C., Delegrange, A., and Henschke, N. 2021. Pelagic food web structure in high nutrient low chlorophyll (HNLC) and naturally iron fertilized waters in the Kerguelen Islands region, Southern Ocean. Journal of Marine Systems, 224: 103625.

Huntley, M. E., and Escritor, F. 1992. Ecology of Metridia gerlachei Giesbrecht in the western Bransfield Strait, Antarctica. Deep Sea Research Part A. Oceanographic Research Papers, 39: 1027–1055.

Huntley, M. E. 1992. Temperature-Dependent Production of Marine Copepods: A Global Synthesis. The American Naturalist, 140: 201–242. The University of Chicago Press.

Iversen, M. H., and Poulsen, K. L. 2007. Coprorhexy, coprophagy, and coprochaly in the copepods Calanus helgolandicus, Pseudocalanus elongatus, and Oithona similis. Marine Ecology Progress Series, 350: 79–89.

Jackson, A. L., Inger, R., Parnell, A. C., and Bearhop, S. 2011. Comparing isotopic niche widths among and within communities: SIBER – Stable Isotope Bayesian Ellipses in R. Journal of Animal Ecology, 80: 595–602. John Wiley & Sons, Ltd.

Jakobsen, H. H., Thoisen, C., and Hansen, B. W. 2018. Crypthecodinium cohnii: a promising prey toward large-scale intensive rearing of the live feed copepod Acartia tonsa (Dana). Aquaculture international, 26: 237–251. Springer.

Janssen, D. J., Sieber, M., Ellwood, M. J., Conway, T. M., Barrett, P. M., Chen, X., de Souza, G. F., *et al.* 2020a. Trace metal and nutrient dynamics across broad biogeochemical gradients in the Indian and Pacific sectors of the Southern Ocean. Marine Chemistry, 221: 103773.

Janssen, D. J., Sieber, M., Ellwood, M. J., Conway, T. M., Barrett, P. M., Chen, X., de Souza, G. F., *et al.* 2020b. Dissolved trace metal (Fe, Ni, Cu, Zn, Cd, Pb) concentrations in the Indian and Pacific sectors of the Southern Ocean from the Antarctic Circumnavigation Expedition (2016-2017).

Jasper, J. P., and Hayes, J. M. 1990. A carbon isotope record of CO2 levels during the late Quaternary. Nature, 347: 462–464. Springer.

Jena, B. 2016. Satellite remote sensing of the island mass effect on the Sub-Antarctic Kerguelen Plateau, Southern Ocean. Frontiers of Earth Science, 10: 479–486.

Jenkins, S. G., Partridge, S. T., Stephenson, T. R., Farley, S. D., and Robbins, C. T. 2001. Nitrogen and carbon isotope fractionation between mothers, neonates, and nursing offspring. Oecologia, 129: 336–341.

Jiang, H.-B., Fu, F.-X., Rivero-Calle, S., Levine, N. M., Sañudo-Wilhelmy, S. A., Qu, P.-P., Wang, X.-W., *et al.* 2018. Ocean warming alleviates iron limitation of marine nitrogen fixation. Nature Climate Change, 8: 709–712.

Johnson, K. S., Plant, J. N., Dunne, J. P., Talley, L. D., and Sarmiento, J. L. 2017. Annual nitrate drawdown observed by SOCCOM profiling floats and the relationship to annual net community production. Journal of Geophysical Research: Oceans, 122: 6668–6683. John Wiley & Sons, Ltd.

Johnston, N. M., Murphy, E. J., Atkinson, A., Constable, A. J., Cotté, C., Cox, M., Daly, K. L., *et al.* 2022. Status, Change, and Futures of Zooplankton in the Southern Ocean.

Jones, E. M., Bakker, D. C. E., Venables, H. J., and Watson, A. J. 2012. Dynamic seasonal cycling of inorganic carbon downstream of South Georgia, Southern Ocean. Deep-Sea Research Part II: Topical Studies in Oceanography, 59–60: 25–35. Elsevier.

Jouandet, M. P., Blain, S., Metzl, N., Brunet, C., Trull, T. W., and Obernosterer, I. 2008. A seasonal carbon budget for a naturally iron-fertilized bloom over the Kerguelen Plateau in the Southern Ocean. Deep Sea Research Part II: Topical Studies in Oceanography, 55: 856–867.

Joubert, W. R., Thomalla, S. J., Waldron, H. N., Lucas, M. I., Boye, M., Le Moigne, F. A. C., Planchon, F., *et al.* 2011. Nitrogen uptake by phytoplankton in the Atlantic sector of the Southern Ocean during late austral summer. Biogeosciences, 8: 2947–2959. Copernicus Publications.

Kaehler, S., Pakhomov, E. A., and Mcquaid, C. D. 2000. Trophic structure of the marine food web at the Prince Edward Islands (Southern Ocean) determined by δ13 C and δ15 N analysis. Marine Ecology Progress Series, 208: 13–20.

Kaiser, J., Reuer, M. K., Barnett, B., and Bender, M. L. 2005. Marine productivity estimates from continuous O2/Ar ratio measurements by membrane inlet mass spectrometry. Geophysical Research Letters, 32. John Wiley & Sons, Ltd.

Kang, S., and Lee, S. 1995. Antarctic phytoplankton assemblage in the western Bransfield Strait region, February 1993: composition, biomass, and mesoscale distributions. Marine Ecology Progress Series, 129: 253–267.

Karl, D., Letelier, R., Tupas, L., Dore, J., Christian, J., and Hebel, D. 1997. The role of nitrogen fixation in biogeochemical cycling in the subtropical North Pacific Ocean. Nature, 388: 533–538. Nature Publishing Group.

Karsh, K. L., Trull, T. W., Lourey, M. J., and Sigman, D. M. 2003. Relationship of nitrogen isotope fractionation to phytoplankton size and iron availability during the Southern Ocean Iron RElease Experiment (SOIREE). Limnology and Oceanography, 48: 1058–1068. John Wiley & Sons, Ltd.

Kattner, G., Thomas, D. N., Haas, C., and Kennedy, H. 2004. Surface ice and gap layers in Antarctic sea ice: highly productive

habitats. Marine Ecology Progress Series, 277: 1–12.

Kattner, G. 2012. The expedition of the research vessel 'Polarstern' to the Antarctic in 2011/12 (ANT-XXVIII/2) , Berichte zur Polar- und Meeresforschung. Reports on polar and marine research, Bremerhaven, Alfred Wegener Institute for Polar and Marine Research, 646: 97.

Keller, K. 1999. A model of carbon isotopic fractionation and active carbon uptake in phytoplankton. Marine Ecology Progress Series, 182: 295–298.

Kerkar, A. U., Tripathy, S. C., Minu, P., Baranval, N., Sabu, P., Patra, S., Mishra, R. K., *et al.* 2020. Variability in primary productivity and bio-optical properties in the Indian sector of the Southern Ocean during an austral summer. Polar Biology, 43: 1469–1492.

Kiørboe, T. 1993. Turbulence, phytoplankton cell size, and the structure of pelagic food webs. *In* Advances in marine biology, pp. 1–72. Elsevier.

Kiørboe, T. 1997. Population regulation and role of mesozooplankton in shaping marine pelagic food webs. Hydrobiologia, 363: 13–27.

Knapp, A. N. 2012. The sensitivity of marine N2 fixation to dissolved inorganic nitrogen. Frontiers in microbiology, 3: 374. Frontiers Media SA.

Kopczynska, E. E., Weber, L. H., and El-Sayed, S. Z. 1986. Phytoplankton species composition and abundance in the Indian sector of the Antarctic Ocean. Polar Biology, 6: 161–169.

Kopczyńska, E. E., Savoye, N., Dehairs, F., Cardinal, D., and Elskens, M. 2007. Spring phytoplankton assemblages in the Southern Ocean between Australia and Antarctica. Polar Biology, 31: 77–88. Springer.

Korb, R. E., Whitehouse, M. J., and Ward, P. 2004. SeaWiFS in the southern ocean: Spatial and temporal variability in phytoplankton biomass around South Georgia. Deep-Sea Research Part II: Topical Studies in Oceanography, 51: 99–116.

Koski, M., Boutorh, J., and de La Rocha, C. 2017. Feeding on dispersed vs. aggregated particles: the effect of zooplankton feeding behavior on vertical flux. PloS one, 12: e0177958. Public Library of Science San Francisco, CA USA.

Koubbi, P. 1993. Influence of the frontal zones on ichthyoplankton and mesopelagic fish assemblages in the Crozet Basin (Indian sector of the Southern Ocean). Polar Biology, 13: 557–564.

Kroopnick, P. M. 1985. The distribution of 13C of ΣCO2 in the world oceans. Deep Sea Research Part A. Oceanographic Research Papers, 32: 57–84.

Kustka, A., Sañudo-Wilhelmy, S., Carpenter, E. J., Capone, D. G., and Raven, J. A. 2003. A revised estimate of the iron use efficiency of nitrogen fixation, with special reference to the marine cyanobacterium Trichodesmium spp.(Cyanophyta) 1. Journal of Phycology, 39: 12–25. Wiley Online Library.

Lalli, C., and Parsons, T. 1997. Biological oceanography: an introduction. Elsevier.

Lamont, T., Berg, M. A. Van Den, Tutt, G. C. O., and Ansorge, I. J. 2019. Impact of deep-ocean eddies and fronts on the shelf seas of a sub-Antarctic Archipelago : The Prince Edward Islands. Continental Shelf Research, 177: 1–14.

Lamont, T., and van den Berg, M. A. 2020. Mesoscale eddies influencing the sub-Antarctic Prince Edward Islands Archipelago: Origin, pathways, and characteristics. Continental Shelf Research, 210: 104257.

Lamont, T., and Toolsee, T. 2022. Spatial and Seasonal Variations of the Island Mass Effect at the Sub-Antarctic Prince Edward Islands Archipelago.

Lamont, T., Tutt, G. C. O., and Barlow, R. G. 2022. Phytoplankton biomass and photophysiology at the sub-Antarctic Prince Edward Islands ecosystem in the Southern Ocean. Journal of Marine Systems, 226: 103669.

Lampert, W. 1989. The adaptive significance of diel vertical migration of zooplankton. Functional ecology: 21–27. JSTOR.

Landry, M. R., Selph, K. E., Brown, S. L., Abbott, M. R., Measures, C. I., Vink, S., Allen, C. B., *et al.* 2002. Seasonal dynamics of phytoplankton in the Antarctic Polar Front region at 170°W. Deep Sea Research Part II: Topical Studies in Oceanography, 49: 1843–1865.

Landwehr, S., Volpi, M., Haumann, F. A., Robinson, C. M., Thurnherr, I., Ferracci, V., Baccarini, A., *et al.* 2021. Exploring the coupled ocean and atmosphere system with a data science approach applied to observations from the Antarctic Circumnavigation Expedition. Earth Syst. Dynam., 12: 1295–1369. Copernicus Publications.

Lange, L., Froneman, W. P., and McQuaid, C. D. 2005. Feeding dynamics and distribution of the hyperiid amphipod, Themisto gaudichaudii (Guérin, 1828) in the Polar Frontal Zone, Southern Ocean. Citeseer.

Lannuzel, D., Vancoppenolle, M., van der Merwe, P., de Jong, J., Meiners, K. M., Grotti, M., Nishioka, J., *et al.* 2016. Iron in sea ice: Review and new insights. Elementa: Science of the Anthropocene, 4: 130.

Lara, R. J., Alder, V., Franzosi, C. A., and Kattner, G. 2010. Characteristics of suspended particulate organic matter in the southwestern Atlantic: Influence of temperature, nutrient and phytoplankton features on the stable isotope signature. Journal of Marine Systems, 79: 199–209.

Laubscher, R. K., Perissinotto, R., and McQuaid, C. D. 1993. Phytoplankton production and biomass at frontal zones in the Atlantic sector of the Southern Ocean. Polar Biology, 13: 471–481.

Laufkötter, C., Vogt, M., Gruber, N., Aita-Noguchi, M., Aumont, O., Bopp, L., Buitenhuis, E., *et al.* 2015. Drivers and uncertainties of future global marine primary production in marine ecosystem models. Biogeosciences, 12: 6955–6984. Copernicus GmbH.

Laurenceau-Cornec, E. C., Trull, T. W., Davies, D. M., Bray, S. G., Doran, J., Planchon, F., Carlotti, F., *et al.* 2015. The relative importance of phytoplankton aggregates and zooplankton fecal pellets to carbon export: insights from free-drifting sediment trap deployments in naturally iron-fertilised waters near the Kerguelen Plateau. Biogeosciences, 12: 1007–1027. Copernicus Publications.

Laws, E. A., Popp, B. N., Bidigare, R. R., Kennicutt, M. C., and Macko, S. A. 1995. Dependence of phytoplankton carbon isotopic composition on growth rate and [CO2) aq: theoretical considerations and experimental results. Geochimica et cosmochimica acta, 59: 1131–1138. Citeseer.

Laws, E. A., Bidigare, R. R., and Popp, B. N. 1997. Effect of growth rate and CO2 concentration on carbon isotopic fractionation by the marine diatom Phaeodactylum tricornutum. Limnology and Oceanography, 42: 1552–1560. John Wiley & Sons, Ltd.

Laws, E. A., Falkowski, P. G., Smith Jr., W. O., Ducklow, H., and McCarthy, J. J. 2000. Temperature effects on export production in the open ocean. Global Biogeochemical Cycles, 14: 1231–1246. John Wiley & Sons, Ltd.

Laws, E. A., Popp, B. N., Cassar, N., and Tanimoto, J. 2002. 13C discrimination patterns in oceanic phytoplankton: likely influence of CO2 concentrating mechanisms, and implications for palaeoreconstructionse. Functional Plant Biology, 29: 323–333.

Layman, C. A., Arrington, D. A., Montaña, C. G., and Post, D. M. 2007. Can stable isotope ratios provide for community-wide measures of trophic structure? Ecology, 88: 42–48. John Wiley & Sons, Ltd.

Layman, C. A., Araujo, M. S., Boucek, R., Hammerschlag-Peyer, C. M., Harrison, E., Jud, Z. R., Matich, P., *et al.* 2012. Applying stable isotopes to examine food-web structure: an overview of analytical tools. Biological Reviews, 87: 545–562. John Wiley & Sons, Ltd.

Le Moigne, F. A. C., Henson, S. A., Cavan, E., Georges, C., Pabortsava, K., Achterberg, E. P., Ceballos-Romero, E., *et al.* 2016. What causes the inverse relationship between primary production and export efficiency in the Southern Ocean? Geophysical Research Letters, 43: 4457–4466. John Wiley & Sons, Ltd.

Le Roux, P. C., and McGeoch, M. A. 2008. Changes in climate extremes, variability and signature on sub-Antarctic Marion Island. Climatic Change, 86: 309–329. Springer.

Leblanc, K., Quéguiner, B., Fiala, M., Blain, S., Morvan, J., and Corvaisier, R. 2002. Particulate biogenic silica and carbon production rates and particulate matter distribution in the Indian sector of the Subantarctic Ocean. Deep Sea Research Part II: Topical Studies in Oceanography, 49: 3189–3206.

Lee, R. F., and Hagen, W. 2006. Lipid storage in marine zooplankton. Marine Ecology Progress Series, 307: 273–306.

Lehette, P., and Hernández-León, S. 2009. Zooplankton biomass estimation from digitized images: a comparison between subtropical and Antarctic organisms. Limnology and Oceanography: Methods, 7: 304–308. John Wiley & Sons, Ltd.

Lehmann, M. F., Bernasconi, S. M., Barbieri, A., and McKenzie, J. A. 2002. Preservation of organic matter and alteration of its carbon and nitrogen isotope composition during simulated and in situ early sedimentary diagenesis. Geochimica et Cosmochimica Acta, 66: 3573–3584.

Leibold, M. A. 1995. The Niche Concept Revisited: Mechanistic Models and Community Context. Ecology, 76: 1371–1382. John Wiley & Sons, Ltd.

Leichter, J. J., Stewart, H. L., and Miller, S. L. 2003. Episodic nutrient transport to Florida coral reefs. Limnology and Oceanography, 48: 1394–1407. John Wiley & Sons, Ltd.

Lesage, V. 1999. Trophic relationships, seasonal diving activity and movements of harbour seals, Phoca vitulina concolor, in the St. Lawrence River Estuary, Canada. University of Waterloo.

Leung, S., Cabré, A., and Marinov, I. 2015. A latitudinally banded phytoplankton response to 21st century climate change in the Southern Ocean across the CMIP5 model suite. Biogeosciences, 12: 5715–5734. Copernicus GmbH.

Lin, H., Rauschenberg, S., Hexel, C. R., Shaw, T. J., and Twining, B. S. 2011. Free-drifting icebergs as sources of iron to the Weddell Sea. Deep Sea Research Part II: Topical Studies in Oceanography, 58: 1392–1406. Elsevier.

Lipschultz, F. 2001. A time-series assessment of the nitrogen cycle at BATS. Deep Sea Research Part II: Topical Studies in Oceanography, 48: 1897–1924. Elsevier.

Litchman, E., Klausmeier, C. A., Schofield, O. M., and Falkowski, P. G. 2007. The role of functional traits and trade-offs in structuring phytoplankton communities: scaling from cellular to ecosystem level. Ecology letters, 10: 1170–1181. Wiley Online Library.

Liu, K.-K., Kao, S.-J., Chiang, K.-P., Gong, G.-C., Chang, J., Cheng, J.-S., and Lan, C.-Y. 2013. Concentration dependent nitrogen isotope fractionation during ammonium uptake by phytoplankton under an algal bloom condition in the Danshuei estuary, northern Taiwan. Marine Chemistry, 157: 242–252.

Liu, Y., Xie, L., Morrison, J. M., Kamykowski, D., and Sweet, W. V. 2014. Ocean circulation and water mass characteristics around the Galápagos Archipelago simulated by a multiscale nested ocean circulation model. International Journal of Oceanography, 2014. Hindawi.

Llort, J., Lévy, M., Sallée, J.-B., and Tagliabue, A. 2015. Onset, intensification, and decline of phytoplankton blooms in the Southern Ocean. ICES Journal of Marine Science, 72: 1971–1984.

Loisel, H., and Morel, A. 1998. Light scattering and chlorophyll concentration in case 1 waters: A reexamination. Limnology and Oceanography, 43: 847–858. John Wiley & Sons, Ltd.

Lomas, M. W., and Glibert, P. M. 1999. Temperature regulation of nitrate uptake: A novel hypothesis about nitrate uptake and reduction in cool-water diatoms. Limnology and Oceanography, 44: 556–572. John Wiley & Sons, Ltd.

Lomas, M. W., and Glibert, P. M. 2000. Comparisons of nitrate uptake, storage, and reduction in marine diatoms and flagellates. Journal of Phycology, 36: 903–913. John Wiley & Sons, Ltd.

Lombard, A. T., Reyers, B., Schonegevel, L. Y., Cooper, J., Smith-Adao, L. B., Nel, D. C., Froneman, P. W., *et al.* 2007. Conserving pattern and process in the Southern Ocean: designing a Marine Protected Area for the Prince Edward Islands. Antarctic Science, 19: 39–54. Cambridge University Press.

Longhurst, A. R., and Glen Harrison, W. 1989. The biological pump: Profiles of plankton production and consumption in the upper ocean. Progress in Oceanography, 22: 47–123.

Longhurst, A. R. 1991. Role of the marine biosphere in the global carbon cycle. Limnology and Oceanography, 36: 1507–1526. John Wiley & Sons, Ltd.

Lonsdale, D. J., Caron, D. A., Dennett, M. R., and Schaffner, R. 2000. Predation by Oithona spp. on protozooplankton in the Ross Sea, Antarctica. Deep Sea Research Part II: Topical Studies in Oceanography, 47: 3273–3283.

Lorenzen, C. J. 1967. Determination of Chlorophyll and Pheo-Pigments : Spectrophotometric Equations ~. Limnology and oceanography, 12(2): 343–346.

Lorrain, A., Graham, B. S., Popp, B. N., Allain, V., Olson, R. J., Hunt, B. P. V, Potier, M., *et al.* 2015. Nitrogen isotopic baselines and implications for estimating foraging habitat and trophic position of yellowfin tuna in the Indian and Pacific Oceans. Deep Sea Research Part II: Topical Studies in Oceanography, 113: 188–198.

Louise Allan, E., William Froneman, P., Durgadoo, J. V., Mcquaid, C. D., Ansorge, I. J., and Richoux, N. B. 2013. Critical indirect effects of climate change on sub-Antarctic ecosystem functioning. Ecology and Evolution, 3: 2994–3004.

Lourantou, A., and Metzl, N. 2011. Decadal evolution of carbon sink within a strong bloom area in the subantarctic zone. Geophysical Research Letters, 38. John Wiley & Sons, Ltd.

Lourey, M. J., Trull, T. W., and Sigman, D. M. 2003. Sensitivity of δ15N of nitrate, surface suspended and deep sinking particulate nitrogen to seasonal nitrate depletion in the Southern Ocean. Global Biogeochemical Cycles, 17. John Wiley & Sons, Ltd.

Louw, D. V. S., Walker, D. R., and Fawcett, S. E. 2022. Factors influencing sea-ice algae abundance, community composition, and distribution in the marginal ice zone of the Southern Ocean during winter. Deep Sea Research Part I: Oceanographic Research

Papers, 185: 103805.

Lovenduski, N. S., and Gruber, N. 2005. Impact of the Southern Annular Mode on Southern Ocean circulation and biology. Geophysical Research Letters, 32. Wiley Online Library.

Lübcker, N., Whiteman, J. P., Newsome, S. D., Millar, R. P., and de Bruyn, P. J. N. 2020. Can the carbon and nitrogen isotope values of offspring be used as a proxy for their mother's diet? Using foetal physiology to interpret bulk tissue and amino acid δ15N values. Conservation Physiology, 8: coaa060.

Lusher, A. L., Welden, N. A., Sobral, P., and Cole, M. 2017. Sampling, isolating and identifying microplastics ingested by fish and invertebrates. Analytical Methods, 9: 1346–1360. The Royal Society of Chemistry.

Lutjeharms, J. R. E., and Valentine, H. R. 1984. Southern ocean thermal fronts south of Africa. Deep Sea Research Part A. Oceanographic Research Papers, 31: 1461–1475.

Lutjeharms, J. R. E. 1985. Location of frontal systems between Africa and Antarctica: some preliminary results. Deep Sea Research Part A. Oceanographic Research Papers, 32: 1499–1509. Elsevier.

M. Franck, V., Brzezinski, M. A., Coale, K. H., and Nelson, D. M. 2000. Iron and silicic acid concentrations regulate Si uptake north and south of the Polar Frontal Zone in the Pacific Sector of the Southern Ocean. Deep Sea Research Part II: Topical Studies in Oceanography, 47: 3315–3338.

Mackas, D., and Bohrer, R. 1976. Fluorescence analysis of zooplankton gut contents and an investigation of diel feeding patterns. Journal of experimental marine biology and ecology, 25: 77–85. Elsevier.

MacKenzie, K. M., Palmer, M. R., Moore, A., Ibbotson, A. T., Beaumont, W. R. C., Poulter, D. J. S., and Trueman, C. N. 2011. Locations of marine animals revealed by carbon isotopes. Scientific reports, 1: 1–6. Nature Publishing Group.

Macko, S. A., Estep, M. L. F., Engel, M. H., and Hare, P. E. 1986. Kinetic fractionation of stable nitrogen isotopes during amino acid transamination. Geochimica et Cosmochimica Acta, 50: 2143–2146.

Maksym, T., Stammerjohn, S. E., Ackley, S., and Massom, R. 2012. Antarctic Sea Ice— A Polar Opposite? Oceanography, 25: 140–151. JSTOR.

Maldonado, M., and Price, N. M. 1996. Influence of N substrate on Fe requirements of marine centric diatoms. Marine Ecology Progress Series, 141: 161–172.

Manganelli, M., Malfatti, F., Samo, T. J., Mitchell, B. G., Wang, H., and Azam, F. 2009. Major Role of Microbes in Carbon Fluxes during Austral Winter in the Southern Drake Passage. PLOS ONE, 4: e6941. Public Library of Science.

Manno, C., Stowasser, G., Enderlein, P., Fielding, S., and Tarling, G. A. 2015. The contribution of zooplankton faecal pellets to deep-carbon transport in the Scotia Sea (Southern Ocean). Biogeosciences, 12: 1955–1965. Copernicus Publications.

Marañón, E., Steele, J. H., Turekian, K. K., and Thorpe, S. A. 2009. Encyclopedia of Ocean Sciences. Academic Press, Oxford.

Marañón, E., Cermeño, P., López-Sandoval, D. C., Rodríguez-Ramos, T., Sobrino, C., Huete-Ortega, M., Blanco, J. M., *et al.* 2013. Unimodal size scaling of phytoplankton growth and the size dependence of nutrient uptake and use. Ecology letters, 16: 371–379. Wiley Online Library.

Marañón, E. 2015. Cell size as a key determinant of phytoplankton metabolism and community structure. Annual review of marine science, 7: 241–264. Annual Reviews.

Marinov, I., Doney, S. C., and Lima, I. D. 2010. Response of ocean phytoplankton community structure to climate change over the 21st century: partitioning the effects of nutrients, temperature and light. Biogeosciences, 7: 3941–3959. Copernicus Publications.

Mariotti, A., Germon, J. C., Hubert, P., Kaiser, P., Letolle, R., Tardieux, A., and Tardieux, P. 1981. Experimental determination of nitrogen kinetic isotope fractionation: Some principles; illustration for the denitrification and nitrification processes. Plant and Soil, 62: 413–430.

Martin, J. H., Gordon, R. M., and Fitzwater, S. E. 1990a. Iron in Antarctic waters. Nature, 345: 156–158.

Martin, J. H., Fitzwater, S. E., and Gordon, R. M. 1990b. Iron deficiency limits phytoplankton growth in Antarctic waters. Global Biogeochemical Cycles, 4: 5–12. John Wiley & Sons, Ltd.

Matear, R. J., and Hirst, A. C. 1999. Climate change feedback on the future oceanic CO2 uptake. Tellus B: Chemical and Physical Meteorology, 51: 722–733. Taylor & Francis.

Mateo, M. A., Serrano, O., Serrano, L., and Michener, R. H. 2008. Effects of sample preparation on stable isotope ratios of carbon and nitrogen in marine invertebrates: implications for food web studies using stable isotopes. Oecologia, 157: 105–115.

Matthews, B., and Mazumder, A. 2005a. Consequences of large temporal variability of zooplankton δ15N for modeling fish trophic position and variation. Limnology and Oceanography, 50: 1404–1414. Wiley Online Library.

Matthews, B., and Mazumder, A. 2005b. Temporal variation in body composition (C: N) helps explain seasonal patterns of zooplankton δ13C. Freshwater Biology, 50: 502–515. John Wiley & Sons, Ltd.

Mayewski, P. A., Meredith, M. P., Summerhayes, C. P., Turner, J., Worby, A., Barrett, P. J., Casassa, G., *et al.* 2009. State of the Antarctic and Southern Ocean climate system. Reviews of Geophysics, 47. John Wiley & Sons, Ltd.

Mayzaud, P., and Pakhomov, E. A. 2014. The role of zooplankton communities in carbon recycling in the Ocean: the case of the Southern Ocean. Journal of Plankton Research, 36: 1543–1556.

Mazloff, M. R., Heimbach, P., and Wunsch, C. 2010. An Eddy-Permitting Southern Ocean State Estimate. Journal of Physical Oceanography, 40: 880–899. American Meteorological Society, Boston MA, USA.

McBride, M. M., Stokke, O. S., Renner, A. H. H., Krafft, B. A., Bergstad, O. A., Biuw, M., Lowther, A. D., *et al.* 2021. Antarctic krill Euphausia superba: spatial distribution, abundance, and management of fisheries in a changing climate. Marine Ecology Progress Series, 668: 185–214.

McCartney, M. S. 1976. The interaction of zonal currents with topography with applications to the Southern Ocean. *In* Deep Sea Research and Oceanographic Abstracts, pp. 413–427. Elsevier.

McCartney, M. S. 1979. Subantarctic mode water. Woods Hole Oceanographic Institution Contribution, 3773: 103–119. Woods Hole Oceanographic Institution.

McConnaughey, T., and McRoy, C. P. 1979. Food-web structure and the fractionation of carbon isotopes in the Bering Sea. Marine biology, 53: 257–262. Springer.

McCorkle, D. C., Emerson, S. R., and Quay, P. D. 1985. Stable carbon isotopes in marine porewaters. Earth and Planetary Science Letters, 74: 13–26.

McCormack, S. A., Melbourne-Thomas, J., Trebilco, R., Griffith, G., Hill, S. L., Hoover, C., Johnston, N. M., *et al.* 2021a. Southern Ocean Food Web Modelling: Progress, Prognoses, and Future Priorities for Research and Policy Makers.

McCormack, S. A., Melbourne-Thomas, J., Trebilco, R., Blanchard, J. L., Raymond, B., and Constable, A. 2021b. Decades of dietary data demonstrate regional food web structures in the Southern Ocean. Ecology and Evolution, 11: 227–241. John Wiley & Sons, Ltd.

McCutchan Jr, J. H., Lewis Jr, W. M., Kendall, C., and McGrath, C. C. 2003. Variation in trophic shift for stable isotope ratios of carbon, nitrogen, and sulfur. Oikos, 102: 378–390. Wiley Online Library.

McIlvin, M. R., and Casciotti, K. L. 2011. Technical updates to the bacterial method for nitrate isotopic analyses. Analytical Chemistry, 83: 1850–1856. ACS Publications.

McKinley, G. A., Pilcher, D. J., Fay, A. R., Lindsay, K., Long, M. C., and Lovenduski, N. S. 2016. Timescales for detection of trends in the ocean carbon sink. Nature, 530: 469–472. Nature Publishing Group.

McKinney, C. R., McCrea, J. M., Epstein, S., Allen, H. A., and Urey, H. C. 1950. Improvements in mass spectrometers for the measurement of small differences in isotope abundance ratios. Review of Scientific Instruments, 21: 724–730. American Institute of Physics.

McMahon, K. W., Hamady, L. L., and Thorrold, S. R. 2013. A review of ecogeochemistry approaches to estimating movements of marine animals. Limnology and Oceanography, 58: 697–714. John Wiley & Sons, Ltd.

McMeans, B. C., McCann, K. S., Humphries, M., Rooney, N., and Fisk, A. T. 2015. Food Web Structure in Temporally-Forced Ecosystems. Trends in Ecology & Evolution, 30: 662–672.

Mcquaid, C. D., and Froneman, W. P. 2008. Biology in the oceanographic environment. The Prince Edward Islands: land–sea interactions in a changing ecosystem. Sun Press, Stellenbosch, South Africa: 97–120.

Mdutyana, M., Thomalla, S. J., Philibert, R., Ward, B. B., and Fawcett, S. E. 2020. The Seasonal Cycle of Nitrogen Uptake and Nitrification in the Atlantic Sector of the Southern Ocean. Global Biogeochemical Cycles, 34: e2019GB006363. John Wiley & Sons, Ltd.

Mdutyana, M., Sun, X., Burger, J. M., Thomalla, S. J., Ward, B. B., Sarah, F., Flynn, R. F., *et al.* 2022. The kinetics of ammonium uptake and oxidation across the Southern Ocean. Limnology and Oceanography, 67: 973–991. AGU.

Meijers, A. J. S. 2014. The Southern Ocean in the coupled model intercomparison project phase 5. Philosophical Transactions of the Royal Society A: Mathematical, Physical and Engineering Sciences, 372: 20130296. The Royal Society Publishing.

Melbourne-Thomas, J., Constable, A. J., Fulton, E. A., Corney, S. P., Trebilco, R., Hobday, A. J., Blanchard, J. L., *et al.* 2017. Integrated modelling to support decision-making for marine social–ecological systems in Australia. ICES Journal of Marine Science, 74: 2298–2308. Oxford University Press.

Melice, J. L., Rouault, M., Lutjeharms, J. R. E., and Ansorge, I. J. 2003. Sea-surface temperatures at the sub-Antarctic islands Marion and Gough during the past 50 years. South African Journal of Science, 99: 363–366.

Ménard, F., Benivary, H. D., Bodin, N., Coffineau, N., Le Loc'h, F., Mison, T., Richard, P., *et al.* 2014. Stable isotope patterns in micronekton from the Mozambique Channel. Deep Sea Research Part II: Topical Studies in Oceanography, 100: 153–163.

Menden-Deuer, S., and Lessard, E. J. 2000. Carbon to volume relationships for dinoflagellates, diatoms, and other protist plankton. Limnology and Oceanography, 45: 569–579. John Wiley & Sons, Ltd.

Mengesha, S., Dehairs, F., Fiala, M., Elskens, M., and Goeyens, L. 1998. Seasonal variation of phytoplankton community structure and nitrogen uptake regime in the Indian Sector of the Southern Ocean. Polar Biology, 20: 259–272.

Michel, L. N., Danis, B., Dubois, P., Eleaume, M., Fournier, J., Gallut, C., Jane, P., *et al.* 2019. Increased sea ice cover alters food web structure in East Antarctica. Scientific Reports, 9: 8062.

Michener, R. H., and Lajtha, K. 2007. Stable isotopes in ecology and environmental science. Wiley Online Library.

Middelburg, J. J. 2014. Stable isotopes dissect aquatic food webs from the top to the bottom. Biogeosciences, 11: 2357–2371. Copernicus GmbH.

Miller, J. F., Millar, J. S., and Longstaffe, F. J. 2011. Stable nitrogen and carbon isotope discrimination between juveniles and adults in an income-breeding small mammal (Peromyscus maniculatus). Mammalian Biology, 76: 563–569.

Mirkin, J., Flynn, R. F., West, A. G., Smith, S., Altieri, K., Granger, J., and Fawcett, S. E. 2023. Msc Thesis: Nitrogen cycle-based estimates of carbon export potential in the waters adjacent to Larsen C Ice Shelf in the western Weddell Sea, Antarctica. Unpublished MSc dissertation, Faculty of Science, Deparment of Oceanography, University of Cape Town.

Mizutani, H., Hasegawa, H., and Wada, E. 1986. High nitrogen isotope ratio for soils of seabird rookeries. Biogeochemistry, 2: 221–247. Springer.

Möbius, J. 2013. Isotope fractionation during nitrogen remineralization (ammonification): Implications for nitrogen isotope biogeochemistry. Geochimica et Cosmochimica Acta, 105: 422–432.

Mongin, M., Molina, E., and Trull, T. W. 2008. Seasonality and scale of the Kerguelen plateau phytoplankton bloom: A remote sensing and modeling analysis of the influence of natural iron fertilization in the Southern Ocean. Deep Sea Research Part II: Topical Studies in Oceanography, 55: 880–892.

Mongin, M. M., Abraham, E. R., and Trull, T. W. 2009. Winter advection of iron can explain the summer phytoplankton bloom that extends 1000 km downstream of the Kerguelen Plateau in the Southern Ocean. Journal of Marine Research, 67: 225–237. Sears Foundation for Marine Research.

Mook, W. G., Bommerson, J. C., and Staverman, W. H. 1974. Carbon isotope fractionation between dissolved bicarbonate and gaseous carbon dioxide. Earth and Planetary Science Letters, 22: 169–176.

Moore, C. M., Mills, M. M., Arrigo, K. R., Berman-Frank, I., Bopp, L., Boyd, P. W., Galbraith, E. D., *et al.* 2013. Processes and patterns of oceanic nutrient limitation. Nature Geoscience, 6: 701–710.

Morel, F. M. M., Hudson, R. J. M., and Price, N. M. 1991. Limitation of productivity by trace metals in the sea. Limnology and Oceanography, 36: 1742–1755. Wiley Online Library.

Morley, S. A., Abele, D., Barnes, D. K. A., Cárdenas, C. A., Cotté, C., Gutt, J., Henley, S. F., *et al.* 2020. Global drivers on Southern Ocean ecosystems: changing physical environments and anthropogenic pressures in an earth system. Frontiers in Marine Science, 7: 547188. Frontiers Media SA.

Murphy, E. J. 1995. Spatial Structure of the Southern Ocean Ecosystem: Predator-Prey Linkages in Southern Ocean Food Webs. Journal of Animal Ecology, 64: 333–347. [Wiley, British Ecological Society].

Nakatsuka, T., Handa, N., Wada, E., and Wong, C. S. 1992. The dynamic changes of stable isotopic ratios of carbon and nitrogen in suspended and sedimented particulate organic matter during a phytoplankton bloom. Journal of Marine Research, 50: 267–296. Sears Foundation for Marine Research.

Naselli-Flores, L., and Padisák, J. 2022. Ecosystem services provided by marine and freshwater phytoplankton. Hydrobiologia.

Needoba, J. A., Sigman, D. M., and Harrison, P. J. 2004. The mechanism of isotope fractionation during algal nitrate assimilation as illuminated by the 15N/14N of intracellular nitrate. Journal of Phycology, 40: 517–522. John Wiley & Sons, Ltd.

Nejstgaard, J. C., Båmstedt, U., Bagøien, E., and Solberg, P. T. 1995. Algal constraints on copepod grazing. Growth state, toxicity, cell size, and season as regulating factors. ICES Journal of Marine Science, 52: 347–357.

Newsome, S. D., Clementz, M. T., and Koch, P. L. 2010. Using stable isotope biogeochemistry to study marine mammal ecology. Marine Mammal Science, 26: 509–572. John Wiley & Sons, Ltd.

Nicholson, S.-A., Lévy, M., Jouanno, J., Capet, X., Swart, S., and Monteiro, P. M. S. 2019. Iron Supply Pathways Between the Surface and Subsurface Waters of the Southern Ocean: From Winter Entrainment to Summer Storms. Geophysical Research Letters, 46: 14567–14575. John Wiley & Sons, Ltd.

Nielsen, T., and Sabatini, M. 1996. Role of cyclopoid copepods Oithona spp. in North Sea plankton communities. Marine Ecology Progress Series, 139: 79–93.

Not, F., Siano, R., Kooistra, W. H. C. F., Simon, N., Vaulot, D., and Probert, I. 2012. Chapter One - Diversity and Ecology of Eukaryotic Marine Phytoplankton. *In* Genomic Insights into the Biology of Algae, pp. 1–53. Ed. by G. B. T.-A. in B. R. Piganeau. Academic Press.

Nowicki, M., DeVries, T., and Siegel, D. A. 2022. Quantifying the carbon export and sequestration pathways of the ocean's biological carbon pump. Global Biogeochemical Cycles, n/a: e2021GB007083. John Wiley & Sons, Ltd.

O'Leary, M. H. 1981. Carbon isotope fractionation in plants. Phytochemistry, 20: 553–567.

O'Leary, M. H. 1988. Carbon Isotopes in Photosynthesis. BioScience, 38: 328–336. [American Institute of Biological Sciences, Oxford University Press].

O'Reilly, C. M., Hecky, R. E., Cohen, A. S., and Plisnier, P.-D. 2002. Interpreting stable isotopes in food webs: Recognizing the role of time averaging at different trophic levels. Limnology and Oceanography, 47: 306–309. John Wiley & Sons, Ltd.

Oke, P. R., and England, M. H. 2004. Oceanic response to changes in the latitude of the Southern Hemisphere subpolar westerly winds. Journal of Climate, 17: 1040–1054.

Omori, M. 1969. Weight and chemical composition of some important oceanic zooplankton in the North Pacific Ocean. Marine Biology, 3: 4–10.

Øresland, V. 1991. Feeding of the carnivorous copepod Euchaeta antarctica in Antarctic waters. Mar Ecol Prog Ser, 78: 41–47.

Øresland, V., and Ward, P. 1993. Summer and winter diet of four carnivorous copepod species around South Georgia. Marine Ecology Progress Series, 98: 73–78. Inter-Research Science Center.

Orr, J. C., Fabry, V. J., Aumont, O., Bopp, L., Doney, S. C., Feely, R. A., Gnanadesikan, A., *et al.* 2005. Anthropogenic ocean acidification over the twenty-first century and its impact on calcifying organisms. Nature, 437: 681–686.

Orsi, A. H., Whitworth, T., and Nowlin, W. D. 1995. On the meridional extent and fronts of the Antarctic Circumpolar Current. Deep-Sea Research Part I, 42: 641–673.

Otero, X. L., De La Peña-Lastra, S., Pérez-Alberti, A., Ferreira, T. O., and Huerta-Diaz, M. A. 2018. Seabird colonies as important global drivers in the nitrogen and phosphorus cycles. Nature Communications, 9: 246.

Paasche, E., Bryceson, I., and Tangen, K. 1984. Interspecific variation in dark nitrogen uptake by dinoflagellates 1. Journal of Phycology, 20: 394–401. Wiley Online Library.

Paffenhöfer, G.-A. 1983. Vertical zooplankton distribution on the northeastern Florida shelf and its relation to temperature and food abundance. Journal of Plankton Research, 5: 15–33. Oxford University Press.

Pakhomov, E. A., and McQuaid, C. D. 1996. Distribution of surface zooplankton and seabirds across the Southern Ocean. Polar Biology, 16: 271–286.

Pakhomov, E. A., and Froneman, P. W. 1999. The Prince Edward Islands pelagic ecosystem, south Indian Ocean: a review of

achievements, 1976–1990. Journal of Marine Systems, 18: 355–367. Elsevier.

Pakhomov, E. A., Perissinotto, R., and Froneman, P. W. 1999. Predation impact of carnivorous macrozooplankton and micronekton in the Atlantic sector of the Southern Ocean. Journal of Marine Systems, 19: 47–64.

Pakhomov, E. A., Ansorge, I. J., and Froneman, P. W. 2000a. Variability in the inter-island environment of the Prince Edward Islands (Southern Ocean). Polar Biology, 23: 593–603.

Pakhomov, E. A., Froneman, P. W., Ansorge, I. J., and Lutjeharms, J. R. E. 2000b. Temporal variability in the physico-biological environment of the Prince Edward Islands (Southern Ocean). Journal of Marine Systems, 26: 75–95. Elsevier.

Pakhomov, E. A., Perissinotto, R., McQuaid, C. D., and Froneman, P. W. 2000c. Zooplankton structure and grazing in the Atlantic sector of the Southern Ocean in late austral summer 1993: Part 1. Ecological zonation. Deep Sea Research Part I: Oceanographic Research Papers, 47: 1663–1686.

Pakhomov, E. A. 2000. Demography and life cycle of Antarctic krill, Euphausia superba, in the Indian sector of the Southern Ocean: long-term comparison between coastal and open-ocean regions. Canadian Journal of Fisheries and Aquatic Sciences, 57: 68–90. NRC Research Press.

Pakhomov, E. A., Froneman, P. W., and Perissinotto, R. 2002. Salp/krill interactions in the Southern Ocean: spatial segregation and implications for the carbon flux. Deep Sea Research Part II: Topical Studies in Oceanography, 49: 1881–1907.

Pakhomov, E. A., Dubischar, C. D., Strass, V., Brichta, M., and Bathmann, U. V. 2006. The tunicate Salpa thompsoni ecology in the Southern Ocean. I. Distribution, biomass, demography and feeding ecophysiology. Marine Biology, 149: 609–623. Springer.

Pakhomov, E. A., Henschke, N., Hunt, B. P. V, Stowasser, G., and Cherel, Y. 2019. Utility of salps as a baseline proxy for food web studies. Journal of Plankton Research, 41: 3–11.

Palter, J. B., Marinov, I., Sarmiento, J. L., and Gruber, N. 2013. Large-Scale, Persistent Nutrient Fronts of the World Ocean: Impacts on Biogeochemistry. *In* The Handbook of Environmental Chemistry, pp. 1–38. Springer Berlin Heidelberg, Berlin, Heidelberg.

Pantoja, S., Repeta, D. J., Sachs, J. P., and Sigman, D. M. 2002. Stable isotope constraints on the nitrogen cycle of the Mediterranean Sea water column. Deep Sea Research Part I: Oceanographic Research Papers, 49: 1609–1621.

Parker, P. L. 1964. The biogeochemistry of the stable isotopes of carbon in a marine bay. Geochimica et Cosmochimica Acta, 28: 1155–1164. Elsevier.

Parkinson, C. L., and Cavalieri, D. J. 2012. Antarctic sea ice variability and trends, 1979–2010. The Cryosphere, 6: 871–880. Copernicus GmbH.

Pasciak, W. J., and Gavis, J. 1974. Transport limitation of nutrient uptake in phytoplankton 1. Limnology and Oceanography, 19: 881–888. Wiley Online Library.

Pasotti, F., Saravia, L. A., De Troch, M., Tarantelli, M. S., Sahade, R., and Vanreusel, A. 2015. Benthic Trophic Interactions in an Antarctic Shallow Water Ecosystem Affected by Recent Glacier Retreat. PLOS ONE, 10: e0141742. Public Library of Science.

Pasternak, A. F., and Schnack-Schiel, S. B. 2001. Seasonal feeding patterns of the dominant Antarctic copepods Calanus propinquus and Calanoides acutus in the Weddell Sea. Polar Biology, 24: 771–784.

Pauli, N.-C., Metfies, K., Pakhomov, E. A., Neuhaus, S., Graeve, M., Wenta, P., Flintrop, C. M., *et al.* 2021. Selective feeding in Southern Ocean key grazers—diet composition of krill and salps. Communications Biology, 4: 1061.

Pearce, I., Davidson, A. T., Thomson, P. G., Wright, S., and van den Enden, R. 2010. Marine microbial ecology off East Antarctica (30-80° E): Rates of bacterial and phytoplankton growth and grazing by heterotrophic protists. Deep Sea Research Part II: Topical Studies in Oceanography, 57: 849–862. Elsevier.

Pearce, I., Davidson, A. T., Thomson, P. G., Wright, S., and van den Enden, R. 2011. Marine microbial ecology in the sub-Antarctic Zone: Rates of bacterial and phytoplankton growth and grazing by heterotrophic protists. Deep Sea Research Part II: Topical Studies in Oceanography, 58: 2248–2259.

Pedentchouk, N., and Zhou, Y. 2018. Factors controlling carbon and hydrogen isotope fractionation during biosynthesis of lipids by phototrophic organisms. Hydrocarbons, Oils and Lipids: Diversity, Origin, Chemistry and Fate. Handbook of Hydrocarbon and Lipid Microbiology, edited by: Wilkes, H: 1–24.

Peloquin, J. A., and Smith Jr., W. O. 2007. Phytoplankton blooms in the Ross Sea, Antarctica: Interannual variability in magnitude,

temporal patterns, and composition. Journal of Geophysical Research: Oceans, 112. John Wiley & Sons, Ltd.

Pennock, J. R., Velinsky, D. J., Ludlam, J. M., Sharp, J. H., and Fogel, M. L. 1996. Isotopic fractionation of ammonium and nitrate during uptake by Skeletonema costatum: Implications for δ15N dynamics under bloom conditions. Limnology and Oceanography, 41: 451–459. John Wiley & Sons, Ltd.

Pérez-Tribouillier, H., Noble, T. L., Townsend, A. T., Bowie, A. R., and Chase, Z. 2020. Quantifying lithogenic inputs to the Southern Ocean using long-lived thorium isotopes. Frontiers in Marine Science, 7: 207. Frontiers Media SA.

Perissinotto, R., Rae, C. M. D., Boden, B. P., and Allanson, B. R. 1990. Vertical stability as a controlling factor of the marine phytoplankton production at the Prince Edward Archipelago (Southern Ocean). Marine Ecology Progress Series, 60: 205–209. Inter-Research Science Center.

Perissinotto, R., and Duncombe Rae, C. M. 1990. Occurrence of anticyclonic eddies on the Prince Edward Plateau (Southern Ocean): effects on phytoplankton biomass and production. Deep Sea Research Part A. Oceanographic Research Papers, 37: 777–793. Elsevier.

Perissinotto, R., Laubscher, R. K., and McQuaid, C. D. 1992. Marine productivity enhancement around Bouvet and the South Sandwich Islands (Southern Ocean). Marine Ecology-Progress Series, 88: 41. INTER RESEARCH.

Perissinotto, R. 1992. Mesozooplankton size-selectivity and grazing impact on the phytoplankton community of the Prince Edward Archipelago (Southern Ocean). Marine ecology progress series. Oldendorf, 79: 243–258.

Peterson, B. J., and Fry, B. 1987. Stable isotopes in ecosystem studies. Annual Review of Ecology and Systematics, 18: 293–320. Annual Reviews.

Peterson, W. T., Tiselius, P., and Kiørboe, T. 1991. Copepod egg production, moulting and growth rates, and secondary production, in the Skagerrak in August 1988. Journal of Plankton Research, 13: 131–154.

Pethybridge, H., Choy, C. A., Logan, J. M., Allain, V., Lorrain, A., Bodin, N., Somes, C. J., *et al.* 2018. A global meta-analysis of marine predator nitrogen stable isotopes: Relationships between trophic structure and environmental conditions. Global Ecology and Biogeography, 27: 1043–1055. John Wiley & Sons, Ltd.

Petrou, K., Kranz, S. A., Trimborn, S., Hassler, C. S., Ameijeiras, S. B., Sackett, O., Ralph, P. J., *et al.* 2016. Southern Ocean phytoplankton physiology in a changing climate. Journal of Plant Physiology, 203: 135–150.

Pinnegar, J. K., and Polunin, N. V. C. 1999. Differential fractionation of δ13C and δ15N among fish tissues: implications for the study of trophic interactions. Functional ecology, 13: 225–231. Wiley Online Library.

Planquette, H., Statham, P. J., Fones, G. R., Charette, M. A., Moore, C. M., Salter, I., Nédélec, F. H., *et al.* 2007. Dissolved iron in the vicinity of the Crozet Islands, Southern Ocean. Deep Sea Research Part II: Topical Studies in Oceanography, 54: 1999–2019.

Planquette, H., Sanders, R. R., Statham, P. J., Morris, P. J., and Fones, G. R. 2011. Fluxes of particulate iron from the upper ocean around the Crozet Islands: A naturally iron-fertilized environment in the Southern Ocean. Global Biogeochemical Cycles, 25. John Wiley & Sons, Ltd.

Polito, M. J., Reiss, C. S., Trivelpiece, W. Z., Patterson, W. P., and Emslie, S. D. 2013. Stable isotopes identify an ontogenetic niche expansion in Antarctic krill (Euphausia superba) from the South Shetland Islands, Antarctica. Marine Biology, 160: 1311–1323.

Pollard, R. T., Lucas, M. I., and Read, J. F. 2002. Physical controls on biogeochemical zonation in the Southern Ocean. Deep Sea Research Part II: Topical Studies in Oceanography, 49: 3289–3305.

Pollard, R. T., Salter, I., Sanders, R. J., Lucas, M. I., Moore, C. M., Mills, R. A., Statham, P. J., *et al.* 2009. Southern Ocean deep-water carbon export enhanced by natural iron fertilization. Nature, 457: 577–580.

Popp, B. N., Takigiku, R., Hayes, J. M., Louda, J. W., and Baker, E. W. 1989. The post-Paleozoic chronology and mechanism of 13 C depletion in primary marine organic matter. American Journal of Science, 289: 436–454. American Journal of Science.

Popp, B. N., Laws, E. A., Bidigare, R. R., Dore, J. E., Hanson, K. L., and Wakeham, S. G. 1998. Effect of Phytoplankton Cell Geometry on Carbon Isotopic Fractionation. Geochimica et Cosmochimica Acta, 62: 69–77.

Popp, B. N., Trull, T., Kenig, F., Wakeham, S. G., Rust, T. M., Tilbrook, B., Griffiths, B., *et al.* 1999. Controls on the carbon isotopic composition of southern ocean phytoplankton. Global Biogeochemical Cycles, 13: 827–843. John Wiley & Sons, Ltd.

Post, A. L., Meijers, A. J. S., Fraser, A. D., Meiners, K. M., Ayers, J., Bindoff, N. L., Griffiths, H. J., *et al.* 2014. Chapter 4.

Environmental Setting. Biogeographic Atlas of the Southern Ocean: 46–64. Scientific Committee on Antarctic Research Cambridge.

Post, D. M. 2002. Using stable isotopes to estimate trophic position: Models, Methods, and Assumptions. Ecology, 83: 703–718. John Wiley & Sons, Ltd.

Post, D. M., Layman, C. A., Arrington, D. A., Takimoto, G., Quattrochi, J., and Montaña, C. G. 2007. Getting to the fat of the matter: models, methods and assumptions for dealing with lipids in stable isotope analyses. Oecologia, 152: 179–189.

Prakash, S., Ramesh, R., Sheshshayee, M. S., Mohan, R., and Sudhakar, M. 2015. Nitrogen uptake rates and f-ratios in the Equatorial and Southern Indian Ocean. Current Science, 108: 239–245. Current Science Association.

Prend, C. J., Gray, A. R., Talley, L. D., Gille, S. T., Haumann, F. A., Johnson, K. S., Riser, S. C., *et al.* 2022. Indo-Pacific Sector Dominates Southern Ocean Carbon Outgassing. Global Biogeochemical Cycles, 36: e2021GB007226. John Wiley & Sons, Ltd.

Prézelin, B. B., Hofmann, E. E., Mengelt, C., and Klinck, J. M. 2000. The linkage between Upper Circumpolar Deep Water (UCDW) and phytoplankton assemblages on the west Antarctic Peninsula continental shelf. Journal of Marine Research, 58: 165–202. Sears Foundation for Marine Research.

Price, L. M. 2012. Microzooplankton Community Structure and Grazing Impact along the Western Antarctic Peninsula - Thesis. Master of Science (M.Sc.) - Virginia Institute of Marine Science.

Price, N. M., Andersen, L. F., and Morel, F. M. M. 1991. Iron and nitrogen nutrition of equatorial Pacific plankton. Deep Sea Research Part A. Oceanographic Research Papers, 38: 1361–1378. Elsevier.

Primer-E. 2009. Plymouth routines in multivariate ecological research. Plymouth Marine Laboratory Plymouth.

Priscu, J. C., and Sullivan, C. W. 1998. Nitrogen metabolism in Antarctic fast-ice microalgal assemblages. Antarctic sea ice: biological processes, interactions and variability, 73: 147–160. Wiley Online Library.

Probyn, T. A. 1985. Nitrogen uptake by size-fractionated phytoplankton populations in the southern Benguela upwelling system. Marine ecology progress series. Oldendorf, 22: 249–258.

Puccinelli, E., McQuaid, C. D., and Ansorge, I. J. 2018. Factors affecting trophic compositions of offshore benthic invertebrates at a sub-Antarctic archipelago. Limnology and Oceanography, 63: 2206–2228. John Wiley & Sons, Ltd.

Puccinelli, E., Smart, S. M., and Fawcett, S. E. 2020. Temporal variability in the trophic composition of benthic invertebrates in the Indian Sub-Antarctic Ocean. Deep Sea Research Part I: Oceanographic Research Papers, 163: 103340.

Putt, M., and Stoecker, D. K. 1989. An experimentally determined carbon: volume ratio for marine “oligotrichous” ciliates from estuarine and coastal waters. Limnology and Oceanography, 34: 1097–1103. Wiley Online Library.

Quéguiner, B. 2013. Iron fertilization and the structure of planktonic communities in high nutrient regions of the Southern Ocean. Deep Sea Research Part II: Topical Studies in Oceanography, 90: 43–54.

R Core Team, Rf. 2018. R: A language and environment for statistical computing. R foundation for statistical computing Vienna, Austria.

Rafter, P., Bagnell, Aa., DeVries, T., and Marconi, D. 2019. Dataset: Estimated nitrate d15N modeled using an ensemble of artificial neural networks (EANNs).

Rafter, P. A., DiFiore, P. J., and Sigman, D. M. 2013. Coupled nitrate nitrogen and oxygen isotopes and organic matter remineralization in the Southern and Pacific Oceans. Journal of Geophysical Research: Oceans, 118: 4781–4794. John Wiley & Sons, Ltd.

Ratnarajah, L., Nicol, S., and Bowie, A. R. 2018. Pelagic Iron Recycling in the Southern Ocean: Exploring the Contribution of Marine Animals.

Rau, G. H., Takahashi, T., and Marais, D. J. Des. 1989. Latitudinal variations in plankton δ13C: implications for CO2 and productivity in past oceans. Nature, 341: 516–518.

Rau, G. H., Teyssie, J. L., Rassoulzadegan, F., and Fowler, S. W. 1990. C-13/C-12 and N-15/N-14 variations among size-fractionated marine particles-Implications For their origin and trophic relationships. Marine Ecology Progress Series, 59: 33–38.

Rau, G. H., Sullivan, C. W., and Gordon, L. I. 1991a. δ13C and δ15N variations in Weddell Sea particulate organic matter. Marine

Chemistry, 35: 355–369.

Rau, G. H., Takahashi, T., Des Marais, D. J., and Sullivan, C. W. 1991b. Particulate organic matter δ13C variations across the Drake Passage. Journal of Geophysical Research: Oceans, 96: 15131–15135. John Wiley & Sons, Ltd.

Rau, G. H., Takahashi, T., Des Marais, D. J., Repeta, D. J., and Martin, J. H. 1992a. The relationship between δ13C of organic matter and [CO2(aq)] in ocean surface water: Data from a JGOFS site in the northeast Atlantic Ocean and a model. Geochimica et Cosmochimica Acta, 56: 1413–1419.

Rau, G. H., Ainley, D. G., Bengtson, J. L., Torres, J. J., and Hopkins, T. L. 1992b. 15 N/ 14 N and 13 C/ 12 C in Weddell Sea birds, seals, and fish: implications for diet and trophic structure. Marine Ecology Progress Series, 84: 1–8. Inter-Research Science Center.

Raven, J. A. 1988. The iron and molybdenum use efficiencies of plant growth with different energy, carbon and nitrogen sources. New Phytologist, 109: 279–287. Wiley Online Library.

Raven, J. A., and Johnston, A. M. 1991. Mechanisms of inorganic-carbon acquisition in marine phytoplankton and their implications for the use of other resources. Limnology and Oceanography, 36: 1701–1714. John Wiley & Sons, Ltd.

Raven, J. A., Wollenweber, B., and Handley, L. L. 1992. A comparison of ammonium and nitrate as nitrogen sources for photolithotrophs. New Phytologist, 121: 19–32. John Wiley & Sons, Ltd.

Raven, J. A. 1997. Inorganic Carbon Acquisition by Marine Autotrophs. *In* Classic Papers, pp. 85–209. Ed. by J. A. B. T.-A. in B. R. Callow. Academic Press.

Raven, J. A. 1998. The twelfth Tansley Lecture. Small is beautiful: the picophytoplankton. Functional ecology, 12: 503–513. Wiley Online Library.

Raven, J. A., Cockell, C. S., and De La Rocha, C. L. 2008. The evolution of inorganic carbon concentrating mechanisms in photosynthesis. Philosophical Transactions of the Royal Society B: Biological Sciences, 363: 2641–2650. Royal Society.

Redfield, A. C. 1934. On the proportions of organic derivatives in sea water and their relation to the composition of plankton. James Johnstone Memorial Volume: 176–192. The University Press.

Rembauville, M., Blain, S., Armand, L., Quéguiner, B., and Salter, I. 2014. Export fluxes in a naturally fertilized area of the Southern Ocean, the Kerguelen Plateau: ecological vectors of carbon and biogenic silica to depth (Part 2). Biogeosciences Discuss, 11: 17089–17150. Citeseer.

Rembauville, M., Blain, S., Armand, L., Quéguiner, B., and Salter, I. 2015. Export fluxes in a naturally iron-fertilized area of the Southern Ocean – Part 2: Importance of diatom resting spores and faecal pellets for export. Biogeosciences, 12: 3171–3195. Copernicus Publications.

Reynolds, C. S. 2006. The ecology of phytoplankton. Cambridge University Press.

Richoux, N. B., and Froneman, P. W. 2009. Plankton trophodynamics at the subtropical convergence, Southern Ocean. Journal of Plankton Research, 31: 1059–1073.

Rickaby, R. E. M., Henderiks, J., and Young, J. N. 2010. Perturbing phytoplankton : response and isotopic fractionation with changing carbonate chemistry in two coccolithophore species. Climate of the Past, 6: 771–785. Copernicus Publications on behalf of the European Geosciences Union, Palaeobiology, Department of Earth Sciences, Earth Sciences, Disciplinary Domain of Science and Technology, Uppsala University.

Rigual-Hernández, A. S., Trull, T. W., Bray, S. G., Cortina, A., and Armand, L. K. 2015. Latitudinal and temporal distributions of diatom populations in the pelagic waters of the Subantarctic and Polar Frontal zones of the Southern Ocean and their role in the biological pump. Biogeosciences, 12: 5309–5337. Copernicus Publications.

Roberts, D., Hopcroft, R. R., and Hosie, G. W. 2014. Southern Ocean Pteropods. Citeseer.

Robinson, C., Steinberg, D. K., Anderson, T. R., Arístegui, J., Carlson, C. A., Frost, J. R., Ghiglione, J.-F., *et al.* 2010. Mesopelagic zone ecology and biogeochemistry – a synthesis. Deep Sea Research Part II: Topical Studies in Oceanography, 57: 1504–1518.

Roeske, C. A., and O'Leary, M. H. 1984. Carbon isotope effects on enzyme-catalyzed carboxylation of ribulose bisphosphate. Biochemistry, 23: 6275–6284. American Chemical Society.

Rönner, U., Sörensson, F., and Holm-Hansen, O. 1983. Nitrogen assimilation by phytoplankton in the Scotia Sea. Polar Biology, 2: 137–147. Springer.

Rouault, M., Mélice, J.-L., Reason, C. J. C., and Lutjeharms, J. R. E. 2005. Climate variability at Marion Island, Southern Ocean, since 1960. Journal of Geophysical Research: Oceans, 110. John Wiley & Sons, Ltd.

Roukaerts, A., Cavagna, A.-J., Fripiat, F., Lannuzel, D., Meiners, K. M., and Dehairs, F. 2016. Sea-ice algal primary production and nitrogen uptake rates off East Antarctica. Deep Sea Research Part II: Topical Studies in Oceanography, 131: 140–149.

Saage, A., Altin, D., Vadstein, O., and Sommer, U. 2008. Trophic position of Calanus finmarchicus (Copepoda, Calanoida) in the Trondheim Fjord. Journal of Sea Research, 59: 162–172.

Safi, K. A., Brian Griffiths, F., and Hall, J. A. 2007. Microzooplankton composition, biomass and grazing rates along the WOCE SR3 line between Tasmania and Antarctica. Deep Sea Research Part I: Oceanographic Research Papers, 54: 1025–1041.

Sambrotto, R. N., and Mace, B. J. 2000. Coupling of biological and physical regimes across the Antarctic Polar Front as reflected by nitrogen production and recycling. Deep Sea Research Part II: Topical Studies in Oceanography, 47: 3339–3367.

Sarakinos, H. C., Johnson, M. L., and Zanden, M. J. Vander. 2002. A synthesis of tissue-preservation effects on carbon and nitrogen stable isotope signatures. Canadian Journal of Zoology, 80: 381–387. NRC Research Press.

Sarmiento, J. L., and Toggweiler, J. R. 1984. A new model for the role of the oceans in determining atmospheric P CO2. Nature, 308: 621–624. Nature Publishing Group.

Sarmiento, J. L., and Le Quere, C. 1996. Oceanic carbon dioxide uptake in a model of century-scale global warming. Science, 274: 1346–1350. American Association for the Advancement of Science.

Sarmiento, J. L. 2013. Ocean biogeochemical dynamics. *In* Ocean Biogeochemical Dynamics. Princeton University Press.

Scambos, T. A., Hulbe, C., Fahnestock, M., and Bohlander, J. 2000. The link between climate warming and break-up of ice shelves in the Antarctic Peninsula. Journal of Glaciology, 46: 516–530. Cambridge University Press.

Schallenberg, C., Bestley, S., Klocker, A., Trull, T. W., Davies, D. M., Gault-Ringold, M., Eriksen, R., *et al.* 2018. Sustained Upwelling of Subsurface Iron Supplies Seasonally Persistent Phytoplankton Blooms Around the Southern Kerguelen Plateau, Southern Ocean. Journal of Geophysical Research: Oceans, 123: 5986–6003.

Schlitzer, R. 2002. Carbon export fluxes in the Southern Ocean: results from inverse modeling and comparison with satellite-based estimates. Deep Sea Research Part II: Topical Studies in Oceanography, 49: 1623–1644.

Schlitzer, R. 2021. Ocean Data View.

Schmidt, K., Atkinson, A., Stübing, D., McClelland, J. W., Montoya, J. P., and Voss, M. 2003. Trophic relationships among Southern Ocean copepods and krill: Some uses and limitations of a stable isotope approach. Limnology and Oceanography, 48: 277–289. John Wiley & Sons, Ltd.

Schmidt, K., McClelland, J. W., Mente, E., Montoya, J. P., Atkinson, A., and Voss, M. 2004. Trophic-level interpretation based on δ15N values: implications of tissue-specific fractionation and amino acid composition. Marine Ecology Progress Series, 266: 43–58.

Schmidt, K., Atkinson, A., Petzke, K.-J., Voss, M., and Pond, D. W. 2006. Protozoans as a food source for Antarctic krill, Euphausia superba: Complementary insights from stomach content, fatty acids, and stable isotopes. Limnology and Oceanography, 51: 2409–2427. John Wiley & Sons, Ltd.

Schmidt, K., Atkinson, A., Pond, D. W., and Ireland, L. C. 2014. Feeding and overwintering of Antarctic krill across its major habitats: The role of sea ice cover, water depth, and phytoplankton abundance. Limnology and Oceanography, 59: 17–36. John Wiley & Sons, Ltd.

Schmidt, K., Brown, T. A., Belt, S. T., Ireland, L. C., Taylor, K. W. R., Thorpe, S. E., Ward, P., *et al.* 2018. Do pelagic grazers benefit from sea ice? Insights from the Antarctic sea ice proxy IPSO25. Biogeosciences, 15: 1987–2006. Copernicus Publications.

Schmidt, S. N., Olden, J. D., Solomon, C. T., and Zanden, M. J. Vander. 2007. Quantitative aproaches to the analysis of stable isotope food web data. Ecology, 88: 2793–2802. John Wiley & Sons, Ltd.

Schmoker, C., Hernández-León, S., and Calbet, A. 2013. Microzooplankton grazing in the oceans: impacts, data variability, knowledge gaps and future directions. Journal of Plankton Research, 35: 691–706.

Schoffman, H., Lis, H., Shaked, Y., and Keren, N. 2016. Iron–nutrient interactions within phytoplankton. Frontiers in plant science, 7: 1223. Frontiers Media SA.

Schwamborn, R., and Giarrizzo, T. 2015. Stable Isotope Discrimination by Consumers in a Tropical Mangrove Food Web: How Important Are Variations in C/N Ratio? Estuaries and Coasts, 38: 813–825.

Seeyave, S., Lucas, M. I., Moore, C. M., and Poulton, A. J. 2007. Phytoplankton productivity and community structure in the vicinity of the Crozet Plateau during austral summer 2004/2005. Deep Sea Research Part II: Topical Studies in Oceanography, 54: 2020–2044.

Séférian, R., Berthet, S., Yool, A., Palmiéri, J., Bopp, L., Tagliabue, A., Kwiatkowski, L., *et al.* 2020. Tracking Improvement in Simulated Marine Biogeochemistry Between CMIP5 and CMIP6. Current Climate Change Reports, 6: 95–119.

Sekerci, Y., and Petrovskii, S. 2015. Mathematical Modelling of Plankton–Oxygen Dynamics Under the Climate Change. Bulletin of Mathematical Biology, 77: 2325–2353.

Semeneh, M., Dehairs, F., Elskens, M., Baumann, M. E. M., Kopczynska, E. E., Lancelot, C., and Goeyens, L. 1998. Nitrogen uptake regime and phytoplankton community structure in the Atlantic and Indian sectors of the Southern Ocean. Journal of Marine Systems, 17: 159–177.

Seyboth, E., Botta, S., Mendes, C. R. B., Negrete, J., Dalla Rosa, L., and Secchi, E. R. 2018. Isotopic evidence of the effect of warming on the northern Antarctic Peninsula ecosystem. Deep Sea Research Part II: Topical Studies in Oceanography, 149: 218–228.

Sharp, Z. 2017. Principles of stable isotope geochemistry.

Shatova, O., Wing, S. R., Gault-Ringold, M., Wing, L., and Hoffmann, L. J. 2016. Seabird guano enhances phytoplankton production in the Southern Ocean. Journal of Experimental Marine Biology and Ecology, 483: 74–87. Elsevier.

Shaw, T. J., Raiswell, R., Hexel, C. R., Vu, H. P., Moore, W. S., Dudgeon, R., and Smith Jr, K. L. 2011. Input, composition, and potential impact of terrigenous material from free-drifting icebergs in the Weddell Sea. Deep Sea Research Part II: Topical Studies in Oceanography, 58: 1376–1383. Elsevier.

Sherr, E., and Sherr, B. 2007. Heterotrophic dinoflagellates: a significant component of microzooplankton biomass and major grazers of diatoms in the sea. Marine Ecology Progress Series, 352: 187–197.

Sherr, E. B., and Sherr, B. F. 2002. Significance of predation by protists in aquatic microbial food webs. Antonie Van Leeuwenhoek, 81: 293–308. Springer.

Sherrell, R. M., Annett, A. L., Fitzsimmons, J. N., Roccanova, V. J., and Meredith, M. P. 2018. A 'shallow bathtub ring' of local sedimentary iron input maintains the Palmer Deep biological hotspot on the West Antarctic Peninsula shelf. Philosophical Transactions of the Royal Society A: Mathematical, Physical and Engineering Sciences, 376: 20170171. Royal Society.

Siegel, D. A., Buesseler, K. O., Doney, S. C., Sailley, S. F., Behrenfeld, M. J., and Boyd, P. W. 2014. Global assessment of ocean carbon export by combining satellite observations and food-web models. Global Biogeochemical Cycles, 28: 181–196. Wiley Online Library.

Sigman, D. M., Altabet, M. A., McCorkle, D. C., François, R., and Fischer, G. 1999. The δ15N of nitrate in the southern ocean: Consumption of nitrate in surface waters. Global Biogeochemical Cycles, 13: 1149–1166. John Wiley & Sons, Ltd.

Sigman, D. M., Altabet, M. A., McCorkle, D. C., François, R., and Fischer, G. 2000. The δ15N of nitrate in the Southern Ocean: Nitrogen cycling and circulation in the ocean interior. Journal of Geophysical Research: Oceans, 105: 19599–19614. John Wiley & Sons, Ltd.

Sigman, D. M., Casciotti, K. L., Andreani, M., Barford, C., Galanter, M., and Böhlke, J. K. 2001. A Bacterial Method for the Nitrogen Isotopic Analysis of Nitrate in Seawater and Freshwater. Analytical Chemistry, 73: 4145–4153. American Chemical Society.

Sigman, D. M., Hain, M. P., and Haug, G. H. 2010. The polar ocean and glacial cycles in atmospheric CO2 concentration. Nature, 466: 47–55. Nature Publishing Group.

Sigman, D. M., and Fripiat, F. 2019. Nitrogen isotopes in the ocean. Encyclopedia of Ocean Sciences, 1: 263–278.

Silfer, J. A., Engel, M. H., and Macko, S. A. 1992. Kinetic fractionation of stable carbon and nitrogen isotopes during peptide bond hydrolysis: Experimental evidence and geochemical implications. Chemical Geology: Isotope Geoscience section, 101: 211–221.

Sink, K. J., Holness, S., Harris, L., Majiedt, P. A., Atkinson, L., Robinson, T., Kirkman, S., *et al.* 2012. National Biodiversity Assessment 2011: Technical Report. Volume 4: Marine and Coastal Component. South African National Biodiversity Institute, Pretoria.

Sixth Assessment Report of the Intergovernmental Panel on Climate Change. 2022. IPCC, 2022: Climate Change 2022: Impacts, Adaptation, and Vulnerability. 3056 pp.

Smart, S. M., Fawcett, S. E., Thomalla, S. J., Weigand, M. A., Reason, C. J. C., and Sigman, D. M. 2015. Isotopic evidence for nitrification in the Antarctic winter mixed layer. Global Biogeochemical Cycles, 29: 427–445. John Wiley & Sons, Ltd.

Smart, S. M., Fawcett, S. E., Ren, H., Schiebel, R., Tompkins, E. M., Martínez-García, A., Stirnimann, L., *et al.* 2020. The Nitrogen Isotopic Composition of Tissue and Shell-Bound Organic Matter of Planktic Foraminifera in Southern Ocean Surface Waters. Geochemistry, Geophysics, Geosystems, 21: e2019GC008440. John Wiley & Sons, Ltd.

Smetacek, V., Assmy, P., and Henjes, J. 2004. The role of grazing in structuring Southern Ocean pelagic ecosystems and biogeochemical cycles. Antarctic Science, 16: 541–558. Cambridge University Press.

Smith, R. C., and Stammerjohn, S. E. 2001. Variations of surface air temperature and sea-ice extent in the western Antarctic Peninsula region. Annals of Glaciology, 33: 493–500. Cambridge University Press.

Smith, R. E. H., and Kalff, J. 1982. Size-dependent phosphorus uptake kinetics and cell quota in phytoplankton 1. Journal of Phycology, 18: 275–284. Wiley Online Library.

Smith, S. 2020. Biogeochemical data - 2017 Winter Cruise Atlantic-Indian Southern Ocean [Data set]. Zenodo.

Smith, S., Altieri, K., Mdutyana, M., Walker, D., Parrott, R., Gallie, S., Spence, K., *et al.* 2022. Biogeochemical controls on ammonium accumulation in the surface layer of the Southern Ocean. Biogeosciences, 19: 715–741.

Smith, V. R. 2002. Climate change in the sub-Antarctic: an illustration from Marion Island. Climatic Change, 52: 345–357. Springer.

Smith, W. O., and Lancelot, C. 2004. Bottom-up versus top-down control in phytoplankton of the Southern Ocean. Antarctic Science, 16: 531–539. Cambridge University Press.

Sokolov, S., and Rintoul, S. R. 2009a. Circumpolar structure and distribution of the Antarctic Circumpolar Current fronts: 2. Variability and relationship to sea surface height. Journal of Geophysical Research: Oceans, 114: C11019.

Sokolov, S., and Rintoul, S. R. 2009b. Circumpolar structure and distribution of the Antarctic Circumpolar Current fronts: 1. Mean circumpolar paths. Journal of Geophysical Research: Oceans, 114: C11018.

Somes, C. J., Schmittner, A., Galbraith, E. D., Lehmann, M. F., Altabet, M. A., Montoya, J. P., Letelier, R. M., *et al.* 2010. Simulating the global distribution of nitrogen isotopes in the ocean. Global Biogeochemical Cycles, 24. John Wiley & Sons, Ltd.

Squire, V. A. 1998. The marginal ice zone.

St John Glew, K., Espinasse, B., Hunt, B. P. V, Pakhomov, E. A., Bury, S. J., Pinkerton, M., Nodder, S. D., *et al.* 2021. Isoscape Models of the Southern Ocean: Predicting Spatial and Temporal Variability in Carbon and Nitrogen Isotope Compositions of Particulate Organic Matter. Global Biogeochemical Cycles, 35: e2020GB006901. John Wiley & Sons, Ltd.

Stammerjohn, S., Massom, R., Rind, D., and Martinson, D. 2012. Regions of rapid sea ice change: An inter-hemispheric seasonal comparison. Geophysical Research Letters, 39. Wiley Online Library.

Steinberg, D. K., and Landry, M. R. 2017. Zooplankton and the Ocean Carbon Cycle. Annual Review of Marine Science, 9: 413–444. Annual Reviews.

Stirnimann, L., Bornman, T. G., Verheye, H. M., Bachèlery, M.-L., van der Poel, J., and Fawcett, S. E. 2021. Plankton community composition and productivity near the Subantarctic Prince Edward Islands archipelago in autumn. Limnology and Oceanography, 66: 4140–4158. John Wiley & Sons, Ltd.

Stoecker, D. K. 1999. Mixotrophy among Dinoflagellates1. Journal of Eukaryotic Microbiology, 46: 397–401. John Wiley & Sons, Ltd.

Stoecker, D. K., Hansen, P. J., Caron, D. A., and Mitra, A. 2017. Mixotrophy in the marine plankton. Annual Review of Marine Science, 9: 311–335. Annual Reviews.

Stolte, W., and Riegman, R. 1995. Effect of phytoplankton cell size on transient-state nitrate and ammonium uptake kinetics. Microbiology, 141: 1221–1229. Microbiology Society.

Storlazzi, C. D., Cheriton, O. M., Van Hooidonk, R., Zhao, Z., and Brainard, R. 2020. Internal tides can provide thermal refugia that will buffer some coral reefs from future global warming. Scientific reports, 10: 1–9. Nature Publishing Group.

Stowasser, G., Atkinson, A., McGill, R. A. R., Phillips, R. A., Collins, M. A., and Pond, D. W. 2012. Food web dynamics in the Scotia Sea in summer: A stable isotope study. Deep Sea Research Part II: Topical Studies in Oceanography, 59–60: 208–221.

Strickland, J. D. H., and Parsons, T. R. 1972. A practical handbook of seawater analysis. Fisheries research board of Canada.

Strutton, P. G., Lovenduski, N. S., Mongin, M., and Matear, R. 2012. Quantification of Southern Ocean phytoplankton biomass and primary productivity via satellite observations and biogeochemical models. Ccamlr Science, 19: 247–265.

Suaria, G., Perold, V., Lee, J. R., Lebouard, F., Aliani, S., and Ryan, P. G. 2020. Floating macro- and microplastics around the Southern Ocean: Results from the Antarctic Circumnavigation Expedition. Environment International, 136: 105494.

Sullivan, C. W., Arrigo, K. R., McClain, C. R., Comiso, J. C., and Firestone, J. 1993. Distributions of Phytoplankton Blooms in the Southern Ocean. Science, 262: 1832–1837. American Association for the Advancement of Science.

Sun, J., and Liu, D. 2003. Geometric models for calculating cell biovolume and surface area for phytoplankton. Journal of Plankton Research, 25: 1331–1346.

Sunda, W. G., and Huntsman, S. A. 1997. Interrelated influence of iron, light and cell size on marine phytoplankton growth. Nature, 390: 389–392.

Sunda, W. G., and Hardison, R. D. 2007. Ammonium uptake and growth limitation in marine phytoplankton. Limnology and Oceanography, 52: 2496–2506. John Wiley & Sons, Ltd.

Sutherland, K. R., Madin, L. P., and Stocker, R. 2010. Filtration of submicrometer particles by pelagic tunicates. Proceedings of the National Academy of Sciences, 107: 15129–15134. Proceedings of the National Academy of Sciences.

Suttle, C. A., Chan, A. M., Taylor, W. D., and Harrison, P. J. 1986. Grazing of planktonic diatoms by microflagellates. Journal of Plankton Research, 8: 393–398. Oxford University Press.

Swart, S., Thomalla, S. J., and Monteiro, P. M. S. 2015. The seasonal cycle of mixed layer dynamics and phytoplankton biomass in the Sub-Antarctic Zone: A high-resolution glider experiment. Journal of Marine Systems, 147: 103–115.

Sweeting, C. J., Polunin, N. V. C., and Jennings, S. 2004. Tissue and fixative dependent shifts of δ13C and δ15N in preserved ecological material. Rapid Communications in Mass Spectrometry, 18: 2587–2592. John Wiley & Sons, Ltd.

Syväranta, J., Vesala, S., Rask, M., Ruuhijärvi, J., and Jones, R. I. 2008. Evaluating the utility of stable isotope analyses of archived freshwater sample materials. Hydrobiologia, 600: 121–130.

Syväranta, J., and Rautio, M. 2010. Zooplankton, lipids and stable isotopes: importance of seasonal, latitudinal, and taxonomic differences. Canadian Journal of Fisheries and Aquatic Sciences, 67: 1721–1729.

Tagliabue, A., Sallée, J.-B., Bowie, A. R., Lévy, M., Swart, S., and Boyd, P. W. 2014. Surface-water iron supplies in the Southern Ocean sustained by deep winter mixing. Nature Geoscience, 7: 314–320.

Tagliabue, A., and Arrigo, K. R. 2016. Decadal trends in air-sea CO2 exchange in the Ross Sea (Antarctica). Geophysical Research Letters, 43: 5271–5278. John Wiley & Sons, Ltd.

Takahashi, T., Sutherland, S. C., Wanninkhof, R., Sweeney, C., Feely, R. A., Chipman, D. W., Hales, B., *et al.* 2009. Climatological mean and decadal change in surface ocean pCO2, and net sea–air CO2 flux over the global oceans. Deep Sea Research Part II: Topical Studies in Oceanography, 56: 554–577. Elsevier.

Talley, L. D. 2011. Descriptive physical oceanography: an introduction. Academic press.

Tamelander, T., Kivimäe, C., Bellerby, R. G. J., Renaud, P. E., and Kristiansen, S. 2009. Base-line variations in stable isotope values in an Arctic marine ecosystem: effects of carbon and nitrogen uptake by phytoplankton. Hydrobiologia, 630: 63–73.

Tarling, G. A., and Johnson, M. L. 2006. Satiation gives krill that sinking feeling. Current Biology, 16: R83–R84. Elsevier.

Teinturier, S., Stegner, A., Didelle, H., and Viboud, S. 2010. Small-scale instabilities of an island wake flow in a rotating shallow-water layer. Dynamics of atmospheres and oceans, 49: 1–24. Elsevier.

Thibodeau, P., Song, B., Moreno, C., and Steinberg, D. K. 2022. Feeding ecology and microbiome of the pteropod Limacina helicina antarctica. Aquatic Microbial Ecology, 88: 19–24.

Thomalla, S. J., Waldron, H. N., Lucas, M. I., Read, J. F., Ansorge, I. J., and Pakhomov, E. 2011. Phytoplankton distribution and nitrogen dynamics in the southwest indian subtropical gyre and Southern Ocean waters. Ocean Science, 7: 113–127.

Thomas, D. N., and Dieckmann, G. S. 2002. Antarctic Sea Ice--a Habitat for Extremophiles. Science, 295: 641–644. American Association for the Advancement of Science.

Tieszen, L. L., Boutton, T. W., Tesdahl, K. G., and Slade, N. A. 1983. Fractionation and turnover of stable carbon isotopes in animal tissues: implications for δ13C analysis of diet. Oecologia, 57: 32–37. Springer.

Timmermans, K. R., Stolte, W., and de Baar, H. J. W. 1994. Iron-mediated effects on nitrate reductase in marine phytoplankton. Marine Biology, 121: 389–396.

Timmermans, K. R., Van Leeuwe, M. A., De Jong, J. T. M., McKay, R. M. L., Nolting, R. F., Witte, H. J., Van Ooyen, J., *et al.* 1998. Iron stress in the Pacific region of the Southern Ocean: evidence from enrichment bioassays. Marine Ecology Progress Series, 166: 27–41.

Timmermans, K. R., van der Wagt, B., and de Baar, H. J. W. 2004. Growth rates, half-saturation constants, and silicate, nitrate, and phosphate depletion in relation to iron availability of four large, open-ocean diatoms from the Southern Ocean. Limnology and Oceanography, 49: 2141–2151. John Wiley & Sons, Ltd.

Tortell, P. D., Reinfelder, J. R., and Morel, F. M. M. 1997. Active uptake of bicarbonate by diatoms. Nature, 390: 243–244.

Tortell, P. D., Payne, C. D., Li, Y., Trimborn, S., Rost, B., Smith, W. O., Riesselman, C., *et al.* 2008. CO2 sensitivity of Southern Ocean phytoplankton. Geophysical Research Letters, 35. Wiley Online Library.

Tortell, P. D., Long, M. C., Payne, C. D., Alderkamp, A.-C., Dutrieux, P., and Arrigo, K. R. 2012. Spatial distribution of pCO2, ΔO2/Ar and dimethylsulfide (DMS) in polynya waters and the sea ice zone of the Amundsen Sea, Antarctica. Deep Sea Research Part II: Topical Studies in Oceanography, 71–76: 77–93.

Traganza, E. D., Nestor, D. A., and McDonald, A. K. 1980. Satellite observations of a nutrient upwelling off the coast of California. Journal of Geophysical Research: Oceans, 85: 4101–4106. Wiley Online Library.

Trathan, P. N., and Hill, S. L. 2016. The Importance of Krill Predation in the Southern Ocean BT - Biology and Ecology of Antarctic Krill. *In* pp. 321–350. Ed. by V. Siegel. Springer International Publishing, Cham.

Treasure, A. M., Ruzicka, J. J., Moloney, C. L., Gurney, L. J., and Ansorge, I. J. 2015. Land–Sea Interactions and Consequences for Sub-Antarctic Marine Food Webs. Ecosystems, 18: 752–768.

Treasure, A. M., Ruzicka, J. J., Pakhomov, E. A., and Ansorge, I. J. 2019. Physical Transport Mechanisms Driving Sub-Antarctic Island Marine Ecosystems. Ecosystems, 22: 1069–1087.

Trebilco, R., Melbourne-Thomas, J., and Constable, A. J. 2020. The policy relevance of Southern Ocean food web structure: Implications of food web change for fisheries, conservation and carbon sequestration. Marine Policy, 115: 103832. Elsevier.

Tréguer, P., and Pondaven, P. 2000. Silica control of carbon dioxide. Nature, 406: 358–359.

Tréguer, P. J. 2014. The Southern Ocean silica cycle. Comptes Rendus Geoscience, 346: 279–286.

Treibergs, L. A., Fawcett, S. E., Lomas, M. W., and Sigman, D. M. 2014. Nitrogen isotopic response of prokaryotic and eukaryotic phytoplankton to nitrate availability in Sargasso Sea surface waters. Limnology and Oceanography, 59: 972–985. John Wiley & Sons, Ltd.

Trenberth, K. E., Large, W. G., and Olson, J. G. 1990. The mean annual cycle in global ocean wind stress. Journal of Physical Oceanography, 20: 1742–1760. American Meteorological Society.

Trueman, C. N., and St John Glew, K. 2019. Chapter 6 - Isotopic Tracking of Marine Animal Movement. *In* pp. 137–172. Ed. by K. A. Hobson and L. I. B. T.-T. A. M. with S. I. (Second E. Wassenaar. Academic Press.

Trull, T. W., and Armand, L. 2001. Insights into Southern Ocean carbon export from the δ13C of particles and dissolved inorganic carbon during the SOIREE iron release experiment. Deep Sea Research Part II: Topical Studies in Oceanography, 48: 2655–2680.

Trull, T. W., Davies, D., and Casciotti, K. 2008. Insights into nutrient assimilation and export in naturally iron-fertilized waters of the Southern Ocean from nitrogen, carbon and oxygen isotopes. Deep Sea Research Part II: Topical Studies in Oceanography, 55: 820–840.

Tuerena, R. E., Ganeshram, R. S., Humphreys, M. P., Browning, T. J., Bouman, H., and Piotrowski, A. P. 2019. Isotopic fractionation of carbon during uptake by phytoplankton across the South Atlantic subtropical convergence. Biogeosciences, 16: 3621–3635. Copernicus Publications.

Turner, J., Bracegirdle, T. J., Phillips, T., Marshall, G. J., and Hosking, J. S. 2013. An initial assessment of Antarctic sea ice extent in the CMIP5 models. Journal of Climate, 26: 1473–1484.

Turner, J. T. 2015. Zooplankton fecal pellets, marine snow, phytodetritus and the ocean's biological pump. Progress in Oceanography, 130: 205–248.

Uitz, J., Claustre, H., Morel, A., and Hooker, S. B. 2006. Vertical distribution of phytoplankton communities in open ocean: An assessment based on surface chlorophyll. Journal of Geophysical Research: Oceans, 111. John Wiley & Sons, Ltd.

UKMO. 2005. GHRSST Level 4 OSTIA Global Foundation Sea Surface Temperature Analysis. NASA Physical Oceanography DAAC.

Uye, S., and Kayano, Y. 1994. Predatory Feeding Behavior of Tortanus (Copepoda: Calanoida): Life-stage Differences and the Predation Impact on Small Planktonic Crustaceans. Journal of Crustacean Biology, 14: 473–483.

Van Ballegooyen, R. C., Perissinotto, R., Ismail, A., Boden, B. R., Lucas, M., Allanson, B. R., and Lutjeharms, J. R. E. 1989. Data report of the second cruise of the Marion Offshore Ecological Study (MOES II). CSIR Report EMA-D, 8910.

van Leeuwe, M. A., Webb, A. L., Venables, H. J., Visser, R. J. W., Meredith, M. P., Elzenga, J. T. M., and Stefels, J. 2020. Annual patterns in phytoplankton phenology in Antarctic coastal waters explained by environmental drivers. Limnology and Oceanography, 65: 1651–1668. John Wiley & Sons, Ltd.

Van Oostende, N., Fawcett, S. E., Marconi, D., Lueders-Dumont, J., Sabadel, A. J. M., Woodward, E. M. S., Jönsson, B. F., *et al.* 2017. Variation of summer phytoplankton community composition and its relationship to nitrate and regenerated nitrogen assimilation across the North Atlantic Ocean. Deep Sea Research Part I: Oceanographic Research Papers, 121: 79–94.

van Rossum, G. 1995. Python reference manual. Department of Computer Science [CS]. CWI.

Vander Zanden, M. J., Cabana, G., and Rasmussen, J. B. 1997. Comparing trophic position of freshwater fish calculated using stable nitrogen isotope ratios (δ15N) and literature dietary data. Canadian Journal of Fisheries and Aquatic Sciences, 54: 1142–1158. NRC Research Press.

Vargas, C. A., and Madin, L. P. 2004. Zooplankton feeding ecology: clearance and ingestion rates of the salps Thalia democratica, Cyclosalpa affinis and Salpa cylindrica on naturally occurring particles in the Mid-Atlantic Bight. Journal of Plankton Research, 26: 827–833.

Vargas, C. A., Escribano, R., and Poulet, S. 2006. phytoplankton food quality determines time windows for successful zooplankton reproductive pulses. Ecology, 87: 2992–2999. John Wiley & Sons, Ltd.

Venkatachalam, S., Matcher, G. F., Lamont, T., van den Berg, M., Ansorge, I. J., and Dorrington, R. A. 2019. Influence of oceanographic variability on near-shore microbial communities of the sub-Antarctic Prince Edward Islands. Limnology and Oceanography, 64: 258–271. John Wiley & Sons, Ltd.

Ventura, M., and Catalan, J. 2008. Incorporating life histories and diet quality in stable isotope interpretations of crustacean zooplankton. Freshwater Biology, 53: 1453–1469. John Wiley & Sons, Ltd.

Ventura, M., and Jeppesen, E. 2009. Effects of fixation on freshwater invertebrate carbon and nitrogen isotope composition and its arithmetic correction. Hydrobiologia, 632: 297–308.

Verdy, A., and Mazloff, M. R. 2017. A data assimilating model for estimating Southern Ocean biogeochemistry. Journal of Geophysical Research: Oceans, 122: 6968–6988. John Wiley & Sons, Ltd.

Vereshchaka, A., Musaeva, E., and Lunina, A. 2021. Biogeography of the Southern Ocean: environmental factors driving mesoplankton distribution South of Africa. PeerJ, 9: e11411. PeerJ Inc.

Verheye, H. M., and Makhado, A. B. 2014. 2014 Marion Relief Voyage 011 of MV SA Agulhas II, Voyage Report: Ship- and Shore-based Research, 02 April – 06 May 2014. 175 pp.

Verheye, H. M. 2017. 2017 Marion Island Relief Voyage 024 of MV SA Agulhas II. Cruise Report: Ship-based science programme: Oceanographic and benthic monitoring and research in the Southern Ocean, 06 April-12 May 2017. Department of Environmental Affairs: Oceans and Coasts Research, Cape Town. 122 pp.

Verity, P. G., and Lagdon, C. 1984. Relationships between lorica volume, carbon, nitrogen, and ATP content of tintinnids In Narragansett Bay. Journal of Plankton Research, 6: 859–868.

Vernet, M., Sines, K., Chakos, D., Cefarelli, A. O., and Ekern, L. 2011. Impacts on phytoplankton dynamics by free-drifting icebergs in the NW Weddell Sea. Deep Sea Research Part II: Topical Studies in Oceanography, 58: 1422–1435. Elsevier.

Vernet, M., Smith Jr, K. L., Cefarelli, A. O., Helly, J. J., Kaufmann, R. S., Lin, H., Long, D. G., *et al.* 2012. Islands of ice: Influence of free-drifting Antarctic icebergs on pelagic marine ecosystems. Oceanography, 25.

Vidussi, F., Claustre, H., Manca, B. B., Luchetta, A., and Marty, J.-C. 2001. Phytoplankton pigment distribution in relation to upper thermocline circulation in the eastern Mediterranean Sea during winter. Journal of Geophysical Research: Oceans, 106: 19939–19956. John Wiley & Sons, Ltd.

Villinski, J. C., Hayes, J. M., Brassell, S. C., Riggert, V. L., and Dunbar, R. B. 2008. Sedimentary sterols as biogeochemical indicators in the Southern Ocean. Organic Geochemistry, 39: 567–588.

Volk, T., and Hoffert, M. I. 1985. Ocean Carbon Pumps: Analysis of Relative Strengths and Efficiencies in Ocean-Driven Atmospheric CO2 Changes. The Carbon Cycle and Atmospheric CO2: Natural Variations Archean to Present: 99–110.

von der Meden, C. E. O., Atkinson, L. J., Branch, G. M., Asdar, S., Ansorge, I. J., and van den Berg, M. 2017. Long-term change in epibenthic assemblages at the Prince Edward Islands: a comparison between 1988 and 2013. Polar Biology, 40: 2171–2185.

Voronina, N. M. 1998. Comparative abundance and distribution of major filter-feeders in the Antarctic pelagic zone. Journal of Marine Systems, 17: 375–390. Elsevier.

Voss, M., Bange, H. W., Dippner, J. W., Middelburg, J. J., Montoya, J. P., and Ward, B. 2013. The marine nitrogen cycle: recent discoveries, uncertainties and the potential relevance of climate change. Philosophical Transactions of the Royal Society B: Biological Sciences, 368: 20130121. Royal Society.

Wada, E., Terazaki, M., Kabaya, Y., and Nemoto, T. 1987. 15N and 13C abundances in the Antartic Ocean with emphasis on the biogeochemical structure of the food web. Deep Sea Research Part A. Oceanographic Research Papers, 34: 829–841.

Wada, E., and Hattori, A. 1991. Variation of 15N/14N in nitrogen cycling and its significance in marine environments. Nitrogen in the Sea: Forms, Abundances, and Rate Processes: 141–176. CRC Press Boca Raton, Fla.

Wada, E. 2009. Stable δ15N and δ13C isotope ratios in aquatic ecosystems. Proceedings of the Japan Academy, Series B, 85: 98–107. The Japan Academy.

Wafar, M., L'Helguen, S., Raikar, V., Maguer, J.-F., and Corre, P. Le. 2004. Nitrogen uptake by size-fractionated plankton in permanently well-mixed temperate coastal waters. Journal of Plankton Research, 26: 1207–1218.

Wainman, B. C. 1997. Lipids in freshwater ecosystems. Springer: NY.

Wainright, S. C., Haney, J. C., Kerr, C., Golovkin, A. N., and Flint, M. V. 1998. Utilization of nitrogen derived from seabird guano by terrestrial and marine plants at St. Paul, Pribilof Islands, Bering Sea, Alaska. Marine Biology, 131: 63–71.

Wallace, M. I., Cottier, F. R., Brierley, A. S., and Tarling, G. A. 2013. Modelling the influence of copepod behaviour on faecal pellet export at high latitudes. Polar Biology, 36: 579–592. Springer.

Wallschuss, S., Mdutyana, M., Parrott, R. G., Forrer, H. J., Roman, R., Walker, D. R., Ansorge, I. J., *et al.* 2022. The influence of Agulhas leakage on primary production and nitrogen cycling in the southeastern Atlantic Ocean. Journal of Geophysical Research: Oceans, 127: e2022JC018971. Wiley Online Library.

Walsh, J., and Reiss, C. 2020. Lipid content and stable isotopes of zooplankton during five winters around the northern Antarctic Peninsula. Scientific Data, 7: 380.

Walton, D. W. H., and Thomas, J. 2018. Cruise Report-Antarctic Circumnavigation Expedition (ACE) 20th December 2016-19th March 2017. OpenAIRE: Birmingham, UK: 1–380.

Wang, S., Kranz, S. A., Kelly, T. B., Song, H., Stukel, M. R., and Cassar, N. 2020. Lagrangian Studies of Net Community Production: The Effect of Diel and Multiday Nonsteady State Factors and Vertical Fluxes on O2/Ar in a Dynamic Upwelling Region. Journal of Geophysical Research: Biogeosciences, 125: e2019JG005569. John Wiley & Sons, Ltd.

Ward, P., and Shreeve, R. S. 1995. Egg production in three species of Antarctic Calanoid Copepods during an austral summer. Deep Sea Research Part I: Oceanographic Research Papers, 42: 721–735.

Waser, N. A., Yin, K., Yu, Z., Tada, K., Harrison, P. J., and Turpin, D. H. 1998. Nitrogen isotope fractionation during nitrate, ammonium and urea uptake by marine diatoms and coccolithophores under various conditions of N availability. Marine Ecology Progress Series, 169: 29–41.

Wassmann, P. 1997. Retention versus export food chains: processes controlling sinking loss from marine pelagic systems. Hydrobiologia, 363: 29–57.

Weigand, M. A., Foriel, J., Barnett, B., Oleynik, S., and Sigman, D. M. 2016. Updates to instrumentation and protocols for isotopic analysis of nitrate by the denitrifier method. Rapid Communications in Mass Spectrometry, 30: 1365–1383. Wiley Online Library.

Weldrick, C. K., Trebilco, R., Davies, D. M., and Swadling, K. M. 2019. Trophodynamics of Southern Ocean pteropods on the southern Kerguelen Plateau. Ecology and Evolution, 9: 8119–8132. John Wiley & Sons, Ltd.

Welschmeyer, N. A. 1994. Fluorometric analysis of chlorophyll a in the presence of chlorophyll b and pheopigments. Limnology and Oceanography, 39: 1985–1992. John Wiley & Sons, Ltd.

Welti, N., Striebel, M., Ulseth, A. J., Cross, W. F., DeVilbiss, S., Glibert, P. M., Guo, L., *et al.* 2017. Bridging food webs, ecosystem metabolism, and biogeochemistry using ecological stoichiometry theory. Frontiers in microbiology, 8: 1298. Frontiers Media SA.

West, J. B., Bowen, G. J., Dawson, T. E., and Tu, K. P. 2009. Isoscapes: understanding movement, pattern, and process on Earth through isotope mapping. Springer.

Westwood, K. J., Griffiths, F. B., Meiners, K. M., and Williams, G. D. 2010. Primary productivity off the Antarctic coast from 30°–80° E; BROKE-West survey, 2006. Deep Sea Research Part II: Topical Studies in Oceanography, 57: 794–814. Elsevier.

Whitworth III, T., and Nowlin Jr., W. D. 1987. Water masses and currents of the Southern Ocean at the Greenwich Meridian. Journal of Geophysical Research: Oceans, 92: 6462–6476. John Wiley & Sons, Ltd.

Williams, T. J., Wagner, A. J., Sikes, E. L., and Martin, E. E. 2021. Evolution of the Oceanic 13C Suess Effect in the Southeastern Indian Ocean Between 1994 and 2018. Geochemistry, Geophysics, Geosystems, 22: e2020GC009402. John Wiley & Sons, Ltd.

Wing, S. R., Jack, L., Shatova, O., Leichter, J. J., Barr, D., Frew, R. D., and Gault-Ringold, M. 2014. Seabirds and marine mammals redistribute bioavailable iron in the Southern Ocean. Marine Ecology Progress Series, 510: 1–13.

Wong, W. W., and Sackett, W. M. 1978. Fractionation of stable carbon isotopes by marine phytoplankton. Geochimica et Cosmochimica Acta, 42: 1809–1815.

Wright, S. W., Thomas, D. P., Marchant, H. J., Higgins, H. W., and Mackey, M. D. 1996. Analysis of phytoplankton of the Australian sector of the Southern Ocean: comparisons of microscopy and size frequency data with interpretations of pigment HPLC data using the \'CHEMTAX\' matrix factorisation program. Marine Ecology Progress Series, 144: 285–298.

Yang, E. J., Jiang, Y., and Lee, S. 2016. Microzooplankton herbivory and community structure in the Amundsen Sea, Antarctica. Deep Sea Research Part II: Topical Studies in Oceanography, 123: 58–68.

Yang, G., Atkinson, A., Hill, S. L., Guglielmo, L., Granata, A., and Li, C. 2021. Changing circumpolar distributions and isoscapes of Antarctic krill: Indo-Pacific habitat refuges counter long-term degradation of the Atlantic sector. Limnology and Oceanography, 66: 272–287. John Wiley & Sons, Ltd.

Yen, J. 1991. Predatory feeding behavior of an Antarctic marine copepod, Euchaeta antarctica. Polar research, 10: 433–442. Wiley Online Library.

Yool, A., Martin, A. P., Fernández, C., and Clark, D. R. 2007. The significance of nitrification for oceanic new production. Nature, 447: 999–1002. Nature Publishing Group.

Yoshikawa, C., Ogawa, N. O., Chikaraishi, Y., Makabe, A., Matsui, Y., Sasai, Y., Wakita, M., *et al.* 2022. Nitrogen Isotopes of Sinking Particles Reveal the Seasonal Transition of the Nitrogen Source for Phytoplankton. Geophysical Research Letters, 49: e2022GL098670. John Wiley & Sons, Ltd.

Yoshioka, T., Wada, E., and Hayashi, H. 1994. A Stable Isotope Study on Seasonal Food Web Dynamics in a Eutrophic Lake. Ecology, 75: 835–846. John Wiley & Sons, Ltd.

Zanden, M. J. Vander, and Rasmussen, J. B. 1999. Primary Consumer δ 13C and δ 15N and the Trophic Position of Aquatic Consumers. Ecology, 80: 1395–1404. Ecological Society of America.

Zeldis, J., James, M. R., Grieve, J., and Richards, L. 2002. Omnivory by copepods in the New Zealand Subtropical Frontal Zone. Journal of Plankton Research, 24: 9–23.

Zeldis, J. R., and Décima, M. 2020. Mesozooplankton connect the microbial food web to higher trophic levels and vertical export in the New Zealand Subtropical Convergence Zone. Deep Sea Research Part I: Oceanographic Research Papers, 155: 103146.

Zhang, L., Altabet, M. A., Wu, T., and Hadas, O. 2007. Sensitive Measurement of NH4+ 15N/14N (δ15NH4+) at Natural Abundance

Levels in Fresh and Saltwaters. Analytical Chemistry, 79: 5297–5303. American Chemical Society.

Zhang, R., Ma, Q., Chen, M., Zheng, M., Cao, J., and Qiu, Y. 2019. Nitrogen uptake regime regulated by ice melting during austral summer in the Prydz Bay, Antarctica. Acta Oceanologica Sinica, 38: 1–7.

Zhang, Y., Lacan, F., and Jeandel, C. 2008. Dissolved rare earth elements tracing lithogenic inputs over the Kerguelen Plateau (Southern Ocean). Deep Sea Research Part II: Topical Studies in Oceanography, 55: 638–652.

Appendices

Appendix A - A circum-Antarctic plankton isoscape I: Carbon export potential across the Southern Ocean

a. Observed versus satellite-derived measurements of sea surface temperature

In this study, two estimates of Sea Surface Temperature (SST) were considered:

1) Measurements from sensors installed on the ship's Aqualine Ferrybox system that was connected to the underway seawater supply during the Antarctic Circumnavigation Expedition (ACE). Data were collected continuously except for during periods when the underway system pump was switched off. Data are provided at 1-minute intervals along the cruise track (Haumann *et al.*, (2020); https://zenodo.org/record/3660852).
2) Daily high-resolution sea surface temperature (GHRSST) Level 4 data on a global 0.054° grid from the Operational Sea Surface Temperature and Sea Ice Analysis (OSTIA) database (https://podaac.jpl.nasa.gov/dataset/UKMO-L4HRfnd-GLOB-OSTIA; UKMO 2005).

Both SST data types were merged at the closest geographical point to yield a record for the entire cruise track. The data show roughly the same geographical distribution (Figure A.1) with a median difference between the two datasets of 0.99±0.8°C, indicating very good agreement. However, because of some irregularities in the data from the Aqualine Ferrybox system (e.g., between 40 and 50°S, from 56 to 67°S, and at 150°E; red dots in Figure A.1), we chose to use the GHRSST product in our analysis.

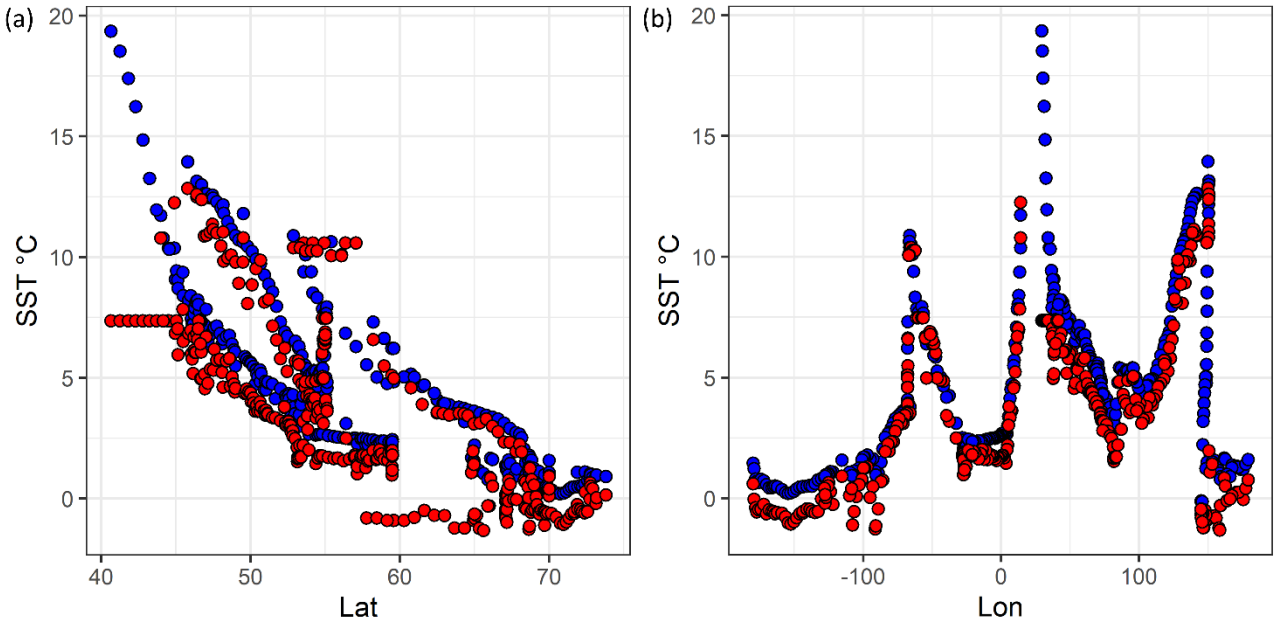

Figure A.1 Sea Surface Temperature (SST; °C) from Aqualine Ferrybox system (Red dots) and from GHRSST product (Blue dots) distributed along (a) latitude (Lat; °S) and (b) longitude (Lon; °E).

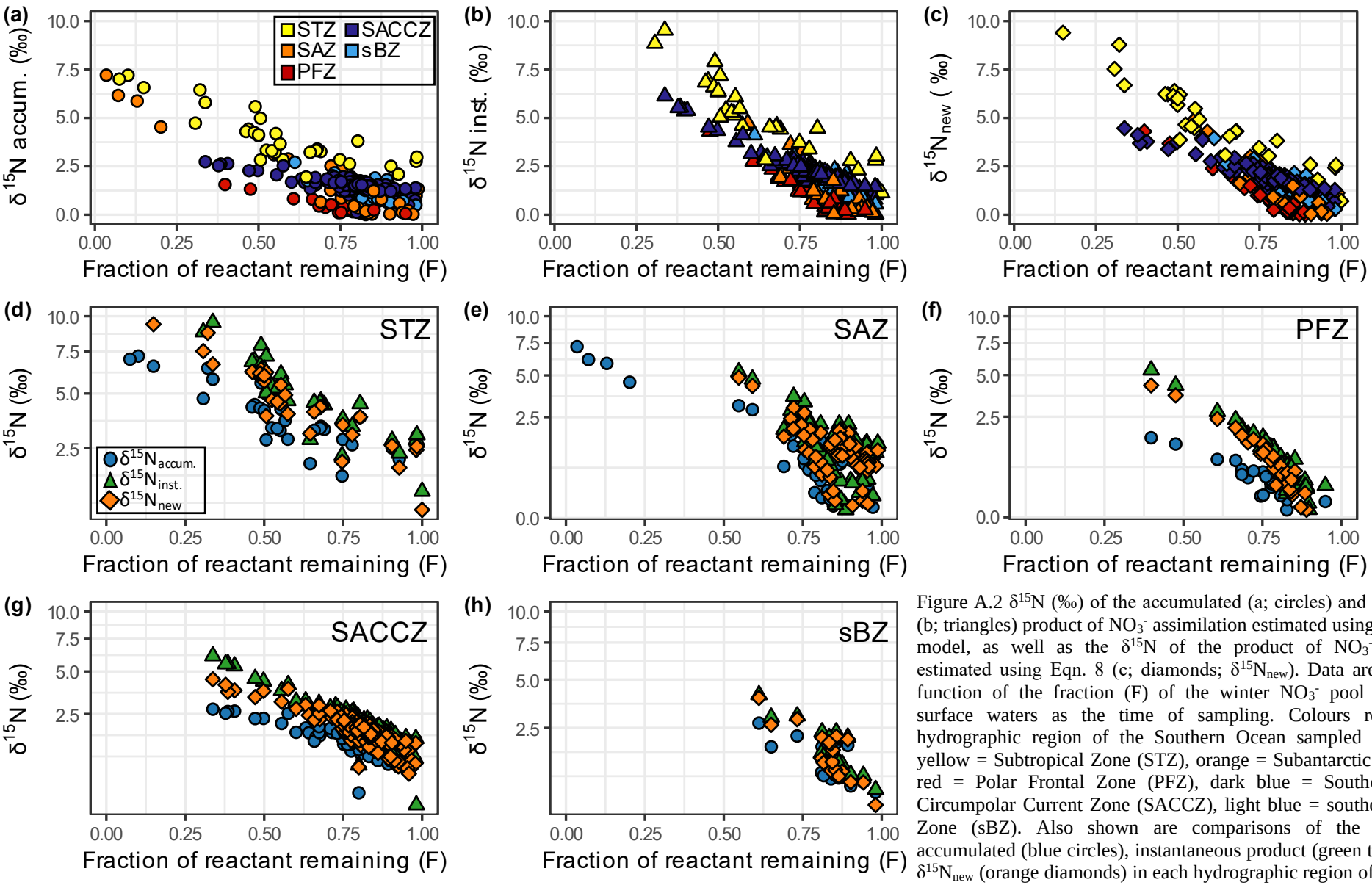

Figure A.2 $\delta^{15}N$ (‰) of the accumulated (a; circles) and instantaneous (b; triangles) product of NO_3^- assimilation estimated using the Rayleigh model, as well as the $\delta^{15}N$ of the product of NO_3^- assimilation estimated using Eqn. 8 (c; diamonds; $\delta^{15}N_{new}$). Data are plotted as a function of the fraction (F) of the winter NO_3^- pool remaining in surface waters as the time of sampling. Colours refer to each hydrographic region of the Southern Ocean sampled during ACE: yellow = Subtropical Zone (STZ), orange = Subantarctic Zone (SAZ), red = Polar Frontal Zone (PFZ), dark blue = Southern Antarctic Circumpolar Current Zone (SACCZ), light blue = southern Boundary Zone (sBZ). Also shown are comparisons of the $\delta^{15}N$ of the accumulated (blue circles), instantaneous product (green triangles), and $\delta^{15}N_{new}$ (orange diamonds) in each hydrographic region of the Southern Ocean sampled during ACE: STZ (d), SAZ (e), PFZ (f), SACCZ (g), and sBZ (h). Y-axes of panels d-h are squared root transformed.

b. Comparison of the observed and b-SOSE-derived source NO_3^- concentrations

During the Antarctic Circumnavigation Expedition, samples for NO_3^- concentration were collected throughout the water column at 31 stations during CTD and trace metal rosette (TMR) deployments, then analysed by flow injection following standard methods (Hassler and Ellwood, 2020; https://zenodo.org/record/3923586). Since our analysis required a far larger NO_3^- concentration dataset than that generated during ACE, we used a data-constrained model output, the biogeochemical-Southern Ocean State Estimate (b-SOSE; Verdy and Mazloff, 2017; Mazloff *et al.*, 2010), to estimate $[NO_3^-]_{source}$ (http://sose.ucsd.edu/SO6/ITER135/bsose_I135_2013to2019_monthly_NO3.nc) at each underway station, computed as the mean NO_3^- concentration over the source layer (i.e., the winter mixed layer, which we define as the waters between the winter and summer mixed layer depths). We also derived the summer and winter mixed layer depths (MLD) from b-SOSE (http://sose.ucsd.edu/SO6/ITER135/bsose_I135_2013to2019_monthly_MLD.nc) by averaging the b-SOSE MLDs from June to August 2016 (winter) and January to March 2017 (summer). For the stations at which the NO_3^- supply likely originated below the winter MLD (e.g., those influenced by topographic upwelling due to the Island Mass Effect (IME)), we used the average b-SOSE-derived NO_3^- concentration data between 200 and 300m).

We compared the b-SOSE-derived $[NO_3^-]_{source}$ with the measured $[NO_3^-]_{source}$ (i.e., the observed $[NO_3^-]$ in the sub-summer mixed layer waters) at the ACE CTD/TMR stations (Figure A.3). In the open ocean (i.e., the stations at which we used $[NO_3^-]_{W\text{-}S}$ as the source NO_3^-), the average difference between the two datasets was 1.33±2.08 µM (Figure A.3a). For the stations at which we used $[NO_3^-]_{200\text{-}300}$, the average difference was 1.42±1.24 µM (Figure A.3b). The two datasets thus agree well, with no clear bias of one towards higher or lower concentrations, which validates our use of the b-SOSE data in our analysis.

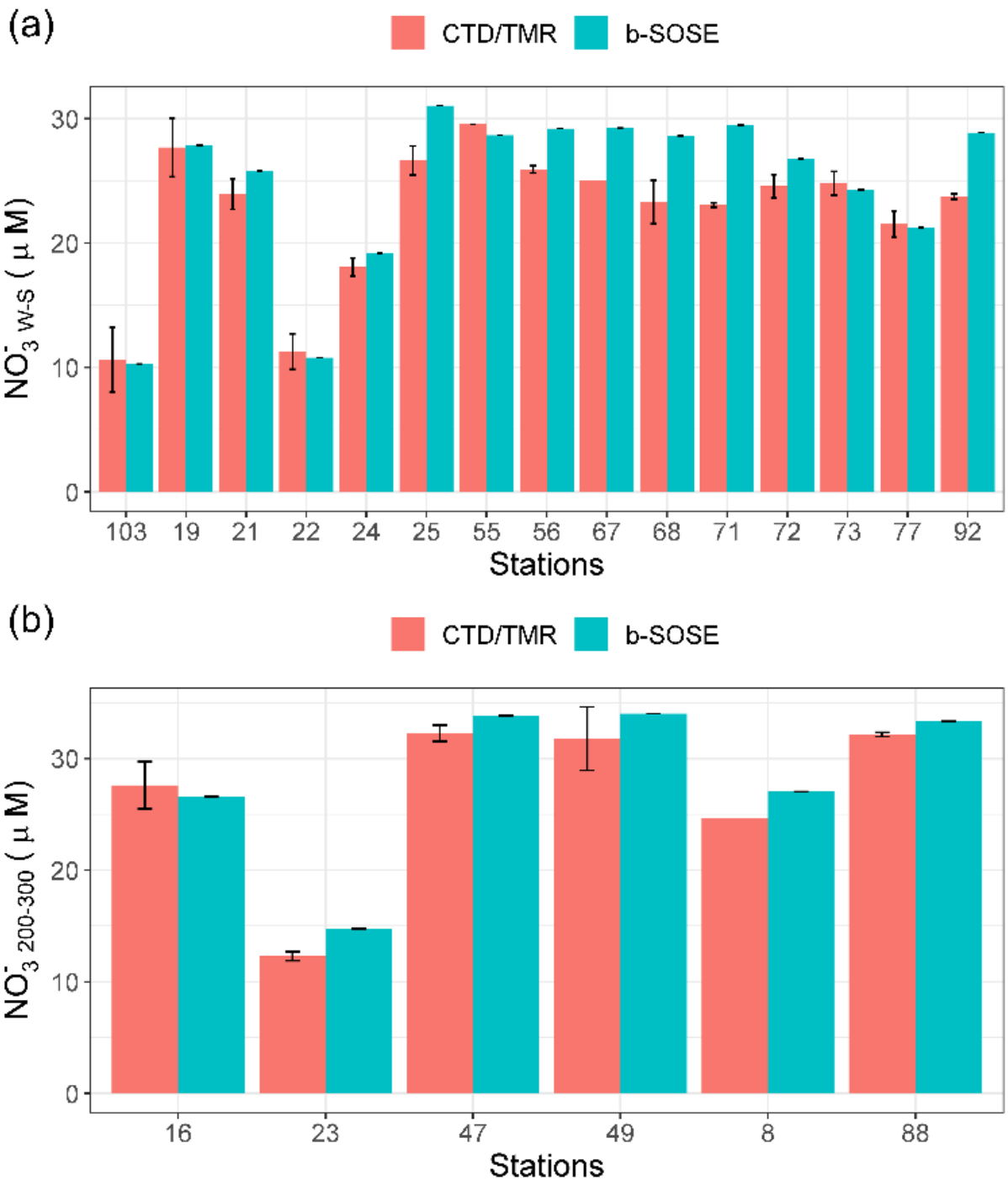

Figure A.3 Comparison of the average source NO_3^- concentrations measured from ACE CTD/TMR sample collections (red bars) and derived from b-SOSE (blue bars) for (a) the open ocean stations where the source NO_3^- was assumed to be that below the summer mixed layer, and (b) the stations influenced by the IME at which we took the data from 200-300 m at representative of the source NO_3^-.

c. Comparison of the observed and modelled source NO_3^- $\delta^{15}N$

During ACE, samples were collected for $\delta^{15}N_{NO_3^-}$ over the upper 1000 m at seven stations during Leg1 (Forrer, 2021), then analysed using the denitrifier method (Sigman *et al.*, 2001; McIlvin and Casciotti, 2011; Weigand *et al.*, 2016). Due to the paucity of spatial-resolved $\delta^{15}N_{NO_3^-}$ measurements from ACE, we used a data-constrained model output from the neural-network-based global ocean NO_3^- $\delta^{15}N$ climatology of Rafter *et al.* (2019) to determine the source $\delta^{15}N_{NO_3^-}$ at each of our stations. Comparing the observed and modelled $\delta^{15}N_{NO_3^-}$ for the seven CTD stations at which NO_3^- isotope samples were collected reveals non-significant differences between the two datasets for $\delta^{15}N_{NO_3^-\,(source)}$ over both the W-S and 200-300m depth layers (t-test; p-value > 0.05; Figure A.4).

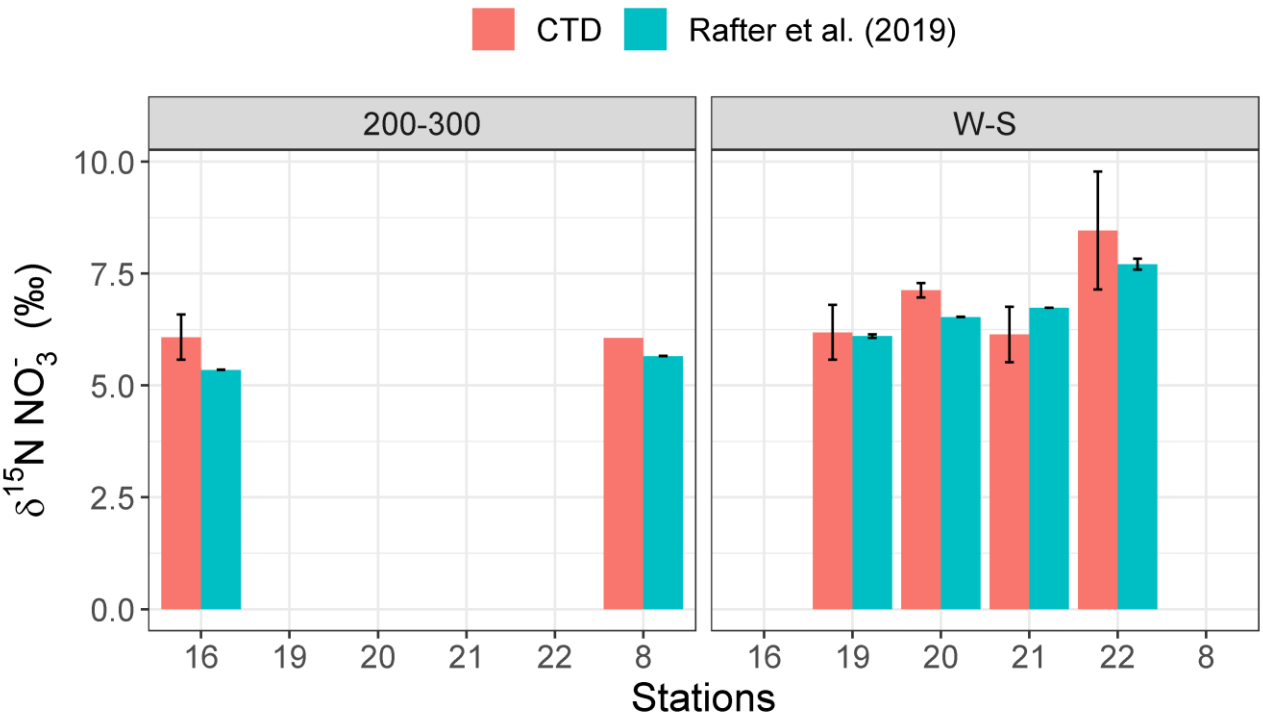

Figure A.4. Comparison of the source NO_3^- $\delta^{15}N$ ($\delta^{15}N_{NO_3^-\,(source)}$; ‰) determined through direct measurements (Forrer, 2021; red bars) versus from the neural-network-based global ocean NO_3^- $\delta^{15}N$ climatology of Rafter *et al.* (2019; blue bars) for stations occupied during Leg1 of the ACE cruise. The left panel bars show the source NO_3^- that was estimated as the concentration-weighted average $\delta^{15}N$ from the 200-300 m layer, while right panel bars show the source NO_3^- that was estimated as the concentration-weighted average $\delta^{15}N$ for the layer between the winter and summer MLDs (W-S). While the NO_3^- $\delta^{15}N$ was measured at one additional station near the PEIs (i.e., Station 2), a neural network- derived estimate of $\delta^{15}N_{NO_3^-\,(source)}$ is lacking because the neural network at times becomes unreliable proximate to the islands due to sharp changes in bathymetry.

d. Assessment isotope effects

For our analysis, we assessed the isotopic effect (ε_{assim}) occurring in NO_3^- assimilation by phytoplankton following the formula defined by (DiFiore *et al.*, 2010) (Table 2.4):

$$\varepsilon_{assim} = 0.07 \times MLD_{summer} + 4‰$$

The ε_{assim} used in Eqn. 2.10 was then calculated for each of the five hydrographic zones as the median of all station-specific ε_{assim} values within each zone (Table 2.4 and Figure 2.9).

Table A.1 Median and interquartile range (IQR) values of the isotopic fractionation during assimilation of NO_3^- (ε_{assim}; ‰) in each oceanographic zone, assessed using the formula from DiFiore *et al.*, (2010). STZ = Subtropical Zone, SAZ = Subantarctic Zone, PFZ = Polar Frontal Zone, SACCZ = Southern Antarctic Circumpolar Current Zone, and sBZ = southern Boundary Zone of ACC. n = number of observations.

Zone	n	Median (‰)	IQR
STZ	34	5.8	1.1
SAZ	77	6.5	1.3
PFZ	78	7.2	2.0
SACCZ	138	5.3	0.5
sBZ	20	5.3	0.0

Thomas *et al.* (*in prep.*) assessed ε_{assim} at 7 stations of Leg1 (Table A.2) by linearly regressing NO_3^- $\delta^{15}N$ measured between the subsurface source and mixed layer of the ACE Leg1 hydrocast stations on $\ln([NO_3^-])$, providing values of samples collected from CTD casts only and values averaged to samples collected from the underwater supply system (UDW) of the ship in the vicinity of the same station.

Table A.2 Values of the isotopic fractionation during assimilation of NO_3^- (ε_{assim}; ‰) assessed by Thomas et al (*in prep*) using data values from CTD stations only and from both CTD and UDW (CTD+UDW), and assessed using the formula from DiFiore *et al.* (2010) at each station. STZ = Subtropical Zone, SAZ = Subantarctic Zone, PFZ = Polar Frontal Zone, SACCZ = Southern Antarctic Circumpolar Current Zone, and sBZ = Southern Boundary of ACC.

ACE Station	Zone	CTD only	CTD+UDW	$\varepsilon_{assim} = 0.07 \times MLD_{summer} + 4‰$
2	SAZ	5.2 ± 2.1	5.4 ± 2.0	6.5
8	SAZ	6.8 ± 1.2	6.9 ± 0.6	6.5
16	PFZ	4.0 ± 1.2	3.5 ± 1.0	7.9
19	SACCZ	4.7 ± 1.3	4.7 ± 1.1	5.8
20	PFZ	5.3 ± 0.5	5.3 ± 0.6	5.8
21	SAZ	4.6 ± 0.6	4.9 ± 1.7	5.8
22	STZ	8.5 ± 0.8	8.7 ± 1.4	5.8

While for most of the stations the differences between values assessed using the MLD linear function and the results from Thomas *et al.* (*in prep.*) range between 0.3 and 1.3‰ only, in stations 16 and 22 the two assessments differenced by as much as 3.9 - 4.4‰ and -2.7 - -2.9‰ respectively.

e. Comparison of the nitrogen isotope ratios of surface nitrate ($\delta^{15}N_{NO_3^-}$) from Rayleigh model and observed data

Both methods showed similar values and gradients along Leg1 (Figure A.5a and b), where average differences were 0.3 ± 1.3‰, ranging between -2 and 6‰ (Figure A.5c). Highest differences (> ± 3‰) were estimated at one station only, in the open ocean close to Tasmania, where $\delta^{15}N_{NO_3^-(surf)}$ was 5.5‰ higher than the measured values. $\delta^{15}N_{NO_3^-(surf)}$ in the vicinity of Kerguelen Island were 1.2 ± 0.2‰ lower than the measured values (Figure A.5c). The small and non-significant difference (p-value >0.05) between the measured and the modelled values of $\delta^{15}N_{NO_3^-}$ indicates a very good agreement between the two datasets, validating our results of $\delta^{15}N_{NO_3^-(surf)}$ assessed using the Rayleigh model.

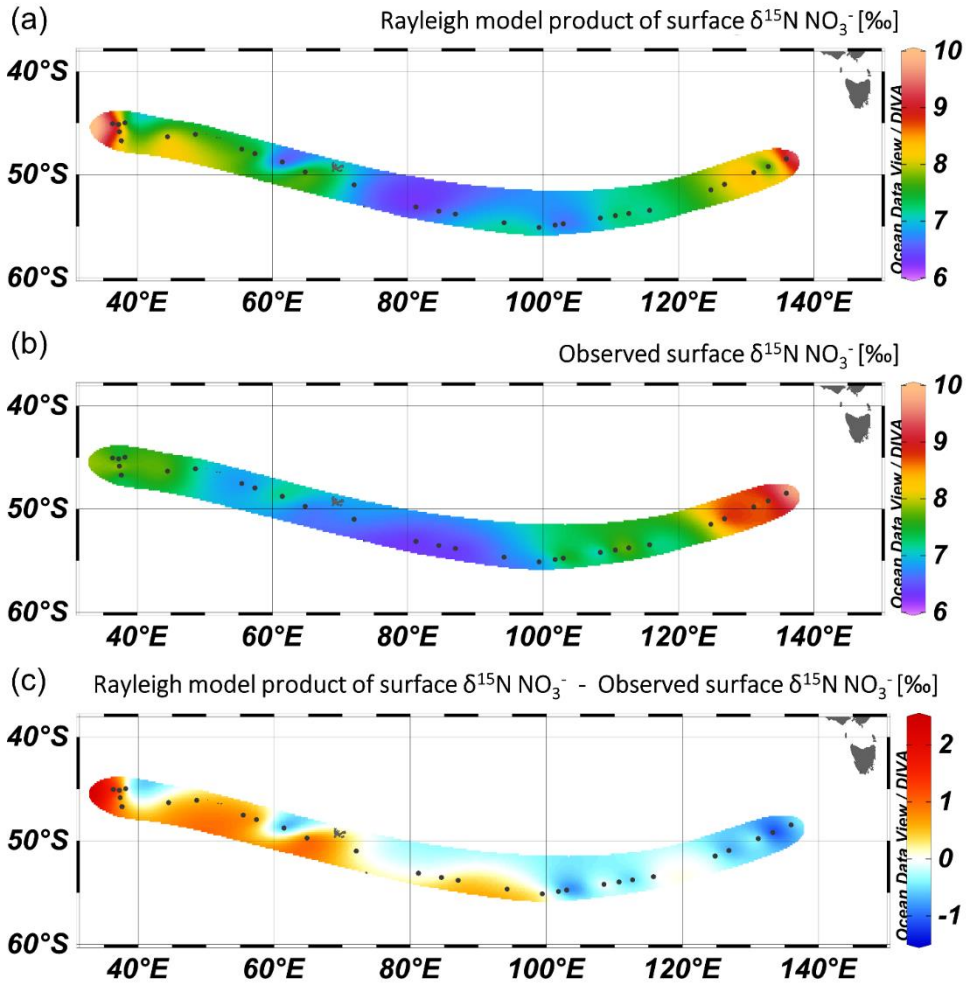

Figure A.5 (a-b) Surface NO_3^- $\delta^{15}N$ assessed along the Leg1 of the Antarctic Circumnavigation Expedition (ACE) using the (a) Rayleigh model ($\delta^{15}N_{NO_3^-(surf)}$; ‰) and (b) from direct observed measurements from underway sampling during ACE. (c) Difference between the modelled surface $\delta^{15}N_{NO_3^-(surf)}$ and the observed surface NO_3^- $\delta^{15}N$.

Surface distribution of fCO_2

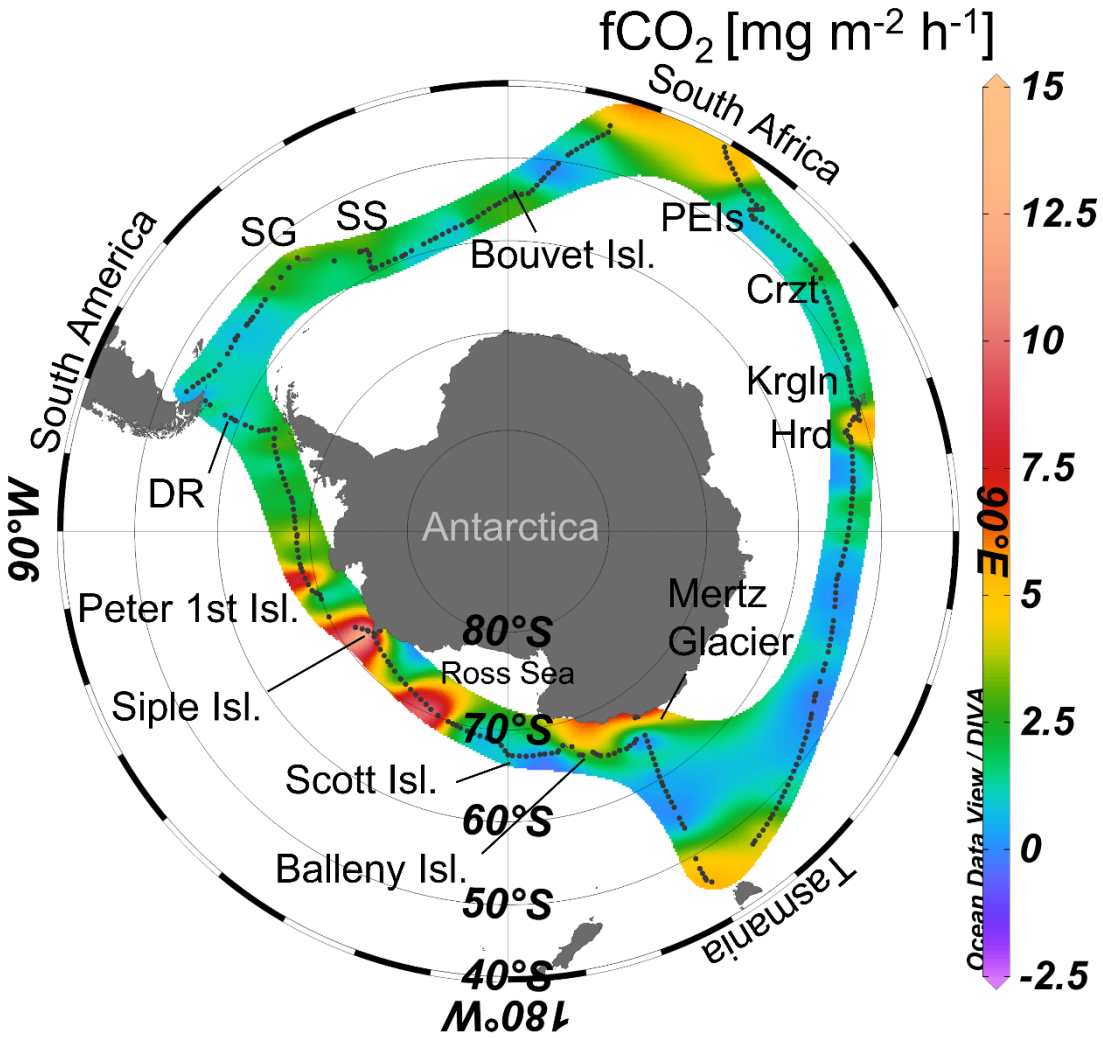

Figure A.6 Surface distribution of the air-sea fluxes of CO_2 (i.e., surface ocean downward mass flux of CO_2 expressed as fCO_2; mg m^{-2} h^{-1}) obtained from a monthly 1-degree resolution global reconstructed product (resources.marine.copernicus.eu/ product-detail/ MULTIOBS_GLO_BIO_CARBON_SURFACE_REP_015_008) and interpolated using ODV, with positive values indicating air-to-sea fluxes (i.e., ocean uptake) and negative values indicating sea-to-air fluxes. The islands visited during the ACE cruise are indicated on the plot: PEIs = Prince Edward Islands, Crzt = Crozet Island, Krgln = Kerguelen Island, Hrd = Heard Island, DR = Diego Ramirez Island, SG = South Georgia Island, and SS = South Sandwich Islands.

f. Longitudinal variability of $\delta^{13}C_{SPM}$ and $\delta^{15}N_{SPM}$

On average for the entire Southern Ocean, $\delta^{13}C_{SPM}$ was significantly higher for samples collected during Leg1 than Leg2 and Leg3 (-25.1 ± 1.8‰, -27.5 ± 1.9‰, and -27.9 ± 2.8‰; mean±1SD; *p*-values <0.001; Figure A.7a). By contrast, the average whole-Southern Ocean $\delta^{15}N_{SPM}$ did not vary significantly among sampling legs or with longitude (*p*-value = 0.11), with values of 0.8 ± 3.1‰, 0.1 ± 2.2‰, and 0.7 ± 2.4‰ for Leg1, Leg2, and Leg3, respectively (Figure A.7b). We note that most of the Leg1 observations are from the Subantarctic rather than the Antarctic (128 *versus* 13), that fewer Subantarctic than Antarctic samples were collected during Leg2 (19 *versus* 103), and that on Leg3, the number of Subantarctic and Antarctic measurements are similar (40 *versus* 57). As such, the apparent longitudinal trends in $\delta^{13}C_{SPM}$ and $\delta^{15}N_{SPM}$ may be partly driven by latitudinal changes. Additionally, because the ACE cruise proceeded temporally along a longitudinal transect, analysing our dataset for longitudinal variability means analysing it for temporal variability (see Appendix A.g).

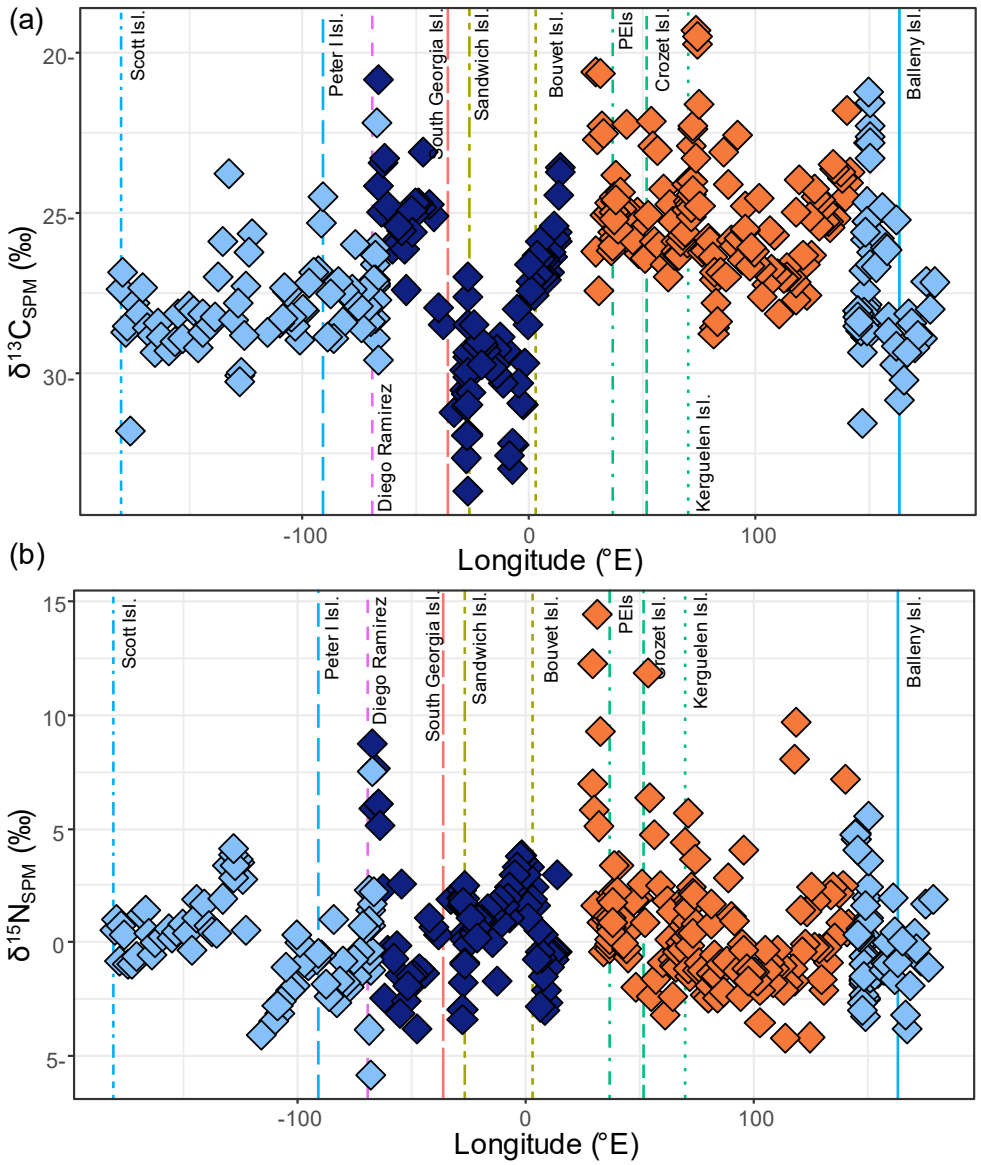

Figure A.7 Longitudinal variability of (a) carbon and (b) nitrogen isotope ratios of the SPM ($\delta^{13}C_{SPM}$ and $\delta^{15}N_{SPM}$; ‰) measured at the surface mixing layer during the Antarctic Circumnavigate Expedition. Colours of diamonds = legs of ACE: Leg1 = orange, Leg2 = light blue, Leg3 = dark blue. Vertical lines = position of islands crossed during ACE, whose names are labelled at the top. The line type and colour are associated with each Island.

g. Spatial distribution of POC:PON ratio and temporal trends in $\delta^{13}C_{SPM}$, $\delta^{15}N_{SPM}$, SST, pCO_2, f_{new}, phytoplankton composition, and NH_4^+

Average POC:PON ratio (Table A.3) along the cruise track in the entire SO is equal to 7.42 ± 1.90 (median=7.14), but in the Subantarctic Ocean the values were significantly higher than in the Antarctic Ocean (respectively, 7.46 ± 2.23 and 6.97 ± 1.29; pairwise t-test: *p*-value < 0.001). In the Subantarctic Ocean there was a slight negative relationship with Latitude, although the linear model explained only 9% of the data variation (lm: y ~ *15.2 - 0.147 * Lat*, σ = 2.17, R^2 = 0.09, *p*-value < 0.001). This is in contrast to the POC:PON ratio in the Antarctic Ocean that did not show any relationship. POC:PON ratio in the STZ were significantly similar to values in the SAZ (respective averages, 8.18 ± 3.72 and 7.63 ± 1.8; pairwise t-test: *p*-value = 1), and both higher than values from PFZ, SACCZ and sBZ which were also significant similar (pairwise t-test: *p*-value > 0.05). POC:PON ratio differed in average between all legs (ANOVA: *p*-value < 0.001). Ratio values are on average higher during Leg1 (8.06 ± 2.60), followed by Leg2 (7.26 ± 1.18) and Leg3, which had the lowest values (6.70 ± 0.98; pairwise t-test: *p*-values < 0.05).

For the entire dataset, $\delta^{13}C_{SPM}$ decreased with time from -24.5±1.8‰ (mean±1SD) at the beginning of the cruise (first two weeks; n = 68) to -28.7 ± 2.3‰ at the end (last two weeks; n = 66; Figure A.8a). Moreover, $\delta^{13}C_{SPM}$ decreased with time in both the Subantarctic and Antarctic, although the calculated regressions explain only 3.5% and 18%, respectively, of the variability (Table A.1). $\delta^{13}C_{SPM}$ remained roughly constant with time in the STZ, SAZ, and sBZ, while in the PFZ and SACCZ, $\delta^{13}C_{SPM}$ declined (R^2 = 9.7% and 20%; red and light blue regressions in Figure A.8a). $\delta^{15}N_{SPM}$ also decreased with time, from 1.7±3.3‰ in the first two weeks to 0.7±1.8‰ in the last two weeks (Figure A.8b). $\delta^{15}N_{SPM}$ decreased significantly in both the Subantarctic and Antarctic, although as for $\delta^{13}C_{SPM}$, the calculated regressions were weak (R^2 = 4.8% and 8.9%, respectively). Additionally, $\delta^{15}N_{SPM}$ decreased significantly with time in the SAZ, PFZ, and sBZ (R^2 = 10%, 7.4%, and 80%, respectively; orange, red, and light blue regressions in Figure A.8b), increased significantly in the SACCZ (R^2 =18%; dark blue regression), and did not change in the STZ where the variability with time was greatest.

The graphical representations of the temporal trends and variations in SST, pCO_2, f_{new}, phytoplankton composition, and NH_4^+ are presented below (Figure A.9, A.10, A.11 and A.12, respectively) and discussed in detail in section 4.3 of the main manuscript.

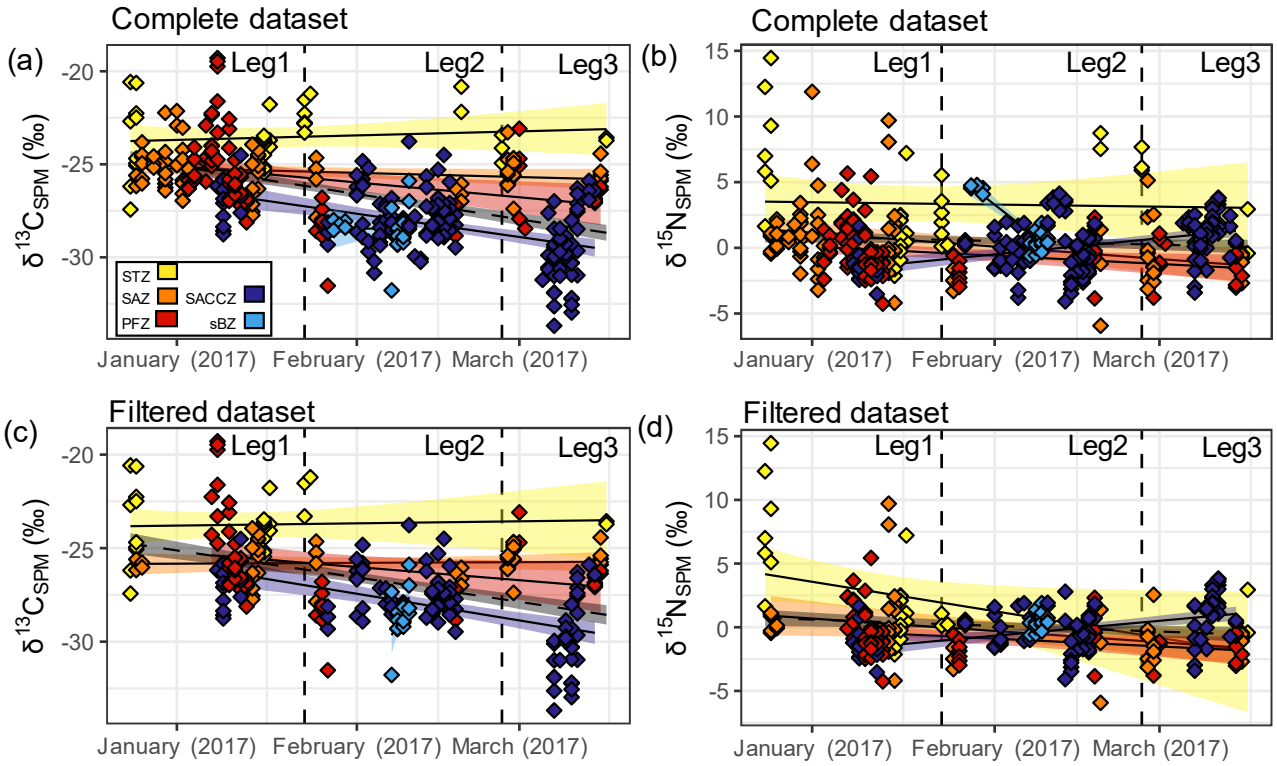

Figure A.8 Temporal variability in $\delta^{13}C_{SPM}$ (‰) and $\delta^{15}N_{SPM}$ (‰) for surface samples collected during ACE: (a-b) whole data set (n=364); (c-d) dataset filtered to remove observations near islands and continents (n=247). The symbol colours represent the hydrographic zones: yellow = Subtropical Zone (STZ), orange = Subantarctic Zone (SAZ), red = Polar Frontal Zone (PFZ), dark blue = Southern Antarctic Circumpolar Current Zone (SACCZ), light blue = southern Boundary Zone (sBZ). Linear regressions with 95% confidence intervals are similarly coloured for each hydrographic zone. The vertical dashed lines delimit each leg of the cruise.

Table A.3 Linear regressions for $\delta^{13}C_{SPM}$, $\delta^{15}N_{SPM}$ and POC:PON ratio for each region of the Southern Ocean. Statistical parameters are also shown: σ = residual standard error, *p*-value = statistical significance, and R^2 = coefficient of determination.

$\delta^{13}C_{SPM}$ (‰)

Zone	Linear regression	σ	p-value	R^2
Subantarctic	*y ~ 215.7 - 0.014 * Time*	1.83	**0.00909**	0.035
Antarctic	*y ~ 692.3 - 0.0419 * Time*	1.58	**2.03E-08**	0.18
STZ	*y ~ -158.1 + 0.00783 * Time*	1.6	0.503	0.013
SAZ	*y ~ 113.3 - 0.00807 * Time*	1.12	0.0912	0.038
PFZ	*y ~ 464.6 - 0.0285 * Time*	2	**0.00462**	0.097
SACCZ	*y ~ 740 - 0.0446 * Time*	1.64	**2.98E-08**	0.2
sBZ	*y ~ -56.9 + 0.00165 * Time*	1.04	0.973	0.000052

$\delta^{15}N_{SPM}$ (‰)

Zone	Linear regression	σ	p-value	R^2
Subantarctic	*y ~ 468 - 0.0272 * Time*	3.01	**0.00219**	0.048
Antarctic	*y ~ -570.9 + 0.0332 * Time*	1.84	**9.66E-05**	0.089
STZ	*y ~ 102.3 - 0.00576 * Time*	3.97	0.842	0.0012
SAZ	*y ~ 579.6 - 0.0337 * Time*	2.76	**0.00478**	0.1
PFZ	*y ~ 383.6 - 0.0223 * Time*	1.82	**0.014**	0.074
SACCZ	*y ~ -752.7 + 0.0437 * Time*	1.74	**2.39E-07**	0.18
sBZ	*y ~ 6027.4 - 0.35 * Time*	0.79	**1.28E-09**	0.8

POC:PON ratio

Zone	Linear regression	σ	p-value	R^2
Subantarctic	*y ~ 501.4 - 0.0287 * Time*	2.15	**8.03E-06**	0.098
Antarctic	*y ~ 220.9 - 0.0124 * Time*	1.29	**0.0337**	0.027
STZ	*y ~ 1185.9 - 0.0685 * Time*	3.65	**0.0134**	0.16
SAZ	*y ~ 355.9 - 0.0202 * Time*	1.68	**0.00529**	0.099
PFZ	*y ~ 355.6 - 0.0203 * Time*	1.33	**0.00243**	0.11
SACCZ	*y ~ 242 - 0.0136 * Time*	1.23	**0.0179**	0.04
sBZ	*y ~ -1845.7 + 0.108 * Time*	1.53	0.138	0.093

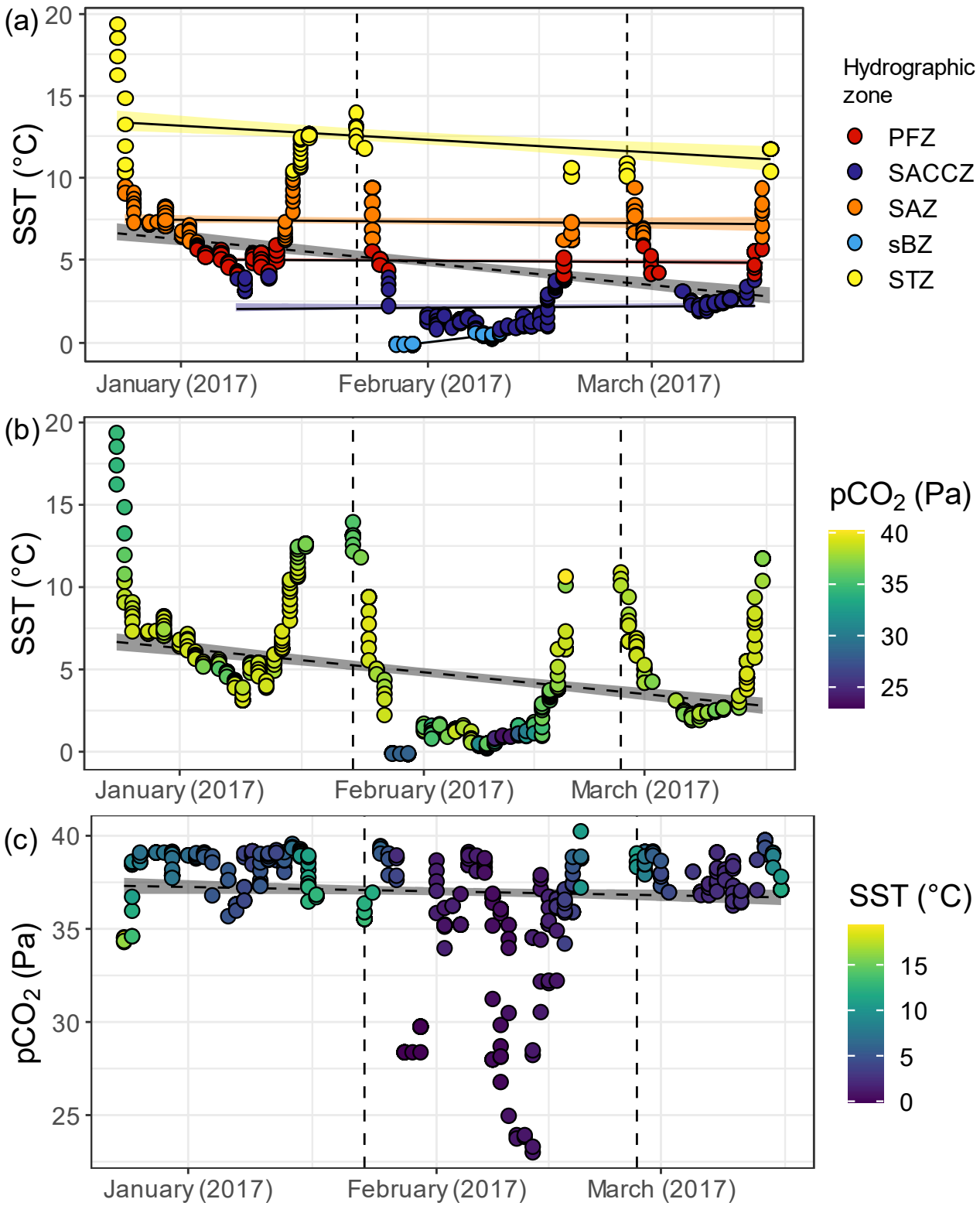

Figure A.9 Temporal variability in (a-b) sea surface temperature (SST; °C) and the partial pressure of CO_2 (pCO_2; Pa) for samples collected at the surface during the Antarctic Circumnavigation Expedition (ACE). (a) The symbol colours represent the hydrographic zones: yellow = Subtropical Zone (STZ), orange = Subantarctic Zone (SAZ), red = Polar Frontal Zone (PFZ), dark blue = Southern Antarctic Circumpolar Current Zone (SACCZ), light blue = southern Boundary Zone (sBZ). (b) The symbol colours represent the pCO_2 (Pa). (c) The symbol colours represent the SST (°C). Dashed linear regressions with their respective 95% confidence intervals (grey areas). In (a) solid linear regressions with their respective 95% confidence intervals for each hydrographic zone (colours according to hydrographic zones). Vertical dashed lines split the ACE legs: Leg1 = left sector, Leg2 = central sector, Leg3 = right sector.

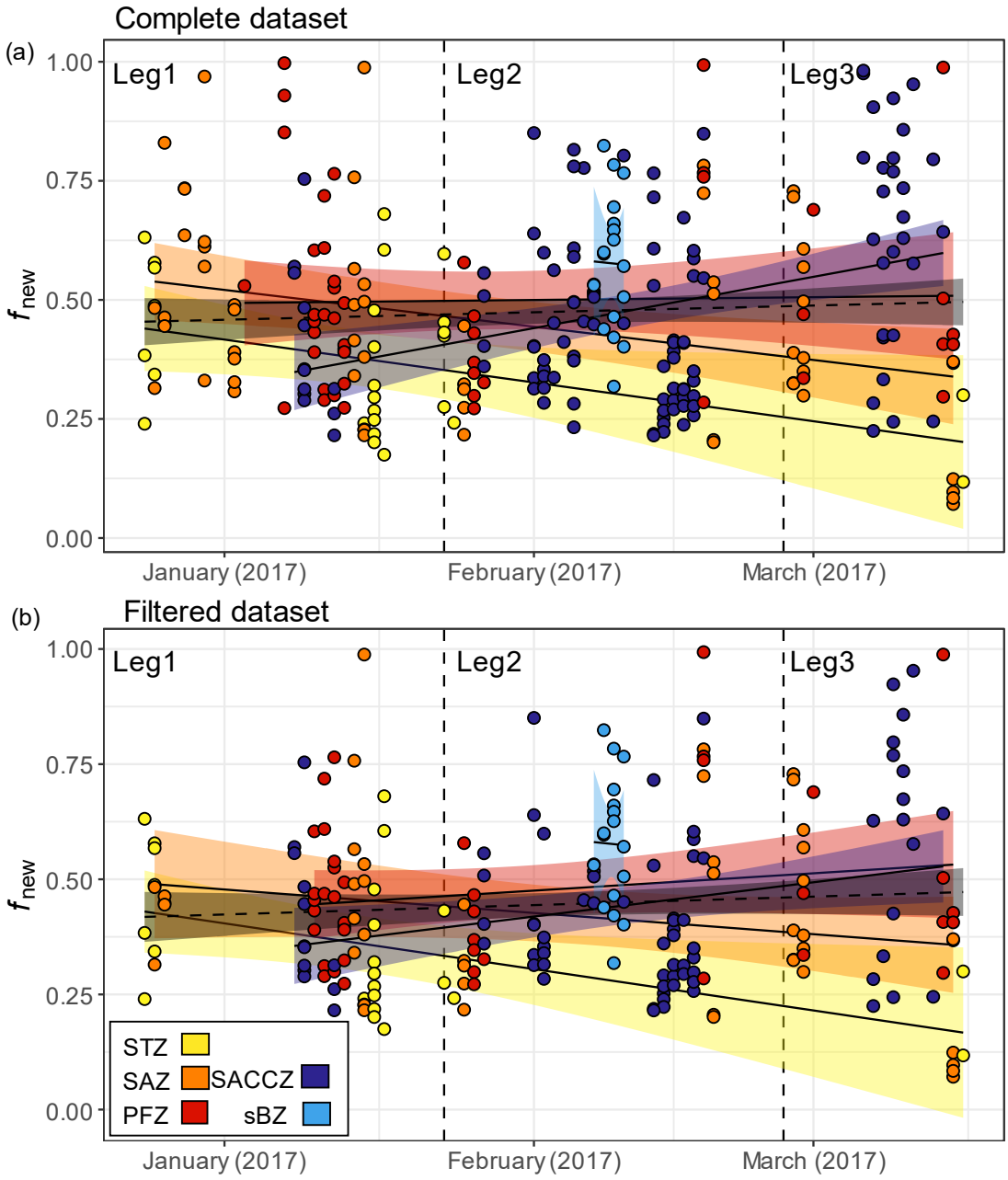

Figure A.10 Temporal variability in f_{new} derived for surface samples collected during ACE: (a) complete dataset (n=270) and (b) dataset filtered to remove observations near islands and continents (n=211). The symbol colours represent the hydrographic zones: yellow = Subtropical Zone (STZ), orange = Subantarctic Zone (SAZ), red = Polar Frontal Zone (PFZ), dark blue = Southern Antarctic Circumpolar Current Zone (SACCZ), light blue = southern Boundary Zone (sBZ). Linear regressions with 95% confidence intervals are similarly coloured for each hydrographic zone. The vertical dashed lines delimit each leg of the cruise.

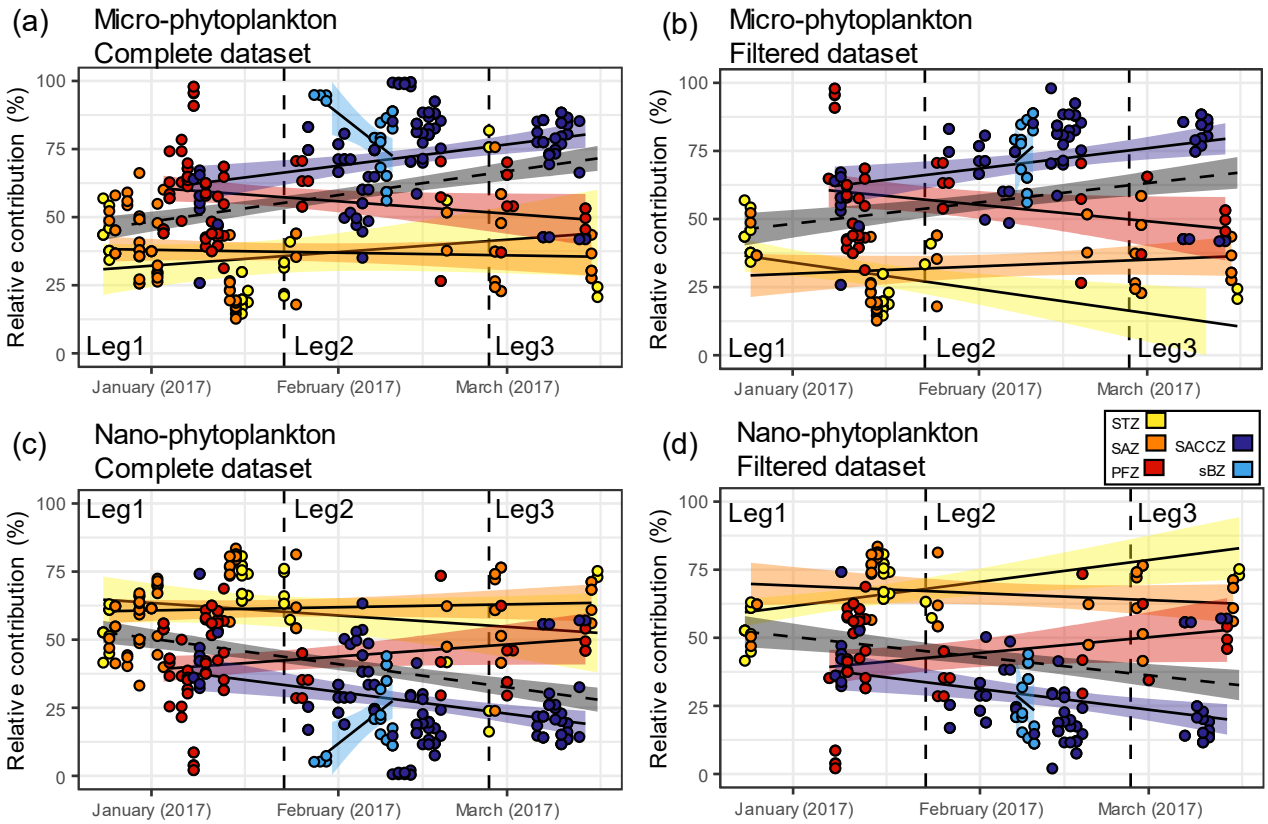

Figure A.11 Pigment data collected during ACE (Antoine *et al.*, 2020). Temporal variability in the percent contribution to total Chl-a of (a-b) micro-phytoplankton and (c-d) nano-phytoplankton: Panels (a-c) show the complete dataset (n=364) and (b-d) show the dataset filtered to remove observations near islands and continents (n=247). The symbol colours represent the hydrographic zones: yellow = Subtropical Zone (STZ), orange = Subantarctic Zone (SAZ), red = Polar Frontal Zone (PFZ), dark blue = Southern Antarctic Circumpolar Current Zone (SACCZ), light blue = southern Boundary Zone (sBZ). Linear regressions with 95% confidence intervals are similarly coloured for each hydrographic zone. The vertical dashed lines delimit each leg of the cruise.

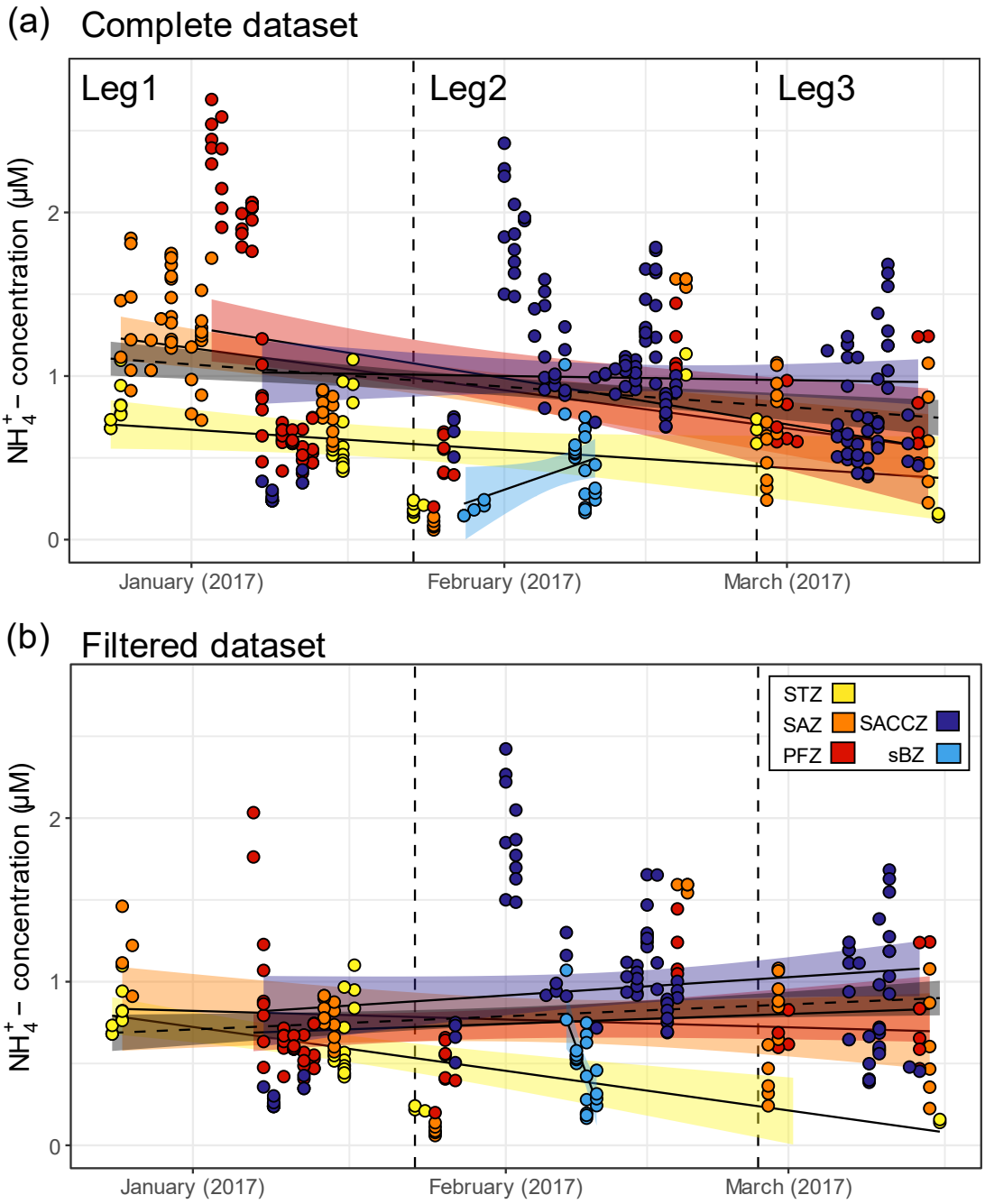

Figure A.12 Temporal variability in NH_4^+ concentrations measured at the surface during ACE: (a) complete dataset (n=364) and (b) dataset filtered to remove observations near islands and continents (n=247). The symbol colours represent the hydrographic zones: yellow = Subtropical Zone (STZ), orange = Subantarctic Zone (SAZ), red = Polar Frontal Zone (PFZ), dark blue = Southern Antarctic Circumpolar Current Zone (SACCZ), light blue = southern Boundary Zone (sBZ). Linear regressions with 95% confidence intervals are similarly coloured for each hydrographic zone. The vertical dashed lines delimit each leg of the cruise.

Phytoplankton composition from HPLC pigment data

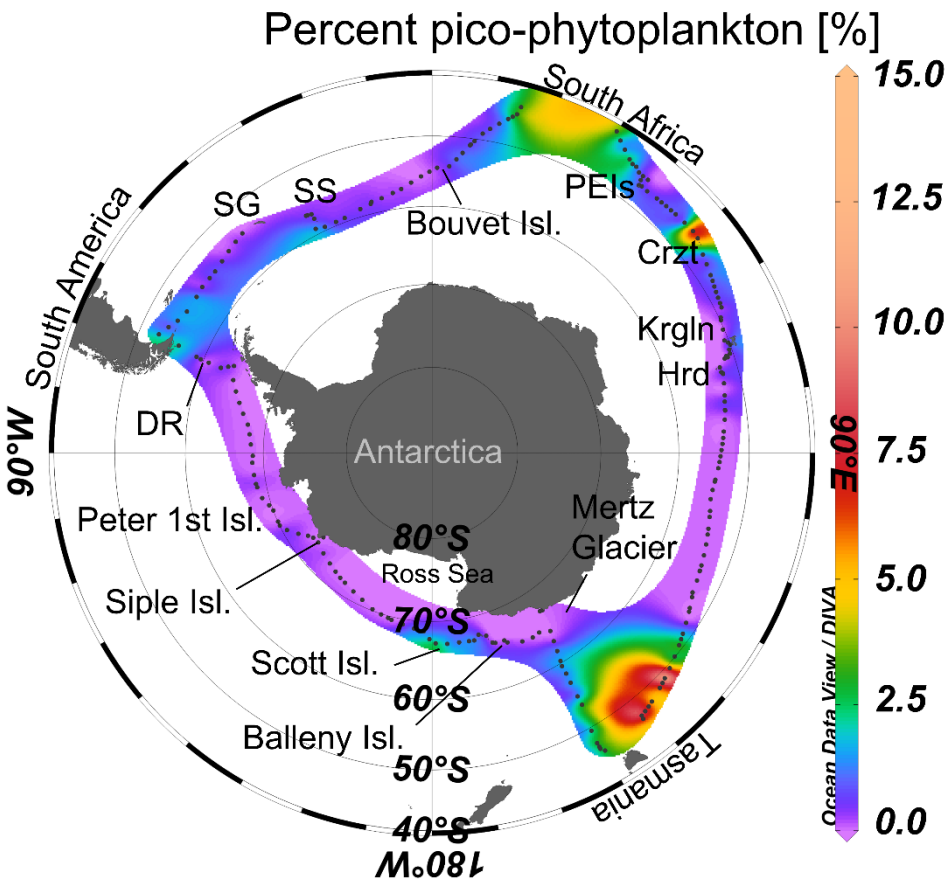

Figure A.13 Surface distribution of the percent contribution of pico-phytoplankton (<2 µm; %) relative to total Chl-a during ACE, determined using the HPLC data (Antoine *et al.*, 2020). PEIs = Prince Edward Islands, Crzt = Crozet Island, Krgln = Kerguelen Island, Hrd = Heard Island, DR = Diego Ramirez Island, SG = South Georgia Island, and SS = South Sandwich Island.

Numerical and taxonomic analysis of micro-phytoplankton community composition

Table A.4 Averaged abundance (cells L^{-1}), 1SD and relative contribution (%) of different micro-phytoplankton species at each hydrographic zone of the Southern Ocean during the Antarctic Circumnavigation Expedition (ACE) cruise: STZ = Subtropical Zone, SAZ = Subantarctic Zone, PFZ = Polar Frontal Zone, SACCZ = Southern Antarctic Circumpolar Current Zone, and sBZ = southern Boundary Zone.

SO zone	Group	Species	Averaged abundance (Cells L^{-1})	1SD	Relative percentage (%)
STZ	Dinoflagellate	*Ceratium extensum fusus*	12.3	17.5	58.3
STZ	Diatom	*Fragilariopsis kerguelensis*	2.1	4.7	10.0
STZ	Diatom	*Fragilariopsis pseudonana*	2.1	4.7	10.0
STZ	Diatom	*Thalassiothrix antarctica*	1.7	2.7	8.1
STZ	Diatom	*Corethron pennatum*	1.5	2.7	7.1
STZ	Diatom	Centric unknown	0.6	0.9	2.8
STZ	Dinoflagellate	*Protoperidium* sp.	0.4	0.9	1.9
STZ	Diatom	*Rhizosolenia* sp.	0.2	0.5	0.9
STZ	Dinoflagellate	*Dinophysis antarctica*	0.2	0.5	0.9
SAZ	Diatom	*Fragilariopsis kerguelensis*	961.4	1409.8	66.5
SAZ	Dinoflagellate	*Ceratium pentagonum*	45.0	119.9	3.1
SAZ	Diatom	*Chaetoceros dichaeta*	43.3	147.2	3.0
SAZ	Diatom	*Fragilariopsis pseudonana*	37.6	150.8	2.6
SAZ	Diatom	*Chaetoceros atlanticus*	36.2	149.6	2.5
SAZ	Diatom	*Chaetoceros compressus*	31.6	181.3	2.2
SAZ	Diatom	*Eucampia antarctica var antarctica*	25.1	112.1	1.7
SAZ	Diatom	*Pseudonitzschia heimii*	24.8	56.7	1.7
SAZ	Diatom	*Thalassiothrix antarctica*	24.4	52.2	1.7
SAZ	Dinoflagellate	*Ceratium lineatum*	15.6	49.3	1.1
SAZ	Diatom	*Chaetoceros neglectus*	12.6	72.5	0.9
SAZ	Diatom	*Nitzschia closterium*	11.6	54.5	0.8
SAZ	Dinoflagellate	*Ceratium extensum fusus*	11.2	46.6	0.8
SAZ	Diatom	*Pseudonitzschia* sp.	10.4	41.8	0.7
SAZ	Diatom	*Asteromphalus roperanus*	7.7	24.3	0.5
SAZ	Dinoflagellate	*Peridinium* sp.	7.6	42.3	0.5
SAZ	Diatom	*Thalassiosira eccentrica*	7.5	14.7	0.5
SAZ	Dinoflagellate	*Dinophysis antarctica*	6.7	29.0	0.5
SAZ	Diatom	*Fragilariopsis* sp.	6.1	34.8	0.4
SAZ	Diatom	*Corethron pennatum*	6.0	20.3	0.4
SAZ	Diatom	*Chaetoceros bulbosus*	5.8	21.2	0.4
SAZ	Dinoflagellate	*Protoperidium* sp.	5.2	13.2	0.4
SAZ	Diatom	Centric unknown	5.1	16.1	0.4
SAZ	Diatom	*Chaetoceros densus*	4.9	28.0	0.3
SAZ	Diatom	*Chaetoceros radicans*	4.7	27.2	0.3
SAZ	Diatom	Small centric unknown	4.7	11.8	0.3
SAZ	Dinoflagellate	*Ceratium furca*	4.7	27.2	0.3
SAZ	Dinoflagellate	*Prorocentrum* sp.	4.3	7.6	0.3
SAZ	Diatom	*Membraneis challengeri*	4.2	17.0	0.3
SAZ	Diatom	*Asteromphalus hookeri*	4.0	11.6	0.3
SAZ	Diatom	*Chaetoceros concavicornis*	3.4	18.1	0.2

SAZ	Diatom	*Coscinodiscus radiatus*	3.4	18.1	0.2
SAZ	Diatom	*Fragilariopsis curta*	3.2	18.1	0.2
SAZ	Diatom	*Fragilariopsis cylindrus*	3.2	18.1	0.2
SAZ	Diatom	*Pseudonitzschia delicatissima*	3.2	18.1	0.2
SAZ	Diatom	*Fragilaria islandica* var. *producta*	2.9	16.9	0.2
SAZ	Diatom	*Thalasionema nitzschiodes*	2.9	10.0	0.2
SAZ	Diatom	*Thalassiosira lentignosa*	2.9	13.2	0.2
SAZ	Diatom	*Dactyliosolen antarcticus*	2.8	9.1	0.2
SAZ	Diatom	*Rhizosolenia imbricata*	2.5	8.0	0.2
SAZ	Diatom	*Chaetoceros* sp.	2.2	6.8	0.2
SAZ	Dinoflagellate	*Protoperidium latistriatum*	2.1	10.9	0.1
SAZ	Diatom	*Pseudonitzschia subcurvata*	2.0	7.1	0.1
SAZ	Silicoflagellate	*Distephanus speculum*	2.0	9.7	0.1
SAZ	Dinoflagellate	*Protoperidium antarcticum*	1.8	5.5	0.1
SAZ	Diatom	*Chaetoceros convolutus*	1.6	9.1	0.1
SAZ	Diatom	*Fragilaria* sp.	1.6	9.1	0.1
SAZ	Diatom	*Cylindrotheca closterium*	1.5	7.6	0.1
SAZ	Diatom	*Grammatophora* sp.	1.3	7.3	0.1
SAZ	Diatom	*Paralia sulcata*	1.3	7.3	0.1
SAZ	Diatom	*Guinardia cylindrus*	1.1	6.0	0.1
SAZ	Diatom	*Rhizosolenia* sp.	1.1	4.3	0.1
SAZ	Diatom	*Thalassiosira maculata*	1.1	2.4	0.1
SAZ	Diatom	*Thalassiosira oliveriana*	1.1	4.1	0.1
SAZ	Diatom	*Asteromphalus hyalinus*	0.8	3.7	0.1
SAZ	Diatom	*Pseudonitzschia lineola*	0.8	4.4	0.1
SAZ	Dinoflagellate	*Dinophysis* sp.	0.8	3.4	0.1
SAZ	Diatom	Pennate unknown	0.7	4.2	<0.1
SAZ	Diatom	*Rhizosolenia styliformis*	0.7	3.6	<0.1
SAZ	Diatom	*Chaetoceros flexuosus*	0.6	3.6	<0.1
SAZ	Diatom	*Pseudonitzschia antarctica*	0.6	3.6	<0.1
SAZ	Diatom	*Cocconeis* sp.	0.5	2.5	<0.1
SAZ	Diatom	*Corethron inerme*	0.5	3.1	<0.1
SAZ	Diatom	*Plagiotropis gaussii*	0.4	1.8	<0.1
SAZ	Dinoflagellate	*Prorocentrum antarcticum*	0.4	2.4	<0.1
SAZ	Diatom	*Actinocyclus actinochilus*	0.3	1.8	<0.1
SAZ	Diatom	*Actinocyclus curvatulus*	0.3	1.3	<0.1
SAZ	Diatom	*Entomoneis paludosa*	0.3	1.8	<0.1
SAZ	Diatom	*Fragilariopsis rhombica*	0.3	1.8	<0.1
SAZ	Diatom	*Navicula criophila*	0.3	1.8	<0.1
SAZ	Diatom	*Odontella* sp.	0.3	1.8	<0.1
SAZ	Diatom	*Proboscia inermis*	0.3	1.8	<0.1
SAZ	Diatom	*Rhizosolenia delicatula*	0.3	1.8	<0.1
SAZ	Diatom	*Rhizosolenia stolterfothii*	0.3	1.8	<0.1
SAZ	Dinoflagellate	*Polykrikos schwartzii*	0.3	1.8	<0.1
SAZ	Diatom	*Actinocyclus divisus*	0.2	1.0	<0.1
SAZ	Diatom	*Actinocyclus exiguus*	0.2	1.2	<0.1
SAZ	Diatom	*Asteromphalus parvulus*	0.2	1.1	<0.1
SAZ	Diatom	*Azpeitia tabularis*	0.2	0.9	<0.1
SAZ	Diatom	*Nitzschia* sp.	0.2	1.2	<0.1
SAZ	Diatom	*Plagiotropis* sp.	0.2	0.8	<0.1

SAZ	Diatom	*Rhabdonema arcuatum*	0.2	1.0	<0.1
SAZ	Diatom	*Rhizosolenia chunii*	0.2	0.9	<0.1
SAZ	Diatom	*Thalassiosira ritscheri*	0.2	0.9	<0.1
SAZ	Diatom	*Tropidoneis antarctica*	0.2	1.2	<0.1
SAZ	Diatom	*Coscinodiscus centralis*	0.1	0.6	<0.1
SAZ	Diatom	*Coscinodiscus commutatus*	0.1	0.3	<0.1
SAZ	Diatom	*Licmophora* sp.	0.1	0.7	<0.1
SAZ	Diatom	*Nitzschia lecontei*	0.1	0.5	<0.1
SAZ	Diatom	*Rhizosolenia antennata f. semispina*	0.1	0.8	<0.1
SAZ	Diatom	*Thalassiosira symmetrica*	0.1	0.4	<0.1
SAZ	Dinoflagellate	*Blepharocysta splendor-maris*	0.1	0.6	<0.1
SAZ	Dinoflagellate	*Dinophysis operculoides*	0.1	0.6	<0.1
SAZ	Dinoflagellate	*Gonyaulax* sp.	0.1	0.7	<0.1
SAZ	Dinoflagellate	*Katodinium* sp.	0.1	0.6	<0.1
SAZ	Dinoflagellate	*Protoperidium pellucidum*	0.1	0.8	<0.1
SAZ	Silicoflagellate	*Dictyocha fibula*	0.1	0.6	<0.1
PFZ	Diatom	*Fragilariopsis kerguelensis*	757.5	709.9	36.2
PFZ	Diatom	*Chaetoceros radicans*	353.2	1634.4	16.9
PFZ	Diatom	*Odontella weissflogii*	219.2	1021.7	10.5
PFZ	Diatom	*Eucampia antarctica* var. *antarctica*	205.2	567.6	9.8
PFZ	Diatom	*Pseudonitzschia heimii*	119.9	180.8	5.7
PFZ	Diatom	*Chaetoceros atlanticus*	116.9	337.8	5.6
PFZ	Diatom	*Thalassiothrix antarctica*	42.7	47.8	2.0
PFZ	Diatom	*Dactyliosolen antarcticus*	27.8	76.7	1.3
PFZ	Diatom	*Pseudonitzschia turgidula*	19.0	76.3	0.9
PFZ	Diatom	*Corethron pennatum*	18.4	30.9	0.9
PFZ	Diatom	*Fragilariopsis cylindrus*	17.6	89.9	0.8
PFZ	Diatom	*Corethron inerme*	15.8	61.6	0.8
PFZ	Diatom	*Pseudonitzschia* sp.	14.0	71.5	0.7
PFZ	Diatom	*Pseudonitzschia australis*	9.6	49.0	0.5
PFZ	Diatom	Centric unknown	8.4	11.5	0.4
PFZ	Dinoflagellate	*Ceratium pentagonum*	7.9	18.7	0.4
PFZ	Diatom	*Thalassiosira eccentrica*	7.8	13.4	0.4
PFZ	Diatom	*Leptocylindrus* sp.	7.5	38.4	0.4
PFZ	Diatom	*Chaetoceros danicus*	7.3	21.0	0.3
PFZ	Diatom	*Asteromphalus roperanus*	6.3	12.6	0.3
PFZ	Diatom	*Membraneis challengeri*	5.8	9.9	0.3
PFZ	Dinoflagellate	*Ceratium lineatum*	5.7	17.6	0.3
PFZ	Diatom	*Asteromphalus hookeri*	5.5	8.6	0.3
PFZ	Diatom	*Chaetoceros decipiens*	5.4	20.4	0.3
PFZ	Diatom	*Pseudonitzschia lineola*	4.8	24.5	0.2
PFZ	Diatom	*Proboscia inermis*	4.6	8.2	0.2
PFZ	Diatom	Pennate unknown	4.5	20.5	0.2
PFZ	Diatom	*Thalassiosira lentignosa*	4.2	7.7	0.2
PFZ	Dinoflagellate	*Protoperidium* sp.	4.1	7.7	0.2
PFZ	Dinoflagellate	*Prorocentrum* sp.	3.8	6.6	0.2
PFZ	Diatom	*Thalasionema nitzschiodes*	3.0	14.3	0.1
PFZ	Diatom	*Chaetoceros bulbosus*	2.7	7.0	0.1
PFZ	Diatom	*Thalassiosira oliveriana*	2.7	6.7	0.1
PFZ	Diatom	*Chaetoceros dichaeta*	2.5	7.3	0.1

PFZ	Diatom	*Rhizosolenia chunii*	2.5	8.5	0.1
PFZ	Silicoflagellate	*Distephanus speculum*	2.3	3.5	0.1
PFZ	Diatom	*Fragilariopsis rhombica*	2.1	8.3	0.1
PFZ	Diatom	*Haslea trompii*	2.1	4.5	0.1
PFZ	Diatom	*Asteromphalus parvulus*	1.9	5.9	0.1
PFZ	Diatom	*Cerataulina pelagica*	1.9	9.5	0.1
PFZ	Diatom	*Plagiotropis gaussii*	1.9	6.7	0.1
PFZ	Diatom	*Thalassiosira maculata*	1.7	3.3	0.1
PFZ	Diatom	*Cylindrotheca closterium*	1.6	8.2	0.1
PFZ	Diatom	*Asteromphalus hyalinus*	1.3	3.9	0.1
PFZ	Dinoflagellate	*Protoperidium latistriatum*	1.3	3.8	0.1
PFZ	Diatom	*Actinocyclus divisus*	1.2	4.1	0.1
PFZ	Diatom	*Chaetoceros hendeyi*	1.2	6.1	0.1
PFZ	Diatom	*Chaetoceros peruvianus*	1.2	2.8	0.1
PFZ	Diatom	*Pseudonitzschia seriata*	1.2	5.9	0.1
PFZ	Diatom	*Rhizosolenia antennata f. semispina*	1.2	6.1	0.1
PFZ	Dinoflagellate	*Dinophysis antarctica*	1.2	3.8	0.1
PFZ	Diatom	*Chaetoceros pendulus*	1.1	4.3	0.1
PFZ	Diatom	*Fragilaria* sp.	1.1	4.9	0.1
PFZ	Diatom	*Pseudonitzschia subcurvata*	1.1	3.2	0.1
PFZ	Diatom	*Rhizosolenia alata*	1.0	4.1	<0.1
PFZ	Diatom	*Thalassiosira gracilis* var. *gracilis*	1.0	2.3	<0.1
PFZ	Diatom	*Rhizosolenia imbricata*	0.9	3.2	<0.1
PFZ	Diatom	*Proboscia alata*	0.8	3.4	<0.1
PFZ	Diatom	*Rhizosolenia styliformis*	0.8	2.4	<0.1
PFZ	Dinoflagellate	*Alexandrium* sp.	0.8	4.1	<0.1
PFZ	Diatom	*Chaetoceros* sp.	0.7	2.4	<0.1
PFZ	Diatom	*Coscinodiscus oppositus*	0.7	2.6	<0.1
PFZ	Diatom	*Coscinodiscus radiatus*	0.7	2.8	<0.1
PFZ	Diatom	*Fragilariopsis pseudonana*	0.7	3.7	<0.1
PFZ	Dinoflagellate	*Prorocentrum antarcticum*	0.7	2.3	<0.1
PFZ	Diatom	*Chaetoceros adelianus*	0.6	3.1	<0.1
PFZ	Diatom	*Chaetoceros lorenzianus*	0.6	3.1	<0.1
PFZ	Diatom	*Hemidiscus cuneiformis*	0.6	3.1	<0.1
PFZ	Diatom	*Plagiotropis* sp.	0.6	1.7	<0.1
PFZ	Dinoflagellate	*Dinophysis operculoides*	0.6	3.3	<0.1
PFZ	Diatom	*Coscinodiscus commutatus*	0.5	2.5	<0.1
PFZ	Diatom	*Odontella* sp.	0.5	2.1	<0.1
PFZ	Diatom	*Rhizosolenia* sp.	0.5	2.5	<0.1
PFZ	Diatom	Small centric unknown	0.5	1.5	<0.1
PFZ	Diatom	*Actinocyclus exiguus*	0.4	2.0	<0.1
PFZ	Diatom	*Coscinodiscus oculus-iridis*	0.4	1.6	<0.1
PFZ	Diatom	*Chaetoceros castracanei*	0.3	1.4	<0.1
PFZ	Diatom	*Chaetoceros tetrasticon*	0.3	1.5	<0.1
PFZ	Diatom	*Guinardia cylindrus*	0.3	1.5	<0.1
PFZ	Diatom	*Haslea* sp.	0.3	1.1	<0.1
PFZ	Diatom	*Planktonella sol*	0.3	1.2	<0.1
PFZ	Dinoflagellate	*Dinophysis* sp.	0.3	1.4	<0.1
PFZ	Dinoflagellate	*Polykrikos schwartzii*	0.3	1.6	<0.1
PFZ	Dinoflagellate	*Protoperidium pellucidum*	0.3	1.1	<0.1

PFZ	Diatom	*Azpeitia tabularis*	0.2	0.8	<0.1
PFZ	Diatom	*Coscinodiscus oculoides*	0.2	1.0	<0.1
PFZ	Diatom	*Guinardia delicatula*	0.2	1.0	<0.1
PFZ	Diatom	*Nitzschia closterium*	0.2	1.0	<0.1
PFZ	Diatom	*Pleurosigma directum*	0.2	0.8	<0.1
PFZ	Diatom	*Thalassiosira gerloffii*	0.2	1.0	<0.1
PFZ	Diatom	*Thalassiosira oestrupi*	0.2	1.0	<0.1
PFZ	Diatom	*Thalassiosira ritscheri*	0.2	0.8	<0.1
PFZ	Diatom	*Thalassiosira symmetrica*	0.2	0.8	<0.1
PFZ	Diatom	*Tropidoneis antarctica*	0.2	0.9	<0.1
PFZ	Diatom	*Actinocyclus curvatulus*	0.1	0.3	<0.1
PFZ	Diatom	*Rhizosolenia delicatula*	0.1	0.5	<0.1
PFZ	Diatom	*Rhizosolenia hebetata f. semispina*	0.1	0.6	<0.1
PFZ	Diatom	*Rhizosolenia setigera*	0.1	0.6	<0.1
PFZ	Diatom	*Thalassiosira frenguellii*	0.1	0.7	<0.1
PFZ	Dinoflagellate	*Peridinium* sp.	0.1	0.4	<0.1
PFZ	Dinoflagellate	*Preperidinium meunierii*	0.1	0.4	<0.1
SACCZ	Diatom	*Fragilariopsis kerguelensis*	1060.3	1243.5	42.6
SACCZ	Diatom	*Chaetoceros atlanticus*	758.8	1663.2	30.5
SACCZ	Diatom	*Corethron pennatum*	134.2	337.4	5.4
SACCZ	Diatom	*Chaetoceros concavicornis*	82.4	208.6	3.3
SACCZ	Diatom	*Fragilariopsis pseudonana*	81.5	293.0	3.3
SACCZ	Diatom	*Thalassiothrix antarctica*	66.3	80.9	2.7
SACCZ	Diatom	*Pseudonitzschia lineola*	33.3	92.7	1.3
SACCZ	Diatom	*Corethron inerme*	33.1	140.3	1.3
SACCZ	Diatom	*Chaetoceros atlanticus f. audax*	25.1	98.1	1.0
SACCZ	Diatom	*Dactyliosolen antarcticus*	23.2	46.7	0.9
SACCZ	Diatom	*Pseudonitzschia heimii*	22.7	66.3	0.9
SACCZ	Diatom	*Rhizosolenia hebetata f. semispina*	12.3	49.0	0.5
SACCZ	Diatom	*Pseudonitzschia* sp.	10.8	42.5	0.4
SACCZ	Dinoflagellate	*Prorocentrum* sp.	10.1	14.1	0.4
SACCZ	Diatom	*Fragilariopsis rhombica*	10.0	28.2	0.4
SACCZ	Diatom	*Thalassiosira gracilis* var. *gracilis*	9.7	23.0	0.4
SACCZ	Dinoflagellate	*Protoperidium* sp.	8.5	10.8	0.3
SACCZ	Diatom	Centric unknown	8.0	16.1	0.3
SACCZ	Diatom	*Fragilariopsis* sp.	7.9	30.9	0.3
SACCZ	Diatom	*Chaetoceros convolutus*	7.7	32.7	0.3
SACCZ	Diatom	*Rhizosolenia antennata f. semispina*	7.3	22.9	0.3
SACCZ	Dinoflagellate	*Gymnodinium* sp.	6.6	16.9	0.3
SACCZ	Diatom	*Asteromphalus hookeri*	6.0	11.5	0.2
SACCZ	Diatom	*Chaetoceros dichaeta*	4.1	13.5	0.2
SACCZ	Dinoflagellate	*Dinophysis* sp.	4.0	13.4	0.2
SACCZ	Diatom	*Thalassiosira eccentrica*	3.8	11.7	0.2
SACCZ	Diatom	*Asteromphalus hyalinus*	3.6	7.4	0.1
SACCZ	Diatom	*Plagiotropis gaussii*	3.2	6.3	0.1
SACCZ	Diatom	*Rhizosolenia styliformis*	3.1	7.9	0.1
SACCZ	Diatom	*Asteromphalus parvulus*	3.0	8.9	0.1
SACCZ	Diatom	*Coscinodiscus oculoides*	2.9	11.9	0.1
SACCZ	Diatom	*Chaetoceros decipiens*	2.8	11.8	0.1
SACCZ	Silicoflagellate	*Distephanus speculum*	2.6	3.9	0.1

SACCZ	Diatom	*Proboscia inermis*	2.5	7.5	0.1
SACCZ	Diatom	*Thalassiosira lentignosa*	2.4	6.2	0.1
SACCZ	Diatom	*Proboscia alata*	2.1	5.7	0.1
SACCZ	Diatom	*Chaetoceros* sp.	2.0	4.7	0.1
SACCZ	Diatom	*Rhizosolenia* sp.	1.9	5.2	0.1
SACCZ	Diatom	*Thalassiosira gerloffii*	1.9	6.6	0.1
SACCZ	Diatom	*Odontella weissflogii*	1.7	7.1	0.1
SACCZ	Diatom	*Chaetoceros castracanei*	1.5	6.5	0.1
SACCZ	Diatom	*Eucampia antarctica* var. *antarctica*	1.2	3.1	<0.1
SACCZ	Diatom	*Chaetoceros adelianus*	1.1	4.5	<0.1
SACCZ	Diatom	*Plagiotropis* sp.	1.1	3.5	<0.1
SACCZ	Diatom	*Chaetoceros bulbosus*	1.0	2.4	<0.1
SACCZ	Diatom	*Fragilariopsis cylindrus*	1.0	4.2	<0.1
SACCZ	Diatom	*Actinocyclus divisus*	0.9	4.0	<0.1
SACCZ	Diatom	*Azpeitia tabularis*	0.8	3.3	<0.1
SACCZ	Diatom	*Fragilaria islandica* var. *stricta*	0.8	3.3	<0.1
SACCZ	Dinoflagellate	*Ceratium lineatum*	0.8	2.0	<0.1
SACCZ	Diatom	*Odontella* sp.	0.7	2.5	<0.1
SACCZ	Diatom	*Thalassiosira* sp.	0.7	2.9	<0.1
SACCZ	Dinoflagellate	*Dinophysis antarctica*	0.7	2.9	<0.1
SACCZ	Diatom	*Membraneis challengeri*	0.6	1.7	<0.1
SACCZ	Diatom	*Asteromphalus roperanus*	0.5	1.2	<0.1
SACCZ	Diatom	*Cylindrotheca closterium*	0.5	2.0	<0.1
SACCZ	Diatom	*Thalassiosira oliveriana*	0.5	1.1	<0.1
SACCZ	Diatom	*Actinocyclus actinochilus*	0.4	1.0	<0.1
SACCZ	Diatom	*Chaetoceros radicans*	0.4	1.6	<0.1
SACCZ	Diatom	*Thalasionema nitzschiodes*	0.4	1.4	<0.1
SACCZ	Diatom	*Coscinodiscus oppositus*	0.3	1.4	<0.1
SACCZ	Diatom	*Actinocyclus curvatulus*	0.2	0.8	<0.1
SACCZ	Diatom	*Chaetoceros danicus*	0.2	0.8	<0.1
SACCZ	Diatom	*Navicula directa* var. *directa*	0.2	0.7	<0.1
SACCZ	Diatom	*Odontella sinensis*	0.2	0.7	<0.1
SACCZ	Diatom	*Pseudonitzschia turgidula*	0.2	0.8	<0.1
SACCZ	Diatom	*Rhizosolenia imbricata*	0.2	0.7	<0.1
SACCZ	Diatom	*Diploneis* sp.	0.1	0.2	<0.1
SACCZ	Diatom	*Planktonella sol*	0.1	0.2	<0.1
SACCZ	Diatom	Small centric unknown	0.1	0.6	<0.1
SACCZ	Diatom	*Thalassiosira maculata*	0.1	0.5	<0.1
SACCZ	Diatom	*Thalassiosira ritscheri*	0.1	0.5	<0.1
sBZ	Diatom	*Pseudonitzschia lineola*	45.8		34.4
sBZ	Diatom	*Thalassiothrix antarctica*	29.2		21.9
sBZ	Diatom	*Fragilariopsis kerguelensis*	20.8		15.6
sBZ	Diatom	*Chaetoceros concavicornis*	12.5		9.4
sBZ	Diatom	*Rhizosolenia* sp.	8.3		6.2
sBZ	Diatom	*Trichotoxon reinboldii*	8.3		6.2
sBZ	Diatom	*Corethron pennatum*	4.2		3.2
sBZ	Diatom	*Nitzschia closterium*	4.2		3.2

h. Isotope mixing model

h.1. Inputs to the Rayleigh model

In the open ocean, the b-SOSE derived $NO_{3\,(W-S)}^{-}$ concentration increased with latitude in the Subantarctic (STZ = $14.2_{11.4}^{16.2}$ µM, SAZ = $21.7_{20.1}^{23.6}$ µM, PFZ = $26.1_{24.5}^{27.2}$ µM; pairwise Wilcoxon test, *p*-value < 0.001) to reach a maximum in the Antarctic (SACCZ = $28.7_{27.3}^{29.2}$ µM and sBZ = $29.0_{28.7}^{29.4}$ µM; pairwise Wilcoxon test, *p*-value = 0.55; Table 2.4). By contrast, the $\delta^{15}N_{NO_3^-(W-S)}$ was highest in the STZ ($8.2_{7.9}^{8.5}$‰) and decreased polewards (SAZ = $7.1_{6.7}^{7.5}$‰, PFZ = $6.4_{6.1}^{6.5}$‰, SACCZ = $6.2_{5.9}^{6.3}$‰, and sBZ = $5.9_{5.7}^{6.5}$‰). The $NO_{3\,(200-300)}^{-}$ concentrations and $\delta^{15}N_{NO_3^-(200-300)}$ were higher and lower, respectively, than the W-S values at the same stations (Figure A.14). The lowest $NO_{3\,(200-300)}^{-}$ concentrations occurred near South America and Tasmania ($19.3_{19.1}^{19.4}$ and $14.7_{14.4}^{14.8}$µM) while the $NO_{3\,(200-300)}^{-}$ was $25.3_{23.6}^{26.6}$µM over the Indian archipelago and $34.0_{33.6}^{34.4}$µM at the Atlantic archipelago. The $\delta^{15}N_{NO_3^-(200-300)}$ ranged from 4.8‰ to 7.2‰, with higher values at the stations located near lower-latitude landmasses such as near Tasmania ($6.7_{6.6}^{6.7}$‰) and South America ($6.9_{6.7}^{7.0}$‰), and within the Indian archipelago ($5.7_{5.5}^{6.0}$‰). The $\delta^{15}N_{NO_3^-(200-300)}$ near landmasses south of 50°S was $4.9_{4.8}^{5.0}$‰.

The derived isotope effects (ε_{assim}) ranged from 4.5‰ to 10.6‰. Lower values of ε_{assim} were determined for the Antarctic stations (SACCZ = $5.3_{5.0}^{5.8}$‰ and sBZ = $5.3_{5.3}^{5.3}$‰; Wilcoxon test, *p*-value = 0.045; Table 2.4). By contrast, ε_{assim} at the PFZ stations was fairly high ($7.2_{5.8}^{7.9}$‰) and statistically similar to the ε_{assim} determined for the SAZ ($\varepsilon = 6.5_{5.8}^{7.2}$‰; pairwise Wilcoxon test, *p*-value = 1; Table 2.4). A lower median ε_{assim} was estimated for the STZ ($5.8_{5.8}^{7.0}$‰; pairwise Wilcoxon test, *p*-value < 0.001). In general, both the values and latitudinal trend that we determine here for ε_{assim} are consistent with previous observations from the summertime Southern Ocean (e.g., ε_{assim} has been shown to decrease poleward from values of 6‰ to 9‰ in the Subantarctic to 4.5‰ to 6.1‰ in the Antarctic) (DiFiore *et al.*, 2010; Fripiat *et al.*, 2019).

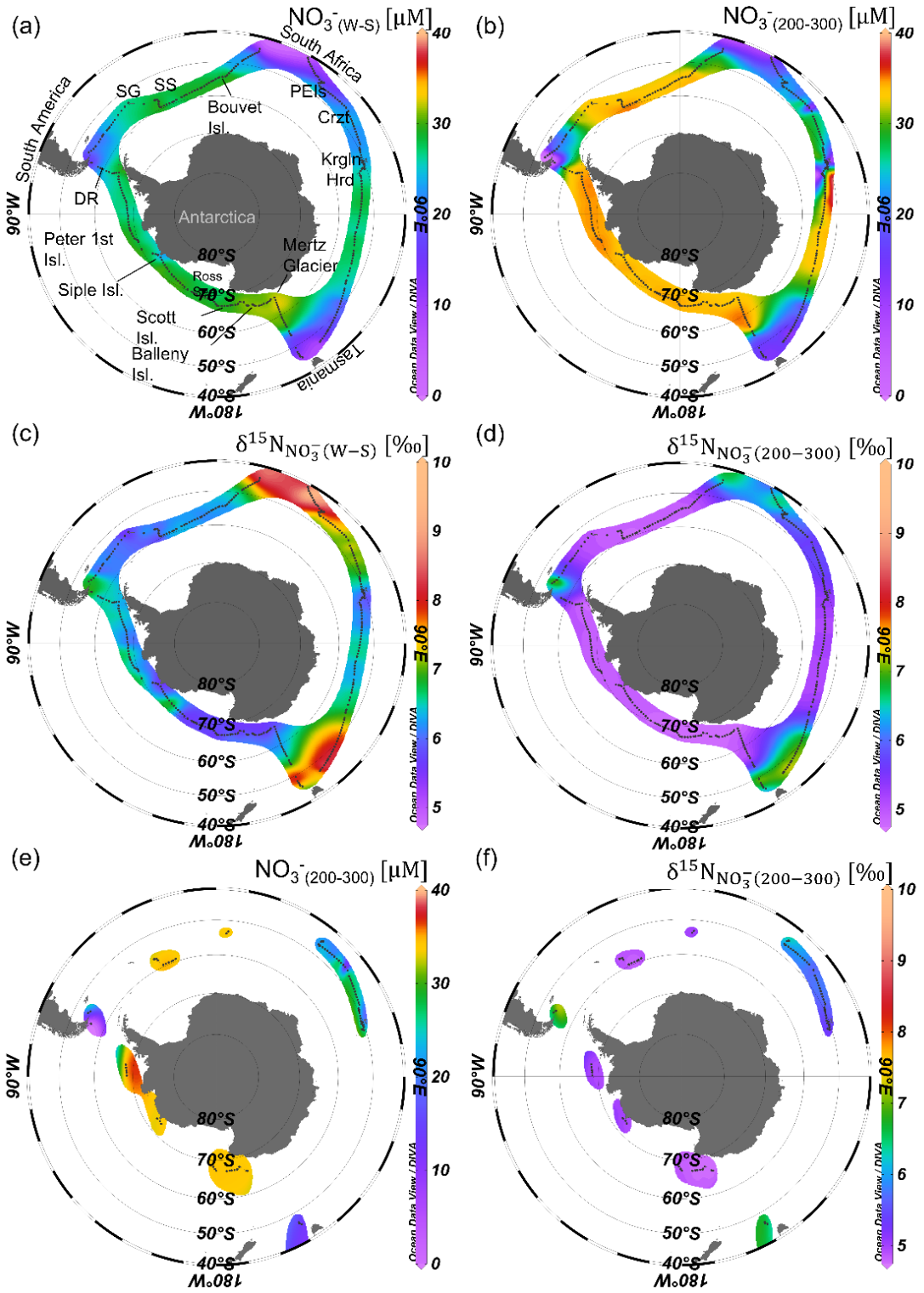

Figure A.14 Inputs to the Rayleigh model. The (a-b) concentration (µM) and (c-d) $\delta^{15}N$ (‰) of the source NO_3^- to summertime surface waters determined as (a-c) the water mass between the MLD_{summer} and the MLD_{winter} ($NO_{3(W-S)}^-$ and $\delta^{15}N_{NO_3^-(W-S)}$) or (b-d) the water mass between 200 and 300 m, typically below the MLD_{winter} ($NO_{3(200-300)}^-$ and $\delta^{15}N_{NO_3^-(200-300)}$). Panels (e-b) show the $NO_{3(200-300)}^-$ and $\delta^{15}N_{NO_3^-(200-300)}$ in the upwelling regions only (i.e., near islands and continental shelves). The NO_3^- concentrations are taken from the biogeochemical-Southern Ocean State Estimate (b-SOSE) (Mazloff *et al.*, 2010; Verdy and Mazloff, 2017) and the $\delta^{15}N$ of NO_3^- from the neural-network-based global ocean database of Rafter *et al.* (2019). PEIs = Prince Edward Islands archipelago, Crzt = Crozet Island, Krgln = Kerguelen Island, Hrd = Heard Island, DR = Diego Ramirez Island, SG = South Georgia Island and SS = South Sandwich Island.

h.2. Outputs of the Rayleigh model

Not unexpectedly, the computed $\delta^{15}N_{NO_3^-(surf)}$ (i.e., the $\delta^{15}N$ of surface NO_3^- expected for the degree of phytoplankton NO_3^- consumption implied by *F;* Eqn. 4a) and $\delta^{15}N_{new}$ varied in concert across the transect (Figure A.15; Table 2.4). Maximum values of $\delta^{15}N_{NO_3^-(surf)}$ were computed for the STZ ($8.9^{9.7}_{8.5}$‰), while for the rest of the transect, the median $\delta^{15}N_{NO_3^-(surf)}$ was $6.8^{7.1}_{6.5}$‰. In the open ocean, $\delta^{15}N_{new}$ ranged from -1.5 to 19.1‰ (whole Southern Ocean median of $1.4^{2.1}_{0.5}$‰; Figure A.15b), with the highest median values also computed for the STZ ($4.4^{6.2}_{2.9}$‰). $\delta^{15}N_{new}$ decreased southwards across the Subantarctic, reaching a minimum in the PFZ (SAZ = $1.0^{1.6}_{0.5}$‰ and PFZ = $0.8^{+1.4}_{-0.3}$‰) before increasing again into the Antarctic (SACCZ = $1.8^{2.1}_{1.3}$‰ and sBZ = $1.5^{2.1}_{1.0}$‰; pairwise Wilcoxon Test, *p*-value = 0.50). The $\delta^{15}N_{new}$ over the eastern Indian archipelago (Leg1) and the first part of Leg3 were the lowest of the transect ($-0.7^{-0.2}_{-1.0}$‰ and $+0.1^{+0.6}_{-0.3}$‰, respectively), reaching -1.5‰ near Kerguelen Island and -0.8% to the west of South Georgia. On Leg3, the waters east of the South Sandwich Islands to Bouvet Island had a relatively high $\delta^{15}N_{new}$ ($2.0^{2.2}_{1.8}$‰, reaching a local maximum of 2.9‰), as did the open-ocean waters on Leg2 (range of 0.9‰ to 5.0‰, maximum near Siple Island) except near Scott Island and the mouth of the Ross Sea ($\delta^{15}N_{new}$ of 0.4‰ to 1.4‰).

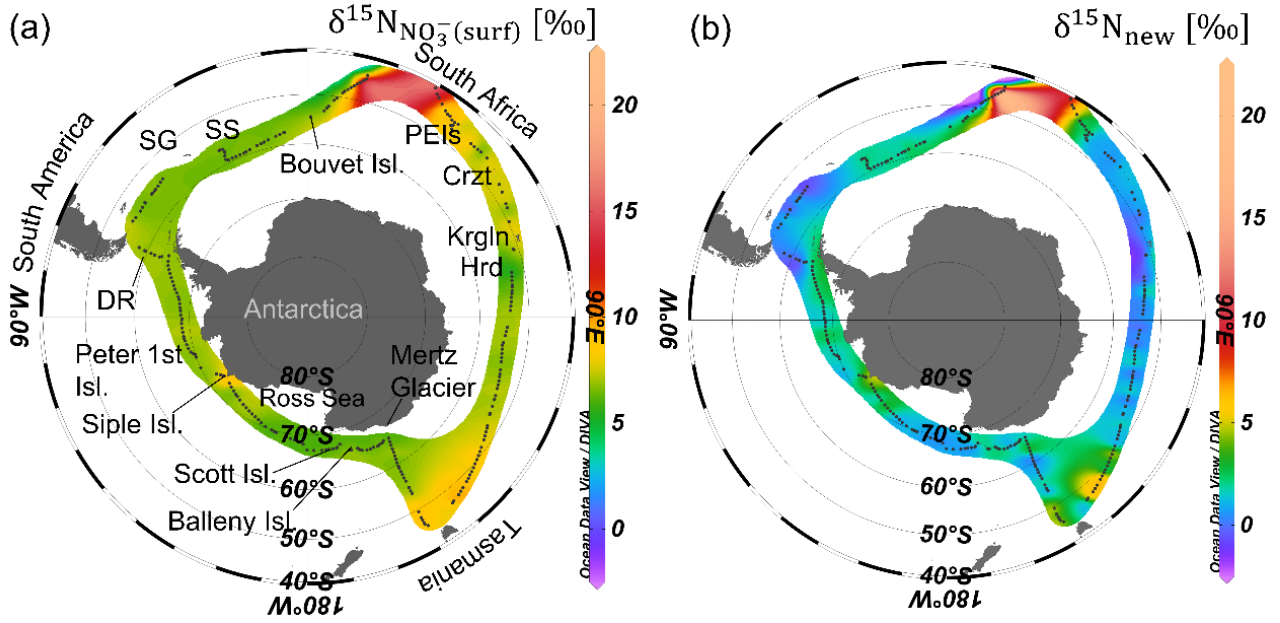

Figure A.15 Outputs of the Rayleigh model. (a) Distribution of the computed surface NO_3^- $\delta^{15}N$ ($\delta^{15}N_{NO_3^-(surf)}$; ‰) and (b) $\delta^{15}N_{new}$ (‰). PEIs = Prince Edward Islands archipelago, Crzt = Crozet Island, Krgln = Kerguelen Island, Hrd = Heard Island, DR = Diego Ramirez Island, SG = South Georgia Island, and SS = South Sandwich Islands. Note that the colour bars have different scales.

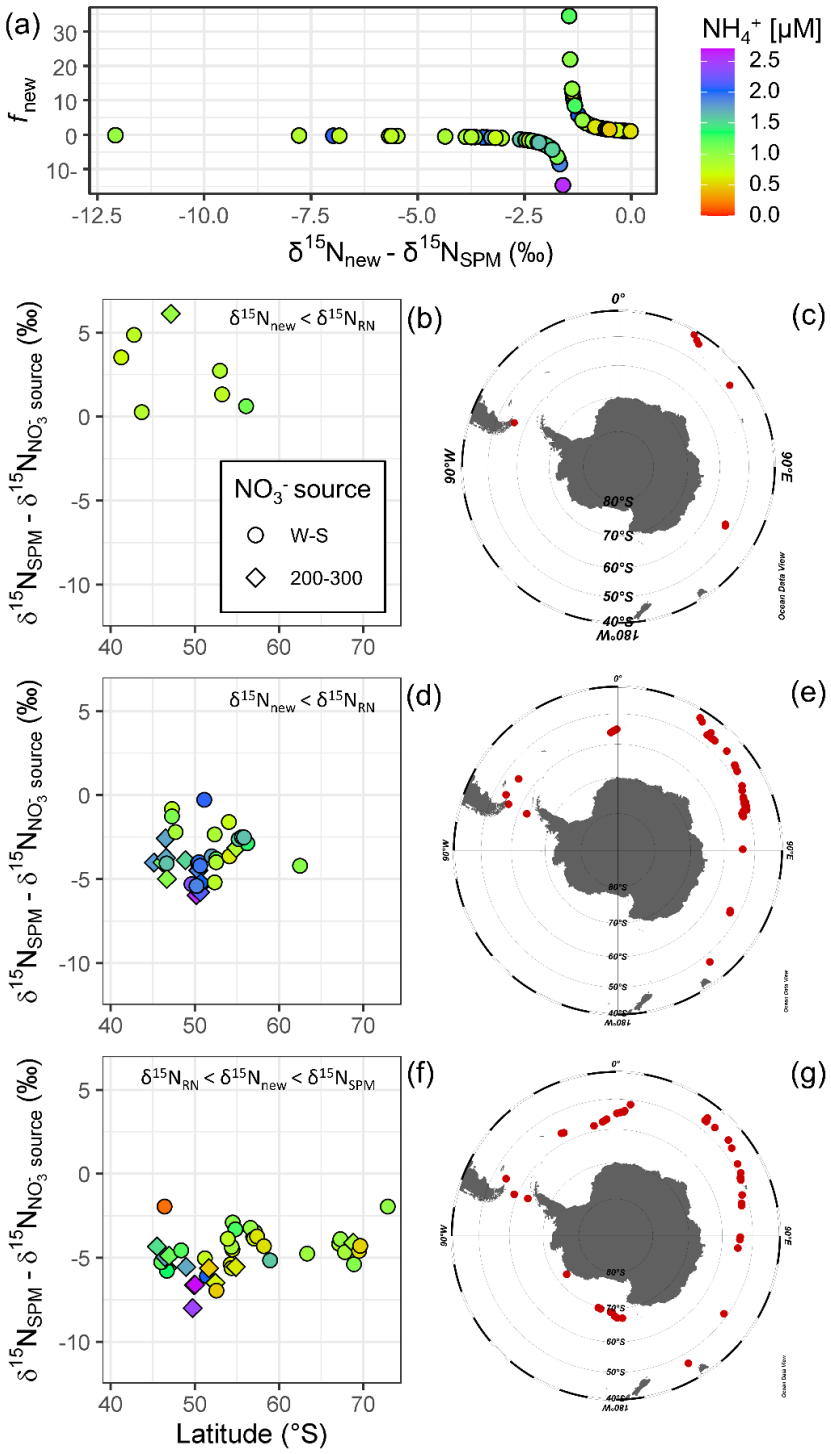

Figure A.16 Data that violate the Rayleigh model ($f_{new} \notin (0,1)$; n = 86). (a) Representation of the rational function f_{new} (i.e., $f_{new} = (\delta^{15}N_{SPM} - \delta^{15}N_{RN})/(\delta^{15}N_{new} - \delta^{15}N_{RN})$ where $\delta^{15}N_{SPM} > \delta^{15}N_{RN}$; Eqns 2 and 3) with a horizontal translation of the x-axis by $\delta^{15}N_{new} - \delta^{15}N_{SPM}$ to visualize local behaviour near the point where $\delta^{15}N_{new} = \delta^{15}N_{SPM}$. The domain of this function is $\delta^{15}N_{new} \neq \delta^{15}N_{RN}$. The function has a horizontal asymptote at y = 0. The function f_{new} is between 0 and 1 for values of $\delta^{15}N_{new} > \delta^{15}N_{SPM}$ (data not shown in the graph), $f_{new} > 1$ for values of $\delta^{15}N_{new}$ in the interval ($\delta^{15}N_{RN}$, $\delta^{15}N_{SPM}$), and $f_{new} < 0$ for values of $\delta^{15}N_{new} < \delta^{15}N_{RN}$. Symbol colours show the NH_4^+ concentrations (µM). (b-g) Latitudinal and spatial distribution of the "standardized" $\delta^{15}N_{SPM}$ (i.e., $\delta^{15}N_{SPM} - \delta^{15}N_{NO_3^- source}$) for observations that violate the Rayleigh model: (b-c) $\delta^{15}N_{new} < \delta^{15}N_{RN}$ and $\delta^{15}N_{SPM} > \delta^{15}N_{NO_3^- source}$, (d-e) $\delta^{15}N_{new} < \delta^{15}N_{RN}$ and $\delta^{15}N_{SPM} > \delta^{15}N_{NO_3^- source}$, and (f-g) $\delta^{15}N_{RN} < \delta^{15}N_{new} < \delta^{15}N_{SPM}$. Symbol shapes indicate source NO_3^- depth: circles = winter MLD – summer MLD and diamonds = 200-300 m layer.

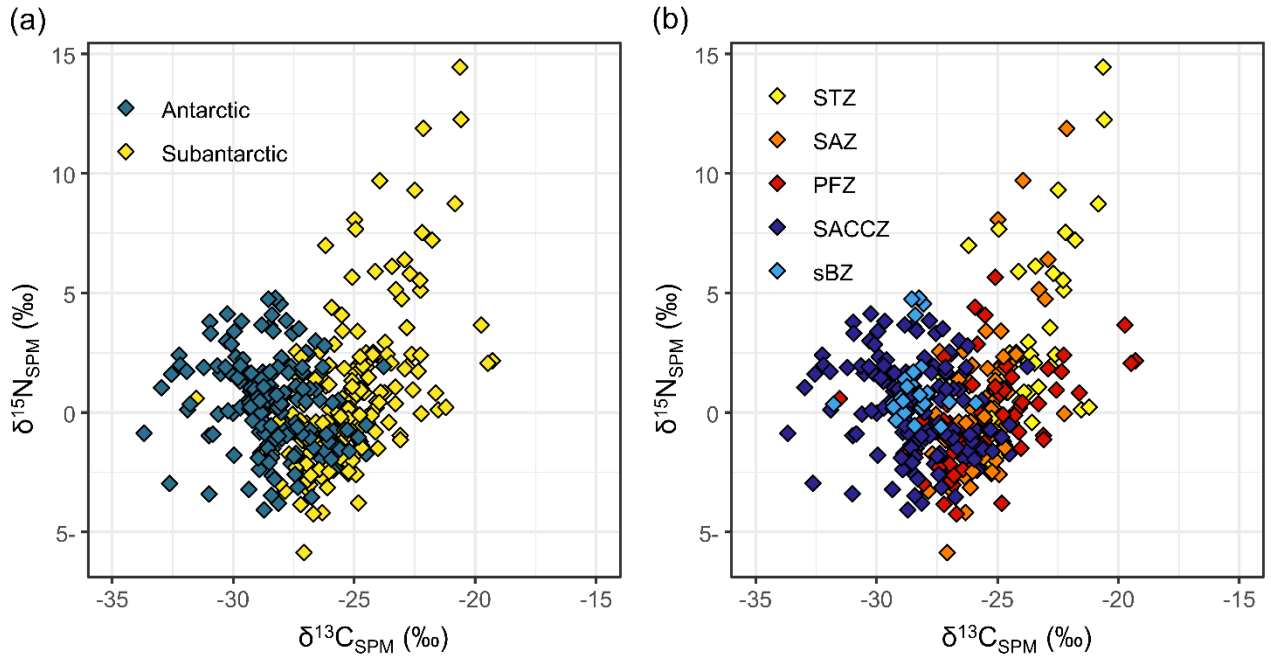

Figure A.17. Surface $\delta^{15}N_{SPM}$ versus $\delta^{13}C_{SPM}$ for all samples collected during ACE. Symbol colours show the different oceans and hydrographic zones: (a) yellow = Subantarctic Ocean, blue = Antarctic Ocean; (b) yellow = Subtropical Zone (STZ), orange = Subantarctic Zone (SAZ), red = Polar Frontal Zone (PFZ), dark blue = Southern Antarctic Circumpolar Current Zone (SACCZ), light blue = southern Boundary Zone (sBZ).

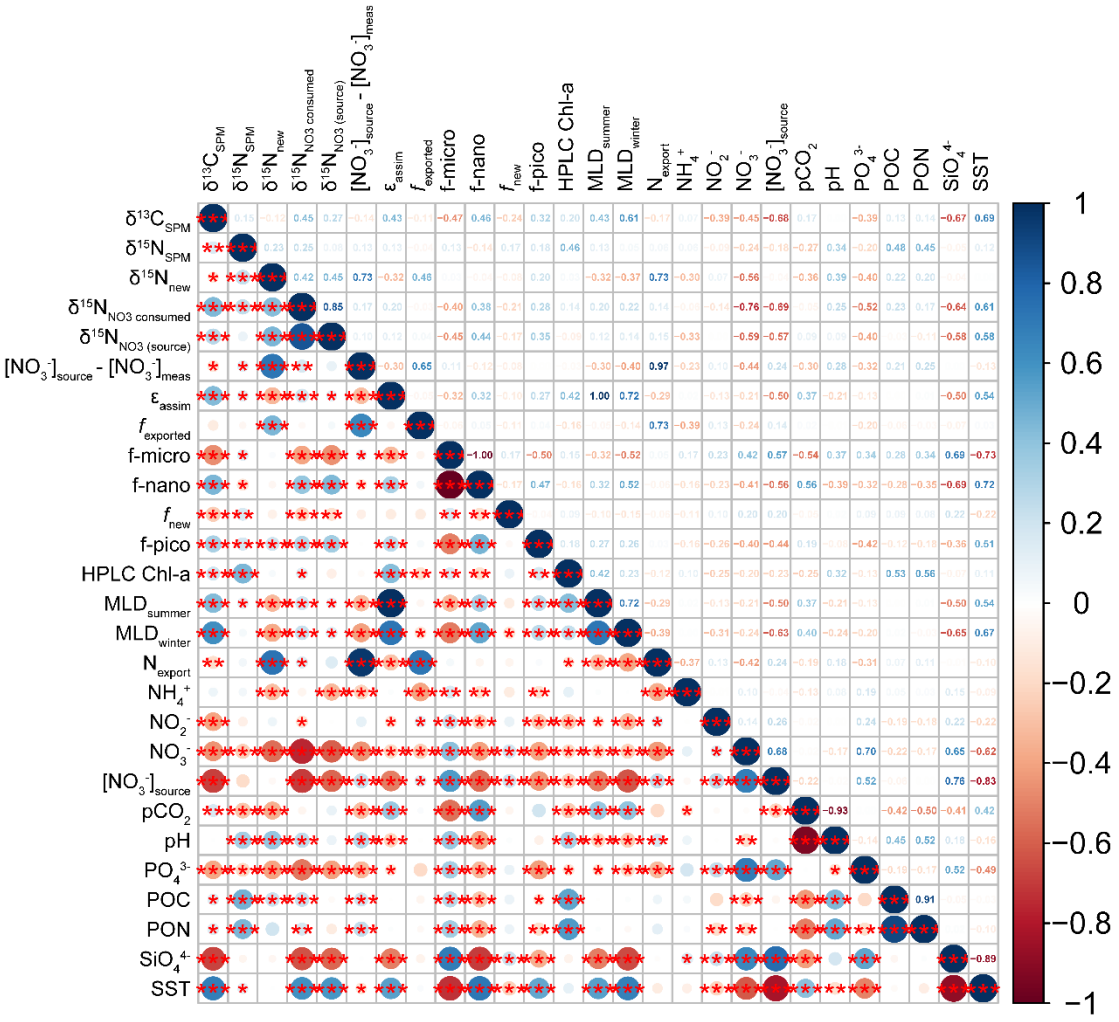

Figure A.18 Spearman's rank correlation analysis of 27 variables measured during ACE in the entire Southern Ocean transect, with no distinction of hydrographic zones or oceans. From the total dataset (n=364), 61 observations with NA values were dropped even if NA was associated with only one parameter, resulting in a final dataset of 303 observations. Correlation tests between the two parameters investigated are reported in the main text. The colour bar shows the correlation coefficient with red indicating negative correlations and blue showing positive correlations, and the red stars indicate the statistical significance at a *p*-value: * = 0.05, ** = 0.01, and *** = 0.001.

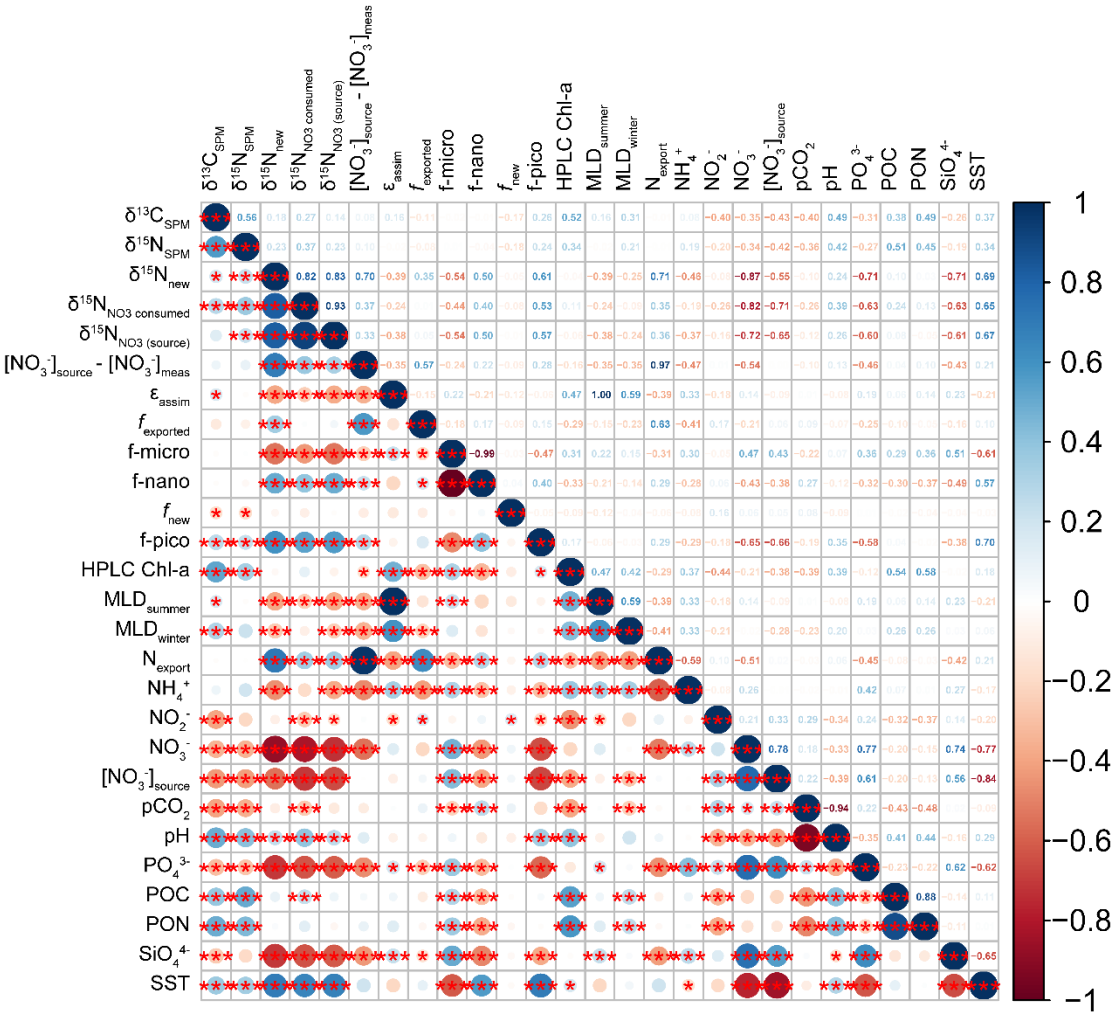

Figure A.19. Spearman's rank correlation analysis of 27 variables collected during ACE, on the dataset from the Subantarctic Ocean only. From the total dataset (n=198), 29 observations with NA values were dropped even if of one parameter, resulting in a final dataset of 169 observations. Correlation tests between the two parameters investigated are reported in the main text using the full dataset. The colour bar shows correlation coefficient where the red shows negative correlations and blue shows positive correlations, and the red stars indicate the statistical significance at a *p*-value: * = 0.05, ** = 0.01, and *** = 0.001.

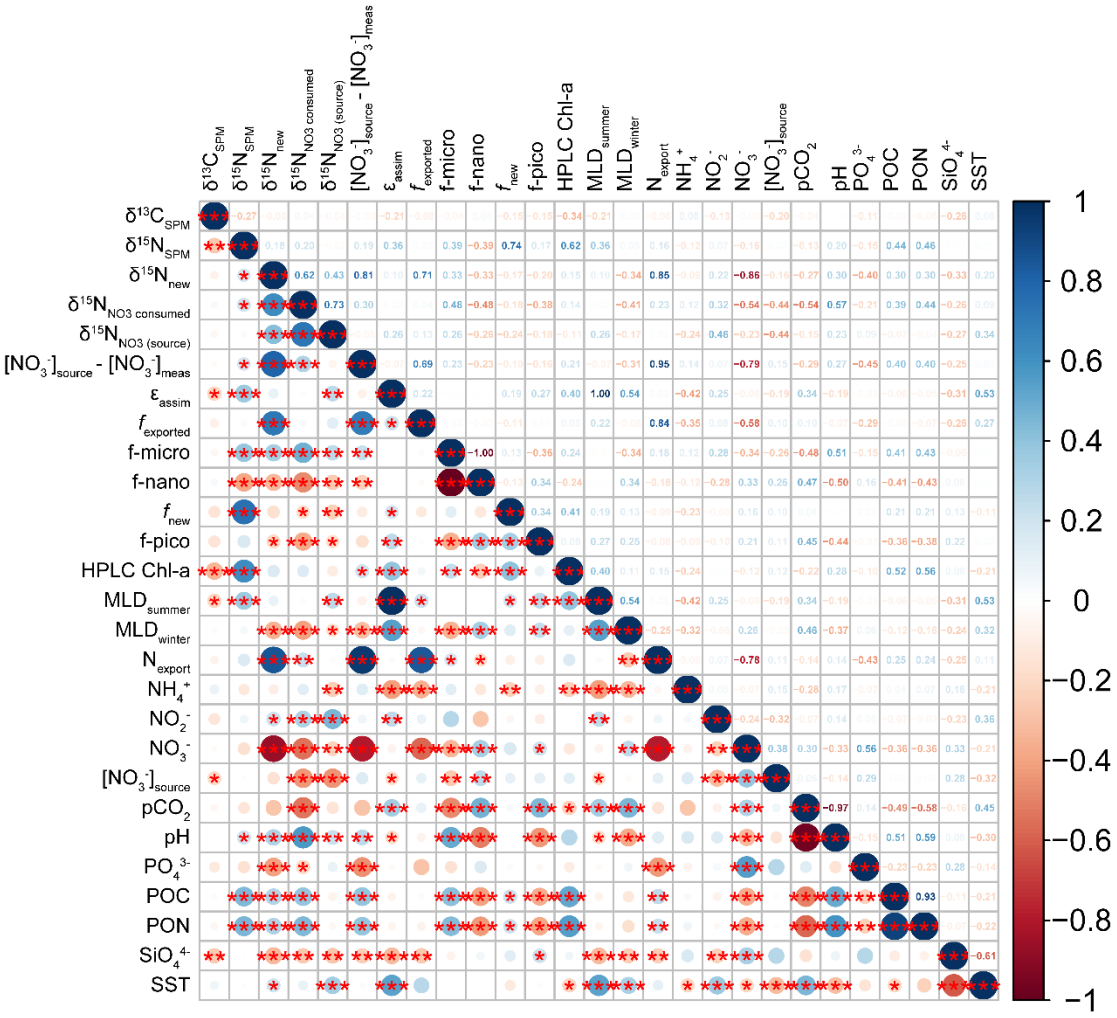

Figure A.20 Spearman's rank correlation analysis of 27 variables collected during ACE, on the dataset from the Antarctic Ocean only. From the total dataset (n=166), 35 observations with NA values were dropped even if of one parameter, resulting in a final dataset of 134 observations. The colour bar shows correlation coefficient where the red shows negative correlations and blue shows positive correlations, and the red stars indicate the statistical significance at a *p*-value: * = 0.05, ** = 0.01, and *** = 0.001.

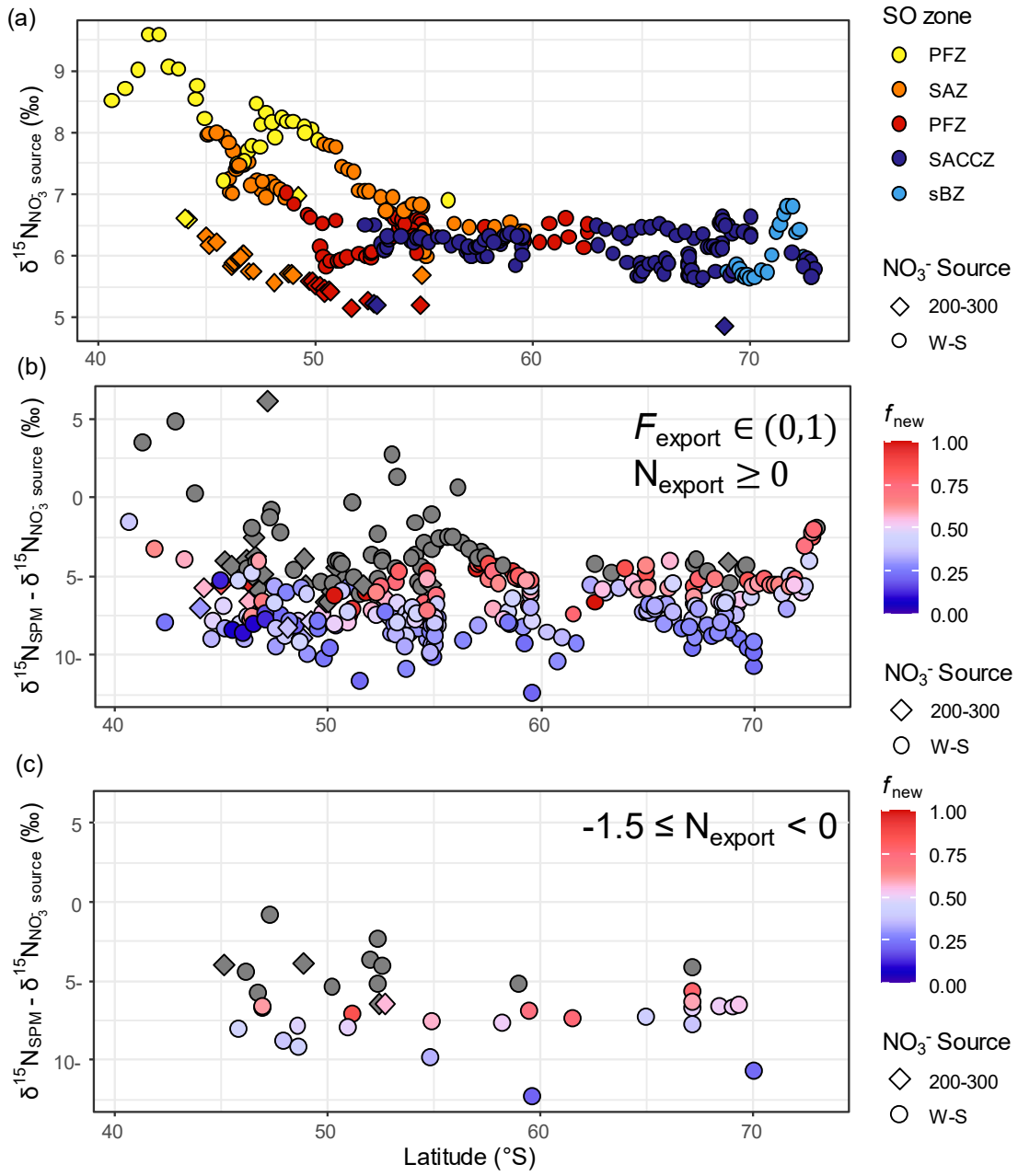

Figure A.21 (a) Latitudinal variability in the $\delta^{15}N_{NO_3^-\,(source)}$ used as the input to the Rayleigh model for the observations that satisfy the conditions of $F_{export} \in (0, 1)$ and $N_{export} \geq 0$ (-1.5) µM (n=306), with symbol colours showing the hydrographic zones: yellow = Subtropical Zone (STZ), orange = Subantarctic Zone (SAZ), red = Polar Frontal Zone (PFZ), dark blue = Southern Antarctic Circumpolar Current Zone (SACCZ), light blue = southern Boundary Zone (sBZ). (b-c) Latitudinal variability and dependence of $\delta^{15}N_{SPM}$ on $\delta^{15}N_{NO_3^-\,(source)}$ with symbol colours showing f_{new}. The grey symbols indicate observations that resulted in an estimate of f_{new} outside the expected range of 0 to 1, with panel (b) showing all observations for which $F_{export} \in (0, 1)$ and $N_{export} \geq 0$ µM, and panel (c) showing the observations for which -1.5 µM $\leq N_{export} < 0$ µM (see main text for details).

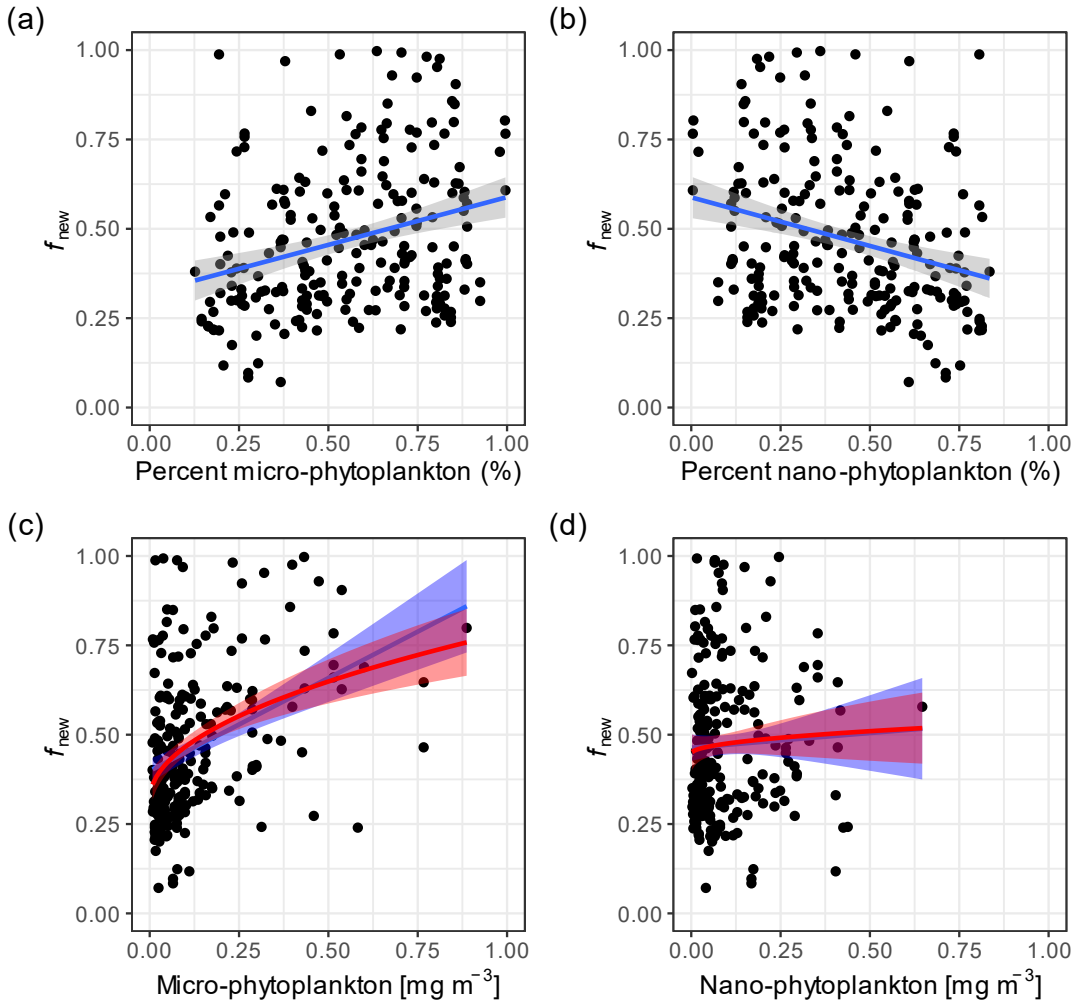

Figure A.22 f_{new} as a function of (a-b) the relative contribution to Chl-a and (c-d) the Chl-a biomass (mg m^{-3}) of micro-phytoplankton (>20 µm) and nano-phytoplankton (2-20 µm). The solid blue lines show a linear regression of the data and the solid red lines show the square root-transformed linear regression. The 95% confidence intervals are indicated by the similarly coloured shading.

Appendix B - A circum-Antarctic plankton isoscape II: zooplankton isotope niches and trophic structure across Southern Ocean hydrographic zones

a. Zooplankton abundances and percentage compositions

Table B.1 Total abundance (Ind. m^{-3}) and relative percentage composition (%) of zooplankton taxa collected from the neuston layer at each station during the Antarctic Circumnavigation Expedition. STZ = Subtropical Zone, SAZ = Subantarctic Zone, PFZ = Polar Frontal Zone, SACCZ = Southern Antarctic Circumpolar Current Zone, and sBZ = southern Boundary Zone.

Zone	Station	Taxa	Abundance (Ind. m^{-3})	Relative percentage (%)
SAZ	2	Pisces	46.6	51.6
SAZ	2	Copepoda	38.3	42.5
SAZ	2	Amphipoda	3.5	3.8
SAZ	2	Polychaeta	1.7	1.9
SAZ	2	Appendicularia	0.1	0.1
SAZ	2	Chaetognatha	0.1	0.1
SAZ	2	Hydrozoa	0.1	0.1
PFZ	16	Copepoda	142.8	99.4
PFZ	16	Polychaeta	0.5	0.4
PFZ	16	Hydrozoa	0.2	0.2
PFZ	16	Appendicularia	0.1	0.1
PFZ	16	Euphausiacea	<0.1	<0.1
SACCZ	19	Copepoda	1182.2	99.4
SACCZ	19	Enteropneusta	5.4	0.5
SACCZ	19	Appendicularia	0.4	<0.1
SACCZ	19	Thaliacea	0.4	<0.1
SACCZ	19	Amphipoda	0.2	<0.1
SACCZ	19	Euphausiacea	0.2	<0.1
SACCZ	19	Pteropoda	0.2	<0.1
SACCZ	19	Polychaeta	0.1	<0.1
PFZ	20	Copepoda	127.8	89.1
PFZ	20	Polychaeta	13.0	9.0
PFZ	20	Appendicularia	2.3	1.6
PFZ	20	Euphausiacea	0.2	0.1
PFZ	20	Hydrozoa	0.2	0.1
PFZ	20	Amphipoda	<0.1	<0.1
PFZ	20B	Copepoda	0.9	93.8
PFZ	20B	Polychaeta	<0.1	4.2
PFZ	20B	Hydrozoa	<0.1	2.1
SAZ	21	Copepoda	3.0	80.3
SAZ	21	Polychaeta	0.4	9.9
SAZ	21	Amphipoda	0.3	7.5
SAZ	21	Thaliacea	<0.1	0.9
SAZ	21	Appendicularia	<0.1	0.5
SAZ	21	Hydrozoa	<0.1	0.5
SAZ	21	Lepadiformes	<0.1	0.5
STZ	22	Copepoda	<0.1	38.9

STZ	22	Euphausiacea	<0.1	27.8
STZ	22	Hydrozoa	<0.1	27.8
STZ	22	Thaliacea	<0.1	5.6
STZ	23	Copepoda	118.2	97.7
STZ	23	Amphipoda	1.9	1.5
STZ	23	Pteropoda	0.7	0.6
STZ	23	Euphausiacea	0.1	0.1
STZ	23	Chaetognatha	<0.1	<0.1
STZ	23	Hydrozoa	<0.1	<0.1
STZ	23	Lepadiformes	<0.1	<0.1
STZ	23	Pisces	<0.1	<0.1
STZ	23	Thaliacea	<0.1	<0.1
SACCZ	25	Copepoda	56.0	91.5
SACCZ	25	Amphipoda	5.0	8.2
SACCZ	25	Euphausiacea	0.1	0.2
sBZ	54	Appendicularia	1.6	94.3
sBZ	54	Euphausiacea	0.1	3.1
sBZ	54	Hydrozoa	<0.1	1.5
sBZ	54	Chaetognatha	<0.1	<0.1
sBZ	56	Copepoda	68.1	99.5
sBZ	56	Appendicularia	0.3	0.5
SACCZ	67	Copepoda	0.4	91.4
SACCZ	67	Appendicularia	<0.1	6.4
SACCZ	67	Amphipoda	<0.1	1.4
SACCZ	67	Euphausiacea	<0.1	0.7
SACCZ	68	Copepoda	541.4	99.6
SACCZ	68	Amphipoda	2.0	0.4
SACCZ	68	Euphausiacea	0.1	<0.1
SACCZ	68	Pisces	<0.1	<0.1
SACCZ	71	Copepoda	36.1	99.5
SACCZ	71	Amphipoda	0.1	0.4
SACCZ	71	Euphausiacea	<0.1	0.1
SAZ	73	Copepoda	55.5	80.7
SAZ	73	Euphausiacea	3.7	5.3
SAZ	73	Acantharia	3.5	5.1
SAZ	73	Pteropoda	3.2	4.6
SAZ	73	Amphipoda	1.1	1.5
SAZ	73	Foraminifera	0.8	1.1
SAZ	73	Chaetognatha	0.5	0.7
SAZ	73	Appendicularia	0.4	0.6
SAZ	73	Ostracoda	0.1	0.2
SAZ	73	Polychaeta	<0.1	<0.1
SAZ	77	Copepoda	43.3	75.6
SAZ	77	Amphipoda	12.1	21.2
SAZ	77	Pteropoda	0.5	0.9
SAZ	77	Euphausiacea	0.5	0.9
SAZ	77	Appendicularia	0.4	0.7
SAZ	77	Chaetognatha	0.4	0.7

SAZ	77	Hydrozoa	<0.1	0.1
SAZ	77	Lepadiformes	<0.1	0.1
SAZ	78	Appendicularia	1.3	50.9
SAZ	78	Copepoda	1.0	39.2
SAZ	78	Pteropoda	0.1	5.0
SAZ	78	Chaetognatha	0.1	3.7
SAZ	78	Amphipoda	<0.1	0.8
SAZ	78	Lepadiformes	<0.1	0.5
SACCZ	94	Radiozoa	15.7	51.4
SACCZ	94	Pteropoda	11.4	37.4
SACCZ	94	Copepoda	2.5	8.0
SACCZ	94	Appendicularia	0.7	2.3
SACCZ	94	Euphausiacea	0.3	0.9
PFZ	100	Copepoda	13.0	96.9
PFZ	100	Appendicularia	0.3	2.5
PFZ	100	Chaetognatha	<0.1	0.3
PFZ	100	Amphipoda	<0.1	0.1
PFZ	100	Lepadiformes	<0.1	0.1
PFZ	100	Pteropoda	<0.1	0.1

Table B.2 Average (± 1SD) abundances [Ind. m^{-3}] and relative percentage composition [%] of zooplankton taxa collected from the neuston layer during the Antarctic Circumnavigation Expedition at each hydrographic zone: STZ = Subtropical Zone, SAZ = Subantarctic Zone, PFZ = Polar Frontal Zone, SACCZ = Southern Antarctic Circumpolar Current Zone, and sBZ = southern Boundary Zone. Each sampling station was considered as single replicate for the relative hydrographic zone, and the absent species were counted as null abundance. Average (± standard error) of the relative percentage composition [%] of zooplankton taxa assessed for each station within the same hydrographic zone (see Table B.1).

Zone	Taxa	n	Average abundance (Ind. m^{-3})	Relative percentage (%)	Average relative percentage among stations (%)
STZ	Copepoda	13	59.1 ± 83.6	97.7	68.3 ± 41.6
STZ	Amphipoda	9	0.9 ± 1.3	1.5	0.8 ± 1.
STZ	Pteropoda	9	0.4 ± 0.5	0.6	0.3 ± 0.4
STZ	Euphausiacea	13	<0.1	0.1	13.9 ± 19.6
STZ	Hydrozoa	13	<0.1	<0.1	13.9 ± 19.6
STZ	Chaetognatha	9	<0.1	<0.1	<0.1
STZ	Lepadiformes	9	<0.1	<0.1	<0.1
STZ	Thaliacea	13	<0.01	<<0.1	2.8 ± 3.9
STZ	Pisces	9	<0.01	<<0.1	<<0.1
STZ	Acantharia	0	0.0	0.0	-
STZ	Appendicularia	0	0.0	0.0	-
STZ	Enteropneusta	0	0.0	0.0	-
STZ	Foraminifera	0	0.0	0.0	-
STZ	Ostracoda	0	0.0	0.0	-
STZ	Polychaeta	0	0.0	0.0	-
STZ	Radiozoa	0	0.0	0.0	-
SAZ	Copepoda	38	28.2 ± 24.8	63.4	63.6 ± 21.0
SAZ	Pisces	7	9.3 ± 20.8	21.0	10.3 ± 23.1
SAZ	Amphipoda	38	3.4 ± 5.08	7.6	7.0 ± 8.4
SAZ	Euphausiacea	18	0.8 ± 1.6	1.9	1.2 ± 2.3
SAZ	Pteropoda	24	0.8 ± 1.4	1.7	2.1 ± 2.5
SAZ	Acantharia	10	0.7 ± 1.6	1.6	1.0 ± 2.3
SAZ	Appendicularia	38	0.4 ± 0.5	0.1	10.6 ± 22.6
SAZ	Polychaeta	24	0.4 ± 0.7	0.1	2.4 ± 4.3
SAZ	Chaetognatha	31	0.2 ± 0.2	<0.1	1.0 ± 1.5
SAZ	Foraminifera	10	0.2 ± 0.3	<0.1	0.2 ± 0.5
SAZ	Ostracoda	10	<0.1	<<0.1	<0.1
SAZ	Hydrozoa	22	<0.1	<<0.1	0.1 ± 0.2
SAZ	Lepadiformes	21	<0.1	<<0.1	0.2 ± 0.3
SAZ	Thaliacea	7	<<0.1	<<0.1	0.2 ± 0.4
SAZ	Enteropneusta	0	0.0	0.0	-
SAZ	Radiozoa	0	0.0	0.0	-
PFZ	Copepoda	20	71.1 ± 74.5	94.3	94.8 ± 4.43
PFZ	Polychaeta	14	3.4 ± 6.4	4.5	3.4 ± 4.2
PFZ	Appendicularia	17	0.7 ± 1.1	0.9	1.1 ± 1.2
PFZ	Hydrozoa	14	0.1 ± 0.1	0.1	0.6 ± 1.0
PFZ	Euphausiacea	11	<0.1	0.1	<0.1
PFZ	Amphipoda	12	<0.1	<0.1	<0.1
PFZ	Chaetognatha	6	<0.1	<0.1	0.1 ± 0.2

PFZ	Lepadiformes	6	<<0.1	<<0.1	<0.1
PFZ	Pteropoda	6	<<0.1	<<0.1	<0.1
PFZ	Acantharia	0	0.0	0.0	-
PFZ	Enteropneusta	0	0.0	0.0	-
PFZ	Foraminifera	0	0.0	0.0	-
PFZ	Ostracoda	0	0.0	0.0	-
PFZ	Pisces	0	0.0	0.0	-
PFZ	Radiozoa	0	0.0	0.0	-
PFZ	Thaliacea	0	0.0	0.0	-
SACCZ	Copepoda	27	303.0 ± 478.0	97.7	81.6 ± 36.3
SACCZ	Radiozoa	5	2.6 ± 6.4	0.9	8.6 ± 21
SACCZ	Pteropoda	13	1.9 ± 4.7	0.6	6.2 ± 15.2
SACCZ	Amphipoda	22	1.22 ± 2.02	0.4	1.74 ± 3.22
SACCZ	Enteropneusta	8	1.0 ± 2.2	0.3	0.1 ± 0.2
SACCZ	Appendicularia	17	0.2 ± 0.3	0.1	1.5 ± 2.6
SACCZ	Euphausiacea	27	0.1 ± 0.1	<0.1	0.3 ± 0.4
SACCZ	Thaliacea	8	<<0.1	<0.1	<<0.1
SACCZ	Polychaeta	8	<<0.1	<<0.1	<<0.1
SACCZ	Pisces	4	<<0.1	<<0.1	<<0.1
SACCZ	Acantharia	0	0.0	0.0	-
SACCZ	Chaetognatha	0	0.0	0.0	-
SACCZ	Foraminifera	0	0.0	0.0	-
SACCZ	Hydrozoa	0	0.0	0.0	-
SACCZ	Lepadiformes	0	0.0	0.0	-
SACCZ	Ostracoda	0	0.0	0.0	-
sBZ	Copepoda	2	34.0 ± 48.1	97.1	49.8 ± 70.4
sBZ	Appendicularia	6	1.0 ± 1.0	2.8	47.4 ± 66.4
sBZ	Euphausiacea	4	<0.1	0.1	1.6 ± 2.2
sBZ	Hydrozoa	4	<<0.1	<0.1	0.7 ± 1.1
sBZ	Chaetognatha	4	<<0.1	<0.1	0.5 ± 0.7
sBZ	Acantharia	0	0.0	0.0	-
sBZ	Amphipoda	0	0.0	0.0	-
sBZ	Enteropneusta	0	0.0	0.0	-
sBZ	Foraminifera	0	0.0	0.0	-
sBZ	Lepadiformes	0	0.0	0.0	-
sBZ	Ostracoda	0	0.0	0.0	-
sBZ	Pisces	0	0.0	0.0	-
sBZ	Polychaeta	0	0.0	0.0	-
sBZ	Pteropoda	0	0.0	0.0	-
sBZ	Radiozoa	0	0.0	0.0	-
sBZ	Thaliacea	0	0.0	0.0	-

Table B.3 Average (± standard error) abundances [Ind. m^{-3}] and relative percentage (%) of zooplankton taxa collected from the neuston layer during the Antarctic Circumnavigation Expedition, at each hydrographic zone: STZ = Subtropical Zone, SAZ = Subantarctic Zone, PFZ = Polar Frontal Zone, SACCZ = Southern Antarctic Circumpolar Current Zone, and sBZ = southern Boundary Zone; m = male; f = female; CI-CV= Copepodite stage level from 1 to 5. Each sampling station was considered as single replicate for the relative hydrographic zone, and the absent species were counted as null abundance.

STZ

Taxa	Species	Life stage	Average abundance (Ind. m^{-3})	Relative percentage (%)
Amphipoda	*Cyllopus* spp.	adult	0.2 ± 0.2	0.3
Amphipoda	Hyperiidae	adult	0.3 ± 0.3	0.5
Amphipoda	*Themisto gaudichaudii*	adult	0.4 ± 0.4	0.7
Chaetognatha	Chaetognatha	adult	<0.1	<0.1
Copepoda	Calanidae	CI - CII	<<0.1	<<0.1
Copepoda	Calanidae	CII	<<0.1	<<0.1
Copepoda	Calanidae	CIII	0.6 ± 0.6	1.0
Copepoda	*Calanus propinquus*	CV	<<0.1	<<0.1
Copepoda	*Clausocalanus laticeps*	adult	<<0.1	<<0.1
Copepoda	Copepoda Und.	eggs	<<0.1	<<0.1
Copepoda	*Microcalanus* spp.	adult	58.0 ± 57.8	95.7
Copepoda	*Oithona* spp.	adult	0.6 ± 0.6	1.0
Euphausiacea	Euphausiacea (0-5mm)	adult	<<0.1	<<0.1
Euphausiacea	Euphausiacea (10-20mm)	adult	<0.1	<0.1
Euphausiacea	Euphausiacea (5-10 mm)	adult	<0.1	<0.1
Hydrozoa	*Physalia physalis*	adult	<0.1	<0.1
Hydrozoa	Siphonophorae	adult	<0.1	<0.1
Lepadiformes	Lepadiformes larva	larvae	<0.1	<0.1
Pisces	Fish larvae	larvae	<0.1	<0.1
Pteropoda	Euthecosomata	adult	<0.1	<0.1
Pteropoda	Gymnosomata	adult	0.4 ± 0.4	0.7
Thaliacea	*Salpa* spp.	adult	<<0.1	0.0

SAZ

Taxa	Species	Life stage	Average abundance (Ind. m^{-3})	Relative percentage (%)
Acantharia	Acantharia	adult	0.7 ± 0.7	1.6
Amphipoda	*Cyllopus* spp.	adult	0.7 ± 0.7	1.6
Amphipoda	Hyperiidae	adult	<<0.1	<<0.1
Amphipoda	*Themisto gaudichaudii*	adult	2.7 ± 2.4	6.0
Appendicularia	Appendicularia	adult	<0.1	<0.1
Appendicularia	*Oikopeura* spp.	adult	0.4 ± 0.2	0.9
Chaetognatha	Chaetognatha	adult	0.2 ± 0.1	0.4
Copepoda	Calanidae	CI	0.2 ± 0.2	0.4
Copepoda	Calanidae	CI - CII	<0.1	<0.1
Copepoda	Calanidae	CII	0.7 ± 0.6	1.6
Copepoda	Calanidae	CIII	3.1 ± 1.9	6.9
Copepoda	Calanidae	CIV	2.1 ± 1.2	4.7
Copepoda	*Calanus propinquus*	CV	0.4 ± 0.4	0.9
Copepoda	*Calanus simillimus*	CV	2.8 ± 2.8	6.3
Copepoda	*Candacia varicans* s.l.	f	<0.1	<0.1
Copepoda	*Clausocalanus laticeps*	adult	<<0.1	<<0.1
Copepoda	Copepoda Und.	eggs	0.5 ± 0.5	1.1
Copepoda	Exuvia		<0.1	<0.1
Copepoda	*Metridia gerlachei*	CV	0.1 ± 0.1	0.2
Copepoda	*Metridia lucens*	adult	0.5 ± 0.5	1.1
Copepoda	*Metridia* spp.	CIV	0.9 ± 0.9	2.0
Copepoda	*Microcalanus* spp.	adult	6.3 ± 3.9	14.1
Copepoda	Nauplii	nauplius	0.3 ± 0.3	0.7
Copepoda	Nauplii*	nauplius	<<0.1	<<0.1
Copepoda	*Oithona* spp.	adult	9.0 ± 4.2	20.1
Copepoda	*Oithona* spp.	juvenile	<0.1	<0.1
Copepoda	*Oithona* spp.	m	<0.1	<0.1
Copepoda	*Oithona* spp.	adult	0.1 ± 0.1	0.2
Copepoda	*Paraeuchaeta antarctica*	CV	<0.1	<0.1
Copepoda	Copepoda Und.	adult	0.9 ± 0.9	2.0
Euphausiacea	Euphausiacea (10-20mm)	adult	0.1 ± 0.1	0.2
Euphausiacea	Euphausiacea (5-10 mm)	adult	0.8 ± 0.8	1.8
Foraminifera	Foraminifera	adult	0.2 ± 0.2	0.4
Hydrozoa	Hydrozoa	adult	<<0.1	<<0.1
Hydrozoa	Scyphozoa	adult	<<0.1	<<0.1
Hydrozoa	Siphonophorae	adult	<0.1	<0.1
Lepadiformes	Lepadiformes larva	larvae	<0.1	<0.1
Ostracoda	Ostracoda	adult	<0.1	<0.1
Pisces	Fish larvae	larvae	9.3 ± 9.32	20.8
Polychaeta	Polychaeta	larvae	0.1 ± 0.1	0.2
Polychaeta	*Tomopteris* spp.	larvae	0.3 ± 0.3	0.7
Pteropoda	Euthecosomata	adult	<<0.1	<<0.1
Pteropoda	*Limacina* spp.	adult	0.8 ± 0.6	1.8
Thaliacea	*Salpa* spp.	adult	<<0.1	<<0.1

PFZ

Taxa	Species	Life stage	Average abundance (Ind. m^{-3})	Relative percentage (%)
Amphipoda	*Themisto gaudichaudii*	adult	<0.1	0.1
Appendicularia	Appendicularia	adult	0.6 ± 0.6	0.8
Appendicularia	*Frittillaria* spp.	adult	<<0.1	<<0.1
Appendicularia	*Oikopeura* spp.	adult	0.1 ± 0.1	0.1
Chaetognatha	Chaetognatha	adult	<0.1	<0.1
Copepoda	Calanidae	CI	0.8 ± 0.5	1.1
Copepoda	Calanidae	CI - CII	4.1 ± 2.7	5.4
Copepoda	Calanidae	CII	4.0 ± 2.4	5.3
Copepoda	Calanidae	CIII	0.2 ± 0.2	0.3
Copepoda	Calanidae	CIV	0.4 ± 0.4	0.5
Copepoda	*Calanus propinquus*	CV	1.1 ± 0.7	1.5
Copepoda	Clausocalanidae		<0.1	<0.1
Copepoda	*Clausocalanus laticeps*	adult	6.9 ± 5.3	9.1
Copepoda	Copepoda Und.	eggs	3.5 ± 3.1	4.6
Copepoda	Exuvia		2.2 ± 1.3	2.9
Copepoda	Harpacticoida	Juvenile	0.7 ± 0.5	0.9
Copepoda	Nauplii*	nauplius	1.6 ± 1.6	2.1
Copepoda	*Oithona* spp.	adult	2.5 ± 2.5	3.3
Copepoda	*Oithona* spp.	juvenile	43.0 ± 25.1	56.9
Copepoda	Copepoda Und.	adult	0.1 ± 0.1	0.1
Euphausiacea	Euphausiacea	adult	<0.1	<0.1
Euphausiacea	Euphausiacea (caliptopis)	larvae	<0.1	<0.1
Hydrozoa	Hydrozoa	adult	<0.1	<0.1
Hydrozoa	Siphonophorae	adult	<0.1	<0.1
Lepadiformes	Lepadiformes larva	larvae	<<0.1	<<0.1
Polychaeta	Polychaeta	larvae	3.4 ± 3.2	4.5
Pteropoda	*Limacina* spp.	adult	<<0.1	<0.1

SACCZ

Taxa	Species	Life stage	Average abundance (Ind. m^{-3})	Relative percentage (%)
Amphipoda	*Cyllopus* spp.	adult	<<0.1	<<0.1
Amphipoda	Hyperiidae	adult	<<0.1	<<0.1
Amphipoda	*Themisto gaudichaudii*	adult	1.2 ± 0.82	0.4
Appendicularia	Appendicularia	adult	0.1 ± 0.1	<0.1
Appendicularia	*Oikopeura* spp.	adult	0.1 ± 0.1	<0.1
Copepoda	Calanidae	CI - CII	1.3 ± 1.3	0.4
Copepoda	Calanidae	CII	1.5 ± 1.3	0.5
Copepoda	Calanidae	CIII	3.1 ± 1.8	1.0
Copepoda	Calanidae	CIV	0.8 ± 0.5	0.3
Copepoda	*Calanus propinquus*	CV	0.1 ± 0.1	<0.1
Copepoda	*Calanus simillimus*	CV	<<0.1	<<0.1
Copepoda	Clausocalanidae		6.6 ± 6.6	2.1
Copepoda	*Clausocalanus laticeps*	adult	89.0 ± 89.0	28.6
Copepoda	Copepoda Und.	eggs	0.3 ± 0.3	0.1
Copepoda	Exuvia		24.0 ± 23.6	7.7
Copepoda	Harpacticoida	Juvenile	0.9 ± 0.9	0.3
Copepoda	*Metridia gerlachei*	CV	<0.1	<0.1
Copepoda	*Metridia lucens*	adult	0.3 ± 0.3	0.1
Copepoda	*Microcalanus* spp.	adult	18.0 ± 17.3	5.8
Copepoda	Nauplii	nauplius	1.2 ± 0.9	0.4
Copepoda	Nauplii*	nauplius	0.2 ± 0.2	0.1
Copepoda	*Oithona* spp.	adult	76.0 ± 69.0	24.4
Copepoda	*Oithona* spp.	juvenile	80.0 ± 80.4	25.7
Copepoda	*Oithona* spp.	m	0.3 ± 0.3	0.1
Copepoda	Copepoda Und.	adult	<0.1	0.3
Enteropneusta	Enteropneusta	larvae	0.9 ± 0.9	0.3
Euphausiacea	Euphausiacea	adult	<0.1	<0.1
Euphausiacea	Euphausiacea (>20mm)	adult	<0.1	<0.1
Euphausiacea	Euphausiacea (>5 cm)	adult	<<0.1	<<0.1
Euphausiacea	Euphausiacea (0-5mm)	adult	<<0.1	<<0.1
Euphausiacea	Euphausiacea (caliptopis)	larvae	0.1 ± 0.1	<0.1
Pisces	Fish larvae	larvae	<<0.1	<<0.1
Polychaeta	Polychaeta	larvae	<0.1	<<0.1
Pteropoda	*Creseis* spp.	adult	<0.1	<<0.1
Pteropoda	*Limacina* spp.	adult	1.9 ± 1.9	0.6
Radiozoa	Radiozoa	adult	2.6 ± 2.6	0.8
Thaliacea	*Salpa* spp.	adult	0.1 ± 0.1	<0.1

sBZ

Taxa	Species	Life stage	Average abundance (Ind. m^{-3})	Relative percentage (%)
Appendicularia	*Oikopeura* spp.	adult	1.00 ± 0.7	2.9
Chaetognatha	Chaetognatha	adult	<<0.1	<0.1
Copepoda	Calanidae	CIII	0.4 ± 0.4	1.2
Copepoda	Exuvia		0.4 ± 0.4	1.2
Copepoda	Nauplii	nauplius	0.8 ± 0.8	2.3
Copepoda	*Oithona* spp.	adult	32.0 ± 32.5	92.3
Euphausiacea	Euphausiacea (10-20mm)	adult	<0.1	0.1
Hydrozoa	*Physalia physalis*	adult	<0.1	0.1

b. Temporal variability of stable isotopes

Longitudinal gradient analysis was performed to determine any geographical differences between Southern Ocean sectors (Indian, Pacific, and Atlantic). Since the expedition was conducted proceeding almost always longitudinally, a longitudinal analysis also allows the calculation of temporal variabilities in zooplankton SIs.

Figure B.1 shows the $\delta^{15}N$ and $\delta^{13}C$ values of the zooplankton (full coloured dots) and SPM (opaque grey diamonds) distributed across time, for each oceanic zone (different panels). Linear regressions were determined considering each taxon as singular data points and referring to the whole zooplankton communities; however, only the SAZ, SACCZ and PFZ had sufficient stations and data points spread across time to allow the calculation of a clear temporal trend in SIs. While zooplankton results are explained in the main manuscript and summarized in Table B4, temporal trends for SPM are comprehensively explained by Chapter 2 and in the associated Appendix A.

Table B.4 also contains the temporal variability of carbon to nitrogen (C:N) ratio of zooplankton for each hydrographic region investigated. The analysis did not reveal a linear relationship between C:N and time (*lm*, *p*-values > 0.05).

Table B.4 Temporal variability of zooplankton $\delta^{13}C$ [‰], $\delta^{15}N$ [‰] and C:N ratio assessed for each hydrographic region investigated. σ = estimated standard deviation of the errors (or residual standard deviation); *p*-value = probabilistic test to reject the Null Hypothesis; R-squared (R^2) = coefficient of determination.

$\delta^{13}C$ (‰)

Region	Linear regression	σ	*p*-value	R^2
Subantarctic	y ~ 692.66 - 0.0416 * Time	3.37	**0.00403**	0.092
Antarctic	y ~ -50.38 + 0.00136 * Time	3.55	0.955	0.000041
STZ	y ~ -2073.61 + 0.119 * Time	1.42	0.286	0.076
SAZ	y ~ 650.46 - 0.0391 * Time	3.94	0.132	0.068
PFZ	y ~ 645.44 - 0.0389 * Time	3.27	**0.0435**	0.11
SACCZ	y ~ -226.57 + 0.0116 * Time	3.07	0.584	0.0059
sBZ	y ~ 7602.13 - 0.443 * Time	4.06	0.329	0.035

$\delta^{15}N$ (‰)

Region	Linear regression	σ	*p*-value	R^2
Subantarctic	y ~ 900.75 - 0.0522 * Time	2.33	**1.35E-06**	0.25
Antarctic	y ~ -153.52 + 0.00921 * Time	2.25	0.536	0.0049
STZ	y ~ -5112.87 + 0.298 * Time	1.39	**0.013**	0.35
SAZ	y ~ 794.22 - 0.046 * Time	2.11	**0.00213**	0.26
PFZ	y ~ 899.04 - 0.0521 * Time	2.67	**0.00239**	0.25
SACCZ	y ~ -271.15 + 0.016 * Time	2.00	0.235	0.028
sBZ	y ~ -619.9 + 0.0364 * Time	2.24	0.885	0.00081

C:N ratio

Region	Linear regression	σ	*p*-value	R^2
Subantarctic	y ~ -18.49 + 0.00136 * Time	2.35	0.893	0.00022
Antarctic	y ~ 45.5 - 0.00238 * Time	1.49	0.809	0.00075
STZ	y ~ -1382.51 + 0.0807 * Time	1.21	0.395	0.049
SAZ	y ~ 293.16 - 0.0168 * Time	2.75	0.356	0.027
PFZ	y ~ -188.38 + 0.0113 * Time	2.23	0.400	0.022
SACCZ	y ~ 44.61 - 0.00233 * Time	1.43	0.808	0.0012
sBZ	y ~ -338.35 + 0.0199 * Time	1.65	0.915	0.00045

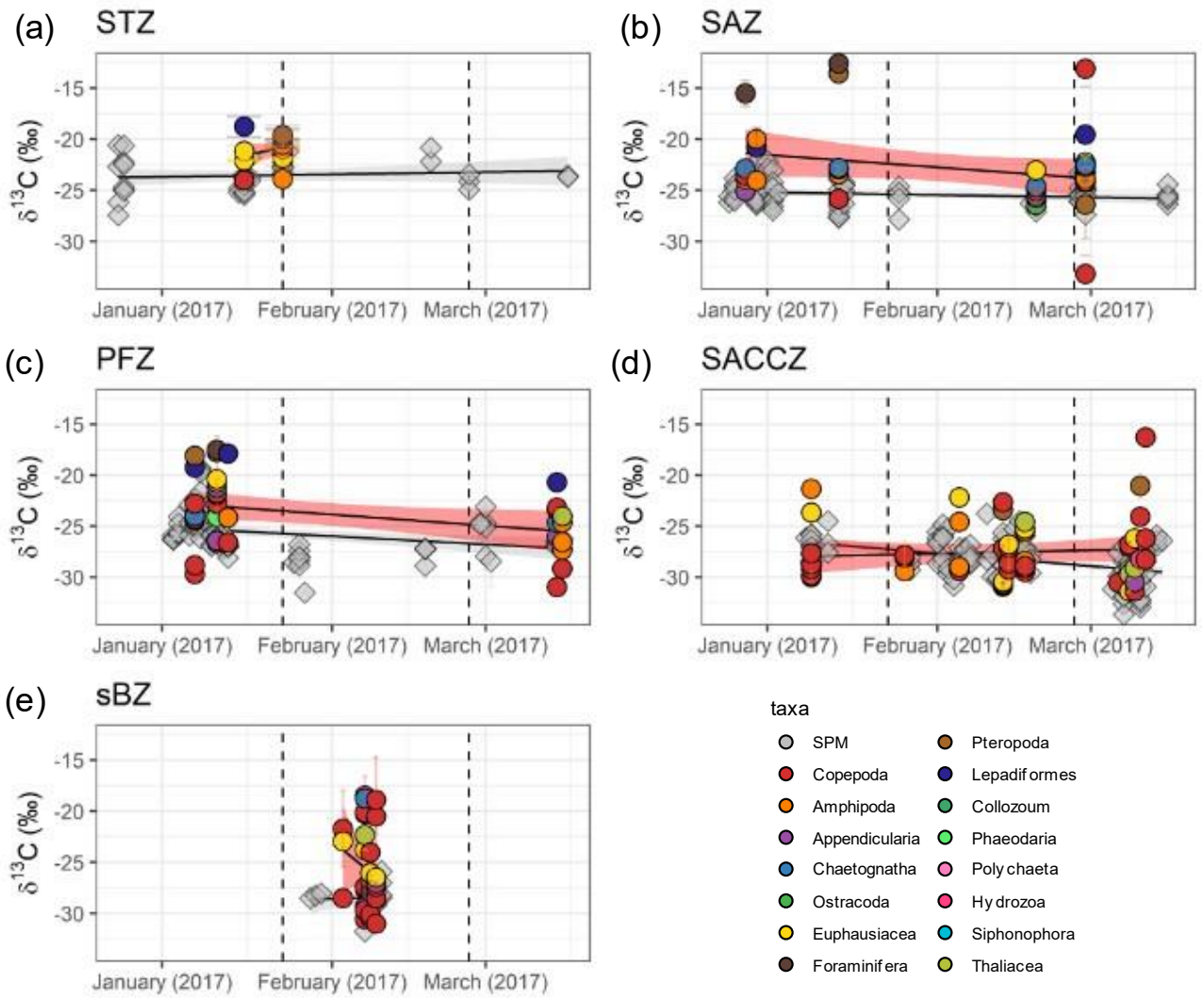
(a) STZ
(b) SAZ
(c) PFZ
(d) SACCZ
(e) sBZ
δ13C (‰)
-15
-20
-25
-30
January (2017)
February (2017)
March (2017)
taxa
SPM
Copepoda
Amphipoda
Appendicularia
Chaetognatha
Ostracoda
Euphausiacea
Foraminifera
Pteropoda
Lepadiformes
Collozoum
Phaeodaria
Polychaeta
Hydrozoa
Siphonophora
Thaliacea

Continues…

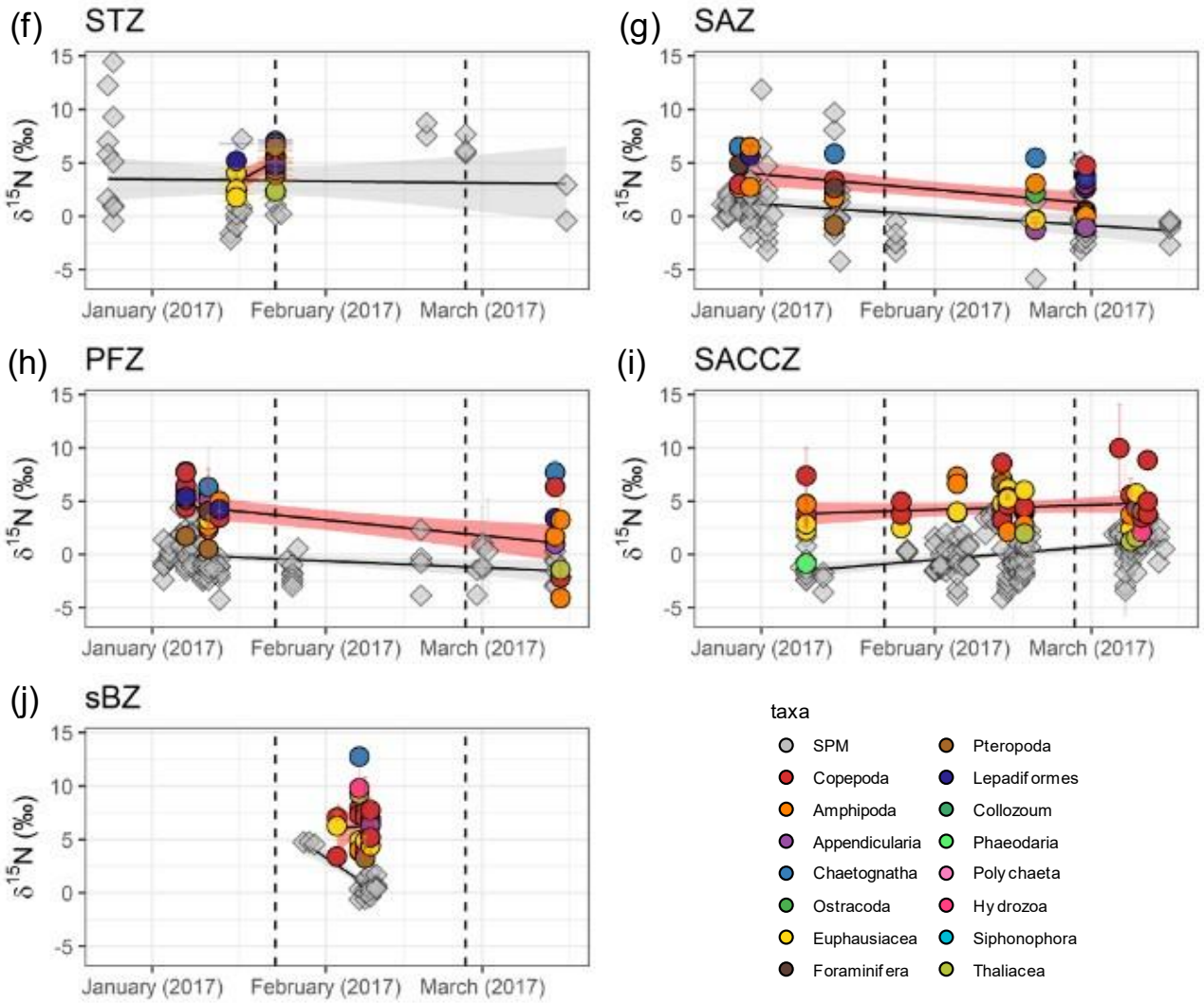

Figure B.1 Temporal varaibility of $\delta^{13}C$ (a-e) and $\delta^{15}N$ (f-l) of SPM (grey diamonds) and zooplankton (coloured circles) during the Antarctic Circumnavigation Expedition. Solid black lines are linear regressions with the respective 95% confidence intervals (grey = SPM, red = zooplankton). Colour dots = zooplankton taxa. SAZ = Subantarctic Zone, PFZ = Polar Frontal Zone, SACCZ = Southern Antarctic Circumpolar Current Zone, and sBZ = southern Boundary Zone . Vertical dashed lines limit each leg, from left to right: Leg1, Leg2 and Leg3.

Zooplankton $\delta^{13}C$ decreased across/over time within the PFZ, from -22.8 ± 3.1‰ (07/01/2017 - 22/01/2017) to -25.7 ± 3.1‰ (28/02/2017 - 15/03/2017; Table B.4). Zooplankton $\delta^{13}C$ from the other zones were more constant (*lm*, *p*-values > 0.05), even though values seemed to decrease and increase respectively in the SAZ and the SACCZ.

The temporal trend of zooplankton $\delta^{13}C$ in the SAZ appeared to be negatively correlated with time (*p*-value < 0.005); however, this regression is possibly affected by the large variability of $\delta^{13}C$ values between zooplankton taxa collected at station 78 (28/02/2017). In fact, the values of two Copepoda (red colours. i.e., *Oithona* spp. and *Candacia* spp.) showed particularly lower values that influenced the calculation of the regression. Removing those two, the trend becomes constant ($y \sim 467.89 - 0.028 * \text{Time}$, *p*-value = 0.23, $R^2 = 0.013$). Zooplankton $\delta^{13}C$ in the PFZ decreased over time from -22.8 ± 3.1‰ (07/01/2017 - 22/01/2017) to -25.7 ± 3.1‰ (28/02/2017 - 15/03/2017; Figure 3.6a, Figure B.1c and Table B.4), in contrast to the $\delta^{13}C$ from all the other zones that were more constant (*lm*, p-values > 0.05), even though values seemed to decease and increase respectively in the SAZ and the SACCZ.

Zooplankton $\delta^{15}N$ significantly decreased in the SAZ and the PFZ (*lm*, p-values < 0.01) respectively from 4.7 ± 1.6‰ (28/12/2016 – 12/01/2017) to 2.2 ± 0.4‰ (13/02/2017 – 28/02/2017) and from 4.3 ± 1.8‰ to 0.7 ± 3.9‰ (Figure 3.6b, Figure B.1g-h and Table B.4). In contrast, $\delta^{15}N$ in the SACCZ appeared to slightly increase (from 3.4 ± 2.3‰ to 4.3 ± 2.6), although the calculated trend is not significant and describes only 3% of the data (Table B.4).

The amount of data for the STZ and the sBZ is too limited to warrant any meaningful analysis (Figure B.1).

c. Isotopic niche of the zooplankton system in the Subantarctic Ocean and the Antarctic Ocean

Table B.5 Layman metric outputs for zooplankton from Neuston stations from the Antarctic Circumnavigation Expedition for each hydrographic region: STZ = Subtropical Zone, SAZ = Subantarctic Zone, PFZ = Polar Frontal Zone, SACCZ = Southern Antarctic Circumpolar Current Zone, and sBZ = southern Boundary Zone

Region	δ^{15}N-range (‰)	δ^{13}C-range (‰)	TA (‰^{2})	CD (‰)	MNND (‰)	SDNND
Southern Ocean	13.9	15.0	141.3	3.6	1.0	1.1
Antarctic	13.6	12.0	77.2	3.4	1.0	0.8
Subantarctic	11.1	13.6	105.1	3.0	1.2	1.2
STZ	5.3	4.9	15.2	1.8	0.8	0.5
SAZ	5.5	13.0	62.4	3.2	1.5	1.3
PFZ	11.6	11.5	85.8	3.8	1.5	1.0
SACCZ	9.4	9.0	49.0	2.7	0.9	0.8
sBZ	9.5	12.0	71.1	4.4	1.5	1.0

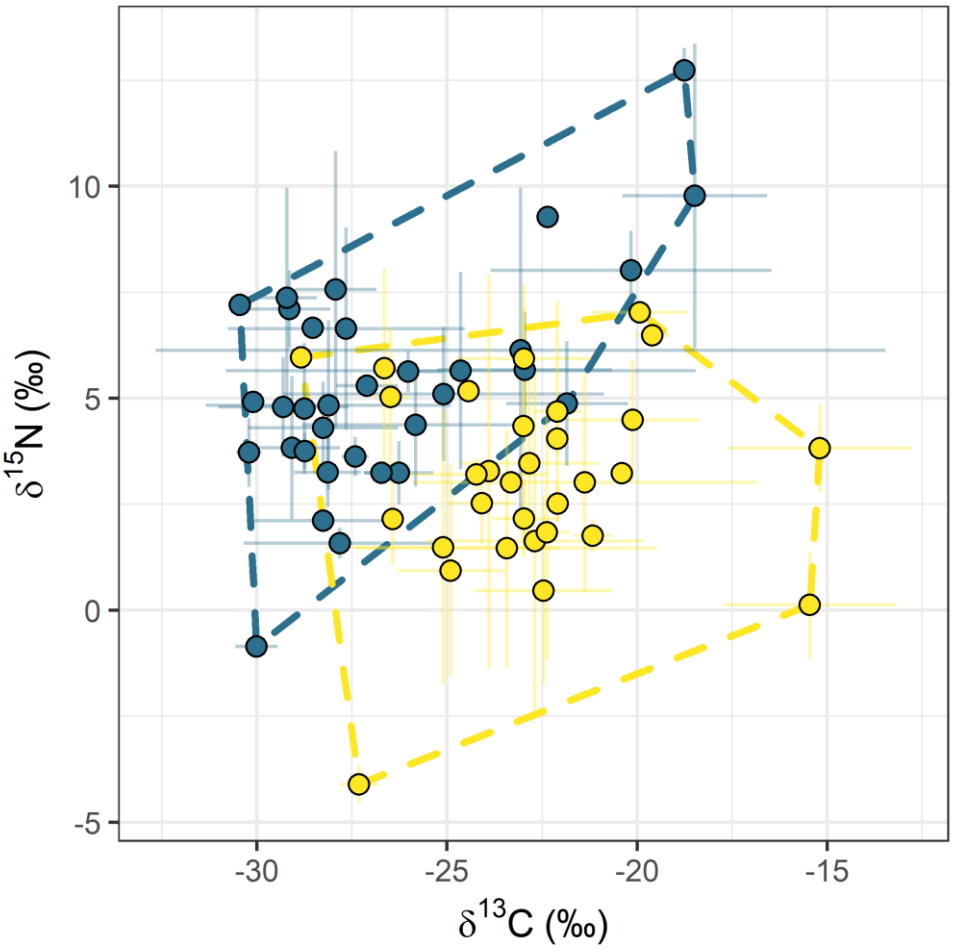

Figure B.2 Average $\delta^{13}C$ [‰] and $\delta^{15}N$ [‰] of zooplankton collected from the neuston layer during the Antarctic Circumnavigation Expedition in each hydrographic zone: Isotopic niches based on Layman metrics analysis of zooplankton species collected during the Antarctic Circumnavigation Expedition. Isotopic niches are. Yellow = Subantarctic Ocean, and Blue = Antarctic Ocean.

d. Island Mass Effect on zooplankton stable isotopes and trophic structure

Table B.6 Layman metrics computed for the $\delta^{13}C$ and $\delta^{15}N$ of zooplankton from the Neuston stations of the open ocean or in the vicinity of island systems, in each hydrographic zone: STZ = Subtropical Zone, SAZ = Subantarctic Zone, PFZ = Polar Frontal Zone, SACCZ = Southern Antarctic Circumpolar Current Zone, and sBZ = southern Boundary Zone. $\delta^{15}N$-range and $\delta^{13}C$-range = distances between the two species with the most enriched and most depleted $\delta^{15}N$ or $\delta^{13}C$ values (e.g., maximum $\delta^{15}N$ − minimum $\delta^{15}N$); TA = total area; MNND = mean nearest neighbour distance; SDNND = standard deviation of the nearest neighbour distance.

Zone	region	$\delta^{15}N$-range (‰)	$\delta^{13}C$-range (‰)	TA (‰^{2})	CD (‰)	NND (‰)	SDNND (‰)
STZ	Islands	-	-	-	-	-	-
	Open Ocean	5.3	4.9	15.2	1.7	0.7	0.6
SAZ	Islands	6.4	10.9	37.0	3.2	1.7	1.4
	Open Ocean	5.1	13.8	57.7	3.7	1.8	1.3
PFZ	Islands	6.1	10.7	28.6	3.1	2.3	1.5
	Open Ocean	11.4	11.7	86.4	4.0	1.5	1.1
SACCZ	Islands	6.7	13.0	45.0	3.4	1.9	2.2
	Open Ocean	9.4	9.4	51.9	2.6	1.0	1.0
sBZ	Islands	3.6	6.8	0.4	3.1	3.1	2.8
	Open Ocean	9.5	12.0	71.1	4.3	1.5	0.9

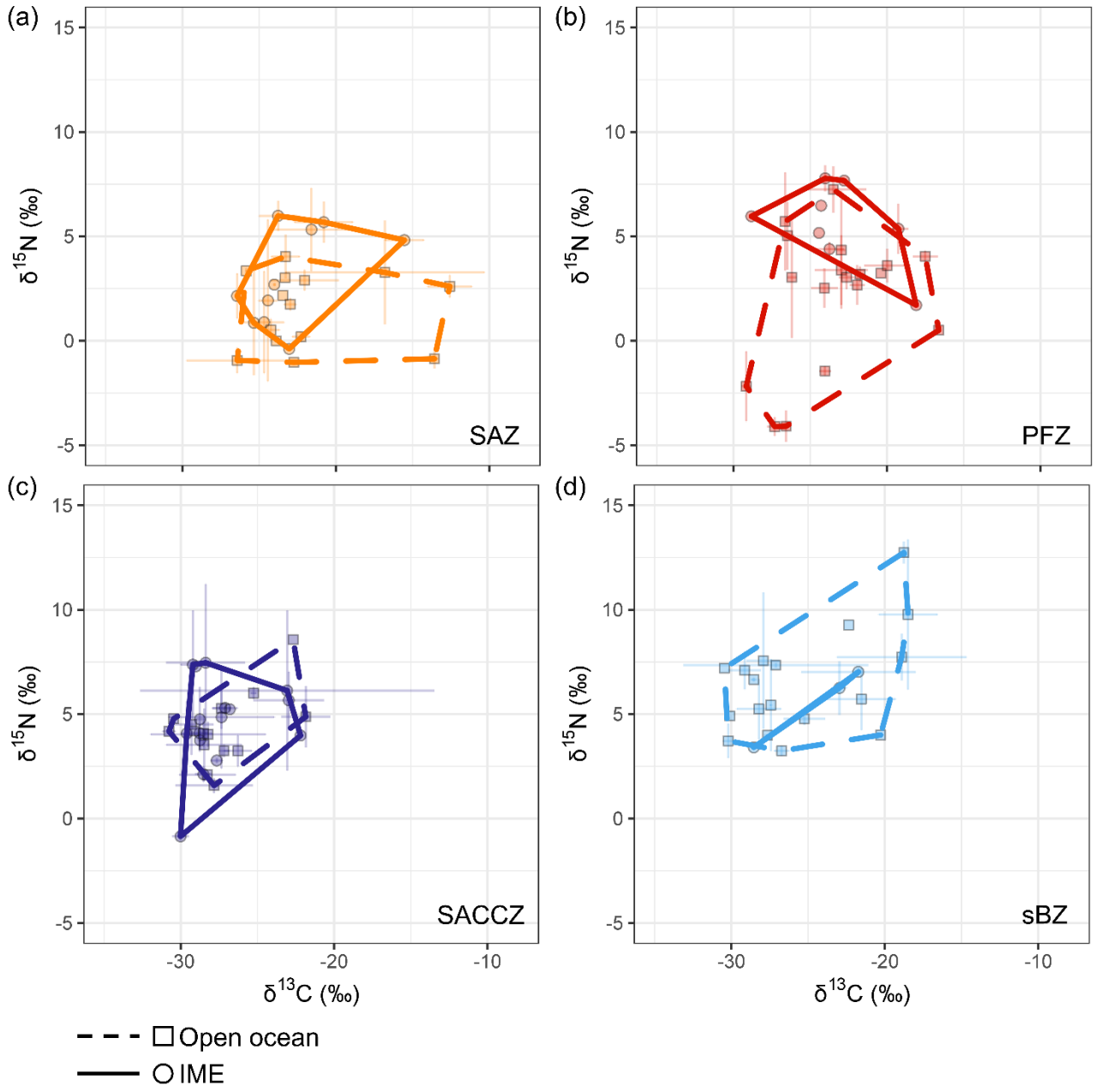

Figure B.3 Isotopic niches based on Layman metrics analysis for zooplankton collected during the Antarctic Circumnavigation Expedition in the vicinity of the island systems (solid lines and circles), and from station in the open ocean (dashed lines and squares), for each hydrographic zone, excluding the Subtropical Zone: (a) orange = Subantarctic Zone (SAZ), (b) red = Polar Frontal Zone (PFZ), c) dark blue = Southern Antarctic Circumpolar Current Zone (SACCZ), and (c) light blue = southern Boundary Zone (sBZ). Error bars = standard deviation (1SD).

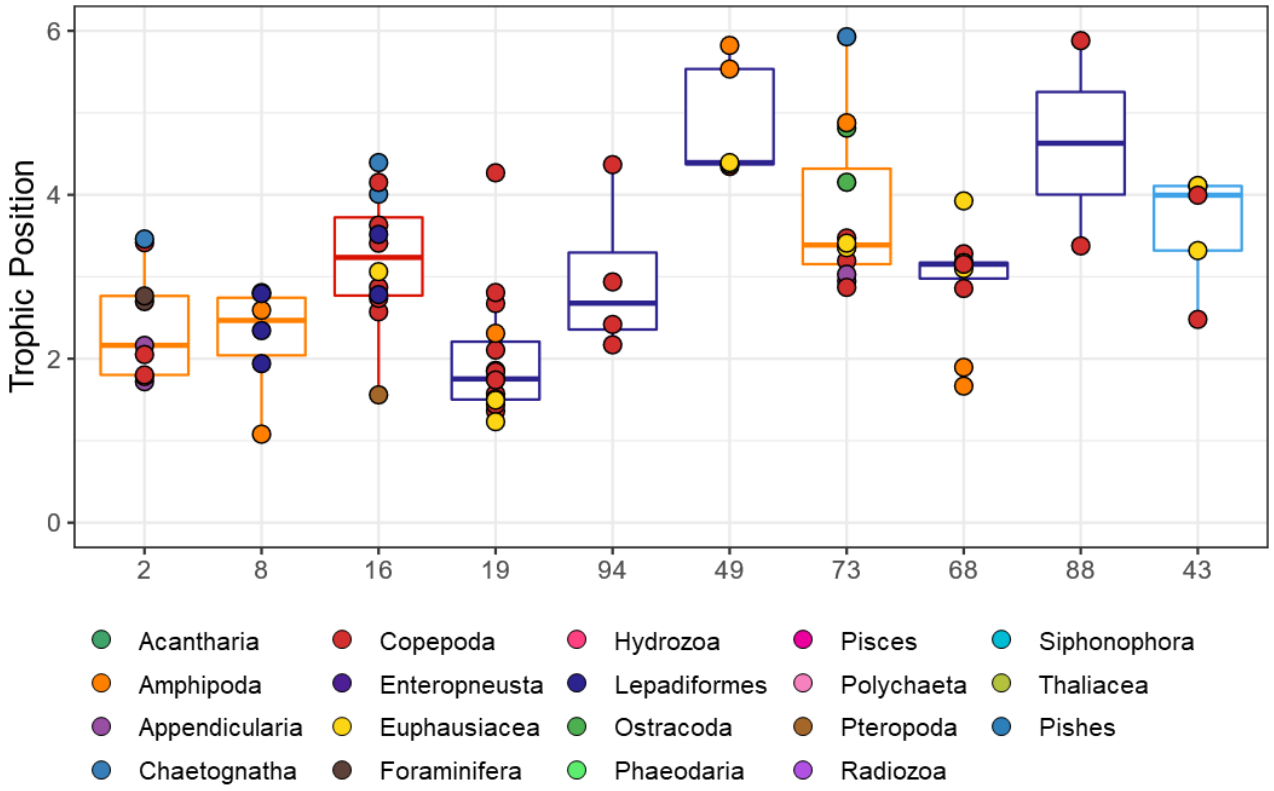

Figure B.4 Boxplots of zooplankton trophic positions (TPs) assessed using $\delta^{15}N_{SPM}$ as baseline for samples collected during the Antarctic Circumnavigation Expedition. Dots correspond to different zooplankton taxa (colours). Middle horizontal lines in the boxes are the medians. Colours of the box = Hydrographic zone: orange = Subantarctic Zone, red = Polar Frontal Zone, dark blue = Southern Antarctic Circumpolar Current Zone, and light blue = southern Boundary Zone.

e. Comparing the carbon and nitrogen isotope ratios ($\delta^{13}N$ and $\delta^{15}N$) of SPM and zooplankton

For each oceanic region (i.e., Subantarctic Ocean, Antarctic Ocean and each hydrographic zone), $\delta^{13}N_{SPM}$ and $\delta^{15}N_{SPM}$ were significantly lower than the zooplankton $\delta^{13}N$ and $\delta^{15}N$ (Student t-tests with Bonferroni adjustment, *p*-values < 0.001). Equivalent statistical differences (*p*-value < 0.001) were obtained testing isotope ratio values through Nested ANOVA, in which the plankton groups (zooplankton and SPM) were *nested* in the factor 'ocean' (Subantarctic and Antarctic). This test also showed that $\delta^{15}N$ of the whole plankton community (SPM + zooplankton) do not differ between Oceans (F = 2.42, *p*-value = 0.121), while $\delta^{13}C$ is higher in the Sub-Antarctic than in the Antarctic (F = 341.34, *p*-value < 2.0 E^{-16}). However, *nesting* within the five ocean 'zones' (STZ, SAF, PFZ, SACCZ and sBZ), shows that each zone statically influences the SIs of both the SPM and the zooplankton ($\delta^{15}N$ - zones: F = 34.73, *p*-value < 2.0 E^{-16}; $\delta^{13}C$ - zones: F = 124.77, *p*-value < 2.0 E^{-16}).

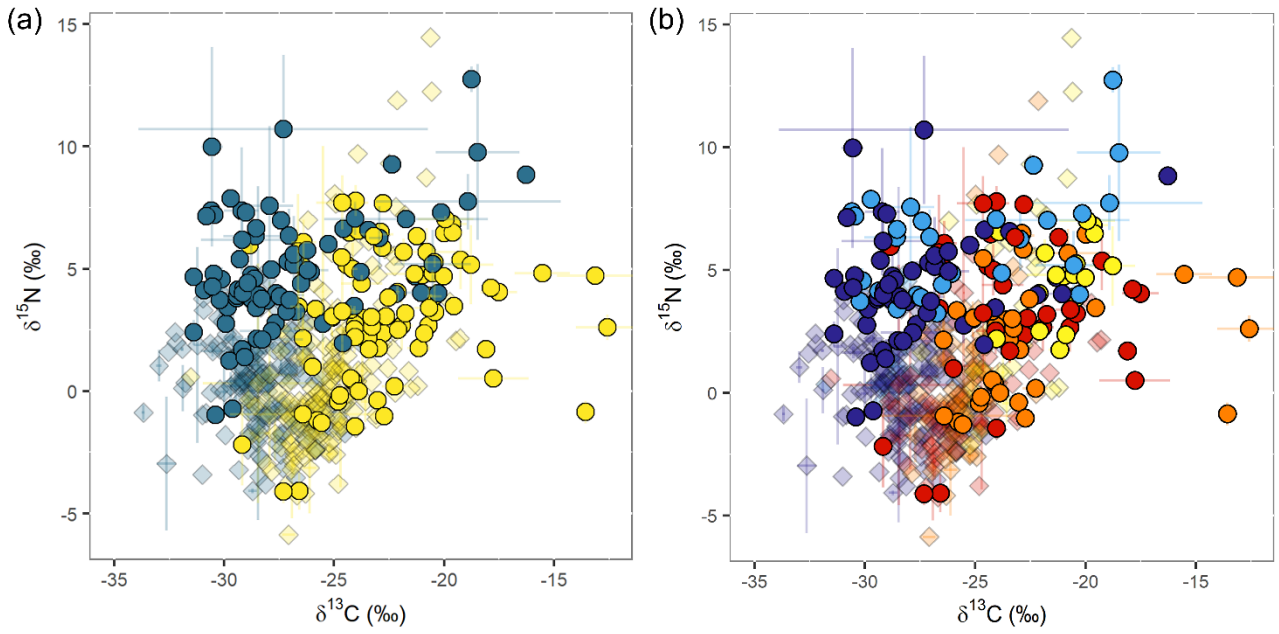

Figure B.5. $\delta^{13}C$ [‰] and $\delta^{15}N$ [‰] of SPM (opaque diamonds) and zooplankton (circles) collected during the Antarctic Circumnavigation Expedition. Colours = hydrographic regions. a) yellow = Subantarctic Ocean, and blue = Antarctic Ocean. b) yellow = Subtropical Zone (STZ), orange = Subantarctic Zone (SAZ), red = Polar Frontal Zone (PFZ), dark blue = Southern Antarctic Circumpolar Current Zone (SACCZ), and sBZ = southern Boundary Zone.

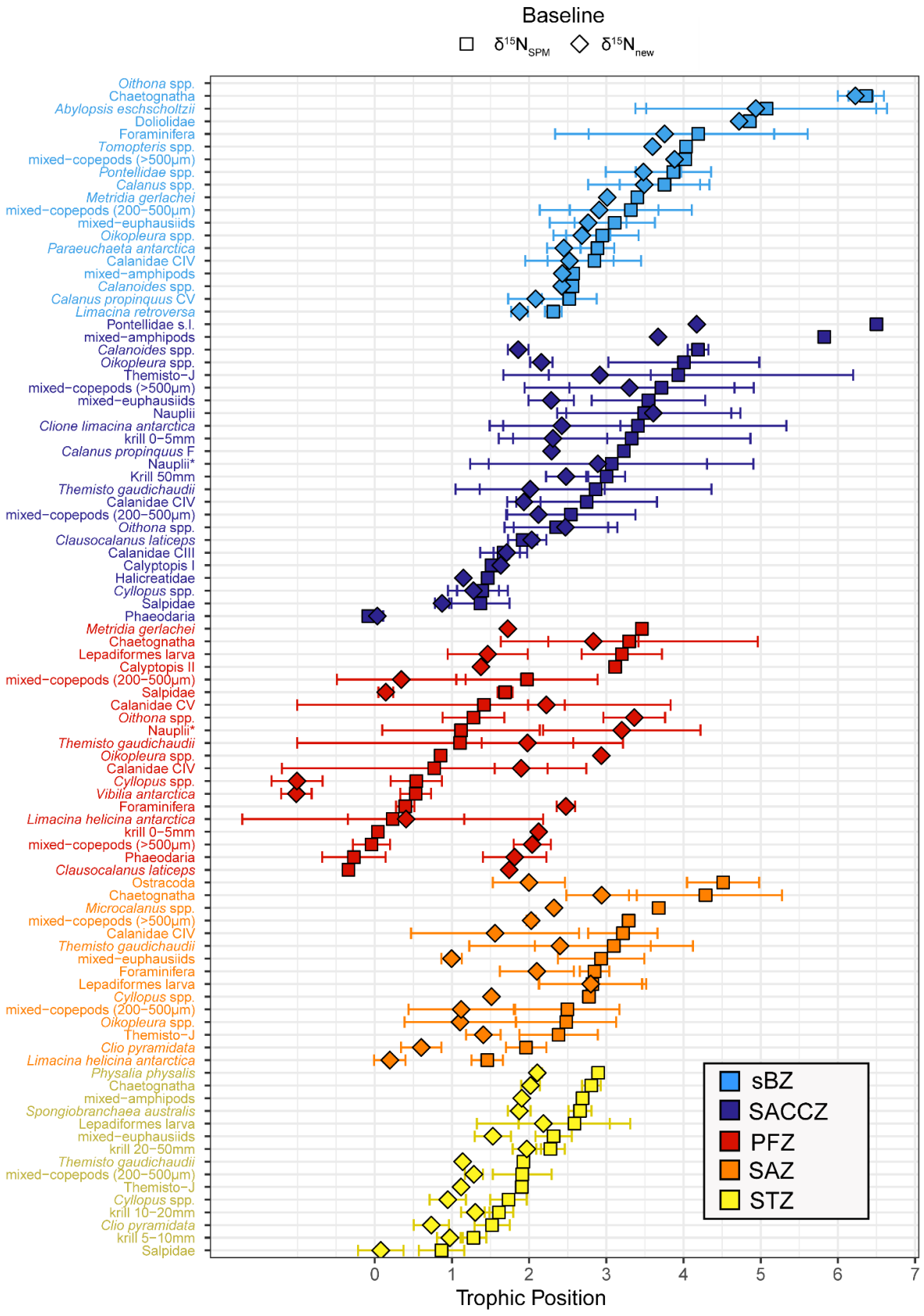

Figure B.6. Trophic Positions of species-specific zooplankton assessed using two baselines: $\delta^{15}N_{SPM}$ (squares) and $\delta^{15}N_{new}$ (diamonds). Samples collected in the neuston layer during the Antarctic Circumnavigation Expedition for each hydrographic zone: yellow = Subtropical Zone (STZ), orange = Subantarctic Zone (SAZ), red = Polar Frontal Zone (PFZ), dark blue = Southern Antarctic Circumpolar Current Zone (SACCZ), and light blue = southern Boundary Zone (sBZ).

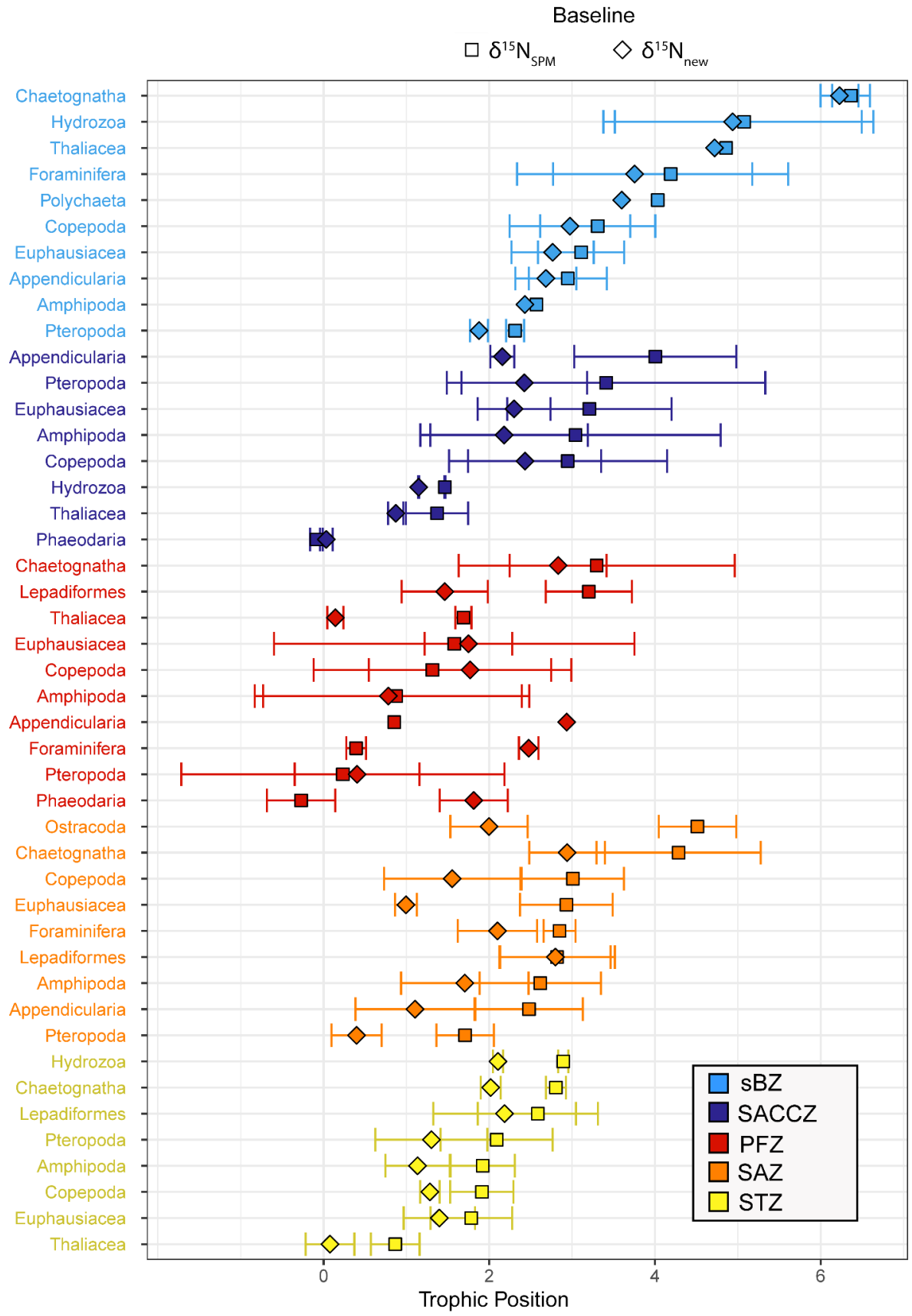

Figure B.7. Trophic Positions of zooplankton (at Order levels) assessed using two baselines: $\delta^{15}N_{SPM}$ (squares) and $\delta^{15}N_{new}$ (diamonds). Samples collected in the neuston layer during the Antarctic Circumnavigation Expedition for each hydrographic zone: yellow = Subtropical Zone (STZ), orange = Subantarctic Zone (SAZ), red = Polar Frontal Zone (PFZ), dark blue = Southern Antarctic Circumpolar Current Zone (SACCZ), and sBZ = southern Boundary Zone.

Table B.7 Averages (± 1SD) of the trophic positions of zooplankton assessed using $\delta^{15}N_{SPM}$ and $\delta^{15}N_{new}$ as baselines. Samples collected in the neuston layer during the Antarctic Circumnavigation Expedition

Order	Species/Taxa	STZ		SAZ		PFZ		SACCZ		sBZ	
		TP (δ^{15N}_{SPM})	TP ($\delta^{15}N_{new}$)	TP (δ^{15N}_{SPM})	TP ($\delta^{15}N_{new}$)	TP (δ^{15N}_{SPM})	TP ($\delta^{15}N_{new}$)	TP (δ^{15N}_{SPM})	TP ($\delta^{15}N_{new}$)	TP (δ^{15N}_{SPM})	TP ($\delta^{15}N_{new}$)
Amphipoda	*Cyllopus* spp.	1.7 ± 0.9	0.2 ± 0.2	2.8 ± 1.5		0.5 ± 1.0	0.3 ± 0.3	1.4 ± 1.3	0.3 ± 0.3		
Amphipoda	mixed-amphipods	2.7 ± 1.9						5.8 ± 3.7		2.6 ± 2.4	
Amphipoda	Themisto-J	1.9 ± 1.1		2.4 ± 1.4	0.5 ± 0.2			3.9 ± 2.9	2.3 ± 0.7		
Amphipoda	*Themisto gaudichaudii*	1.9 ± 1.1		3.1 ± 2.4	1.0 ± 1.2	1.1 ± 2.0	2.1 ± 0.6	2.9 ± 2.0	1.5 ± 1.0		
Amphipoda	*Vibilia antarctica*					0.5 ± 1.0	0.2 ± 0.2				
Appendicularia	*Oikopleura* spp.			2.5 ± 1.1	0.6 ± 0.7	0.9 ± 2.9		4.0 ± 2.2	1.0 ± 0.1	2.9 ± 2.7	0.5 ± 0.4
Chaetognatha	Chaetognatha	2.8 ± 2.0	0.1 ± 0.1	4.3 ± 2.9	1.0 ± 0.5	3.3 ± 2.8	1.7 ± 0.6			6.4 ± 6.2	0.2 ± 0.2
Copepoda	Calanidae CIII							1.7 ± 1.7	0.3 ± 0.2		
Copepoda	Calanidae CIV			3.2 ± 1.6	0.4 ± 1.1	0.8 ± 1.9	2.0 ± 0.3	2.7 ± 1.9	0.9 ± 0.2	2.8 ± 2.5	0.6 ± 0.6
Copepoda	Calanidae CV					1.4 ± 2.2	2.4 ± 0.2				
Copepoda	Calanoides spp.							4.2 ± 1.9	0.1 ± 0.1	2.6 ± 2.4	0.0 ± 0.0
Copepoda	*Calanus propinquus* CV									2.5 ± 2.1	0.4 ± 0.4
Copepoda	*Calanus propinquus* F							3.2 ± 2.3	0.0 ± 0.0		
Copepoda	*Calanus* spp.									3.8 ± 3.5	0.6 ± 0.7
Copepoda	*Clausocalanus laticeps*					-0.3 ± 1.7		1.9 ± 2.0	0.2 ± 0.2		
Copepoda	*Metridia gerlachei*					3.5 ± 1.7				3.4 ± 3.0	0.0 ± 0.0
Copepoda	*Microcalanus* spp.			3.7 ± 2.3							
Copepoda	mixed-copepods (>500µm)			3.3 ± 2.0	0.1 ± 0.1	0.0 ± 2.0	0.2 ± 0.2	3.7 ± 3.3	1.2 ± 1.4	4.0 ± 3.9	0.1 ± 0.1
Copepoda	mixed-copepods (200-500µm)	1.9 ± 1.3	0.4 ± 0.1	2.5 ± 1.1	0.7 ± 0.7	2.0 ± 0.3	0.9 ± 0.8	2.5 ± 2.1	0.8 ± 0.4	3.3 ± 2.9	0.8 ± 0.8
Copepoda	Nauplii							3.5 ± 3.6	1.1 ± 1.1		
Copepoda	Nauplii*					1.1 ± 3.2	1.0 ± 1.0	3.1 ± 2.9	1.8 ± 1.4		
Copepoda	*Oithona* spp.					1.3 ± 3.4	0.4 ± 0.4	2.4 ± 2.5	0.7 ± 0.7		
Copepoda	*Paraeuchaeta antarctica*									2.9 ± 2.4	0.2 ± 0.2
Copepoda	*Pontellidae* spp.							6.5 ± 4.2		3.9 ± 3.5	0.5 ± 0.5
Euphausiacea	krill 0-5 mm					0.0 ± 2.1		3.3 ± 2.3	1.5 ± 0.7		
Euphausiacea	krill 5-10 mm	1.3 ± 1.0	0.2 ± 0.2								

Euphausiacea	krill 10-20 mm	1.6 ± 1.3	0.2 ± 0.2								
Euphausiacea	krill 20-50 mm	2.3 ± 2.0	0.2 ± 0.2								
Euphausiacea	Krill 50 mm							3.0 ± 2.5	0.2 ± 0.3		
Euphausiacea	Calyptopis I							1.5 ± 1.6			
Euphausiacea	Calyptopis II					3.1 ± 1.4					
Euphausiacea	mixed-euphausiids	2.3 ± 1.5	0.2 ± 0.2	2.9 ± 1.0	0.6 ± 0.1			3.5 ± 2.3	0.7 ± 0.3	3.1 ± 2.8	0.5 ± 0.5
Foraminifera	Foraminifera			2.8 ± 2.1	0.2 ± 0.5	0.4 ± 2.5	0.1 ± 0.1			4.2 ± 3.8	1.4 ± 1.4
Hydrozoa	*Abylopsis eschscholtzii*									5.1 ± 4.9	1.6 ± 1.6
Hydrozoa	Halicreatidae							1.5 ± 1.1	0.0 ± 0.0		
Hydrozoa	*Physalia physalis*	2.9 ± 2.1	0.1 ± 0.1								
Lepadiformes	Lepadiformes larva	2.6 ± 2.2	0.7 ± 0.9	2.8 ± 2.8	0.7 ± 0.7	3.2 ± 1.5	0.5 ± 0.5				
Ostracoda	Ostracoda			4.5 ± 2.0	0.5 ± 0.5						
Phaeodaria	Phaeodaria					-0.3 ± 1.8	0.4 ± 0.4	-0.1 ± 0.0	0.1 ± 0.1		
Polychaeta	*Tomopteris* spp.									4.0 ± 3.6	
Pteropoda	*Clio pyramidata*	1.5 ± 0.7	0.2 ± 0.2	2.0 ± 0.6	0.3 ± 0.3						
Pteropoda	*Clione limacina antarctica*							3.4 ± 2.4	1.9 ± 0.8		
Pteropoda	*Limacina helicina antarctica*			1.5 ± 0.2	0.2 ± 0.2	0.2 ± 0.4	1.9 ± 0.8				
Pteropoda	*Limacina retroversa*									2.3 ± 1.9	0.1 ± 0.1
Pteropoda	*Spongiobranchaea australis*	2.7 ± 1.9	0.1 ± 0.1								
Thaliacea	Doliolidae									4.9 ± 4.7	
Thaliacea	Salpidae	0.9 ± 0.1	0.3 ± 0.3			1.7 ± 0.1	0.1 ± 0.1	1.4 ± 0.9	0.4 ± 0.1		

Appendix C - Plankton community composition and productivity near the Subantarctic Prince Edward Islands archipelago in autumn

a. Contribution of the Prince Edward Islands to the Subantarctic's biological pump

From our incubation experiments, we determined that phytoplankton retained between the two islands experienced light-replete but iron-limited conditions that drove them to rely mainly on reduced nitrogen (N) forms that, at least in the case of ammonium (NH_4^+), were available in surface waters at elevated concentrations (Figure C.1c). Despite this, our results show that the average whole-plateau average integrated rate of NPP and the *f*-ratio$_{NPP}$ were equal to 1.14 mmol C m^{-2} h^{-1} and 0.24 ± 0.09, respectively. This latter value implies that roughly a quarter of the carbon biomass was potentially available for export. We calculate the carbon export flux as:

$$Carbon\ export\ flux\ = NPP\ \times\ f - \text{ratio}_{NPP} \times\ T$$

where T is the number of daylight hours in April and May at the archipelago (8-10 h).

The calculation above yields a carbon export flux estimate of 2.2-2.7 mmol C m^{-2} d^{-1} for the archipelago, which is higher than the annual mean carbon export flux in the open Subantarctic, away from the influence of landmasses, that was estimated using a Community Earth System Model to range from 0.8-1.6 mmol C m^{-2} d^{-1} (Harrison *et al.* 2018; see also main text section 4.4.1).

In addition, we can independently estimate the contribution of the Prince Edward Islands archipelago to total Subantarctic carbon export using nitrate-based estimates of net community production measured by profiling floats (Johnson *et al.*, 2017). These float data indicate that the whole-Subantarctic carbon export flux ranges from 2 to 3 Pg C yr^{-1} (0.17-0.25 Pg C month^{-1} on average, recognizing that some months [e.g., spring and summer] will be more important for carbon export than others), over an area of ~27.5 million km^2 (calculated taking the Subantarctic to extend from 46°S to 58°S (~30.6 million km^2), between the approximate positions of the Subtropical Front and the APF (Orsi *et al.*, 1995; Giglio and Johnson, 2016), minus 10% to account for land masses and fluctuations in frontal positions). We further estimate (based on satellite Chl-a maps; Figure 2E-G) that the area around the Prince Edward Islands influenced by the island

mass effect in autumn is ~40000 km^2, which amounts to 0.13% of the whole-Subantarctic area. This region contributes 0.003-0.0036 Pg C $month^{-1}$, or 1.2-2.2% of Subantarctic export production. In other words, the carbon export flux at the Prince Edward Islands plateau in autumn is roughly 10-times higher than its contribution to the area of the Subantarctic, consistent with the comparison of our Prince Edward Islands carbon export flux to the Harrison *et al.* (2018) open-Subantarctic estimates. We thus conclude that the Prince Edward Islands archipelago enhances the productivity of the Subantarctic Ocean.

b. Grazing rates of Euphausiacea

Individual grazing rates estimated for Euphausiacea (<4 cm in length) were not correlated with body length (R^2 = 0.09) and the maximum grazing rates of 0.04 and 0.02 µg Chl-a $ind.^{-1}$ h^{-1} were associated with smaller specimens with average lengths of 31 mm (station H5N) and 8 mm (station H13N), respectively. Overall, the grazing rates for individual Euphausiacea averaged 0.013 ± 0.003 µg Chl-a $ind.^{-1}$ h^{-1} (Figure C.5). Using the median abundance of Euphausiacea across the plateau (0.88 ind. m^{-3}) and their average grazing rate, we estimate their contribution to grazing over the upper 200 m to be 2.3 µg Chl-a m^{-2} h^{-1} (i.e., 0.88 ind. m^{-3} × 0.013 µg Chl-a $ind.^{-1}$ h^{-1} × 200 m), corresponding to ~20% of the community grazing rate (12.5 µg Chl-a m^{-2} h^{-1}) and reaching a maximum of 20.2 µg Chl-a m^{-2} h^{-1} at station P11N. The median abundance and grazing rates of krill upstream and in the inter-island region were, respectively, 0.60 ind. m^{-3} and 1.5 µg Chl-a m^{-2} h^{-1} (~13% of the upstream grazing rate of 12.1 µg Chl-a m^{-2} h^{-1}) and 1.18 ind. m^{-3} and 3.1 µg Chl-a m^{-2} h^{-1} (~20% of the inter-island grazing rate of 15.6 µg Chl-a m^{-2} h^{-1}). Downstream, krill abundances and grazing rates were 1.74 ind. m^{-3} and 4.5 µg Chl-a m^{-2} h^{-1} at night (~9.5% of the night-time grazing rate of 47.2 µg Chl-a m^{-2} h^{-1}) and 0.11 ind. m^{-3} and 0.3 µg Chl-a m^{-2} h^{-1} during the day (~4% of the daytime grazing rate of 7.8 µg Chl-a m^{-2} h^{-1}).

Table C.1 Samples and data collected at each station during the autumn 2017 Prince Edward Islands expedition. CTD = location of stations at which conductivity-temperature-depth, dissolved oxygen, and fluorescence were measured; PP = primary production experiments; SP = secondary production experiments; D = day; N = night.

Station	Latitude (°N)	Longitude (°E)	Date	Day time	Hydrography	NO_3^-	SiO_4^{4-}	NH_4^-	Chl-a bulk	Chl-a size class fractionation	Abundance and biomass		PP	SP	Grazing
											Phytoplankton	Mesozooplankton			
H1	45°44.964'	37°17.969'	17/04/2017	D	x	x	x		x						
H2	46°00.035'	37°17.906'	17/04/2017	D	x	x	x		x						
H3	46°14.982'	37°17.935'	17/04/2017	N	x	x	x		x						
H4	46°29.927'	37°17.988'	17/04/2017	N	x	x	x		x						
H5	46°44.948'	37°18.052 '	26/04/2017	N	x	x	x		x	x	x	x			x
H5	46°45.218'	37° 18.270'	27/04/2017	D	x	x	x		x	x	x	x	x	x	x
H5	46°45.218'	37° 18.270'	18/04/2017	D								x			x
H6	46°59.9167'	37°17.880'	27/04/2017	D	x							x			x
H7	47°14.990’	37°18.014’	19/04/2017	D	x	x	x	x	x	x	x	x	x	x	x
H8	47°30.856'	37°18.000'	19/04/2017	N	x										
H13	46°44.988'	38°30.022'	20/04/2017	N	x	x	x		x	x	x	x		x	x
H17	46°44.991'	38°18.010'	20/04/2017	N	x	x	x		x	x	x	x			x
H18	46°44.991	38°06.042'	20/04/2017	D	x	x	x	x	x	x	x	x	x		x
H19	46°44.991'	37°54.058'	20/04/2017	D	x	x	x		x	x	x	x			x
H20	46°44.978'	37°42.076'	20/04/2017	D	x				x	x	x	x			x
H21	46°44.978'	37°42.076'	20/04/2017	N	x				x	x	x	x			x
P10	46°53.953'	37° 57.552'	24/04/2017	D	x			x	x	x	x	x	x	x	x
P10	46°53.989'	37° 57.512'	24/04/2017	N	x			x	x	x	x	x			x
P11	46°53.963'	38°06.144'	28/04/2017	D	x			x	x	x	x	x	x	x	x
P11	46°54.072'	38°06.123'	28/04/2017	N	x			x	x	x	x	x			x
P12	46°56.983'	38°18.430'	25/04/2017	D	x			x	x	x	x	x	x		x
C35	46 42.650'	37 48.310'	22/04/2017	D	x								x		
D2	46°43.721'	37°45.058'	02/05/2017	N	x				x						
D3	46°43.085'	37° 49.928'	02/05/2017	D	x				x						
D4	46°48.201'	37° 59.103'	13/04/2017	D	x				x						

D7	46°43.510'	38°04.419'	02/05/2017	D	x				x			
D8	46°51.513'	37°03.515'	24/04/2017	D	x				x			
D9	46°48.470'	38°04.362'	25/04/2017	N	x				x			
D11	46°36.444'	37°58.224'	03/05/2017	D	x	x	x		x			
D12	46°48.494'	38°04.198'	13/04/2017	D	x				x			
D13	46°48.115'	38°04.764'	13/04/2017	D	x				x			x
MT1	46°42.092'	37°42.114'	27/04/2017	N	x							x
MT5	46°48.042'	37°42.000'	28/04/2017	N	x							x

Table C.2 Cell volume-carbon conversions for the different plankton (~3-200 μM) taxonomic groups.

Group	**Carbon conversion**	**Conversion reference**
Diatoms	Log_{10} (pg C $cell^{-1}$) = 0.76 log_{10} V (μm^3) – 0.352	Eppley *et al.* (1970)
Dinoflagellates	log_{10} (pg C $cell^{-1}$) = 0.864 log_{10} V (μm^3) – 0.353	Menden-Deuer and Lessard (2000)
Other phytoplankton	log_{10} (pg C $cell^{-1}$) = 0.94 log_{10} V (μm^3) – 0.60	Eppley *et al.* (1970)
Aloricate ciliates	log_{10} (pg C $cell^{-1}$) = 0.984 log_{10} V (μm^3) – 0.639	Putt and Stoecker (1989), modified by Menden-Deuer and Lessard (2000)
Loricate ciliates	log_{10} (pg C $cell^{-1}$) = 0.841 log_{10} V (μm^3) – 0.168	Verity and Lagdon (1984), modified by Menden-Deuer and Lessard (2000)

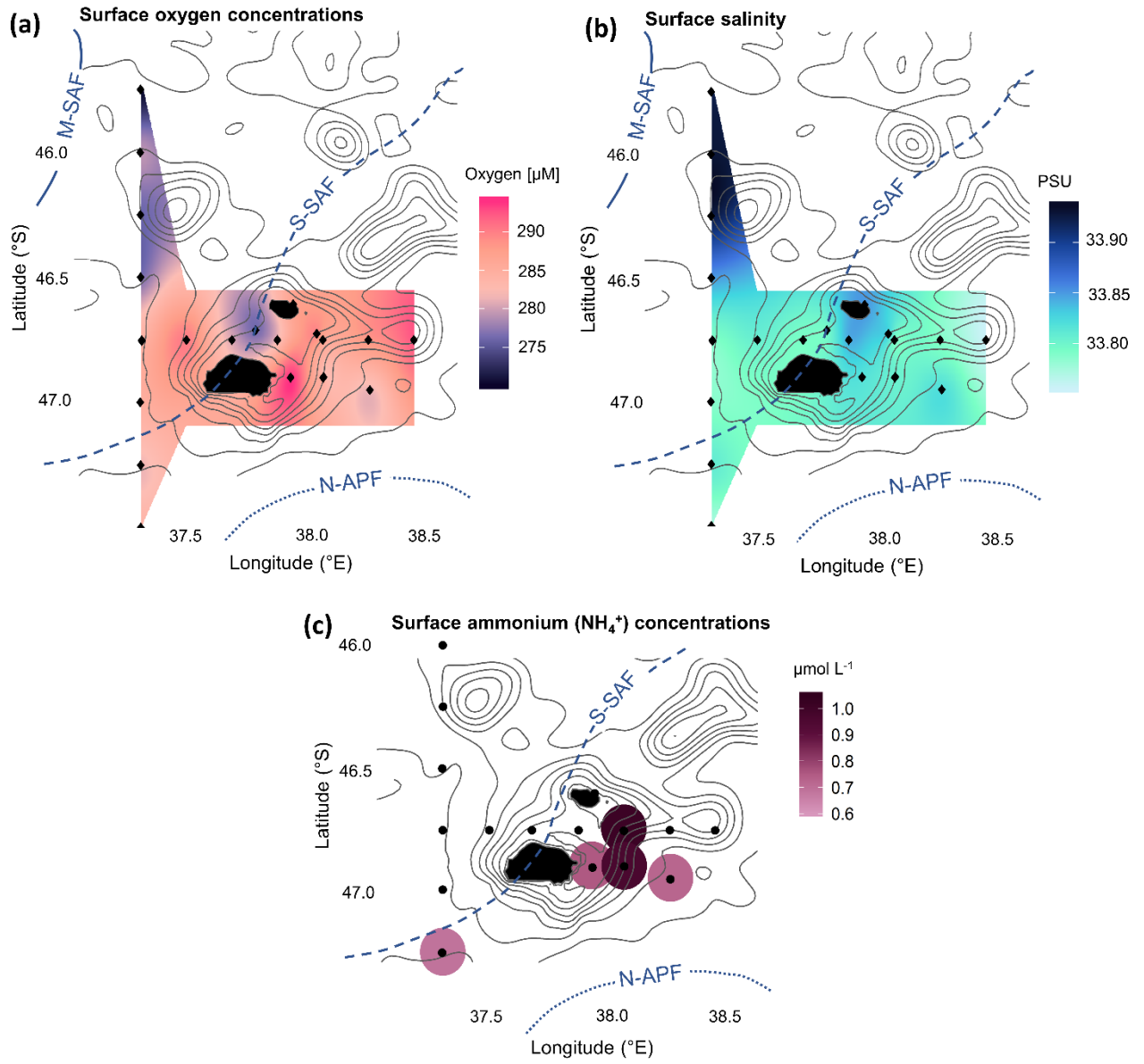

Figure C.1 Surface maps of hydrographic and biogeochemical parameters measured around the Prince Edward Islands archipelago: (a) oxygen, (b) salinity, and (c) ammonium (NH_4^+). Solid grey lines = bathymetry (see Figure 4.1 for depths); solid blue line = M-SAF; dashed blue line = S-SAF; dotted blue line = N-APF. The black dots indicate the positions of the stations; see Figure 4.3a for station numbers.

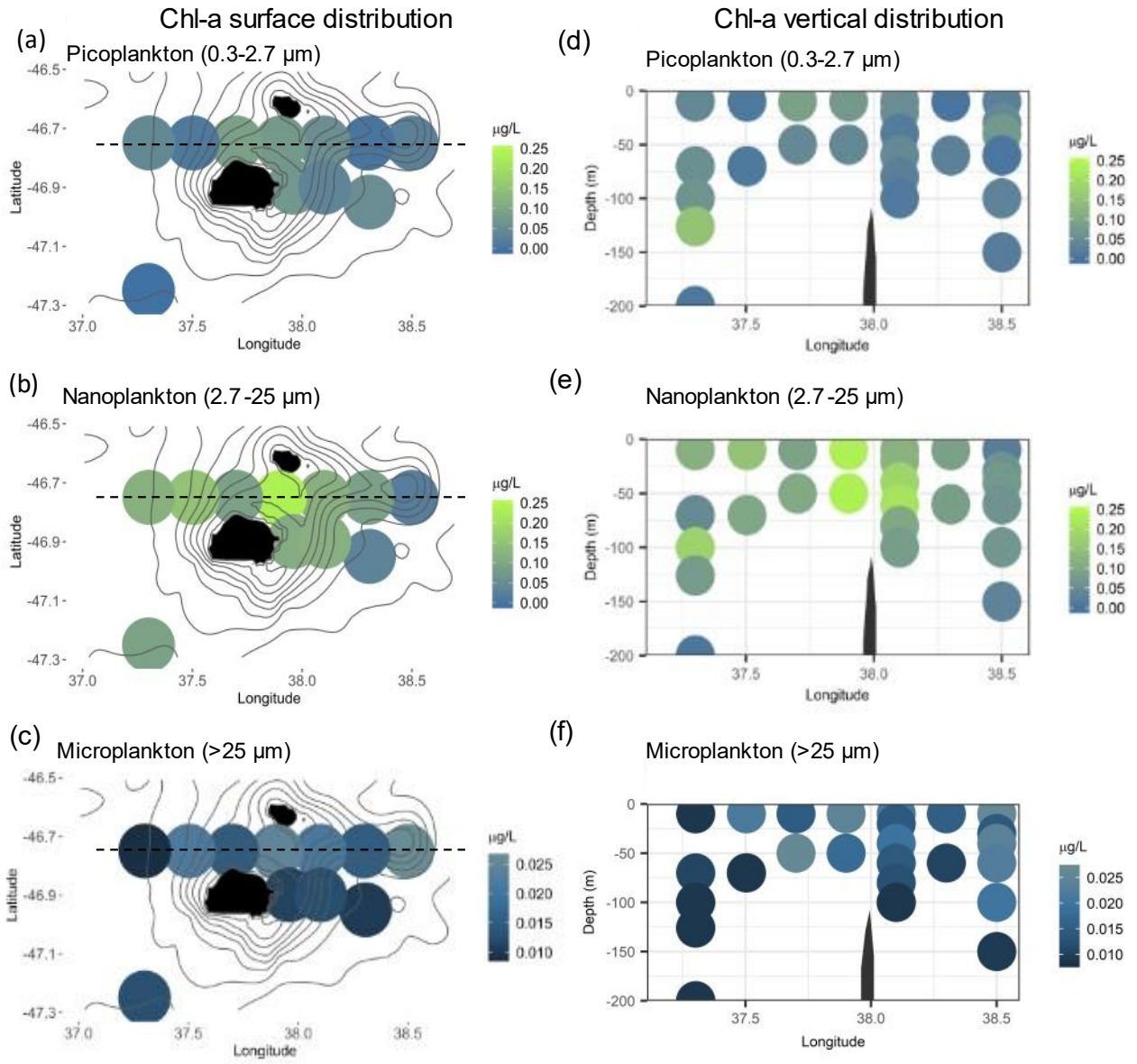

Figure C.2 Size-fractionated Chl-a concentrations for picoplankton (a and d), nanoplankton (b and e), and microplankton (c and f) at the surface (a-c) and throughout the upper 200 m of the water column (d-f) along an east-west inter-island transect (dashed black line in panels a-c) of the Prince Edward Islands archipelago. The bathymetric feature in panels (d-f) is the Natal Bank.

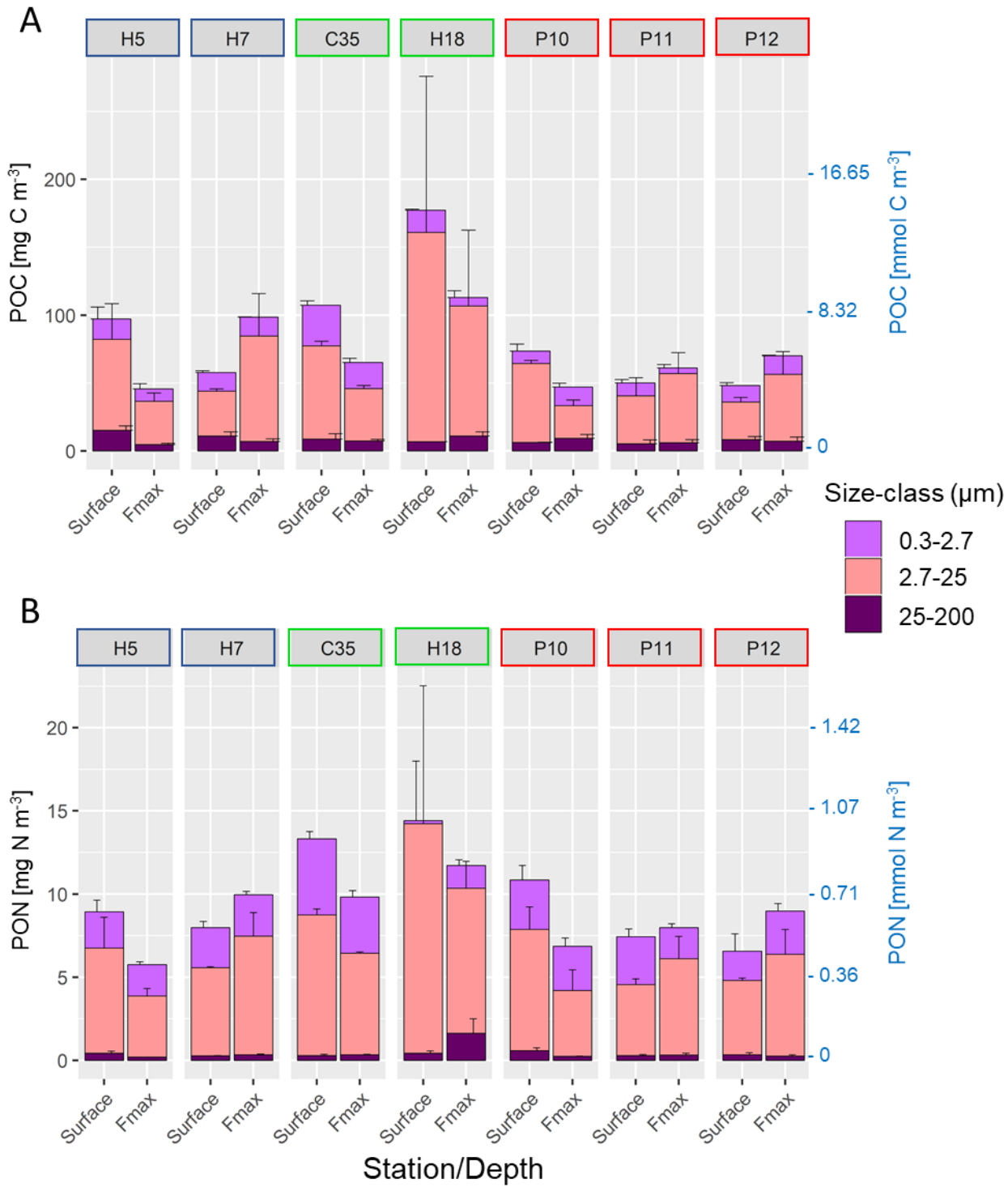

Figure C.3 Concentrations of particulate organic (a) carbon (POC) and (b) nitrogen (PON) for samples collected at two water depths (surface and F-max) and for three size-classes (0.3-2.7 µm, 2.7-25 µm, and 25-200 µm) over the Prince Edward Islands archipelago. Colours of the bars indicate the different size-classes: bright purple = picoplankton (0.3-2.7 µm), pink = nanoplankton (2.7-25 µm), and dark purple = microplankton (25-200 µm). Colours of the boxes around the station numbers at the top of the panels refer to the area of sampling: blue = upstream, green = inter-island and red = downstream. Error bars indicate ± 1 SE.

Table C.3Rates of NPP and NO_3^- uptake for bulk and size-fractionated phytoplankton at seven stations near the Prince Edward Islands, averaged (over the surface and F-max depths) or integrated (over the mixed layer; see text for details). 'BDL' = below detection limit

Station	Area	MLD (m)	Class	Max rate of NPP	Max NO_3^- uptake rate	Average rate of NPP	Average NO_3^- uptake rate	Integrated NPP by size class	Integrated NO_3^- uptake rate by size class	Biomass C:N	*f*-ratio$_{NPP}$
		F-max (m)	µm	nmol C L^{-1} h^{-1}	nmol NO_3^- L^{-1} h^{-1}	nmol C L^{-1} h^{-1}	nmol NO_3^- L^{-1} h^{-1}	mg C m^{-2} h^{-1}	mg NO_3^- m^{-2} h^{-1}		
H5D	Upstream	110	Bulk	9	0.45	6.82 ± 3.08	0.35 ± 0.00	6.38 ± 0.79	0.37 ± 0.05	10.9	0.38 ± 0.03
			0.3-2.7	0.9	0.15	0.79 ± 0.14	0.10 ± 0.07	0.75 ± 0.09	0.11 ± 0.06	7.2	0.83 ± 0.11
		70	2.7-25	8.2	0.3	5.65 ± 3.61	0.25 ± 0.07	5.29 ± 0.65	0.27 ± 0.06	8.4	0.30 ± 0.14
			25-200	0.12	1.03 E^{-2}	0.37 ± 0.56	6.31 E^{-3} ± 3.09 E^{-3}	0.35 ± 0.04	6.89 E^{-3} ± 3.46 E^{-3}	30.1	0.11 ± 0.09
H7D	Upstream	110	Bulk	9.05	0.2	5.42 ± 5.13	0.16 ± 0.00	5.57 ± 1.45	0.17 ± 0.04	9.9	0.20 ± 0.06
			0.3-2.7	2.1	0.05	1.30 ± 1.13	0.03 ± 0.04	1.3 ± 0.25	0.03 ± 4.0 E^{-3}	2.3	0.13 ± 0.04
		70	2.7-25	6.95	0.15	4.13 ± 4.00	0.13 ± 0.04	4.24 ± 0.92	0.14 ± 0.01	13.1	0.20 ± 0.03
			25-200	BDL	1.01 E^{-3}	BDL	6.83 E^{-3} ± 3.09 E^{-3}	BDL	7.13 E^{-3} ± 3.20 E^{-3}	-	-
C35D	Inter-island	100	Bulk	61.95	1.4	55.27 ± 9.44	1.3 ± 0.07	43.55 ± 2.85	1.19 ± 0.04	8.5	0.18 ± 0.01
			0.3-2.7	26.05	0.45	22.2 ± 5.44	0.40 ± 0.07	17.49 ± 2.33	0.37 ± 0.05	6.9	0.12 ± 0.05
		50	2.7-25	35.7	0.95	32.775 ± 4.14	0.90 ± 0.07	25.82 ± 0.04	0.83 ± 0.14	11.2	0.18 ± 0.04
			25-200	0.49	1.31 E^{-2}	0.32 ± 0.14	6.52 E^{-3} ± 5.93 E^{-3}	0.38 ± 0.21	7.01 E^{-3} ± 6.74 E^{-3}	34.1	0.13 ± 0.08
H18D	Inter-island	100	Bulk	17.7	0.6	13.8 ± 5.51	0.50 ± 0.02	12.18 ± 0.75	0.51 ± 0.03	12.1	0.23 ± 0.01
			0.3-2.7	3.6	0.1	2.55 ± 1.48	0.10 ± 0.00	2.25 ± 0.27	0.10 ± 0.02	6.6	0.26 ± 0.03
		50	2.7-25	13.83	0.5	11.06 ± 3.91	0.40 ± 0.14	9.77 ± 1.46	0.41 ± 0.06	9.9	0.24 ± 0.01
			25-200	0.27	2.63 E^{-2}	0.19 ± 0.11	1.38 E^{-2} ± 8.18 E^{-3}	0.20 ± 1.29	1.88 E^{-2} ± 8.30 E^{-3}	35.3	0.48 ± 0.19
P10D	Downstream	110	Bulk	10.75	0.15	7.02 ± 5.27	0.13 ± 0.04	6.33 ± 1.44	0.13 ± 0.03	8.2	0.13 ± 0.04
			0.3-2.7	2.48	0.02	1.87 ± 0.87	0.01 ± 0.01	1.68 ± 0.35	0.01 ± 0.1 E^{-2}	4.6	0.03 ± 0.01
		75	2.7-25	8.12	0.13	5.08 ± 4.29	0.12 ± 0.02	4.58 ± 0.74	0.12 ± 0.016	8.5	0.15 ± 0.03
			25-200	0.18	0.02	0.14 ± 7.67 E^{-2}	8.41 E^{-3} ± 5.36 E^{-3}	0.14 ± 0.01	8.43 E^{-3} ± 6.01 E^{-3}	27.4	0.41 ± 0.18
P11D	Downstream	100	Bulk	18.4	0.8	13.30 ± 7.21	0.55 ± 0.21	12.88 ± 0.95	0.63 ± 0.18	8.4	0.32 ± 0.04
			0.3-2.7	3.7	0.2	3.00 ± 0.99	0.15 ± 0.07	2.91 ± 0.50	0.17 ± 0.03	2.6	0.33 ± 0.05
		75	2.7-25	14.4	0.6	10.08 ± 6.12	0.40 ± 0.28	9.76 ± 1.32	0.46 ± 0.05	10.4	0.26 ± 0.03
			25-200	0.37	8.88 E^{-3}	0.21 ± 0.12	6.50 E^{-3} ± 2.63 E^{-3}	0.22 ± 0.04	6.51 E^{-3} ± 3.34 E^{-3}	21.1	0.20 ± 0.09
P12D	Downstream	110	Bulk	10.5	0.35	9.40 ± 1.55	0.33 ± 0.04	8.65 ± 0.72	0.35 ± 0.05	8.4	0.27 ± 0.02
			0.3-2.7	2.2	0.05	2.20 ± 0.00	0.05 ± 0.00	2.02 ± 0.42	0.05 ± 0.01	1.9	0.15 ± 0.07
		60	2.7-25	8.15	0.3	7.08 ± 1.52	0.28 ± 0.04	6.51 ± 0.82	0.30 ± 0.04	8.8	0.23 ± 0.02
			25-200	0.21	7.65 E^{-3}	0.13 ± 0.06	4.80 E^{-3} ± 2.37 E^{-3}	0.13 ± 0.10	5.33 E^{-3} ± 2.79 E^{-3}	30.5	0.25 ± 0.21

Table C.4 Total abundance (cells L^{-1}) of planktonic organisms (<200 µm) collected at the surface (~10 m) and F-max near the Prince Edward Islands in autumn 2017

Station	**H5D**	**H5N**	**H7D**	**H20D**	**H18D**	**H17N**	**H13N**	**P10D**	**P10N**	**P11D**	**P11N**	**P12D**
Level	Surface	Surface	Surface	Surface	Surface	Surface	Surface	Surface	Surface	Surface	Surface	Surface
Nanoplankton	85.33	255.98	341.30	0.00	853.26	255.98	938.59	767.93	170.65	341.30	85.33	255.98
Coccolitophores	853.26	341.30	2389.13	5802.17	0.00	3242.39	85.33	511.96	0.00	511.96	0.00	1535.87
Nanoflagellates	4948.91	7252.72	11433.70	2133.15	31570.65	10580.43	13396.20	17833.15	6143.48	10523.55	4052.99	24915.22
Microflagellates	0.00	0.00	85.33	0.00	511.96	0.00	0.00	0.00	0.00	56.88	0.00	255.98
Cryptophytes	341.30	938.59	938.59	255.98	2559.78	2218.48	0.00	597.28	853.26	511.96	469.29	853.26
Dinoflagellates	4692.93	5887.50	6655.43	4351.63	15700.00	11092.39	4180.98	7764.67	5034.24	6086.59	6826.09	5631.52
Diatoms	255.98	170.65	170.65	170.65	511.96	341.30	1109.24	682.61	85.33	511.96	213.32	1109.24
Pennate Diatoms	1109.24	1194.57	853.26	85.33	2389.13	1365.22	853.26	341.30	170.65	853.26	1279.89	1279.89
Ciliates	1023.91	2133.15	2303.80	85.33	1194.57	341.30	1535.87	1621.20	1109.24	682.61	1066.58	1023.91
Thalassiosira	341.30	0.00	0.00	0.00	0.00	0.00	0.00	0.00	0.00	0.00	0.00	0.00
other	0.00	0.00	170.65	85.33	341.30	255.98	85.33	0.00	0.00	56.88	42.66	0.00
Level	Fmax	Fmax	Fmax	Fmax	Fmax	Fmax	Fmax	Fmax	Fmax	Fmax	Fmax	Fmax
Nanoplankton	341.30	170.65	0.00	0.00	0.00	341.30	42.66	1080.80	85.33	42.66	682.61	1791.85
Coccolitophores	511.96	0.00	1365.22	8617.93	341.30	341.30	42.66	1877.17	0.00	383.97	511.96	938.59
Nanoflagellates	10523.55	6655.43	9385.87	1194.57	19625.00	10068.48	4138.32	10694.20	7167.39	4948.91	8959.24	12201.63
Microflagellates	0.00	0.00	0.00	0.00	0.00	0.00	127.99	56.88	85.33	0.00	0.00	0.00
Cryptophytes	511.96	938.59	767.93	85.33	1877.17	1194.57	85.33	398.19	511.96	938.59	1023.91	1194.57
Dinoflagellates	6086.59	5716.85	5887.50	2559.78	7850.00	5972.83	2901.09	5802.17	4180.98	5460.87	7508.70	6655.43
Diatoms	398.19	170.65	255.98	0.00	511.96	255.98	298.64	568.84	85.33	298.64	170.65	255.98
Pennate Diatoms	853.26	767.93	170.65	170.65	2047.83	1109.24	1365.22	2047.83	170.65	554.62	1109.24	511.96
Ciliates	682.61	1023.91	682.61	170.65	2730.43	682.61	426.63	967.03	1023.91	1194.57	1023.91	938.59
Thalassiosira	0.00	0.00	0.00	0.00	170.65	0.00	0.00	56.88	0.00	0.00	85.33	0.00
other	56.88	85.33	85.33	0.00	0.00	85.33	383.97	113.77	0.00	0.00	0.00	85.33

Table C.5 Total abundance (ind. m^{-3}) of Copepoda sampled near the Prince Edward Islands in autumn 2017

Copepods	H5D	H5N	H5D*	H6D	H7D	H21D	H20D	H18D	H17N	H13N	P10D	P10N	P11D	P11N	P12D
Aetideus armatus	0	0	0	0	0	0	0	0	0	0	0	0	0	0	0.88
Calanidae	5.31	4.42	8.84	13.26	8.84	10.61	5.31	2.21	12.38	73.39	0.03	12.03	8.84	13.26	4.42
Calanoides macrocarinatus s.l.	0	0	0	0	0.88	0	0	0	0	0	0	0	0	0	0
Calanus propinquus	0	0	0	0	0	0	0	0	0	6.19	0	0	0	0	0
Calanus simillimus	0	0	0	0	0	0	0	0	9.73	7.07	0	0	4.42	12.38	0
Candacia varicans s.l.	0	0	0	0	0	0	0	0	0	0.88	0	0	0	0	0
Clausocalanidae	2.65	0.00	17.68	8.84	38.02	6.19	4.42	4.86	9.73	76.92	2.84	53.05	21.22	46.86	14.15
Clausocalanus brevipes	0	1.77	5.31	0.00	4.42	2.65	21.22	0	0	0	0.29	0	0	65.43	6.19
Clausocalanus laticeps	0	0	0	0	0	0	0.88	0	0	0	0	0	0	0	0
Clausocalanus spp.	0	0.00	12.38	6.19	0.88	3.54	0	0.88	0	7.07	0.00	2.83	1.77	0	0
Ctenocalanus spp.	0	16.80	0	0.88	0	5.31	0	1.33	0	9.73	0.26	16.98	2.65	0	5.31
Ctenocalanus vanus	0	0	0	0	0	0	0	0	0	0	0	0	0	25.64	0
Euchaetidae	0	0	0	0	0	0	0	0	0	0	0	0	0	0.88	0
Heterorhabdus austrinus	0	0	0	0	0	0	0	0	0	0.88	0	0	0	0	0.88
Heterorhabdus spp.	0	6.19	0	0	2.65	0	0	0	0	2.65	0	0	0	0	0
Metridia sp.	0	0.88	10.61	0	0.88	3.54	2.65	0.88	1.77	1.77	0	0.71	0	0	0
Metridia gerlachei	0	0	0	0	0	0	0	0	0	0	0	0.71	0	0	0
Metridia lucens	0.44	2.65	0	0	3.54	1.77	1.77	0.44	0	6.19	0.03	1.41	0	3.54	0
Nauplii	0	0	1.77	1.77	2.65	0	1.77	0.44	0	0.00	0.06	3.54	0	6.19	0
Oithona spp.	78.69	114.06	171.53	75.16	85.77	95.49	6.19	39.35	70.74	279.41	2.06	204.43	53.94	185.68	57.47
Oncaea spp.	0	0	0	0	0	1.77	107.87	0	2.65	0.88	0.20	0	0	0	0
Paraeuchaeta antarctica	0	0.88	0	0	0.88	0	0	0	0.88	0	0	0	0	0	0
Pleuromamma robusta	0	11.49	0	0	7.07	7.96	4.42	0	0	7.96	0	0	0	1.77	0
Rhincalanus gigas	0.44	0	0	0	0	0	0	0	0	5.31	0	0	0.88	0	0
Sapphirina spp.	0	0	0.88	0	0	0	0	0	0	0	0	0	0	0	0
Unidentified	0	0	0	0	0	0.88	0	0	0	0.88	0	0	0	0	0

Table C.6 Percent abundance of copepod species relative to total copepod abundance (total abundance = 2526 ind.) across the Prince Edward Islands in autumn 2017

Taxa	Stage	H5D	H5N	H5D*	H6D	H7D	H20D	H20D	H18D	H17N	H13N	P10D	P10N	P11D	P11N	P12D	Sum (%)
Aetidaus armatus	**Adult**	0.00	0.00	0.00	0.00	0.00	0.00	0.00	0.00	0.00	0.00	0.00	0.00	0.00	0.00	0.04	**0.04**
Calanidae	**Adult**	0.00	0.00	0.00	0.00	0.04	0.00	0.00	0.00	0.21	0.42	0.00	0.00	0.11	0.49	0.00	**1.26**
Calanidae	**Juvenile**	0.21	0.18	0.35	0.53	0.35	0.42	0.21	0.09	0.67	3.01	0.00	0.48	0.42	0.53	0.18	**7.61**
Clausocalanidae	**Adult**	0.00	0.28	0.70	0.28	0.21	0.46	0.88	0.04	0.00	0.28	0.02	0.73	0.18	3.61	0.46	**8.11**
Clausocalanidae	**Juvenile**	0.11	0.46	0.70	0.35	1.51	0.25	0.18	0.25	0.39	3.43	0.11	2.16	0.84	1.86	0.56	**13.13**
Euchaetidae	**Adult**	0.00	0.04	0.00	0.00	0.04	0.00	0.00	0.00	0.00	0.00	0.00	0.00	0.00	0.04	0.00	**0.11**
Euchaetidae	**Juvenile**	0.00	0.00	0.00	0.00	0.00	0.00	0.00	0.00	0.04	0.00	0.00	0.00	0.00	0.00	0.00	**0.04**
Metrinidae	**Adult**	0.02	0.56	0.00	0.00	0.32	0.39	0.21	0.00	0.00	0.46	0.00	0.08	0.00	0.21	0.00	**2.24**
Metrinidae	**Juvenile**	0.00	0.04	0.42	0.00	0.14	0.14	0.14	0.05	0.07	0.18	0.00	0.03	0.00	0.00	0.00	**1.20**
Cyclopoida	**Adult**	0.77	4.52	2.21	2.98	1.05	3.78	0.25	1.56	2.80	7.85	0.00	0.22	2.14	1.93	0.21	**32.26**
Cyclopoida	**Juvenile**	2.35	0.00	4.59	0.00	2.35	0.00	3.40	0.00	0.00	3.22	0.08	7.87	0.00	5.43	2.07	**31.35**
Poecilostomatoida	**Adult**	0.00	0.00	0.00	0.00	0.00	0.07	0.88	0.00	0.11	0.04	0.01	0.00	0.00	0.00	0.00	**1.09**
Candaciidae	**Adult**	0.00	0.00	0.00	0.00	0.00	0.00	0.00	0.00	0.00	0.04	0.00	0.00	0.00	0.00	0.00	**0.04**
Eucalanidae	**Adult**	0.02	0.00	0.00	0.00	0.00	0.00	0.00	0.00	0.00	0.07	0.00	0.00	0.04	0.00	0.00	**0.12**
Eucalanidae	**Juvenile**	0.00	0.00	0.00	0.00	0.00	0.00	0.00	0.00	0.00	0.14	0.00	0.00	0.00	0.00	0.00	**0.14**
Heterorhabdidae	**Adult**	0.00	0.25	0.00	0.00	0.11	0.00	0.00	0.00	0.00	0.14	0.00	0.00	0.00	0.00	0.04	**0.53**
Sapphirinidae	**Juvenile**	0.00	0.00	0.04	0.00	0.00	0.00	0.00	0.00	0.00	0.00	0.00	0.00	0.00	0.00	0.00	**0.04**
Nauplii	**Juvenile**	0.00	0.00	0.07	0.07	0.11	0.00	0.07	0.02	0.00	0.00	0.00	0.14	0.00	0.25	0.00	**0.72**
																	100
Sum (%)		2.00	6.30	5.50	0.23	14.33	3.54	6.20	9.07	6.20	19.26	3.47	4.27	11.71	3.71	4.20	100

Table C.7 Total abundance (ind. m^{-3}) of non-copepod mesozooplankton collected near the Prince Edward Islands during autumn 2017

Non copepod Taxa	H5D	H5N	H5D*	H6D	H7D	H21D	H20D	H18D	H17N	H13N	P10D	P10N	P11D	P11N	P12D
Amphipoda (large)	0.05	0.04	0	0.04	0	0	0	0	0	0	0	0	0	0	0
Amphipoda (small)	0.11	0	0.50	0.46	0.39	0.39	0.32	0.71	0.39	1.70	0.58	1.53	0.50	1.63	0.18
Appendicularia.	0	0.04	2.02	0	0	0	0	0	0	0	0	0	0	0	0
Cryptoniscus	0.05	0.07	0.04	0.04	0.21	0.21	0.18	0.18	0.21	0.21	0	0.06	0.04	0	0.25
Ostracoda indet.	0.07	0	0	0	0	0.07	0.04	0	0	0.07	0	0.06	0	0	0.04
Ostracoda indet.	0.64	1.49	1.31	2.72	5.69	2.76	1.84	3.93	8.21	33.39	0.26	1.75	5.62	8.98	8.70
Chaetognatha	0	0	0	0	0	0	0	0	0	0	0.09	0.06	0.04	0	0
Cnidaria	0	0	0	0	0	0	0	0	0	0	0	0	0.11	0	0
Creseis spp.	0	0	0	0	0	0	0	0	0	0.07	0	0	0	0	0
Enteropneusta	0	0	0	0	0	1.03	0	0	0	0	0	0	0	0	0
Euphausiacea	0	0	0	0.11	0	0	0	0	0	0	0	0	0	0	0
Euphausiacea (0-5 mm)	0.02	0.85	0.18	0	0.32	0	0.35	0	0	0.07	0	0.06	0	5.66	0.07
Euphausiacea (10-20 mm)	0.23	1.10	0.46	0.00	0.74	0.00	0.39	1.27	0.11	0.35	0.06	1.92	0.04	2.12	0.04
Euphausiacea (5-10 mm)	0.02	0	0.07	0.07	0.07	0.14	0	0.04	0	0.71	0	0.06	0.14	0	0
Euphausiacea (>20 mm)	0.07	0.07	0.25	0.04	0.28	0	0.35	0	0.14	0.85	0.12	0.23	0.04	0	0
Euphausiacea (calyptopis)	0	0	0.04	0	0	0	0	0	0	0	0	0	0	0.07	0
Euphausiacea (furcilia)	0	0	0	0	0	0	0	5.38	0	0	1.97	0	0	0	0
Faecal pellet	0.07	0.04	0.21	0.07	0.07	0.25	0.28	0.07	0.14	0.28	0.06	0.23	0.11	0.35	0.04
Fish larvae	4.90	5.20	10.43	17.75	3.75	3.36	1.63	0.21	5.48	3.54	2.09	0.11	4.24	15.92	5.34
Foraminifera	0	0	0	0	0	0	0	0.04	0	0	0	0	0.07	0	0
Fritillaria spp.	0.25	8.56	0.35	0.85	0.71	0.18	0.21	0.25	3.22	13.44	2.46	0.45	2.62	13.72	0.21
Limacina spp.	0	0.04	0.07	0.39	0.04	0	0.04	0	0	0	0	0	0.14	0	0
Medusae	0	0.11	0	0.07	0	0	0	0	0	0	0	0.23	0	0	0
Nematoda	0.02	0	0	0.04	0	0.14	0	0.07	0.04	0.35	0	0.28	0.14	0.35	0.04
Oikopleura spp.	4.39	7.32	6.26	7.71	9.69	5.80	4.77	3.71	13.23	22.28	1.28	2.26	7.75	21.43	9.62
Polychaeta (benthic)	0	0	0	0.04	0	0	0.04	0	0	0	0	0.06	0.07	0	0.11
Polychaeta (holoplanktonic)	0	0	0	0.07	0	0	0	0	0.04	0.64	0	0	0	0	0
Salpae	0	0	0	0	0	0	0	0.04	0	0	0	1.53	0	0	0.21
Siphonophora	0	0	0.14	0.18	0.21	0	0	0	0	0.07	0.03	0	0.11	0	0
Phaeodaria	1.77	0	2.69	0	1.70	1.03	3.54	3.54	0	0.07	0.06	1.70	3.54	0.28	3.54
Trochophora	0	0	0	0	0	0	0	0	0	0.28	0	0	0	0	0

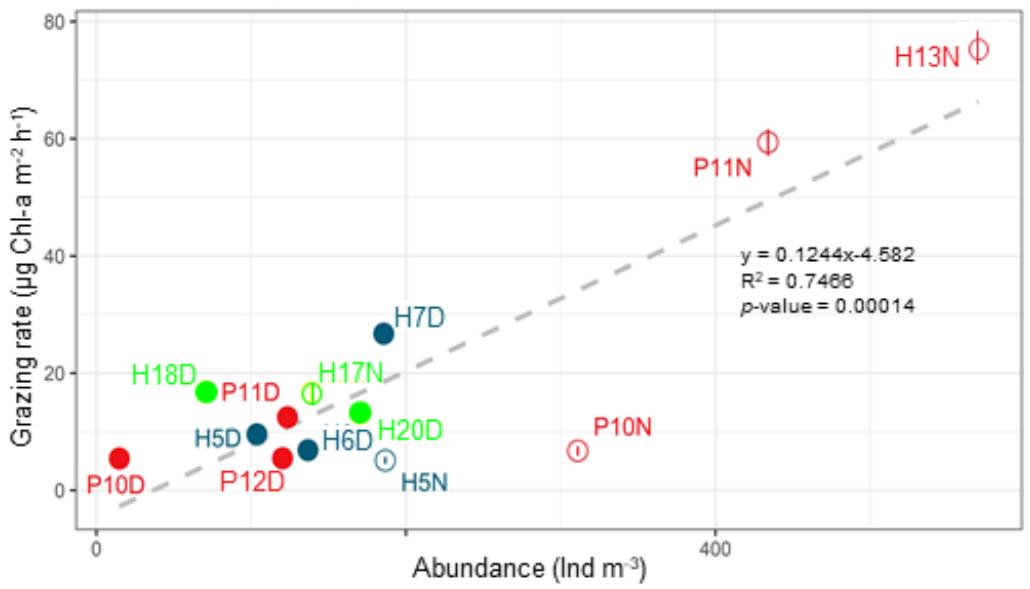

Figure C.4 Relationship between total mesozooplankton abundance (ind. m^{-3}) and grazing rate (µg Chl-a m^{-2} h^{-1}). The dashed grey line indicates a linear relationship between the two parameters. Dark blue = upstream, green = inter-island, and red = downstream stations. Open circles and N = night, filled circles and D = day. Vertical error bars (± 1 SE of duplicate experiments) are shown for the grazing rates only.

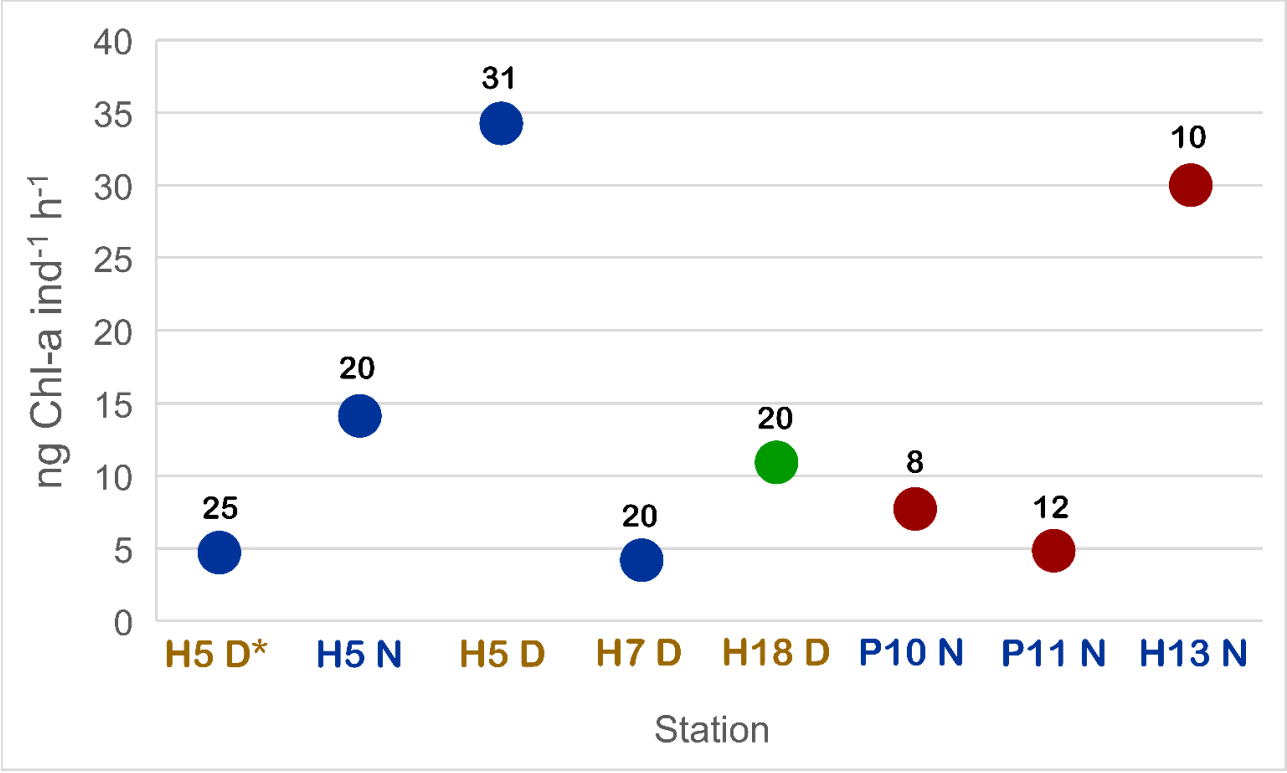

Figure C.5 Grazing rate (ng Chl-a ind^{-1} h^{-1}) for single individuals of *Euphausiacea* collected from the waters surrounding the Prince Edward Islands, with the numbers above the points indicating the length of each specimen in mm. With respect to data-point colour, dark blue = upstream, green = inter-island, and red = downstream. The x-axis shows station numbers, with N = night and D = day.

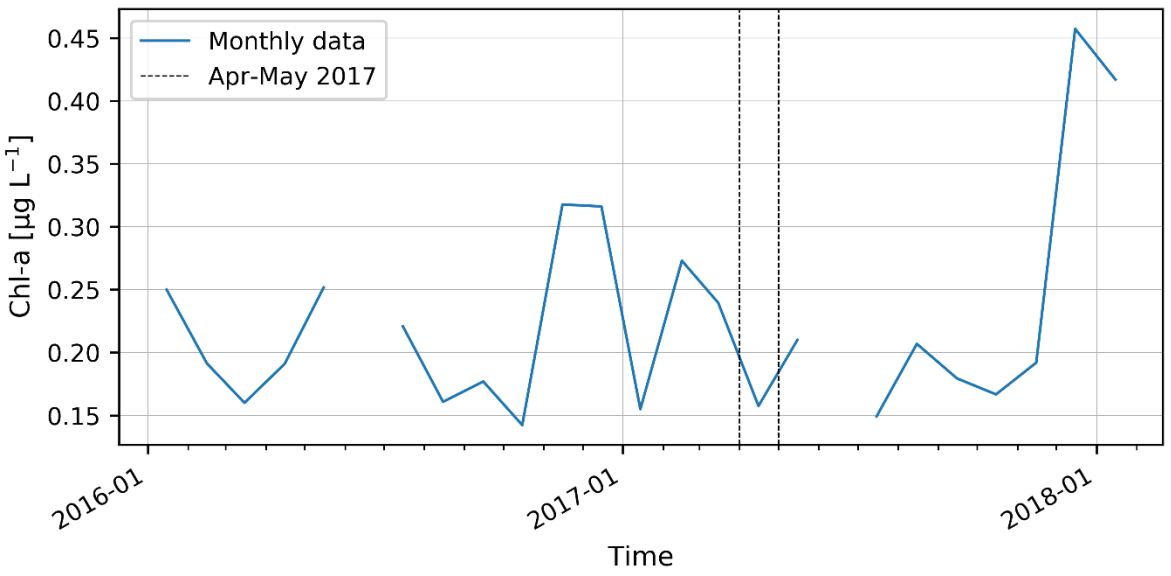

Figure C.6 Time-series of monthly MODIS Aqua satellite level-3 Chl-a product at 4 km spatial resolution (https://oceandata.sci.gsfc.nasa.gov/MODIS-Aqua/Mapped/Monthly/4km/chlor_a/) averaged over the region surrounding the Prince Edward Islands (between 46.40°S and 47.40°S, 37.40°E and 38.20°E) from October 2016 to January 2018. The black dashed lines indicate the expedition sampling period (April-May 2017) while the thin grey vertical lines indicate the start of each calendar year.

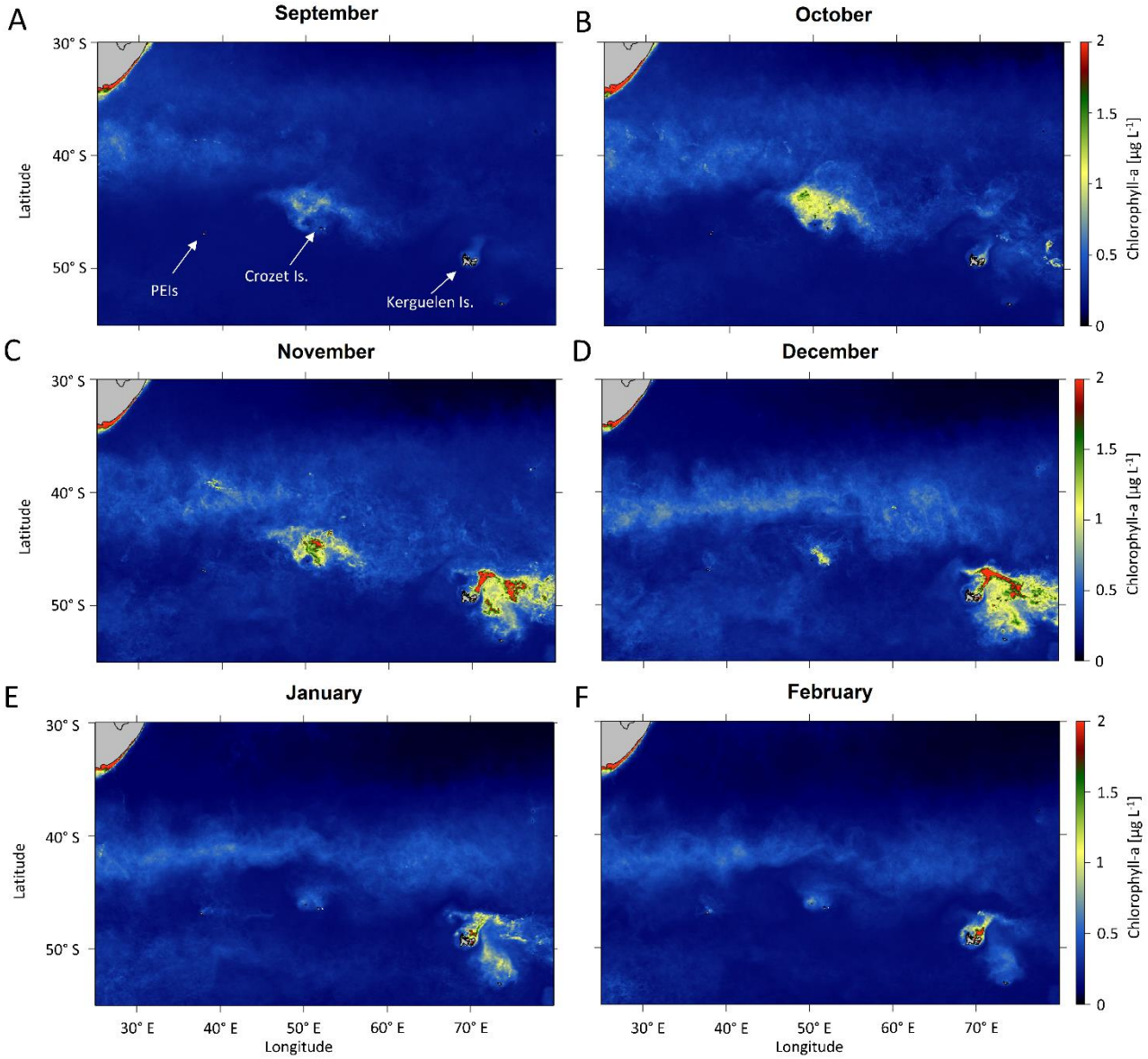
A
September
B
October
C
November
D
December
E
January
F
February
30° S
40° S
50° S
Latitude
PEIs
Crozet Is.
Kerguelen Is.
30° E
40° E
50° E
60° E
70° E
Longitude
Chlorophyll-a [µg L-1]
0
0.5
1
1.5
2

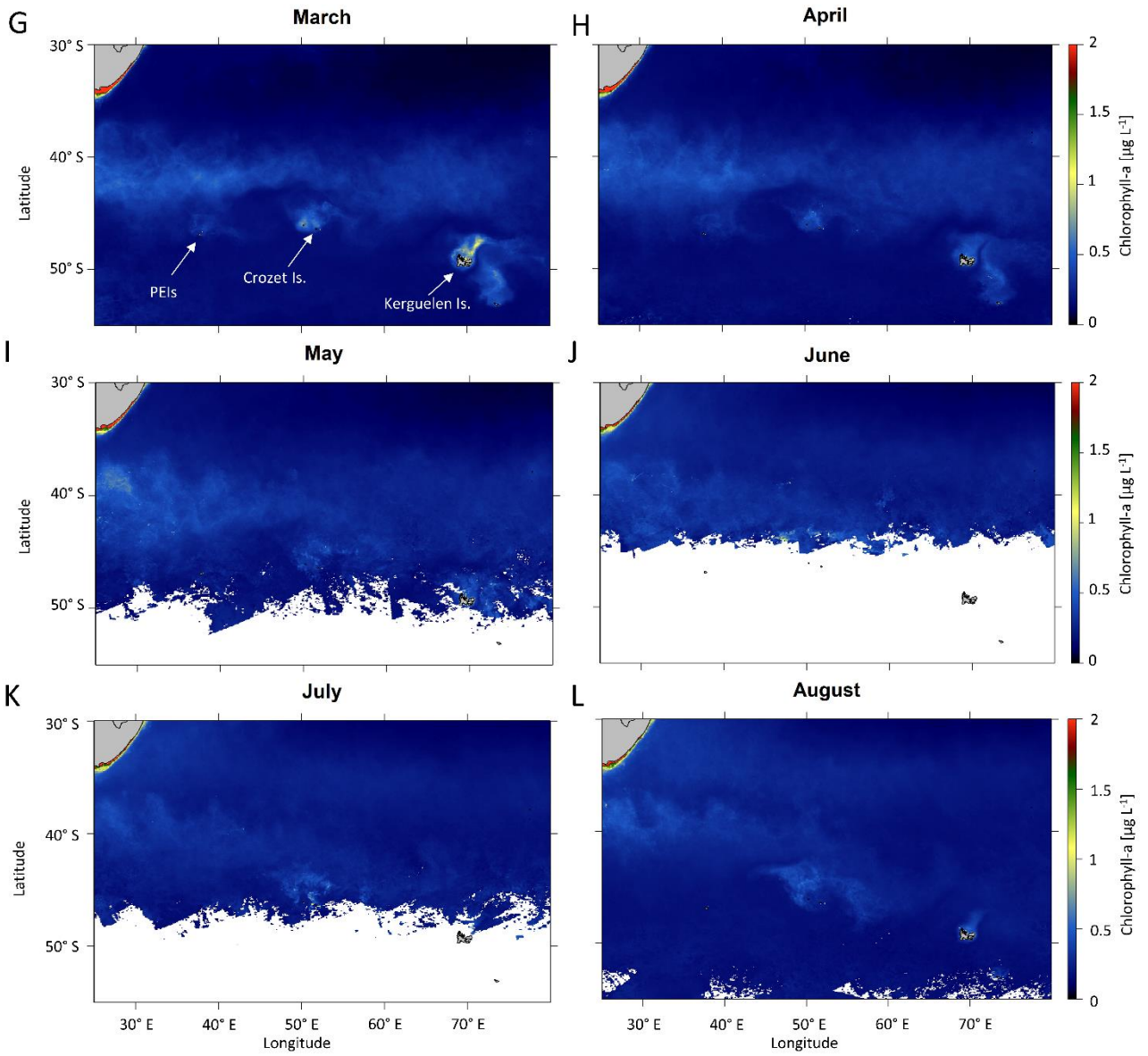

Figure C.7 Monthly average surface Chl-a concentrations in the Indian sector of the Subantarctic Ocean derived from the MODIS Aqua satellite level-3 Chl-a product at 4 km spatial resolution, for the period 2002-2019. A-F) September to February and G-L) March to August. The Prince Edward Islands (PEIs), Crozet Island, and Kerguelen Island are labelled on panels A and G. White region = no data available because of cloud cover.

Table C.8 Historical minimum and maximum total surface Chl-a concentrations ('Phytoplankton biomass') and rates of primary production measured around the Prince Edward Islands archipelago, along with our new measurements ('This study'). 'Cell carbon' = carbon biomass estimated from summed individual cellular carbon contents. ND = not determined. Table modified from McQuaid and Froneman (2008) and Ansorge *et al.* (2012).

Source	**Season/Year**	**Region**	**Phytoplankton biomass (mg Chl-a m^{-3})**		**Primary production (mg C m^{-2} d^{-1})**
El-Sayed *et al.* (1979)	Autumn 1976	Inter-island	0.09-1.88		211
Allanson *et al.* (1985)	Autumn 1983	Inter-island	0.10 –2.30		84-2100
Perissinotto and Duncombe Rae (1990)	Autumn 1985	Inter-island	0.10-2.80		70-3000
Van Ballegooyen *et al.* (1989)	Autumn 1987	Inter-island	0.05-0.45		47-312
Froneman and Balarin (1998)	Autumn 1997	Open ocean	0.29-0.52		ND
Balarin (1999)	Autumn 1998	Inter-island	0.20-0.81		119-353
Bernard and Froneman (2005)	Autumn 2003	Open ocean	0.15-0.28		ND
Bernard (2006)	Autumn 2005	Inter-island	0.24-0.71		ND
Allan (2011)	Autumn 2009	Inter-island	0.13-0.29		ND
			Phytoplankton biomass (mg Chl-a m^{-3})	**Cell carbon* (mg C m^{-3})**	
This study	Autumn 2017	Upstream	0.08-0.15	0.72-1.64	133-151
		Inter-island	0.18-0.33	0.96-2.78	292-1045
		Downstream	0.09-0.15	0.92-2.29	151-307

*mixotrophic and heterotrophic organisms <200 µm not included; see main text for details.

Table C.9 Historical estimates of mesozooplankton abundance and biomass in the waters surrounding the Prince Edward Islands archipelago, along with our new measurements ('This study'). 'vPEI' = in the vicinity of the Prince Edward Islands. PFZ = Polar Frontal Zone (between the SAF and APF). 'DW' = dry weight. We note that the 'summed carbon content' (i.e., sum of carbon contained in each zooplankton organism) is lower than the dry weight estimates – bulk zooplankton carbon content is expected to be ~40% of dry weight, although the percentage varies among taxa (Omori, 1969). Table modified from McQuaid and Froneman (2008) and Ansorge *et al.* (2012).

Source	**Season**	**Region**	**Abundance (ind. m^{-3})**	**Dry weight biomass (mg DW m^{-3})**	**Net type**
Grindley and Lane (1979)	Autumn 1976	vPEI	400 - 4850	8.70 - 28.40	WP-2
	Spring 1976	vPEI	1575 - 1854	14.60 - 34.90	
Boden and Parker (1986)	Autumn 1982 and Autumn 1983	vPEI	22 - 594	12.90 - 53	N70V
Allanson *et al.* (1985)	Autumn 1983	vPEI	ND	23.85 ± 10.3	WP-2
Perissinotto (1992)	Autumn 1985	Inter-island	150-229	17.4 – 30.0	Bongo
Perissinotto (1992)	Autumn 1989	Interisland	130-191	32.3 – 56.8	Bongo
Ansorge *et al.* (1999)	Autumn 1989	vPEI	10 - 312	2.47 - 62.70	Bongo
Froneman *et al.* (1998)	Autumn 1997	vPEI	5 - 263	0.60 - 15.70	Bongo
Bernard and Froneman (2002)	Autumn 2001	PFZ Open ocean	49 - 1512	0.70 – 25.0	Bongo
(Bernard and Froneman, 2003)	Autumn 2002	PFZ Open ocean	78 - 1034	9.80 - 27.90	Bongo
Bernard and Froneman (2009)	Autumn 2002	PFZ Open ocean	19.06 - 657.53	1.31 - 33.22	WP-2
	Autumn 2004		51.07 - 870.83	2.61 - 38.42	Bongo
	Autumn 2005		16.75 - 605.27	0.76 - 32.26	WP-2
				Summed carbon content (mg C m^{-3})	
This study	Autumn 2017	Upstream	104 - 254	1.71 - 13.36	Bongo
		Inter-island	71 - 156	3.88 - 13.36	Bongo
		Downstream	15 - 570	0.37 - 31.82	Bongo

Appendix D - Short-term variations in plankton biomass $\delta^{13}C$ and $\delta^{15}N$ and trophic structure near the Subantarctic Prince Edward Islands archipelago

Table D.1. Surface averages (mean ± 1SD) of particulate organic carbon and nitrogen concentrations (POC and PON [µM]), POC to PON ratio (C:N) and carbon and nitrogen isotope ratios of the suspended particulate matter ($\delta^{13}C_{SPM}$ $\delta^{15}N_{SPM}$ [‰]) for observations collected in the open ocean and in the vicinity of the Prince Edward Islands archipelago, during the five periods, July-August 2015, April-May 2016, December 2016, April-May 2017, and June-July 2017, at two hydrographic zones of the Southern Ocean: Subantarctic Zone (SAZ) and Polar Frontal Zone (PFZ).

Sampling period	Hydrographic zone	POC (µM)	PON (µM)	C:N	$\delta^{13}C$ (‰)	$\delta^{15}N$ (‰)
July-August 2015	SAZ	5.4 ± 1.5	0.7 ± 0.2	7.7 ± 0.5	-21.8 ± 1.5	0.8 ± 0.2
	PFZ	5.5 ± 2.2	0.7 ± 0.2	7.5 ± 0.8	-23.7 ± 7.7	3.9 ± 1.8
April-May 2016	SAZ	7.2 ± 0.7	1.1 ± 0.1	6.4 ± 0.2	-23.0 ± 0.5	-2.2 ± 0.3
	PFZ	6.1 ± 1.0	1.0 ± 0.2	6.1 ± 0.4	-23.7 ± 1.1	-3.1 ± 1.0
December 2016	SAZ	5.7 ± 0.3	0.9 ± 0.1	6.0 ± 0.0	-26.3 ± 0.3	-0.5 ± 0.1
	PFZ	6.5 ± 2.8	1.1 ± 0.5	6.1 ± 0.5	-25.7 ± 2.0	0.9 ± 1.9
April-May 2017	SAZ	5.7 ± 0.2	0.9 ± 0.2	6.6 ± 1.1	-22.2 ± 0.0	0.9 ± 1.5
	PFZ	6.6 ± 0.2	1.0 ± 0.3	6.6 ± 0.2	-21.6 ± 0.1	-2.0 ± 1.0
June-July 2017	SAZ	3.4 ± 4.1	0.5 ± 0.7	7.2 ± 1.2	-24.3 ± 1.5	1.9 ± 12.8
	PFZ	3.2 ± 1.0	0.4 ± 0.3	7.4 ± 0.6	-25.4 ± 1.9	1.3 ± 2.4

Table D.2 Surface averages (mean ± 1SD) of particulate organic carbon and nitrogen concentrations (POC and PON [µM]), POC to PON ratio (C:N) and carbon and nitrogen isotope ratios of the suspended particulate matter ($\delta^{13}C_{SPM}$ $\delta^{15}N_{SPM}$ [‰]) for observations collected in the open ocean and three areas in the vicinity of the Prince Edward Islands archipelago, according to the main ACC stream flow: upstream, inter-island, and downstream, during the five periods, July-August 2015, April-May 2016, December 2016, April-May 2017, and June-July 2017.

Sampling period	Area	POC (µM)	PON (µM)	C:N	$\delta^{13}C$ (‰)	$\delta^{15}N$ (‰)
July-August 2015	Open ocean	5.5 ± 3.6	0.7 ± 0.4	7.5 ± 0.7	-23.3 ± 9.2	3.2 ± 2.3
April-May 2016	Downstream	6.3 ± 0.2	1.0 ± 0.1	6.3 ± 0.0	-23.8 ± 0.5	-2.7 ± 0.2
	Inter-island	7.1 ± 0.3	1.2 ± 0.0	6.0 ± 0.0	-23.4 ± 0.1	-3.1 ± 0.5
	Upstream	6.4 ± 1.2	1.0 ± 0.2	6.3 ± 0.4	-23.4 ± 1.0	-2.6 ± 0.6
December 2016	Downstream	4.8 ± 0.2	0.9 ± 0.1	5.3 ± 0.0	-24.7 ± 0.0	0.4 ± 0.7
	Inter-island	7.4 ± 2.6	1.2 ± 0.3	6.4 ± 0.4	-25.0 ± 1.1	1.4 ± 1.7
	Upstream	5.8 ± 0.6	1.0 ± 0.1	6 ± 0.1	-26.9 ± 1.1	0.0 ± 0.2
April-May 2017	Downstream	5.6 ± 0.1	0.9 ± 0.2	6.5 ± 0.2	-21.2 ± 0.0	-2.6 ± 0.3
	Inter-island	8.5 ± 0.1	1.3 ± 0.1	6.8 ± 0.0	-22.1 ± 0.0	-1.2 ± 0.5
	Upstream	5.7 ± 0.2	0.9 ± 0.2	6.6 ± 1.1	-22.2 ± 0.0	0.9 ± 1.5
June-July 2017	Open ocean	3.3 ± 5.0	0.5 ± 0.9	7.2 ± 1.0	-24.7 ± 3.3	1.7 ± 14.5

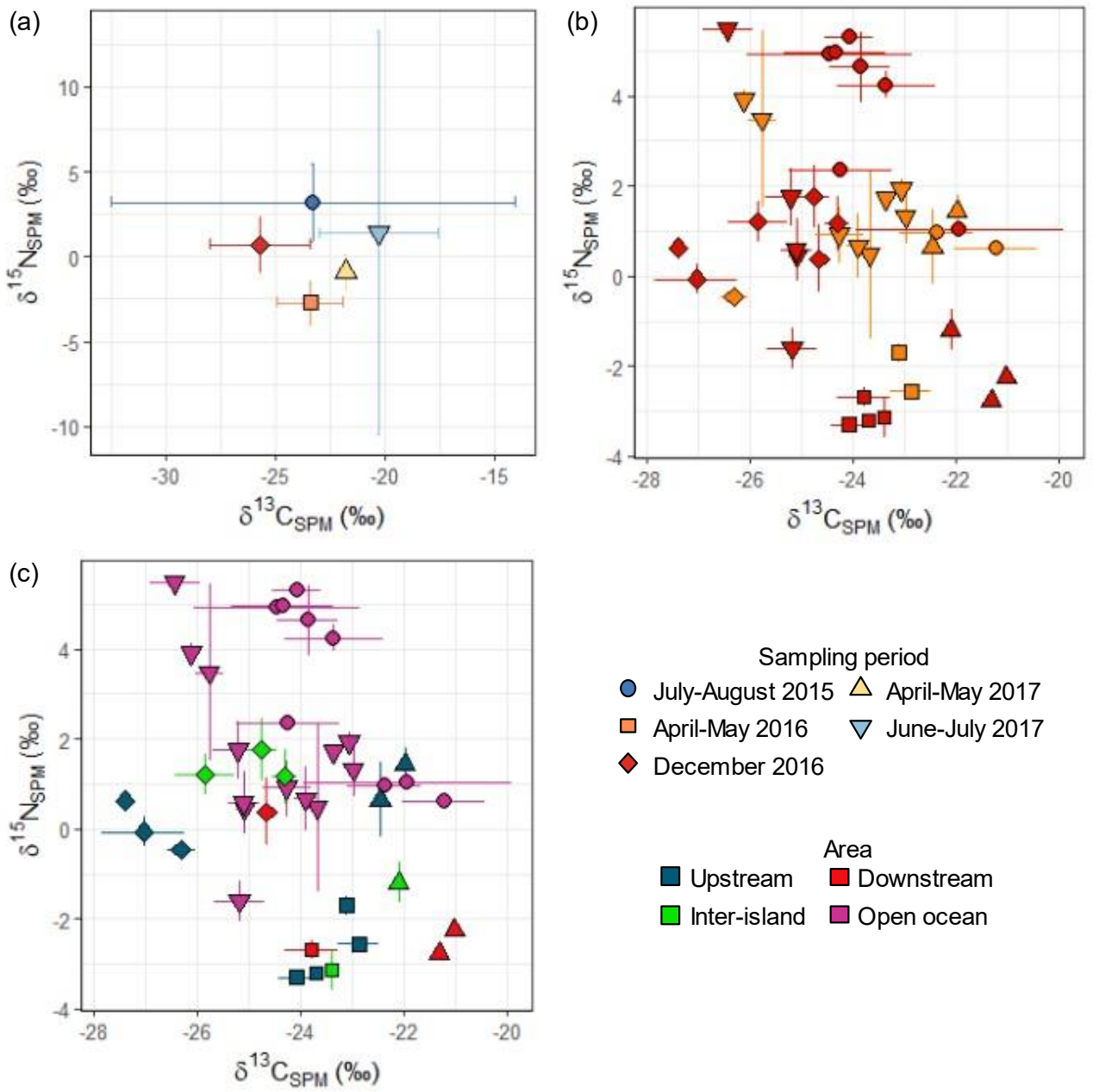

Figure D.1(a) carbon and nitrogen isotope ratios of particulate suspended matter ($\delta^{13}C_{SPM}$ and $\delta^{15}N_{SPM}$ [‰]) averaged within each of the five periods (shapes): July-August 2015 (circle), April-May 2016 (square), December 2016 (diamond), April-May 2017 (up-side triangle), and June-July 2017 (down-side triangle). colours = period of investigation and tonality refers to the seasons: cold colours (light and dark blue) = winter (July-August 2015 and June-July 2017, respectively) and warm colours (orange, red and yellow) = summer to autumn (April-May 2016, December 2016, and April-May 2017, respectively). (b) Carbon and nitrogen isotope ratios of particulate suspended matter ($\delta^{13}C_{SPM}$ and $\delta^{15}N_{SPM}$ [‰]) collected at surface at each period (shapes) and grouped by hydrographic zones (colours): Subantarctic Zone (SAZ; orange) and Polar Frontal Zone (PFZ; Red). (c) Carbon and nitrogen isotope ratios of particulate suspended matter ($\delta^{13}C_{SPM}$ and $\delta^{15}N_{SPM}$) collected at surface at each period (shapes) and grouped by areas (colours): within the open ocean (purple) or within the three areas in the vicinity of the Prince Edward Islands archipelago, according to the main ACC stream flow: upstream (blue), inter-island (green) and downstream (red).

Table D.3 Median [± interquartile range] of carbon to nitrogen ratio (C:N), and carbon and nitrogen isotope ratios ($\delta^{13}C$ and δ15N [‰]) of zooplankton taxa collected in the vicinity of the Prince Edward Islands archipelago (PEIs) during April-May 2016, December 2016 and April-May 2017.

Taxa	April-May 2016				December 2016				April-May 2017			
	C:N	$\delta^{13}C$ (‰)	$\delta^{15}N$ (‰)	N	C:N	$\delta^{13}C$ (‰)	$\delta^{15}N$ (‰)	N	C:N	$\delta^{13}C$ (‰)	$\delta^{15}N$ (‰)	N
Amphipoda					3.5	-23.9	2.6	1	4.4 ± 0.4	-23 ± 2.5	2.8 ± 2.8	6
Appendicularia					4.3	-25.1	3 .0	1				
Chaetognatha	4 ± 0.2	-21.9 ± 1.5	3.2 ± 0.9	2	3.2	-22.9	6.5	1	3.7 ± 0.1	-23.4 ± 0.0	5.0 ± 2.0	2
Copepoda	3.8	-21.3	6.6	1	4.4 ± 0.0	-23.4 ± 0.2	4.7 ± 1.7	2	3.8 ± 0.2	-24.5 ± 0.6	4.7 ± 1.2	14
Euphausiacea	4.1 ± 0.3	-23.7 ± 1.7	1.8 ± 2.0	3					3.7 ± 0.1	-22.8 ± 0.9	1.5 ± 4.0	13
Foraminifera					11.0	-15.5	4.8	1				
Lepadiformes									11.8 ± 0.8	-24.4 ± 1.2	5.0 ± 1.4	2
Ostracoda									4.2	-23.2 L29	4.4	1
Phaeodaria									4.3 ± 0.4	-23 ± 0.5	4.1 ± 1.2	2
Pisces	4.6	-23.1	0.8	1								
Pteropoda									7.2	-12.6	-2.3	1

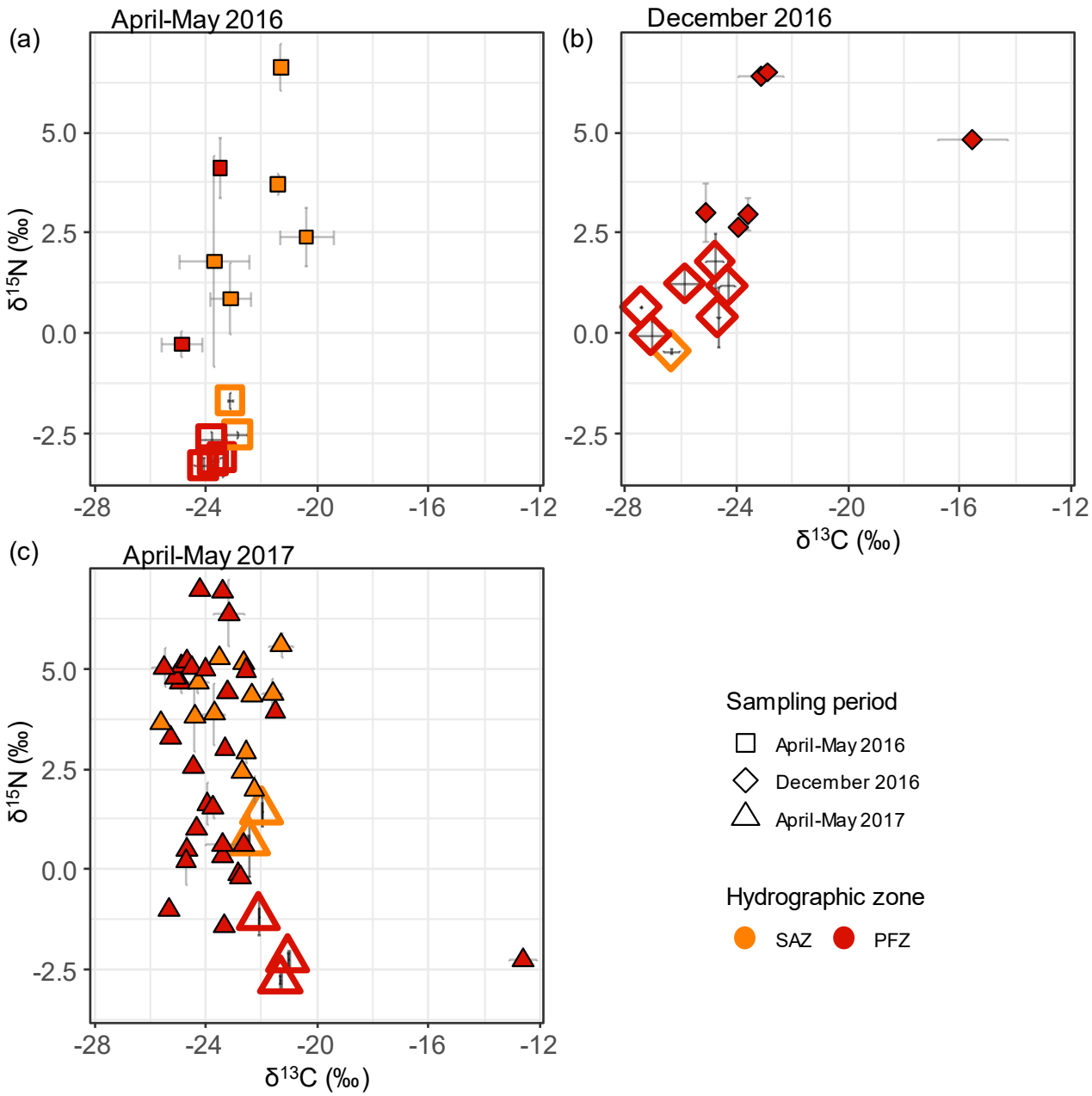

Figure D.2 Carbon and nitrogen isotope ratios of zooplankton specimens ($\delta^{13}C$ and $\delta^{15}N$ [‰]) observed at three periods (shapes): (a) April-May (squares), (b) December 2016 (diamond), and (c) April-May 2017 (up-side triangle) and grouped by hydrographic zones (colours): Subantarctic Zone (SAZ; orange) and Polar Frontal Zone (PFZ; Red).

Table D.4 Average [± 1SD] of carbon to nitrogen ratio (C:N), and carbon and nitrogen isotope ratios ($\delta^{13}C$ and $\delta^{15}N$ [‰]) of zooplankton taxa collected in the vicinity of the Prince Edward Islands archipelago (PEIs) during April-May 2016, December 2016 and April-May 2017 at different hydrographic zones: Subantarctic Zone (SAZ) and Polar Frontal Zone (PFZ).

Period	Family/Order	Hydrographic zone	C:N	$\delta^{13}C$ (‰)	$\delta^{15}N$ (‰)	N
April-May 2016	Euphausiacea	PFZ	4.3	-24.9	-0.3	1
	Chaetognatha	PFZ	3.8	-23.5	4.1	1
	Chaetognatha	SAZ	4.2	-20.4	2.4	1
	Euphausiacea	SAZ	3.9 ± 0.2	-22.6 ± 1.1	2.7 ± 1.0	2
	Pisces	SAZ	4.6	-23.1	0.8	1
	Copepoda	SAZ	3.8	-21.3	6.6	1
December 2016	Appendicularia	PFZ	4.3	-25.1	3.0	1
	Amphipoda	PFZ	3.5	-23.9	2.6	1
	Copepoda	PFZ	4.4 ± 0.0	-23.4 ± 0.2	4.7 ± 1.7	2
	Chaetognatha	PFZ	3.2	-22.9	6.5	1
	Foraminifera	PFZ	11.0	-15.5	4.8	1
April-May 2017	Copepoda	PFZ	3.9 ± 0.1	-24.7 ± 0.6	5.0 ± 1.5	11
	Amphipoda	PFZ	4.2 ± 0.5	-24.0 ± 1.9	1.9 ± 3.4	4
	Euphausiacea	PFZ	3.7 ± 0.1	-23.4 ± 1.0	0.6 ± 1.3	9
	Lepadiformes	PFZ	12.6	-23.2	6.4	1
	Euphausiacea	SAZ	3.7 ± 0.1	-22.3 ± 0.3	4.4 ± 0.8	4
	Phaeodaria	SAZ	4.3 ± 0.4	-23 ± 0.5	4.1 ± 1.2	2
	Copepoda	SAZ	3.7 ± 0.0	-24.3 ± 0.3	3.9 ± 0.4	3
	Amphipoda	SAZ	4.4 ± 0.0	-22.0 ± 0.7	4 ± 1.6	2
	Lepadiformes	SAZ	11	-25.6	3.6	1
	Ostracoda	PFZ	4.2	-23.2	4.4	1
	Chaetognatha	PFZ	3.7 ± 0.1	-23.2 ± 0.1	5.0 ± 2.0	2
	Pteropoda	PFZ	7.2	-23.2 ± 0.2	-2.3	1

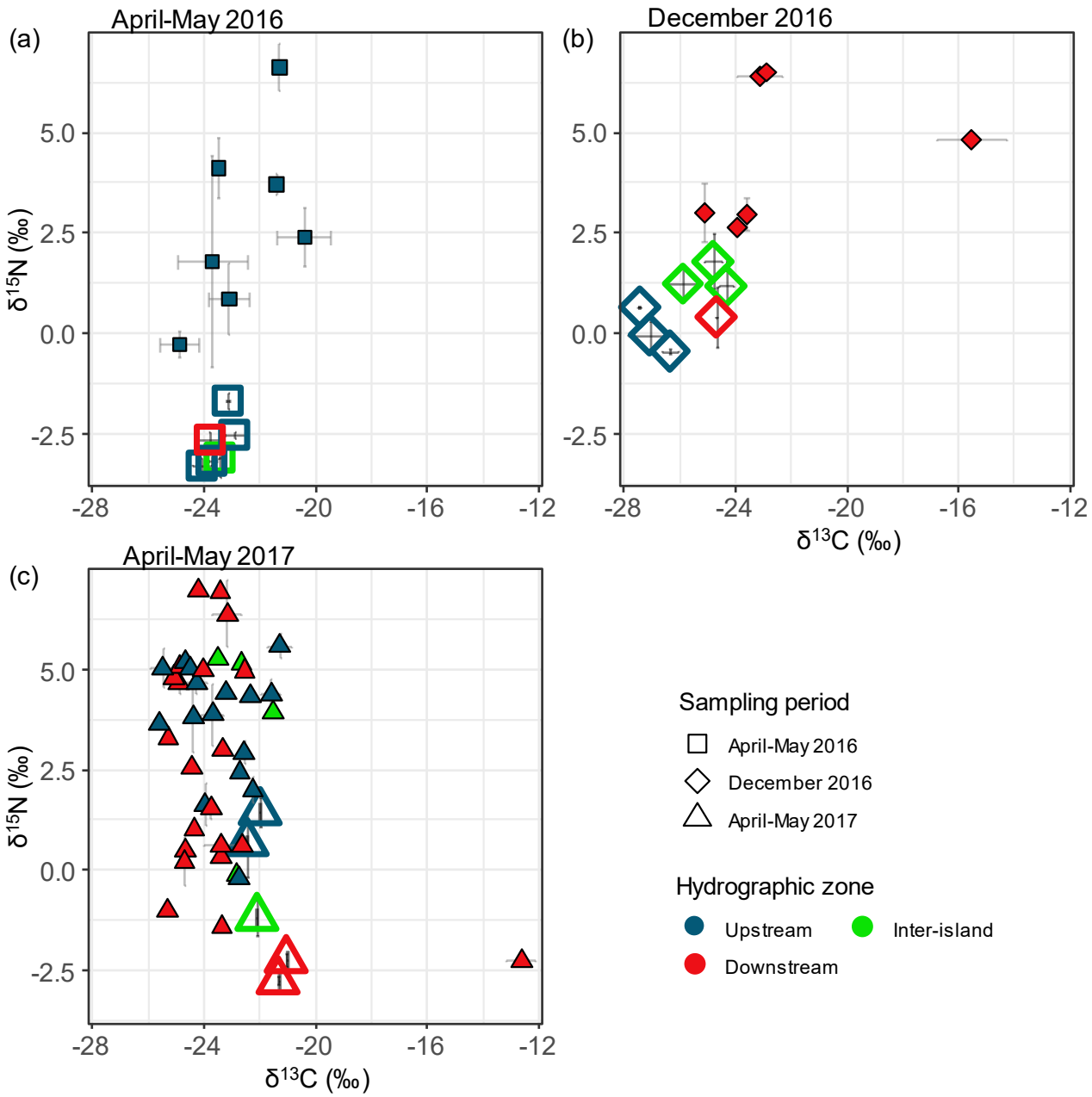

Figure D.3 Carbon and nitrogen isotope ratios of zooplankton specimens ($\delta^{13}C$ and $\delta^{15}N$ [‰]) observed at three periods (shapes): (a) April-May (squares), (b) December 2016 (diamond), and (c) April-May 2017 (up-side triangle) and grouped by areas in the vicinity of the Prince Edward Islands archipelago (colours): within the open ocean (purple) or within the three areas in the vicinity of the Prince Edward Islands archipelago, according to the main ACC stream flow: upstream (blue), inter-island (green) and downstream (red).

Table D.5 Average [± 1SD] of carbon to nitrogen ratio (C:N), and carbon and nitrogen isotope ratios ($\delta^{13}C$ and $\delta^{15}N$ [‰]) of zooplankton taxa collected in the vicinity of the Prince Edward Islands archipelago (PEIs) during April-May 2016, December 2016 and April-May 2017 at the open ocean and at three areas in the vicinity of the Prince Edward Islands archipelago, according to the main ACC stream flow: upstream, inter-island and downstream.

Sampling period	Family/Order	Area	C:N	$\delta^{13}C$ (‰)	$\delta^{15}N$ (‰)	N
April-May 2016	Euphausiacea	Upstream	4.1 ± 0.3	-23.7 ± 1.7	1.8 ± 2.0	3
	Chaetognatha	Upstream	4.0 ± 0.2	-21.9 ± 1.5	3.2 ± 0.9	2
	Pisces	Upstream	4.6	-23.1	0.8	1
	Copepoda	Upstream	3.8	-21.3	6.6	1
December 2016	Appendicularia	Downstream	4.3	-25.1	3.0	1
	Amphipoda	Downstream	3.5	-23.9	2.6	1
	Copepoda	Downstream	4.4	-23.4 ± 0.2	4.7 ± 1.7	2
	Chaetognatha	Downstream	3.2	-22.9	6.5	1
	Foraminifera	Downstream	11.0	-15.5	4.8	1
April-May 2017	Copepoda	Downstream	3.8 ± 0.1	-24.7 ± 0.6	4.7 ± 2.8	8
	Amphipoda	Downstream	4.4 ± 0.4	-24.7 ± 1.0	0.5 ± 2.3	3
	Euphausiacea	Downstream	3.7 ± 0.1	-23.4 ± 0.8	0.6 ± 0.9	6
	Lepadiformes	Downstream	12.6	-23.2	6.4	1
	Euphausiacea	Inter-island	3.6 ± 0.0	-22.7 ± 0.1	2.5 ± 2.6	2
	Amphipoda	Inter-island	4.0	-21.5	3.9	1
	Phaeodaria	Inter-island	4.7	-23.5	5.3	1
	Euphausiacea	Upstream	3.7 ± 0.1	-22.3 ± 0.5	2.0 ± 2.7	5
	Copepoda	Upstream	3.8 ± 0.2	-24.4 ± 0.3	4.8 ± 1.0	6
	Amphipoda	Upstream	4.4 ± 0.0	-22.0 ± 0.7	4.0 ± 1.6	2
	Phaeodaria	Upstream	4.0	-22.6	2.9	1
	Lepadiformes	Upstream	11.0	-25.6	3.6	1
	Ostracoda	Upstream	4.2	-23.2	4.4	1
	Chaetognatha	Downstream	3.7 ± 0.1	-23.4 ± 0.0	5.0 ± 2.0	2
	Pteropoda	Downstream	7.2	-12.6	-2.3	1